Surveyor Spacecraft System

SURVEYOR IV FLIGHT PERFORMANCE FINAL REPORT

JPL Contract 950056/September 1967

SSD 68189-4

N68-18659

K C Beall for

J. D. Cloud
Manager
System Engineering and Analysis Laboratory

T B Van Horne

T. B. Van Horne
Manager
Analysis Department

R. H. Leuschner

R. H. Leuschner
Head
Post Flight Analysis Section

HUGHES

HUGHES AIRCRAFT COMPANY
SPACE SYSTEMS DIVISION

CONTENTS

1.0 INTRODUCTION AND SCOPE

At 11 hours 53 minutes 29.215 seconds GMT (4 hours 53 minutes 29.215 seconds PDT) on Friday, 14 July 1967, the fourth Surveyor spacecraft was launched from pad 36A at AFETR. The launch was near perfect with the spacecraft being injected into its translunar trajectory by the single burn Centaur at 12 hours 4 minutes 57 seconds GMT. All subsequent spacecraft operations (separation, sun and star acquisition, midcourse correction, and coast and preterminal descent maneuvers) were performed in a "text book" manner with no significant anomalies until a sudden loss of signal from the spacecraft near the end of the retro burn period. Contact with the spacecraft was never regained subsequent to this signal loss, even though all conceivable nonstandard procedures were attempted.

The basic purpose of this report is to document the actual performance of this spacecraft throughout the mission, compare its performance with that predicted from spacecraft design, summarize preliminary failure investigations, and recommend any changes or modifications that should be made to the spacecraft design. This report is based on both real-time and postmission data analysis.

2.0   DESCRIPTION OF SURVEYOR SYSTEM

The Surveyor spacecraft is designed and built by Hughes Aircraft Company for the National Aeronautics and Space Administration under the direction of the California Institute of Technology Jet Propulsion Laboratory. It has been conceived and designed to effect a transit from earth to the moon, perform a soft landing, and transmit to earth basic scientific and engineering data relative to the moon's environment and characteristics. A brief description of the Surveyor vehicle design is given in the "Surveyor I Final Performance Report" (Reference 1).

2.1   SURVEYOR IV MISSION OBJECTIVES

The primary objectives of the Surveyor IV spacecraft system, as defined in Reference 2, were as follows:

1)   Accomplish a soft landing on the moon at a site east of the Surveyor III landing site.

2)   Demonstrate spacecraft capability to soft land on the moon with an oblique approach angle not greater than 35 degrees.

3)   Obtain postlanding television pictures.

4)   Obtain data on radar reflectivity, thermal characteristics, touchdown dynamics, and other measurements of the lunar surface through the use of various payload equipment, including the soil mechanics/surface sampler.

Surveyor IV was apparently unable to achieve its objectives due to the problem that caused the abrupt loss of telemetry during the retro phase.

2.2   SURVEYOR IV FLIGHT CONFIGURATION

For a summary description of the major Surveyor functions and design mechanization, consult the "Surveyor I Final Performance Report" or the "Surveyor Spacecraft Equipment Specification," Section 2.3 (References 1 and 3). In this report, design discussion has been limited to those changes first incorporated into Surveyor IV.   Table 2-1 lists those changes

TABLE 2-1. MAJOR SURVEYOR IV HARDWARE CHANGES

Change Title	ECA Number	Unit	Discussion
Incorporation of cross-coupled sidelobe logic in RADVS for all beams	113010	RADVS	Reduce probability that RADVS would reacquire a cross-coupled sidelobe return and thus supply incorrect data to FCSG, if loss of signal acquisition should occur during terminal descent. This change will also remove a previous operational constraint on spacecraft roll attitude during initial acquisition.
Disable RADVS cross-coupled sidelobe logic below 1000 feet	113469	RADVS	RADVS crosscoupled sidelobe logic (CCSLL) has been disabled below 1000 feet. This will prevent recurrence of the Surveyor III problem in which a loss of lock occurred at low altitude due to CCSLL action which prevented the 14-foot mark from being generated. CCSLL is most effective at higher altitudes and is known to produce erroneous outputs near the lunar surface.
Extend conditional reliable logic to 1000 feet	113469	RADVS	The enabling of conditional reliable logic (CRODVS) has been extended to 1000 feet. Previously, variations in spacecraft approach and roll angles, burnout velocity, and SDC tracker nonlinearity could have resulted in a main lobe being rejected. If such a rejection occurs after RODVS, the spacecraft will be without steering signals for an indeterminate time and will not maneuver to alleviate the main lobe rejection condition. Enabling of CRODVS until the spacecraft is in essentially vertical flight will provide proper steering signals continuously to reacquire in an unlocked condition. One thousand feet was the only practical point for terminating the CRODVS extension.
Add EP-40	113058	Spacecraft	EP-4 was a 10-ampere shunt that measured all spacecraft unregulated loads except RADVS, AMR, A/SPP motors, and squibs. With so many loads, it was difficult to analyze any particular one, especially vernier engine solenoid current during midcourse and terminal descent. Thus, all flight control unregulated current (roll actuator, gas jets, gyro thermal control, and gyro heaters) were removed from EP-4 (which became a 6-ampere shunt) and put on a new shunt, EP-40. The mission sequence was also changed to command off all heaters before midcourse and terminal descent.
New SM/SS temperature sensor	113257	Spacecraft	A new SM/SS temperature sensor (SS-13) was added on the mechanism substructure for more accurate measurement of mechanism temperature before turn-on while on the lunar surface. SM/SS motor torque rises at low temperatures to a point where gears and motor shafts do not have adequate margins of safety at operating temperature below -4°F. Previously, it had been difficult to assess whether this restraint was met without using large margins for possible errors which might severely limit SM/SS lunar operation.
RF transfer switch	113064	Transmitter	RF transfer microswitch failures occurred in test, probably due to their use in breaking coil current when switching RF modes. This change eliminates microswitches from the current interrupting function and uses existing circuitry in the transmitters instead. The microswitches will be retained to supply a switch position indicator signal required for the high voltage interlock in low power mode.

Table 2-1 (continued)

Change Title	ECA Number	Unit	Discussion
OCR trickle charge	111876	BCR	OCR trickle charge voltage was lowered to a range of 27.1 to 27.3 volts. The previous value of 27.5 volts caused excessive gas generation which is much reduced at the present value without any significant effect on total battery energy stored.
Add magnet to footpad 2	113546	Spacecraft	A magnet (80 to 100 Gauss) and a nonmagnetized bar have been added to the upper surface of footpad 2 per JPL Action Directive 315. This will permit investigation of the magnetic properties of soil placed on the footpad by the SM/SS.
Improved television azimuth and elevation drive motors	113336	Television	The elevation and azimuth drive motors for the TV survey camera mirror have been improved. In the elevation motor, there is a new drive shaft and flexible coupling, larger bearings, and a modified anti-backlash spring. The azimuth motor now uses machined parts instead of cast, and a new lubricant.
Add grounding to propellant tank superinsulation blankets	112182	Spacecraft	A conductive mesh has been installed in the outer surface of the propellant tank superinsulation blanket and will be grounded to the spaceframe. This will comply with range safety requirements to eliminate possible static charge buildup that could ignite fuel or spacecraft squibs. This mesh is essentially identical to that already installed on the retro rocket.
Power subsystem efficiency redesign	111301	Power (OCR)	The optimum charge regulator (OCR) has been redesigned for improved efficiency (80 percent versus the previous 77 percent). The new unit is electrically interchangeable with the old.

that have a significant effect on spacecraft performance, with a brief explanation of the reason for change. Additional minor differences of Surveyor IV compared with Surveyor III are given in Table 2-2. For completeness, a summary of major changes for each preceding spacecraft is given in Table 2-3. To define the spacecraft configuration at launch, a list of Surveyor IV control items, separated by subsystem or function, is given in Table 2-4.

2.3 REFERENCES

1. "Surveyor I Flight Performance Final Report," Hughes Aircraft Company, SSD 68189R, October 1966.

2. "Space Flight Operations Plan, Surveyor Mission D," Jet Propulsion Laboratory, EPD-180-S/MD, 26 June 1967.

3. "Surveyor Spacecraft Equipment Specification," Hughes Aircraft Company 224832, Revision A.

TABLE 2-2.   SURVEYOR IV/SURVEYOR III MINOR
HARDWARE DIFFERENCES

Change Description	ECA Number
Spacecraft armature plating of bellows	112439
Control of thermal blanket and tank insulation thickness	113008 and 113025
Add leg potentiometer support bracket	113259
Provide strain relief for various connectors	113242, 113298, 113208
Thermal wrap certain connectors	113281
Propellant tank and standpipe kit	113306
Redesign of regulator-ECU chassis for AMR	110349
Modify platenuts and add clamp on AMR	112675
Redimension antenna lower support bracket	110605
Elimination of elevation and roll axis interference	112591
Revise output connector pins (same as 274100 series)	112843
Eliminate interference between strain relief and EMA	113189
Thermal paint requirements on FCSG	111288
Add trimming resistor in IRU	113354
Wrap main battery to prevent compartment damage	112900
Allow coax tube adjustment and remove cable shrink sleeving	231729
New brackets for RADVS waveguide installation and antenna alignment	112416
Replace thermal surface of aluminized teflon with white paint on SDC cover	113156

Table 2-2 (continued)

Change Description	ECA Number
Addition of spacer to waveguide support	113243
Correct identification of switch	113272
Remove SM/SS ballast and repaint to eliminate TV view interference	113061
Vacuum bake of thermal switch contact	112830
Change eyelet length	112626 and 112694
Change vidicon tube type from 988925-1 to 988937-1	112213
Delete balls, plunger spring, and screws in 273663 subassembly	113308
Add stiffener to wire bundle on basic bus 1	113356
Replace self-locking nuts with hex nuts, as required	113340
Relieve flange above auxiliary battery compartment, if required	113392
Modify paint pattern for footpads and footpad ballast	113419
Change ground lugs and length of pinpuller ground wires	113422
Relax alignment tolerances for omnidirectional antenna A	113441
Remove lanyard assembly from test connector dust covers	113459
Use combination of lubricated and unlubricated screws and inserts in compartments A and B	113490
Add antistatic spray to nonconductive covers	113538
Enlarge inner diameter on caps protecting attitude jets	113578
Torque retaining nuts "finger tight" and bond	113447
Rework receivers when in unit area	113500
Change method of locking studs from locktite to epoxy	113411

TABLE 2-3.   MAJOR CHANGES IN PRECEDING SPACECRAFT

Item	Description
Surveyor III Major Changes	
1) Add two special viewing mirrors	On Surveyor III, enables TV survey camera to view as much as possible in area of crushable blocks and vernier engines.
2) Landing gear kickout springs	Add kickout spring to overcome initial static friction during initial leg deployment.
3) Install new retro	High impulse main retro installed in spacecraft.
4) Sidelobe frequency discrimination	Surveyor III only. Antenna sidelobe skewing of 2.0 instead of 0.2 degree necessitated crosscoupled sidelobe logic modification since rejection logic circuitry was designed for a frequency rejection criteria based upon 0.2 degree.
5) Compartment B harness	Addition of zener diode limiter to V_x and V_y outputs to prevent possible erroneous readings in other telemetry channels.
6) SM/SS added	Approach camera TV-4 replaced with simplified SM/SS subsystem.
7) Addition of sun bonnet on TV camera	Sun shade added to mirror assembly to prevent direct sunlight from entering mirror hood at sun angles from zenith to 45 degrees.
Surveyor II Major Changes	
1) Boost regulator overload trip circuit	In Surveyor I, the overload trip circuit in the boost regulator had to be disabled because it would trip with a 2-millisecond transient. The Surveyor II boost regulator has an overload trip circuit that does not trip unless the transient is 20 to 30 milliseconds.
2) a) Filter chokes on input to ESP and AESP b) Filter on A/D converter 2 nulling amplifier in CSP	Both of these design improvements eliminate the large variations in temperature readouts on telemetry which were present on Surveyor I.

Table 2-3 (continued)

	Item	Description
3)	Omnidirectional antenna latch and release mechanism	Surveyor II release mechanisms for omnidirectional antennas A and B have been redesigned to prevent deployment problem that occurred in Surveyor I flight. Clevis opening has been broadened, and a kickout spring has been added.
4)	Telemetry of flight control return signal	In Surveyor II, flight control return signal is telemetered so that varying harness voltage drops can be corrected to provide more accurate data on flight control telemetry signals.
5)	RADVS sidelobe rejection logic	Two resistors in Surveyor II signal data converter were removed in order to lower the point at which the sidelobe signals are rejected from 28 to 25 db.
6)	Canopus sun reference filter change	Surveyor I had a Canopus sun filter with a reduction of 50 percent (filter factor of 1.5) to compensate for any possible fogging of Canopus sensor window in accordance with recent measurements of Canopus brightness at Tucson. Surveyor II has a filter factor of 1.2. This has been reduced from 1.5 to 1.2 because the fogging problem did not materialize at the Canopus sensor temperature of 79° F for the Surveyor I flight.
7)	Auxiliary battery cover paint pattern	The paint pattern of the auxiliary battery container was changed to increase the temperature of this unit, which became too low during coast mode II for Surveyor I.

TABLE 2-4. SPACECRAFT UNIT CONFIGURATION AT LAUNCH

Subsystem	Part Name, Number, S/N
Electrical Power	
	Main battery, 237900, S/N 123
	Auxiliary battery, 237921-1, S/N 93
	Auxiliary battery compartment, 263730, S/N 3
	Auxiliary battery control, 273000-2, S/N 13
	Thermal container and heater A, 232210-1, S/N 19
	Thermal container and heater B, 232210-2, S/N 15
	Boost regulator, 274200-12, S/N 13
	Boost regulator filter, unregulated bus, 290080, S/N 15
	Boost regulator input choke, 290390, S/N 13
	Battery charge regulator, 284100-1, S/N 11
	Solar panel, 237760-3, S/N 5
	Main power switch, 254112, S/N 10
	Engineering mechanisms auxiliary, 263500-6, S/N 13
Flight Control	
	Flight control sensor group, 235000-5, S/N 2
	Inertial reference unit, 235100-1, S/N 7
	Roll actuator, 235900-3, S/N 8
	Gas supply, attitude jet, 235600-2, S/N 7
	Attitude jets, 235700-3, S/N 16 and 5

Table 2-4 (continued)

Subsystem	Part Name, Number, S/N
	Attitude jet, 235700-2, S/N 13
	Secondary solar sensor, 235450-1, S/N 6
Radar	
	Altitude marking radar, 283827-1, S/N 11
	KPSM (RADVS), 232909, S/N 10
	SDC (RADVS), 232908-6, S/N 12
	Altitude velocity sensor antenna (RADVS), 232910, S/N 10
	Velocity sensor antenna (RADVS), 232911-1, S/N 9
	Waveguide assembly (RADVS), 232912-1, S/N 8
Telecommunications	
	Transmitter A, 263220-5, S/N 12
	Transmitter B, 263220-5, S/N 23
	Command receiver A, 231900-3, S/N 17
	Command receiver B, 231900-3, S/N 25
	Omnidirectional antennas A and B, 232400, S/N 23 and 22
	Telemetry buffer amplifiers A and B, 290780-1, S/N 15 and 16
	Planar array antenna, 232300, S/N 17
	Low pass filters A and B, 233466, S/N 32 and 21
	RF switch, SPDT, 284344, S/N 11
	RF transfer switch, 284343, S/N 14

Table 2-4 (continued)

Subsystem	Part Name, Number, S/N
Signal Processing	
	Signal processing auxiliary, 232540-1, S/N 3
	Central command decoder, 232000-5, S/N 5
	Low data rate auxiliary, 264875-2, S/N 7
	Engineering signal processor, 233350-9, S/N 1
	Auxiliary engineering signal processor, 264900-6, S/N 1
	Central signal processor, 232200-8, S/N 5
	TV auxiliary, 232106-5, S/N 12
Television	
	Survey camera, 283712-2, S/N 11
	Photo chart, antenna B, 231051, S/N 15
	Photo chart, leg 2, 230992, S/N 15
	Viewing mirror, 3023928, S/N 2
	Viewing mirror, 3023929, S/N 2
Propulsion	
	Oxidizer tank, 287119, S/N 4
	Oxidizer tank, 287121, S/N 3
	Oxidizer tank, 287120, S/N 3
	Fuel tank, 287117, S/N 7
	Fuel tank, 287118, S/N 5
	Fuel tank, 287117, S/N 8
	Helium tank and valve assembly, 262789-2, S/N 3

Table 2-4 (continued)

Subsystem	Part Name, Number, S/N
	Thrust chamber assembly, 285063-4 (Hughes), S/N 557
	Thrust chamber assembly, 285063-5 (Hughes), S/N 566
	Thrust chamber assembly, 285063-6 (Hughes), S/N 547
	Main retro, 238612-1, S/N 3 (A22-9)
Mechanisms	
	Spaceframe, 264178-3, S/N 1
	Omnidirectional antenna A mechanism, 302800-1, S/N 2
	Omnidirectional antenna B mechanism, 273880-1, S/N 4
	Antenna/solar panel positioner, 287580, S/N 4
	Leg position pots, 988684-1, S/N 989067, 989068, and 989069
	Retro-rocket release mechanisms, 230069-1, S/N 13, 14, and 40
	Separation sensing and arming devices, 293400, S/N 13, 14, and 16
	Shock absorbers, legs 1 through 3, 238927, S/N 7, 9, and 12
	Footpads, legs 1 and 3, 263947, S/N 35, 511
	Footpad, leg 2, 263947-1, S/N 464
	Magnet and control bar assembly, 3050831, S/N 5
	Landing gear, 261278, S/N 6
	Landing gear, 261279, S/N 5

Table 2-4 (continued)

Subsystem	Part Name, Number, S/N
	Landing gear, 261280, S/N 6
	Crushable blocks, 261281, S/N 1, 2, and 3
	Accelerometer amplifier, 239011, S/N 6
	Strain gauge amplifier, 238930, S/N 3
SM/SS Subsystem	
	SM/SS auxiliary, 3024536, S/N 2
	SM/SS mechanism, 3024700, S/N 2
Thermal Control	
	Thermal switch A, 3028200-2, S/N 3
	Thermal switch A, 3028200-1, S/N 1, 2, 5, 6, 7, 9, 12, and 20
	Thermal switch B, 3028200-4, S/N 3
	Thermal switch B, 3028200-3, S/N 1, 2, 4, 5, and 6
	Thermal shell, compartment A, 286459, S/N 4
	Thermal shell, compartment B, 286460, S/N 4
	Thermal tray, compartment A, 264334-1, S/N 6
	Thermal tray, compartment B, 276935, S/N 7
Harness	
	Wiring harness compartment B, 3025332, S/N 1
	Wiring harness compartment A, 3025963, S/N 1
	Wiring harness basic bus 1, 3050651, S/N 1
	Wiring harness TV camera, 292259, S/N 2
	Wiring harness basic bus 2, 286240, S/N 2

Table 2-4 (continued)

Subsystem	Part Name, Number, S/N
	Wiring harness auxiliary battery, 264100, S/N 8
	Wiring harness retro motor, 286984, S/N 2
	Wiring harness battery cell volt, 3025155, S/N 5
	Wiring harness separation squibs, 286926, S/N 2
	Wiring harness A/SPP, 286417, S/N 3
	Cable, retro igniter, 286927, S/N 2

3.0 SYSTEM SUMMARY

3.1 SUMMARY OF SIGNIFICANT ANOMALIES

The anomalies that occurred during Mission D are summarized in Table 3-1. For this report, an anomaly is defined as an unexpected occurence that might be indicative of a spacecraft trouble or failure. The anomalies are discussed in greater detail in the sections noted in this table.

Currently, nine spacecraft anomalies have been identified with the Surveyor IV mission. Only three TFRs are noted in Table 3-1, and these are associated with Failure Review Board investigations of the failure during terminal descent. Disposition of these TFRs is presently open.

TABLE 3-1. SPACECRAFT ANOMALIES

Number	GMT, day:hr:min:sec	Anomaly	Effect on Mission	TFR Number
1	198:02:02:40	Just prior to main burn-out, all RF contact with spacecraft was lost. Attempts to re-establish contact were unsuccessful (see subsections 4.3 and 5.3.2.3).	Catastrophic. Loss of mission.	18262
2	After 198:02:02:00	During retro burn, the thrust commands to the vernier engines showed an apparent periodic (18 Hz) oscillation with a peak-to-peak magnitude of about 7 pounds for engines 1 and 2 and 2 pounds for vernier engine 3 (subsection 5.5.2).	If oscillation was small, mission would not be affected. Large oscillation may cause structural damage with con-sequential catas-trophic effects.	65340

Table 3-1   (continued)

Number	GMT, day:hr:min	Anomaly	Effect on Mission	TFR Number
3	Coast period	Degraded receiver B performance. An approximate -5 db bias existed in either the performance or calibration of the receiver. Lunar recalibration was precluded by mission failure (see subsection 5. 3. 2. 1).	None	None
4	196:22:27	Simultaneous DSS-51 and DSS-11 loss of lock during station transfer in pass 2, possibly due to ground station transmitter tuning (see subsection 5. 3. 2. 2).	Unknown. Did not reoccur during mission; signature in no way compares to that of signal loss during terminal descent.	None
5	Approximately 196:19:22	Temperature of oxidizer tank 1 suddenly increased from 49° to 54°F, and subsequently returned to 49°F (see subsection 5. 1. 3).	None	None
6	Before 198:02:02	During terminal descent, the no-signal AGC voltage for the AMR prior to enable was over 2. 0 volts versus 1. 5 to 1. 6 volts from preflight test experience (see subsection 5. 8. 2).	None, since AMR operated properly in all respects.	29462

Table 3-1   (continued)

Number	GMT, day:hr:min	Anomaly	Effect on Mission	Number
7	195:12:02	Spacecraft boost accelerometer (Z-axis) showed three shocks at 4 minutes 50 seconds after Centaur main engine ignition. One was 3 g and two were 8 g peak-to-peak, with predominate frequency of 1400 Hz. Shock characteristics were not indicative of spacecraft squib firing.	None since magnitude of shock was below that used for spacecraft design and test environment.	None
8	Coast period	At least seven "false Canopus" particles were noted. Cotton smocks used on Surveyor IV for the first time may have caused more spurious particles to be present on the spacecraft (see subsection 5.5.4.4)	None	None
9	198:02:02	An oscillation occurred on RADVS lateral velocity channels (V_x and V_y) of 10 fps peak-to-peak in a period from 36.5 to 40.5 seconds after the AMR mark. No correlation could be found with thrust command oscillations. Equivalent attitude motion is about 0.1 degree (see subsection 5.9.3.12).	Apparently none	None

3.2 SYSTEM PERFORMANCE PARAMETERS

Performance parameters that could be directly determined through analysis of spacecraft telemetry are summarized in Table 3-2. Required or predicted values for these parameters are included in this summary for comparative purposes.

3.3 CONCLUSIONS AND RECOMMENDATIONS

3.3.1 Conclusions

Following a near-perfect injection and equally perfect transit phase and midcourse, the Surveyor IV flight was essentially uneventful until loss of data during terminal descent. Extensive investigation of this failure resulted in the delineation of possible failure modes and the initiation of ancillary studies. Subsection 4.3 highlights the results of the failure review preliminary investigation.

3.3.2 Recommendations

Recommendations from the Surveyor IV flight are primarily associated with the investigations into the sudden loss of RF contact and consequent mission failure. Since no single failure mode could be isolated, the following recommendations are made to ensure better data retrieval, and for additional investigations, where feasible, of all suspected subsystems.

1) Provide emergency ground command tape sequence for loss of RF during terminal descent.

2) Turn on touchdown strain gauges prior to retro ignition for additional continuous telemetry data.

3) Investigate use of mode 2 telemetry data for terminal descent to obtain retro upper and lower case temperatures.

4) Investigate change to spacecraft RF switching to provide capability for simultaneous high and low power transmitter operation on omnidirectional antennas.

5) Investigate feasibility of postinjection transit phase TV damage assessment.

6) Review JPL S-9 "buzz" test data and develop and carry out additional S-9 "buzz" tests required to reverify attitude control loop "buzz" margins for a normal spacecraft and establish such margins for a spacecraft with certain key structural failures.

7) Investigate provisions for continuous accelerometer or thrust command telemetry.

8) Make a special inspection of the 29-volt low ripple lines for correct harness dress and stress relief.

9) Review existing postvibration structural inspection procedures and techniques, and make recommendations for additional procedures, such as X-rays, for those items found to be unaccessible using normal inspection techniques.

10) Complete investigation of improved X-ray procedures for main retro.

11) Investigate additional spacecraft flight acceptance tests that will provide additional confidence in structural integrity of the wire harness.

TABLE 3-2. SYSTEM PERFORMANCE DETAILS AND MISSION EVENTS

			Performance Details			
Item	Description	Actual	Subsection Reference	Predicted or Specified	Reference	Comments
			Launch to Acquisition Summary			
1	Dynamic Flight Environment					
	Ignition-liftoff	0	Flight path analysis and command	0	Preflight nominal trajectory	0 second is 195:11:53:29.215 In seconds referenced to launch
	Booster engine cutoff	141.88		143.66		
	Booster jettison	145.38		147.76		
	Insulation panel jettison	176.18		177.66		
	Nose fairing jettison	203.38		204.66		
	Sustainer engine cutoff	237.98		238.18		
	Atlas/Centaur Separation	241.58		240.18		
	Centaur main engine cutoff 1	687.98		680.67		
	Surveyor					
	Extend landing gear	715.78		713.68		
	Extend omnidirectional antenna	725.28		724.18		
	Transmitter to high power	745.98		744.68		
	Electrical disconnect from Centaur	751.28		750.18		
	Centaur separation	756.88		755.68		
2	Time to null rates to 0.1 deg/sec	<13 seconds	5.5.4.2	Within 50 seconds	224832A (3.5.2.1)	
	Pitch	+0.35 degree				
	Yaw	-2.0 degrees				
	Roll	0 degree				
3	Centaur Retro Maneuver Time	L + 996.88 seconds	Flight path analysis and command	L + 995.98 seconds	Nominal	
4	Solar Axis Deployment Time	348 seconds	5.10.4.3	340 seconds	Preflight test	
5	Spacecraft separated weight	2294.9 pounds	SSD 68252-9			Spacecraft weight, C.G., and moments of inertia at separation
6	Spacecraft C.G. Location		SSD 68252-9			
	X	+0.065 inch				
	Y	-0.239 inch				
	Z	-12.139 inch				

Table 3-2 (continued)

Item	Description	Actual	Subsection Reference	Predicted or Specified	Reference	Comments
Performance Details					
7	Spacecraft Moment of Inertia		SSD 68252-9			
	I_{xx}	213.5 slug/ft^2				
	I_{yy}	209.8 slug/ft^2				
	I_{zz}	225.7 slug/ft^2				
Coast Summary					
	Sun Acquisition		5.5.4.3		224832A (7.3.3.3.4)	Roll maneuver until activation of acquisition sun sensor and then a yaw maneuver until primary sun sensor illumination
1	Roll angle	-59.4 degrees				
2	Yaw angle	+42.1 degrees				
3	Total time	203 seconds		18 minutes maximum		
	Star Acquisition		5.5.4.4		224832A (7.3.3.3.5)	
4	Proper acquisition and Canopus verification	Automatic				
5	Roll angle from beginning of maneuver to Canopus	+210.5 degrees				
6	Objects identified	Eta U Majoris, Delta Veldrum, Gamma Casiopeiae, Canopus, Earth and Moon				
7	Mean roll rate during star map phase	0.5003 deg/sec		0.5 deg/sec		
8	Effective gain of Canopus sensor	1.16 x Canopus			Design	Normally the gain setting is 1 x Canopus
	Attitude Orientation					
9	Average error from sunline		5.5.4.6	Within 0.2 degree	224832A (7.3.3.3.6)	Sensor group roll axis shall be held within 0.2 degree of sun-spacecraft line.
	Pitch	+0.009 degree				
	Yaw	+0.08 degree				
10	Average error from Canopus line of sight	+0.104 degree	5.5.4.6	Within 0.2 degree	224832A (7.3.3.3.6)	Canopus sensor null with respect to sensor group roll pitch plane
11	Limit Cycle Optical Mode		5.5.4.6		224832A (7.3.3.3.3)	
	Average amplitude-roll	0.6 degree		±0.44 degree		
	Average amplitude-pitch	0.44 degree				
	Average amplitude-yaw	0.41 degree				
	Average period	64 seconds				

Table 3-2 (continued)

Item	Description	Actual	Subsection Reference	Predicted or Specified	Reference	Comments
	Performance Details					
12	Limit Cycle Inertial Mode		5.5.4.6		224832A (7.3.3.3.3)	
	Average amplitude-roll	0.48 degree		±0.44 degree		
	Average amplitude-pitch	0.46 degree				
	Average amplitude-yaw	0.53 degree				
	Average period	61 seconds				
13	Gyro Drift		5.5.4.9			
	Roll	-0.5 deg/hr		< 1 deg/hr	224832A (7.3.3.3C)	Non g sensitive
	Pitch	-1.0 deg/hr				
	Yaw	+0.15 deg/hr				
	Midcourse Summary					
1.0	Total Magnitude Errors (RSS)	0.18 fps	5.5.4.8			
1.1	Errors proportional to maneuver magnitude		5.5.4.8			
	Accelerometer accuracy			1.1 percent	234632C	
	Reference signal			0.5 percent	234600E	
	FCE null			0.15 percent	234600E	
	Thrust bias variation			0.09 percent	287105	
	Control channel gain variation	0.17 fps		0.07 percent	234600E	
	Accelerometer misalignment			0.06 percent	234600E	
	Total proportional errors: (RSS)			0.17 percent		
1.2	Errors independent of maneuver magnitude		5.5.4.8			
	Shutdown impulse dispersion	-0.004 fps		±0.63 lb-sec	287015	
	Hysteresis limit cycle	0		3 milli-amperes	287015	
	Ignition transient	0		—	—	
	Timing granularity	-0.06 fps	5.5.4.8	0.05 second	224832A (7.2.1.9)	
	Total independent errors (RSS)	-0.064 fps				
2.0	Total Attitude Errors (RSS)	0.19 degree	5.5.4.6	±0.7 degree		Attitude error prior to ignition (0.1 degree uncertainty)

Table 3-2   (continued)

			Performance Details			
Item	Description	Actual	Subsection Reference	Predicted or Specified	Reference	Comments
2.1	Initial position errors					
	Sensor group roll axis to sun/spacecraft line	Pitch = +0.009 degree		0.2 degree		
		Yaw = +0.08 degree				
	Pitch/yaw limit cycle	-0.06/-0.1 deg/sec		0.3 degree		
	Sensor group roll-pitch plane to Canopus-spacecraft line	+0.104 degree		0.2 degree		
	Roll limit cycle	+0.15 degree		0.3 degree		
2.2	Rotational magnitude errors					
	Gyro torquer scale factor	⎫		0.05 percent		
	Precession current accuracy	⎬ 0.2 percent		0.13 percent		
	Precession current circuit drift	⎭		0.1 percent		
	Timing source accuracy	Roll = 0.15 degree		0.2 percent		
		Yaw = +0.08 degree				
2.3	Rotational axis error					
	Gyro alignment to FCSG, roll axis	Pitch = +0.042 degree		0.14 degree		
		Yaw = +0.119 degree				
2.4	Final position errors					
	Reference axis drift, gyro non-g drift	Roll = -0.12 degree		< 1 deg/hr		
		Yaw = +0.02 degree				
		Pitch = -0.15 degree				
	Midcourse maneuver duration	10.479 seconds	5.5.4.8	10.4628 seconds	Command SSD74108	
3.0	Midcourse ΔV	10.1316 m/sec	5.5.4.8	10.305 m/sec		
4.0	Midcourse ΔV Error	-0.17 m/sec	5.5.4.8			
5.0	Peak Attitude Transient at Engine Ignition					
	Pitch	-0.17 degree				
	Yaw	+0.19 degree				
6.0	Peak Angular Error at Shutdown		5.5.4.8			
	Roll	+1.18 degrees				
	Pitch	+1.09 degrees				
	Yaw	+0.10 degree				

Table 3-2 (continued)

Item	Description	Actual	Subsection Reference	Predicted or Specified	Reference	Comments
			Performance Details			
7.0	Roll Actuator Position Peak at ignition	-1.22 degrees	5.5.4.8			
8.0	Engine Shutoff Impulse Engine 1 Engine 2 Engine 3	-0.18 lb-sec +0.03 lb-sec +0.15 lb-sec	5.5.4.8	Δ impulse < 0.66 lb-sec	224832A (8.3.1.3.2.4.2)	
9.0	Shut Down Angular Rate Pitch Yaw	+0.24 deg/sec -0.01 deg/sec				
			Terminal Descent Summary			
1	Initial Time of First Maneuver	198:01:24:47	TM		Command	Before AMR mark
2	Retro Phase Initial Conditions (Vernier Ignition) Time Attitude Slant range Velocity	198:02:01:59 30.38 degrees 250,907 feet 8605.9 fps	5.12.4.1 5.11.4.1	198:02:01:57 30.38 degrees 250,907 feet 8605.9 fps	SSD74108	Six degree of freedom program prediction
3	Signal Loss Altitude Velocity Flight path angle	49,420 feet 1092 fps 26.8 degrees		49,830 feet 1049 fps 25.5 degrees		
4	Misalignment During Burn	In-plane 0.03 degree Out of plane 0.136 degree	5.11.4.1			
5	Time Between AMR Mark and Vernier Ignition	2.731 seconds	Table 4.1	2.731 seconds	SSD74108	
6	Retro Thrust to CG Offset During Burning	—	5.7.3	< 0.11 inch	224832A (8.3.5.3.2.7)	Total value
7	Retro Action Time (T3500)	≈42 seconds	5.7.3			
8	Maximum Retro Thrust	9250 pounds	5.7.3	9350 pounds	QA firing data	
9	Peak Attitude Transient at Retro Ignition Yaw Pitch	-0.35 degree -0.09 degree	5.5.4.10			

3-10

4.0 SYSTEM PERFORMANCE ANALYSIS

4.1 GENERAL MISSION SUMMARY

The Surveyor IV transit phase, through loss of spacecraft signal, was conducted from 14 July (GMT day 195) through 17 July 1967 with the spacecraft responding to 322 commands. The launch was delayed until the second opportunity on 14 July. The final countdown of the Atlas 1-Centaur/Surveyor on pad 36A proceeded smoothly until approximately T-40 seconds when an approximate 29-second hold was called by Centaur. Liftoff was accomplished at 11 hours 53 minutes 29.215 seconds GMT on day 195, with a launch azimuth of 103.82 degrees. Performance of the Atlas and Centaur AC-11 launch vehicles appeared excellent throughout the flight period as all mark events occurred very close to the predicted times.

A summary of the mission event history is contained in Table 4-1. Injection of the spacecraft occurred at 12 hours 4 minutes 57.2 seconds GMT on a trajectory that would have provided, with no midcourse correction, a total miss of approximately 110 miles from the target landing site within Sinus Medii (Central Bay) of 0.58°N and 0.83°W. All spacecraft operations, including separation, sun acquisition, solar panel deployment, DSIF acquisition, initial commanding and interrogations, Canopus verification and acquisition, midcourse maneuvers and thrusting, and terminal maneuvers, were executed and successfully completed with no major problem. Sixty-two hours 9 minutes and 12 seconds after launch (i.e., approximately only 2 minutes and 20 seconds prior to the predicted touchdown time), all contact was lost with the spacecraft less than 2 seconds before the expected retro engine burnout. Efforts to re-establish contact with the spacecraft were unsuccessful.

The earth track traced by Surveyor IV is shown in Figure 4-1. Specific events, such as sun and Canopus acquisition, midcourse correction, and touchdown, are also shown. The Surveyor and Centaur trajectory in the earth's equatorial plane is shown in Figure 4-2. The predicted and actual view periods for the tracking stations are given in Table 4-2. Operational differences between Surveyors III and IV are summarized in Table 4-3.

Figure 4-1. Surveyor IV Earth Track

Figure 4-2. Surveyor and Centaur Trajectory in Earth's Equatorial Plane

TABLE 4-1. SURVEYOR IV TRANSIT MISSION MILESTONES

Event	GMT, day:hr:min:sec
Launch	195:11:53:29.215
Injection	12:04:57.2
Separation — electrical disconnect	12:06:00.5
Separation — mechanical	12:06:06.1
Automatic sun acquisition completed	12:10:24.2
A/SPP solar panel unlocked	12:06:05.6
A/SPP solar panel locked in transit position	12:11:53.6
A/SPP roll axis locked in transit position	12:16:05.6
Spacecraft visibility at Ascension (one-way)	12:10:21
Initial DSS acquisition (two-way lock) confirmed	12:14:03
First ground command sent to spacecraft	12:29:46
Canopus verification begins	17:51:27
Canopus lockon	18:10:22
First premidcourse attitude maneuver initiated	197:02:15:29
Midcourse thrust executed	02:30:0
Sun reacquired	02:34:40.2
Canopus reacquired	02:40:17.7
Initiation of roll maneuver (terminal descent)	198:01:24:44
Initiation of yaw maneuver	01:29:34
Initiation of roll maneuver	01:35:05
Retro sequence mode on	01:56:20
AMR on	01:57:17.00
Thrust phase power on	01:58:16.40
AMR enable	02:00:16.99
AMR mark	02:01:56.08
Vernier ignition	02:01:58.81
Retro ignition	02:01:59.92
RADVS on	02:02:00.78
Retro burnout	NA
Loss of all spacecraft signal	02:02:41.018

TABLE 4-2. DEEP SPACE STATION VIEW PERIOD SUMMARY

Times are GMT in hr:min

| Station | Date and Pass Number | Number of Commands | Acquisition | | | End of Pass | | |
| | | | Predicted | | Actual Time | Predicted | | Actual Time |
			Event, degrees	Time		Event, degrees	Time	
DSS-72 Ascension	14 July (1)	49	0 rise	12:10	12:10	0 set	02:21	12:49
DSS-51 Johannesburg	14 July (1)	5	5 rise	12:17	12:17	90 HA set	23:07	23:40
DSS-61 Madrid	14 July (1)	24	5 rise	15:46	15:23	5 set	22:53	22:58
DSS-11 Goldstone	14 July (1)	13	5 rise	23:05	23:15	5 set	07:20	07:27
DSS-42 Canberra	14 July (1)	19	5 rise	02:47	03:05	5 set	16:21	16:17
DSS-51 Johannesburg	15 July (2)	11	270 HA rise	11:52	11:59	90 HA set	23:51	23:53
DSS-72 Ascension	15 July (2)	—	0 rise	14:30	—	0 set	02:54	—
DSS-61 Madrid	15 July (2)	0	5 rise	16:07	16:04	5 set	00:00	21:52*
DSS-11 Goldstone	15 July (2)	87	5 rise	23:20	23:20	5 set	07:56	08:06
DSS-42 Canberra	16 July (2)	20	5 rise	03:19	03:40	5 set	16:31	16:34
DSS-51 Johannesburg	16 July (3)	28	270 HA rise	12:07	12:07	90 HA set	00:01	00:02
DSS-72 Ascension	16 July (3)	—	0 rise	14:43	—	—	—	—
DSS-61 Madrid	16 July (3)	0	5 rise	16:08	16:15	5 set	00:19	00:02
DSS-11 Goldstone	16 July (3)	66**	5 rise	23:21	23:20	—	—	00:02

*Due to antenna failure.

**Through time of touchdown only.

4.1.1 Spacecraft Transit Phase Command Log

A detailed list of spacecraft commands sent during the flight are presented in Tables 4-4 and 4-5. Table 4-4 lists the 322 commands transmitted up to loss of contact with the spacecraft. It includes the time the command was sent, as well as the tracking station originating the command. Table 4-5 lists some of the first commands sent after loss of data in an attempt to regain contact with the spacecraft. The standard command to turn on strain gauge modulation preceded the first emergency command (backup for thrust level from programmer) and was transmitted in the blind at 2 hours 3 minutes 26.4 seconds GMT. Sixty-six seconds later, spacecraft modulation was commanded off to increase the change of carrier detection by the tracking stations. A total of 431 additional commands were sent from Goldstone in this initial, unsuccessful turnon effort.

TABLE 4-3. SURVEYOR IV/SURVEYOR III OPERATIONAL DIFFERENCES

1) Surveyor IV was lifted encapsulated off Centaur without disconnecting air conditioning, umbilicals, or thrust chamber assembly vacuum lines.

2) Surveyor IV had a 1-day hold on pad.

3) Surveyor IV was a single-burn Centaur (direct ascent, not parking orbit).

4) Star map was made using omnidirectional antenna B only on Surveyor IV.

5) Midcourse correction was made at L + 39 hours for Surveyor IV instead of L + 16 hours. Full pressure was therefore not applied to the Surveyor IV vernier propellant tanks for 39 hours after launch.

6) There were a larger number of gyro drift checks made on Surveyor IV (13 instead of 11).

7) Both midcourse and terminal maneuvers were initiated when the limit cycle passed through null on Surveyor IV.

8) The lunar approach flight path angle (between velocity vector and the lunar vertical) was larger on Surveyor IV (31.5 versus 23.6 degrees) due to the more easterly landing location.

4.1.2 Prelaunch Countdown

The launch of Surveyor IV was delayed until the second day of the launch window, 14 July, to permit tightening of a connection in the booster's fuel oxidizer system. With the launch rescheduled for 11 hours 53 minutes GMT (4 hours 53 minutes PDT), the final countdown produced just one suspected anomaly. At T-36 minutes, the receiver A automatic gain control (AGC) reading indicated a signal level approximately 14 db lower than that observed during a corresponding period of the Surveyor IV J-FACT test. Testing was then initiated to check the AGC reading at which indexing occurred, as well as the indication for a no-signal condition. Results of these tests led to the conclusion that the receiver performance was satisfactory and that the difference between the observed prelaunch results and the J-FACT data was probably due to nonrepeatable air link results primarily caused by the difficulty in recreating the exact conditions for both tests.

TABLE 4-4. SURVEYOR IV COMMAND SEQUENCE

Command Number	Description	GMT, hr:min:sec	Telemetry Mode	Bit Rate
	Day 195 — DSS-72			
0237	Low Mod SCO's Off	12:29:46	5	550
0216	7.35 Kc SCO On	29:54		
0205	1100 bps	29:58		1100
0107	Xmtr Hi Volt Off	34:08		
0110	Xmtr Fil Pwr Off	34:15		
0130	Xfer Sw B Lo Pwr	34:19		
0623	Accel Amp 1-4 Off	38:14		
0316	SP Deploy Logic Off	38:17		
0522	Prop Str Gage Pwr Off	38:20		
0512	Accel Amp 5-8 Off	38:24		
0516	TD Str Gage Pwr Off	38:27		
0126	Xfer Sw A Lo Pwr	38:31		
0402	Step SP Minus (10)	39:30		
0401	Step SP Plus (5)	39:44		
0405	Step Roll Axis Plus (10)	40:33		
0406	Step Roll Axis Minus (5)	40:45		
0510	AESP Off	41:26		
0226	Mode 1	41:33	1	
0231	Mode 4	43:40	4	
0227	Mode 2	46:49	2	
0232	ESP Off	49:44		
0507	Mode 6	49:49	6	
0506	Mode 5	12:51:47	5	
	Day 195 — DSS-51			
0704	Cruise Mode	15:22:47		
	Day 195 — DSS-61			
0510	AESP Off	17:26:58.1		
0231	Mode 4	27:06.0	4	
0227	Mode 2	29:11.1	2	
0226	Mode 1	31:03.7	1	
0232	ESP Off	33:16.5		
0506	Mode 5	33:22.5	5	
0105	Xmtr B Fil Pwr On	44:50.9		
0127	Xfer Sw B Hi Pwr	46:34.4		
0106	Xmtr B Hi Volt On	46:34.9		
0220	7.35 Kc SCO Off	47:46.9		
0217	33 Kc SCO On	47:53.8		
0206	4400 bps	47:59.3		4400

Table 4-4 (continued)

Command Number	Description	GMT, hr:min:sec	Telemetry Mode	Bit Rate
0704	Cruise Mode	17:50:03.1	5	4400
0715	Man Delay Mode	50:04.4		
0710	Pos Angle Maneuver	50:04.9		
0714	Sun and Roll	17:51:26.9		
0703	Sun-Star Acq Mode	18:07:58.8		
0704	Cruise Mode	12:53.8		
0205	1100 bps	13:34.3		1100
0220	33 Kc SCO Off	13:41.7		
0216	7.35 Kc SCO On	13:49.2		
0107	Xmtr Hi Volt Off	14:49.7		
0110	Xmtr Fil Pwr Off	14:56.2		
0130	Xfer Sw B Lo Pwr	18:14:56.7		

Day 195 — DSS-51

0700	Inertial Mode	18:46:01.0		
0704	Cruise Mode	20:54:14.1		
0700	Inertial Mode	20:57:42.7		
0704	Cruise Mode	22:37:23.7		

Day 195 — DSS-11

| 0510 | AESP Off | 23:59:02.7 | | |
| 0231 | Mode 4 | 23:59:08.7 | 4 | |

Day 196 — DSS-11

0227	Mode 2	00:02:41.5	2	
0232	ESP Off	07:46.5		
0506	Mode 5	07:51.5	5	
0700	Inertial Mode	00:09:25.0		
0704	Cruise Mode	02:09:23.8		
0702	Sun Acq Mode	02:18:51.8		
0510	AESP Off	04:11:27.9		
0231	Mode 4	11:37.6	4	
0227	Mode 2	16:04.6	2	
0232	ESP Off	18:07.3		
0506	Mode 5	04:18:16.5	5	

Day 196 — DSS-42

0503	550 bps	07:52:30.8		550
0204	Coast Phase Clock Rates	52:36.8		
0220	7.35 Kc SCO Off	07:52:41.7		

Table 4-4 (continued)

Command Number	Description	GMT, hr:min:sec	Telemetry Mode	Bit Rate
0215	3.9 SCO On	07:52:47.2	5	550
0704	Cruise Mode	07:54:56.1		
0700	Inertial Mode	08:00:56.0		
0510	AESP Off	02:48.3		
0231	Mode 4	02:55.8	4	
0227	Mode 2	06:05.8	2	
0232	ESP Off	08:16.8		
0506	Mode 5	08:23.3	5	
0704	Cruise Mode	09:58:29.3		
0700	Inertial Mode	10:20:12.2		
0704	Cruise Mode	11:47:00.6		
0510	AESP Off	12:01:35.5		
0231	Mode 4	01:48.0	4	
0227	Mode 2	04:22.6	2	
0232	ESP Off	07:29.6		
0506	Mode 5	12:07:37.0	5	

Day 196 — DSS-51

Command Number	Description	GMT, hr:min:sec	Telemetry Mode	Bit Rate
0510	AESP Off	15:59:50.5		
0231	Mode 4	16:00:00.9	4	
0227	Mode 2	03:56.0	2	
0232	ESP Off	07:13.4		
0506	Mode 5	07:22.4	5	
0700	Inertial Mode	16:08:33.4		
0704	Cruise Mode	17:38:33.1		
0700	Inertial Mode	18:03:17.1		
0704	Cruise Mode	19:42:36.0		
0702	Sun Acq Mode	21:39:49.3		
0704	Cruise Mode	22:27:25.7		

Day 197 — DSS-11

Command Number	Description	GMT, hr:min:sec	Telemetry Mode	Bit Rate
0510	AESP Off	00:11:26.6		
0231	Mode 4	11:33.5	4	
0227	Mode 2	13:44.1	2	
0226	Mode 1	15:45.6	1	
0232	ESP Off	17:28.0		
0506	Mode 5	17:35.0	5	
0220	Hi Data Rate SCO's Off	18:25.5	Off	
0221	Gyro Speed SCO On	18:26.0		
0222	Next Gyro	19:13.0		
0222	Next Gyro	19:55.5		
0222	Next Gyro	00:20:31.5		

Table 4-4 (continued)

Command Number	Description	GMT, hr:min:sec	Telemetry Mode	Bit Rate
0222	Next Gyro	00:21:57.5	Off	550
0223	Gyro Speed SCO Off	22:30.5		
0215	3.9 Kc SCO On	00:22:31.0	5	
0510	AESP Off	01:47:21.0		
0231	Mode 4	47:27.5	4	
0227	Mode 2	49:39.6	2	
0226	Mode 1	01:51:28.5	1	
0105	Xmtr B Fil Pwr On	02:00:34.0		
0127	Xfer Sw B Hi Pwr	02:18.0		
0106	Xmtr Hi Volt On	02:18.5		
0220	Hi Data Rate SCO's Off	03:16.9		
0217	33 Kc SCO On	03:17.4		
0206	4400 bps	03:17.9		4400
0704	Cruise Mode	08:26.5		
0710	Pos Angle Maneuver	08:27.0		
3617	Interlock	08:27.5		
M 1313	Magnitude (363 counts)	08:28.0		
0714	Sun and Roll	15:28.9		
0702	Sun Acq Mode	18:34.5		
3617	Interlock	18:35.0		
M 1202	Magnitude (322 counts)	18:35.5		
0713	Yaw	21:09.9		
0227	Mode 2	24:00.8	2	
0226	Mode 1	25:40.3	1	
0521	Prop Str Gage Pwr On	26:10.3		
0700	Inertial Mode	26:10.8		
0720	Reset Group 4 Outputs	26:22.8		
0135	SMSS Aux Htr Off	27:24.9		
0604	AMR Htr Off	27:25.4		
0613	VL 2 FT 2 Ther Pwr Off	27:25.9		
0616	VL 1 OT 2 Ther Pwr Off	27:26.4		
0621	VL 3 OT 3 Ther Pwr Off	27:26.9		
3617	Interlock	27:27.4		
0605	Unlk Roll Act, Press VPS	27:27.9		
0727	FC Thrust Phase Pwr On	27:53.3		
3617	Interlock	28:16.9		
M 0622	Magnitude (210 counts)	28:17.4		
3617	Interlock	30:01.8		
0721	Vernier Ignition	30:02.3		
0735	Emerg Vernier Eng Off	30:14.7		
0735	Emerg Vernier Eng Off	30:15.7		
0737	FC Thrust Phase Pwr Off	30:29.7		
0737	FC Thrust Phase Pwr Off	30:31.2		
0522	Prop Str Gage Pwr Off	02:30:55.3		

Table 4-4 (continued)

Command Number	Description	GMT, hr:min:sec	Telemetry Mode	Bit Rate
0512	Accel Amp 5-8 Off	02:30:55.8	1	4400
0516	TD Str Gage Pwr Off	30:56.3		
0232	ESP Off	31:17.8		
0506	Mode 5	31:24.3	5	
0611	VL 2 Ther Pwr On	31:49.8		
0614	VL 1 Ther Pwr On	31:50.3		
0617	VL 3 Ther Pwr On	31:50.8		
0624	AMR Htr On	31:51.3		
0136	SMSS Aux Htr On	31:51.8		
0710	Pos Angle Maneuver	32:19.3		
3617	Interlock	32:19.8		
M 1202	Magnitude (322 counts)	32:20.3		
0713	Yaw	32:53.4		
0702	Sun Acq Mode On	35:43.8		
3617	Interlock	36:26.8		
M 1313	Magnitude (363 counts)	36:27.3		
0714	Sun and Roll	37:25.1		
0704	Cruise Mode	40:56.7		
0510	AESP Off	41:22.8		
0227	Mode 2	41:29.3	2	
0231	Mode 4	42:52.7	4	
0232	ESP Off	44:22.9		
0506	Mode 5	44:29.4	5	
0503	550 bps	45:01.3		550
0204	Coast Phase Clock Rates	45:01.8		
0220	Hi Data Rate SCO's Off	45:02.3		
0215	3.9 Kc SCO On	45:02.8		
0107	Xmtr Hi Volt Off	46:03.2		
0110	Xmtr Fil Pwr Off	46:09.7		
0130	Xfer Sw B Lo Pwr	02:46:10.1		
0700	Inertial Mode	04:15:57.7		
0704	Cruise Mode	05:50:44.3		
	Day 197 — DSS-42			
0510	AESP Off	07:10:39.2		
0231	Mode 4	10:46.4	4	
0227	Mode 2	13:12.5	2	
0232	ESP Off	18:17.5		
0506	Mode 5	18:26.5	5	
0317	Aux Batt Mode	07:58:17.1		
0322	Hi Curr Mode On	08:07:58.7		
0320	Restore MB Mode	10:36.7		
0702	Sun Acq Mode	08:50:58.8		

Table 4-4 (continued)

Command Number	Description	GMT, hr:min:sec	Telemetry Mode	Bit Rate
0510	AESP Off	11:58:37.9	5	550
0231	Mode 4	11:58:46.8	4	
0227	Mode 2	12:01:56.4	2	
0232	ESP Off	04:38.9		
0506	Mode 5	12:04:46.8	5	
0317	Aux Batt Mode	13:02:32.1		
0323	Hi Curr Mode Off	07:40.1		
0320	Restore MB Mode	11:07.1		
0322	Hi Curr Mode On	13:21:04.1		
0704	Cruise Mode	14:36:18.3		
0615	OT 2 Ther Pwr On	14:37:24.5		
	Day 197 — DSS-51			
0510	AESP Off	15:16:11.5		
0231	Mode 4	16:19.9	4	
0227	Mode 2	19:58.5	2	
0232	ESP Off	22:42.0		
0506	Mode 5	22:51.4	5	
0700	Inertial Mode	15:40:35.4		
0704	Cruise Mode	17:30:31.0		
0700	Inertial Mode	17:39:41.5		
0704	Cruise Mode	19:12:57.1		
0510	AESP Off	24:04.1		
0231	Mode 4	24:14.5	4	
0227	Mode 2	31:42.1	2	
0232	ESP Off	41:25.5		
0506	Mode 5	19:41:35.0	5	
0317	Aux Batt Mode	20:13:55.4		
0323	Hi Curr Mode Off	27:33.9		
0320	Restore MB Mode	33:44.9		
0322	Hi Curr Mode On	20:42:26.8		
1136	Sur Camera ETC On	21:08:49		
0510	AESP Off	35:41		
0231	Mode 4	35:50	4	
0232	ESP Off	38:37		
0506	Mode 5	21:38:47	5	
0510	AESP Off	22:37:53.9		
0231	Mode 4	38:02.4	4	
0227	Mode 2	40:14.9	2	
0232	ESP Off	42:41.6		
0506	Mode 5	22:42:49.3	5	

Table 4-4 (continued)

Command Number	Description	GMT, hr:min:sec	Telemetry Mode	Bit Rate
	Day 197 — DSS-11			
0510	AESP Off	23:45:37. 7	5	550
0231	Mode 4	45:44. 7	4	
0227	Mode 2	49:32. 2	2	
0226	Mode 1	51:32. 2	1	
0232	ESP Off	53:42. 2		
0506	Mode 5	53:49. 6	5	
0220	Hi Data Rate SCO's Off	54:49. 5	Off	
0221	Gyro Speed SCO On	54:50. 0		
0222	Next Gyro	55:43. 7		
0222	Next Gyro	56:47. 7		
0222	Next Gyro	57:12. 2		
0223	Gyro Speed SCO Off	58:02. 7		
0215	3. 9 Kc SCO On	23:58:03. 2	5	
	Day 198 — DSS-11			
0124	Xpndr Pwr Off	00:00:57. 2		
0123	Xpndr B Pwr On	02:31. 2		
0507	Mode 6	00:59:29. 3	6	
0510	AESP Off	01:04:43. 3		
0231	Mode 4	04:50. 7	4	
1133	Sur Camera V TC On	06:14. 3		
0105	Xmtr B Fil Pwr On	07:43. 3		
0127	Xfer Sw B Hi Pwr	09:26. 3		
0106	Xmtr Hi Volt On	09:26. 8		
0220	Hi Data Rate SCO's Off	09:55. 3		
0216	7. 35 Kc SCO On	09:55. 8		
0205	1100 bps	09:56. 3		1100
0214	Sum Amps Off	10:36. 9		
0211	Phase Sum Amp B On	10:37. 4		
0227	Mode 2	11:38. 3	2	
0232	ESP Off	13:04. 3		
0506	Mode 5 On	13:11. 2	5	
0521	Prop Str Gage Pwr On	15:33. 2		
0515	TD Str Gage Pwr On	16:14. 2		
0517	TD Str Gage D-Ch On	16:14. 7		
0124	Xpndr Pwr Off	17:08. 9		
0704	Cruise Mode	19:24. 7		
0710	Pos Angle Maneuver	19:25. 2		
3617	Interlock	01:19:25. 7		

Table 4-4 (continued)

Command Number	Description	GMT, hr:min:sec	Telemetry Mode	Bit Rate
M 1425	Magnitude (405 counts)	01:19:26. 2	5	1100
0714	Sun and Roll	24:44. 2		
3617	Interlock	27:52. 2		
M 1620	Magnitude (464 counts)	27:52. 7		
0713	Yaw	29:34. 2		
0700	Inertial Mode	33:09. 1		
3617	Interlock	33:09. 6		
M 0337	Magnitude (127 counts)	33:10. 1		
0711	Roll	35:04. 6		
0723	Reset Nom Thrust Bias	40:49. 1		
3617	Interlock	41:52. 6		
M 0127	Magnitude (55 counts)	41:53. 1		
0507	Mode 6	43:41. 6	6	
0720	Reset Group 4 Outputs	45:03. 1		
3617	Interlock	56:20. 0		
0724	Retro Seq Mode	56:20. 5		
0613	VL 2 FT 2 Ther Pwr Off	56:40. 5		
0616	VL 1 OT 2 Ther Pwr Off	56:41. 0		
0621	VL 3 OT 3 Ther Pwr Off	56:41. 5		
0135	SMSS Aux Heater Off	56:42. 0		
1134	Sur Camera VTC Off	56:42. 5		
1137	Sur Camera ETC Off	56:43. 0		
0604	AMR Htr Off	56:43. 5		
0625	AMR Pwr On	57:14. 5		
0727	FC Thrust Phase Pwr On	01:58:14. 5		
0626	AMR Enable	02:00:14. 5		
0730	Emer AMR Signal	01:54. 0		
0730	Emer AMR Signal	01:55. 0		
0730	Emer AMR Signal	02:01:55. 5		

TABLE 4-5.   COMMANDS SENT AFTER LOSS OF DATA

Command Number	Description	GMT, hr:min:sec
0207	PM Pre-Sum Amp On	02:03:26.4
0733	Emerg Start Pgmd Thrust (4)	03:39.9 through 04:03.4
0214	Sum Amps Off	04:45.4
0120	Omni A Select (4)	05:30.9 through 06:57.9
0737	Thrust Phase Pwr Off (4)	07:26.9 through 07:37.9
3617 } 0630 }	Interlock }(4) RADVS Off }	08:11.9 through 08:29.4
3617 } 0311 }	Interlock }(4) FC Off }	08:42.9 through 09:00.4
0305	OTC Enable (4)	11:00.9 through 11:13.4
0117	Xmtr A to Planar Array (4)	12:04.9 through 12:16.9
0130	Xfer Sw B Lo Pwr (4)	12:27.4 through 12:38.3
0104	Xmtr B Lo Pwr On (4)	12:55.3 through 13:08.8
0112	NB VCXO On (4)	13:30.8 through 13:43.8
0111	Xmtr Lo Pwr Off (4)	15:39.8 through 15:54.3
3617 } 0314 }	Interlock }(4) Noness Loads Off }	16:24.3 through 16:41.8
0116	Xmtr B to Planar Array (4)	02:16:58.3 through 17:10.8

4-15

Table 4-5 (continued)

Command Number	Description	GMT, hr:min:sec
0126	Xfer Sw A Lo Pwr (4)	02:17:25. 8 through 17:39. 8
0101	Xmtr A Lo Pwr On (4)	18:06. 8 through 18:20. 3
0112	NB VCXO On (4)	18:30. 3 through 18:43. 3
0305	OTC Enable (4)	19:43. 8 through 19:57. 8
0116	Xmtr B to Planar Array (4)	20:07. 3 through 20:19. 8
0126	Xfer Sw A Lo Pwr (4)	20:27. 3 through 20:39. 3
0101	Xmtr A Lo Pwr On (4)	20:48. 3 through 21:00. 8
0112	NB VCXO On (4)	21:11. 3 through 21:23. 3
0121	Omni B Select	23:17. 3 through 23:29. 3
0111	Xmtr Lo Pwr Off (4)	36:44. 7 through 36:56. 2
3617 0314	Interlock Noness Loads Off ⎬ 4	37:06. 7 through 37:21. 7
0737	FC Thrust Phase Pwr Off (4)	37:35. 7 through 37:46. 2
3617 0630	Interlock RADVS Off ⎬ (4)	37:57. 7 through 38:12. 2

Table 4-5 (continued)

Command Number	Description	GMT, hr:min:sec
3617 } 0311 }	Interlock } (4) FC Off }	02:38:22. 7 through 38:37. 7
0320	Main Batt On (4)	38:47. 2 through 38:59. 2
0323	Hi Curr Mode Off (4)	39:08. 7 through 02:39:19. 2

Following the built-in hold at T-5 minutes, the countdown was resumed. At T-40 seconds, a 29-second hold was called to confirm the proper liquid hydrogen level in the Centaur. The countdown continued after this short hold, and liftoff occurred at 11 hours 53 minutes 29 seconds GMT at a launch azimuth of 103.82 degrees.

4.1.3   Launch, Injection, and Separation

The direct ascent boost phase was normal, with the Atlas roll and pitch programs, as well as the normal opening and closing of the spacecraft inertia switch, being confirmed by spacecraft telemetry. Figure 4-3 diagrams the major events of the trajectory through separation as seen in profile. The times of Atlas/Centaur mark events are given in Table 4-6. Marks 4, 5, 6, and 7 (Centaur nose fairing jettison, Atlas SECO and VECO, Atlas/Centaur separation, and Centaur main engine start) were all verified in real time from spacecraft data. Subsequent to injection and just prior to its separation from the spacecraft, the Centaur issued the preprogrammed commands "extend landing gears," "extend omni antennas," and "transmitter high power on," all of which are verified by spacecraft telemetry. Separation of Centaur and Surveyor occurred immediately thereafter.

The event times and performance parameters of the postseparation phase are given in Tables 4-7 and 4-8, respectively. Following separation, solar panel stepping was initiated. In addition, the cold gas jets were enabled, and the flight control subsystem nulled out the tip-off rates and initiated the roll-yaw sequence to acquire the sun. At L + 16 minutes 55 seconds, primary sun sensor lockon occurred, following a minus roll of approximately 59 degrees and a positive yaw of 46 degrees. Concurrently with the sun acquisition sequence, the antenna/solar panel positioner (A/SPP) was completing its solar-panel and roll-axis deployment, and, at 12 hours 11 minutes 54 seconds GMT (L + 22 minutes 25 seconds), the solar panel was in its proper transit position.
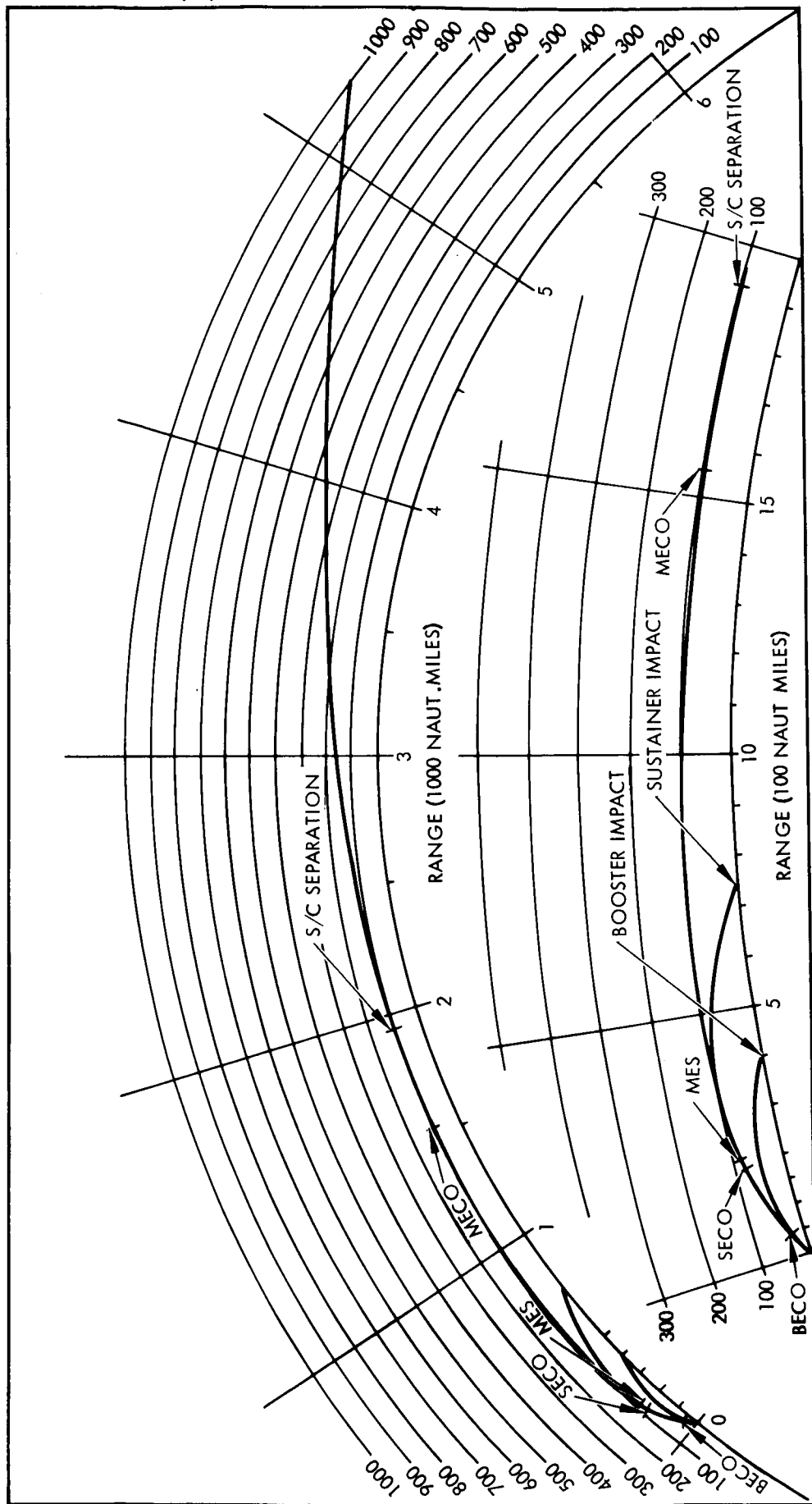
Figure 4-3. AC-11 Launch Phase Trajectory Profile

TABLE 4-6. ATLAS/CENTAUR MARK EVENT TIMES

Mark Number	Event	Nominal Time, seconds	Actual Time, seconds	GMT (Day 195), hr:min:sec
—	Liftoff (2-inch motion)	L + 0.0	0.0	11:53:29.215
1	Atlas booster engine cutoff (BECO)	143.66	141.88	55:51.1
2	Atlas booster engine jettison	147.76	145.38	55:54.6
3	Centaur insulation panel jettison	177.66	176.18	56:25.4
4	Centaur nose fairing jettison	204.66	203.38	56:52.6
5	Atlas sustainer and vernier cutoff (SECO and VECO)	238.18	237.98	57:27.2
6	Atlas/Centaur separation	240.18	241.58	57:30.8
7	Centaur main engine start (MES)	249.68	251.88	57:41.1
8	Centaur main engine cutoff (MECO) (spacecraft injection)	680.67	687.98	12:04:57.2
9	Extend landing gear command	713.68	715.78	05:25.0
—	Landing gear down (telemetry)			05:25.4 ± 1.2
10	Unlock omnidirectional antenna command	724.18	725.28	05:34.5
—	Omnidirectional antennae extended (telemetry)			05:36.8 ± 1.2
11	Turn on Surveyor high power transmitter (command)	744.68	745.98	05:55.2
—	High power on (telemetry)			05:56.1 ± 1.2
12	Centaur/Surveyor electrical disconnect	750.18	751.28	06:00.5
—	Electrical separation (telemetry)			06:01.4 ± 1.2
13	Spacecraft separation	755.68	756.88	06:06.1
14	Begin Centaur turn around maneuver	760.68	No report	— —
15	Start Centaur tank blowdown	995.68	996.88	10:06.1
16	End Centaur tank blowdown	1245.68	1247.58	14:16.8
17	Energize power changeover switch	1246.54	1247.58	14:16.8

TABLE 4-7. SPACECRAFT SEPARATION EVENTS

Events Completed	GMT, day:hr:min:sec
Centaur separation — electrical	195:12:06:02.0
Centaur separation — mechanical	06:06.1
Acquisition sun sensor illuminated	08:53.0
Sun acquisition	10:24.0
Solar panel deployed	11:53.6
A/SPP to roll transit position	16:05.6

TABLE 4-8. SPACECRAFT SEPARATION
AND ACQUISITION PERFORMANCE

Performance	Units	Actual	Predicted Value	Predicted Source
Time to remove separation rates	Seconds	<13	<51	Specification
Solar panel deployment time	Seconds	348	340	Preflight solar thermal vacuum test
A/SPP roll positioning time	Seconds	252	248	Preflight solar thermal vacuum test
Sun acquisition maneuver				
Roll	Degrees	59.4		
Yaw	Degrees	45.6		
Time	Seconds	210	1080	Specification

4.1.4 DSIF Acquisition

At approximately L + 16 minutes 52 seconds, the spacecraft became visible to DSS-72 (Ascension), which achieved one-way lock at this time. Three minutes and 40 seconds later, the acquisition was completed when two-way lock was established by DSS-72 at a signal strength of -90 dbm.

The first ground-controlled sequence ("initial spacecraft operations") was initiated at L + 36 minutes 16 seconds. In accordance with premission plans, this sequence was altered so that the spacecraft transmitter high voltage was not commanded off until the data transmission was switched from the 550-bits/sec low modulation index mode to the 1100-bits/sec normal modulation index mode to ensure satisfactory data reception. In addition to commanding the change in bit rate, commands were sent to turn off equipment required only for the launch-to-DSIF acquisition phase (e.g., transmitter high voltage and filaments off, accelerometer amplifiers off, etc.) to seat the solar panel and roll axis locking pins securely (i.e., by rocking the axes back and forth), and use all telemetry commutator modes for a complete assessment. All spacecraft data and responses to commands were normal.

Because of the high value of the star intensity signal (indicating the presence of the earth in the Canopus sensor field of view, the "cruise mode on" command was delayed and the flight control subsystem was kept in "sun" mode. There was no need to implement the "if required" sequence for permitting receiver A to lock on to the ground transmitter signal since the signal was already well within the receiver pass-band (i.e., receiver A automatic frequency control telemetry indicated only a 6.2-kc error).

4.1.5 Coast Phase I Including Canopus Acquisition

The spacecraft continued to coast normally with its pitch-yaw attitude controlled to track the sun and with its roll axis held inertially fixed. Tracking and telemetry data were being obtained by the use of transmitter B operating in low power in the transponder mode.

By L + 3 hours 27 minutes, the star intensity signal had decreased to a low level (i.e., 0.5 volt), and had remained steady for over 30 minutes. This indication that the earth was no longer in the Canopus sensor field of view, and the "cruise mode on" command was sent to ensure that the attitude control system would revert to inertial mode in the event sun lock was inadvertently lost.

During coast phase I and prior to star map, some unidentified objects passed through the Canopus sensor field of view at approximately 15 hours 27 minutes, 16 hours 4 minutes, 16 hours 16 minutes, and 16 hours 36 minutes 20 seconds GMT. Star map sequence began at 17 hours 51 minutes 27 seconds with one complete roll using omnidirectional antenna B and coast mode commutator data being transmitted at 4400 bits/sec. A Canopus lock signal did appear when Canopus was in the Canopus sensor field of view (after 212 degrees of roll), indicating that automatic lockon should occur on

the next revolution. A possible loss of down link due to rolling through a null did not materialize. Automatic Canopus acquisition was accomplished at 18 hours 10 minutes 22 seconds GMT after some 572 degrees of roll. During the star mapping sequence, four stars (Eta Ursae Majoris, Delta Velorum, Gamma Cassiopeiae, and Canopus), the earth, and the moon were positively identified. In addition to these celestial bodies, several unidentified objects were observed during the star map (see Table 4-9). The vehicle returned to its coasting as before, but with its roll attitude controlled so that its star sensor remained locked to Canopus.

At approximately 20 hours and 8 minutes on day 195 GMT (L + 8 hours 15 minutes 31 seconds), the receiver decoders indexed several times. The station-to-spacecraft vector was known to be in a region of deep nulls on omnidirectional antenna A with receiver A operating near threshold. The antenna gain in these regions is very sensitive to small movements of the spacecraft such as limit cycle. Therefore, some indexing was not unexpected and was not considered a problem since predictions showed that the antenna gain would improve before the next scheduled sequence for commanding the spacecraft.

In coast phase I, there were six standard engineering assessments, nine gyro drift checks, and one gyro speed check. The spacecraft bit rate was reduced from 1100 to 550 bits/sec at 7 hours 52 minutes 47.2 seconds on day 196 when DSS-42 reported a bit error rate of greater than 3×10^{-3}. Spacecraft data continuously gave indications that all subsystems were normal and within their predicted operational limits. However, the vernier oxidizer tank 1 temperature (P-15) showed an unexplainable rapid increase of temperature (rate of 5 BCD/hr) at 19 hours 24 minutes GMT on day 196. At 20 hours and 19 minutes GMT, the temperature stabilized at approximately 52°F, which was well within its upper temperature limit of 100°F.

During the standard Premidcourse Project Management Conferences, it was decided not to execute at L + 15 hours but to delay the midcourse correction until L + 39 hours. This decision was primarily based on the excellent injection conditions of the spacecraft and the expected overall landing site accuracy improvement obtained by executing the maneuvers at 39 hours rather than 15 hours.

4.1.6   Midcourse Correction

All midcourse operations were performed normally. With the spacecraft being controlled by DSS-11 (Goldstone), the maneuver sequence for applying the desired midcourse thrust in the proper direction was a positive roll of 72.5 degrees, followed by a minus yaw of 64.3 degrees (see Table 4-10). During the premidcourse maneuver execution, a new commanding technique was utilized by SPAC for the possible reduction of spacecraft pointing error. This technique was to observe the gyro error limit cycle and execute each maneuver when the respective gyro error was as near to zero as practical.

TABLE 4-9.   DESCRIPTION OF SURVEYOR IV STAR MAP

Roll Angle From Start of Maneuver, degrees	Object in Star Sensor Field of View	Angle From Canopus, degrees	
		Actual	Preflight Prediction
0	(Start of roll)	-210.6	
62.0	Eta U Majoris	-148.6	-148.7
114.1	Moon	-96.5	-97.0
145.5	First particle	-65.1	
189.4	Delta Velorum	-21.3	-21.1
210.6	Canopus	0.0	
315.1	Earth	104.5	103.0
349.7	Gamma Casiopeiae	139.0	139.2
410.5	Second particle	199.9	
421.7	Eta U Majoris	211.1	211.3
474.2	Moon	263.5	263
497.0	Third particle	286.4	
549.2	Delta Velorum	338.6	338.9
572	Canopus	0.0	

TABLE 4-10. SUMMARY OF MIDCOURSE MANEUVER PARAMETERS

| | Maneuver | | | Maneuver Duration, seconds | | As Verified by Telemetry | |
	Axis	Polarity	Angle, degrees	As Computed	As Commanded After Interpolation	Value	Tolerance
First premidcourse maneuver	Sun and roll	Positive	72.5	144.90	145.0	145.0	±0.4
Second premidcourse maneuver	Yaw	Negative	64.3	128.64	128.6	128.7	±0.4
Midcourse thrust	—	—	—	10.4628	10.475	10.499	±0.025
First postmidcourse maneuver	Yaw	Positive	64.3	128.64	128.6	128.45	±0.4
Second postmidcourse maneuver	Sun and roll	Negative	72.5	144.90	145.0	145.1	±0.4

Note:
	Scheduled	Actual
GMT of first maneuver (earliest)	02:15:26	02:15:29
GMT of ignition-nominal	02:30:00	02:30:04.130

With the vehicle thrusting direction now positioned properly, the vernier engine system was pressurized with helium at L + 38 hours 33 minutes 58 seconds. The midcourse velocity correction was applied by ignition of the vernier engines at L + 38 hours 36 minutes 33 seconds, with controlled thrust to achieve a constant acceleration of 0.1 g for 10.475 seconds (a velocity correction of 10.28 m/sec). All sources of data indicated that the midcourse correction was extremely close to its desired value, correcting the miss distance of the in-flight lunar aiming point (1 degree 20 minutes West and 0 degree 25 minutes North) to a calculated miss of 5.6 miles (8.5 kilometers).

Following the midcourse thrusting, the sun and Canopus were reacquired by performing the reverse maneuvers. Thus, confirmation was obtained that the gyros had retained their inertial reference during the vernier engine shut down, and the need to perform a postmidcourse star verification to ensure lockon to the proper star was eliminated.

4.1.7   Coast Phase II

Following the postmidcourse maneuvers, the spacecraft was configured for coast phase II by returning to coast commutator low power and 550 bits/sec (550 bits/sec was utilized up to terminal descent, as was the case with Surveyor I). Coast phase II was very normal as four gyro drift checks, six engineering interrogations, and one gyro speed check were performed. Initial power mode cycling was conducted at 7 hours 58 minutes 17 seconds GMT, and subsequent power mode cycling was conducted at 13 hours 2 minutes 32 seconds and 20 hours 13 minutes 55 seconds GMT, all on day 197. These checks are used to determine battery load sharing when both batteries are placed directly on the bus during terminal descent.

During the transit phase, some 13 gyro drift checks were performed. This large number of drift checks was performed in order to refine the pitch gyro drift rate which indicated near or above specification. In addition to drift rates, the following flight control parameters were made available in real time for terminal descent operations planning:

1)   Amount of nitrogen remaining = 3.92 pounds

2)   Pitch gyro drift rate = -1.0 deg/hr

3)   Yaw gyro drift rate = +0.15 deg/hr

4)   Roll gyro drift rate = -0.5 deg/hr

5)   Pitch optical dead band = 0.437 degree (peak-to-peak)

6)   Yaw optical dead band = 0.412 degree (peak-to-peak)

7)   Roll optical dead band = 0.638 degree (peak-to-peak)

The retro engine bulk temperature was computed to be 56°F, and a temperature of 55°F at retro ignition was predicted. It was estimated that the resulting retro burn time would be 42.53 seconds. For terminal descent maneuvers, the operational procedure was used to control the initiation time of the first two maneuvers so that the limit cycle errors would be minimized (i.e., the same procedure used for premidcourse maneuvers).

4.1.8 Terminal Descent

Terminal descent preparations were initiated by Goldstone (DSS-11) at 57 seconds GMT on day 198 with the turning off of the transponders. The spacecraft was then assessed and configured as follows: 1) high power, 2) 1100 bits/sec, 3) transmitter B, and 4) omnidirectional antenna B. The spacecraft successfully performed the following three terminal maneuvers: 1) plus roll of 80.4 degrees, 2) plus yaw of 92.7 degrees, and 3) minus roll of 25.3 degrees. They were initiated at 1 hour 24 minutes 44 seconds, 1 hour 29 minutes 34 seconds, and 1 hour 35 minutes 4 seconds GMT, respectively, on day 198 (see Table 4-11). The first two maneuvers aligned the retro engine thrust axis to the desired direction, and the third established the preferred spacecraft orientation at retro ignition to reduce the probability of the RADVS breaking lockon, and provided the proper lighting conditions for postlanding viewing of engine 3 by the TV camera. The DSIF signal strength at the end of the third maneuver was reported as -123.9 dbm (prediction of signal strength at this time was within 0.2 dbm), well within the -132.7 dbm touchdown strain gauge turnon criteria.

Other preretro-ignition spacecraft operations (e.g., loading the proper altitude-mark-to-vernier-ignition delay quantity (2.725 seconds), commanding retro sequence mode for automatic flight control sequences following the altitude radar mark, establishing the proper vernier engine thrust level for the retro phase, turning on flight control thrust phase power, etc.) were executed on schedule without difficulty. In addition, the altitude marking radar was turned on at L + 62 hours 3 minutes 46 seconds and enabled at L + 62 hours 6 minutes 46 seconds.

The automatic descent sequence was initiated by the altitude marking radar mark, confirmed on the ground at 2 hours 1 minute 56.080 seconds GMT (L + 62 hours 8 minutes 27 seconds). Vernier engine ignition, retro engine ignition, and RADVS turnon occurred at the proper time. After the retro had been burning for approximately 40.9 seconds (versus a predicted burn time of 42.53 seconds), all spacecraft signals were lost abruptly at 2 hours 2 minutes 41 seconds GMT (L + 62 hours 9 minutes 12 seconds). Subsequent attempts to establish contact with the spacecraft (e.g., by restoring the power control logic by enabling the overload-trip circuit (OTC), by bypassing the OTC, and by taking the auxiliary battery off the bus while commanding various combinations of transmitters, antennas, and transmitter power levels, etc.) were all unsuccessful. Some of the commands sent by Goldstone in its initial revival attempt have already been listed in Table 4-5.

TABLE 4-11. SUMMARY OF TERMINAL MANEUVER PARAMETERS

| | | | | Maneuver Duration, seconds | | | |
| | Maneuver | | | | | As Verified by Telemetry | |
	Axis	Polarity	Angle, degrees	As Computed	As Commanded After Interpolation	Value	Tolerance
First terminal maneuver	Roll	Positive	80.4	161.709	161.8	162.0	±0.4
Second terminal maneuver	Yaw	Positive	92.7	185.362	185.4	185.9	±0.4
Third terminal maneuver	Roll	Negative	25.3	50.472	50.6	50.7	±0.4
Thrust bias/retro delay	—	—		2.73144	2.725	2.730	±0.03

Note:
	Scheduled	Actual
GMT of first maneuver (earliest)	01:25:26	01:24:44
GMT of AMR mark	02:01:53.276	02:01:56.080

TABLE 4-13. SUMMARY OF SIGNIFICANT DEVIATIONS FROM EPD-180, REVISION D (1 JUNE 1967)

Mission Phase	Mission Time	Event/Deviation	Reason for Deviation
DSIF acquisition through star verification	L + 36M 17S	Decision to execute "Initial 1100 BPS Selection" early	Per premission plan to ensure satisfactory data reception by DSIF-12.
DSIF acquisition through star verification	L + 48M 00S	Decision to delay cruise mode on command	Star error signal was fluctuating and star intensity signal level was appreciably above the no-signal level. It was necessary to keep the roll axis in inertial mode to conserve nitrogen gas.
DSIF acquisition through star verification	L + 1H 50M 00S L + 2H 36M 00S	Mode 4 interrogations omitted	Required only if spacecraft passes through earth shadow.
DSIF acquisition through star verification	L + 5H 54M 17S L + 6H 20M 05S	Selection of 4400 bits per second and return to 1100 bits per second for star verification	To increase data rate of star intensity and Canopus error signals during star verification.
Coast phases I and II		Gyro drift checks were run as follows:	Experience has shown that a large data sample is necessary to obtain a value of gyro drift which can be used with confidence in the pre-retro maneuvers to compensate for gyro drift. Only four drift checks are scheduled; the additional checks were performed to increase confidence in the measured values.
	L + 7H 10M 32S	1) 3 axis (110 minutes)	
	L + 9H 4M 14S	2) 3 axis (100 minutes)	
	L + 12H 15M 56S	3) 3 axis (120 minutes)	
	L + 14H 25M 23S	4) Roll only (335 minutes)	
	L + 20H 07M 27S	5) 3 axis (120 minutes)	
	L + 22H 26M 43S	6) 3 axis (90 minutes)	
	L + 28H 15M 04S	7) 3 axis (90 minutes)	
	L + 30H 09M 48S	8) 3 axis (100 minutes)	
	L + 33H 46M 20S	9) Roll only (100 minutes)	
	L + 40H 22M 29S	10) 3 axis (95 minutes)	
	L + 44H 57M 30S	11) Roll only (345 minutes)	
	L + 51H 47M 06S	12) 3 axis (100 minutes)	
	L + 53H 46M 13S	13) 3 axis (95 minutes)	
Coast phase I	L + 9H 30M 00S	Bit rate reduction to 550 bits per second was delayed to L + 19H 59M 2S	Telecommunications performance was adequate to sustain 1100 bits per second.
Coast phase I	L + 12H 05M 34S L + 16H 17M 59S L + 20H 09M 19S L + 24H 08M 07S	Unscheduled engineering interrogations	Additional interrogations were performed in coast phase I because of the delayed midcourse correction.
Coast phase I	L + 36H 28M 29S	Select next gyro speed commanded one extra time	To verify that the correct stepping was accomplished.
Midcourse correction	L + 38H 13M 33S	The second premidcourse gyro speed check was omitted	Previous measurement of gyro speed indicated that the performance was satisfactory.
Coast phase II	L + 42H 06M 33S	Postmidcourse star verification maneuver not performed	Postmidcourse reverse maneuvers resulted in reacquisition of sun and star.
Coast phase II		Five postmidcourse interrogations omitted	Not required because of late midcourse correction.
Coast phase II	L + 45H 50M 00S	Vernier tank thermal control on delayed	Tank temperatures indicated that heating was not required at the scheduled time.
Coast phase II	L + 50H 43M 55S	Vernier oxidizer tank 2 thermal control on	Tank temperature reached a level where heating was required.
Terminal descent	L + 62H 09M 30S	The second preterminal gyro speed check was omitted	Previous measurement of gyro speed indicated that the performance was normal.

Final reliability point estimates for each subsystem are given in Table 4-14.

TABLE 4-14. SUBSYSTEM FINAL RELIABILITY
POINT ESTIMATES

Subsystem		Reliability Estimates
Telecommunications		0.929
Vehicle and mechanisms		0.854
Propulsion		0.947
Electrical power		0.953
Flight control		0.931
Spacecraft	0.667	
Systems interaction reliability factor	0.978	
Spacecraft reliability (0.667)(0.978) = 0.65		

4.2.1.2 Summary of Data Base for Surveyor IV Reliability Estimates

The primary source of data for reliability estimates is the operating time and cycles experienced by Surveyor IV units during systems tests and flight and the accumulated reliability relevant failure data provided by TFRs. Data from Surveyors I, II, and III test and flight experience are included where there are no significant design differences between the units. A failure is considered relevant if it affects equipment reliability and could occur during a mission. Relevance of failures is based upon a joint reliability-systems engineering decision. In addition, relevant failures are weighted as follows:

1.0 Critical — Would normally cause a safety hazard, mission abort, or failure of mission objective.

0.6 Major   — Would significantly degrade system performance but not cause mission abort or failure.

0.1 Minor   — Would not significantly effect ability of system to function as designed.

A summary data base for Surveyor IV reliability estimates is presented in Table 4-15.

Table 4-15 (continued)

Units	Total Weighted Relevant Failures	Test Time (hours) or Cycles	Reliability
Roll actuator	0	190.5	1.0
Attitude jet system	0.1	444,675	0.999
	0	cycles	
Pin puller*	0	16,101 cycles	1.0
Pin puller cartridge*	0	16,101 equivalent firings	1.0
Helium tank and valves assembly*	0.1	36 mission cycles	0.997
Propellant tank assembly*			
Fuel tank	0	58 mission cycles	1.0
Oxidizer tank	0.6	76 mission cycles	0.977
Lines and fittings	0.1	78 mission cycles	0.999
Thrust chamber assembly (JPL supplied)			
Propellant shutoff valve	0	8,033 cycles	1.0
Throttle valve	2.0	698 cycles	0.997
Thrust chamber and injector assembly	1.0	260 cycles	0.996
Helium release valves*	0	16 firings	1.0
Valve cartridge*	0	16,064 equivalent firings	1.0
Shock absorber*	0	400 cycles	1.0
Crushable structure*	0	70 cycles	1.0
System**	0.3	1,174.4	0.978

*Includes unit flight acceptance and type approval test data.

**Based on main power switch operating time in system test.

4.2.1.3 Time/Cycle/Reliability History for all Surveyor I, II, and III Units

Table 4-16 presents a history of time/cycle/reliability data for each major control item for Surveyors I, II, and III.

4.2.2 Future Reliability Predictions

4.2.2.1 Reliability Trends

Surveyor spacecraft realized a steady reliability growth up through Surveyor III, dipped sharply for IV, and has resumed the upward trend for V and SC-6. This can be readily seen from Table 4-17 which presents reliability figures for Surveyors I through V.

Table 4-18 presents the Surveyor IV and V reliability ratio for each subsystem relative to the Surveyor III values. Of particular interest is the V/III column which indicates that the vehicle/mechanisms, propulsion, and flight control subsystems exhibit reliability for Surveyor V below their Surveyor III values. Although flight control reliability is down overall, it has improved somewhat from Surveyor IV to V. The vernier propulsion subsystem is also down overall; however, because of limited testing, the Surveyor IV and V estimates employ the same data base, and hence provide an inconclusive comparison. The vehicle/mechanism reliability is down from Surveyor III to IV and down slightly again from Surveyor IV to V. This decrease was a result of three failures:

1) <u>Wiring Harness Compartment A (TFR 18262)</u>. Surveyor IV mission failure. A possible failure mode has been ascribed to the 29-volt regulated transmitter low ripple wiring from the boost regulator to the transmitter and return. This was a single wire from the boost regulator to both transmitters, and it has been shown that a failure of this wire would produce results very similar to the Surveyor IV mission failure signature. Engineering Change Requests have been initiated to provide redundant wiring and eliminate this potential failure mode. This assignment of the Surveyor IV mission failure to the wiring harness is for reliability calculations only. Subsection 4.3 contains a discussion of all possible Surveyor IV failure modes. The overall reliability estimate is independent of which subsystem is assigned this failure.

2) <u>Wiring Harness Basic Bus 1 (TFR 56439)</u>. Failed pin retention test at umbilical connector. Pin retention failure is a recurring problem during systems testing, but precautions taken prior to final mating of connectors reduces the probability of a connection failure during a mission.

3) <u>Thermal Sensor (TFR 50232)</u>. Temperature sensor test indicated an open circuit for the thermal sensor on thrust chamber assembly (TCA) 1. Revised acceptance specifications include continuity checks on all TCA thermal sensors at El Segundo and AFETR. The addition of continuity checks for thermal sensors during TCA flow checks at AFETR will preclude launching the spacecraft with open connections to any thermal sensors.

Unit	Time (hours) or Cycles			Failures			Reliability		
	I	II	III	I	II	III	I	II	III
Receiver decoder select	2,137.3	4,073.4	5,602.1	0	0	0	1.0	1.0	1.0
Central decoder	2,137.3	4,073.4	5,602.1	0.6	0.6	0.6	0.972	0.987	0.990
Subsystem decoder	10,686.5	20,367.0	28,010.5	0	0	0	1.0	1.0	1.0
Engineering signal processor	691.3	1,300.5	1,711.8	2.2	2.3	0.8	0.752	0.861	0.960
Auxiliary engineering signal processor	838.0	1,478.2	2,290.4	1.0	2.4	2.8	0.893	0.870	0.901
Signal processing auxiliary	292.7	461.8	530.4	0	0	0	1.0	1.0	1.0
Central signal processor	1,828.3	3,133.0	5,836.1	0.7	1.4	0.7	0.960	0.963	0.990
Low data rate auxiliary	449.9	847.1	1,484.3	0	0	0.1	1.0	1.0	0.994
Omnidirectional antenna	716.7	1,068.4	2,075.5	0	0	0	1.0	1.0	1.0
Omnidirectional mechanism	42 cycles	510 cycles	663 cycles	0	0.2	0	1.0	0.999	1.0
Diplexer	2,173.8	5,891.5	8,948.9	0	0	0	1.0	1.0	1.0
Transmitter	1,019.1	2,373.0	3,685.9	2.3	1.0	2.4	0.874	0.961	0.942
Low pass filter	3,176.6	6,822.8	9,880.2	0	0	0	1.0	1.0	1.0
Telemetry buffer amplifier	1,874.4	5,103.3	8,160.7	0	0	0	1.0	1.0	1.0
Receiver	3,580.2	7,297.9	10,355.3	0.2	0.2	0.1	0.995	0.998	0.999
Transponder	529.1	1,153.4	1,663.2	0	0	0	1.0	1.0	1.0
RF transfer switch	1,019.1	2,373.0	3,685.9	0	0	0	1.0	1.0	1.0
SPDT switch	1,019.1	2,373.0	3,685.9	0	0	0	1.0	1.0	1.0
Thermal sensors	40,953.8	76,038.0	104,180.8	0	0	0	1.0	1.0	1.0
Thermal control and heater assembly	1,455.9	1,591.7	2,359.7	0	0	0	1.0	1.0	1.0
Thermal switch	14,755.5	26,196.0	35,373.0	0	1.2	1.2	1.0	0.943	0.958
Thermal shell	1,967.4	3,492.8	4,716.4	0	0	0	1.0	1.0	1.0
Spaceframe	8 cycles	11 cycles	16 cycles	0	0	0	1.0	1.0	1.0
Landing gear	21 cycles	139 cycles	160 cycles	0	0	0	1.0	1.0	1.0
Compartment A thermal tray	8 cycles	11 cycles	17 cycles	0	0	0	1.0	1.0	1.0
Compartment B thermal tray	8 cycles	11 cycles	17 cycles	0	0	0	1.0	1.0	1.0
Auxiliary battery compartment	8 cycles	11 cycles	17 cycles	0	0	0	1.0	1.0	1.0
Wiring harness compartment A	2,587.2	1,868.5	3,332.9	1.0	0	0	0.963	1.0	1.0
Wiring harness compartment B	2,587.2	1,868.5	3,332.9	0.1	0	0	0.997	1.0	1.0
Wiring harness basic bus 1	2,537.2	4,405.7	5,870.1	0.1	2.1	2.1	0.996	0.960	0.970
Wiring harness basic bus 2	2,537.2	4,405.7	5,870.1	1.0	2.0	1.0	0.962	0.962	0.986
Wiring harness A/SPP	1,063.9	1,111.7	1,121.2	0	0	0	1.0	1.0	1.0
Wiring harness auxiliary battery	1,129.1	1,333.8	1,440.2	0	0	0	1.0	1.0	1.0
Wiring harness RF cabling	2,601.3	4,227.5	5,601.0	0.1	0	0	0.996	1.0	1.0
Wiring harness retro rocket	1,053.2	1,059.5	1,070.8	0	0	0	1.0	1.0	1.0
Nitrogen lines	1,147.0	1,963.0	2,814.7	0	0	0	1.0	1.0	1.0
Retro rocket release	540 cycles	575 cycles	578 cycles	0	0	0	1.0	1.0	1.0
Engineering mechanical auxiliary	1,576.3	3,358.6	4,887.3	0	0	0	1.0	1.0	1.0
Antenna/solar panel positioner	240,504 cycles	511,506 cycles	482,446 cycles	22.7	1.4	1.4	0.891	0.995	0.997
Separation sensor and arming device	75 cycles	72 cycles	178 cycles	0	0	0	1.0	1.0	1.0
Retro rocket system	13 cycles	14 cycles	15 cycles	0	0	0	1.0	1.0	1.0
Solar panel	357.1	402.7	467.7	0	0	0	1.0	1.0	1.0
Battery charge regulator	1,128.4	3,072.0	4,600.7	0.1	0.7	0.7	0.989	0.980	0.987
Boost regulator	2,457.8	4,476.1	6,004.8	0.8	1.4	1.4	0.968	0.974	0.982
Auxiliary battery control	1,929.3	3,998.0	5,526.7	0	0.6	0.7	1.0	0.998	0.998
Main power switch	1,475.4	3,354.6	4,883.3	0	0	0	1.0	1.0	1.0
Main battery	1,037.4	1,553.8	2,685.5	1.0	1.0	0	0.882	0.994	1.0
Auxiliary battery	90.7	113.6	248.5	0.6	0.6	0.6	0.880	0.924	0.962
Boost regulator input choke	937.2	2,623.9	4,152.6	0	0	0	1.0	1.0	1.0
Boost regulator unregulated filter	937.2	2,627.9	4,152.6	0	0	0	1.0	1.0	1.0
Flight control sensor group	1,147.2	1,963.2	2,815.1	0	2.0	0	1.0	0.917	1.0
Altitude marking radar	62.9	92.9	106.3	0	0	0	1.0	1.0	1.0
RADVS-signal data convertor	595.1	987.1	1,131.7	6.5	10.3	11.1	0.982	0.989	0.989
Klystron power supply modulator	311.5	725.7	921.0	5.4	5.9	5.9	0.981	0.991	0.993
Attitude and velocity sensing antenna	295.9	522.7	823.9	2.2	2.2	4.4	0.992	0.996	0.994
Velocity sensing antenna	266.6	424.1	652.5	0	1.6	2.2	1.0	0.996	0.996
RADVS waveguide	194.1	278.0	424.2	0	0	0	1.0	1.0	1.0
Roll actuator	56.6	98.1	148.6	0	0	0	1.0	1.0	1.0
Attitude jet system	147,381 cycles	269,576 cycles	370,756 cycles	0.1	0.1	0.1	0.995	0.998	0.998
Pin pullers	16,071 cycles	16,080 cycles	16,092 cycles	0	0	0	1.0	1.0	1.0
Pin puller cartridge	16,071 cycles	16,429 cycles	16,441 cycles	0	0	0	1.0	1.0	1.0
Helium tank and valve assembly	30 cycles	33 cycles	34 cycles	0	0.1	0.1	1.0	0.997	0.997
Fuel tanks	46 cycles	49 cycles	52 cycles	0	0	0	1.0	1.0	1.0
Oxidizer tanks	64 cycles	67 cycles	70 cycles	0	0	0	1.0	1.0	1.0
Lines and fittings	54 cycles	60 cycles	66 cycles	0	0	0.1	1.0	1.0	0.998
Propellant shutoff valve	7,944 cycles	7,947 cycles	7,953 cycles	0	0	0	1.0	1.0	1.0
Throttle valve	693 cycles	694 cycles	697 cycles	2.0	2.0	2.0	0.997	0.997	0.997
Thrust chamber and injector assembly	255 cycles	256 cycles	259 cycles	0	1.0	1.0	1.0	0.996	0.996
Helium release valve	13 cycles	14 cycles	15 cycles	0	0	0	1.0	1.0	1.0
Valve cartridges	16,061 cycles	16,062 cycles	16,063 cycles	0	0	0	1.0	1.0	1.0
Shock absorber	391 cycles	391 cycles	400 cycles	0.2	0	0	0.999	1.0	1.0
Crushable structures	61 cycles	61 cycles	70 cycles	0	0	0	1.0	1.0	1.0
System interaction	1,717.1	1,013.2	1,528.7	5.0	0.6	0.6	0.736	0.949	0.967

TABLE 4-17.   SURVEYOR SPACECRAFT RELIABILITY GROWTH

Subsystem	I	II	III	IV	V
Telecommunications	0.925	0.944	0.965	0.929	0.987
Vehicle and mechanisms	0.816	0.868	0.907	0.854	0.850
Propulsion	0.991	0.991	0.968	0.947	0.947
Electrical power	0.869	0.958	0.935	0.953	0.985
Flight control	0.952	0.889	0.971	0.931	0.944
Systems interaction factor	0.736	0.949	0.967	0.978	1.0
Spacecraft	0.456	0.658	0.745	0.653	0.738

TABLE 4-18.   RELATIVE SUBSYSTEM RELIABILITY FOR
SURVEYORS III, IV, AND V

Subsystem	IV/III	V/IV	V/III
Telecommunications	0.963	1.062	1.023
Vehicle and mechanism	0.942	0.995	0.937
Propulsion	0.978	1.0	0.978
Electrical power	1.019	1.034	1.053
Flight control	0.959	1.014	0.972

The slight decrease in the reliability of the vehicle mechanisms sub-system from Surveyor IV to V is a result of two failures:

1) Thermal Control and Heater Assembly (TFR 53317). The thermal control and heater assembly responded intermittently to turnon commands. The intermittence was a result of poor workmanship on replacement of a failed diode. During subsequent repair to another component, heat transfer caused solder flow and produced the intermittence. No engineering change is required, and production line precaution should prevent repetition of the problem.

2) Thermal Sensor (TFR 53168). The thermal sensor indicated an open circuit. The defective part was replaced and, since detail failure analysis is not practical for thermal sensors, the exact cause of the component failure remains unknown. Thermal sensor performance has been satisfactory and, because the function performed by the sensor is not mission critical, no further engineering action was deemed necessary.

4.2.2.2 Unit Type Permitting Greatest Improvement in Surveyor V Reliability

Table 4-19 lists those units which, with reliability improvement, would have the greatest effect on Surveyor V overall reliability. In particular, this table shows the resulting percent increase in Surveyor V reliability if the listed unit type attained its specification reliability value instead of its current data-based value.

4.2.2.3 Surveyor V Reliability

Estimated reliability for Surveyor V at launch for a 66-hour nominal flight and landing mission is 0.74. This projected estimate is based upon Surveyor V systems test data as of 11 August 1967, and applicable Surveyor I, II, III, and IV test and flight experience.

4.2.2.4 Reliability Estimate Basis

The estimates reported herein are based on equipment failure data and operating time and cycle data generated during spacecraft missions and spacecraft systems testing which are combined in accordance with the "Reliability Math Model Surveyor Spacecraft A-21," SSD 64002-2R, 24 October 1966. The model describes the spacecraft system in terms of block diagrams, mission profile, time/cycle data, and probabilistic equations appropriate to the functional interaction of all spacecraft units. For convenience, the spacecraft is referred to at three basic levels: system, set, and control item or unit. Two mission phases, flight through landing and lunar 80-hour period, are considered. For these phases, reliability is defined as follows:

TABLE 4-19. UNITS HAVING GREATEST EFFECT ON
SURVEYOR V RELIABILITY

Unit Type	Unit Date-Based Reliability	Unit Specification Reliability	Percent Increase Reliability If Unit Specification Is Attained	Reliability If Unit Specification Is Attained
Wiring harness	0.902	0.987	9.4	0.81
Thermal control and heater assembly	0.965	0.998	3.4	0.76
RADVS	0.976	0.998	2.3	0.75
Thermal switch	0.984	0.997	1.2	0.75
Boost regulator	0.985	0.988	0.3	0.74

1) Reliability of the A-21 Surveyor spacecraft for the flight and landing (F and L) phase is the probability that the spacecraft equipment will operate successfully as required from launch through soft landing. Successful soft landing is assumed if two-way communication is established and there is no apparent damage to spacecraft equipment required to support intended lunar operations.

2) Reliability of the A-21 Surveyor spacecraft for the lunar 80-hour (L-80) phase is the probability that the spacecraft equipment will operate successfully as required for 80 hours on the lunar surface given that the spacecraft has successfully soft landed.

In the derivation of the model, the following general assumptions were made:

1) No human errors will occur during the mission which will cause failure.

2) All equipment inspection and test procedures are perfect and comprehensive, and all equipment will be used only in applications within the boundaries of its design parameters.

3) Only standard operating procedures are considered.

4) Every performance characteristic is verified up to the instant of no return in launch operations, and the launch will be aborted if fault exists.

5) All parts and designs are used in applications proven by test.

6) All scheduled changes to improve reliability of performance have been physically incorporated and tested prior to launch.

7) Natural hazards, such as meteorites and deep lunar dust, are nonexistent.

4.3 ANALYSIS OF SURVEYOR IV LOSS-OF-SIGNAL FAILURE

The sudden anomaly that transformed the Surveyor IV mission from a nominal flight to an apparent catastrophic failure has been frequently mentioned in this report. It is the purpose of this section to summarize the considerable effort that has been put into study of this problem, even though no single cause has been (or ever will be, in all probability) isolated. As a reference for this discussion, Table 4-20 gives the last known status of all major spacecraft subsystems and parameters at time of data loss.

4.3.1 Potential Failure Mode Analysis

As the first step in investigating the cause of the Surveyor IV failure, all possible failure modes that could result in the conditions experienced have been identified. Then, as many of these as possible were ruled out either by data, analysis, or subsequent test, thereby leaving only those that are potential candidates. In identifying the potential failure modes, two failure conditions must be considered, neither of which can be ruled out by any data at this time. These conditions are:

1) The failure was such as to cause only the loss of signal and, barring any other second unrelated failure or an extremely damaging lunar terrain, the spacecraft should have continued its descent and soft landed on the moon.

2) The loss of signal was only symptomatic of a more catastrophic spacecraft failure that directly resulted in a lunar crash.

In either event, the ultimate result is the same (i.e., a lost mission), but the potential failure modes are different and the final spacecraft condition is different. In the first case, the spacecraft may now be sitting on the moon intact or toppled over but still essentially intact, while, in the second case, the spacecraft would be demolished by either hitting the lunar surface at approximately 1500 fps or exploding above the lunar surface.

Another division of potential failures that can be made is: 1) the basic failure cause can be electrical in nature (such as a random component failure or a system noise effect), or 2) the basic cause can be structural in nature (such as vibration, shock, collision, or explosion) which then results in a secondary electrical failure.

TABLE 4-20. SURVEYOR IV CONFIGURATION AND STATUS AT TIME OF LOSS OF DATA

	Predicted	Verified	How and When Last Verified
Geometry			
A'titude	49 Kft	—	
Velocity — V_x	-108 fps	-88 fps	} Telemetry at data loss
Velocity — V_y	-26 fps	-19 fps	
Velocity — V_z	1070 fps	$800 < V_2 < 3000$	
Slant range	57.1 Kft	—	
Flight path angle	25.6 degrees	—	
Attitude angle	31.5 degrees	} Confirmed by proper maneuver execution	
Roll angle (X-axis — trajectory plane)	-14 degrees		
Communication link			
Transmitter on	B high	B high	Telemetry at data loss
Antenna selected	Omni B	Omni B	Selected by command prior to launch
Subcarrier oscillators on	7.35 kHz	7.35 kHz	} Telecommunications link at data loss
Bit rate	1100 bits/sec	1100 bits/sec	
Data mode	6	6	
Power system			
Battery mode	High current	High current	
Battery discharge current	12.5 amps	12.5 amps	
Regulated load current	5.3 amps	5.3 amps	} Telemetry at data loss
Unregulated load current	2.2 to 3.7 amps	3.2 amps	
RADVS current	25.0 amps	24.5 amps	
Overload trip circuit	Enabled	Enabled	} Selected by command
Optimum charge regulator	On	On	
Optimum charge regulator current	0	0	} Telemetry at data loss
Bus voltage	20.5 volts	20.7 volts	
Flight control			
Attitude control mode	Inertial	Inertial	
Inertia switch	Armed-open	Armed-open	} Telemetry at data loss
Thrust command	Mid thrust	Mid thrust	
Acceleration	8.4 g	8.50 g	
Retro thrust	≈8000 pounds	8279 pounds	} Calculation from acceleration telemetry at data loss
Retro propellant remaining		67 pounds	
Retro burn time	42.5 seconds	41 seconds	
Vernier thrust 1	≈67 pounds	65.3 pounds	
Vernier thrust 2	≈67 pounds	67.6 pounds	} Telemetry at data loss
Vernier thrust 3	≈67 pounds	66.3 pounds	
	201 pounds	199.2 pounds	
Helium pressure		4020 psi	} Telemetry at data loss
Oxidizer pressure	730 ±30 psi	750 psi	

Table 4-20 (continued)

	Predicted	Verified	How and When Last Verified
Mechanisms			
Landing gear	Down	Down	
Omnidirectional antennas	Extended	Extended	} Telemetry at data loss
Solar panel	Deployed and locked	Deployed and locked	
Planar array	Stowed	Stowed	Telemetry at retro ignition minus 15 minutes
RADVS			
Beam 1 tracker	Locked	Locked	
Beam 2 tracker	Locked	Locked	
Beam 3 tracker	Locked	Locked	
Beam 4 tracker	Not locked	Not locked	
Beam 1 gain state	90 db	90 db	
Beam 2 gain state	90 db	90 db	
Beam 3 gain state	65 db	65 db	} Telemetry at data loss
Beam 4 gain state	80 db	80 db	
Beam 1 signal strength	-95.9 dbm	≈-99 dbm	
Beam 2 signal strength	-92.2 dbm	≈-97 dbm	
Beam 3 signal strength	-87.5 dbm	≈-90 dbm	
Beam 4 signal strength	-99.0 dbm	—	

	Transit Steady State, °F		Actual Just Prior to Retro Ignition, °F
	Predicted	Actual Just Prior to Preretro Maneuver	
Thermal			
Main battery	80 ± 15	77	79
Auxiliary battery	65 ± 15	77	80
Battery charge regulator	104 ± 20	101	91
Boost regulator	98 ± 20	99	120*
Transmitter A	58 ± 20	57	65
Transmitter B	58 ± 20	59	105*
Solar panel	110 ± 10	111	31
Planar array	-60 ± 25	-51	98
Flight control electronics	60 ± 20	62	61
Nitrogen tank	47 ± 15	46	43
Helium tank	68 ± 20	78	65
Lower retro case	} Bulk 55	44	
Upper retro case		66	
Engine 1	57 ± 20	53	179*
Engine 2	78 ± 20	82	127*
Engine 3	60 ± 20	68	134*

*At time of failure

Figure 4-4 is a potential failure tree showing the various possible types of failures. The first two levels of branches are the divisions described above. However, the branches labeled "Prime Failure Electrical" are to be used in two ways, i.e., 1) as a prime electrical failure as described above, and 2) as the potential secondary failure that actually caused the signal loss resulting from a prime structural failure. That is, each structural failure branch should actually be followed by the whole group of electrical failure branches since the ultimate failure (loss of signal) is an electrical failure, but they have been omitted from Figure 4-4 for clarity.

In summary, this tree shows that there are essentially three areas where the ultimate electrical failure that caused the signal to vanish could have occurred: either in the transmitter; the 29-volt power regulation and distribution system; or the 22-volt power generation, control, and distribution system. In the case of loss-of-signal-only failures, only the transmitter (and its associated RF cables) and the nonessential bus portion of the 29-volt system (including the overload trip circuit) are potential failure areas. Failures in the 22-volt system (batteries, battery control, and main power switch) and in the rest of the 29-volt system (the regulator itself and the essential and flight control buses) would cause the more catastrophic spacecraft failure. Notably absent from this tree are flight control, RADVS, and propulsion electrical failures since, while failures in these areas could prevent the spacecraft from landing, they would not cause the simultaneous loss of signal. Also under the loss-of-signal-only branches, the more massive structural failures (large collisions and explosions) have been omitted as it is very unlikely that they would cause such a limited failure. The same information contained in the failure tree for electrical failures is also shown in matrix form in Table 4-21. This table shows general failures and whether or not they could have caused the noted failures, followed by more specific failures on a control item basis.

In the subsystem sections which follow, each of the potential failure modes is expanded and discussed in more detail. The "failure signature" of each of those presently known is identified and compared with the signature experienced in an attempt to eliminate those not compatible with the data. Essentially none of the potential failures in Figure 4-4 can be eliminated except for those tabulated in Table 4-22.

4.3.2   RF Data Link Failure Modes

The Surveyor IV failure signature has been investigated by reducing DSIF DSS-11 magnetic tapes at the time of failure. Per Figure 4-5, the PCM data, the 7.34-kc subcarrier oscillator, and the RF signal all disappeared in a period of 0.25 millisecond or less. With this time period as the basis of investigation, each practical failure mode listed below has been or is being tested to determine the failure signature.

4.3.2.1   Transmitter High Voltage Off Failure

The transmitter high voltage could be removed from the traveling-wave tube (TWT) by any of the following methods, excluding a high voltage arc which is discussed in paragraph 4.3.2.8.
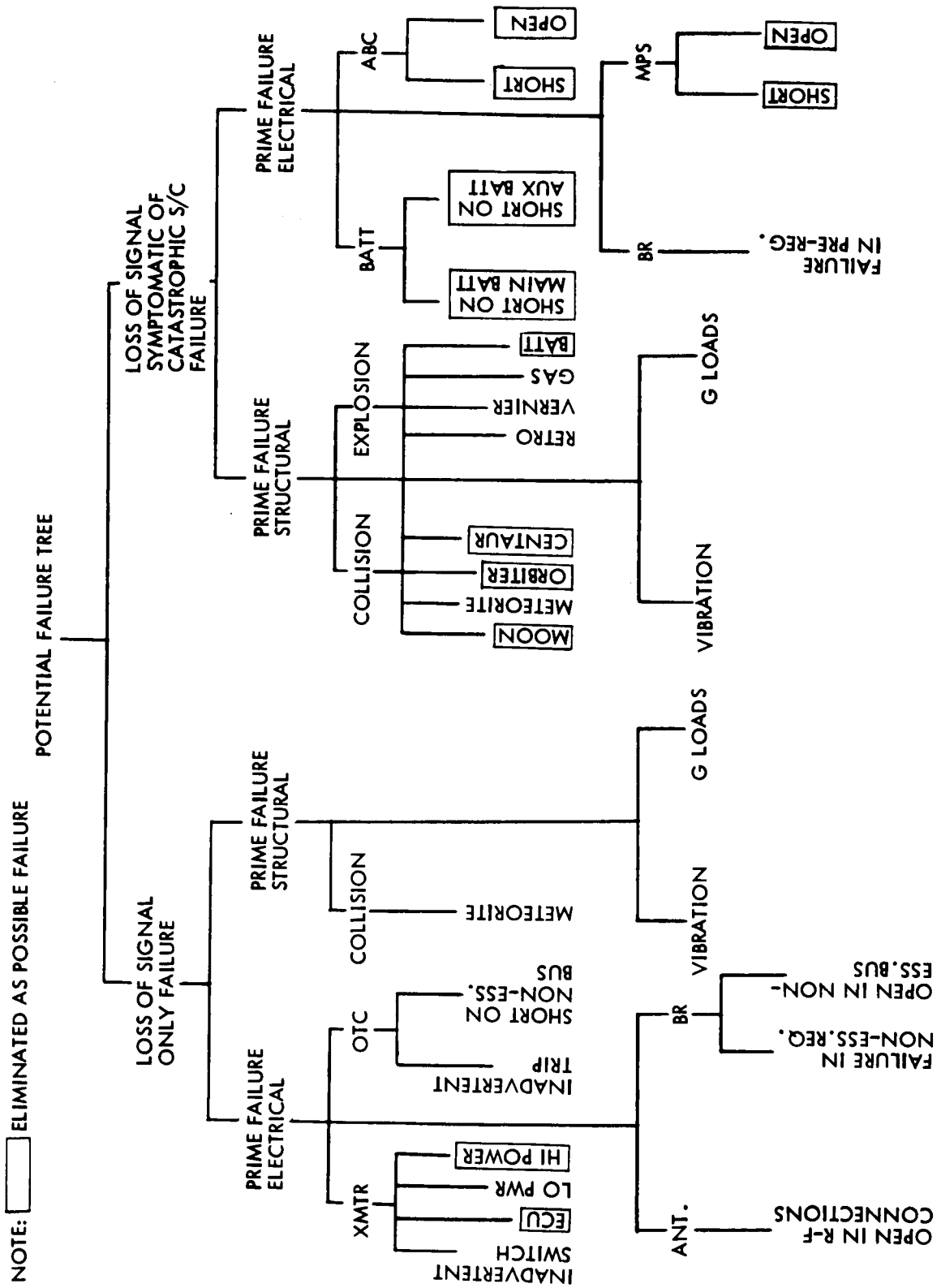
Figure 4-4. Potential Failure Tree

Word
16
0111101001

PCM Data Discriminator Output

7.35 KHz Subcarrier recorded from Phase Detector

500 KHz down-converted to lie within a 1-8 KHz Bandpass Filter

Loss of
Signal

1 msec. 02:02:41.000

1 Khz Timing Code
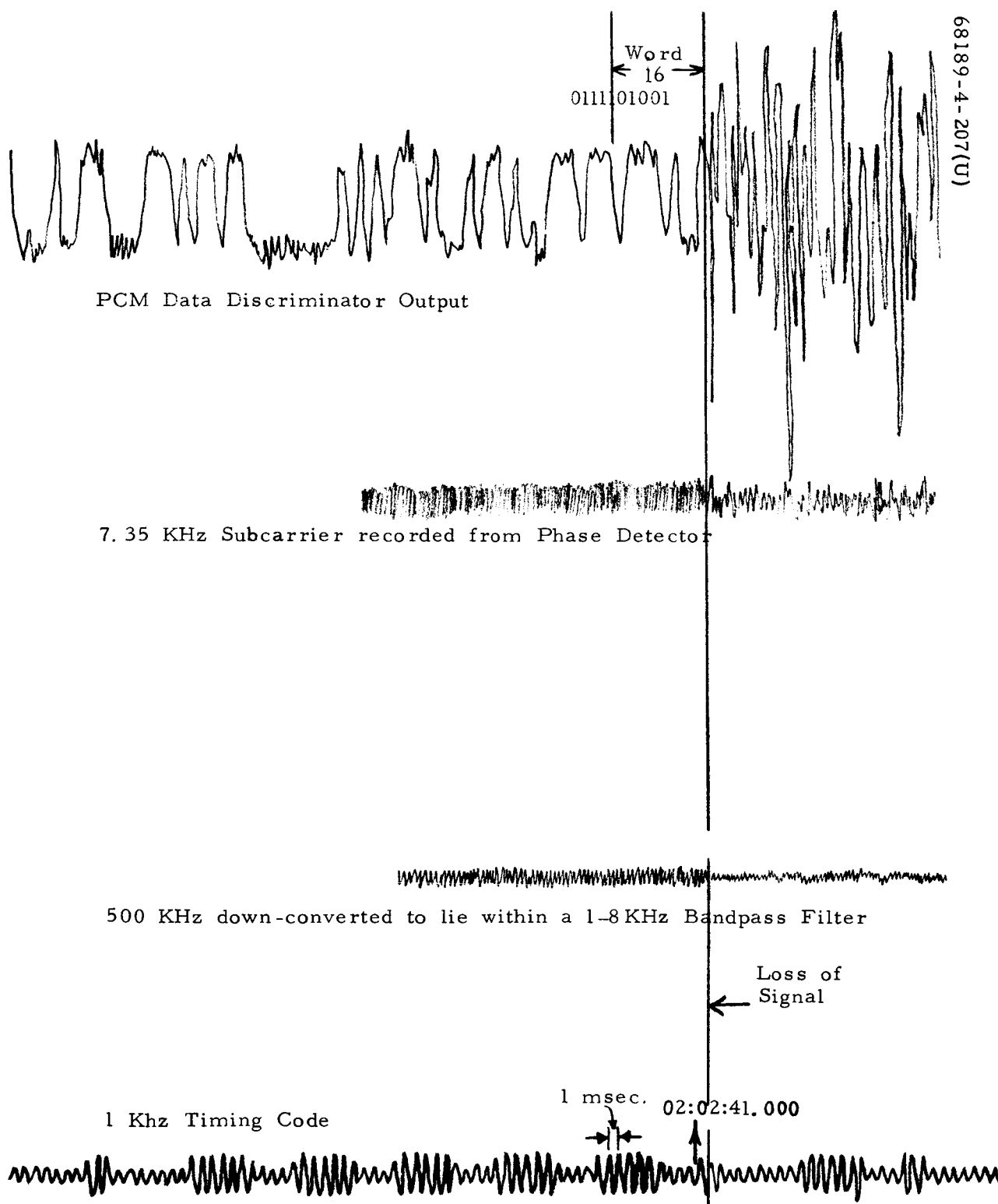
Figure 4-5. DSS-11 60 IPS Tape at Signal Loss

TABLE 4-21.   POTENTIAL FAILURE MATRIX

General Failures	1 Loss of Signal Only	2 Loss of Signal and Failure to Land
1) Short on nonessential bus	Yes	No
2) Short on flight control bus	No	No
3) Short on essential bus	No	No
4) Open on nonessential bus	Yes	No
5) Open on flight control bus	No	No
6) Open on essential bus	No	No
7) Open on unregulated bus	No	Yes

Failures	Main Battery		Auxiliary Battery		Transmitter		Flight Control Sensor Group		Auxiliary Battery Control		Boost Regulator		RADVS		Signal Processor		Command Decoder		Eng. Mech. Auxiliary		TV		Main Power Switch	
	1	2	1	2	1	2	1	2	1	2	1	2	1	2	1	2	1	2	1	2	1	2	1	2
Spurious off condition	N	N	N	N	Y	N	N	N	N	N	N	N	N	N	N	N	—	—	N	N	N	N	(Y)	(Y)
Spurious on condition	N	N	N	N	N	N	N	N	N	N	N	N	N	N	N	N	—	—	N	N	N	N	N	N
Input short	—	—	—	—	Y	N	N	N	N	(Y)	(Y)	(Y)	N	N	Y	N	N	N	?	?	Y	N	N	(Y)
Output short	N	(Y)	N	(Y)	Y	N	N	N	N	(Y)	*	*	N	N	N	N	N	N	N	N	N	N	N	(Y)
Internal short	N	N	N	N	Y	N	N	N	N	(Y)	Y	Y	N	N	N	N	N	N	N	N	N	N	N	(Y)
Spur switch	—	—	—	—	Y	N	N	N	N	N	N	N	N	N	N	N	N	N	N	N	N	N	(Y)	(Y)
Input open	—	—	—	—	Y	N	N	N	N	N	(Y)	(Y)	N	N	N	N	N	N	N	N	N	N	—	—
Output open	N	N	N	N	Y	N	N	N	(Y)	(Y)	*	*	N	N	N	N	N	N	N	N	N	N	(Y)	(Y)
Function failure	—	—	—	—	Y	N	N	N	N	N	Y	Y	N	N	N	N	N	N	N	N	N	N	—	—

Definitions

1   Could cause loss of signal only

2   Could cause loss of signal and failure to land

N   No applicable failure

Y   Yes, possible failure

—   Does not apply

*   General failure

(Y)   Eliminated as possible failure

1)   Inadvertent execution of command 0107 transmitter, "high voltage off," which turns off the high voltage supply to the TWT.

2)   Inadvertent execution of command 0110, "transmitter filament off," which turns the filament and high voltage supplies off. Since the filaments take several seconds to cool, this command is included because the high voltage supply would go off also.

3)   Removal of the 29-volt regulated supply voltage from the high voltage supply for the TWT.   This removal would give the same symptoms as if the supply had been turned off.

4)   Failure of any component in the primary side of the electronic conversion unit (ECU) which transforms the 29-volt regulated supply voltage up to the TWT high voltages.

TABLE 4-22.   POTENTIAL FAILURES ELIMINATED AS
POSSIBLE CAUSE

Failure Mode	Reason Eliminated
Collision with moon	RADVS data, AMR performance, and Lunar Orbit determination accuracy all indicate retro ignition at proper altitude.
Collision with Centaur	Post-spacecraft-separation Centaur retro maneuver has been verified.
Collision with Lunar Orbiter	Location of all three Lunar Orbiters has been confirmed by tracking (one of them only by extrapolation of last orbit prior to its failure) as being not in the Surveyor locale at the time of failure. Also, the two that were still transmitting have been contacted subsequent to the Surveyor failure.
Battery explosion	All known battery failure mechanisms would have signaled their approaching failure prior to the actual explosion.
Transmitter failure due to: 1) High voltage off command 2) Filament off command 3) Open on 29-volt input to high volt electronic conversion units	Signature indicates transmitter carrier power decay is longer than experienced at failure.
22-volt bus system open or short	Signature indicates transmitter carrier power decay is longer than experienced at failure.

This type of failure has been investigated by actually having a transmitter high voltage supply turned off while operating in the SC-6 system. Per Figure 4-6a, the subcarrier decay time is approximately 9 milliseconds. This time far exceeds the less than 0.25-millisecond decay time and is not considered to represent the Surveyor IV decay signature.

In addition, pictures of high voltage turn-off by direct command and by the filament off command have been taken on a transmitter of the Surveyor IV configuration. The results are shown in Figures 4-6b and c. Time to decay exceeds 4 milliseconds. This again does not represent the Surveyor IV signature.

4.3.2.2 Low Power Turn Off

The low power transmitter could be turned off by any of the following modes:

1) Inadvertent execution of the transmitter low power off command

2) Failure of a component in the low power switching circuitry

3) A 29-volt low ripple short within the transmitter

A test was performed to determine the RF carrier signature of turning off the low power transmitter. The results are shown in Figure 4-6d. The carrier disappears instantaneously, exactly duplicating the Surveyor IV failure signature.

This type of failure could have happened on Surveyor IV. However, it is extremely unlikely that the alternate transmitter failed in the same way at the same time. No transmitter has ever failed in this manner during system tests.

4.3.2.3 Inadvertent Transfer Switch Command Execution

Transmitter carrier transmission via the omnidirectional antenna could be interrupted by switching the transmitter in operation from the omnidirectional antenna to the planar array. This switching has been tested on SC-6 at the system level and shows a 47-db decrease in carrier level when switched. In addition, a test was performed on a Surveyor IV configuration transmitter to demonstrate the switching time (Figure 4-6e) which is 250 microseconds or less.

This operation is a possible explanation for the Surveyor IV failure. However, it is not considered the primary failure since the switch could be commanded back to the correct position.

4.3.2.4 Opening of 29-Volt Low Ripple Line to Transmitter

If the wire connecting the boost regulator to the low power transmitter were to break, the low power transmitter would go off. To determine

the signature, a test was performed on a Surveyor IV configuration transmitter. Figure 4-6f shows the carrier decay time of approximately 625 microseconds. Although this time is somewhat in excess of that observed on the Surveyor IV failure, it is not unreasonable and could explain the failure. Since only one wire from the boost regulator services both transmitters, a broken wire could cause both transmitters to become inoperative.

4.3.2.5 Shorting of 29-Volt Low Ripple Line to Transmitter

Although not tested, shorting of the 29-volt low ripple line to the transmitter is expected to give the same signature as opening of the line as discussed above.

4.3.2.6 Opening of Coax From Transfer Switch to Single Pole Double Throw (SPDT) Switch

The single cable routed from the RF transfer switch to the SPDT switch determines the spacecraft capability to transmit on the omni-directional antennas. If this cable were opened, the failure signature would be obtained. Opening at this coax could be due to connector-cable separation or a connector unscrewing and falling out due to vibration. Although this failure mode is considered remote, it is possible.

4.3.2.7 Command Line Susceptibility

Because the command line operations have been considered in the paragraphs above, the susceptibility of each line has been measured on a Surveyor IV configuration transmitter. None of the lines are considered excessively susceptible, but this does not preclude inadvertent operation which is considered possible, but not probable.

4.3.2.8 High Voltage Arc

Transmitters have arced at the unit level during thermal vacuum pumpdown testing at critical pressure. In every instance, the arc was caused by voids in the foam potting compound and the fault has been corrected. It is considered possible that this type of failure could have occurred, but is not probable. In any instance, recovery would be possible by switching to the other transmitter.

4.3.2.9 Practical Failure Mode Summary

The failure signature could be reproduced by four types of transmitter associated failures:

1) Low power turn off (see paragraph 4.3.2.2)

2) Opening or shorting of the 29-volt low ripple line to the transmitter (see paragraphs 4.3.2.4 and 4.3.2.5)

SPEED: 50 M/SEC
7.35 KC SCO OUTPUT

7.35 KC

TIME (1 M SEC/DIV)
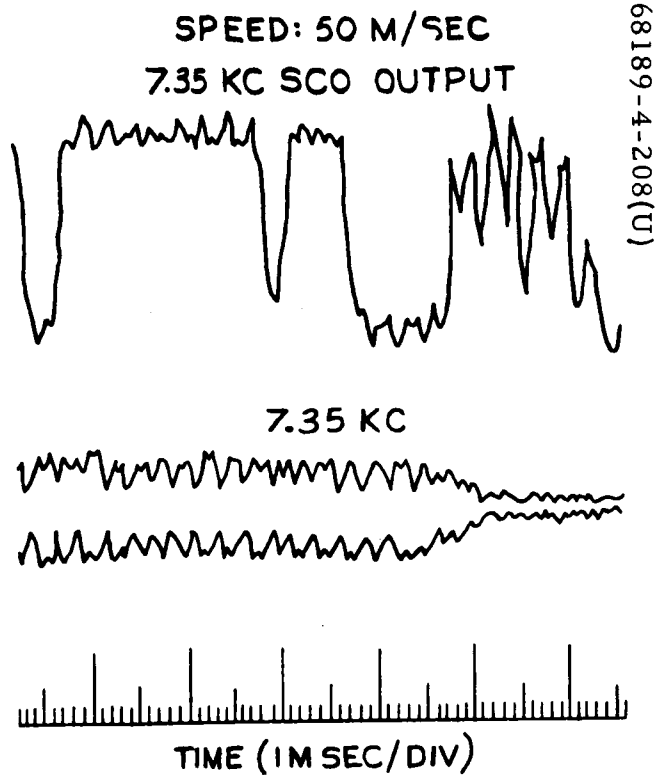
Figure 4-6a. SC-6 High Power Turn-off

68189-4-208(U)

H.V. ON/OFF
STD CMD
IMSEC/DIV

OFF

ON

68189-4-209(U)
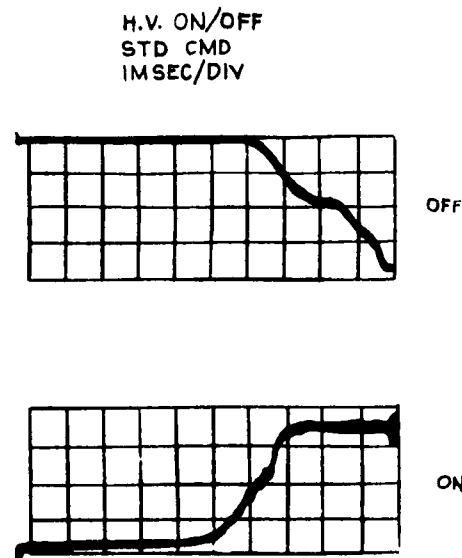
Figure 4-6b. High Voltage Turned
Off by Command

FIL OFF
5/MSEC DIV
STD CMD

68189-4-210(U)
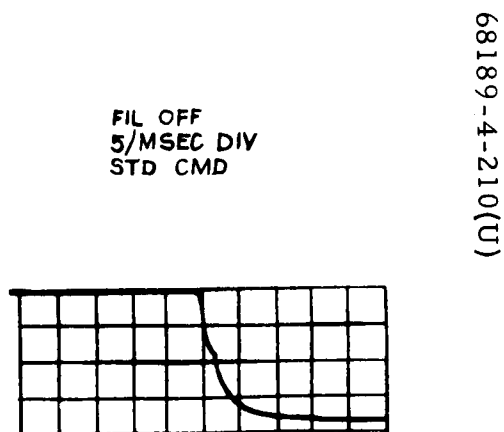
Figure 4-6c. High Voltage Turned
Off by Interlock When Filament Off
Command Is Sent

ON

OFF

68189-4-211(U)

100 USEC/DIV
L.V. ON / OFF
3.3 K
15 MSEC PULSE
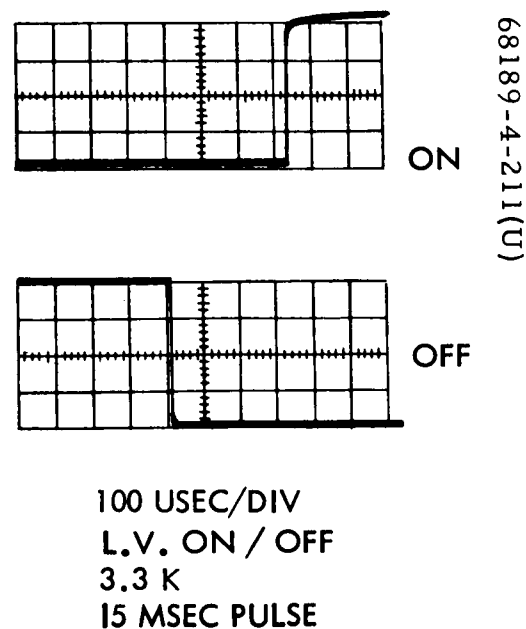
Figure 4-6d. Low Power Transmitter
Turned Off by Command

2 MSEC/DIV
RF X FER SW.
COMM 14-BREAK
COMM 15-MAKE

68189-4-212(U)

BREAK

MAKE
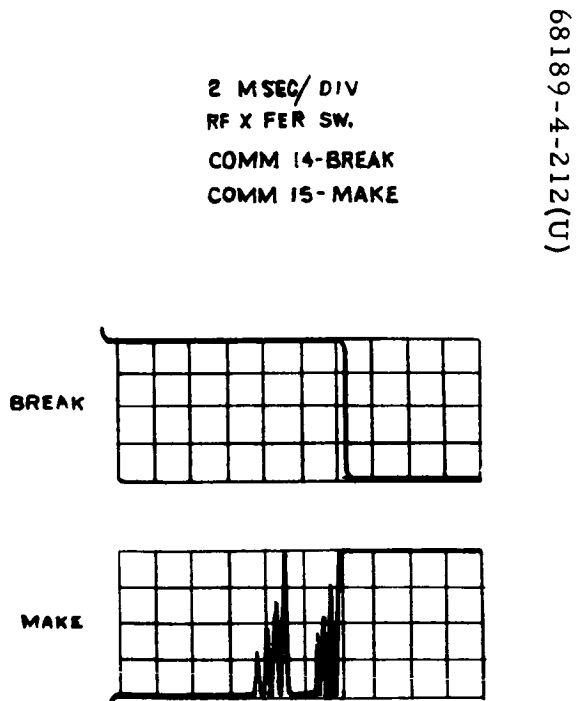
Figure 4-6e. RF Transfer Switch
Command Operation

68189-4-213(U)

ON

OFF

T=0 100 μs/DIV
H.V. OFF
TURN OFF TIME = 650 μSEC
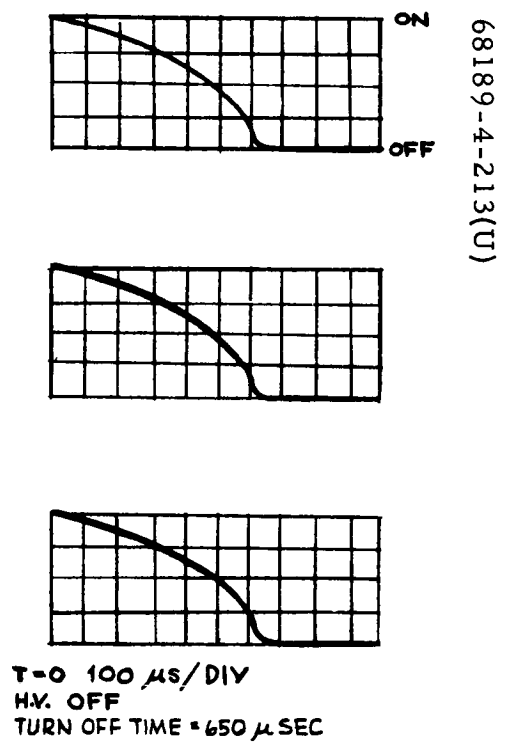
Figure 4-6f. Low Voltage Off,
29-Volt Low Ripple Bus
Opened

4-51

3) Inadvertent operation of the RF transfer switch (see paragraph 4.3.2.3)

4) Opening of the coax from the transfer switch to the SPDT switch (see paragraph 4.3.2.6)

Items 1 and 3 above could reproduce the failure mode, but, in each instance, recovery by command is possible and was tried to no avail after predicted landing time. Although there were inadvertent transfers of the transfer switches in the Surveyor I through Surveyor III configuration, the Surveyor IV configuration switches have not exhibited this problem. The switches were redesigned for Surveyor IV and subsequent spacecraft. To date, no switch has malfunctioned. Items 2 and 4 above could also reproduce the failure mode, but recovery would not be possible.

4.3.3 Propulsion Failure Modes

The propulsion failure mode review is restricted to the propulsion subsystem and does not include other similar sources of failure such as the high pressure shock absorbers, nitrogen tank, explosive bolts, etc.

The failure of either the retro or the vernier propulsion subsystem by itself would not cause the mission failure. The failure of either propulsion subsystem must then cause the transmitting equipment to be damaged or cause another subsystem to be damaged which, in turn, failed the transmitting subsystem.

There are three categories of failure of the propulsion subsystem which could result in loss of communication, and each will be considered in detail:

1) Shock Impulse — Shock input to the spacecraft if the retro nozzle separated from the case.

2) Burnthrough — Hot combustion gas acting as a cutting torch if there were a burnthrough of the retro case.

3) Fragmentation — High velocity fragments from the retro, propellant tanks, or helium tanks.

4.3.3.1 Shock Impulse

If the retro nozzle were severed from the case, there would be a high thrust for a short period. It is estimated that a shock load of 100,000 pounds for 0.003 second could occur before the pressure would decay to the level required to extinguish the burning.

On 30 October 1966, the F-1 apogee motor was ignited to place the Intelsat II communication satellite in a synchronous orbit. Doppler shift data indicated that the motor burned for 4.7 seconds versus the expected 16 seconds and then suddenly terminated by losing its nozzle. The spacecraft was

not damaged except for one whip antenna. Thermal vacuum test at Hughes demonstrated the problem to be low temperature on the aft end of the motor, i. e. , -33°F on the case and -45°F on the nozzle versus the qualification range of 30° to 110°F. Motor A26 tested at Aerojet General Corporation on 23 November 1966 confirmed the failure mode when subjected to these cold temperatures for 96 hours under a simulated altitude of 80, 000 feet. A number of other potential failure modes were investigated both at Hughes and Aerojet General Corporation and found to be of no concern.

Following the design and fabrication of a thermal shield and heater strip to protect the aft end of the motor, additional thermal vacuum tests were run which demonstrated acceptable motor temperatures. Further confirmation was obtained at the Arnold Engineering Development Center where a successful motor test was conducted. Motor A22 was tested with spacecraft T-1 while spinning at 120 rpm. The motor was held at 80, 000 feet simulated altitude for 76 hours and was temperature conditioned to 55°F with nozzle boss flange controlled to 70°F by use of the heater. The next satellite with the new thermal shield performed satisfactorily.

This type of out-of-specification limit thermal failure is not applicable to Surveyor since its temperatures were well within expected values. Analysis indicates that the Surveyor retro support strut would fail under this shock loading but that the retro would not come loose from its main support points. (The highest load to any spacecraft was 40 g accidentally applied during vibration test of Surveyor II. The inert retro support strut failed due to the overload, but no other component in the spacecraft was damaged.)

During development of the retro, two nozzle failures of this type occurred, one of which happened when using a cutoff nozzle. This failure was due to the short nozzle that allowed hot gases leaving the nozzle to overheat the outer structure because of inadequate coupling with the diffuser. As an added safety factor to prevent such failure when using a full-length nozzle, the structure was strengthened. The second nozzle failure (of an obsolete design) occurred when hot gases leaked through a joint in the nozzle, resulting in failure due to overheating. Since the present design was adopted, 31 motors have been fired without any recurrence of these difficulties. In addition, this type of failure would result in a change in velocity or orientation of the spacecraft which may be detectable from flight data. This failure mode is considered an unlikely cause of the failure.

4. 3. 3. 2   Burnthrough

If the retro motor wall became overheated because of excessive heat transfer or improper insulation, the hot combustion gases could cause a burnthrough and allow the gases to act as a cutting torch on the communication subsystem. It should be noted that any gas leak would expand in the surrounding vacuum and appreciably decrease its capability to act as a cutting torch. It is probable that there would be sufficient time to notice a change in thrust vector direction or magnitude before the gas severed the transmission equipment or caused the vernier tanks to fragment and damage the transmitting equipment. In addition, the high temperature would be expected to appear as

noise in the transmitted flight data. Based on these considerations and the fact that this type of burnthrough failure has never occurred in any of these retro motors in the past, the conclusion is that thermal cutting is an unlikely cause of the failure.

Under some conditions, a burnthrough can be followed by the case fragmenting. Such a failure is discussed next.

4. 3. 3. 3   Fragmentation

Fragmentation as a secondary effect to a retro case burnthrough or local overheating could occur. Previous experience with this case material in the first stage Minuteman motor is that, when fragmentation occurs, it is preceded by a flame for a second or more. Unless the burnthrough is aligned with the center of gravity, such a condition should be noticed in the flight data.

The PHOENIX rocket motor is a 15-inch diameter cylindrical motor, also using D6-ac steel at about the same stress level as the Surveyor retro. Early in the program, there were two test failures which are of interest. In the first (motor serial No. 3004) there was an insulation failure which allowed combustion gases to reach a case wall after 16 seconds of a nominal 25-second burn time. The failure mechanism was a simple burnthrough of the case in the area of known insulation breakdown; pressure trace was normal until the burnthrough occurred, at which point it decayed to atmospheric pressure. There was no catastrophic failure.

In the second case (serial No. 3002), a similar insulation failure occurred, but was accompanied by separation between the propellant and liner after 2 seconds of normal burning at 800 psi which caused a pressure rise to about 1450 psi. Pressure decayed for 2 more seconds and then began to drop sharply as if a burnthrough had occurred. High-speed motion pictures show the failure progressing from the area of insulation failure near the head end of the motor all the way to the aft end in about 4 milliseconds, at which point the case ruptured fully and expelled large pieces of propellant and some metal fragments.

There were no failures in this program which fit the Surveyor IV failure conditions; that is, no motor ever failed so near to the end of burning in a way which could have catastrophically damaged surrounding structure and equipment.

There are also instances on Minuteman, Thiokol 26-inch sphere, and PHOENIX motors where a burnthrough did not result in fragmentation. Based on the long time after burnthrough before the case could fragment and since there has never been a burnthrough in the history of this motor, this is an unlikely failure mode.

There are two other methods by which the case can fragment: increased pressure due to nozzle blockage and decreased strength due to over-heating. The case failure due to overheating cannot be completely ruled out as a failure mechanism since no evidence of this type of failure in this motor has been found to date.

There have been failures of a 15-inch spherical motor which are attributed to overheating without burnthrough. In this case, the motor fragmented without previous external indication. The pressure-time history just prior to fracture will be reviewed to see if any appreciable pressure buildup occurred which would be observed as an increased acceleration of the spacecraft. This review will be completed when data become available from NASA-Langley.

Since past history for this retro did not indicate a marginal insulation design and since the preflight X-rays indicated normal bonding of the propellant/linear/insulation/case, this mechanism is not considered a likely failure mode.

In considering nozzle blockage, the three materials in the motor at the time of communcation loss are the propellant slivers, the insulation, and the pyrogen case. The propellant and insulation, if detached from the case, would pass out of the nozzle without blockage. The pyrogen case at the time of failure would be softened so that it too would not be capable of blocking the nozzle. There is a great deal of test data with this motor to show that failure of the graphite insert also would not block the nozzle. Nozzle blockage and resulting case failure by overpressure are considered an unlikely failure mode.

The small amount of propellant remaining in the retro motor at the time of loss of data makes it necessary to burn on all of its surfaces in order to produce sufficient pressure to rupture the retro case at normal temperatures without nozzle blockage. This increase in burning area would require all the propellant slivers to tear loose from the case liner. A pressure increase of this type would require more than 20 milliseconds and would result in an increased thrust and a higher acceleration. The liner held the much higher inertia stress when more propellant was present, and the chamber pressure tends to hold the slivers against the wall. Based on these facts and the history of the motor, this failure is considered very unlikely.

Fragmentation of the vernier helium tank and propellant tanks has also been considered. Since the helium tank had been pressurized to over 5000 psia for several days and at the time of communications loss the pressure was only 4500 psia, it is highly unlikely that the helium tank fragmented from internal pressure. As a result of a Saturn IV B failure, the welds on the nitrogen and helium tanks were examined spectrographically prior to the flight and found to be of the proper weld material. The propellant tanks were pressurized for over a day and similarly are believed to have shown their ability to withstand the internal pressure without failure. This consideration, along with the extensive tests performed during the past year specifically to show that these tanks are not susceptible to stress corrosion, leads to the conclusion that the propellant tanks are unlikely to be the cause of damage to the communication system.

4.3.4   Structural Failure Analysis

   4.3.4.1   Structural History

Structural qualification tests of the design have been conducted on the S-2, S-2A, S-9, and T-21 vehicles for both vibration and landing phases.

TABLE 4-23. STRUCTURAL LOADS AND MARGINS

Spacecraft Element	Design Loads		Margins of Safety	Test Data Available		Loads at Surveyor IV Loss of Signal	Comments
	Vertical	Lateral		Drop	Static		
Omnidirectional antenna A	25 g	25 g	0.23	22 g	12 g	8 g	
Omnidirectional antenna B	25 g	25 g	0.15	31 } g 11 }	12 g	8 g	
Compartment A	18 g	8 g	0.10	18 } g	12 g	8 g	
Compartment B	21 g	9 g	0.10	16 } 10 } g	12 g	8 g	
Auxiliary battery	25 g	25 g	0.11		12 g	8 g	
Retro spacecraft support	3300 pounds		0.30	2540 pounds		2100 pounds	
A/SPP	30 to 40 g		0.11		12 g	8 g	
Vernier brackets	± 35 g	± 18g	Fatigue		12 g	8 g	
Retrorocket motor							
Case	Case pressure 700 psi		0.20	Static Burst pressure 960 and 995 psi		—	Designed for 700 psi Maximum expected operating pressure 582 psi
Skirt	Vertical 4655 pounds	Lateral 1735 pounds	0.15*	Static Diagonal 6455 pounds / Lateral 7355 pounds		3000 pounds	—
Strut	—	—	No failures	Axial 5000 pounds / Lateral 4800 pounds		296 pounds computed	7075-T6 aluminum
Nozzle	Case pressure 700 psi	Torque on closure bolts 200 in-lb	0.16	—		—	Aluminum band phenolic nozzle
Nitrogen tank	5,000 psi proof 11,000 psi burst		1.03 0.01	Drop		Not monitored (5000 psi?)	Titanium spheres: lugs checked and good for 180 g
Helium tank	5,175 psi proof 11,385 psi burst		2.20 0.00	20 g approximately with 250 psi in tanks		4017 psi	
Propellant tank	840 psi proof 1,038 psi burst		0.19 0.05			750 psi	

*Thiokol analysis annealed

These test loads are generally at least 50 percent higher than the 8 g steady-state deceleration load experienced by the vehicle at the time of signal loss. The design and test loads of some of the components of concern are given in Table 4-23.

Surveyor IV had the least amount of fatigue accumulation of any Surveyor flown to that time. Whereas the other vehicles had been subjected to additional vibration tests due to component changes, Surveyor IV was subjected to only one three-axis flight acceptance vibration test. The structural capability remaining, therefore, should have been better than Surveyors I, II, or III. There were no QCHR, MRB, or TFR problems that have any implication on the structural integrity of Surveyor IV.

4.3.4.2 Possible Failure Modes

Some possible modes of structural failure are listed in Table 4-24. Explosion and impact could lead to rapid enough failures so that the flight control data would not indicate the condition. Although structural failure of compartment A or the operating omnidirectional antenna could cause immediate loss of signal, failure of less critical items should have appeared as a control system perturbation. In view of the design margins and large amount of structural testing at 50 percent or more in excess of the loading conditions at the time of signal loss and the fact that this would have been the largest load encountered in the flight to that point, it appears extremely unlikely that structural failure could have occurred earlier in the mission.

Because of the apparent vibratory behavior of the Surveyor IV flight control system during retro fire, the possibility of some structural condition that could explain this condition and ultimately result in failure was sought. The items that could potentially lead to control system buzz problems are listed in Table 4-25. One of the arms of the bipod on compartment B was broken during S-9 torsional vibration tests and resulted in approximately a 2-Hz shift in resonant frequency. Therefore, in order to get significant frequency shifts, either both legs of the bipod must be broken or the attachment to the spaceframe must come loose.

4.3.4.3 Conclusions

Based on the severity and number of qualification tests performed and the lack of any known load environment approaching qualification levels, it seems extremely unlikely that any structural or mechanism failure occurred on Surveyor IV.

4.3.5 Electrical Power Failure Analysis

4.3.5.1 In-flight Status and Timing

Each power subsystem telemetry signal that appears in mode 6 has been analyzed below from AMR mark time until loss of signal. This period covers the last 45 seconds of the mission. All values are nominal. Point-by-point evaluation of the data indicates the power subsystem was operating in a

TABLE 4-24.   STRUCTURAL FAILURE MODE

Possible Failures	Mode of Failure	Surveyor IV Telemetry Signature*	Comments
Explosion of retro, tanks, shock absorber	Shrapnel	1	Assumed propagation of 700 fps
	Shock	1	Propagation velocity = 16,000 fps
	Structural failure	2	
Early impact	Explosion	1	
	Structural failure	1	
	Shock	1	
Structural failure	Compartments	2	
	Auxiliary battery	2	
	Omnidirectional antenna	2	
	Solar panel	2	
	Retro support	2	

*1 — Loss of signal < 10 milliseconds.
 2 — Loss of signal > 10 milliseconds, possibly recognizable by flight control telemetry.

TABLE 4-25. STRUCTURAL CONDITIONS LEADING TO FLIGHT CONTROL BUZZ

Component	Failure	Result on Flight Control Buzz	Final Failure Mode Due to Increasing Deceleration
Retro	None	Resonant frequency about leg 3 axis is 17 Hz, lowest of any direction. As propellant burns, the frequency would increase, reducing any buzz problem. Buzz checked in this configuration on S-2A.	None expected.
A/SPP	Solar axis lock pin without micro-switch not engaged	Lower A/SPP frequency which might lead to buzz. Fundamental mode probably about axis through leg 1.	Solar panel breaks off and hits compartment A. Load capability enough to withstand 8 g.
Compartment A	Upper bipod near leg 1 loose or broken	Significant reduction in resonant frequency possibly giving buzz problem. Compartment center of gravity movement approximately perpendicular to leg 3.	Compartment breaks off. Load capability not known.
Compartment B	Upper bipod near leg 3 loose or broken		

normal manner when the data were terminated. Additionally, data obtained during the transit coast phase and midcourse were reviewed and show no anomalies with all parameters nominal.

EP-14 — Regulated Output Current. Prior to vernier ignition, with the transmitter in high power and flight control thrust phase power on, battery regulated output current was 5.30 amperes. At vernier ignition, approximately 75 milliamperes are applied to the flight control solenoid transistor switch, and EP-14 increases to 5.375 milliamperes.

EP-2 — Unregulated Bus Voltage. With the main battery and auxiliary battery in parallel (high current mode), the unregulated bus was 21.3 volts prior to vernier ignition (total spacecraft load of 14 amperes). After initial RADVS power turnon, the bus dropped to 20.8 volts (total spacecraft load of 27.5 amperes). After RADVS time-in, the bus dropped to 20.6 volts (total spacecraft load of 37 amperes).

EP-17 — Radar Current. Prior to vernier ignition, EP-17 indicates AMR current. The average value is 3.5 amperes with approximately ±0.5 ampere of noise (all spacecraft exhibit this characteristic). After vernier and retro ignition, the AMR is discarded, and EP-17 indicates an initial RADVS current of 15.0 amperes. After 20 seconds, the KPSM times in and the final value of 24.5 amperes is reached.

EP-4 — Unregulated Output Current. Prior to vernier ignition, all cycling heater loads on EP-4 are commanded off. When verniers are ignited, EP-4 indicates solenoid current only. The first readout is a relatively high 1.85 amperes because the solenoids are cool and EP-2 is relatively high because RADVS has not yet been commanded on. After RADVS comes on and the solenoids warm up, their current decreases to 1.68 amperes.

EP-40 — Flight Control Unregulated Current. During coast phase, this shunt measures one constant load of 0.2 ampere — gyro thermal control. Its cycling loads include the three gyro heaters which draw 0.5 ampere each and, occasionally, a gas jet which draws 0.1 ampere. During coast, the average duty cycle of each heater is approximately 25 percent at a cycling rate of approximately 0.5 Hz. During Surveyor IV terminal descent, the spacecraft roll axis was facing away from the sun, and the duty cycle increased to approximately 50 percent for each heater.

Prior to vernier engine burn, thrust phase power is commanded on. This turns on the roll actuator servo amplifier. Its current is measured by EP-40 and indicated 0.34 ampere. Therefore, the minimum EP-40 load was 0.34 ampere for the roll actuator and 0.20 ampere for the gyro thermal control. With one gyro heater on, EP-40 indicates 1.04 amperes; with two gyros on, it indicates 1.54 amperes; and with all three gyros on, it indicates 2.04 amperes. These current values were indicated throughout the last minute of operation with two exceptions. Immediately after vernier ignition, a small torque was applied to the roll actuator, resulting in a 0.14-ampere increase in roll actuator servo current. However, the roll actuator

returned to its null position approximately 3 seconds after vernier ignition. Also, a gas jet came on approximately 3 seconds before loss of signal. (The 2-minute period preceding vernier ignition was also investigated and no indication of gas jet operation could be found.)

EP-9 — Battery Discharge Current. This shunt reads all battery loads, with the exception of the radars, including the boost regulator and the unregulated loads. The cyclic loads once again are the gyro heaters. EP-40 and EP-9 variations are not synchronized because they are separated by 10 words or 120 milliseconds on the commutator frame. Prior to vernier ignition, EP-9 indicates an average of 10.5 amperes. After the solenoids and RADVS come on, the average current is 12.5 amperes.

4.3.5.2 Power Unit Test History

A review of each unit's test history shows no excessive operating time or on-off cycles. All were well under nominal design ratings. Units are subjected to functional and partial flight acceptance test sequences after major rework or redesign, but not to levels exceeding flight acceptance test. No significant relation to the Surveyor IV failure could be established.

4.3.5.3 Spacecraft Harness Failure Modes

An evaluation and review of spacecraft power distribution harnessing was conducted to evaluate failure modes and past test and performance history. The harness is designed without true redundancy; however, in several instances throughout the harness, two or three wires are used to reduce voltage drop between units. A maximum size 12-gauge wire is used in the harnessing to simplify handling and shaping requirements. Wire gauges used in the point-to-point connections are conservative in terms of current rating as a result of efforts to minimize voltage drop.

The primary failure mode in the harnessing is at the connector where connections are made to the pin. Nothing is gained in reliability of the harness by running two redundant wires to the same pin. Redundant connector pins would be necessary to increase reliability.

4.3.5.4 Effects of Wiring Shorts

A study of the 22-volt unregulated bus harnessing has been made to evaluate capability of the harness to carry a short of 125 to 200 amperes. Results show that a short of this magnitude can be carried by the harness through the spacecraft with the exception of the AMR unit. This magnitude short would reduce battery terminal voltage to 16 to 17 volts, with correspondingly lower voltages at the various units in the spacecraft, resulting in loss of the boost regulator and the regulated busses.

A short between almost all +22-volt unregulated bus points and the spaceframe can produce a short circuit in the range of 125 to 200 amperes. The exact value of this current will depend upon the location of the short.
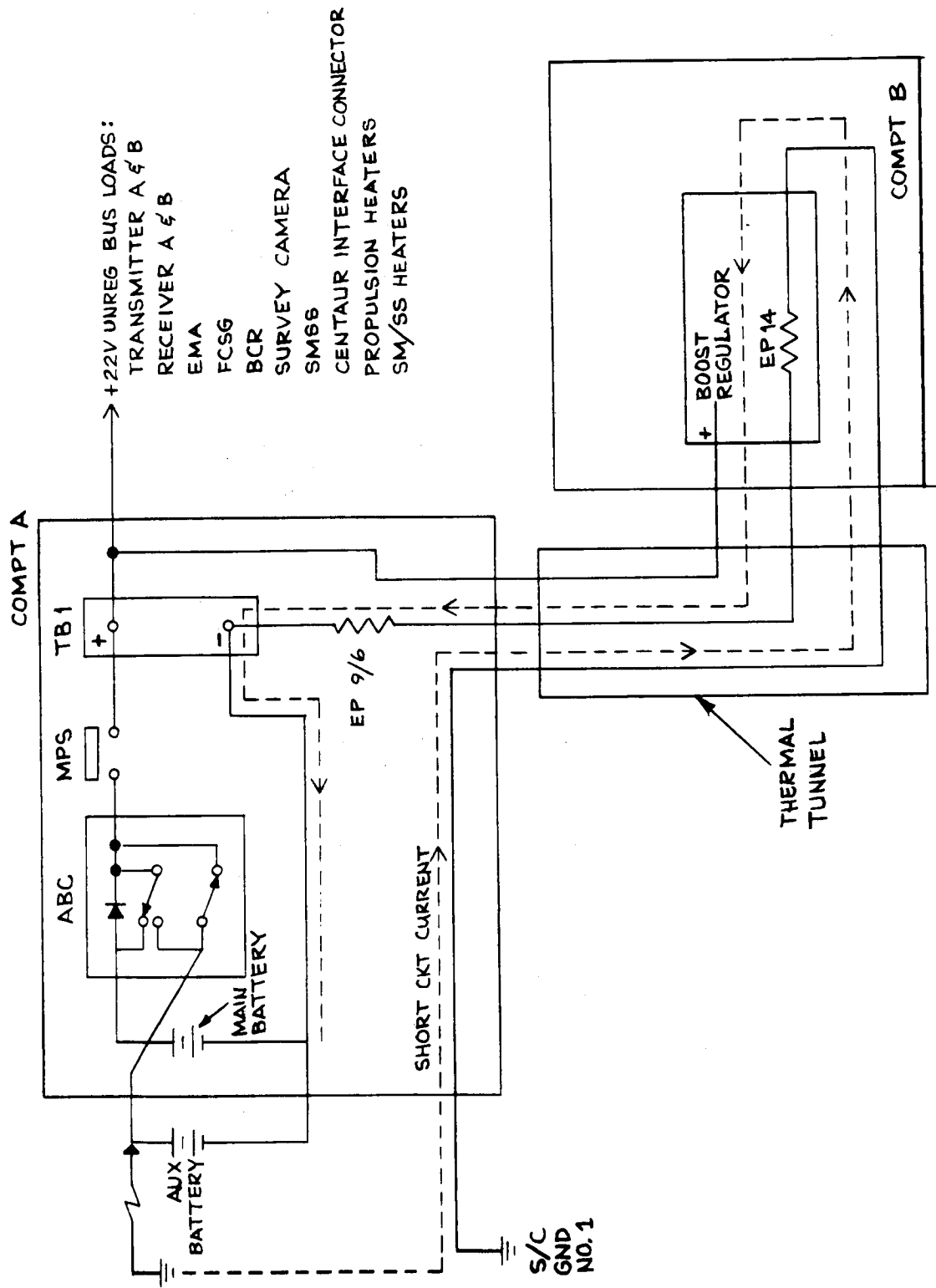
Figure 4-7. Current Path, 29-Volt Unregulated Bus, Short to Ground

Figure 4-7 shows the path of the short circuit current through the spacecraft return leads. It also shows that the harness drop between the negative input terminals of the boost regulator and the negative terminals of the batteries will also lower the input voltage to the boost regulator. When this voltage drops below 17 volts, the overload trip circuit (OTC) will trip with loss of the nonessential bus resulting.

The harness resistance between spacecraft ground 1 and the negative terminals of the main and auxiliary batteries is 0.108 ohm. Therefore, a short circuit at one of the battery positive terminals would result in a short circuit current of 167 amperes if it is assumed that the two batteries will provide an 18-volt terminal voltage with this load (past test history indicates this is a reasonable assumption). The harness resistance between the negative terminal of the boost regulator and the negative terminals of the batteries is 0.0194 ohm, resulting in a voltage drop of 3.2 volts. Boost regulator input voltage would be (18-3.2) = 14.8 volts. This low voltage would cause an OTC trip.

If the short is at the auxiliary battery control, main power switch, or terminal board 1, the short circuit current would be somewhat reduced; but the harness drop between the positive terminals of the batteries and terminal board 1 would also reduce the boost regulator input voltage. A short at terminal board 1 would result in a boost regulator input voltage of 13.4 volts.

Short circuit at the +22-volt terminals of the engineering mechanism auxiliary, battery charge regulator, flight control sensor group, transmitters, receivers, survey camera, soil mechanics/surface sampler Centaur interface connector, or heaters would result in an OTC trip.

Approximately one-half of the short circuit resistance is introduced by a 32-inch length of 24-gauge wire from spacecraft ground 1 to a splice in compartment A. This wire would fuse in 0.2 to 1.0 second and would eventually remove the short. However, approximately only 30 milliseconds are required to trip the OTC.

In order to simplify the above computations, the normal spacecraft load of 40 amperes during terminal descent was not considered. If the computations were to include this current, the boost regulator input voltage calculation would be lower by approximately 0.5 volt.

A study was made to determine if any one single wire open could cause the Surveyor IV failure signature. Based on transmitter test results and a review of the harness wiring, only one wire could cause the failure signature in the +29-volt regulated low ripple segment from compartment B to transmitters A and B in compartment A and its return. This wire consists of segments 391A, 391B, 391C, and 391D per drawing 239535-1, Sheet 1, SC-4 Power Distribution Drawings. An open in this wire could cause loss of RF in approximately 0.6 millisecond.

4.3.5.5 Spacecraft Current Shunts

There are four major current shunts aboard the spacecraft (see Table 4-26).

TABLE 4-26. MAJOR TELEMETERED CURRENT SHUNTS

Unit Designator	Telemetry Channels	Functions Monitored
233R1	EP-17	RADVS, AMR, A/SPP stepper motors.
284R1	EP-6/9	Battery charge/discharge current. Total battery current when EP-17 = 0.
285R1	EP-4	Unregulated current. Unregulated portion of battery and/or solar panel output current not measured on EP-40.
424R1	EP-40	Flight control unregulated current. Includes gyro heater thermal control, gyro heaters, roll actuator, and gas jets.

Two additional current shunts located in the boost regulator are shown below:

Telemetry Channels	Functions Monitored
EP-7	Battery regulator dc-dc converter current. Difference between battery regulator input and output current.
EP-14	Total regulated battery regulator output current.

To date, the only recorded unit failures have been the shearing off of the brass terminal studs due to the application of too great a torque and the stripping of the stud threads for the same reason. These failures have occurred only on the major current shunts: EP-17, 6/9, 4, or 40. No failures have been noted or could be found on either battery regulator shunt EP-7 or EP-14. An open of either EP-7 or EP-14 could cause loss of the battery regulator regulated busses, but the probability of occurrence is highly unlikely. There have been no shunt failures during vibration testing or spacecraft operation.

Since the shunts are in the current return paths, a short from any shunt terminal to spacecraft ground would be detected through telemetry, but would not interrupt it instantaneously. The only shunt failure that could feasibly have caused the observed failure is the opening of 284R1 (EP-6/9). This would have removed power from everything but the RADVS. Although the possibility of a shunt failure seems remote, the reliability of shunt operation could be improved by replacing the brass studs with a stronger material, i.e., stainless steel or beryllium copper.

4.3.5.6 Practical Failure Modes

A summary of power system failure modes is shown in Table 4-27. Major failure modes assumed are 22-volt unregulated bus shorts, 29-volt regulated bus shorts, 22-volt unregulated bus opens, and 29-volt regulated bus opens. Included in these major failure modes are unit, harness, and shunt failures as possible causes.

Conduct of boost regulator tests to establish the signature for the foregoing major failure modes has eliminated the 22-volt bus open mode and the 22-volt bus short mode as a result of the regulated bus decay times. Regulated buses decayed from 0.25 volt/ms to 2.0 volts/ms after holding up for 3 to 10 milliseconds with no change under the 22-volt open and short modes. During this time, it should have been possible to detect a change in the RF link or in one of the subsystems. No change was detected and, therefore, these failure modes are not considered possible.

Signature tests conducted to determine OTC signature as a function of overload on the nonessential regulated bus has eliminated all conditions with the exception of a total load range between 11.2 and 15 amperes. Under loads less than 11.2 the nonessential bus will hold regulation at 29 volts ±1 percent. Under loads greater than this value, initial voltage drop increases with increasing load to an approximately level voltage region. Initial voltage drop ranges from 0.4 to 14.0 volts at a rate of approximately 2 volts/ms.

Duration of the level region increases with increasing load until trip occurs, at which instant the nonessential bus drops to 0 volt in 0.1 to 0.2 millisecond. For loads from the threshold trip value of 11.2 to 20 amperes duration of the level voltage region ranges from 34 to 72 milliseconds. During these time periods, an indication of variation in RF link on other subsystems should have been observed. None was observed. As a result of the Surveyor IV signature being confined to a very small range of possible OTC overload values (less than 4 amperes in the 11.2- to 15-ampere range), it is considered possible, but unlikely, that a short on the nonessential bus caused the failure.

An additional signature test conducted on the boost regulator showed that the flight control bus could support a total load of 6 amperes for 3 to 4 seconds with no noticeable change in regulation or effect on other regulated buses.

TABLE 4-27.   POWER SYSTEM FAILURE MODE SUMMARY

Surveyor IV power subsystem

Assumed Failure Mode	Conditions Necessary	Signature Tests	Estimated Probability of Occurrence	Could Surveyor IV Signature Have Resulted?
22-Volt Bus Short				
Causes				
1) Batteries (main and auxiliary)	125 to 200 amperes required to drop battery terminal voltage to 16 to 17 volts	None recommended	Unlikely	No
2) BR		In process to determine BR signature for a 22-volt bus short	Unlikely	No
3) BCR		None recommended	Unlikely	No
4) ABC		None recommended	Unlikely	No
5) MPS		None recommended	Unlikely	No
6) EMA		None recommended	Unlikely	No
7) TC and HA		None recommended	Unlikely	No
8) Harness		None recommended	Possible	No
Flight Control Bus Shorts				
Causes				
1) Flight control units	10 to 20 ampere short would cause OTC trip	None recommended	Possible	Yes*
2) BR flight control regulator	10 to 20 ampere short would cause OTC trip	None recommended	Possible	Yes*

Table 4-27 (continued)

Assumed Failure Mode	Conditions Necessary	Signature Tests	Estimated Probability of Occurrence	Could Surveyor IV Signature Have Resulted?
Nonessential Bus Short Causes 1) Nonessential loads	If total load was greater than 7.0 amperes for more than 20 milliseconds, would cause OTC trip	BR tests in process to determine OTC signature	Possible	Yes*
2) BR non-essential regulator	If total load was greater than 7.0 amperes for more than 20 milliseconds, would cause OTC trip	None recommended	Possible	Yes*
Essential Bus Short Causes 1) Command decoder	Short of 10 to 20 amperes would cause BR pre-regulated bus to drop and OTC to trip	None recommended	Unlikely	Yes*
2) BR essential regulator (2 series diodes)	Shorted diodes would cause only a rise in essential bus voltage	None recommended	Unlikely	No

Table 4-27 (continued)

Assumed Failure Mode	Conditions Necessary	Signature Tests	Estimated Probability of Occurrence	Could Surveyor IV Signature Have Resulted?
Prevegulator Bus Short				
Cause				
1) BR preregulator	Short of 10 to 20 amperes would cause OTC trip	None recommended	Unlikely	Yes
22-Volt Bus Open				
Causes				
1) Main power switch	1) Application of ≈6 amperes for 60 milliseconds	None recommended	Unlikely	No
	2) Brake release plus mechanical action	None recommended	Unlikely	No
2) ABC	Wire break and both relay contacts open simultaneously	None recommended	Unlikely	No
3) Batteries	Wire break in both batteries simultaneously	None recommended	Unlikely	No
4) Harness	Wire break or connector loose	None recommended	Possible	No
5) Shunts (EP 6/9)	Broken stud	None recommended	Possible	No
Flight Control Bus Open				
	No effect on data loss	—	—	No
Essential Bus Open				
	No effect on data loss	—	—	No

Table 4-27 (continued)

Assumed Failure Mode	Conditions Necessary	Signature Tests	Estimated Probability of Occurrence	Could Surveyor IV Signature Have Resulted?
Preregulator Bus Open				
Cause				
1) BR internal open	Wire or component open	None recommended	Unlikely	Yes
Nonessential Bus Open				
Causes				
1) BR nonessential regulator	Wire or component open	None recommended	Unlikely	Yes
2) OTC trip	1) Total nonessential load greater than 7.0 amperes for more than 20 milliseconds	Test in process on BR to determine signature of open	Possible	Yes*
	2) Short on essential, flight control, or 22-volt bus could cause preregulator bus to drop causing OTC trip	None recommended	Possible	Yes*
Removal of 22-Volts to BR				
	Open on 22-volt bus	Test in process on BR to determine signature of open	Possible	No

*Only over a restricted range of overload.

Tests requiring short circuit currents greater than bus ratings on the essential and flight control regulated buses were not conducted because of their destructive nature. However, based on tests of the other assumed failure modes, it can be stated with reasonable confidence that these types of failures would not have provided the Surveyor IV signature. The only possible exception would be "crowbar" shorts (100 amperes or greater).

4.3.5.7 Conclusions

The following conclusions are made concerning the Surveyor IV failure:

1) A short of approximately 10 to 20 amperes on any regulated bus (29-volt essential, 29-volt nonessential, or flight control) would cause OTC trip (loss of nonessential bus) in 35 to 75 milliseconds, but would not have provided the Surveyor IV signature.

2) A short of 125 to 200 amperes on the 22-volt unregulated bus would cause OTC trip in 35 to 42 milliseconds, but would not have provided the Surveyor IV signature.

3) An open of the 22-volt unregulated bus would cause the OTC trip in 16 milliseconds, but would not have provided the Surveyor IV signature.

4) An open of the 29-volt nonessential regulator or an open of the boost regulator preregulated bus (internal to the boost regulator) would cause loss of the nonessential bus in approximately 10 milliseconds, but would not have provided the Surveyor IV signature.

5) Review of the spacecraft harnessing and shunts shows failures are possible but not likely.

6) Review of all power TFRs shows no reported failure that could have provided the Surveyor IV failure signature.

7) Review of unit discrepancies shows no discrepancy with particular relevance to the Surveyor IV signature.

8) The flight control regulated bus is capable of sustaining a 6-ampere load for 3 to 4 seconds with no effect on regulation or on other regulated busses.

9) The only signal wire open failure in the harness that could have caused the Surveyor IV failure signature is the +29-volt regulated low ripple lead from compartment B to transmitters A and B in compartment A and its return.

4.3.6 Flight Control Failure Analyses

4.3.6.1 Practical Failure Modes

No failure mode has been postulated wherein the flight control subsystem could cause the prime failure noted. There is the possibility, although it is not necessarily obvious, that the thrust command modulation was in some way connected with the ultimate failure. For this reason, this subsection will be devoted to a discussion of the various mechanisms that could cause such a characteristic. These possible causes are shown in Figure 4-8 in a "failure tree" format and are analyzed briefly in Table 4-28.

4.3.6.2 Structural Buzz

Introduction. A plot of the inverse attitude control loop gain is a measure of gain margin from 0-db gain. If the structural transfer function gain were multiplied times the attitude loop gain, it would subtract from the gain margin. Figure 4-9 shows the plot for structural gain measured on spacecraft structural model S-20. The gain margin becomes the distance from the resonant peak of the structural transfer function to the inverse attitude loop gain curve. The root locus stability plot for the attitude loop shows that, in the frequency range of 5 to 25 Hz, the system does not have phase stability and the system is gain stabilized. If a buzz problem were present, suspected structural modes would involve the A/SPP, retro, and/or flight control sensor group, and, in particular, the retro and flight control sensor group because their frequencies of oscillation overlap.

When the data were taken from S2, the outputs of the gyros were used for instrumentation and large forces (14 pounds) were applied to obtain measurable outputs from pitch and yaw torque inputs. Structural gain is a nonlinear function of the input level, and the high level used may have caused the gain to be less. The structural gain for the acceleration loop, which has been tested more, has shown a considerable dependence on the particular structure tested, as well as the input level.

The structural gain is augmented if the motion of the mass effected disturbs the center of gravity during retro firing. The center of gravity effect of A/SPP motion produces an overcenter torque which adds to the torque due to its spring restraint, thus amplifying its effect.

Surveyor IV. The character of the thrust commands during the retro burn looks like a sustained attitude loop oscillation. The high gain of the attitude loops allows the gyro angles to be small (1 to 2 BCD change) and still produce these commands. However, these small gyro angles still represent large rigid body accelerations (1 to 15 rad/sec^2) in the frequency range from 5.0 to 25 Hz. If a nonrigid spaceframe is assumed, these accelerations can be local on individual components such as the flight control sensor group, retro, A/SPP, or compartments.

4-71
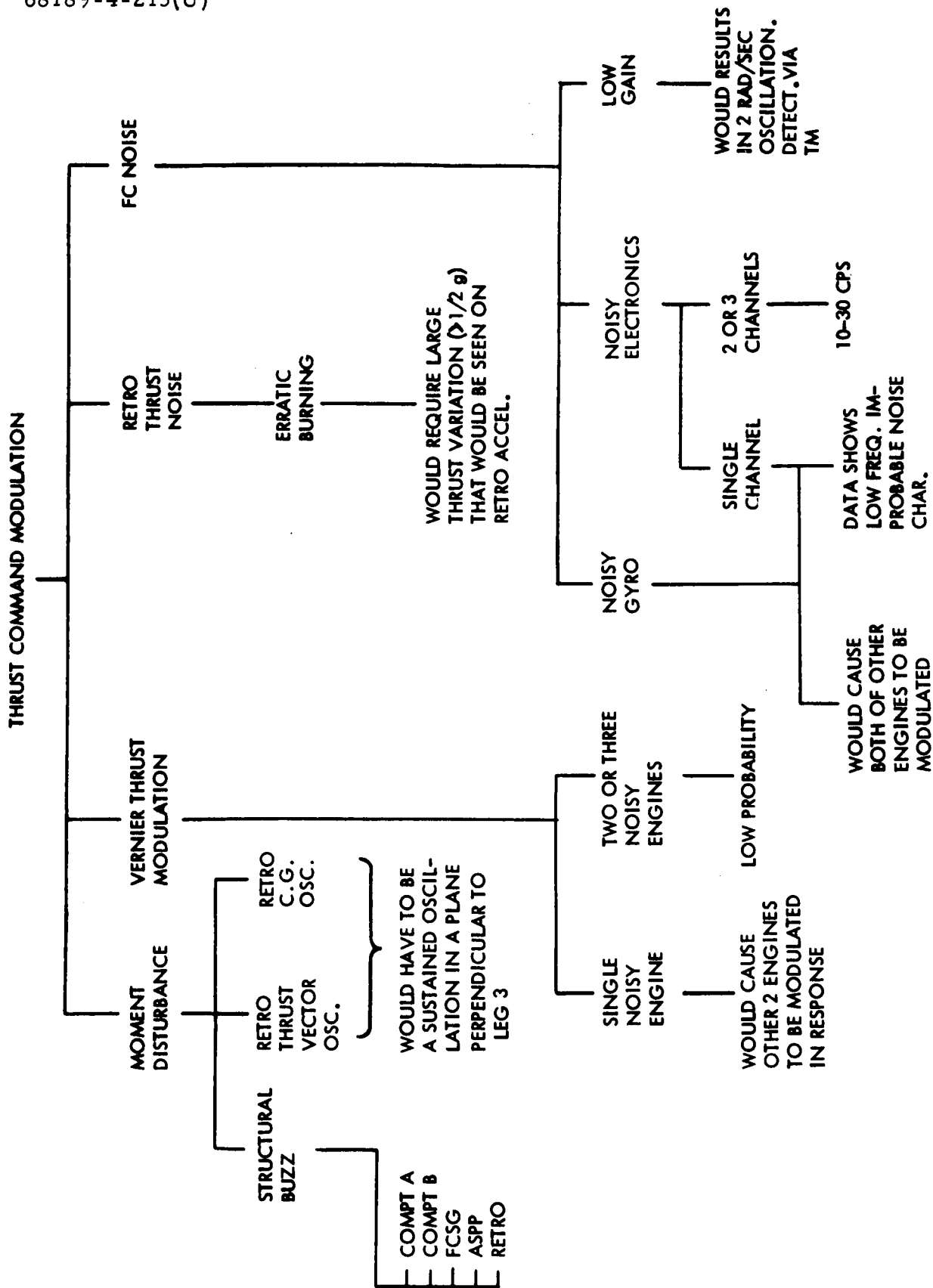
Figure 4-8. Thrust Command Modulation Tree
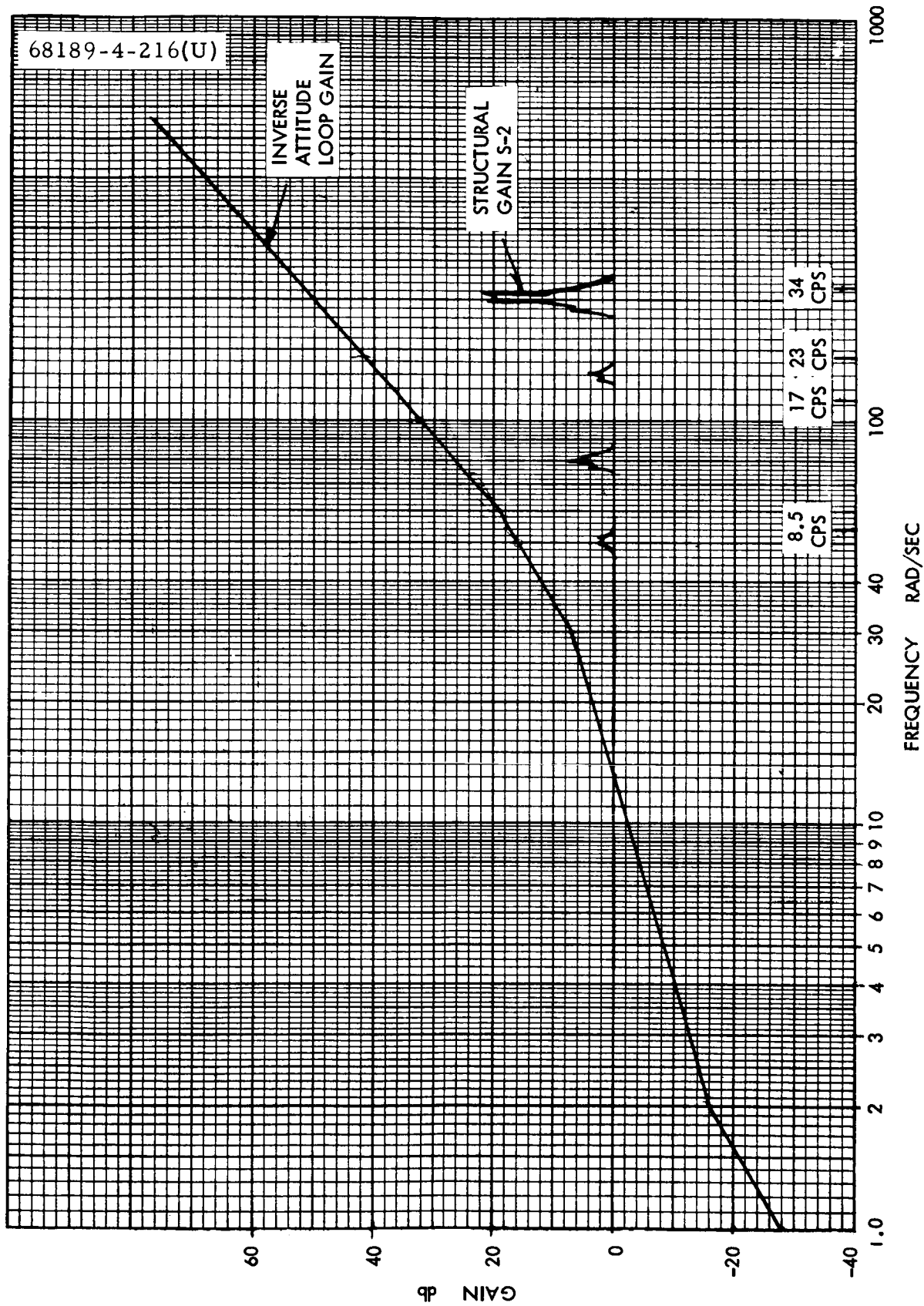
Figure 4-9. Structural Gain Necessary to Maintain Buzz in Attitude Loop

4-73

TABLE 4-28. FLIGHT CONTROL POSSIBLE FAILURE FORMAT

Item	Surveyor IV Signature	Remarks
Noisy gyro	No	Noisy pitch gyro affects engines 1 and 3; yaw affects 2 and 3.
Two noisy gyros	No	Noise would have to be correlated and out of phase.
Noisy electronics	No	Same as for gyros. In addition, low required noise (10 to 30 Hz) improbable.
Low system gain	No	Would result in ~ 2 rad/sec oscillation, readily detectable by telemetry.
Retro-erratic thrust	Low probability	Throttle command yaw data indicate large thrust variation would be required. This would result in detectable (> 1/2 g) change on retro accelerometer. If further analysis of thrust commands reduces moment disturbance, this would be a possible cause.
Noisy vernier engine	No	Would result in other two engines being modulated in response due to flight control sensor mixing; no known mechanism.
Two noisy engines	No	Very low probability; no known mechanism. Data on Surveyors I and III at midcourse and terminal and Surveyor IV at midcourse reveal no such performance characteristic.
Retro thrust vector oscillation Retro center of gravity oscillation	Low probability	Engine thrust command modulation is such as to require the retro thrust vector or center of gravity oscillation to be a sustained one in a plane perpendicular to leg 3.
Structural buzz	Possible	No problem thought to exist for normal spacecraft; could possibly be a problem for damaged structure or improperly installed units.

The frequency range of 15 to 25 Hz must involve the resonance of the flight control sensor group so that the gyro angles are possible. The elastic axis of the flight control sensor group for its low frequency resonance is parallel to the rotational axis assumed for the spacecraft with engine 3 showing the lowest throttling. This flight control sensor group resonance could combine with the retro resonance and provide sufficient gain for a buzz. The low frequency region, 5 to 11 Hz, would probably be an A/SPP resonance.

Analog Simulation of Telemetry Data. An analog simulation was constructed to aid in the buzz problem investigation. The pitch and yaw control loops, including the transfer functions for the three vernier engines, were mechanized on the analog computer. Sampling circuits were built, with the same sampling frequency and phase as the spacecraft, for thrust commands, gyro error, and strain gauge signals. The input to the system was a continuous sine wave disturbance torque into the pitch and yaw loops of the same polarity, resulting in out-of-phase thrust commands on engines 1 and 2 and a small thrust command on engine 3. This is the only way the long-term effect of low thrust on engine 3 could be produced.

The sampling circuit was a sample-hold circuit which sampled the real value in 0.001 second and held it for 0.3 second. The telemetry filters were included between the signal and the sampler.

The signal patterns produced are a function of the sampling phase and frequency. The patterns repeat every 3.33-Hz change in frequency and in the order that they appear in the Surveyor IV data for either an increasing or decreasing rate of change of frequency of 0.05 Hz/sec. The effect of sample phasing on the signals using gyro error signal levels that result in engine 1 and 2 thrust commands were on the order of the observed Surveyor IV levels. Even though the inputs to engines 1 and 2 are out of phase, there is an in-and-out of phase appearance to the signal output due to the sampling. The relationship between thrust commands and strain gauges could not be reproduced exactly. All the computer data were run for a nonelastic structure which makes the acceleration effect larger than the thrust command effects for high frequency. If there was a structural gain between the rigid body and the flight control sensor group, the proportion might be changed.

4.3.6.3   Retro Disturbances

The normal disturbance which the vernier engine system is required to balance in order to maintain attitude stability during the retro phase results from failure of the instantaneous retro thrust vector to pass through the vehicle center of gravity. The abnormal thrust modulation observed on the Surveyor IV vernier engine thrust command telemetry and the shape of the thrust command profile as compared to data from Surveyor I and III flights could result from this disturbance moment.

An analysis to determine the characteristics of the contributors required to produce the indicated disturbance, in the absence of structural buzz considerations, was conducted. The results of this analysis are discussed as follows.

The initial retro disturbance moment acting on the vehicle results from the initial alignment of the retro thrust vector to the vehicle center of gravity. Changes in this disturbance can result from one or a combination of the following: motion of vehicle center of gravity which can be produced by a shift in either retro or spacecraft center of gravity, angular motion or lateral shift of the retro thrust vector, or variation in magnitude of the retro thrust level when an offset between the thrust vector and vehicle center of gravity exists.

In order for thrust magnitude variations alone to produce the moment variations indicated by the Surveyor IV thrust command data, the magnitude of these variations would have to be greater than 3000 pounds. This value is obtained by observing that the average thrust levels are nearly equal, indicating a small average offset ($<$ 0.070 inch), and the thrust variations are sufficient to indicate a significant moment disturbance ($\sim$ 200 in-lb). Thrust level variations of this magnitude would produce substantial modulation in the output of the retro accelerometer and variation in the doppler data which were not indicated by the Surveyor IV data. Thus, retro thrust variations are not indicated as the cause of the vernier engine thrust modulations.

The magnitude of the variations of vehicle center of gravity which would be required to produce the indicated moment disturbance (0.02 inch) are not large enough to preclude this contributor as a cause of the indicated disturbance, although they would be larger than would be expected to occur in a normal flight. A shift in the vehicle center of gravity can be produced by movement of either the retro or the spacecraft (defined as vehicle less retro) center of gravity.

A retro center of gravity shift ($>$ 0.03 inch) would require physical motion of the retro since the retro propellant consumption rate ($\approx$ 32 lb/sec) and the size of the retro is not sufficient to produce the indicated frequency and magnitude of shift under unsymmetrical burning conditions. A spacecraft center of gravity shift of the same order of magnitude would require oscillation of a major component of the spacecraft (i.e., a compartment: 125 pounds shifting 0.3 inch).

Retro thrust motion (angle variations on lateral shift) on the order of three times that measured during retro qualification tests could produce the magnitude of disturbance indicated. What is considered improbable is that these variations would be restricted in direction so as to indicate an oscillatory moment about a constant axis rather than a pitch/yaw moment in a random direction.

Regarding the dc moment disturbance, analysis to date indicates that the data can be best fit by assuming a retro propellant center of gravity shift or a spacecraft minus retro center of gravity shift occurring sometime in the later half of the burn period.

4. 3. 7   Failure Investigation Preliminary Conclusions

Analysis of inflight spacecraft, Centaur, ground data, quality, troubles (TFRs), and test records has been unable to isolate any primary single or multiple cause for the failure of the Surveyor IV mission. Analysis completed to date and summarized in this report includes the following:

1) Complete point-by-point review of all telemetry channels from AMR mark to loss of RF signal

2) Review of all subsystem telemetry plots for midcourse and launch to acquisition phase

3) Review of real-time telemetry data commands and analysis performed by the Space Flight Operations Performance Analysis and Command and Trouble and Failure Analysis groups, which includes all coast phases of flight

4) Review of Centaur and spacecraft data for loads and vibration environment confirmation

5) Review of all Surveyor IV TFRs and quality records for those subsystems which could have lead to loss of RF signal

6) Analysis of ground station tape records

The only significant data anomaly that can be correlated by hypothesis to the final loss of RF signal is the apparent thrust (8 pounds peak to peak) modulation of vernier engines 1 and 2. This telemetry signature is classified as an anomaly or unexpected for Surveyor IV since cyclic thrust modulations of this magnitude were not observed during the Surveyor I and III flights and were not predicted from development model flight spacecraft testing. Without direct indication of the primary cause of failure, all failure modes that could cause RF signal loss within 0.25 millisecond and not disturb previous telemetry data must be considered equally likely.

Signatures obtained from transmitter and power system testing indicate that no reasonable power system short or open, and only a limited number of transmitter problems, such as inadvertent low power or RF transfer switch commands, can match the Mission D loss of signal signature.

All flight loads and vibration data indicate that the in-flight environment was significantly less severe than flight acceptance test levels and, therefore, structural failures are not likely.

Retro and vernier propulsion development, test, and flight hardware quality review indicate no design, manufacturing, or materials problems that lead to suspected tank or case rupture problems. All failure modes are considered unlikely but equally probable.

4.4 REFERENCES AND ACKNOWLEDGMENTS

The material in Section 4 was coordinated (and also originated or compiled) by R. H. Leuschner and W. McIntyre from these sources:

1) "SC-4 Preliminary Post Flight Data Analysis," Hughes Aircraft Company, 1 August 1967.

2) "Surveyor 4 Flight Path Analysis and Command Operations Report," Hughes Aircraft Company SSD 74108, 10 August 1967.

3) "Surveyor Mission D Space Flight Operations Report," Hughes Aircraft Company SSD 74109, August 1967.

Mention is also due L. K. Cooley for the reliability analysis in subsection 4.2

5.0   PERFORMANCE ANALYSIS

5.1   THERMAL CONTROL SUBSYSTEM

5.1.1   INTRODUCTION: SURVEYOR THERMAL CONTROL TECHNIQUES

The Surveyor thermal design utilizes a variety of temperature control techniques. Active, passive, and semiactive mechanisms are employed to provide the required temperature control (storage, operational, and/or survival) throughout the transit and lunar phases of the mission. Each spacecraft subsystem is individually controlled, and the thermal coupling between subsystems is minimized by using conduction and radiation isolation wherever advantageous. Subsystem analyses are accomplished by evaluating in detail the thermal environment for each subsystem, with consideration being given to all significant thermal interactions between the subsystems whenever a high degree of isolation is not possible.

The following temperature control techniques are used on the Surveyor spacecraft:

1)   Passive thermal control utilizing combinations of paints and metal processes to provide surfaces with solar absorptance and infrared emittance characteristics to produce the required subsystem temperatures. Solar energy reflections are used to provide energy in cases where insufficient direct solar illumination exists.

2)   Active thermal control systems utilizing heaters and radiation shields provide energy in cases where:

a)   Sufficient solar illumination is not available

b)   The unit's storage temperature is significantly different from its optimum operational temperature

3)   Subsystems having large heat capacities are thermally decoupled from the transit and lunar environments by utilizing superinsulation blankets to minimize radiative heat transfer and thermal isolators to minimize conductive heat transfer. Such systems never reach equilibrium conditions and therefore depend on heat capacity and a controlled rate of heat rejection to provide optimum operational temperatures.

4) Bimetallically activated thermal switches control the temperature of the electronics compartments during transit and lunar operations.

Combinations of the above techniques are used on many of the subsystems to optimize the temperature control system.

5.1.2 THERMAL ANOMALY: OXIDIZER TANK 1 (P-15)

During Mission D, the temperature of oxidizer tank 1 (sensor P-15) increased from 49° to 54° F at approximately Launch + 30 hours. An examination of the thermal data does not reveal similar temperature perturbations for oxidizer tanks 2 and 3 (sensors P-16 and P-6, respectively).

On all previous spacecraft (Surveyors I through III), the oxidizer tanks have exhibited small temperature perturbations during star acquisition and gyro drift checks. The temperature increase experienced by the Surveyor IV oxidizer tank 1 is greater than any previously observed. Although the excursion occurred during a gyro drift check, the other propellant tanks did not exhibit significant temperature perturbations. Thermal performance of the oxidizer tank before and after the temperature excursion appears normal. Thermal analysts are continuing to examine the tank data; however, it is doubtful at present if the cause of the 5° F increase in tank temperature can be determined. An examination of the propulsion data does not reveal any oxidizer system pressure perturbation at the time of the temperature increase.

5.1.3 SUMMARY AND CONCLUSIONS

The performance of the Surveyor IV thermal control system was excellent. The thermal behavior of all spacecraft subsystems was normal during the transit mission phase. Sixty-three of the 75 thermal sensors onboard the spacecraft were within 5° F of their nominal predicted value, and 70 thermal sensors were within 10° F of their nominal predicted value. The Canopus sensor, attitude gas jet 2, altitude marking radar (AMR) antenna and compartment A thermal switch 2 deviated 13°, 26°, 18°, and 17° F from predictions, respectively; all of these were still within their premission prediction range, however.

A summary of events significant to the thermal subsystem is given in Table 5.1-1. A summary of the actual and predicted transit steady-state temperatures for Missions A through D is presented in Table 5.1-2. Transit thermal profiles for all spacecraft subsystems are presented in Figures 5.1-1 through 5.1-76.

Only thermal performance that is unique or of special interest is discussed in detail. For those units whose temperature is consistent with previous missions, the steady-state temperature summary will be considered sufficient. The oxidizer tank (P-15) temperature increase anomaly is discussed

TABLE 5.1-1. SURVEYOR IV MISSION THERMAL EVENT LOG

Day	GMT, hr:min	Mission Time, hr:min	Event
195 7/14/67	11:53	00:00	Launch
	12:05	00:12	Injection
	12:06	00:13	Separation
	12:08	00:15	Sun acquisition complete
	12:34	00:41	Transmitter high power off
	13:42	01:49	Line 2 heater cycling
	14:00	02:07	SM/SS heater cycling
	17:46	05:53	Transmitter B high power on
	17:51	05:58	Sun and roll
	18:06	06:13	AMR heater cycling
	18:14	06:21	Transmitter B high power off
	18:46	06:53	Start gyro drift check
	20:54	09:01	Terminate gyro drift check
	20:57	09:04	Initiate gyro drift check
	22:37	10:44	Terminate gyro drift check
196 7/15/67	00:09	12:13	Start gyro drift check (all axes)
	02:09	14:13	Terminate gyro drift check
	02:18	14:25	Initiate roll drift check
	07:54	20:01	Terminate roll drift check
	08:02	20:09	Initiate gyro drift check
	09:58	22:05	End gyro drift check
	16:09	28:16	Start gyro drift check

Table 5.1-1 (continued)

Day	GMT, hr:min	Mission Time, hr:min	Event
196 7/15/67	19:42	31:49	End gyro drift check
	21:39	33:46	Roll drift check
	22:27	34:34	End roll drift check
197 7/16/67	02:02	38:09	Transmitter high power on
	02:18	38:25	Sun and roll (+72.5 degrees)
	02:23	38:30	Yaw (-64 degrees)
	02:27	38:34	SM/SS, AMR, VL2FT2, VL1OT2, VL3OT3, heaters off
	02:28	38:35	Thrust phase power on
	02:30	38:37	Midcourse
	02:30	38:37	Thrust phase power off
	02:31	38:38	All heaters enabled after midcourse
	02:37	38:44	Sun and roll
	02:40	38:46	Canopus lock
	02:46	38:53	Transmitter B high power off
	04:16	40:22	Initiate gyro drift check
	05:51	41:57	End gyro drift check
	08:08	44:14	High current mode on
	08:50	44:58	Initiate roll drift check and sun acquisition
	13:21	49:28	High current mode on
	14:36	50:44	End roll drift check
	14:37	50:45	Enable oxidizer tank 2 heater

Table 5. 1-1 (continued)

Day	GMT, hr:min	Mission Time, hr:min	Event
197 7/16/67	15:40	51:47	Initiate gyro drift check
	17:30	53:37	End gyro drift check
	21:08	57:16	TV − 3 electronics heater on
198 7/17/67	01:06	61:13	TV vidicon heater on
	01:09	61:16	Transmitter high power on
	01:24	61:31	Roll (+80. 9 degrees)
	01:27	61:34	End roll
	01:27	61:34	Yaw (+92. 7 degrees)
	01:32	61:39	End yaw
	01:35	61:41	Roll (-25 degrees)
	01:36	61:42	End roll
	01:56	62:03	VL2FT2, VL1OT2, VL3OT3, SM/SS, TV-VTC, TV-ETC, AMR heaters off
	01:57	62:03	AMR power on
	01:58	62:04	Thrust phase power on
	02:00	62:06	AMR enable
	02:01	62:07	Retro ignition

in detail in subsection 5. 1. 4. 5. Vernier Propulsion. Descriptive thermal performance analyses are presented for the various phases of the mission.

5. 1. 4   ANALYSIS OF TRANSIT THERMAL PERFORMANCE

5. 1. 4. 1   Prelaunch Phase

All prelaunch thermal constraints were satisfied. The various spacecraft component heaters were properly configured prior to launch:

Flight Sensor Location by Subsystem		Actual Steady-State Temperature, °F								Operation Allowable Limits
		Mission A Transit		Mission B Premidcourse		Mission C Transit		Mission D Transit		
		Actual	Predicted	Actual	Predicted	Actual	Predicted	Actual	Predicted	
Vehicle and mechanisms										
Compartment A										
Upper tray	V-15	70	78	74	73	49	49	58	59	140/0
Lower tray	V-16	93	98	94	94	70	72	77	79	125/0
Transmitter A	D-13	68	76	71	72	49	47	55	57	210/0
Transmitter B	D-14	68	78	73	73	48	48	58	58	210/0
Main battery	EP-8	97	98	99	99	69	75	75	80	125/40
Battery charge regulator	EP-34	123	125	118	120	94	100	99	104	185/0
Radiators										
No. 5	V-20	42	36	31	42	30	25	26	17	150/-300
No. 8	V-25	44	30	28	35	36	32	42	46	150/-300
No. 2	V-47	35	30	34	36	19	15	21	4	150/-300
Thermal shell inside	V-17	92	102	92	91	68	72	75	74	120/0
Thermal shell outside	V-18	-85	-110	-82	-90	-84	-90	-88	-89	
Thermal switch No. 5 inside	V-19	66	79	69	69	47	47	57	57	150/-300
Compartment B										
Upper tray	V-21	93	97	99	106	76	93	78	77	125/0
Lower tray	V-22	98	102	103	111	81	98	82	80	125/0
Boost regulator	EP-13	115	110	128	123	94	110	99	98	185/0
Radiators										
No. 4	V-24	67	75	70	77	55	67	55	52	150/-300
No. 1	V-45	73	71	84	91	61	74	63	59	150/-300
No. 5	V-46	66	71	70	78	56	72	53	51	150/-300
Thermal shell outside	V-23	-70	-78	-72	-65	-64	-70	-72	-69	125/0
Thermal switch No. 4 inside	V-26	88	93	93	101	74	88	73	72	
Wiring harness	V-29	88		91	94	72	88	75	75	125/0
Auxiliary battery	EP-26	35	60	64*	66	54	60	59	55	130/20
Auxiliary battery compartment	V-48	-2		9*	28	12	5	—	—	130/30
Landing gear assembly										
Leg 2	V-31	83	85	74	55	77	70	72	78	160/-140
Crushable block	V-44	-62	-50	-48	-51	-63	-60	-55	-60	160/-140
Shock absorber										
No. 1	V-30	84	90	76	84	74	84	79	80	125/-20
No. 2	V-32	72	88	73	82	76	72	77	72	125/-20
No. 3	V-33	82	90	82	84	79	84	75	80	125/-20
Antenna/solar panel positioner mechanism										
Solar panel drive	M-10	60	40	45	60	51	47	47	52	165/-225
Elevation axis drive	M-12	1	-86	-17	-8	-11	-7	-19	-10	165/-225
Solar cell array	EP-12	109	118	111	110	112	110	110	110	165/-200
Planar array	M-8	-50	-60	-50	-50	-50	-50	-50	-50	280/-280
A/SPP mast	V-34	-84	-114	-88	-86	-88	-86	-90	-86	160/-140
Spaceframe and substructure										
Upper spaceframe										
Near leg 1	V-27	60	73	53	65	57	56	53	55	160/-140
Near leg 2	V-35	-79	-70	-81	-75	-82	-81	-83	-82	160/-140
Lower spaceframe										
Under compartment B	V-28	48	46	42	50	43	45	39	40	160/-140
Under compartment A	V-36	-27	-21	-24	-24	-32	-25	-36	-30	160/-140

Table 5.1-2 (continued)

Flight Sensor Location by Subsystem		Actual Steady-State Temperature, °F								Operation Allowable Limits
		Mission A Transit		Mission B Premidcourse		Mission C Transit		Mission D Transit		
		Actual	Predicted	Actual	Predicted	Actual	Predicted	Actual	Predicted	
Retro attach points										
Leg 1	V-37	39	46	44	46	42	44	38	38	160/-140
Leg 2	V-38	-36	-21	-32	-24	-52	-50	-53	-55	160/-140
Leg 3	V-39	44	46	44	50	46	46	37	40	160/-140
Propulsion										
Vernier engine thrust chamber assembly										
No. 1	P-7	59	76	54	65	58	60	52	58	125/20
No. 2	P-10	72	81	84	80	81	85	82	76	140/20
No. 3	P-11	59	62	63	70	69	66	66	60	130/20
Propellant tanks										
Oxidizer 1	P-15	75/41†	74/45†	76/50††	49	76/41@	33@	42	42	100/0
Fuel 1	P-13	76/52†	73/48†	77/57††	58	76/55@	48@	56	52	100/0
Oxidizer 2	P-16	77/24†	79/35†	75/35††	38	75/18@	17@	20	22	100/15
Fuel 2	P-5	75/34†	74/30†	83/47††	44	74/33@	19@	36	39	100/15
Oxidizer 3	P-6	79/40†	73/45†	75/46††	50	77/30@	17@	45	40	100/15
Fuel 3	P-14	76/53†	73/51†	75/53††	57	76/52@	42@	51	53	100/0
Propellant lines										
Leg 1	P-8	23 to 29	35	18 to 28	18 to 28	30	19	39	30	100/0
Leg 2	P-4	21 to 26	20 to 27	20 to 27	20 to 27	19 to 22	19 to 24	19 to 24	18 to 26	100/0
Leg 3	P-9	21 to 26	30	20 to 27	20 to 27	19 to 24	19 to 24	19 to 24	18 to 26	100/0
Helium tank	P-17	60	75	72	75	73	75	76	69	100/100
Main retro										
Upper case	P-3	73/67†	74/67†	72/73††	72	73/64@	65@	66	65	70/40
Lower case	P-12	74/46†	74/36†	76/59††	60	78/41@	42@	45	43	70/25
Nozzle	P-22	-124	74/-222†	-118	-120	-130	-120	-127	-134	
Flight control										
Flight control electronics										
Chassis board 1	FC-44	90	100	90	100	71	65	66	65	165/0
Chassis board 6	FC-45	124	135	137	138	60	55	61	60	190/0
Canopus sensor	FC-47	78	90	85	89	74	75	77	65	130/-20
Roll gyro	FC-46	170**	178**	175**	177	173**	177	175	177	185/175
Pitch gyro	FC-54	175**	175**	175**	174	172**	173	175	174	185/170
Yaw gyro	FC-55	180**	177**	174**	177	172**	177	174	177	185/170
Roll actuator	FC-71	79	98	82	88	83	90	80	80	200/0
Nitrogen tank	FC-48	45	71	40	52	50	45	45	47	115/-10
Attitude gas jet	FC-70	88	87	86	77	105	90	94	120	160/-50
RADVS										
KPSM	R-8	12	22	11	15	17	20	18	15	100/-22
SDC	R-9	56	53	63	63	55	59	54	60	140/-18
VS preamplifier	R-10	22	32	14	11	16	13	15	18	112/-42
A/VS preamplifier	R-13	33	45	20	10	27	26	36	36	110/-20
Altitude marking radar										
Electronics	R-7	14 to 16	20 to 22	18	16	14 to 19	18 to 22	13 to 16	15 to 22	120/-5
Antenna dish	R-6	-12	0	-14	-12	3	-15	-5	0	135/-20
Edge of dish	R-27	-185	-160	-191	-185	-202	-180	-183	-200	200/-300
Television and SM/SS										
TV 3 mirror	TV-17	-120	-162	-120	-117	-120	-135	-126	-125	180/-50
TV 3 ECU	TV-16	-134	-150	-128	-123	-128	-134	-125	-125	150/-20
SM/SS structure	SS-13	—	—	—	—	—	—	-104	-98	TBD/0
Auxiliary electronics	SS12	—	—	—	—	-35	-5	-35	-35	158/-4

*Not at steady state.
**Corrected for bit rate error.
+Launch + 63 hours.

††Launch + 15 hours.
@Launch + 65 hours.

SM/SS heater	Enabled
Vernier line heaters	Enabled
AMR heater	Enabled
Survey TV electronics heater	Not enabled
Survey TV vidicon heater	Not enabled
Propellant tank heaters	Not enabled
Compartment A heater	Not enabled, and off
Compartment B heater	Not enabled, and off

5.1.4.2 Midcourse

Surveyor IV's thermal performance during midcourse was normal. All thermal control cyclic heaters were commanded off for approximately 5 minutes during this time. All thermostatically-controlled temperature units (vernier lines, tanks, AMR electronics, etc.) remained within their operational limits during the heater off period.

The vernier engines operated at a thrust level of approximately 78 pounds for 10.5 seconds during the midcourse correction maneuver. Thrust chamber assemblies 1, 2, and 3 reached peak temperatures of 386°, 282°, and 292°F, respectively. The peak temperature of 386°F exhibited by engine 1 is the maximum in-flight temperature recorded on any thrust chamber assembly to date.

The vernier oxidizer lines exhibited temperature increases during the midcourse burn. Propellant line temperature increases are the result of the warmer propellants (stored) flowing through the line past the temperature sensors. Vernier oxidizer line 1 exhibited a temperature increase of from 39° to 60°F. Vernier oxidizer lines 2 and 3, cycling during this period, exhibited temperature increases to 42° and 54°F, respectively. Vernier lines 2 and 3 cycled between 19° and 24°F.

The vernier propellant tank temperature sensors exhibited temperature increases during the midcourse maneuver. Oxidizer tank sensors exhibited peak temperatures of 65°, 43°, and 61°F for legs 1, 2, and 3, respectively. Tank temperatures prior to vernier thrusting were 48°, 26°, and 45°F at legs 1, 2 and 3, respectively. Tank temperature sensors are mounted on the exterior surface of the propellant standpipe fitting (base of the tank). Sensor temperature increases are attributed to propellant thermal stratification and to the flow of warmer propellants past the sensors.

Propellant fuel tanks also exhibited temperature increases. Fuel tanks 1, 2, and 3 temperatures increased to 61°, 42°, and 58°F, respectively. Initial fuel tank temperatures at legs 1, 2, and 3 were 57°, 38° and 51°F, respectively.

The retro nozzle, velocity sensor preamplifier, AMR antenna, crushable blocks, and roll actuator exhibited sizable temperature increases during the midcourse maneuver. The magnitudes of the temperature increases for these subsystems are illustrated in the mission plots.

5.1.4.3 Coast Phases

Performances of the heater controls and heater duty cycles were normal. The first heater cycling was observed on vernier line 2 at Launch + 1 hour 50 minutes. The AMR heater cycled on at Launch + 6 hours. Duty cycle calculations and temperature cycling ranges for vernier line 2 and the AMR are presented in Table 5.1-3.

The soil sampler electronics heater apparently cycled on at Launch + 2 hours 7 minutes, when the electronics temperature (SS-12) dropped to 4°F. The duty cycle remained at 100 percent throughout the remainder of the mission (except when turned off at midcourse and terminal descent), and the electronics temperature (SS-12) continued to decrease to an equilibrium temperature of -35°F.

Vernier line 3 cycled on at Launch + 52 1/2 hours and, based on two cycles, its duty cycle was calculated as 7.1 percent.

Oxidizer tank 2 heater control was enabled at Launch + 50 hours 44 minutes, at which time its temperature (P-16) was 24°F. The heater did not cycle on, and the tank temperature dropped to 19°F at terminal descent. However, this heater normally cycles on at 18°F (per solar thermal vacuum test data), so that observed performance was proper.

The gyro heater duty cycles were measured as 30.6, 19.3, and 19.4 percent for the pitch, roll, and yaw gyros, respectively.

The survey camera mirror assembly and electronics heater were enabled at Launch + 57 hours. Both the electronics and the mirror assembly temperatures increased as predicted. The electronics temperature (TV-16) reached -5°F 1 hour before retro ignition. The vidicon heater was enabled at that time since the constraint that TV-16 be greater than -20°F before commanding vidicon thermal control on was satisfied.

High current mode was initiated at Launch + 44 hours, and the auxiliary battery temperature (EP-26) increased from 59° to 79°F by retro ignition. Both the main and auxiliary batteries were at the same temperature at retro ignition, thus enhancing electrical load sharing.

5.1.4.4 Terminal Phase (to Loss of Data)

Spacecraft thermal response during terminal descent appeared nominal. The spacecraft Z-axis was off the sun for approximately 33 minutes and 7 seconds prior to loss of spacecraft signal. All spacecraft temperature monitored during terminal maneuvers and descent were well within operational limits. The retro-rocket bulk temperature was 55.3°F at retro ignition.

TABLE 5.1-3. HEATER PERFORMANCE

Heater	Mission Time	Duty Cycle, percent	Cycling Range, °F
Vernier line 2	Launch + 19.5 hours	24.7	19 to 24
	Launch + 28 hours	30.3	19 to 24
	Launch + 54 hours	31.7	19 to 24
AMR	Launch + 8.5 hours	55.3	13 to 16
	Launch + 28 hours	63.4	13 to 16
	Launch + 58 hours	64.1	13 to 16

Propulsion system temperatures showed that engine 1 was running considerably hotter (approximately 38 percent) than engines 2 and 3 during the observed period of terminal thrusting. This effect was also noted during midcourse. The temperature decrease observed on engine 2 immediately after thrusting is attributable to the initial flow of cool propellants through the engine.

5.1.4.5 Subsystem Thermal Analyses

Compartments A and B

Thermal performance of compartments A and B agreed well with predictions for Mission D during steady-state operations. It was noted that the transient response early in the mission was slightly different than predicted for compartment A since it reached equilibrium conditions earlier than expected. No definite reason has been cited for this small deviation.

Thermal switch radiator temperatures fluctuated on compartment A throughout the mission due to gyro drift checks. This fluctuation is typical during pitch gyro drift checks since the solar panel shadow line crosses the compartment A radiators. Pitch gyro drift constituted the largest fluctuation during the mission D; consequently, the radiator temperature fluctuations were greater than for previous missions.

The thermal response of some key elements in compartments A and B during high-power transmitter operations is shown in Table 5.1-4. Each of the four high-power transmitter operations was performed using transmitter B. The thermal performance of the compartment system during high-power transmitter operation was as expected.

TABLE 5.1-4. COMPARTMENT THERMAL RESPONSE TO HIGH-POWER TRANSMITTER OPERATION (°F)

| Subsystem and Sensor | Acquisition, 28 minutes 4 seconds | | | Canopus Search, 34 minutes 1 second | | | Midcourse, 43 minutes 26 seconds | | | Terminal Descent, 66 minutes 46 seconds* | | |
| | Peak Temperature | Temperature Rise | | Peak Temperature | Temperature Rise | | Peak Temperature | Temperature Rise | | Peak Temperature Observed | Temperature Rise | |
		Predicted	Actual		Predicted	Actual		Predicted	Actual		Predicted	Actual
Compartment A												
D-13	85	2	0	67	12	9	68	15	13	67	19	10
D-14	125	55	40	107	49	47	107	50	50	107	57	49
EP-8	86	9	7	84	7	0	82	7	5	80	4	3
EP-34	108		23	105	7	2	103	7	5	92	—	-8
V-15	102	25	17	85	30	24	86	35	28	84	30	25
V-16	87	8	5	83	5	2	81	5	5	79	4	1
Compartment B												
EP-13	216	17	13	117	19	17	117	20	20	120	21	17
V-21	93	5	-2	83	4	3	82	6	5	82	3	3
V-22	90	2	3	86	3	2	84	4	3	85	2	2

*Data taken at last date frame and compared with prediction at same time interval of high power.

Vernier Propulsion Subsystem

The effects of maneuvers, midcourse thrusting, and terminal thrusting on propulsion system temperatures are presented in Table 5.1-5. The highest vernier temperature of 386°F resulting from midcourse thrusting was recorded on vernier engine 1 (P-7). The temperature increase observed on this engine was approximately 52 percent greater than noted on engines 2 and 3. However, engine 1 was observed to run characteristically hot in preflight tests due to unit-to-unit variations. Vernier line temperatures increased during midcourse to within 1° to 6°F of their related propellant tank post-thrusting temperatures.

Vernier engine thermal performance was as expected during the transit mission phase. Predicted temperatures for thrust chamber assemblies 1, 2, and 3 were 57°, 76°, and 60°F, respectively. Thrust chamber assemblies 1, 2, and 3 reached steady-state equilibrium temperatures of 50°, 80°, and 66°F, respectively (see Figures 5.1-23, 5.1-26, and 5.1-27).

Thermal performance of the helium pressurization bottle was as expected. Thermal data indicate that the helium tank (temperature sensor P-17) reached a steady-state equilibrium temperature of 76°F during coast phase 1 versus a prediction of 68°F (see Figure 5.1-32). The helium tank thermal sensor exhibited approximately a 2°F increase in temperature during the mission. This increase is attributable to thermal finish (HP4-135, inorganic white paint) degradation; similar temperature increases were observed on Surveyors I through III.

TABLE 5.1-5. PROPULSION SYSTEM TEMPERATURE RESPONSE FROM THRUSTING

	Line			Engine			Oxidizer Tank 1 (P-15)	Fuel Tank 1 (P-13)	Oxidizer Tank 2 (P-16)	Fuel Tank 2 (P-5)	Oxidizer Tank 3 (P-6)	Fuel Tank 3 (P-14)
	1 (P-8)	2 (P-4)	3 (P-9)	1 (P-7)	2 (P-10)	3 (P-11)	1 (P-15)	1 (P-13)	2 (P-16)	2 (P-5)	3 (P-6)	3 (P-14)
Before midcourse yaw, °F	39	22	20	50	80	66	48	57	28	39	46	51
Before midcourse thrusting, °F	39	20	22	57	70	71	48	57	28	39	46	51
After midcourse thrusting, °F	60	42	54	386	281	292	61	61	44	46	60	58
Temperature increase, °F	21	22	32	329	211	221	13	4	16	7	14	7
Before terminal yaw, °F	38	23	23	52	82	67	42	56	18	33	42	51
Before terminal thrusting, °F	38	25	23	52	97	55						
Last data observed, °F	60	40	58	179	127	134						
Premidcourse decrease rate, °F/hr							0.34	0.10	0.40	0.30	0.30	0.16
Postmidcourse decrease rate, °F/hr							0.16	0.07	0.30	0.25	0.25	0.08

Thermal performance of the vernier propulsion propellant tanks was normal during the transit phase. However, oxidizer tank 1 (P-15) exhibited a 5°F increase at approximately L + 31 hours. Oxidizer tanks have shown small temperature perturbations (always increases) during attitude maneuvers on all previous spacecraft. The significance of the temperature increase is that its magnitude is larger than on previous spacecraft, while oxidizer tanks 2 and 3 did not exhibit similar temperature responses. Thermal behavior of oxidizer tank 1 sensor prior and subsequent to the temperature surge was normal. This phenomenon is discussed in subsection 5.1.2.

Propellant temperature stratification was observed on this flight as in all previous flights. However, temperature gradients within the propellants were greatly negated due to the propellant motion induced during thrusting. This results in temperature sensor readings which more accurately reflect bulk propellant temperatures. Thus, the rate of propellant tank temperature decrease is correspondingly reduced during coast phase 2. Premidcourse and postmidcourse decrease rates are shown in Table 5.1-5.

Transit temperature profiles are presented in Figures 5.1-22, 5.1-30, and 5.1-31 for oxidizer tanks 3 (P-6), 1 (P-15), and 2 (P-16), respectively. Transit temperature responses shown in Figures 5.1-21, 5.1-28, and 5.1-29 for vernier fuel tanks 2 (P-5), 1 (P-13), and 3 (P-14), respectively.

Thermal performance of the vernier propulsion propellant lines was as predicted. Oxidizer lines 2 (P-4) and 3 (P-9) cycled as expected, while oxidizer line 1 exhibited a steady-state temperature of 39°F, 9F° above the nominal prediction.

Flight Control Sensor Group (FCSG)

Transit thermal behavior of the flight control sensor group was as expected. Preflight predictions indicated FCSG steady-state temperatures of 65° and 60°F. Actual FCSG steady-state temperatures were 66° and 61°F for flight control electronics chassis boards 1 and 6, respectively.

Nitrogen Tank

Transit thermal performance of the nitrogen gas tank was as expected. The predicted temperature for the tank was 47°F, and the actual flight steady-state temperature was 45°F.

Nitrogen tank temperatures fluctuated between 41° and 46°F during the gyro drift checks. The nitrogen tank is affected during pitch gyro drift checks. The tank transit temperature profile is presented in Figure 5.1-12.

Auxiliary Battery

During the mission the auxiliary battery temperature ran 5°F lower than the nominal prediction of 60°F, but within the ±15°F predictability range. The auxiliary battery warmup (auxiliary battery mode/high current mode) began approximately 6 hours prior to the predicted warmup time. The warmup trend was identical to that of Surveyor III.

Main battery and auxiliary battery temperatures were within 2°F of each other at the time RADVS was activated. This is desirable since it provides optimum load sharing between the two batteries.

Antenna/Solar Panel Positioner

The solar intensities during Surveyors I, III, and IV were, respectively, 431, 441, and 429 Btu/hr-ft². Since solar intensity differed for the various spacecraft, the effect of solar intensity on spacecraft component temperatures was studied. The solar panel temperature was chosen on the basis of its sensitivity to solar intensity. The solar panel temperatures for Surveyors I and IV are approximately the same since the solar intensities were also nearly equal. Surveyor III's solar panel temperature is higher by about 2°F as compared to the other spacecraft, which correlates properly with its higher solar intensity. Analytically, the temperature difference of the solar panel for various spacecraft may be approximated by assuming that the solar panel can be simulated by a flat plate radiating to space and receiving solar intensity. By utilizing the flat

plate method, the temperature difference for a solar intensity between 442 and 428 Btu/hr-ft^2 is 4°F (see Figure 5.1-75).

Comparing actual solar panel temperature with the analytical results indicates that the flight solar panel temperature between Surveyor I and III is about 2°F lower than predicted. This discrepancy between actual and analytical results may be attributed to spacecraft interactions which are not completely simulated in the model. From the above discussion, it can be concluded that variation in solar intensity does affect the solar panel temperature, but not in a significant amount.

5.1.5 REFERENCE

Material in this section was generally prepared in parallel for, or abstracted from the following source:

"Surveyor Mission D Space Flight Operation Report," Hughes Aircraft Company, SSD 74109, August 1967.

5.1.6 ACKNOWLEDGMENT

This section was coordinated by Jerry Lewis of the Surveyor Thermal Control Section.
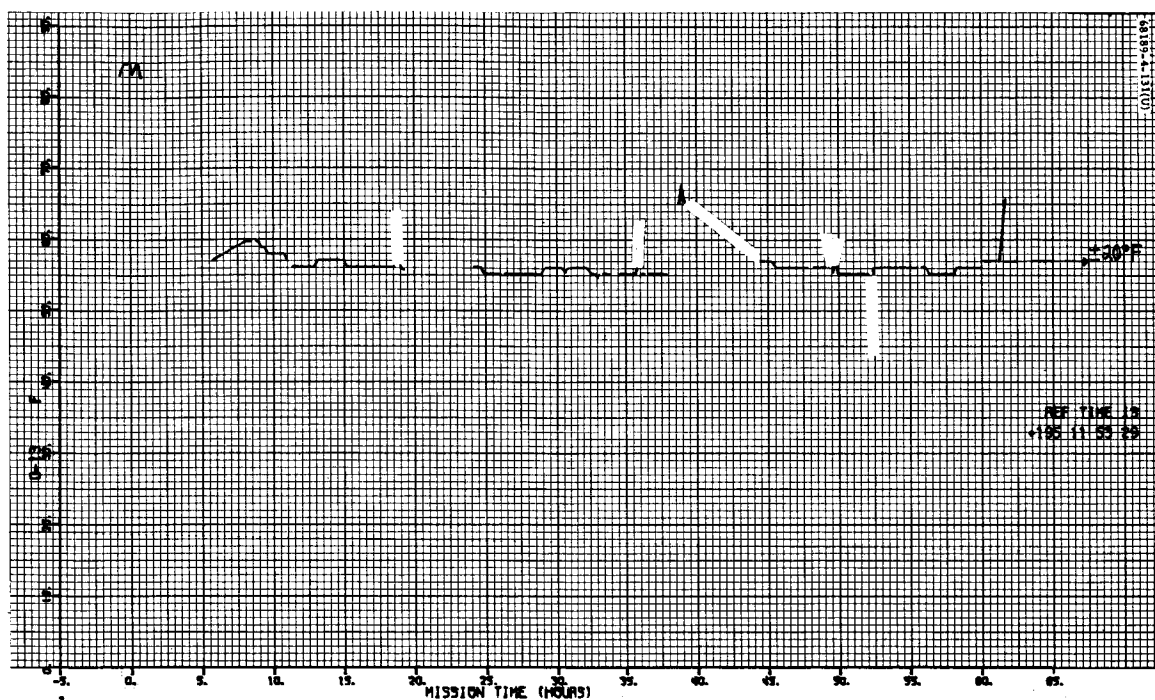
Figure 5.1-1.   Transmitter A Temperature
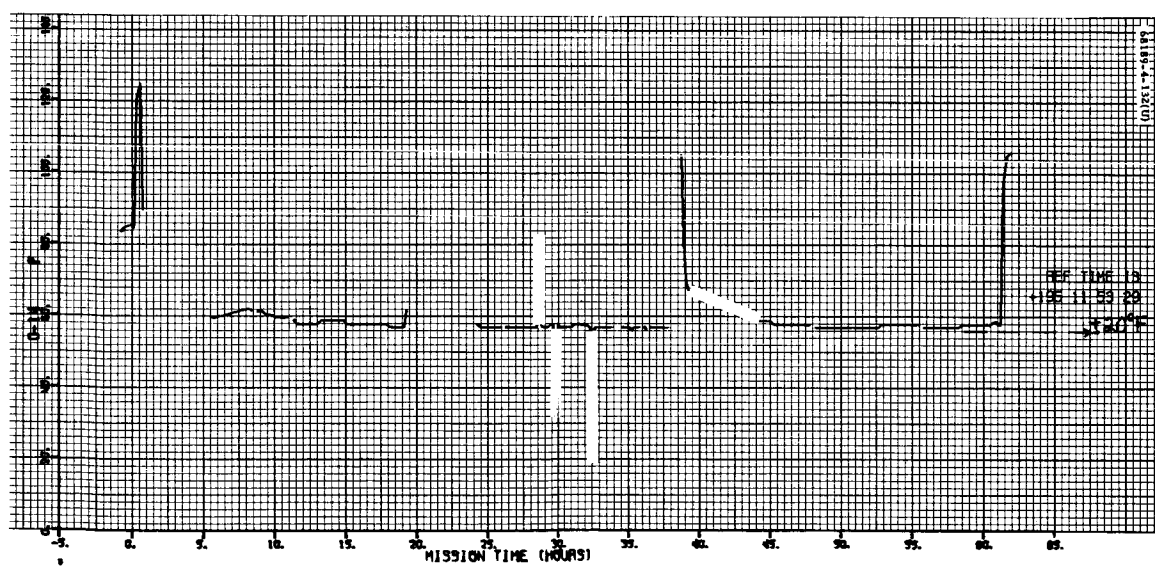
Figure 5.1-2.   Transmitter B Temperature

MISSION TIME (HOURS)
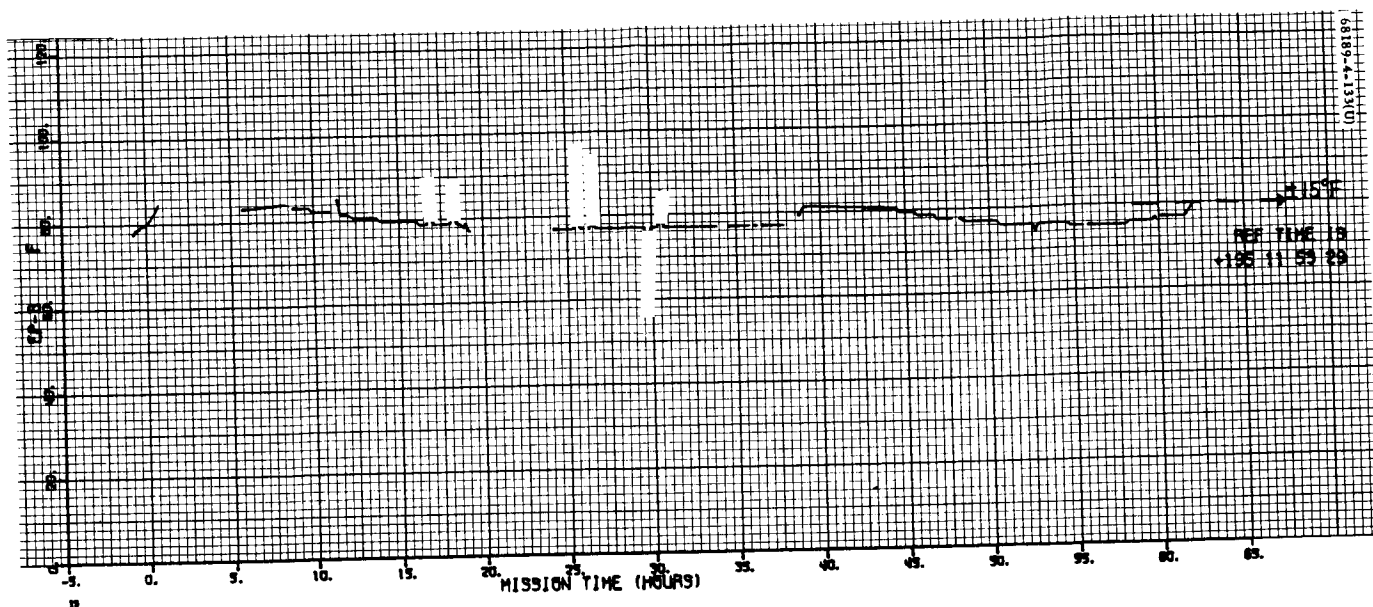
Figure 5.1-3.   Main Battery Temperature

MISSION TIME (HOURS)
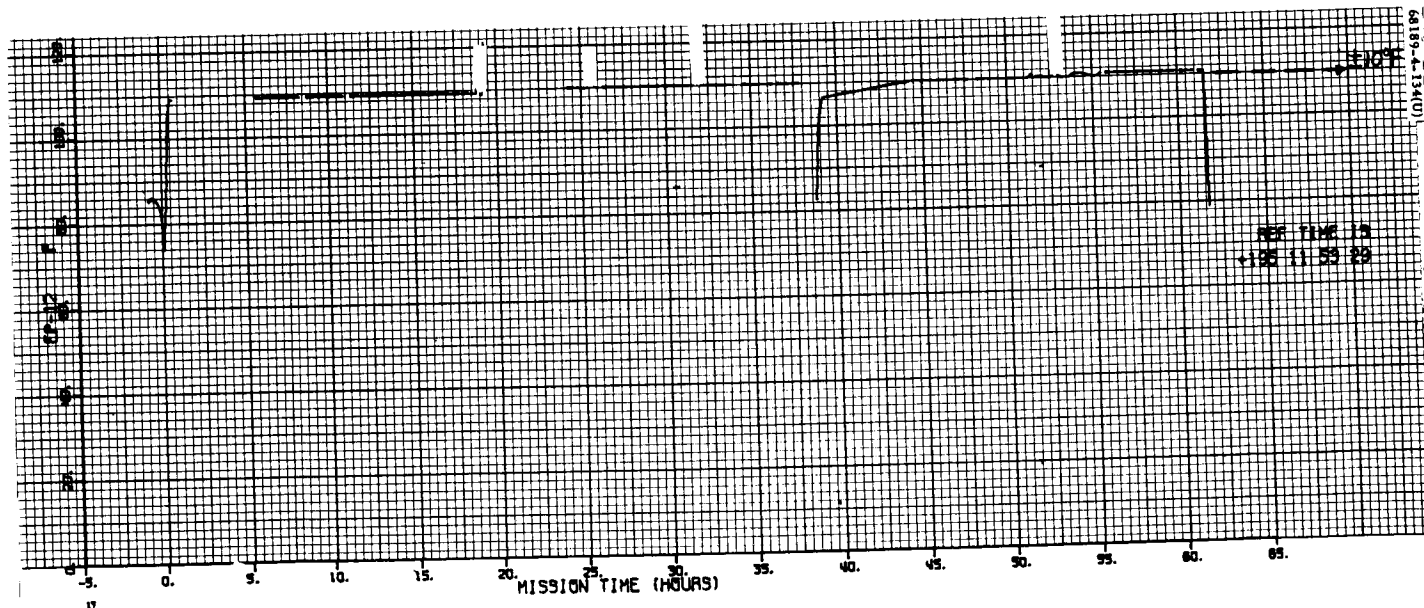
Figure 5.1-4.   Solar Cell Array Temperature
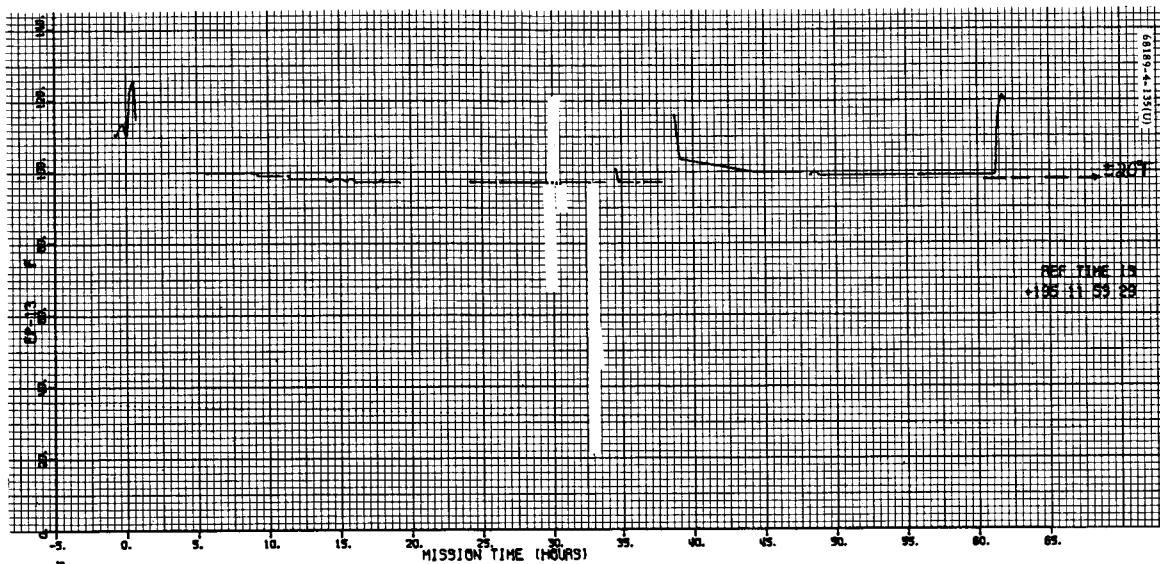
Figure 5.1-5. Boost Regulator Temperature
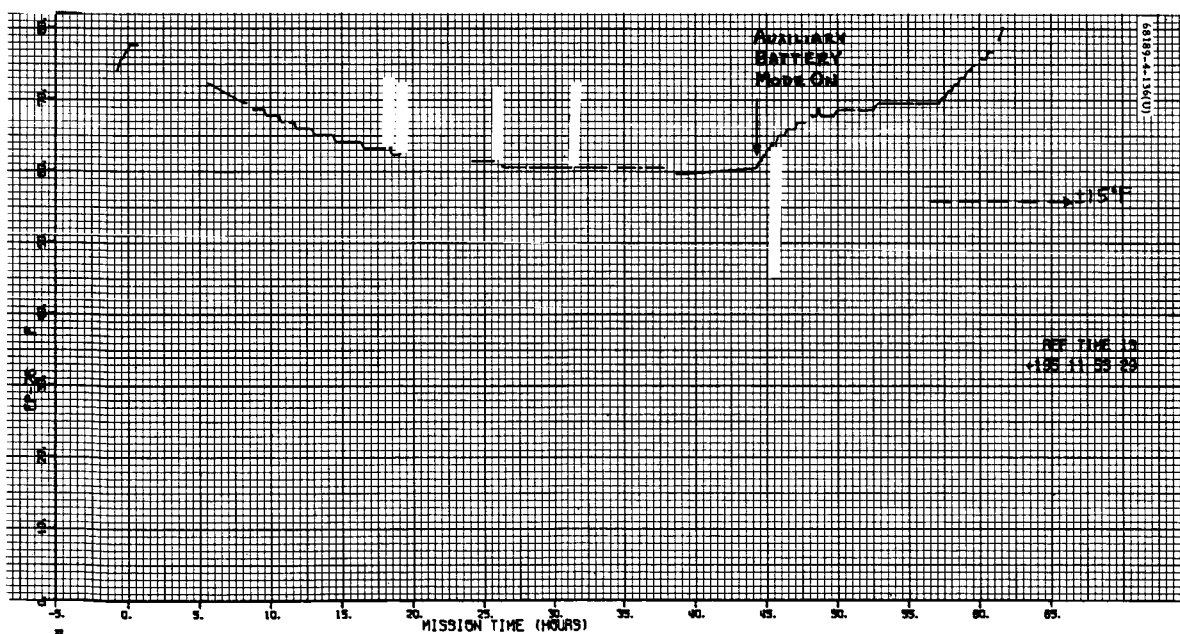
Figure 5.1-6. Auxiliary Battery Temperature
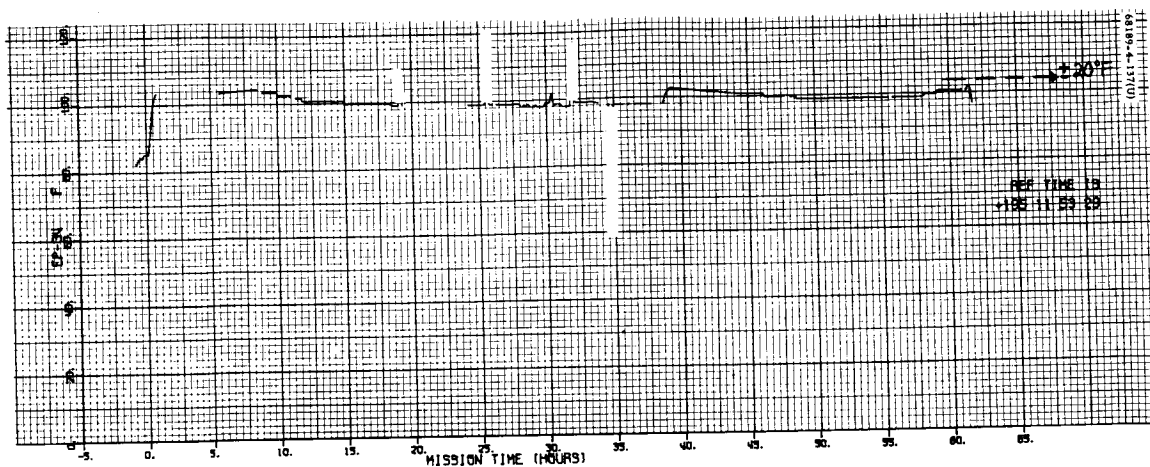
Figure 5.1-7.   Battery Charge Regulator Temperature

Figure 5.1-8.   Flight Control Electronics Temperature 1
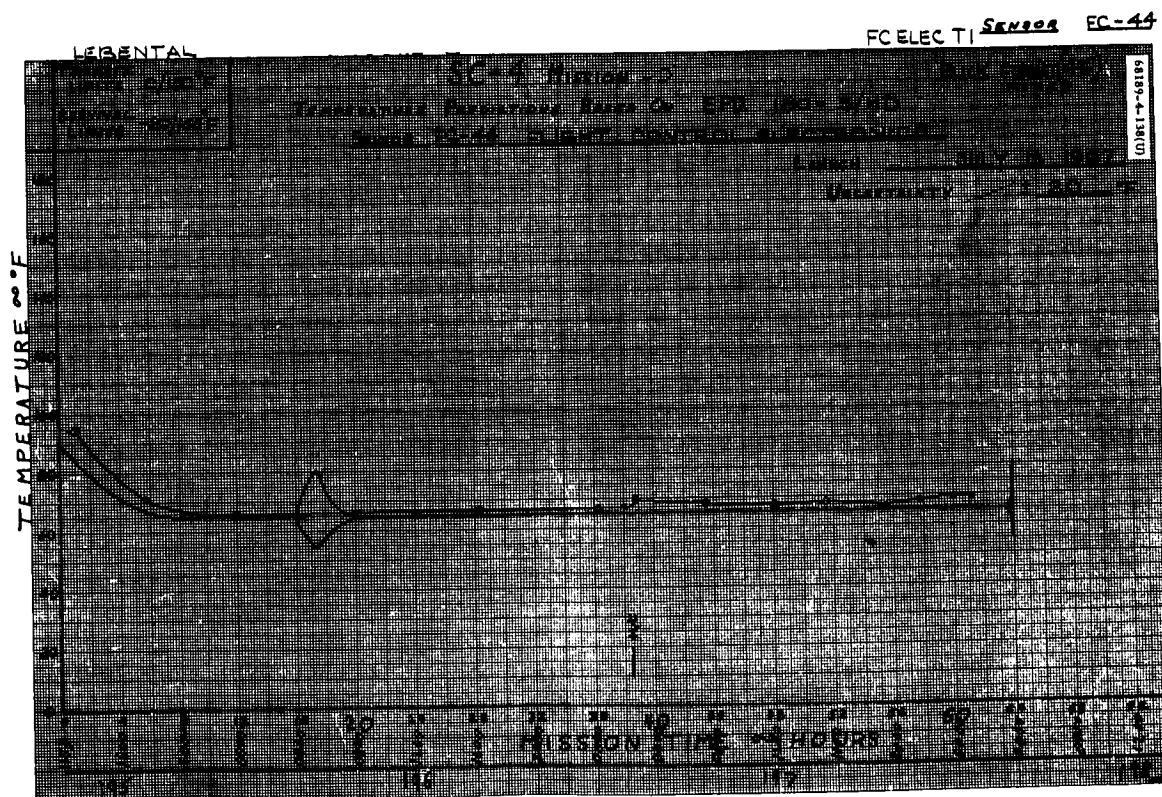
Figure 5.1-9.   Flight Control Electronics Temperature 2
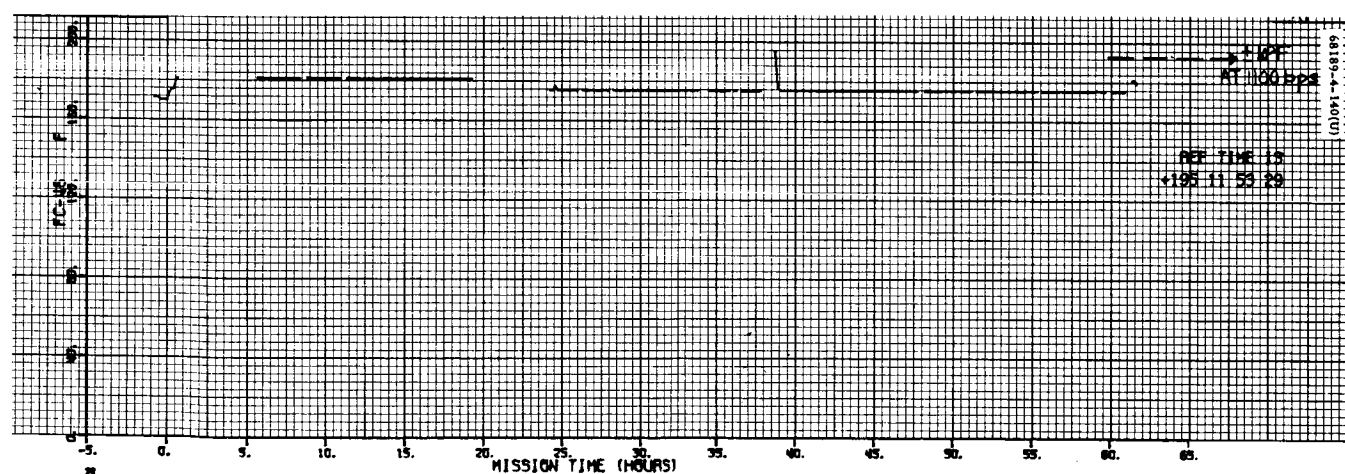
Figure 5.1-10.   Roll Gyro Temperature
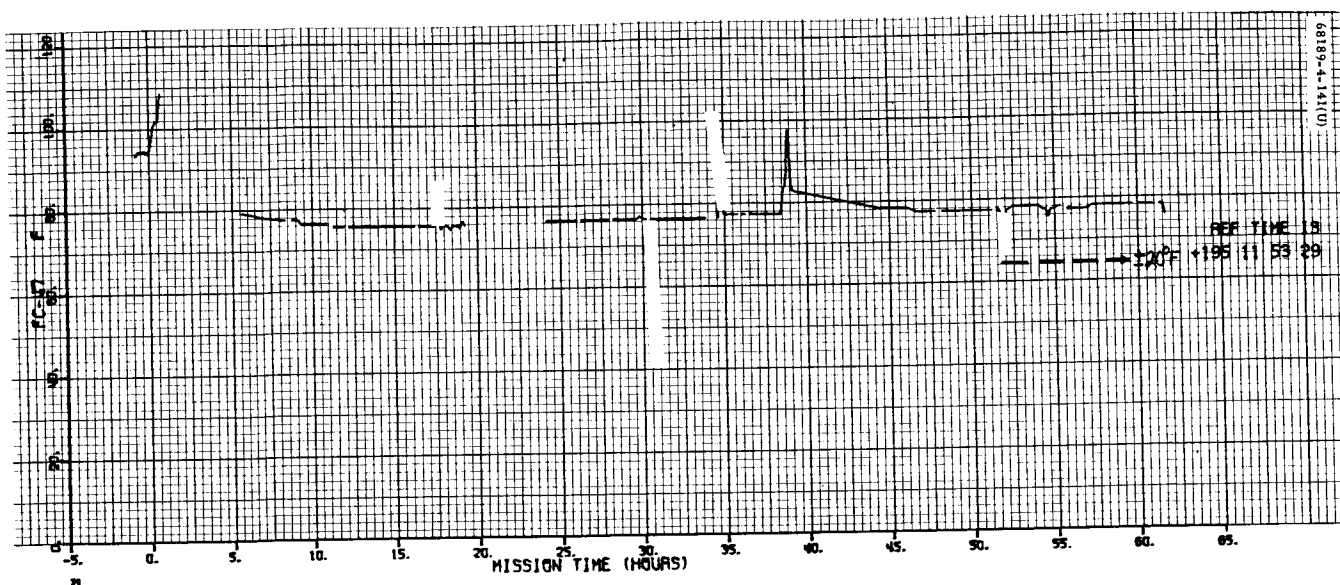
Figure 5.1-11.   Canopus Sensor Temperature

Figure 5.1-12.   Nitrogen Gas Tank Temperature
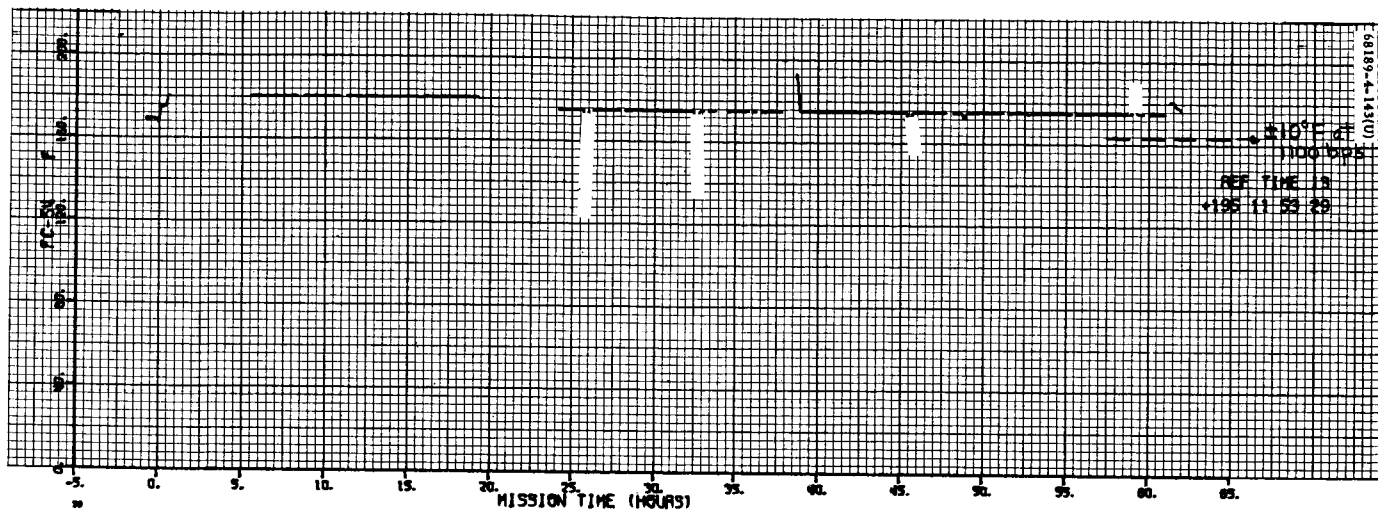
Figure 5. 1-13.   Pitch Gyro Temperature
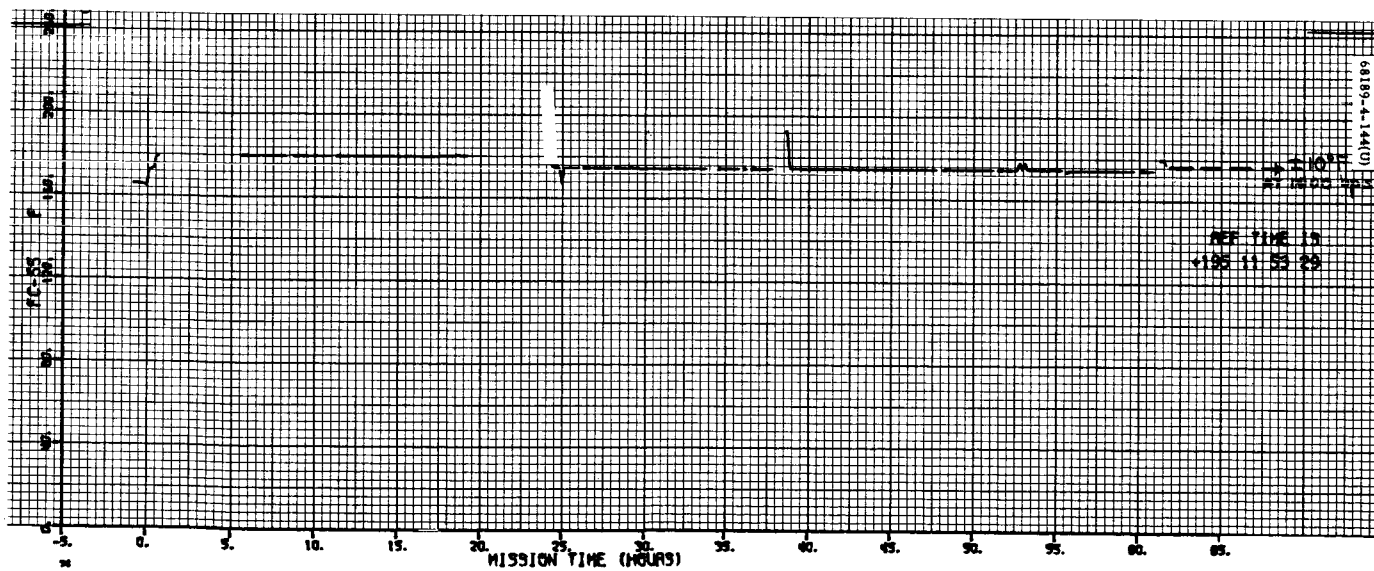
Figure 5. 1-14.   Yaw Gyro Temperature
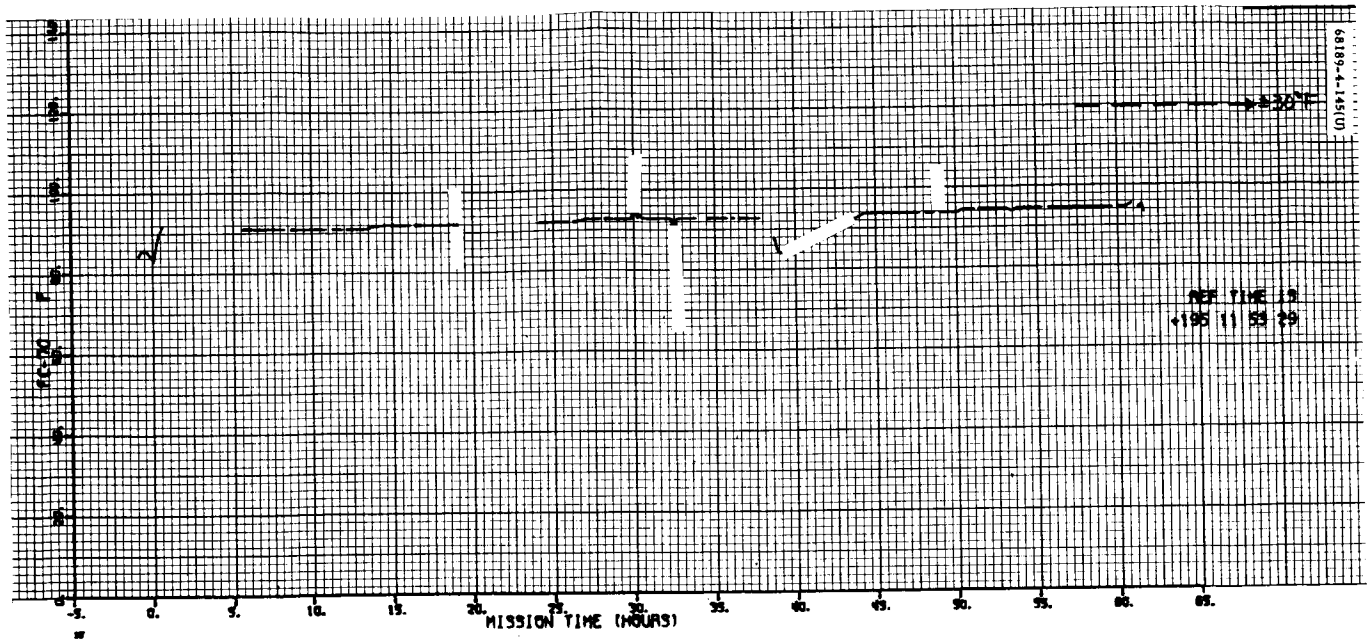
Figure 5.1-15.   Attitude Gas Jet 2 Temperature
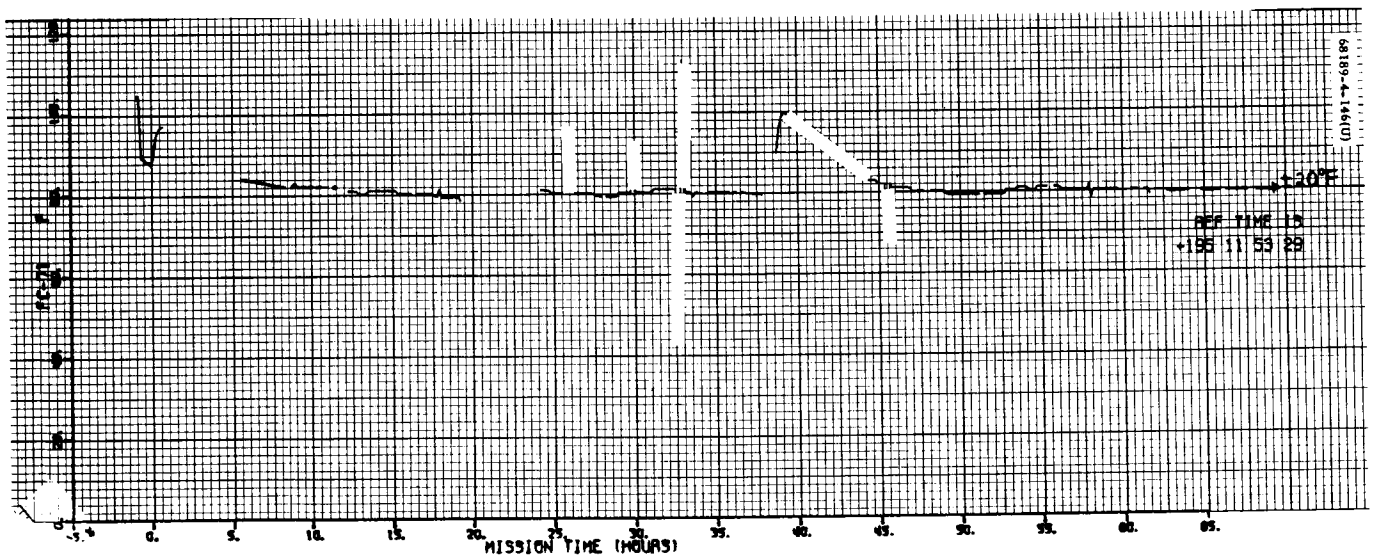
Figure 5.1-16.   Roll Actuator Temperature
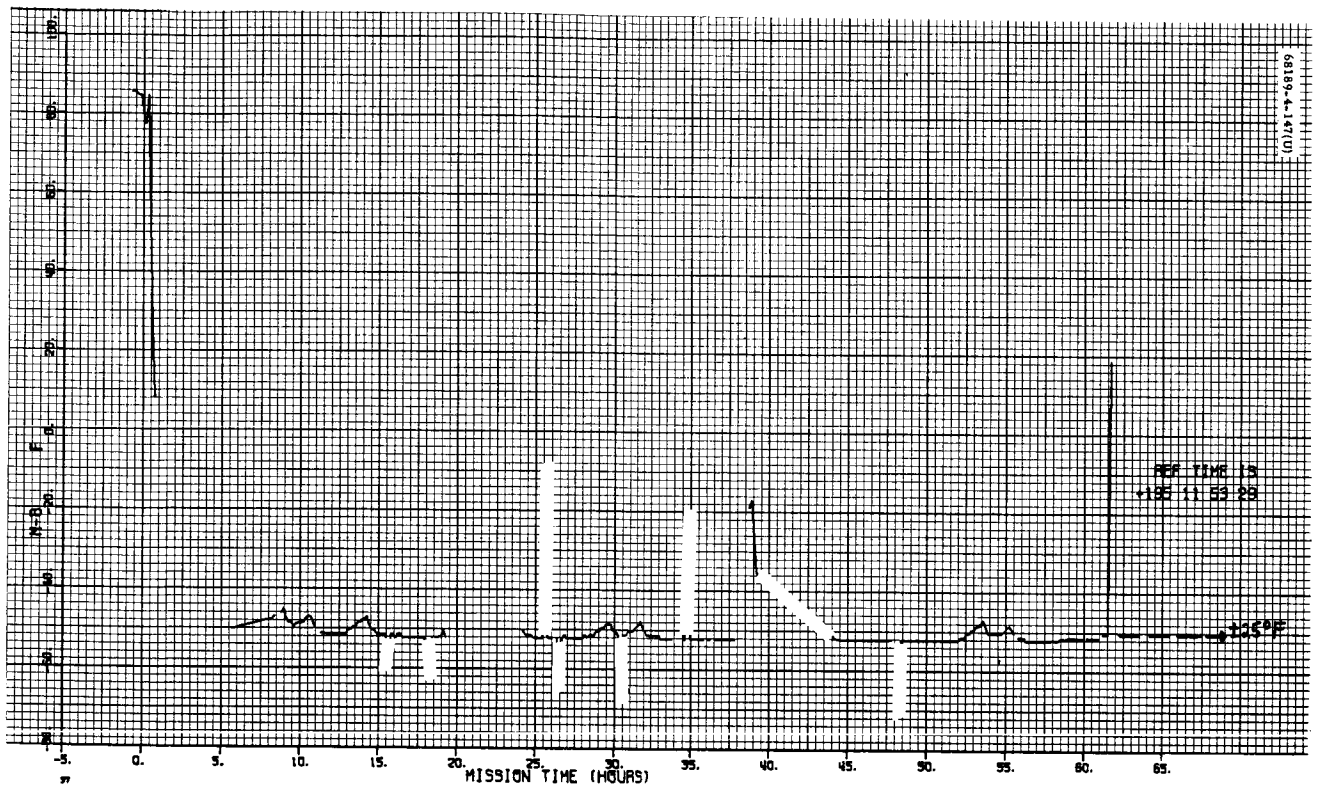
Figure 5.1-17.   Planar Array Temperature
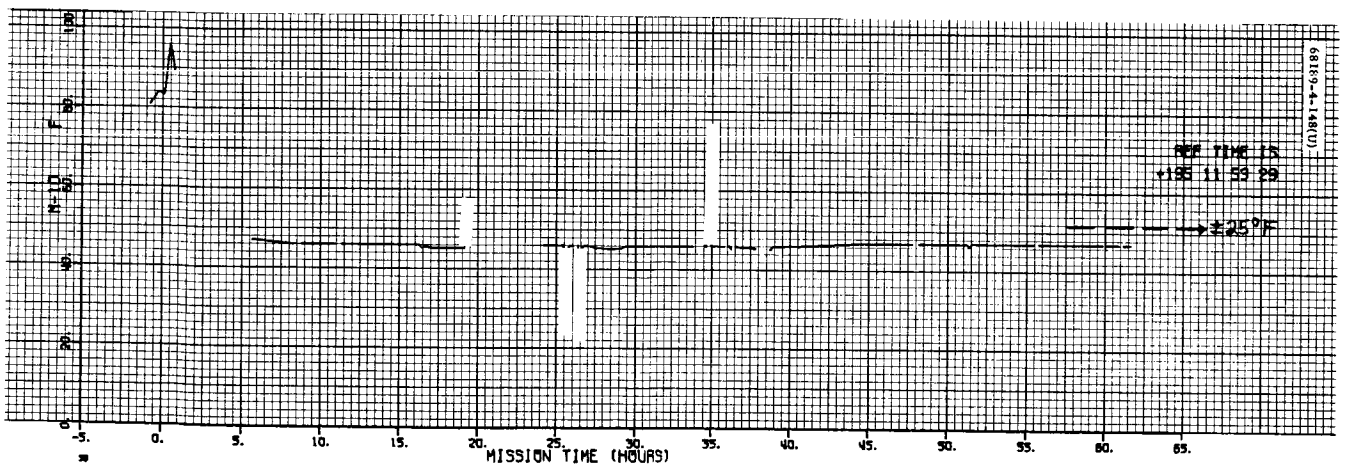
Figure 5.1-18.   Solar Axis Stepping Motor Temperature
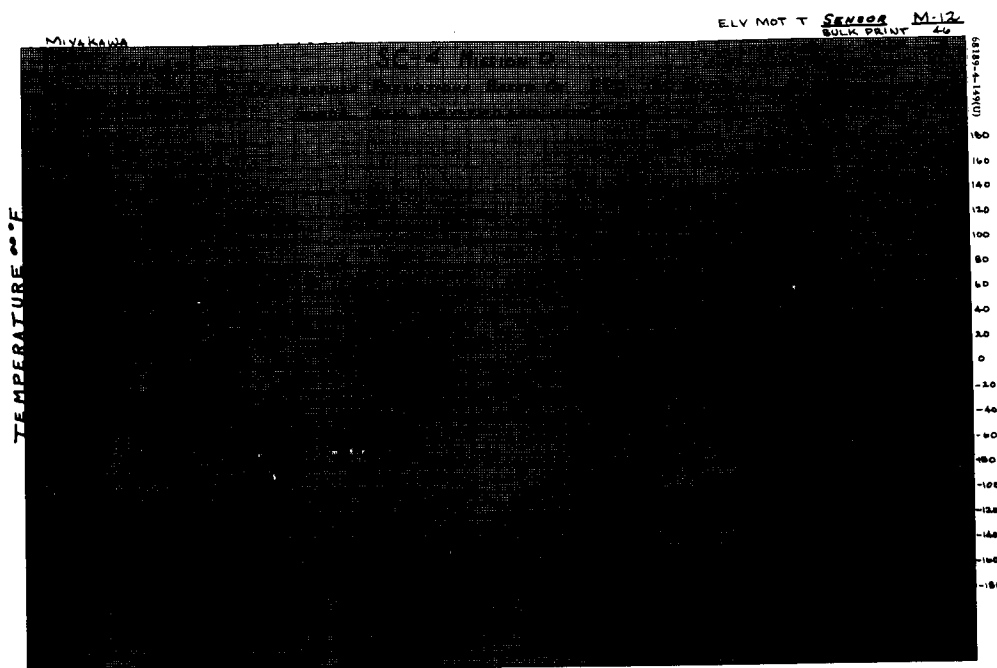
Figure 5.1-19.   Elevation Axis Stepping Motor Temperature
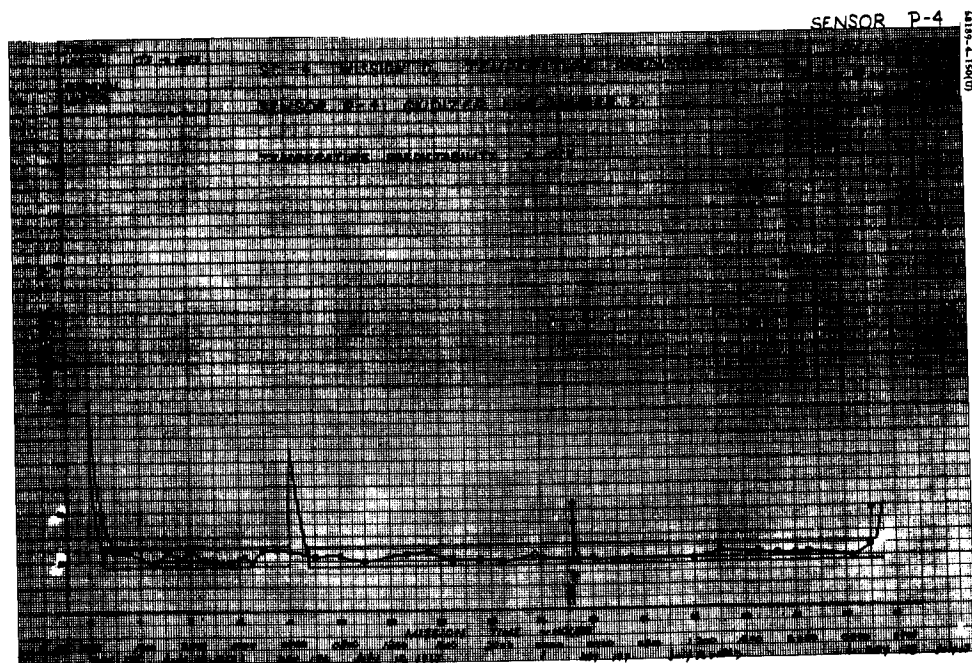
Figure 5.1-20.   Vernier Line 2 Temperature
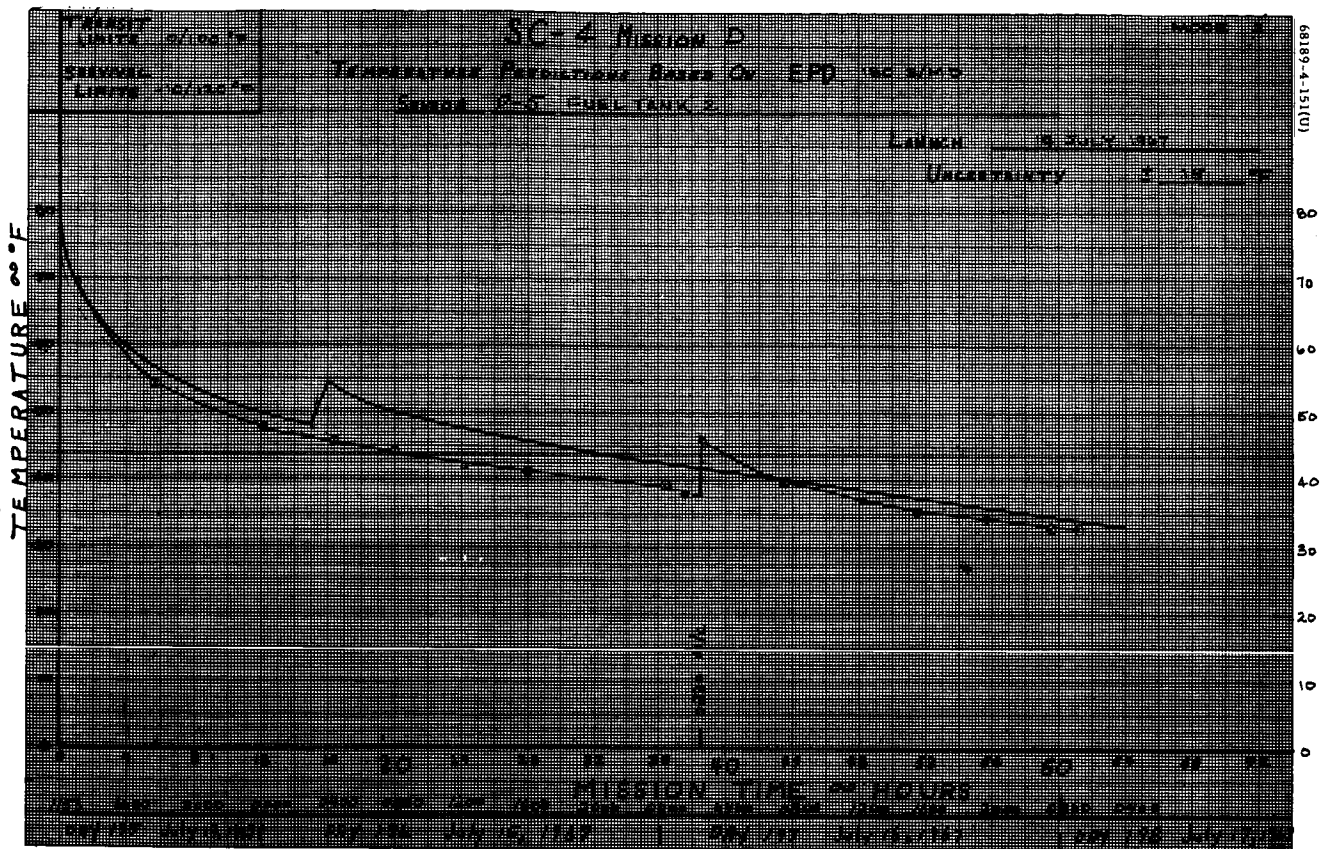
Figure 5.1-21.   Fuel Tank 2 Temperature
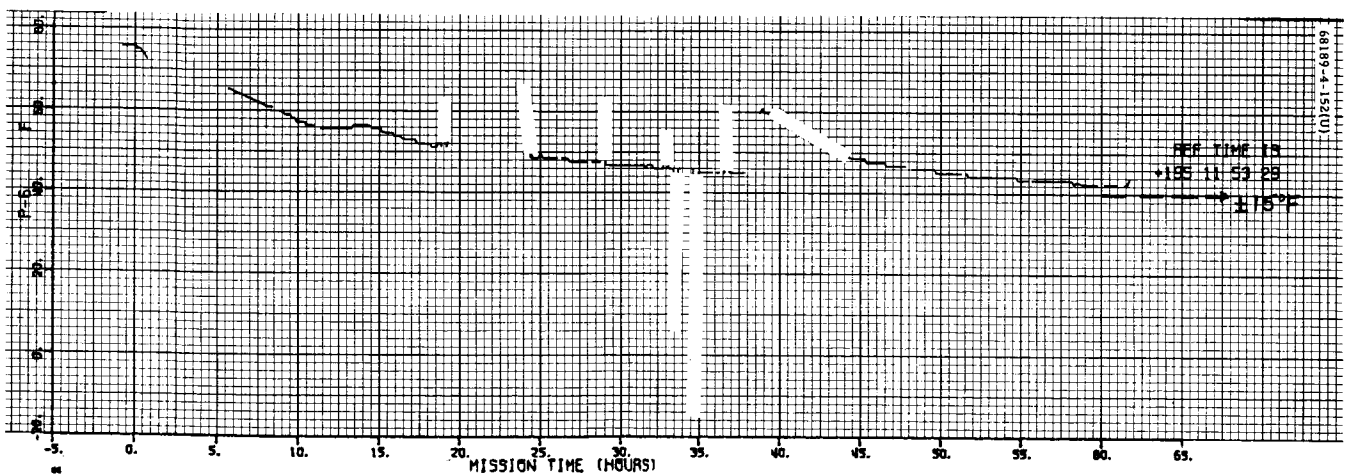
Figure 5.1-22.   Oxidizer Tank 3 Temperature
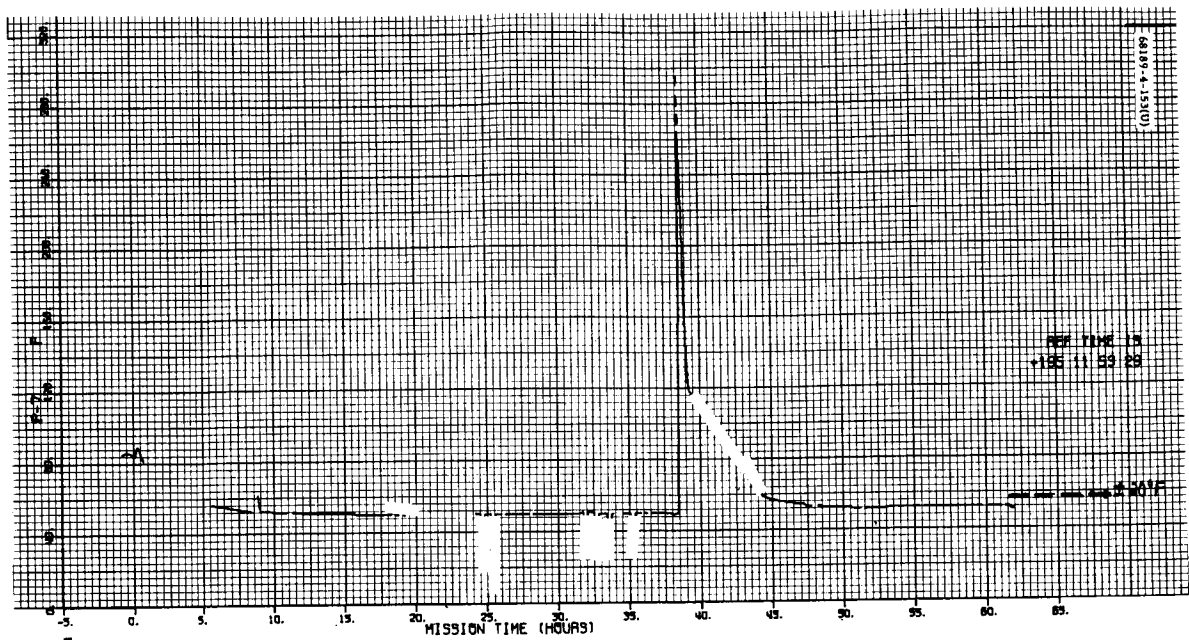
Figure 5.1-23.   Engine 1 Temperature

Figure 5.1-24.   Vernier Line 1 Temperature
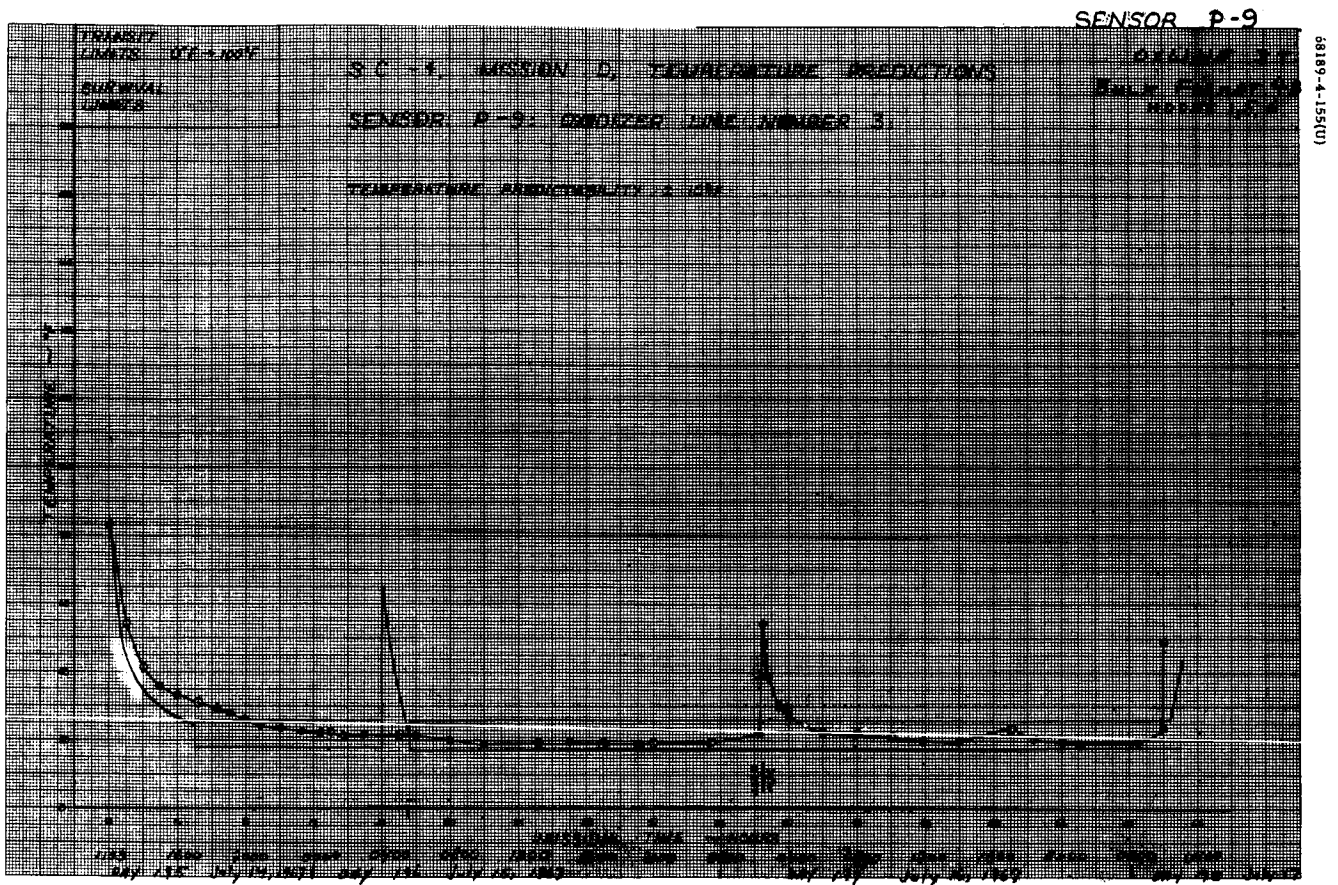
Figure 5.1-25.   Vernier Line 3 Temperature
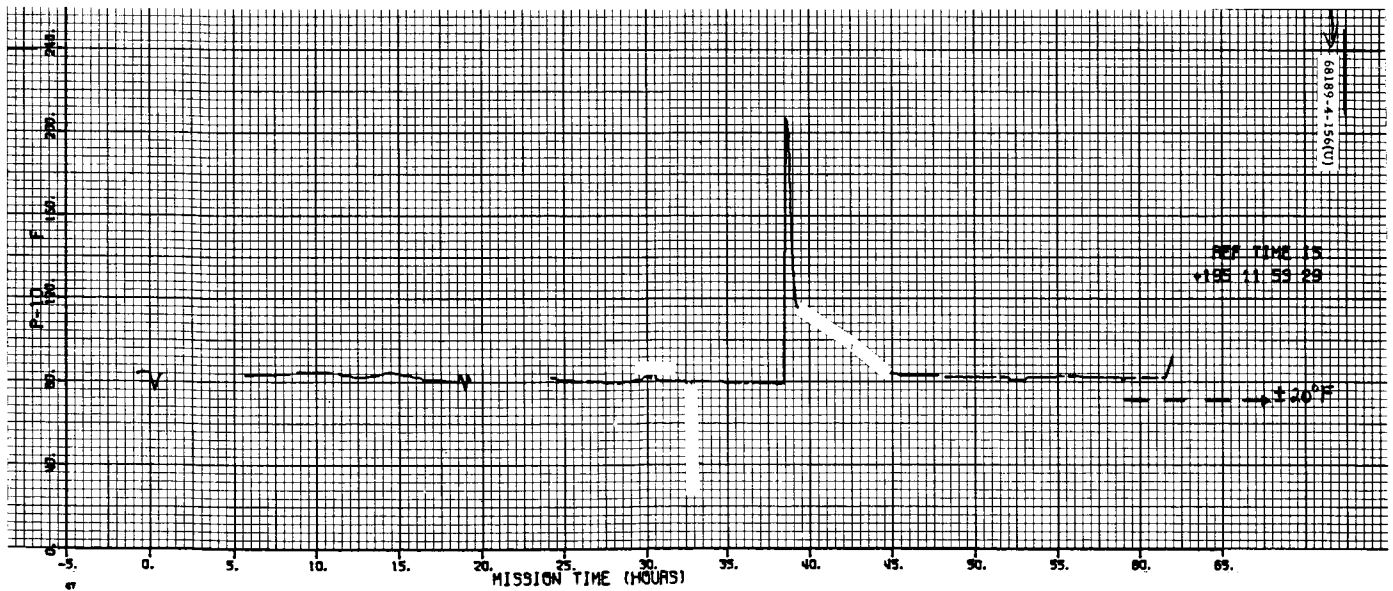
Figure 5.1-26.   Engine 2 Temperature
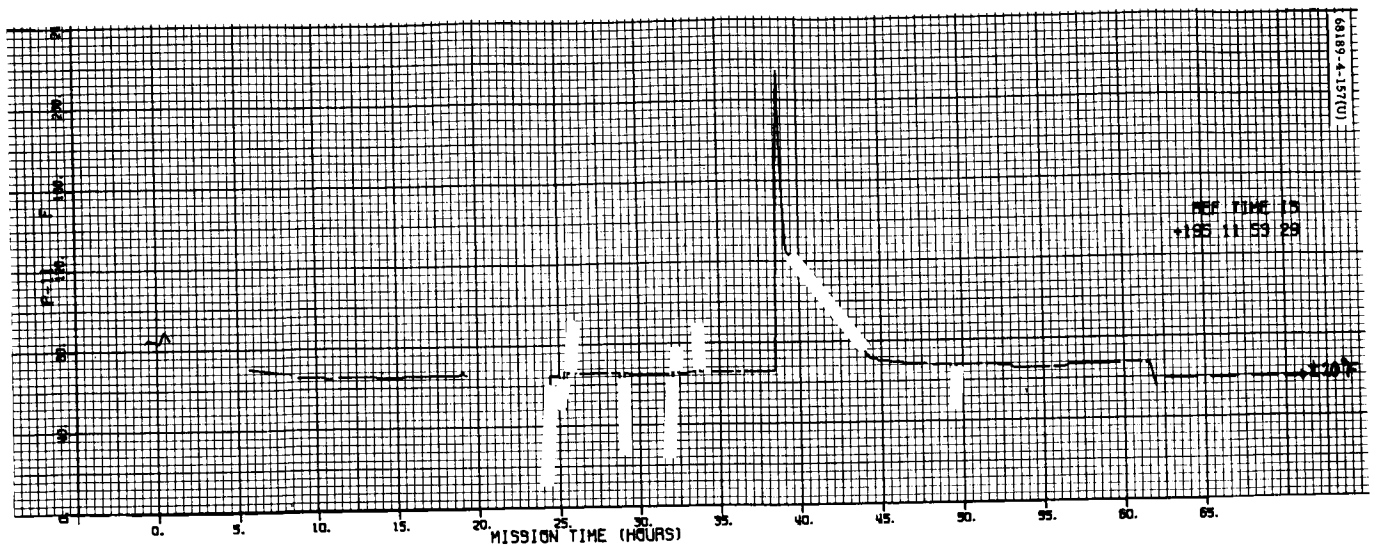
Figure 5.1-27.　Engine 3 Temperature
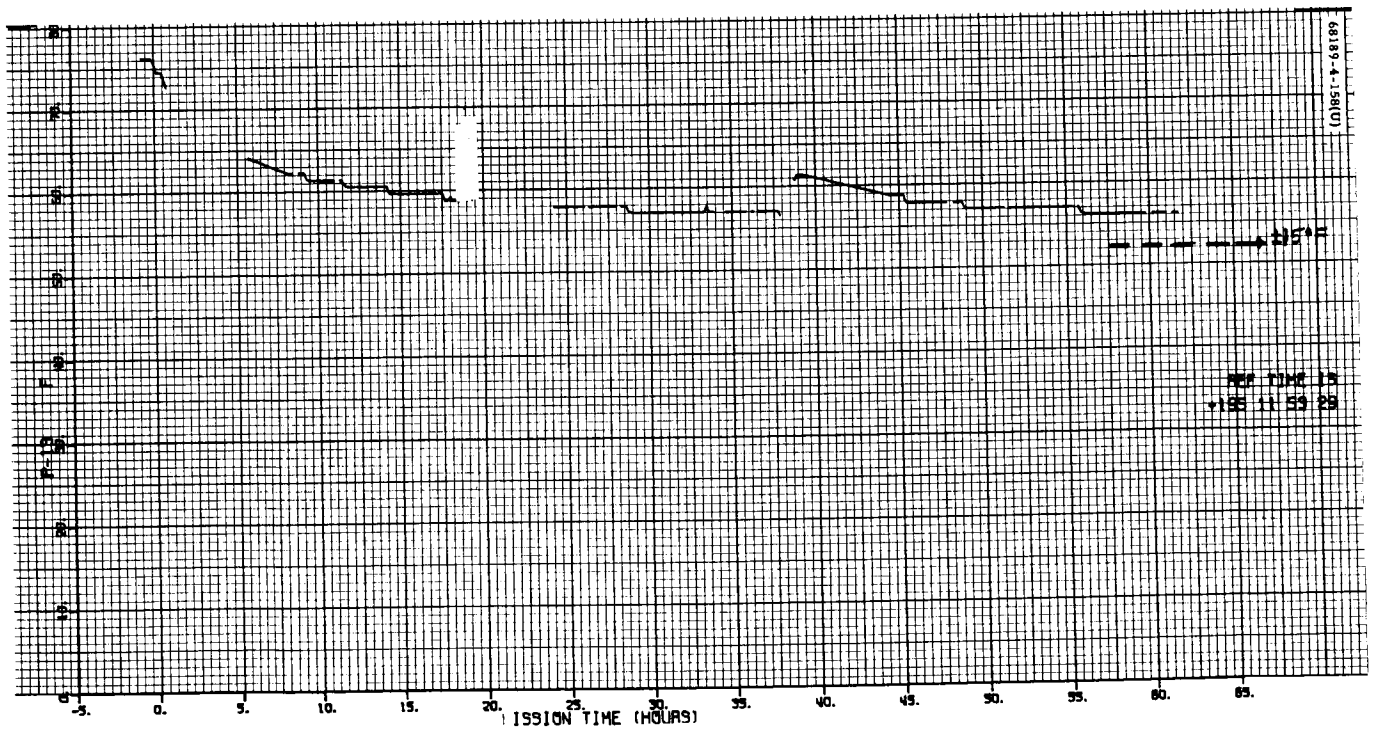
Figure 5.1-28.　Fuel Tank 1 Temperature
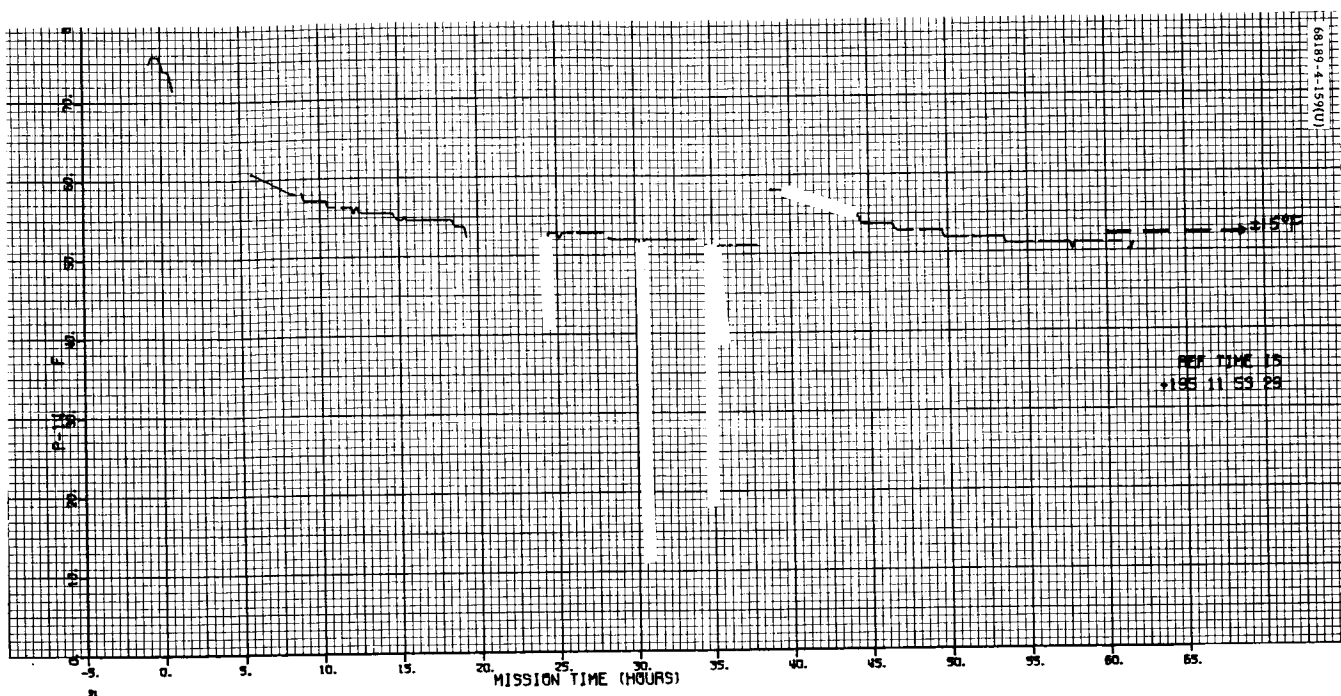
Figure 5.1-29.   Fuel Tank 3 Temperature

Figure 5.1-30.   Oxidizer Tank 1 Temperature
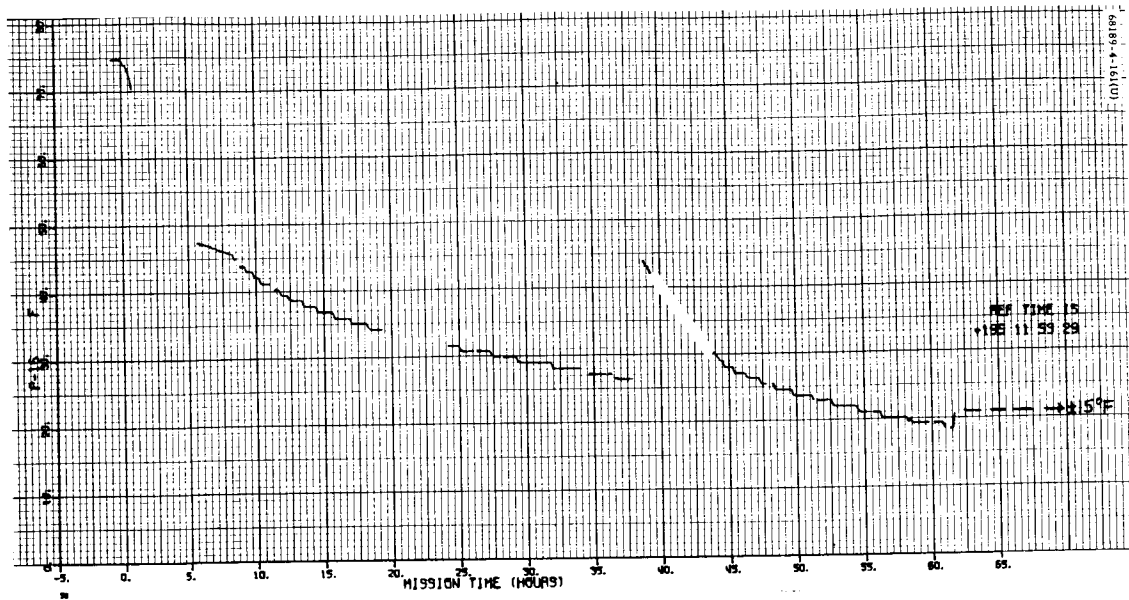
Figure 5.1-31.　Oxidizer Tank 2 Temperature
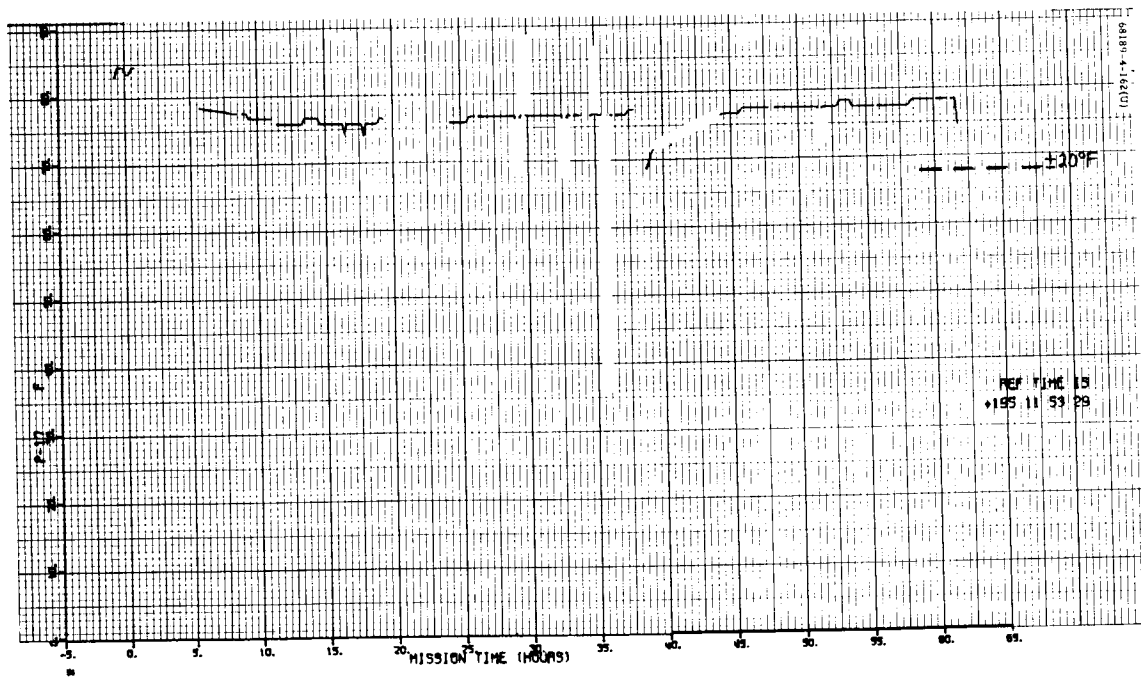
Figure 5.1-32.　Helium Tank Temperature
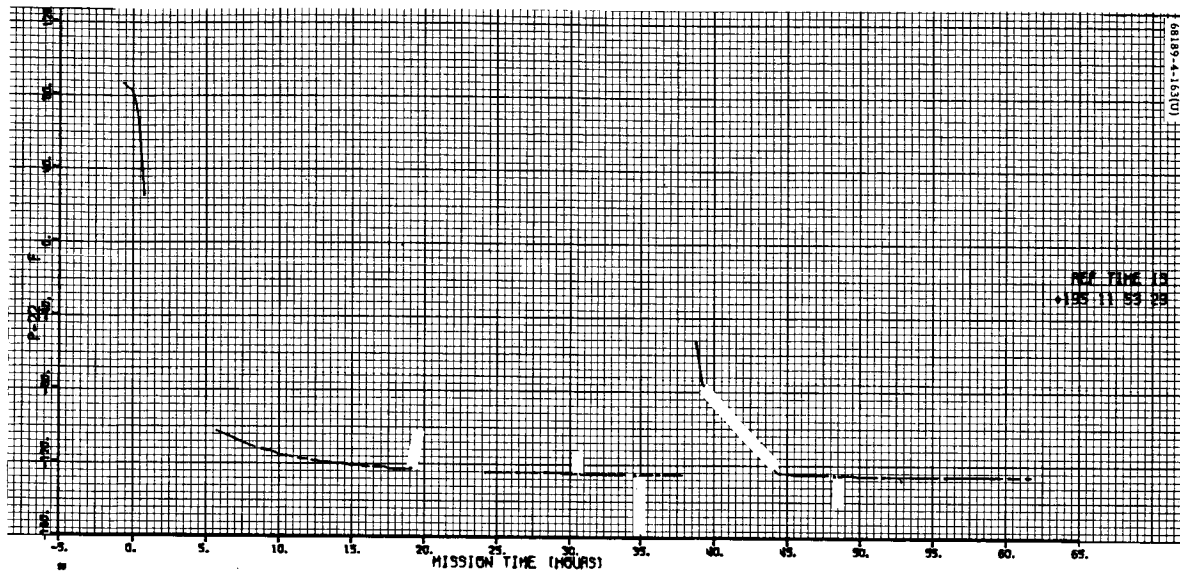
Figure 5.1-33.   Retro Nozzle Temperature
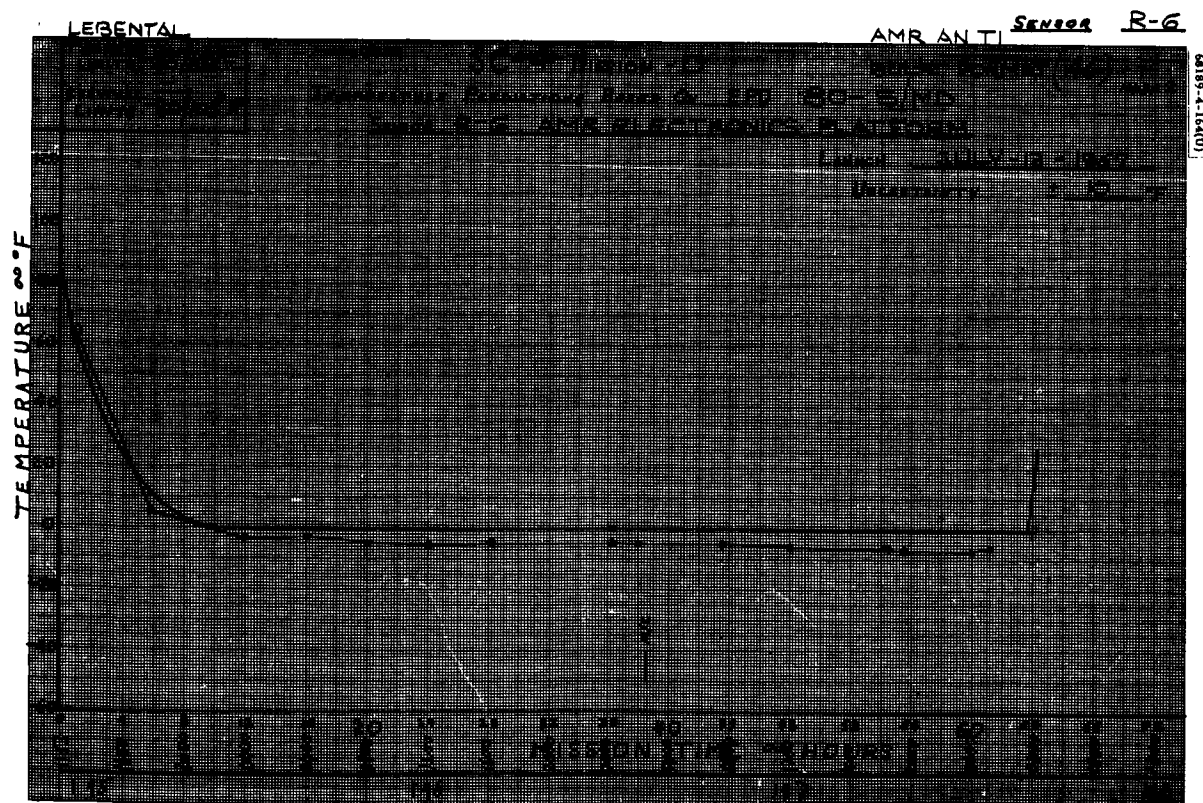
Figure 5.1-34.   AMR Electronics Platform Temperature
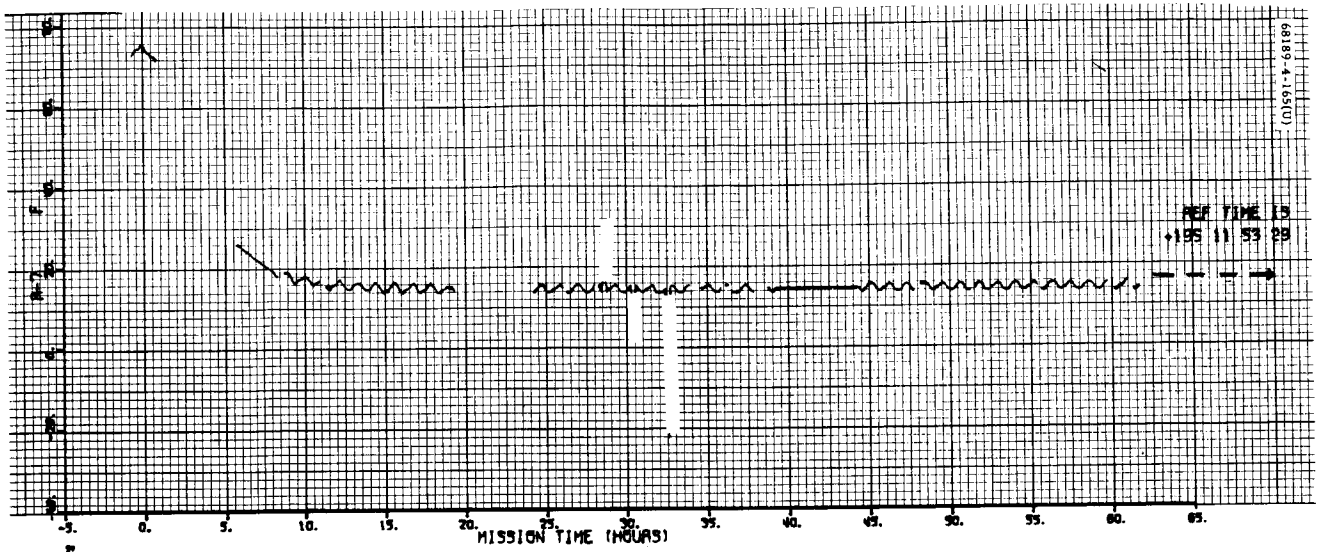
Figure 5.1-35.   AMR Electronics Temperature
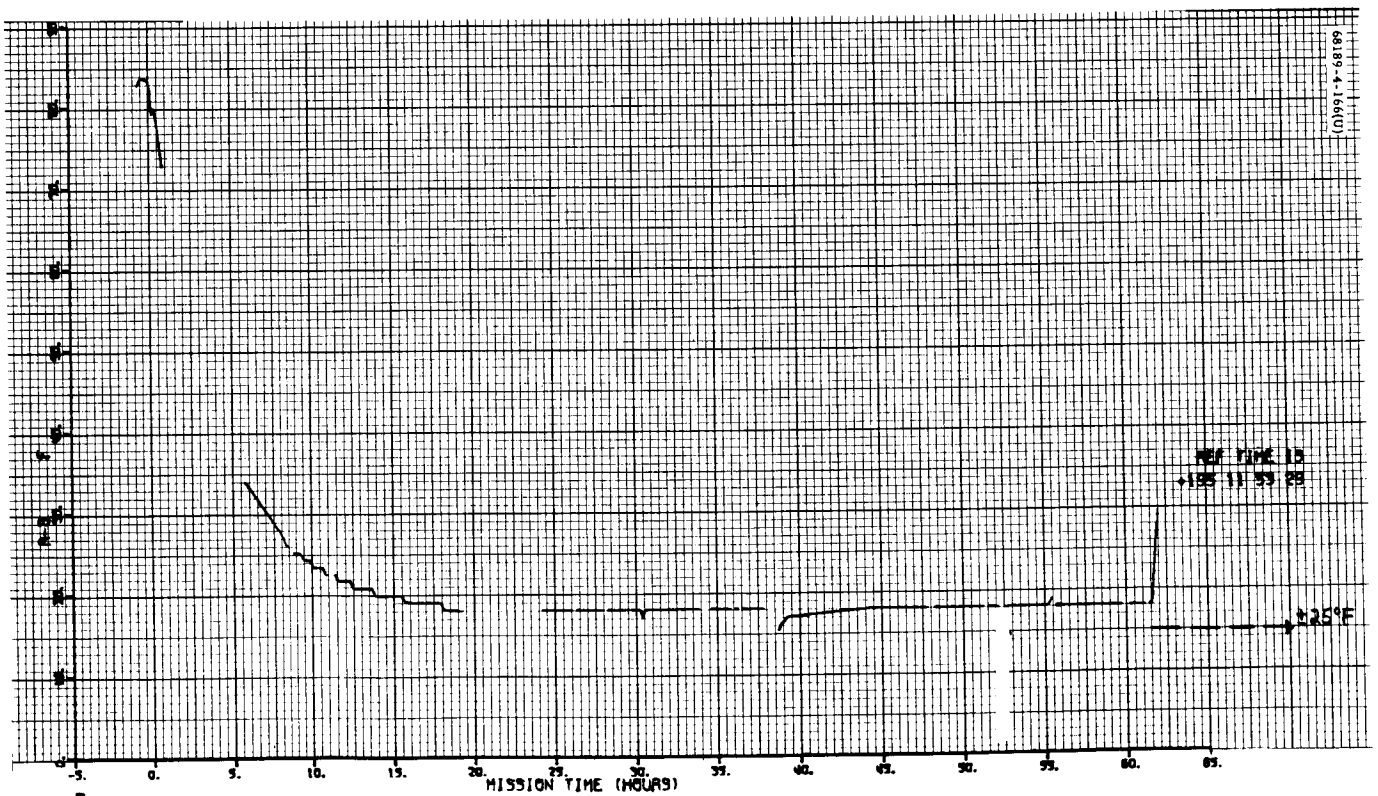
Figure 5.1-36.   RADVS Klystron Unit Temperature

5.1-32
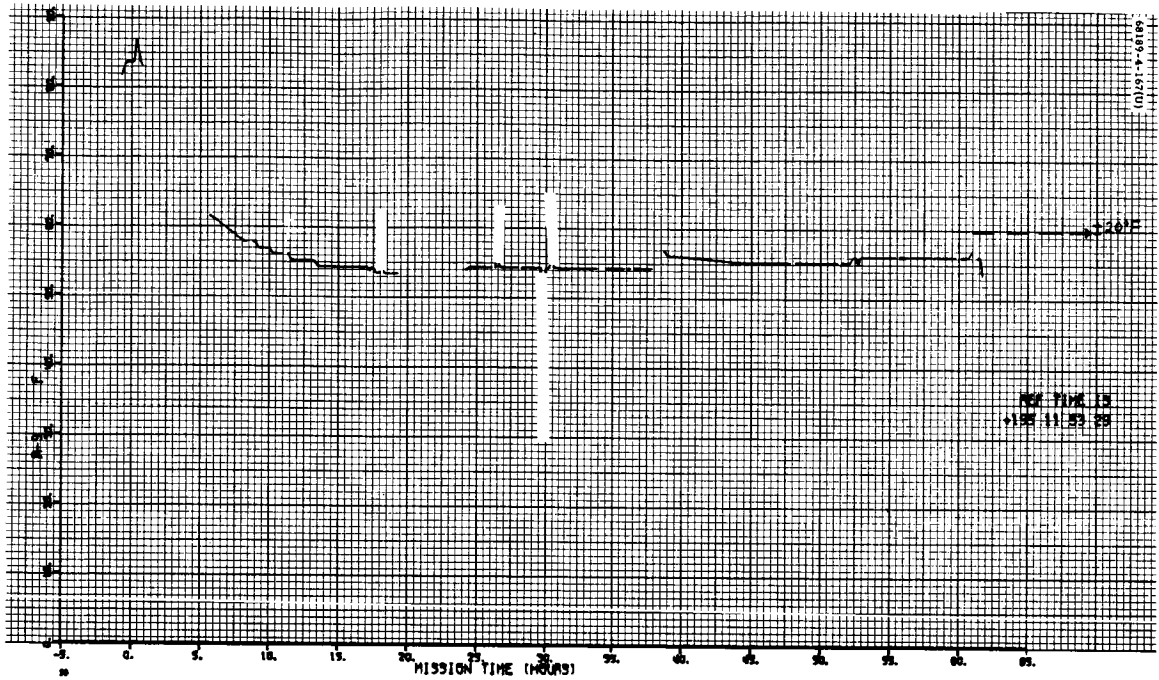
Figure 5.1-37.   RADVS Signal Data Converter Temperature
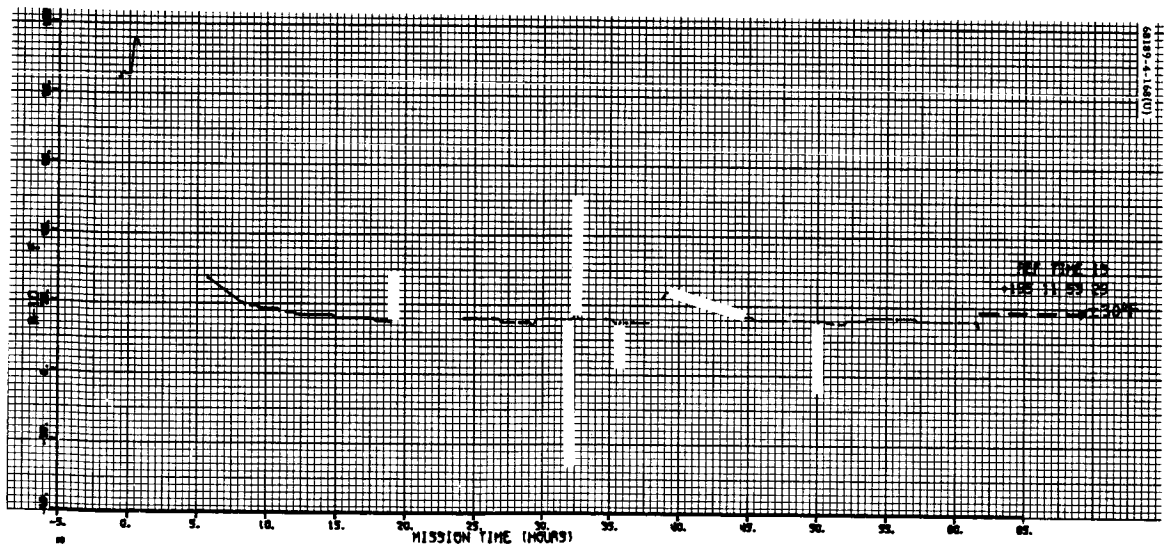
Figure 5.1-38.   Doppler Radar Sensor Temperature
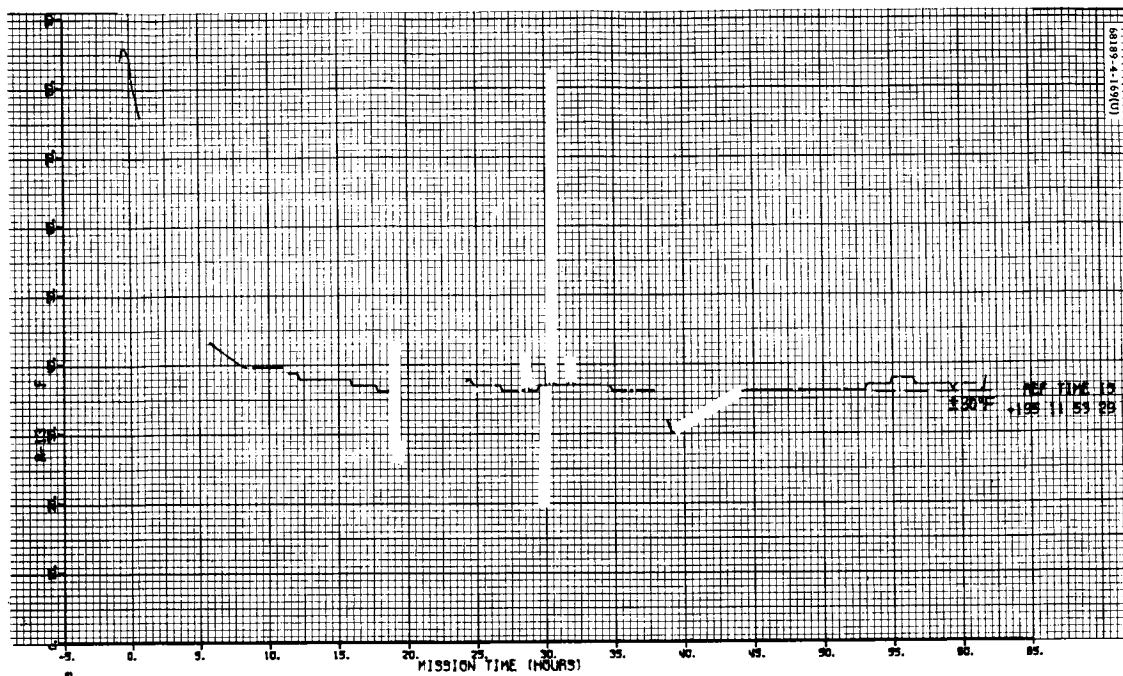
Figure 5.1-39.   Altimeter Radar Sensor Temperature
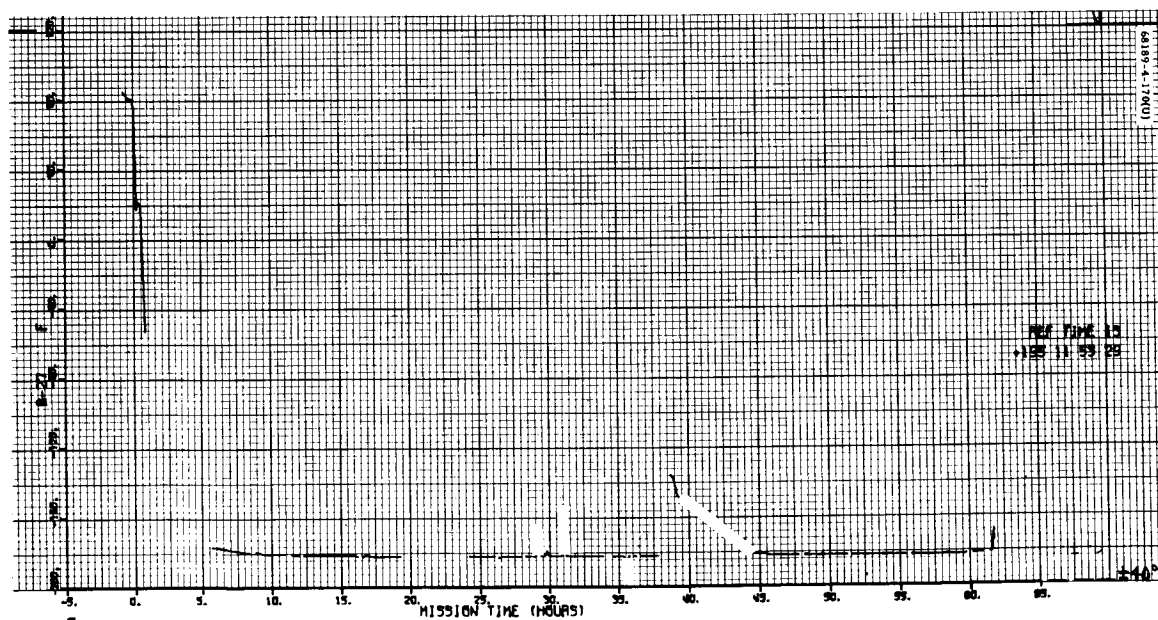
Figure 5.1-40.   AMR Antenna Temperature No. 2
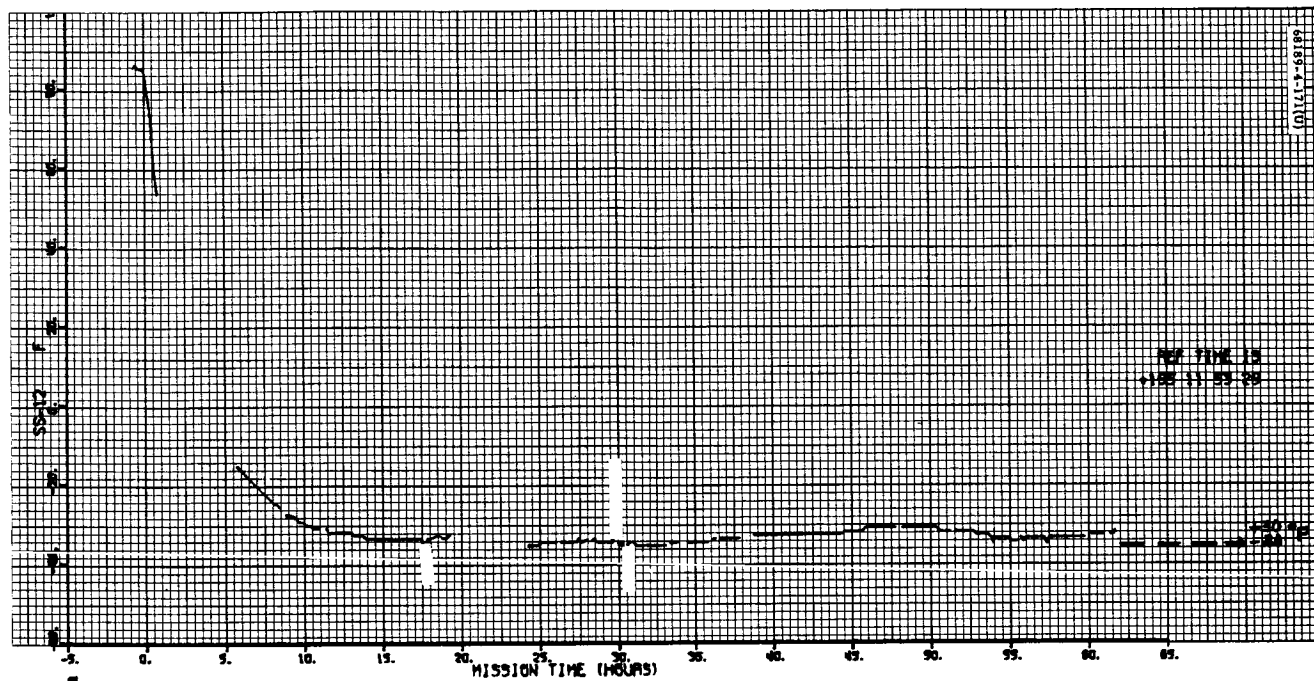
Figure 5.1-41. Soil Sampler Auxiliary Electronics Temperature
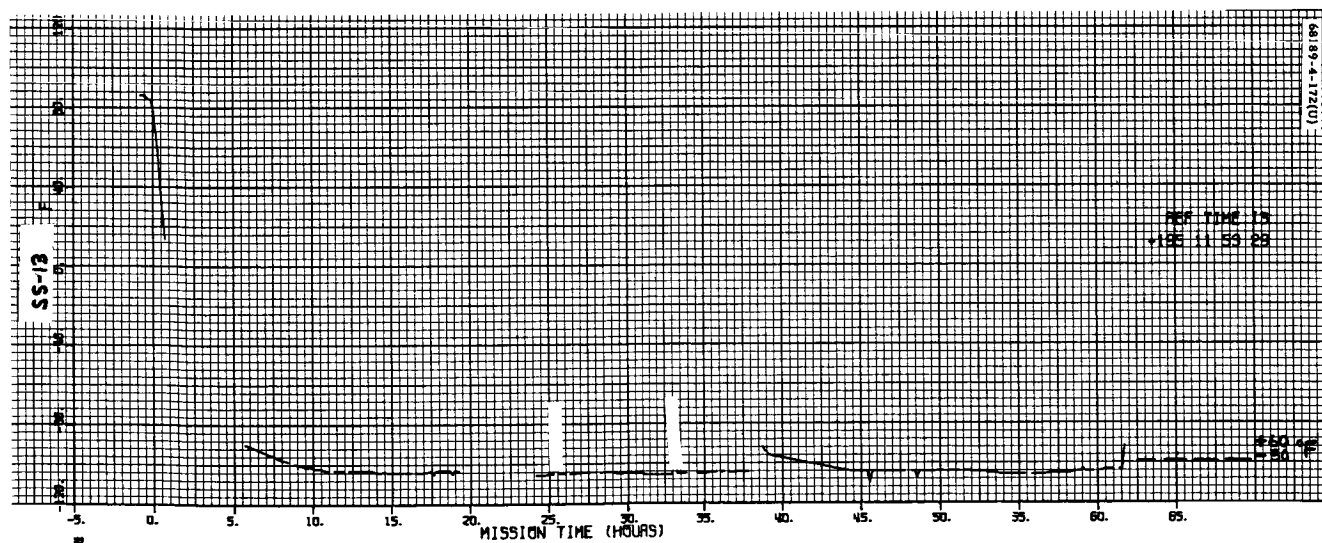
Figure 5.1-42. Soil Sampler Structure Temperature

5.1-35
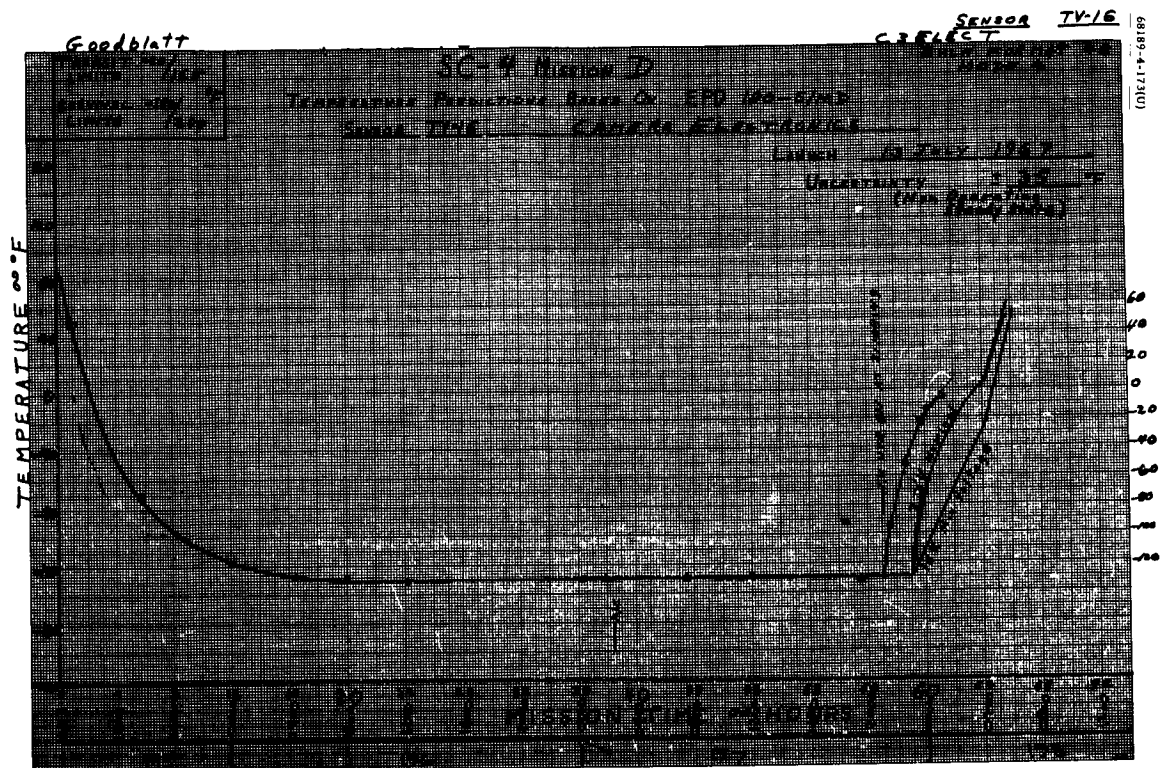
Figure 5. 1-43.   Survey Camera Electronics Temperature

Figure 5. 1-44.   Survey Camera Mirror Assembly Temperature

MISSION TIME (HOURS)
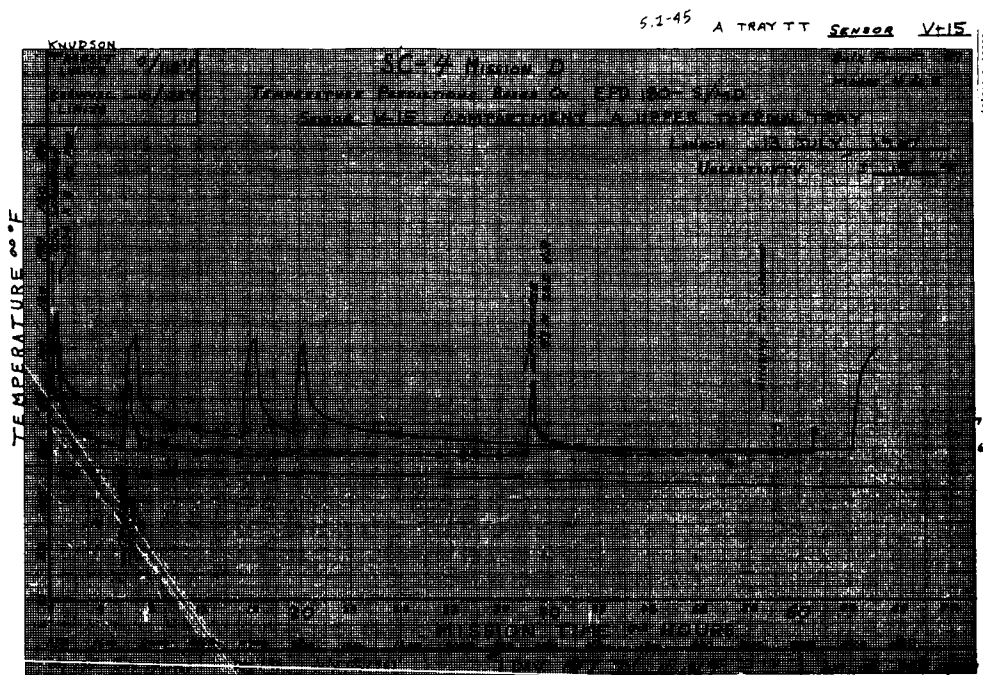
Figure 5.1-45.   Compartment A Tray Top Temperature
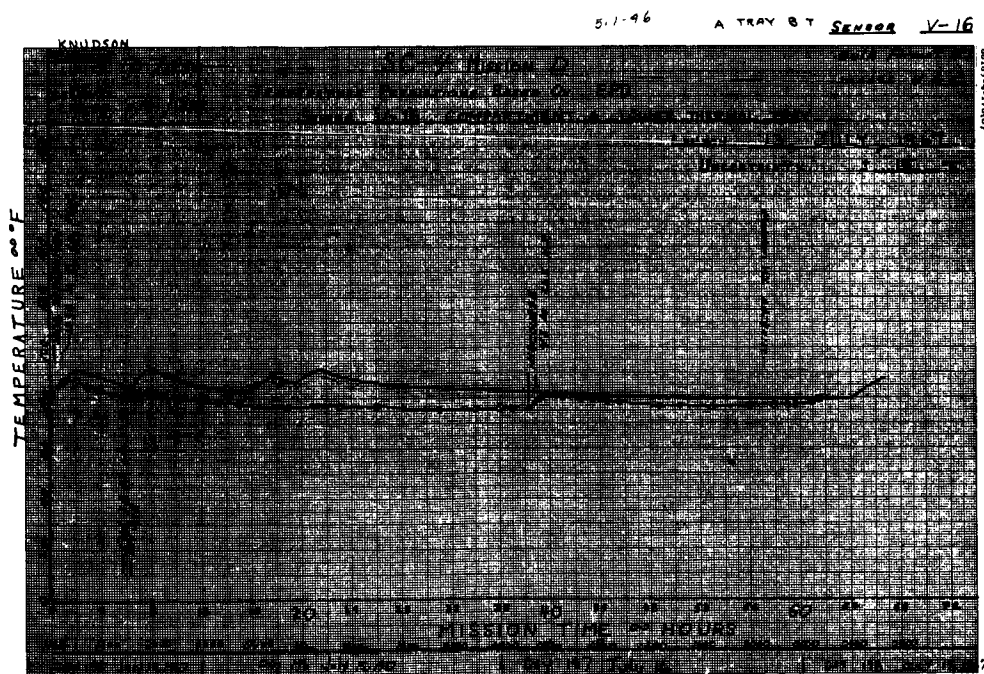
Figure 5.1-46.   Compartment A Lower Support Temperature
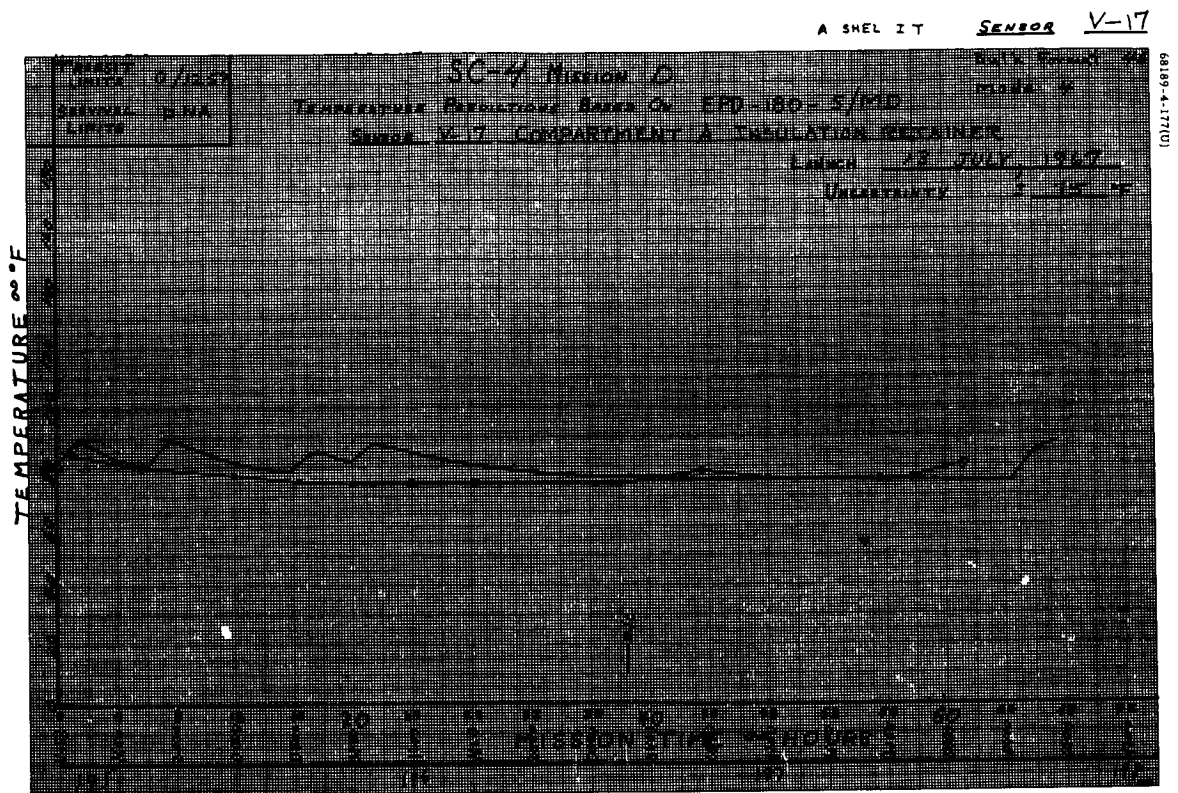
Figure 5.1-47.   Compartment A Insulation

Figure 5.1-48.   Compartment A Canister Temperature
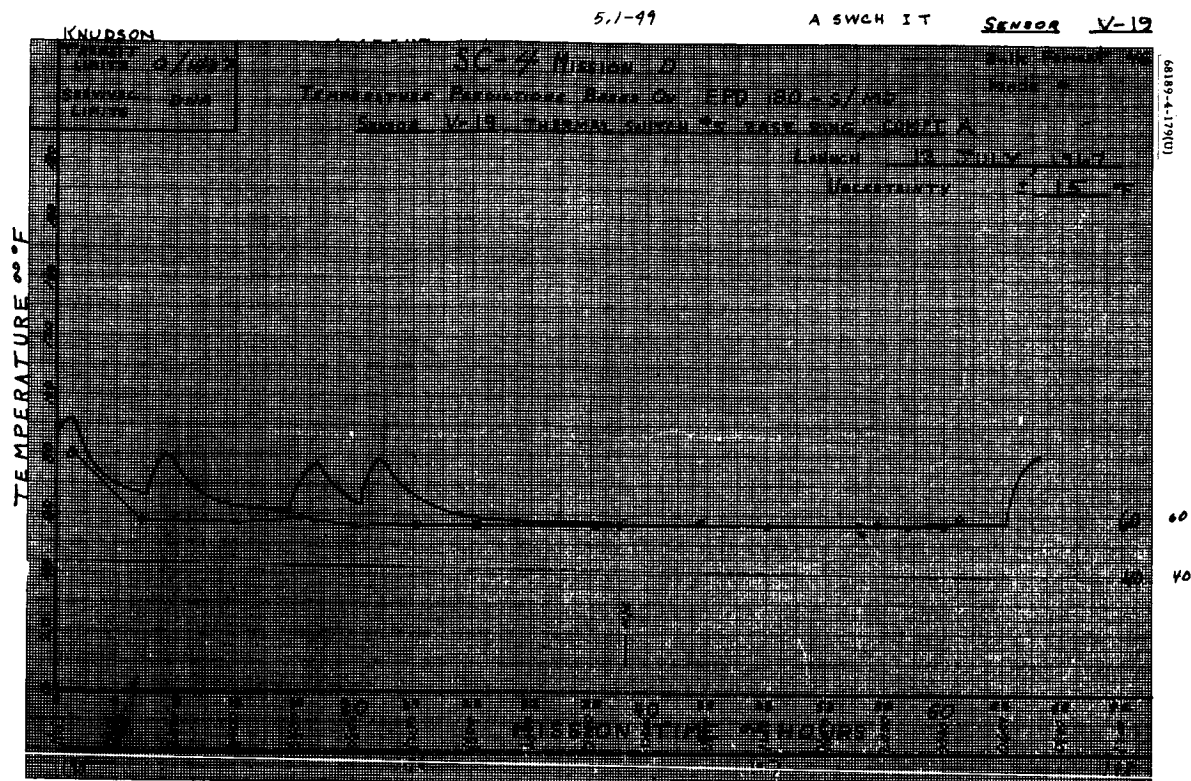
Figure 5.1-49.   Compartment A Switch 5 Base Temperature

Figure 5.1-50.   Compartment A Switch 5 Face Radiator Temperature
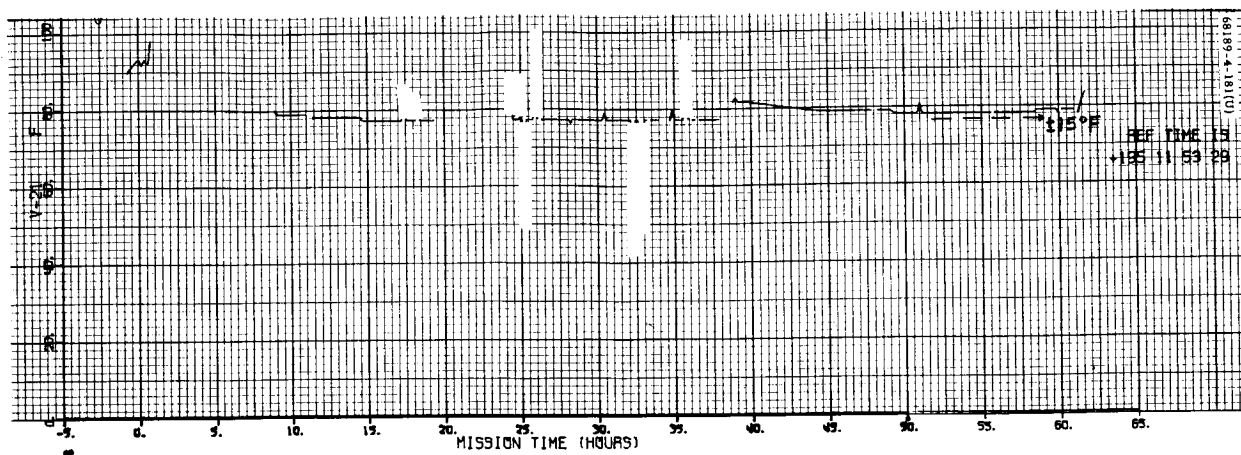
Figure 5.1-51. Compartment B Tray Top Temperature
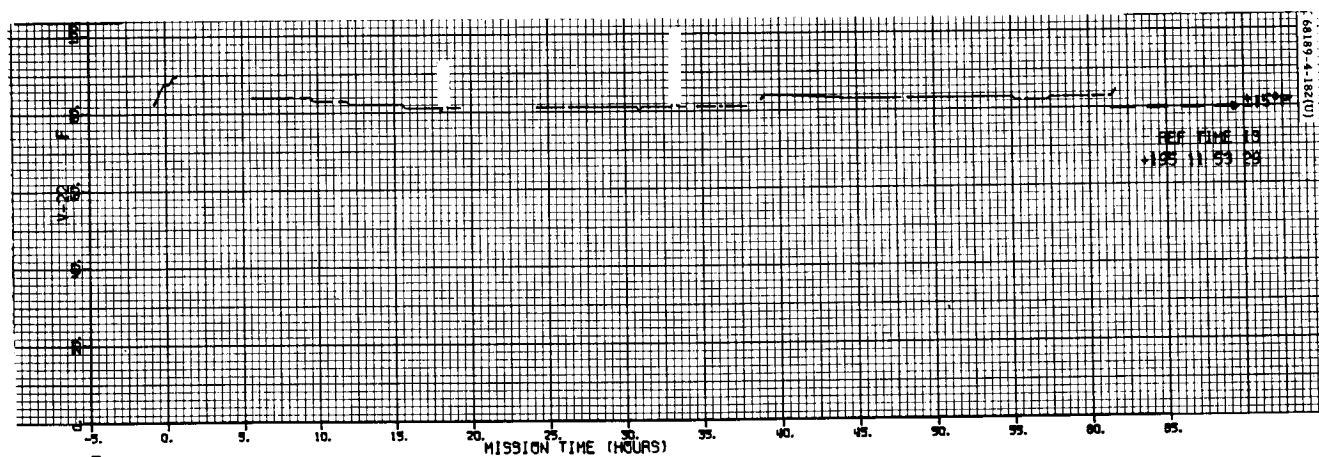
Figure 5.1-52. Compartment B Lower Support Temperature
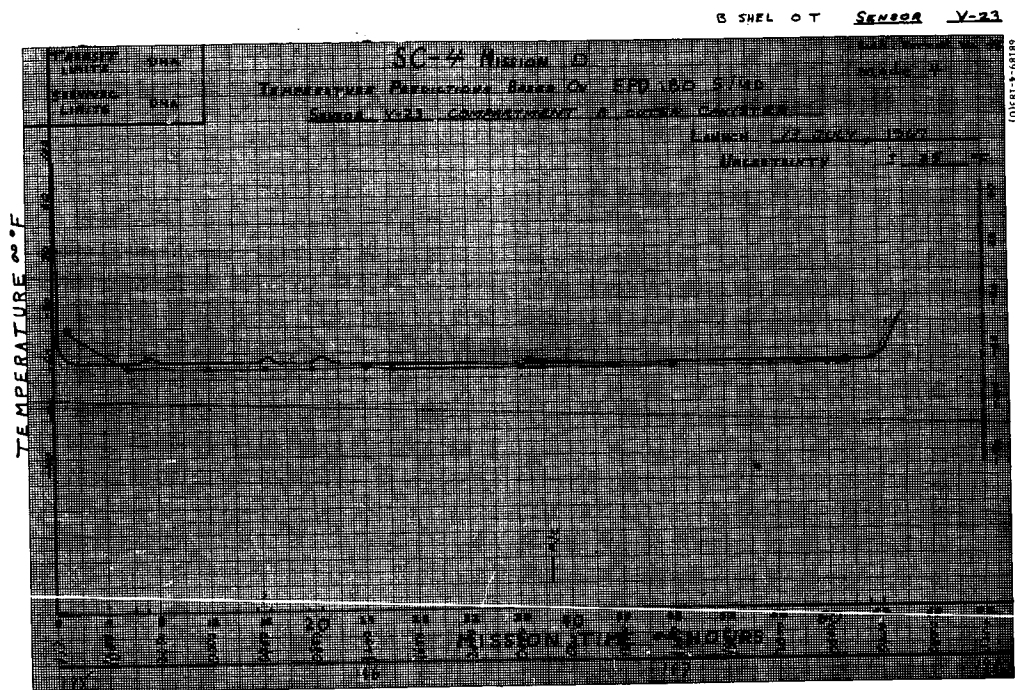
Figure 5.1-53. Compartment B Outer Canister Temperature
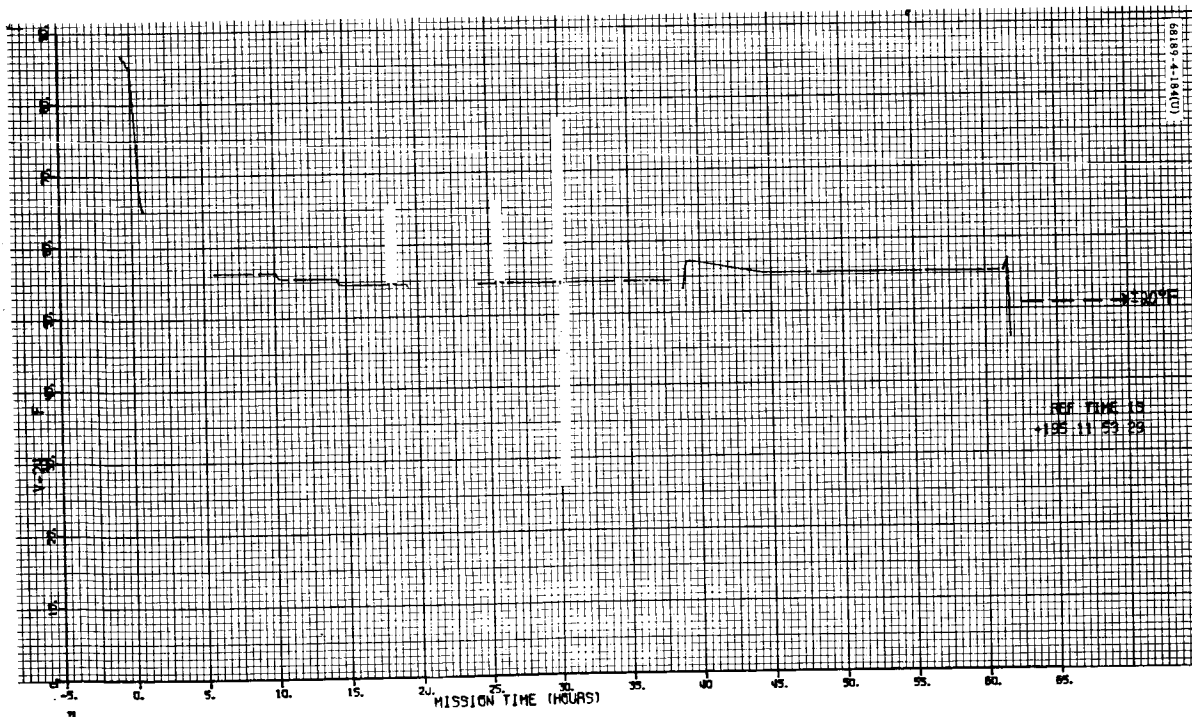
Figure 5.1-54. Compartment B Switch 4 Face Radiator Temperature
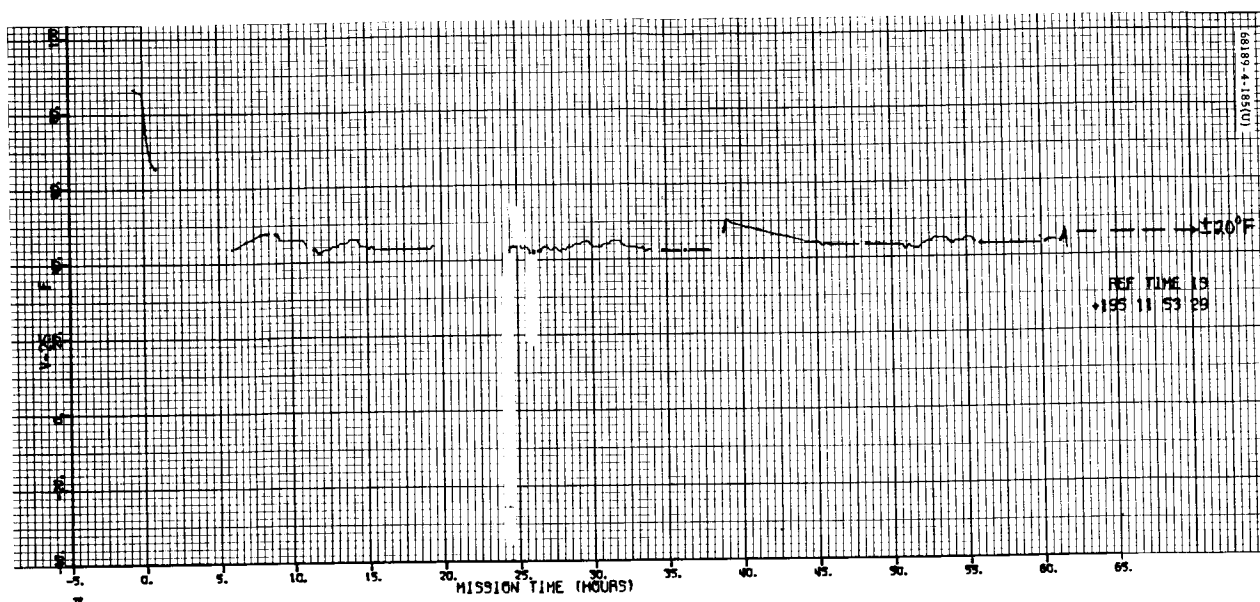
Figure 5.1-55.   Compartment B Switch 8 Face Radiator Temperature

B SWCH IT SENSOR V-26
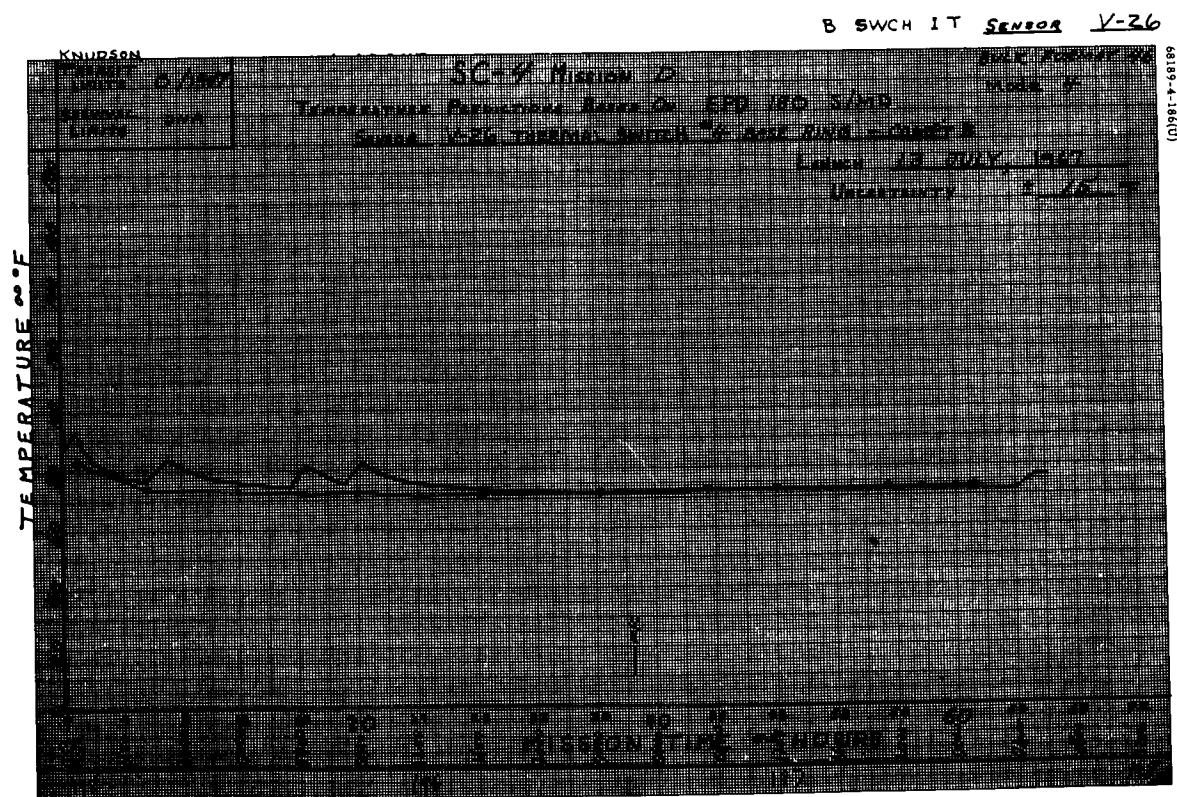
Figure 5.1-56.   Compartment B Switch 4 Base Ring Temperature
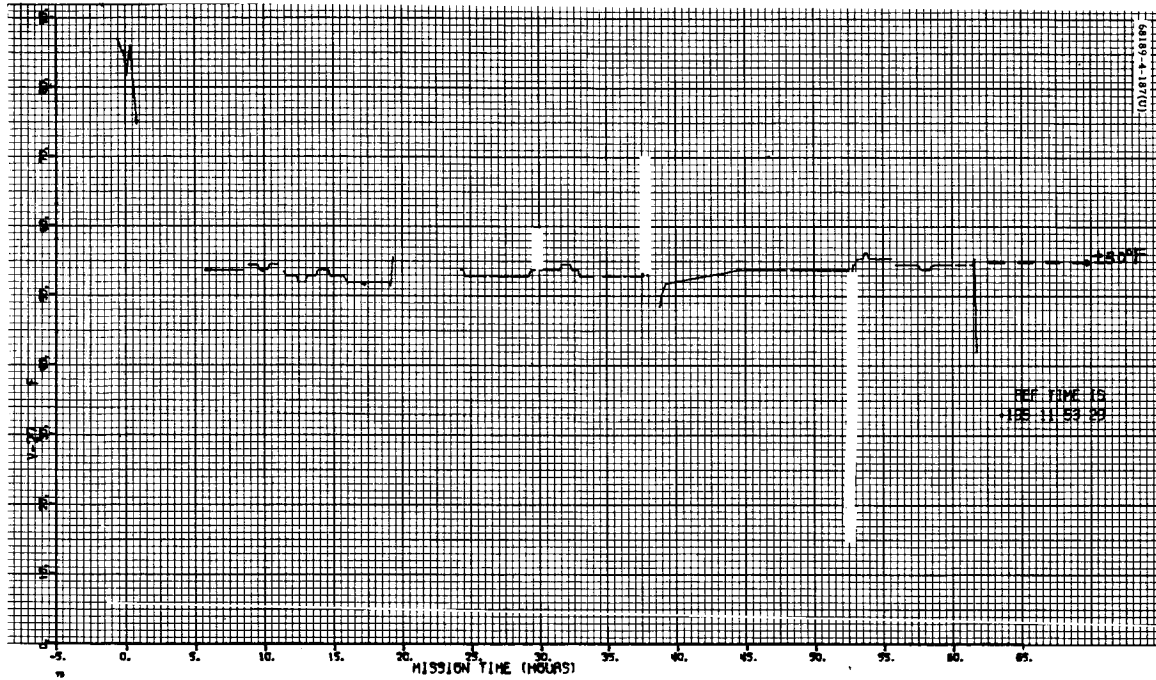
Figure 5.1-57.   Upper Spaceframe Temperature No. 1
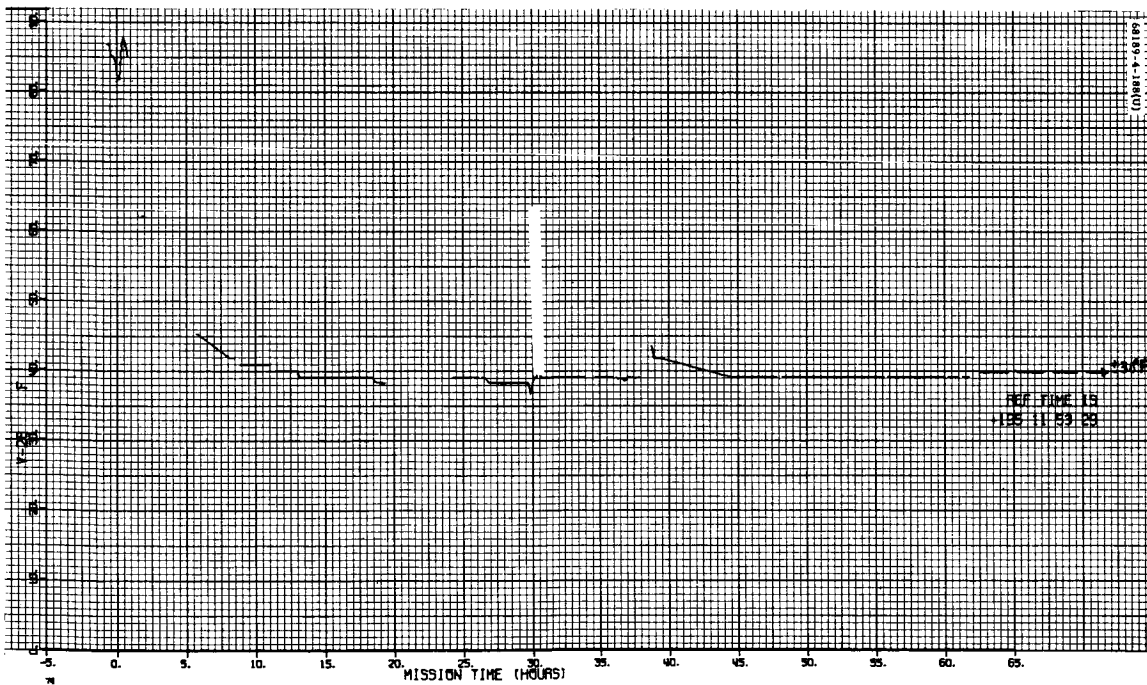
Figure 5.1-58.   Spaceframe Temperature Under Compartment A
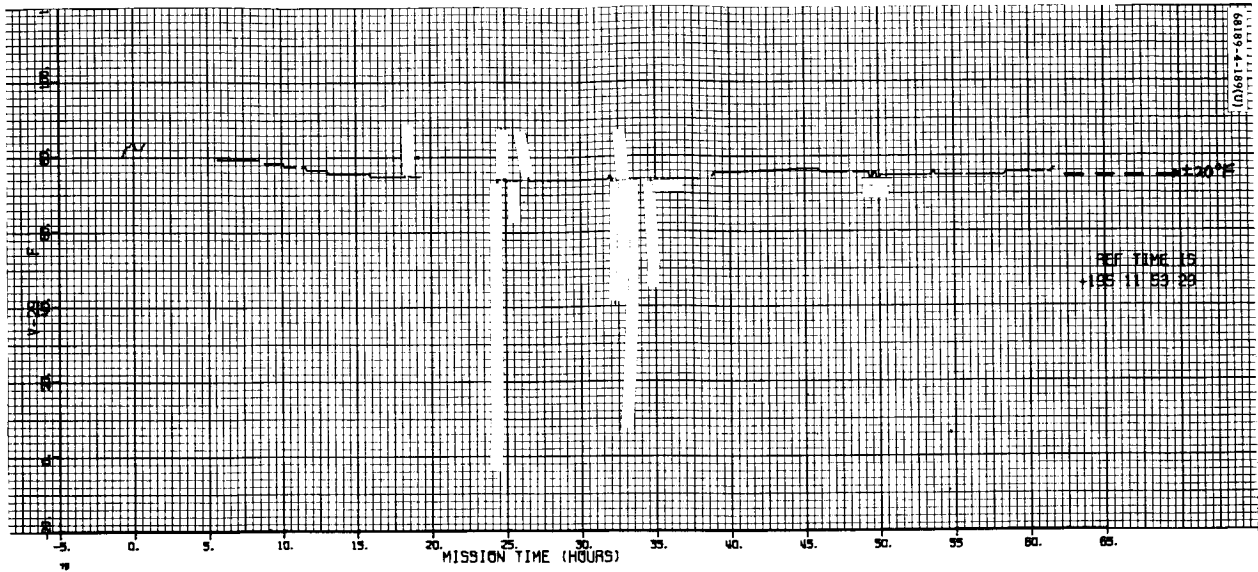
Figure 5.1-59.   Wire Harness Temperature Thermal Tunnel
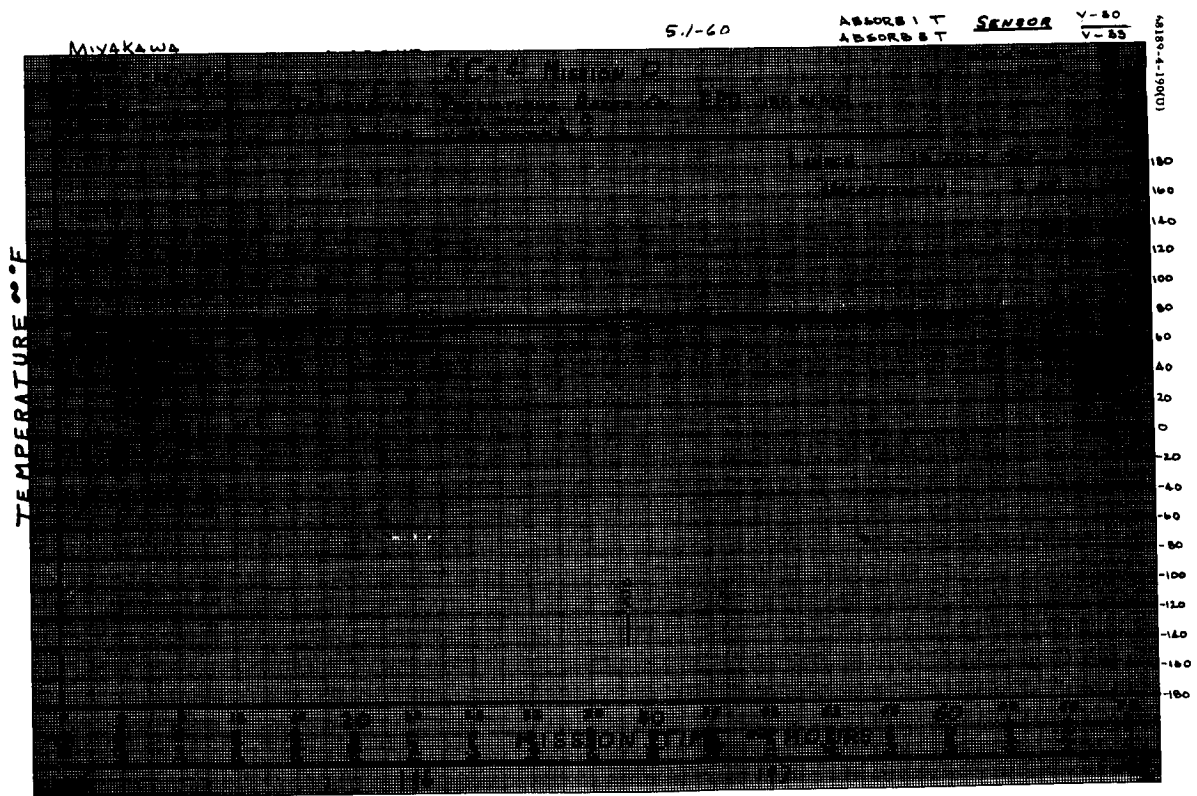
Figure 5.1-60.   Sensor V-30 Shock 1, Sensor V-33 Shock 3
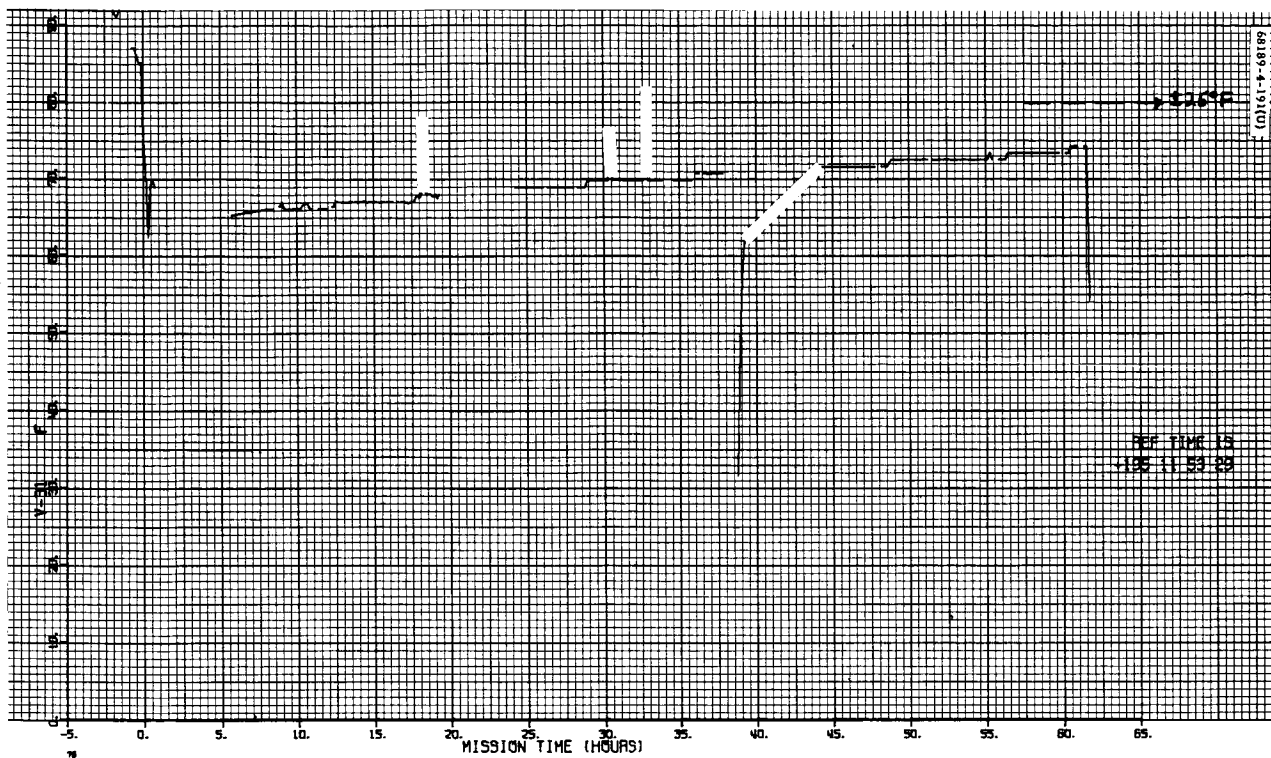
Figure 5.1-61.　Leg 2 Upper Web Temperature
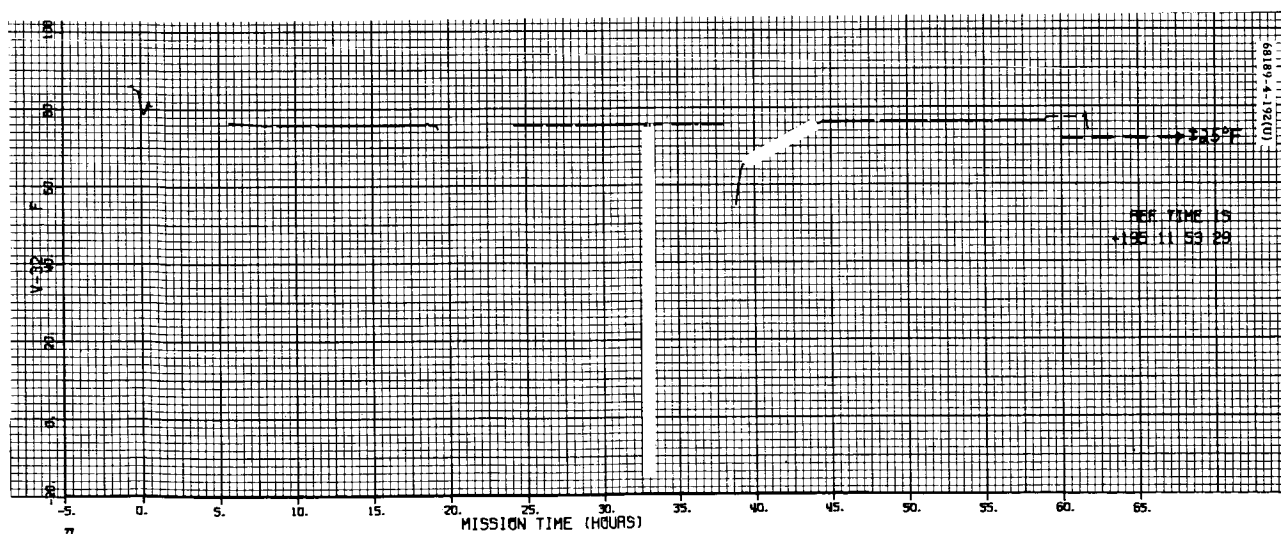
Figure 5.1-62.　Shock Absorber 2 Temperature
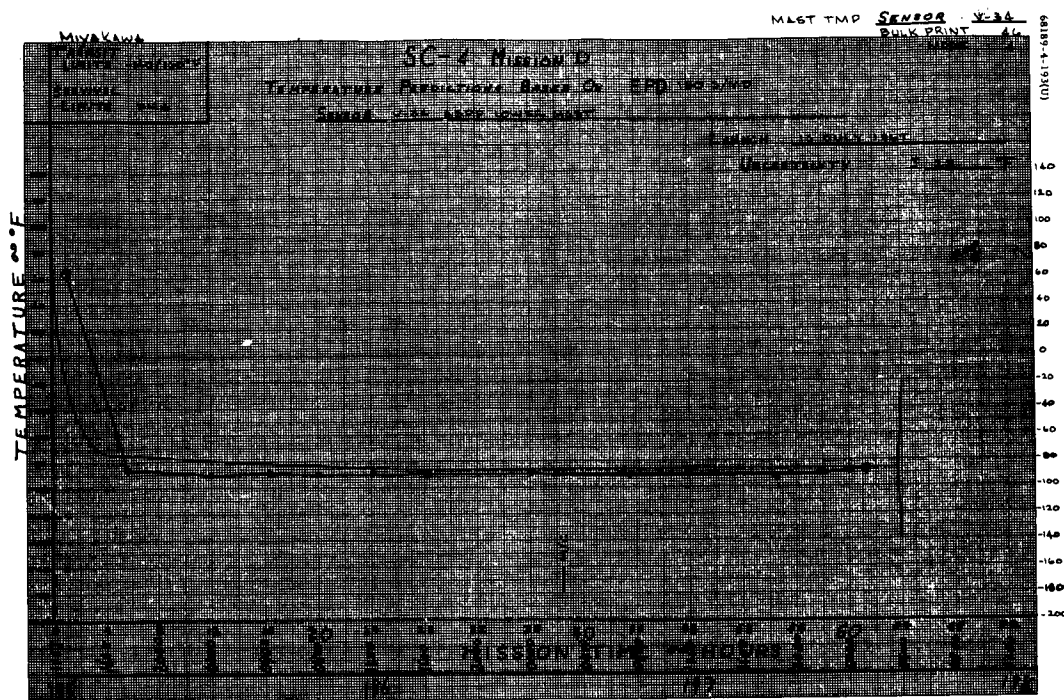
Figure 5.1-63.   A/SPP Lower Mast Temperature
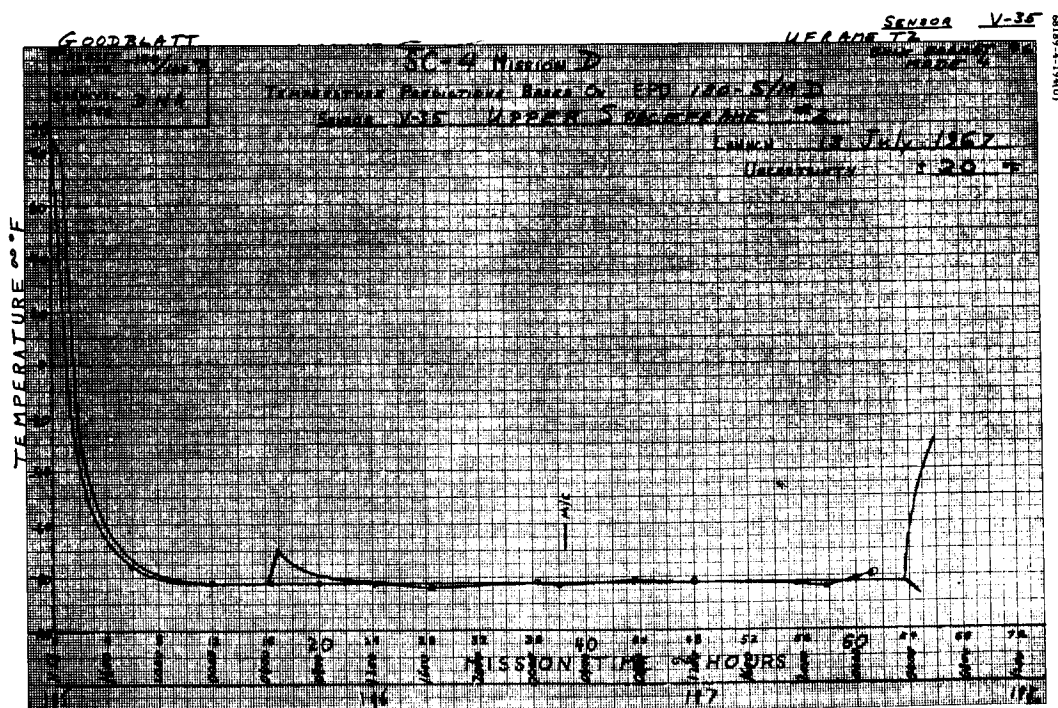
Figure 5.1-64.   Upper Spaceframe, Sensor 2 Temperature
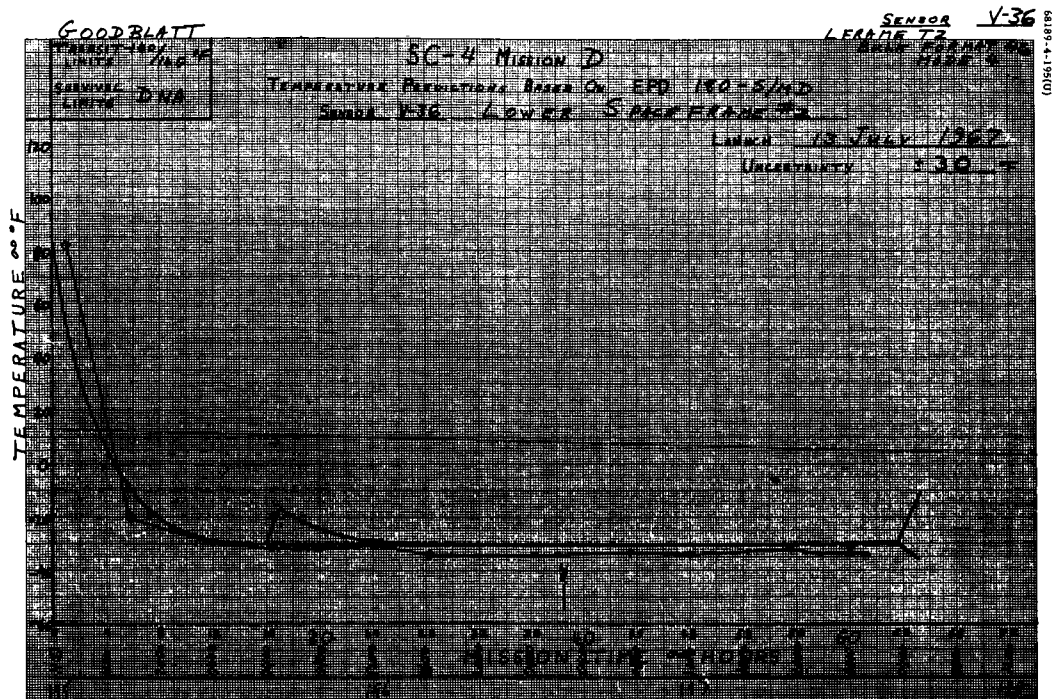
Figure 5.1-65. Lower Spaceframe, Sensor 2 Temperature
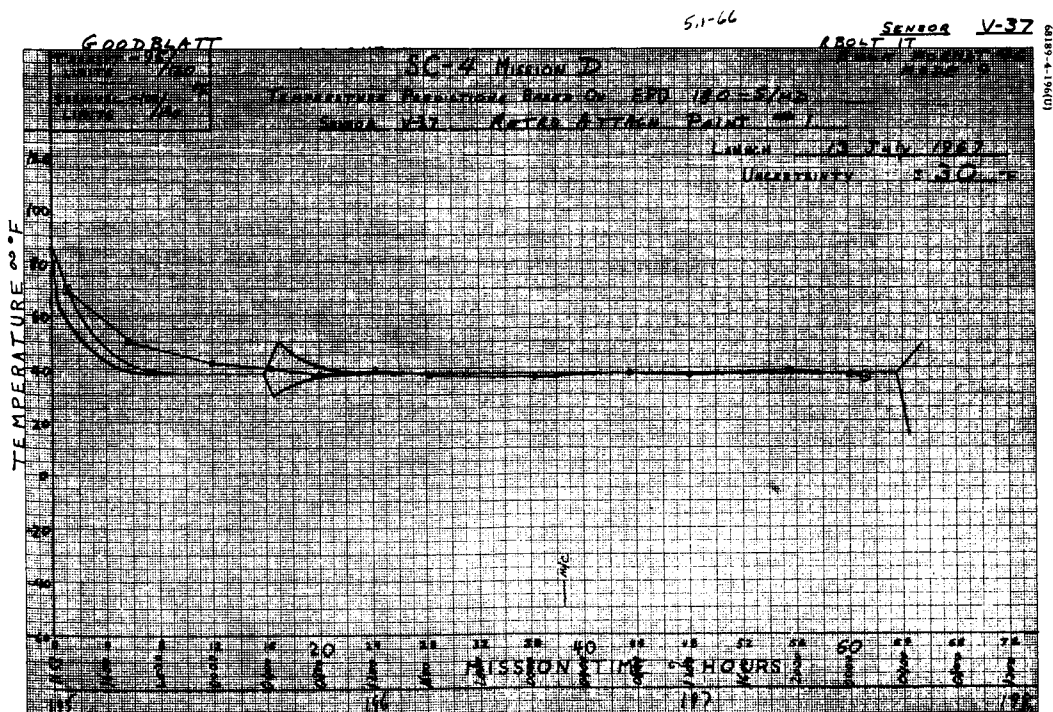
Figure 5.1-66. Retro Attach Point 1 Temperature
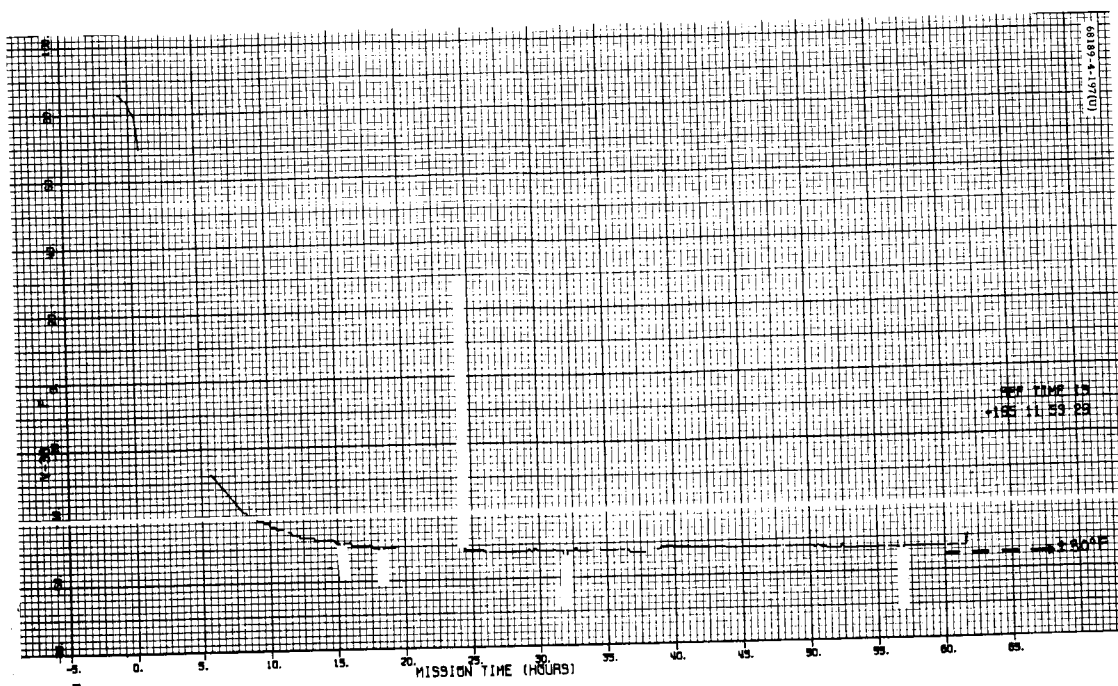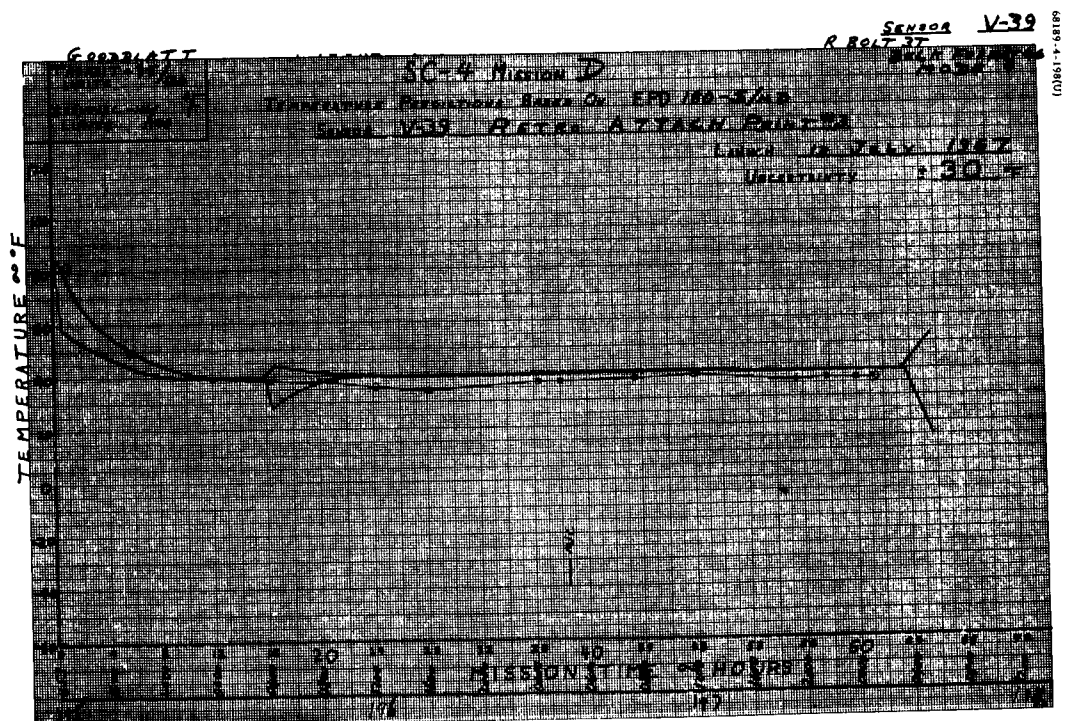
Figure 5.1-67.　Retro Attach Point 2 Temperature
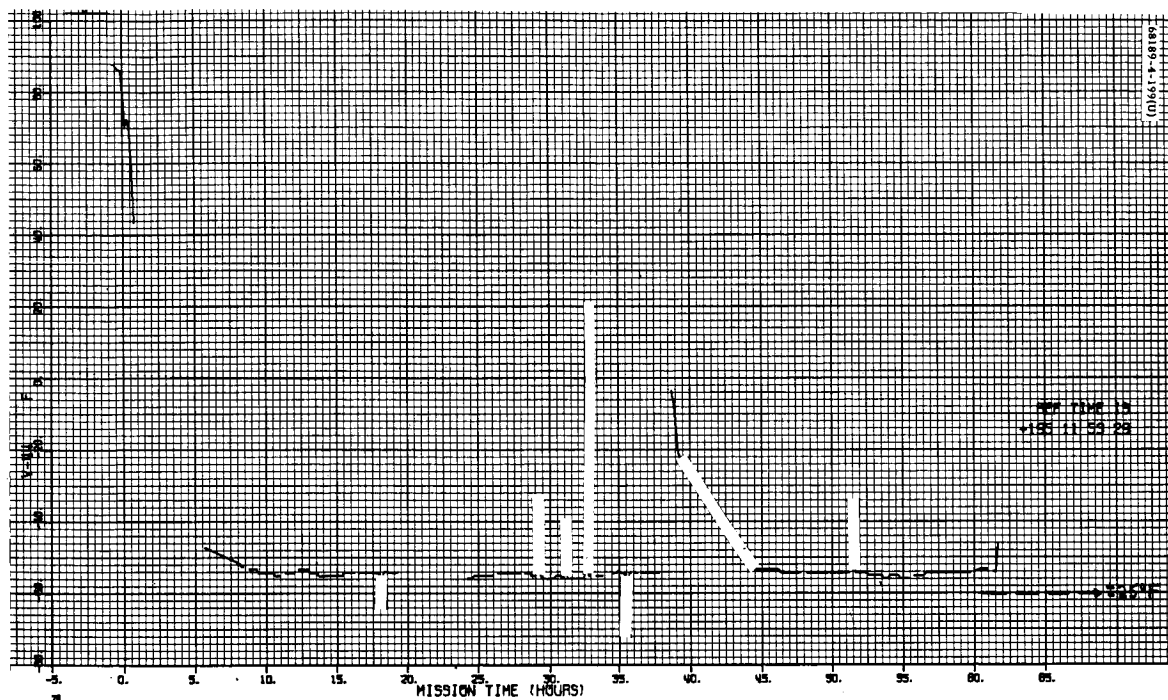

Figure 5.1-68.　Retro Attach Point 3 Temperature

Figure 5.1-69. Crushable Block Temperature
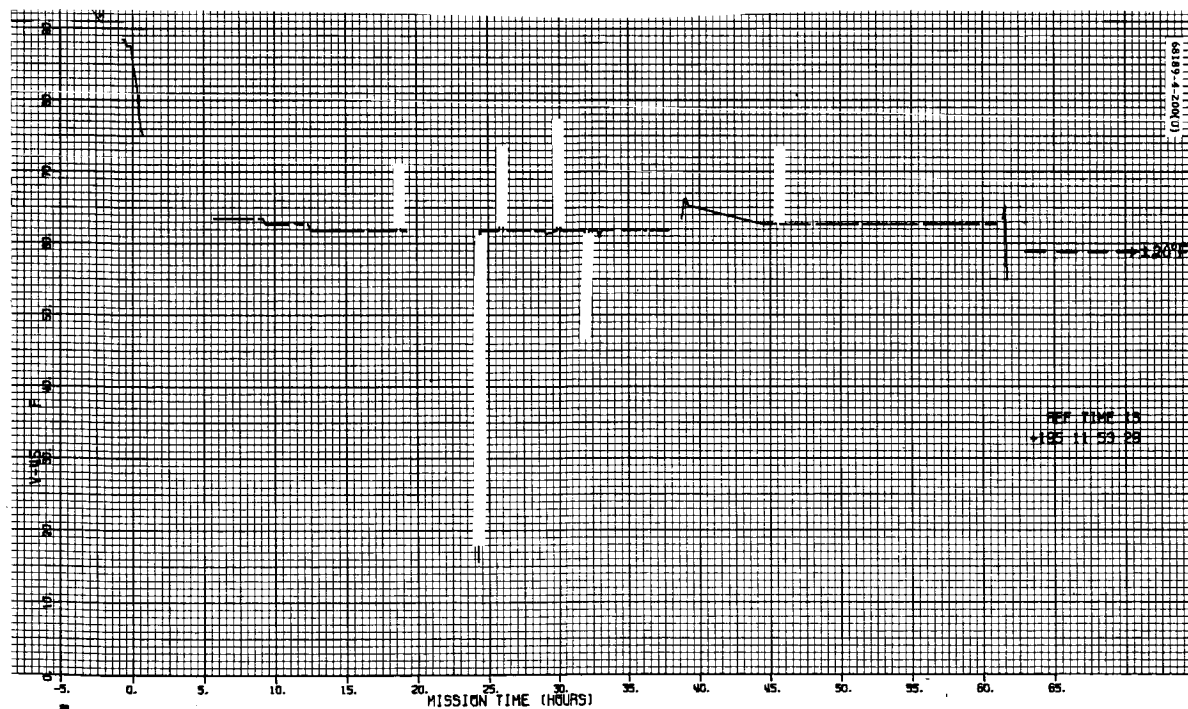

Figure 5.1-70. Compartment B Switch 1 in Face Radiator Temperature
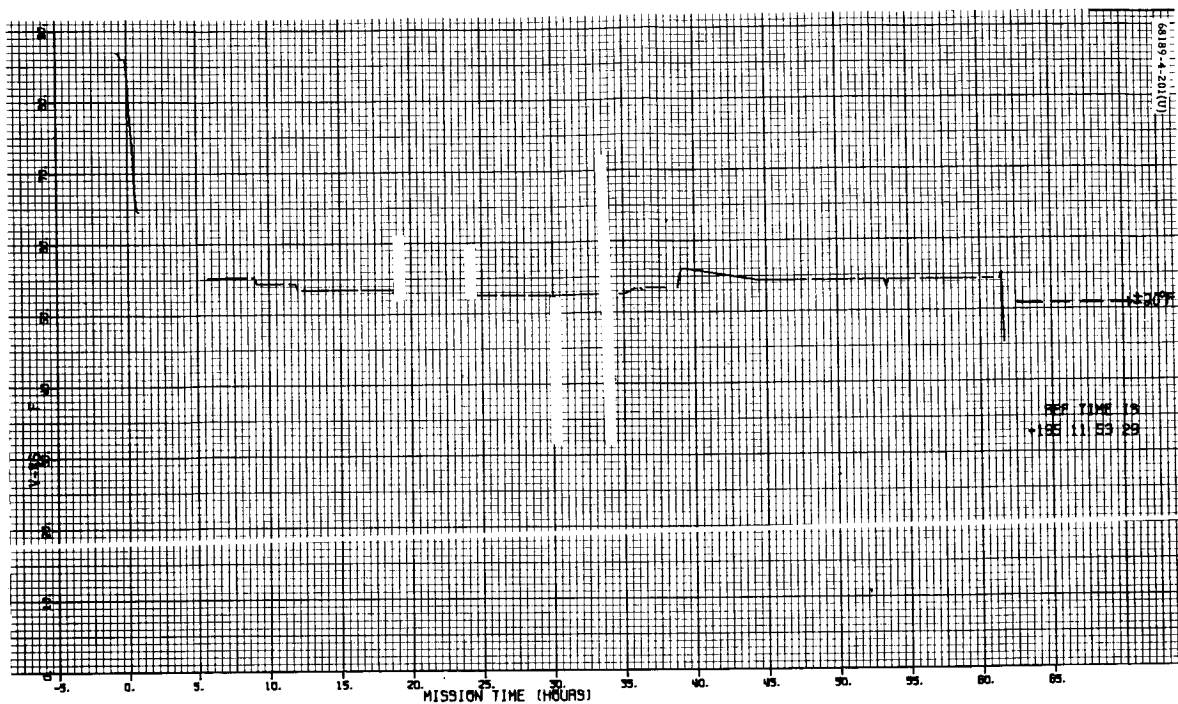
Figure 5.1-71.   Compartment B Switch 5 in Face Radiator Temperature
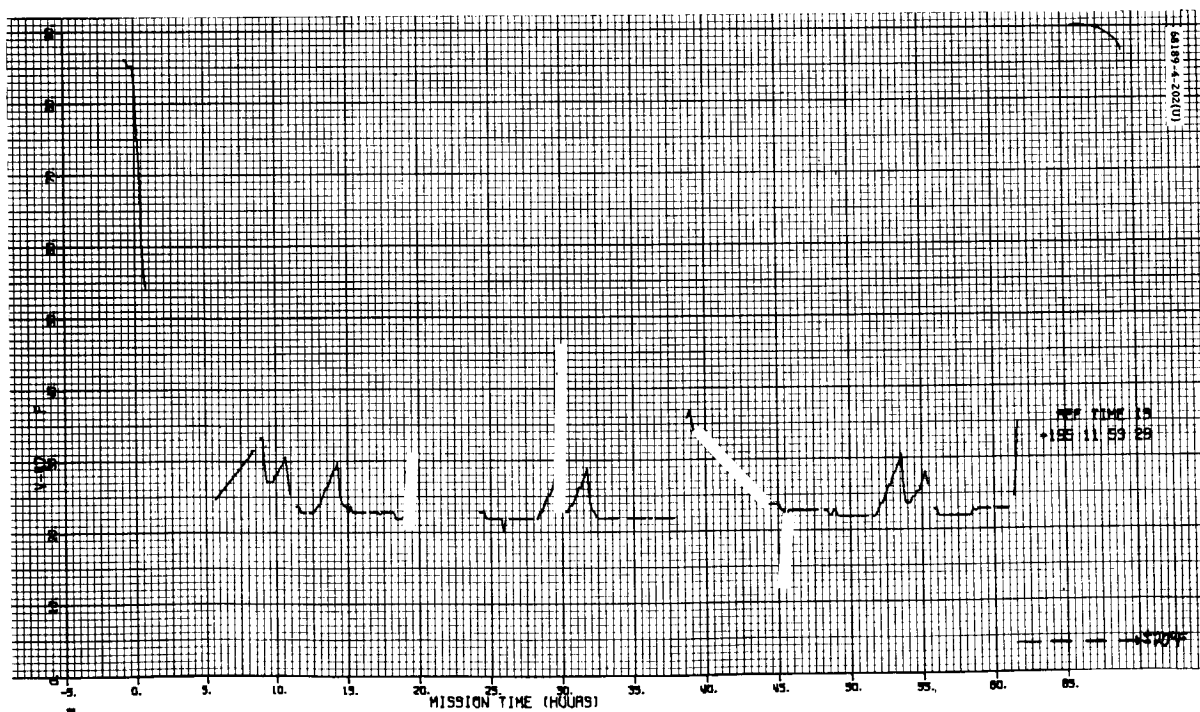

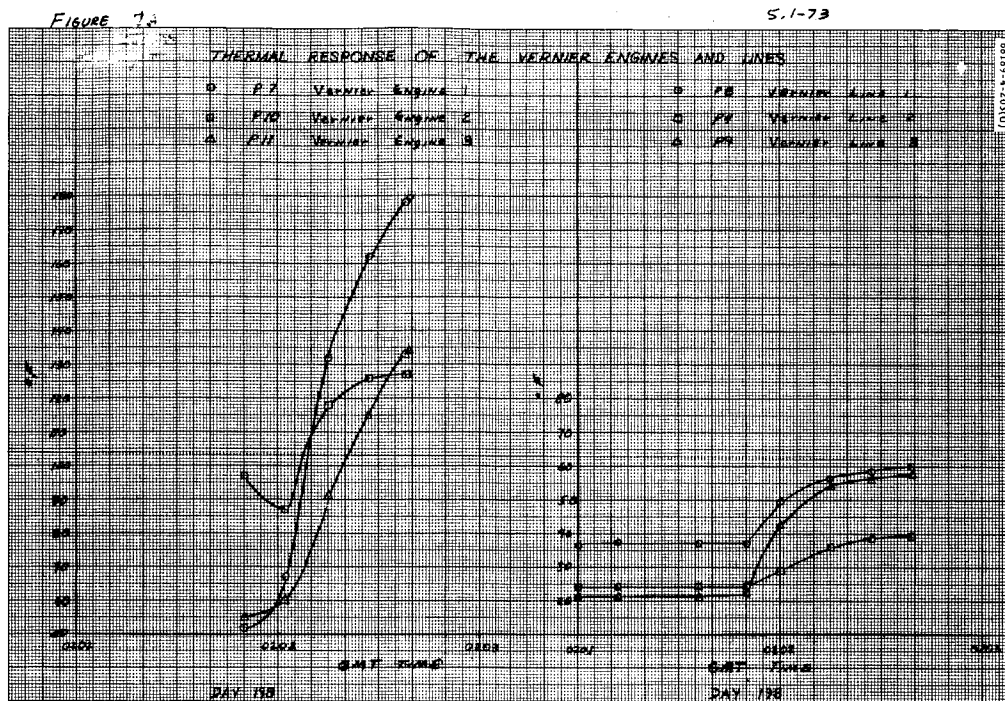Figure 5.1-72.   Compartment A Switch 2 in Face Radiator Temperature

Figure 5.1-73.   Thermal Response of Vernier Engines and Lines
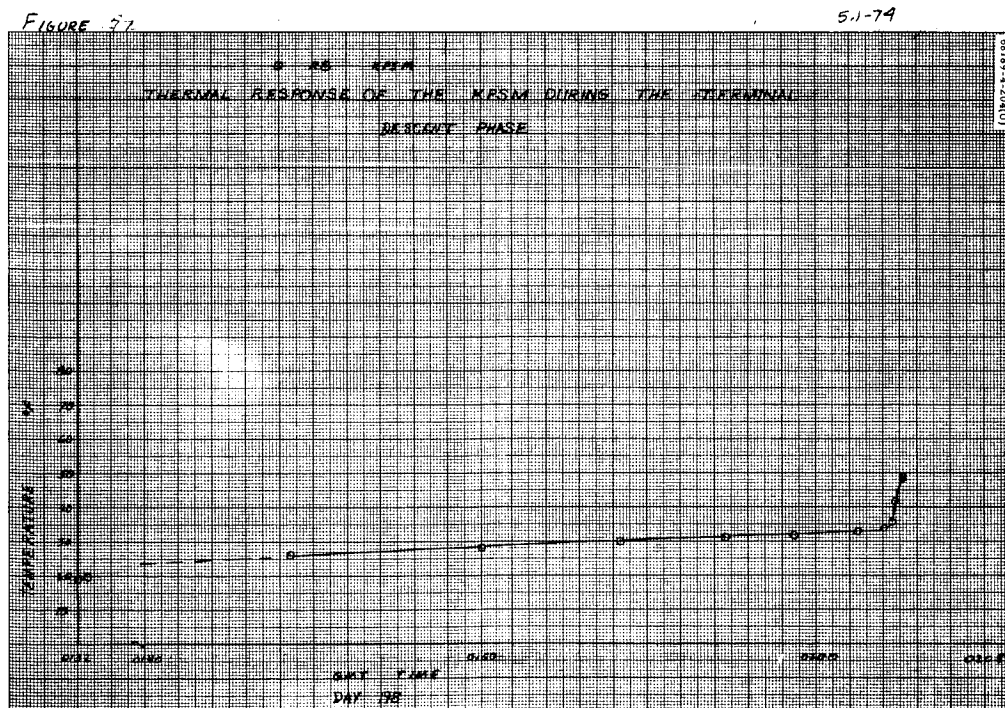
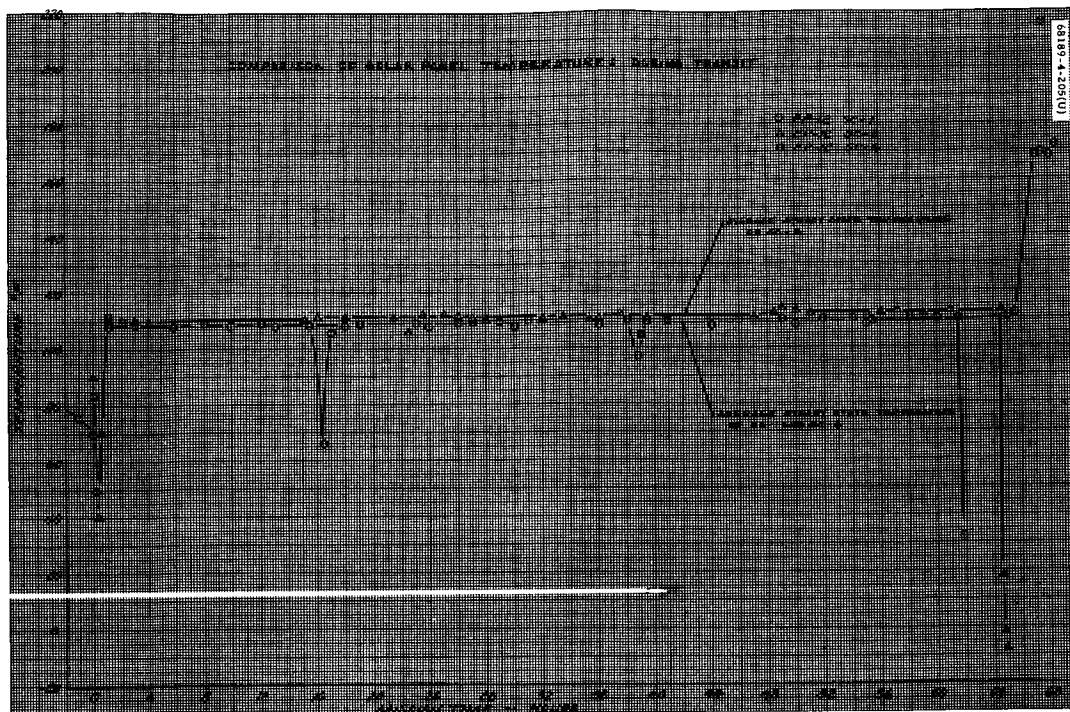Figure 5.1-74.   Thermal Response of KPSM During Terminal Descent

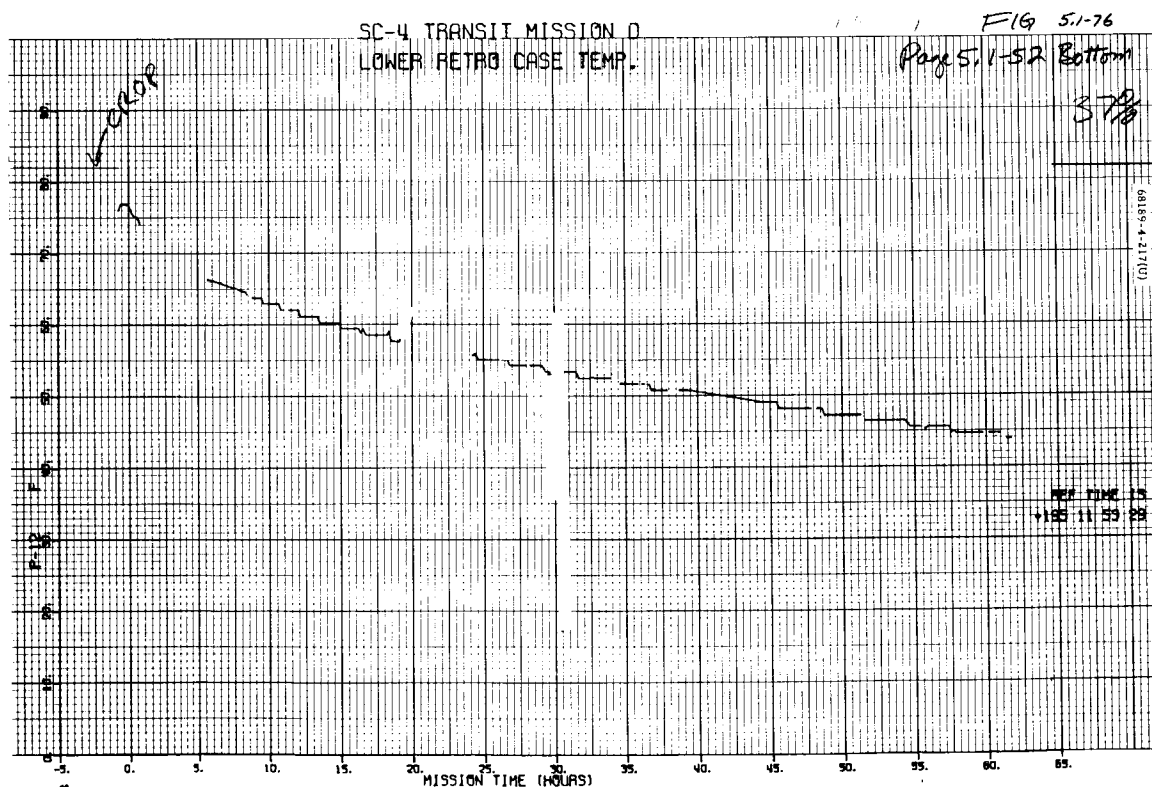Figure 5.1-75.   Comparison of Solar Panel Temperatures During
Terminal Descent

Figure 5.1-76.   Lower Retro Case Temperature

5.2 ELECTRICAL POWER SUBSYSTEM

5.2.1 INTRODUCTION

The electrical power (EP) subsystem generates, stores, converts, and controls electrical energy for distribution to other spacecraft subsystems. There are two sources for this energy: 1) storage batteries and 2) radiant energy converted directly to electrical energy used for system loads or battery charging. During transit, the primary source of power is radiant energy via the solar panels. Figure 5.2-1 shows associated equipment groupings.

The performance of the EP subsystem during the Surveyor IV flight was nominal as compared to test data and simulation analysis predictions. Subsequently, specific comparisons will be made in the body of this subsection.

Flight data were used to calculate solar panel input power and regulator efficiencies. Analysis of specific loads, comparison to prediction, and explanation of discrepancies will be made.

In Table 5.2-1, major events are presented with time in GMT for reference while using mission data processor (MDP) telemetry data. In general, the divisions of Table 5.2-1 correspond to flight phases of importance to the EP subsystem and may not correspond to flight phases in other subsections. Basically, the flight is divided into times corresponding to significant changes in electrical loads. Load changes corresponding to these flight phases are partially illustrated by the regulated current (EP-14) and more completely by the battery discharge current (EP-9).

5.2.2 ANOMALY DESCRIPTION

No anomalies were detected in the electrical power subsystem during flight. TFR 18262 was written against the abrupt loss of spacecraft signal. An engineering change was made in the power subsystem due to a possible failure mode. A single wire open in the (+) 29 volt regulated low ripple lead from the boost regulator to the transmitters and return could cause a catastrophic failure. Redundant wiring will be provided for spacecrafts 6 and 7.
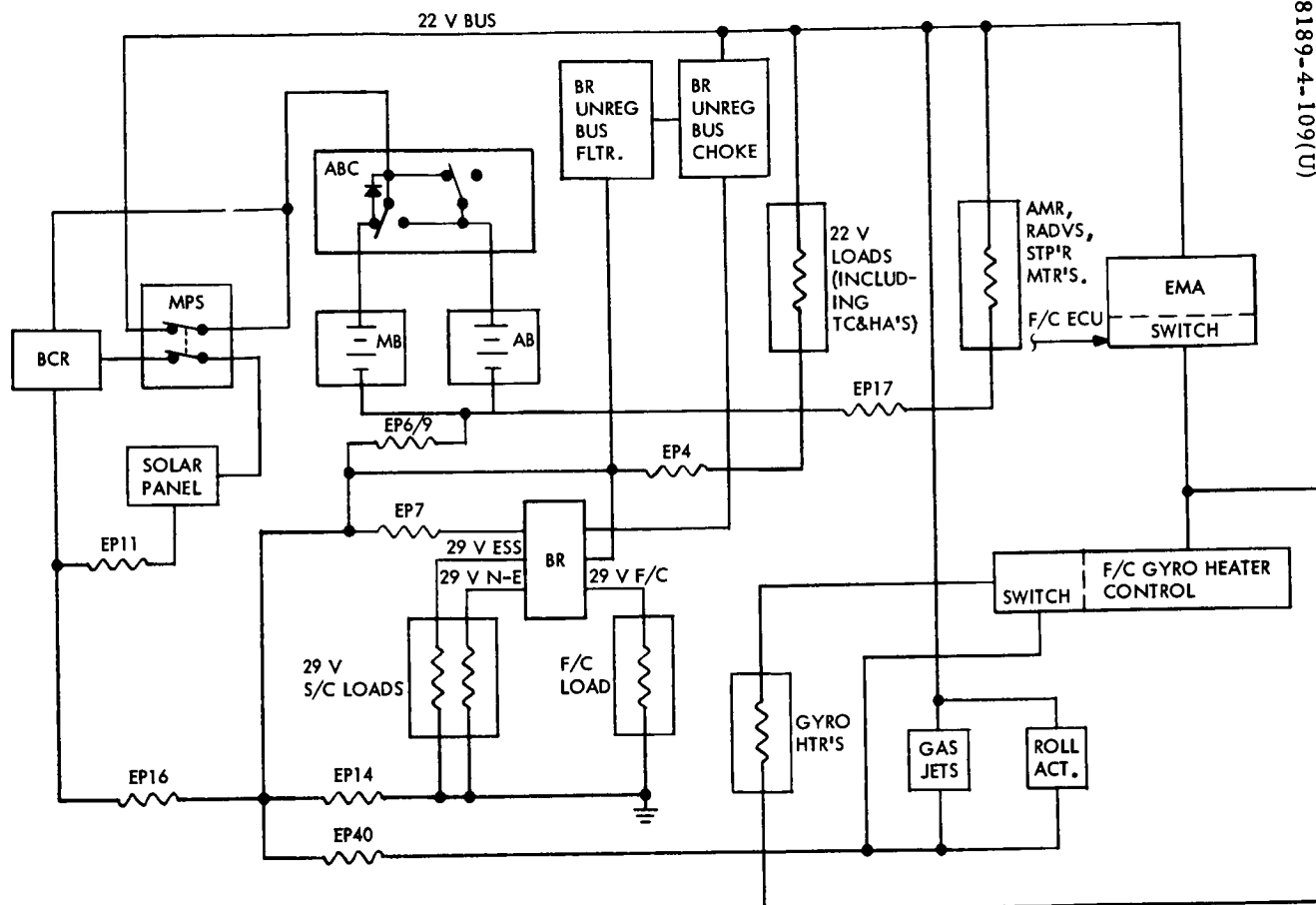
Figure 5.2-1. Power Subsystem Block Diagram, Flight Configuration

TABLE 5.2-1.   ELECTRICAL POWER EVENTS AND TIMES

GMT, day:hr:min:sec*		Comments
From	To	
195:11:53:29	195:12:05:56	Launch and separation
195:12:05:56	195:12:34:08	Transmitter high power
195:12:34:08	195:17:46:34	Coast
195:17:46:34	195:18:14:49	Coast, transmitter high power
195:18:14:49	197:02:02:18	Coast
197:02:02:18	197:02:27:53	Transmitter high power
197:02:27:53	197:02:30:29	Midcourse maneuver, transmitter high power, and flight control thrust phase power on
197:02:30:29	197:02:46:03	Transmitter high power
197:02:46:03	197:07:58:17	Coast
197:07:58:17	197:08:10:36	Coast, power mode cycling, auxiliary battery on
197:08:10:36	197:13:02:32	Coast
197:13:02:32	197:13:21:04	Coast, power mode cycling, auxiliary battery on
197:13:21:04	197:20:13:55	Coast
197:20:13:55	197:20:42:26	Coast, power mode cycling, auxiliary battery on
197:20:42:26	198:01:09:26	Coast
198:01:09:26	198:01:09:26	Transmitter high power, preretro maneuvers
198:01:57:14	198:02:02:41	Transmitter high power, AMR on, terminal descent, loss of data

*Time referenced to sending of appropriate commands.

5.2.3 SUMMARY AND CONCLUSIONS

5.2.3.1 Summary

Table 5.2-2 presents a summary of flight data for Surveyor IV compared to test data for the electrical power subsystem.

5.2.3.2 Conclusion

Operation of the electrical power subsystem was nominal throughout the spacecraft's flight.

5.2.4 ANALYSIS

The analysis considers four areas: mission telemetry plots, power loads and sources budget, comparison of flight loads and flight acceptance test loads, and cyclic loads.

5.2.4.1 Mission Telemetry Plots

Figures 5.2-2 through 5.2-11 are selected mission plots which are pertinent to the electrical power subsystem. They represent line plots of the analog signals averaged at 1-minute intervals. Consequently, due to the scale of these plots and data averaging, they give excellent information for consideration of trends in data flow. Energy load during terminal descent is averaged and will consequently indicate lower than actual. Figure 5.2-21 gives actual RADVS load, and Figure 5.2-6 gives average battery loads during terminal descent.

5.2.4.2 Power Loads and Sources Budget

Energy Used

Table 5.2-2 contains a summary of energy expended as calculated from flight telemetry and predictions indicated in Reference 1. Both the power management prediction and telemetry calculations for battery expended energy are very close (1692 versus 1663 w-hr). Energy obtained from the solar panel is very close to predicted (4336 versus 4383 w-hr) at the time of data loss.

Power Data

Figures 5.2-12 through 5.2-20 present various power parameters as calculated from flight data. The parameters are calculated directly from the following telemetry channels (averaged data):

1) Optimum charge regulator (OCR) efficiency = ((EP-2 * EP-16)/ (EP-10 * EP-11)) * 100

2) Boost regulator efficiency = ((EP-1 * EP-14)/(EP-7 + EP-14) * (EP-2)) * 100

TABLE 5.2-2. ELECTRICAL POWER SUMMARY

Item	Flight Data	Predicted or Specification
Boost regulator efficiency, percent	77	75 (minimum)
Optimum charge regulator efficiency	80	75 (minimum)
Optimum charge regulator output energy, w-hr	4336	4383
Battery energy used, w-hr	1663	1692
Total energy used	5999	6075
Flight control thrust phase power on		
Regulated, watts	33.55	34.22
Unregulated, watts	6.25	7.34
AMR on, watts	35.2 ± 2.2	31.6
AMR enable, watts	40.7 ± 12.3	41.5
RADVS power on, watts	501	551
Vernier ignition		
Midcourse, watts	34.8	39.6
Terminal descent, watts	35.6 ± 1.5	39.6
Vernier line 2 heater, watts	6.6	6.6
Altitude marking radar heater, watts	4.84	5.04
Gyro heater, watts	11.7	11

3) Shunt unbalance current = (EP-9 + EP-16 + EP-17)
    - (EP-4 + EP-40 + EP-14 + EP-7)

4) Regulated power = EP-1 * EP-14

5) Unregulated power = EP-2 * (EP-4 + EP-40)

6) Solar panel power = EP-10 * EP-11

7) Total loads = (EP-9 + EP-16 + EP-17) * EP-2

Figures 5.2-12 and 5.2-13 present mission plots of OCR and boost regulator efficiencies, respectively. The OCR efficiency is approximately 80 percent and the boost regulator efficiency, approximately 77 percent.

Figure 5.2-14 shows the shunt unbalance current throughout the flight. The current is generally biased at about +0.4 ampere.

Figure 5.2-15 is a plot of solar panel power received for 63.5 hours. This represents an energy input of approximately 4521 w-hr — average solar panel power of (88 watts) x (OCR efficiency of 80 percent) x (61.6 hours).

Figure 5.2-16 is a mission plot of unregulated power; Figure 5.2-17 is a similar plot of regulated power. Figure 5.2-18 is a sum of regulated and unregulated power.

Figure 5.2-19 shows the total loads for the electrical power subsystem for the entire Surveyor IV flight. Total energy used during the flight can be estimated from this plot.

Figure 5.2-20 shows total power consumed as well as the sum of regulated and unregulated loads throughout the flight.

5.2.4.3 Comparison of Flight Loads and Flight Acceptance Test Loads

Comparison of telemetry-measured and flight acceptance test-measured loads (Reference 3) will be made for selected units, various heaters, and large current drains.

Selected Equipment Loads

Results of comparing flight and test specification selected equipment loads are presented in Table 5.2-3. The loads and equipments considered are as follows:

1) Flight Control Thrust Phase Power On. Command 0727 is within specification.

2) RADVS Power On. Command 0637 applies power to the RADVS. The power consumed is close to that expected. Figure 5.2-21 (EP-17, radar and squib current) shows the current profile. The average value of EP-17 was about 24.4 amperes.

TABLE 5.2-3. SELECTED EQUIPMENT LOADS

Command(s)*	Command Time, GMT	Current, milliamperes		Power, watts	
	day:hr:min:sec	Flight	Specification (Reference 2)	Flight	Specification (Reference 2)
Flight control thrust phase power on	198:01:58:16				
R 0727		1160	1180	33.55	34.22
U 0727		293	470	6.25	10.34
Vernier ignition					
U 0721	198:02:30:02	1680 ± 5	1800	34.82 ± 0.12	39.6
U 0721	198:02:01:58	1710 ± 070	1800	35.6 ± 1.5	39.6
AMR on	198:01:57:17				
U 0626		1640 ± 100	1439	35.26 ± 2.2	31.6
AMR enable	198:02:00:17				
U 0625		1910 ± 580	1886	40.7 ± 12.3	41.5
RADVS power on	198:02:02:01				
U 0637		24310	29000	501	551

*R = regulated; U = unregulated.

5.2.4.4 Cyclic Loads

Gyro Heater

The periodic loading that occurs in EP-40 contains gyro heater effects. The gyro heaters have a short on-off cycle when compared to the altitude marking radar (AMR) and vernier line heaters (EP-4). Each gyro heater load is approximately 0.5 ampere, which compares favorably to the flight acceptance test data.

AMR and Vernier Line Heaters

Figure 5.2-22 is a plot of EP-4 at 20 min/in. Gyro heater effects are averaged out in this plot. The cyclic load effects of the AMR and vernier line 2 heaters are apparent. Only the AMR and vernier line 2 heaters are cyclic at this time. The vernier line 2 heater uses approximately 300 milliamperes, and the AMR heater draws about 220 milliamperes. This agrees favorably with test data, indicating that vernier line heater 2 should draw about 300 milliamperes and that the AMR heater should draw about 230 milliamperes.

5.2.5 REFERENCES

1. "Surveyor Mission D Space Flight Operations Report," Hughes Aircraft Company, SSD 74109, August 1967.

2. J. Mundy, "System Specification Power Management Data Summary SC-3 Spacecraft," Hughes Aircraft Company, No. 3023930, Revision A, 14 February 1967.

5.2.6 ACKNOWLEDGMENTS

W. McIntyre, Technical coordinator and writer

J. Berger, Signal processing
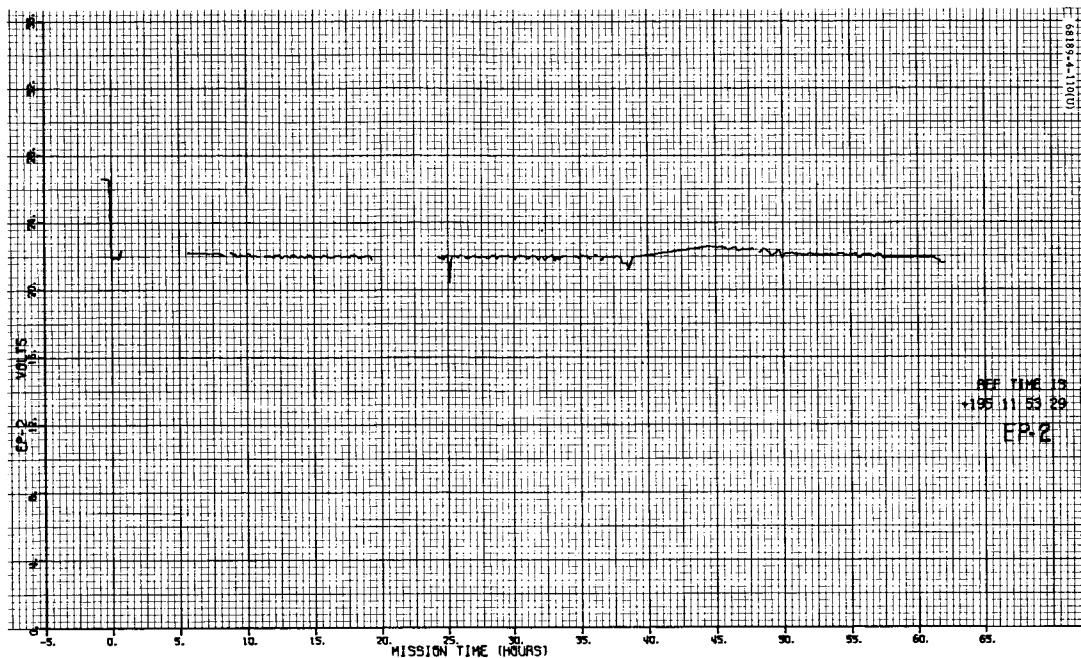
Figure 5.2-2. Unregulated Bus Voltage
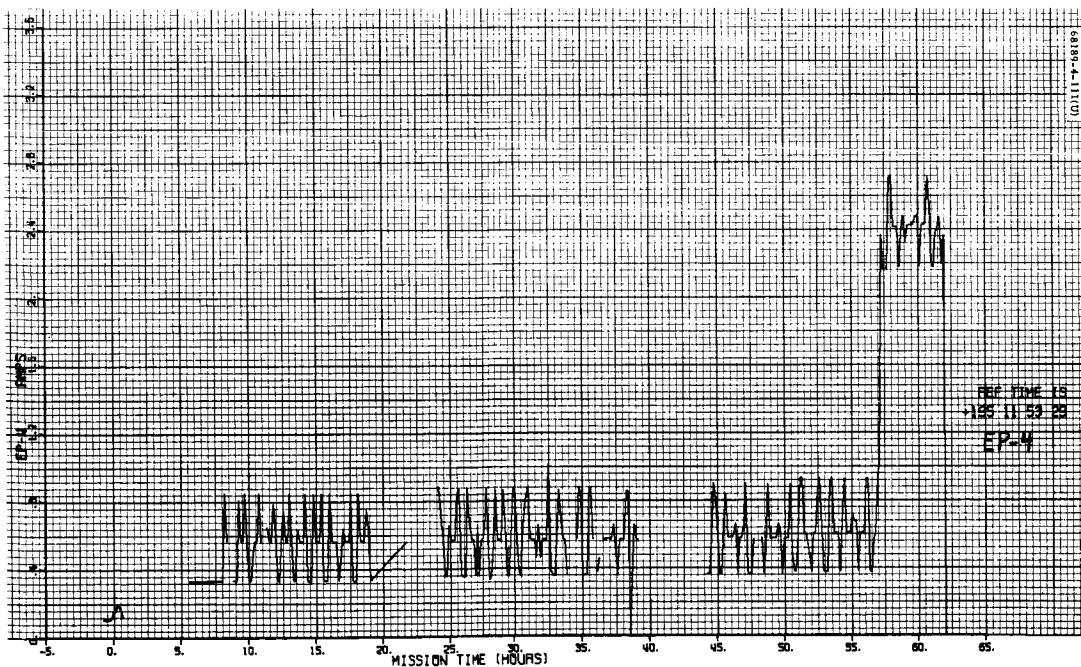
Figure 5.2-3. Unregulated Output Current (EP-4)
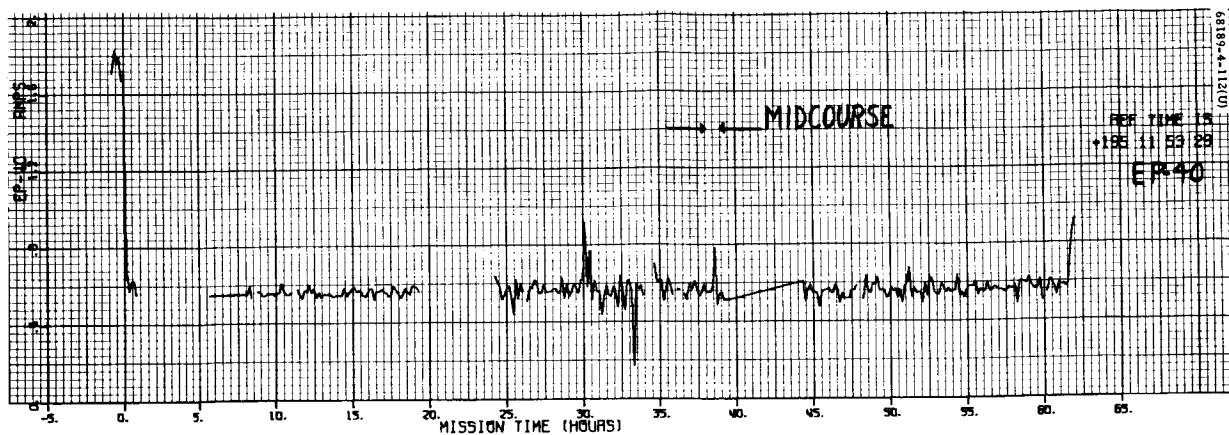
Figure 5. 2-4.   Flight Control Unregulated Current (EP-40)
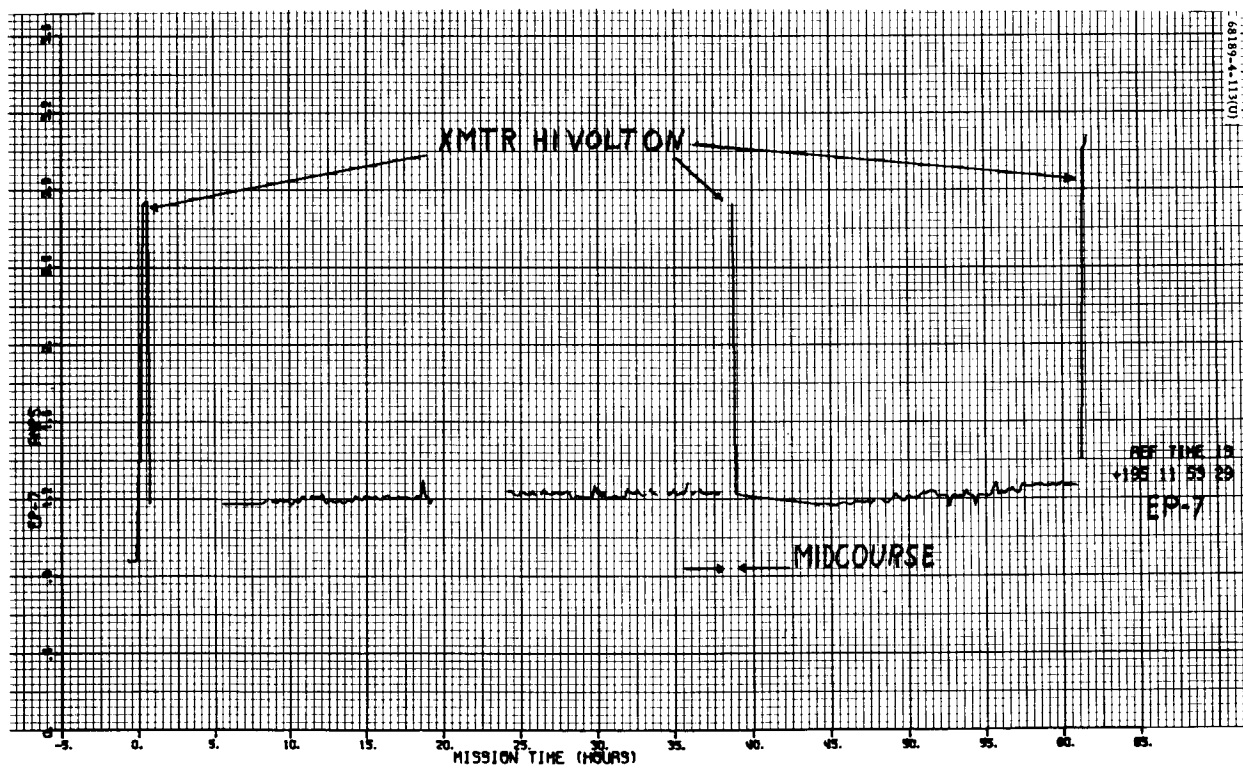
Figure 5. 2-5.   Boost Regulator Difference Current
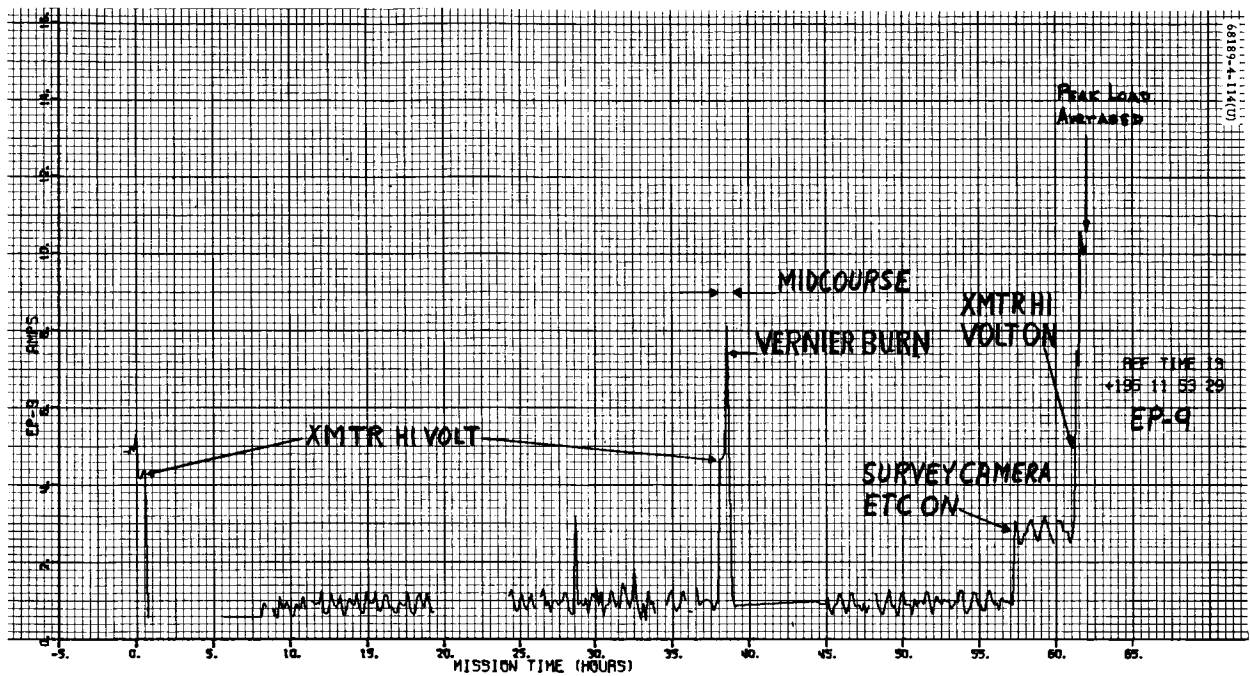
Figure 5.2-6.   Battery Discharge Current
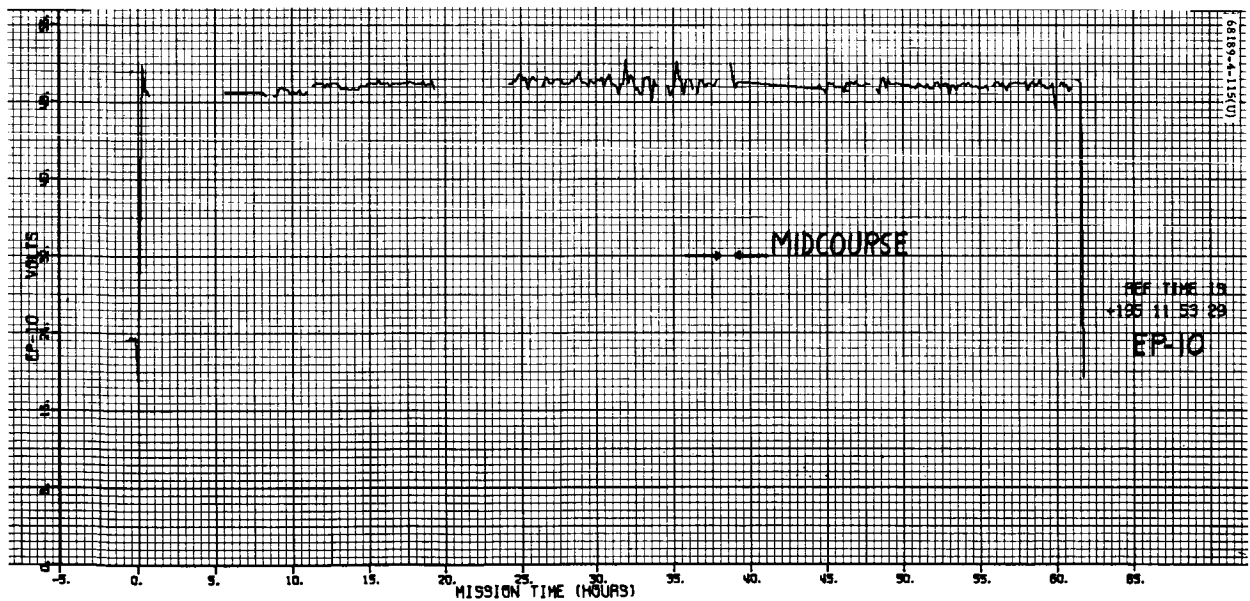
Figure 5.2-7.   Solar Cell Array Voltage
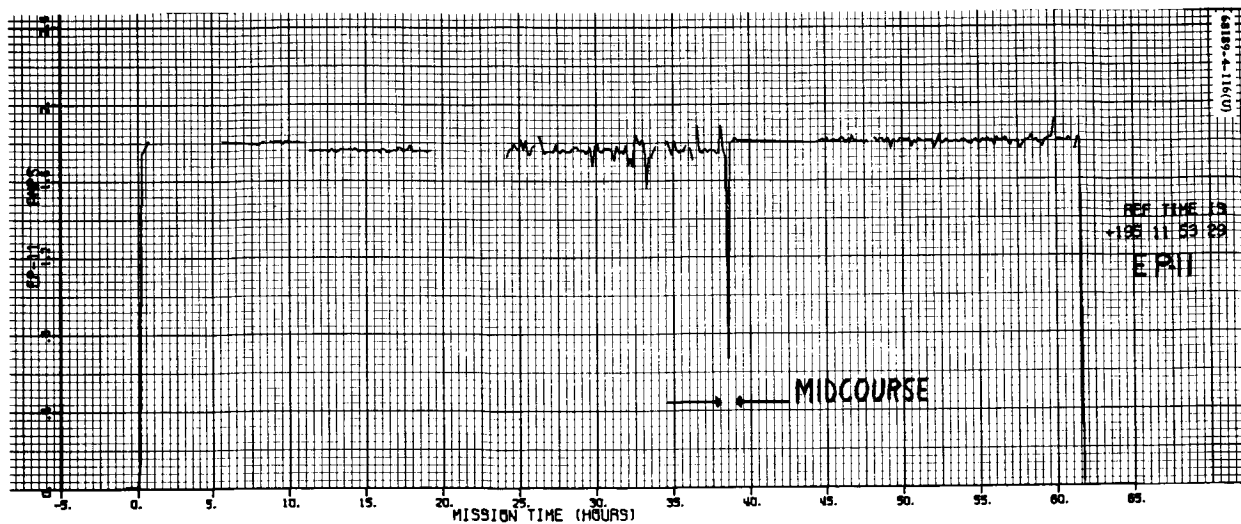
Figure 5.2-8.   Solar Cell Array Current
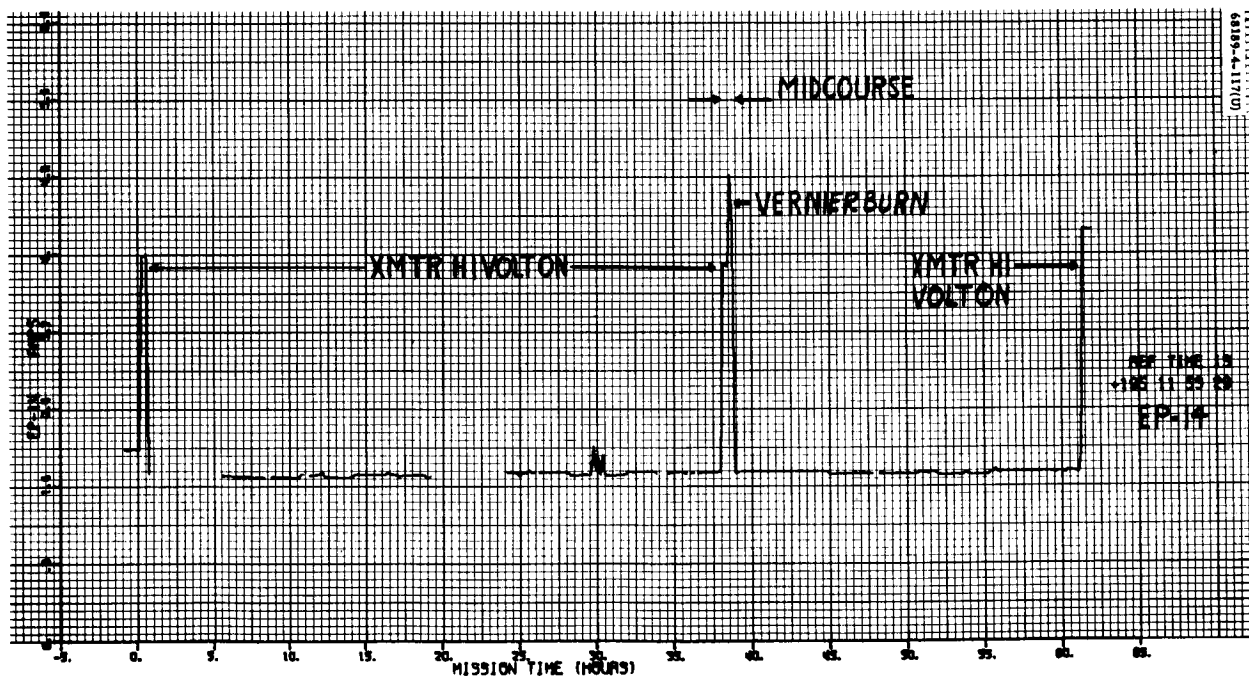
Figure 5.2-9.   Regulated Output Current
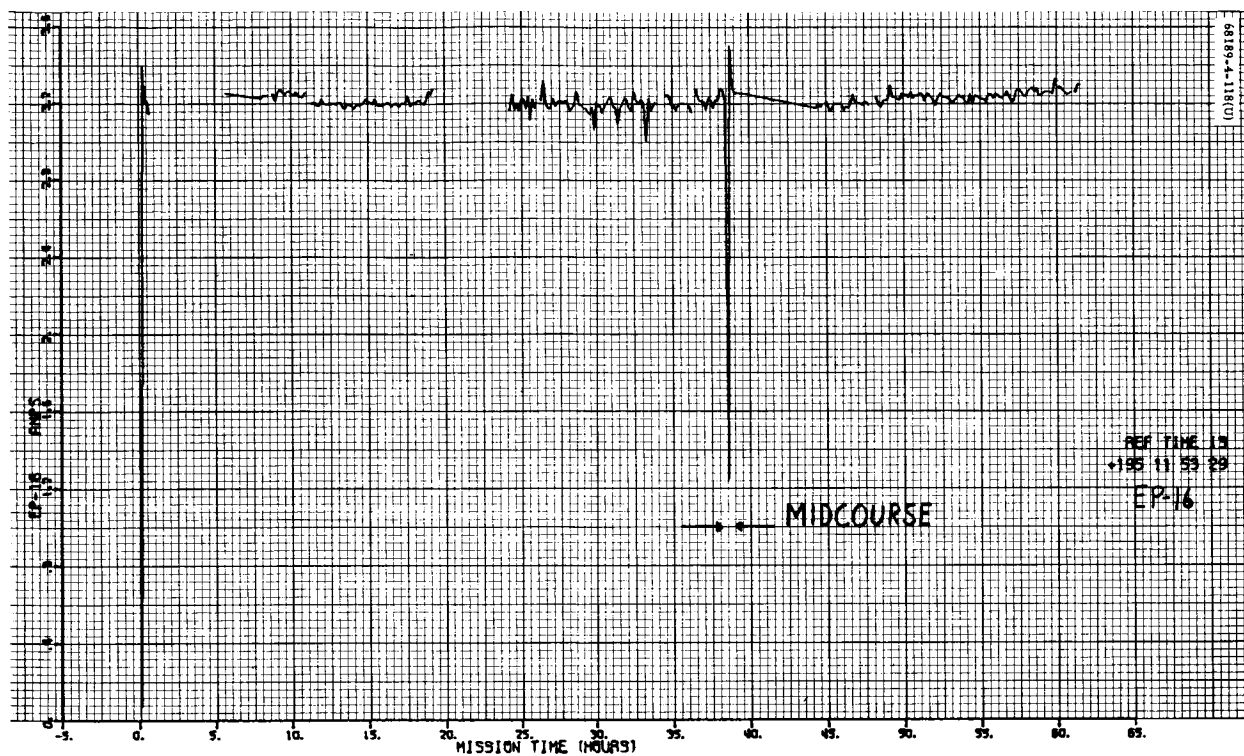
Figure 5.2-10.   Optimum Charge Regulator Output Current
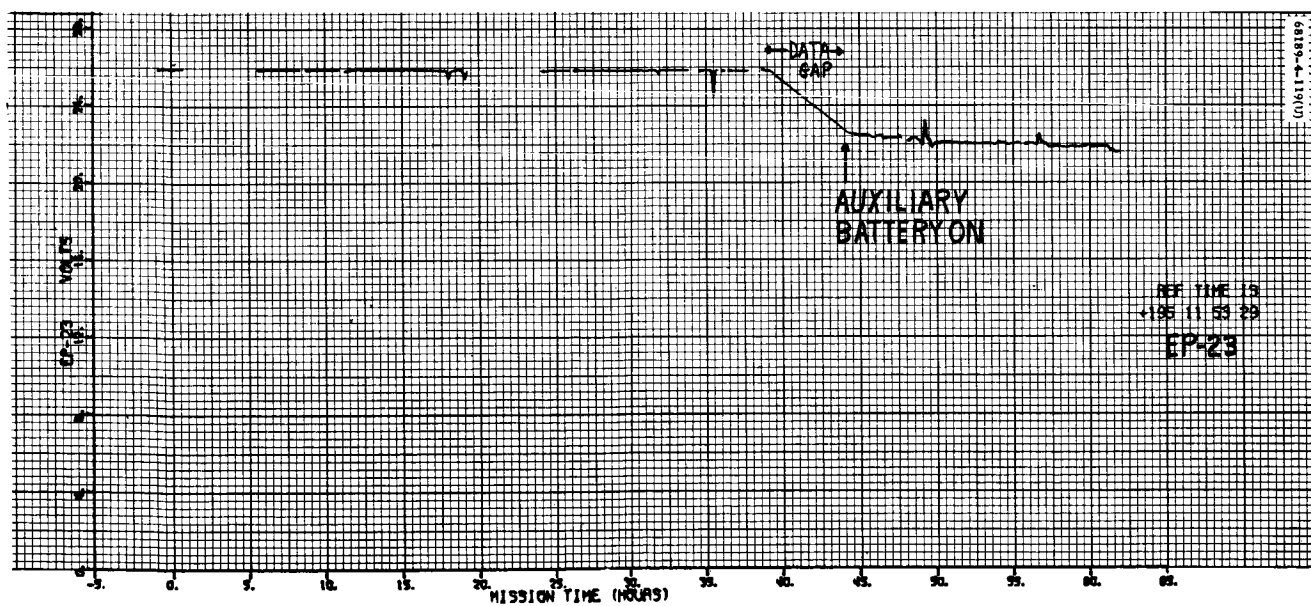
Figure 5.2-11.   Auxiliary Battery Voltage
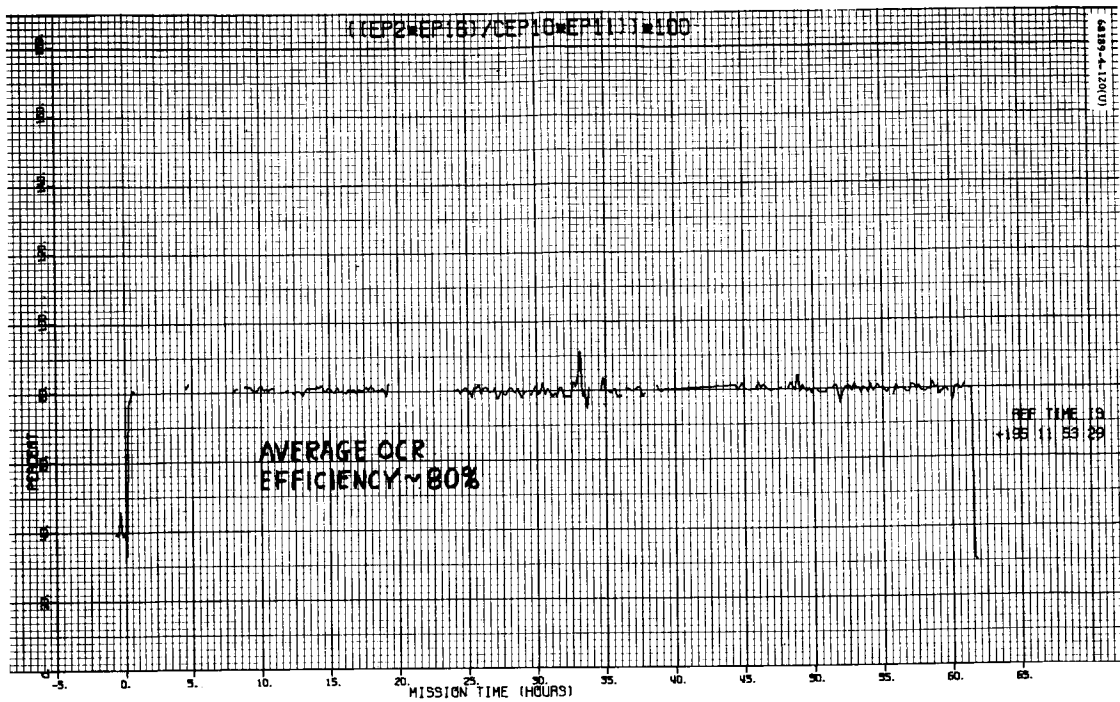
Figure 5.2-12. Optimum Charge Regulator Output Current
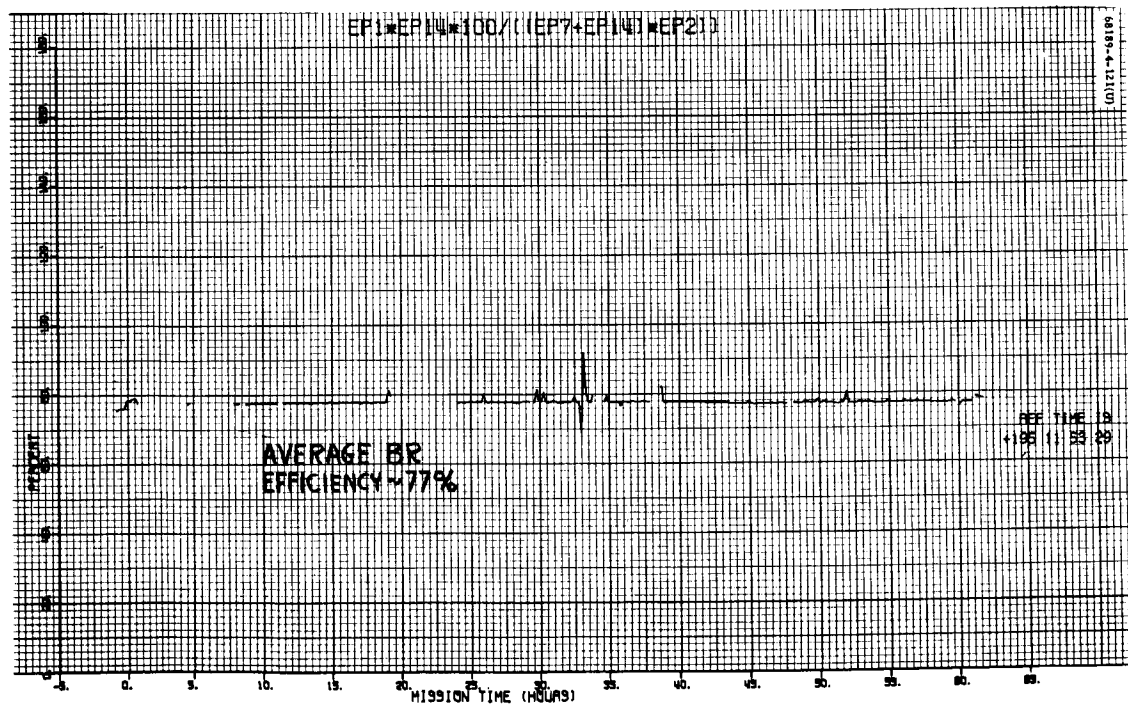
Figure 5.2-13. Boost Regulator Efficiency
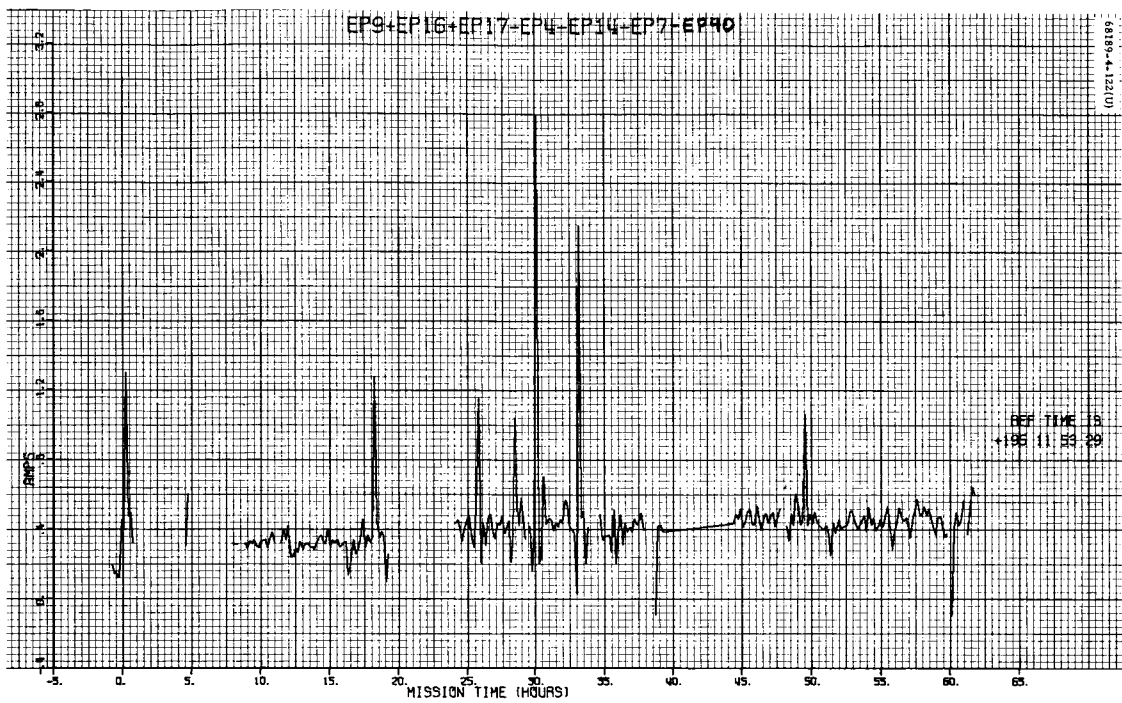
Figure 5.2-14. Shunt Unbalance Current

Figure 5.2-15. Solar Panel Power

Figure 5.2-16.   Unregulated Power
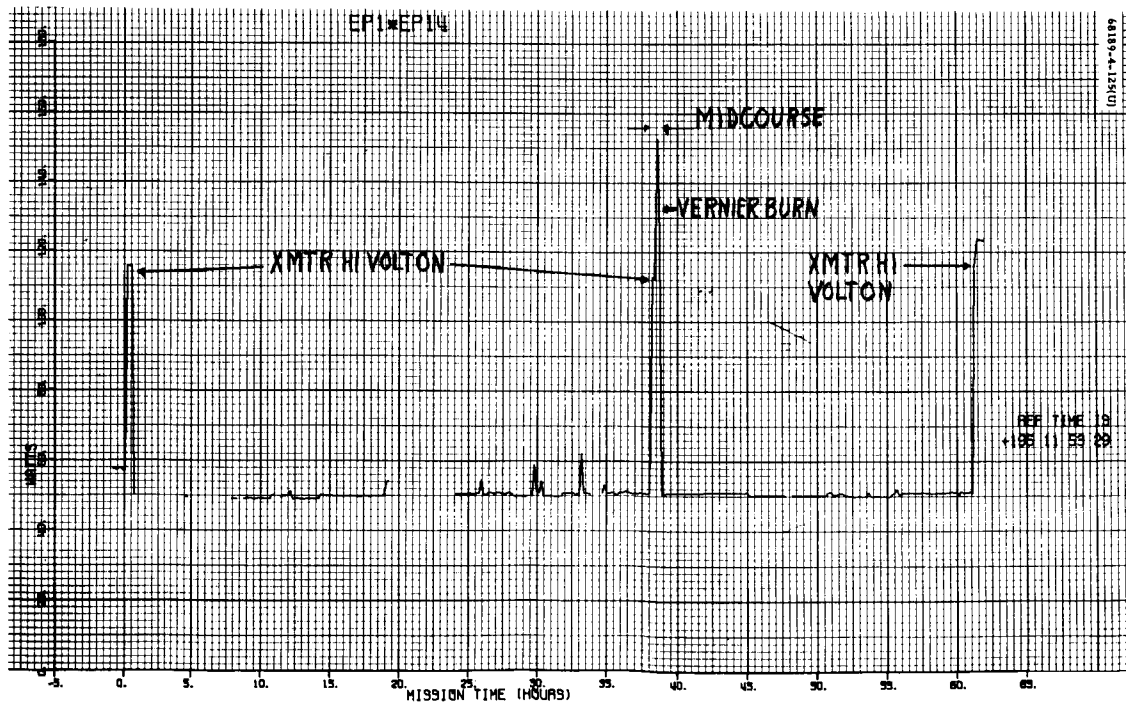
Figure 5.2-17.   Regulated Power
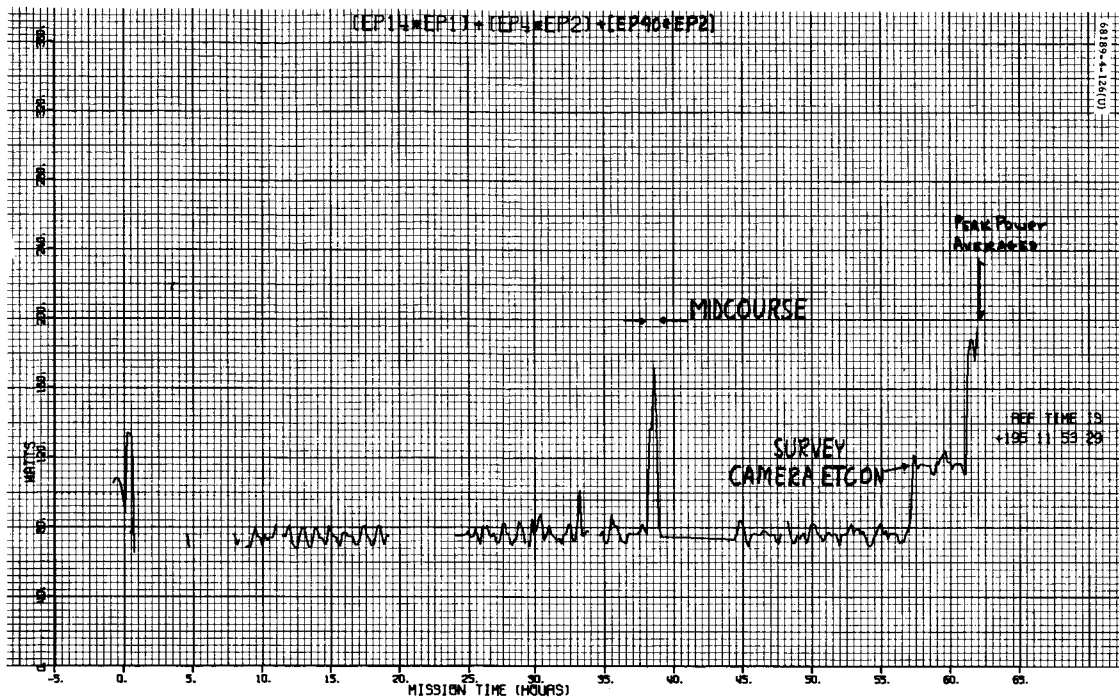
Figure 5.2-18.   Total Power
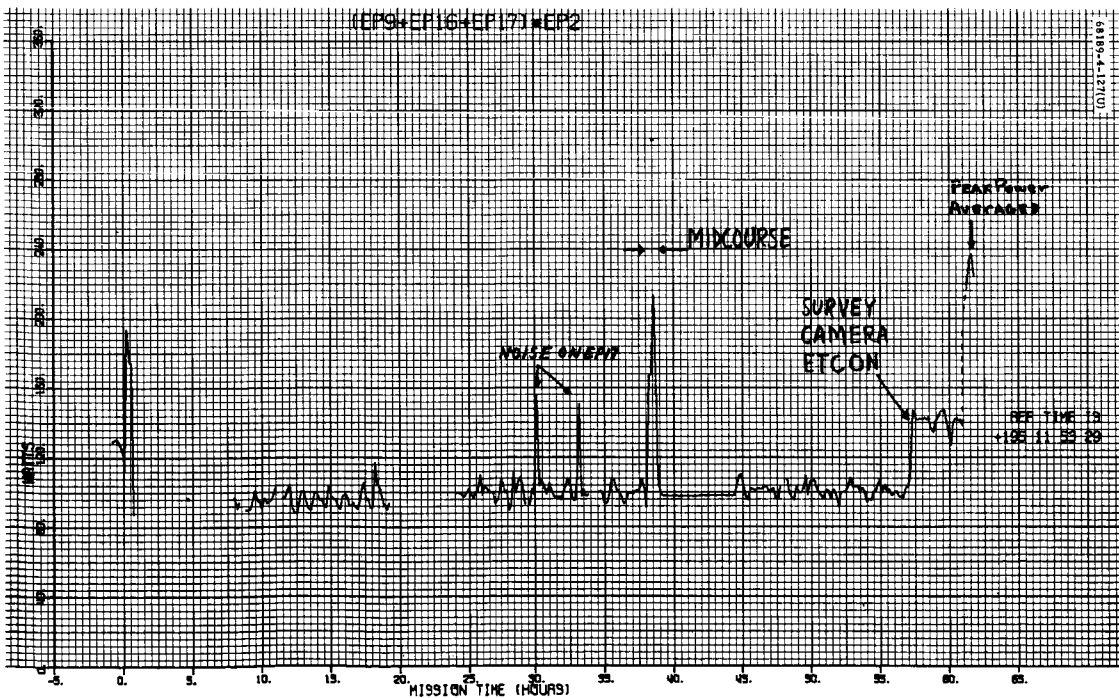
Figure 5.2-19.   Total Loads
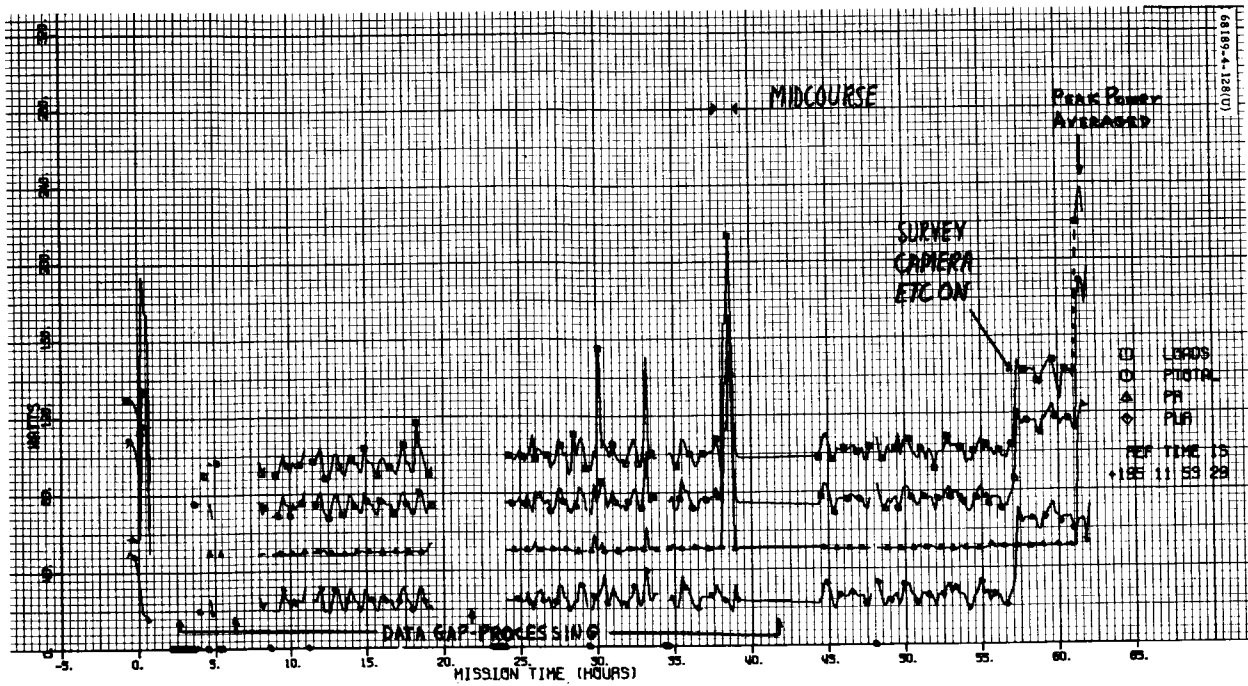
Figure 5.2-20. Power Consumed and Loads
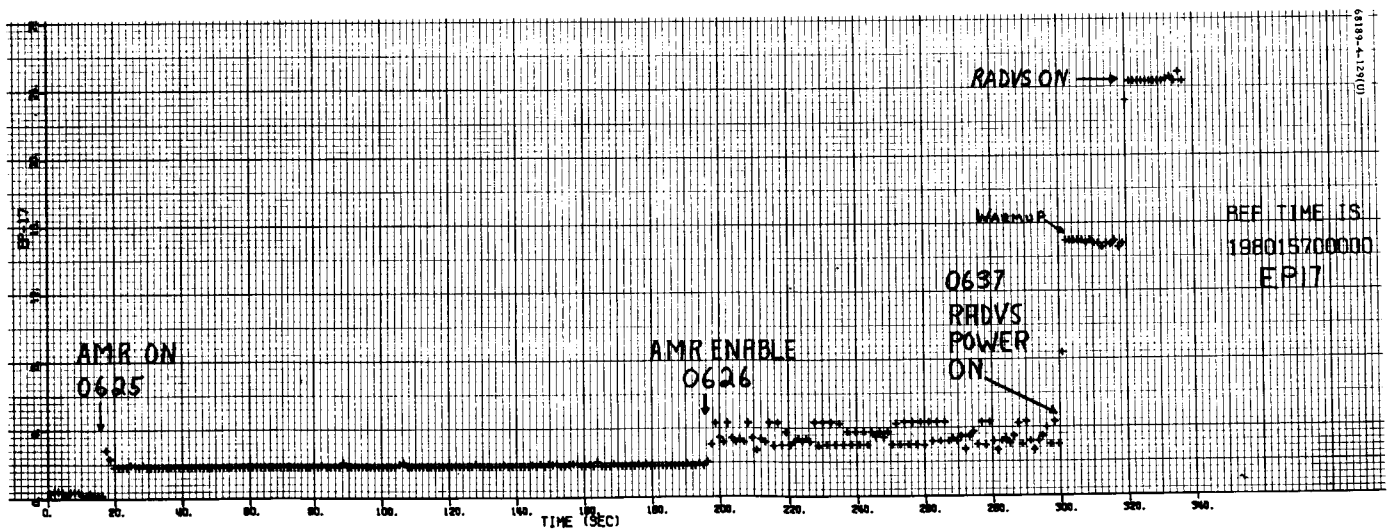
Figure 5.2-21. Radar and Squib Current (RADVS Power On)
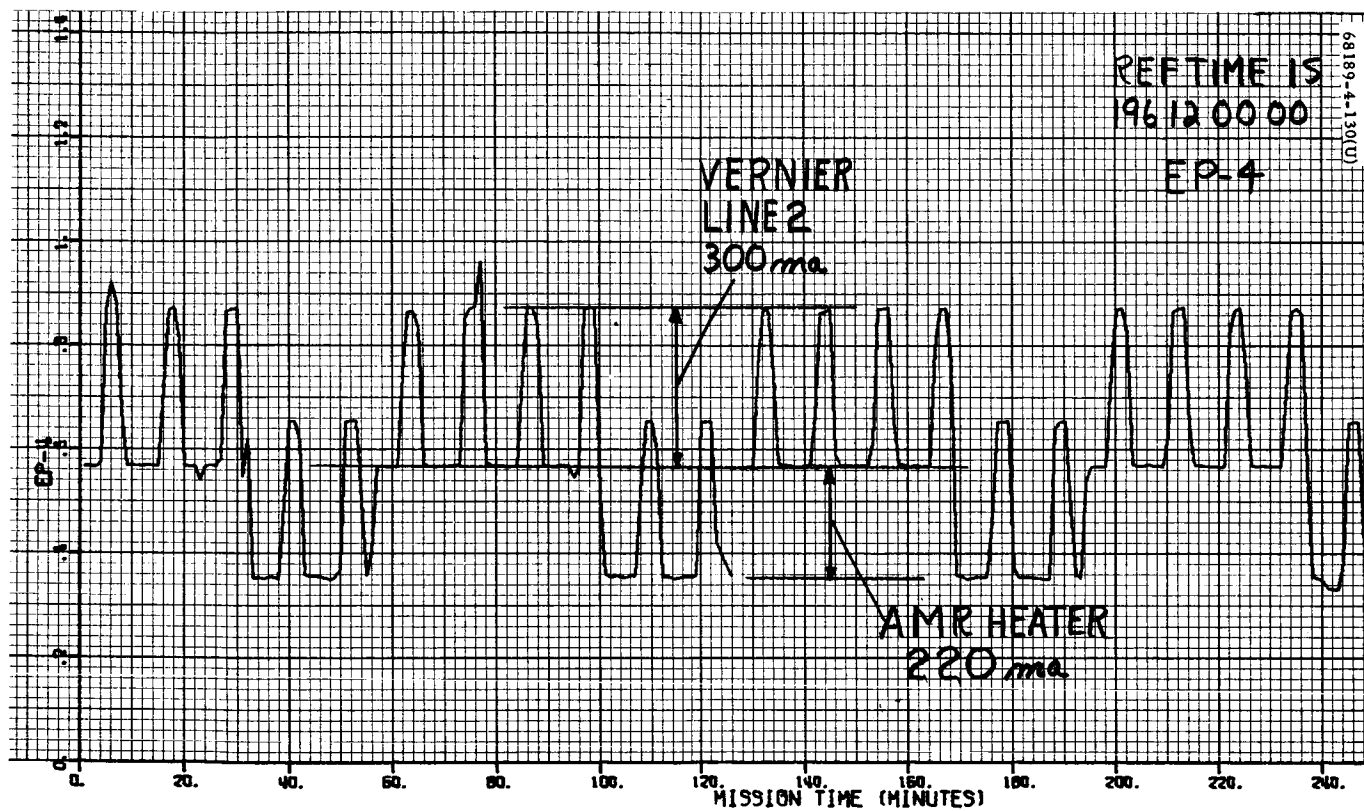
Figure 5. 2-22.   Unregulated Output Current — Coast Phase I

5.3 RF DATA LINK SUBSYSTEM

5.3.1 INTRODUCTION

This section contains a summary and analysis of the performance of the data link subsystem during Surveyor Mission D.

The data link subsystem consists of the transmitters, transponders, receivers, command decoders, and antennas. It is the function of this subsystem to: 1) provide engineering data transmission from the spacecraft at bit rates compatible with specific mission phases, 2) provide analog data, such as that from television and strain gauges, at signal levels high enough for proper discrimination, 3) provide phase coherent two-way doppler for tracking and orbit determination, and 4) provide command reception capability throughout the mission to allow for complete control of the spacecraft from the ground. A simplified block diagram of the communications subsystem is shown in Figure 5.3-1.

The pertinent subsystem units on the spacecraft during the mission are as follows:

Unit	Part Number	Serial Number
Receiver A	231900-3	17
Receiver B	231900-3	25
Transmitter A	263220-5	12
Transmitter B	263220-5	23
Command decoder unit	232000-5	5

Unlike most subsystems, individual data link subsystem parameters, such as losses, threshold sensitivity, modulation index, etc., are not measured or individually determined from mission data. The composite effect of these parameters on the performance is measured as received signal power at the spacecraft and the tracking station (DSS) and as telemetry and command error rates. Consequently, it is impossible to compare individual link parameters to specified performance criteria. The best that can be done is to compare measured signal levels to predicted levels, and telemetry quality and command capability to predicted capabilities. To further cloud the analysis, omnidirectional antenna gain is a major contributor to the uncertainty in received signal levels. Accurate omnidirectional antenna gain
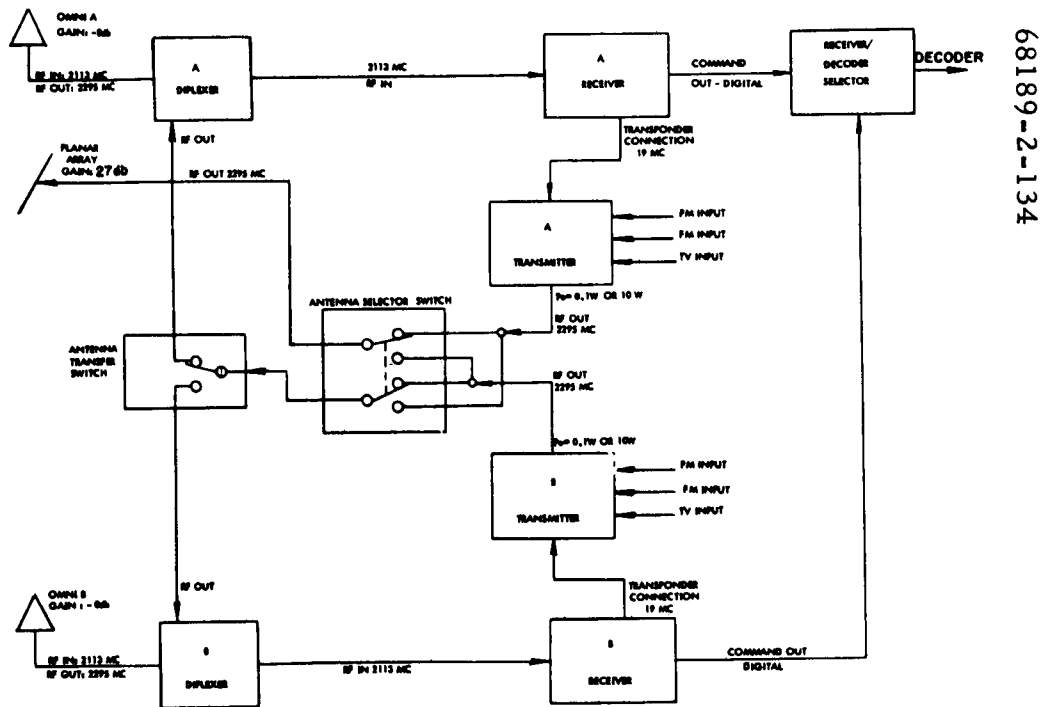
Figure 5.3-1.   Communications Subsystem Block Diagram

measurements are difficult to achieve and, in most cases, deviations from predictions can most likely be attributed to antenna gain uncertainty. Because of the problems outlined above, analysis of the data link subsystem performance will, in general, be a qualitative analysis of the performance of the entire subsystem rather than a quantitative assessment of the performance of the individual subsystem parameters. Equally as important as subsystem performance evaluation in this analysis is the qualitative assessment of the premission and real-time prediction techniques used during the mission, since future missions must rely on these techniques as guidelines during the real-time operation.

In general, the RF data link subsystem performed as expected. The single exception was the performance of receiver B, which, while still within the expected tolerance region, exhibited approximately a -5 db offset from the predicted nominal receiver signal level profile values. All other subsystem units performed very close to the nominal predictions.

The data contained in this report consist of spacecraft telemetered, DSS, and mission event time data. Where meaningful, the data are correlated to and compared with equipment specifications, previous test data, preflight predictions, and in-flight analysis predictions. Specifically, this section contains the following discussions which are shown with the appropriate subsection notation:

Anomaly Discussion (subsection 5. 3. 2) — This subsection primarily contains a discussion of three topics:

1)   The -5 db offset in receiver B received signal levels.

2)   A simultaneous loss of ground receiver lock at both DSS-51 and DSS-11 during the station transfer on day 196.

3)   Determination of the loss of signal signature during retro engine firing at terminal descent.

Summary and Conclusions (subsection 5. 3. 3) — This subsection contains a summary of subsystem performance with conclusions relative to performance and postflight analysis.

Subsystem Performance Analysis (subsection 5. 3. 4) — This subsection contains the following items:

1)   General discussion of data, equations used, and path of the earth vector relative to omnidirectional antenna gain contours.

2)   Discussion of subsystem performance during specific mission phases.

3)   Discussion of pertinent subsystem telemetry signals plotted as a function of time from launch.

The major mission event times relative to the RF data link subsystem are tabulated in Tables 5.3-1 and 5.3-2. Table 5.3-1 contains telemetry mode and bit rate, primary tracking station number, and station automatic gain control values as a function of time. Table 5.3-2 contains a tabulation of the subsystem configuration as a function of time. Both tables cover the mission from launch to the time of loss of signal during retro engine firing at terminal descent. Also, in some cases, the times in these tables are accurate only to the nearest minute.

TABLE 5.3-1. TELEMETRY MODE SUMMARY

GMT, hr:min:sec	Mode	Bit Rate	DSIF Station	DSIF, AGC-dbm	Telemetry Margin, db	Comments
Day 195						
11:53:29	5	550	(Low mod index SCO)			Launch
12:09:56			72			Rcvr 1 in lock
12:10:22						Rcvr 2 in lock (SAA)
12:10:45						Decom lock
12:12:08						Auto track (rcvr 1 on SCM)
12:12:24						Gnd xmtr on
12:12:24						Signal in passband rcvr A
12:12:30				-90/-102		DSS rcvr 1/rcvr 2
12:13:07						Signal in passband rcvr B
12:13:43						DSS-72 two-way lock
12:15:50				-102		Rcvr 2
12:16:48			51			Reports reception of signal
12:16:53				-122.2		Rcvr 2 in lock — SAA/paramp
12:16:53						Rcvr 1 in lock
12:17:24			72			Dropped up link
12:18:30			51			Auto track SAA/ paramp
12:18:50			72			Rcvr 1/SCM/auto track
12:19:00			51			Decom lock
12:19:22			72			Cmd mod on
12:20:00						DSS-72 cannot confirm two-way
12:20:00			51	-85/-121		Rcvr 1/rcvr 2
12:20:50			72			Cmd mod off to reacquire
12:21:45			51			Reports both rcvs out of lock

Table 5.3-1 (continued)

GMT, hr:min:sec	Mode	Bit Rate	DSIF Station	DSIF, AGC-dbm	Telemetry Margin, db	Comments
12:21:46			72	-103/-130.5		Rcvr 1/rcvr 2 two-way lock
12:21:54			51			Rcvr 2 in lock
12:22:05			51			Rcvr 1 in lock
12:22:07			51			Decom in lock
12:22:10			51			Auto SCM
12:25:00			51	-85		Rcvr 1
12:25:15			72			On synthesizer
12:25:28			72			One-way
12:25:50			51	-90		
12:25:52			72			DSS-72 reports out of lock
12:26:41			72			Two-way/cmd mod on
12:30:00			51	-90.2/120.5		Rcvr 1/rcvr 2
12:31:40			72			DSS-72 reports loss of data
12:32:25			72	-107/-135		Rcvr 1/rcvr 2
12:29:59	5	1100				
12:34:15						Xmtr B low power
12:34:15			51			DSS-51 reports both rcvrs out of lock
12:34:41			72	-135		Rcvr 1 (rcvr 2 threshold)
12:34:41						DSS-51 reports both rcvrs in lock
12:36:30			51	-113		
12:40:00			51	-115.3		Rcvr 1
12:40:11			72			Rcvr 2 to 50-Hz bandwidth
12:41:32	1					
12:42:00				-134		
12:42:35				-135		Rcvr 1 (rcvr 2 out of lock)
12:43:17						Decom in and out of lock
12:43:40	4					
12:46:48	2					Decom in and out of lock
12:46:50						Difficulty maintaining RF lock
12:48:30						Cannot confirm two-way
12:49:00			51	-119.2		
12:49:49	6					

Table 5.3-1 (continued)

GMT, hr:min:sec	Mode	Bit Rate	DSIF Station	DSIF, AGC-dbm	Telemetry Margin, db	Comments
12:50:10			72	-136		Rcvr 1 (rcvr 2 out of lock)
12:50:12						Good two-way lock
12:51:46	5					
13:00:00			51	-122.3		
13:03:47			72			Cmd mod off for xfer to DSS-51
13:10:00			51			Xmtr on
13:10:25				-127.3	+11.3	
13:12:18						Exciter on track syn freq
13:12:44						Cmd mod on
14:00:00				-128.0	+10.6	
14:29:36						Tuning to new syn freq
14:31:18						Exciter locked to synthesizer
15:00:00				-129.7		
16:00:00				-132.6		
16:30:30				-133.2	+ 5.6	
16:54:00						Cmd mod off
17:00:00				-133.8	+ 5.0	
17:00:02						Xmtr off for xfer to DSS-61
17:11:00			61	-133.1	+ 5.7	
17:27:02	4					
17:29:08	2					
17:31:02	1					
17:33:21	5					
17:46:13				-135.3		
17:47:20				-114.0		Xmtr B high pwr Δ = 21.3 db
17:47:58		4400				
17:49:00			51	-118.6		
17:49:40			61	-118.8		
18:00:00			51	-115.3		
18:13:47		1100	61			
18:14:25				-113.2		
18:15:04			51	-131.8		
18:15:25			61	-129.8	+ 8.8	Xfer B low pwr Δ = 16.6 db
18:30:00			51			Xmtr on
18:30:02			61			Xmtr off
18:31:12			51			On track syn freq
18:32:20			51			Cmd mod on

Table 5.3-1 (continued)

GMT, hr:min:sec	Mode	Bit Rate	DSIF Station	DSIF, AGC -dbm	Telemetry Margin, db	Comments
18:45:38				-131.7		
18:45:59						Start gyro drift check
19:00:00				-131.9		
19:30:00				-132.8		
20:00:00				-131.1		
20:05:00			72	-143.1		
20:41:56			51	-133.4		
20:41:56			61	-131.1		
20:54:13						Terminate gyro drift check
20:57:42						Start gyro drift check
21:13:00			61	-132.0		
21:13:00			72	-142.0		
21:13:00			51	-134.6		
21:40:00			51	-135.8		
21:40:00			61	-132.8		
22:00:00			51	-136.6		
22:37:00				-136.6		
22:37:22				-136.4		Sun and Canopus lock
23:00:00				-136.0		
23:05:00						Cmd mod off
23:05:10						Xmtr off —xfer to DSS-11
23:44:00			11	-134.9		
23:59:07	4					
Day 196						
00:02:42	2					
00:07:52	5					
00:09:25						Start gyro drift check
00:27:40				-135.4	+ 2.3	
00:57:50				-135.0	+ 2.7	
01:27:20				-134.9	+ 2.8	
02:00:35				-134.8	+ 2.9	
02:09:24						End gyro drift check
02:10:27				-135.7		
02:18:52						Start gyro drift check
02:26:00				-135.9		
02:58:00				-136.1		
03:14:40			42	-137.0		
03:23:30			11	-136.4		
03:55:00	5	1100	11	-136.9		
04:11:38	4					
04:16:05	2					

Table 5.3-1 (continued)

GMT, hr:min:sec	Mode	Bit Rate	DSIF Station	DSIF, AGC-dbm	Telemetry Margin, db	Comments
04:18:17	5			-137.1		
04:53:07				-137.5	+ 1.1	
04:55:10						Cmd mod off
05:04:13						Xmtr off
05:05:47			42			One-way
05:08:20				-137.4	+ 1.2	Two-way
05:53:50				-137.7	+ 0.9	
06:09:00						BER = 1.2 × 10^{-3}
06:20:00			11			BER = 1.7 × 10^{-3}
06:27:00			42	-137.5	+ 1.1	
06:39:00			11	-138.0	+ 0.6	
06:39:00			42	-137.5	+ 1.1	
06:55:00			42			BER = 1.85 × 10^{-3}; T = 53°K
07:00:00			42	-137.6	+ 1.0	
07:41:00			42	-138.4	+ 0.2	
07:45:00			42	-138.5	+ 0.1	BER = 3 × 10^{-3}
07:52:47		550	42	-139.3	+ 4.4	
07:54:56						End gyro drift check
08:00:56						Start gyro drift check
08:02:56	4					
08:06:06	2					
08:08:24	5					
08:27:50				-138.6		
08:58:00				-138.6		
09:25:00				-138.7		
09:57:30				-139.0		
09:58:27						End gyro drift check
10:20:12						Start gyro drift check
10:51:30				-139.0		
11:21:00				-139.1		
11:47:01						Cruise mode on (end drift check)
12:01:48	4					
12:04:23	2					
12:07:37	5					
13:00:00				-139.6		
13:48:50				-139.8		
13:48:50			51	-138.5		
14:01:50			51			Xmtr on
14:03:30						Rcvr out of lock — sideband
14:08:12						Rcvr in lock
14:08:14			51			Decom in lock
14:09:25						On track syn freq

Table 5. 3-1 (continued)

GMT, hr:min:sec	Mode	Bit Rate	DSIF Station	DSIF, AGC -dbm	Telemetry Margin, db	Comments
14:10:40						Cmd mod on
15:00:00			51	-139. 1		
15:00:00			42	-140. 2		
15:38:00			51	-139. 1		
16:00:01	4					
16:03:56	2					
16:06:53			61	-156. 1		(Questionable)
16:07:23	5					
16:08:34						Start gyro drift check
16:34:20			51	-139. 2		
16:34:20			61	-140. 1		
17:00:00			51	-139. 1		
17:04:00			61	-141. 1		
17:30:00			51	-139. 3		
17:38:34						End gyro drift check
17:41:20				-139. 6		
18:03:17						Start gyro drift check
18:30:00				-139. 6		
19:00:00				-139. 4		
19:03:00			61	-141. 1		
19:30:00			51	-139. 7		
19:36:00			61	-141. 6		
19:42:36			51			End gyro drift check
20:00:00			51	-140. 2		
20:30:00			51	-140. 4		
20:30:00			61	-141. 2		
21:00:00			51	-140. 4		
21:10:00			61	-141. 9		
21:30:00			51	-140. 4		
21:31:00			61	-141. 8		
21:39:49			51			Start gyro drift check (roll only)
22:00:00			51	-140. 5		
22:27:26						End gyro drift check
22:30:00			51	-140. 6		
23:00:00			51	-140. 7		
23:29:00			51			Cmd mod off
23:30:00			11	-141. 2		
23:35:02			51			Xmtr off for xfer to DSS-11
23:36:00			11	-141. 1		
Day 197						
00:11:34	4					
00:13:44	2					

Table 5.3-1 (continued)

GMT, hr:min:sec	Mode	Bit Rate	DSIF Station	DSIF, AGC -dbm	Telemetry Margin, db	Comments
00:15:46	1	550	11			
00:17:35	5					
00:18:26	None					Gyro speed sig processing on
00:22:31	5					
00:53:00				-141.2		
01:47:28	4					
01:49:40	2					
01:51:29	1			-141.5		
02:01:24				-141.5		
02:02:19				-120.8		Xmtr B high pwr; $\Delta = 20.7$ db
02:03:18		4400		-124.5		Range=2.68×10^5 km
02:18:37				-125.3		
02:23:54				-125.3		
02:24:01	2					
02:25:41	1					
02:31:50	5					
02:35:36				-125.4		
02:40:27				-124.7		
02:41:29	2					
02:42:53	4					
02:44:30	5					
02:45:03		550		-121.4		High pwr
02:46:11				-142.5	+ 1.3	Low pwr; $\Delta = 21.1$ db
03:28:00				-142.3		
03:28:40			14	-134.2		
04:01:40			11	-142.7		
04:01:40			42	-140.9		
04:01:40			14	-133.9		
04:15:58						Start gyro drift check
05:01:40			11	-142.3		
05:01:40			14	-134.1		
05:41:21			11	-142.6		
05:41:21			14	-134.7		
05:50:44						End gyro drift check
05:51:33			11	-142.2		
06:00:00			42			DSS-42 two-way
06:03:00			42	-140.8		
06:31:10			42	-140.5		
06:31:10			14	-133.9		
06:31:10			11	-142.4		
07:10:47	4					
07:13:13	2					
07:18:27	5					
08:08:30	5	550	42	-141.4		

Table 5. 3-1 (continued)

GMT, hr:min:sec	Mode	Bit Rate	DSIF Station	DSIF, AGC-dbm	Telemetry Margin, db	Comments
08:45:44				-141. 2		
08:50:59						Start gyro drift check (roll only)
09:00:00				-141. 4	+ 2. 3	
10:00:00				-140. 9	+ 2. 8	
11:00:00				-141. 2	+ 2. 5	
11:32:00				-141. 4	+ 2. 3	
11:58:47	4					
12:01:57	2					
12:04:47	5					
12:32:00			42	-141. 6	+ 2. 1	
12:32:00			51	-141. 4	+ 2. 3	
13:00:00			42	-141. 7	+ 2. 0	
13:32:00			42	-141. 5	+ 2. 2	
14:36:18						End gyro drift check
14:44:32			51	-141. 7		
14:44:32			42	-141. 8		
15:00:00			42	-142. 8		Xmtr off for xfer to DSS-51
15:01:20			51	-141. 8		On track syn freq
15:16:20	4					
15:19:59	2					
15:22:55	5					
15:30:00			51	-141. 7	+ 2. 0	
15:38:00				-141. 7		
15:40:35						Start gyro drift check
16:00:00				-141. 7	+ 2. 0	
16:05:00			42	-143. 1		
16:30:00			51	-141. 5	+ 2. 2	
17:00:00			51	-141. 5		
17:07:00			61	-143. 1		
17:07:00			51	-141. 7		
17:30:00			51	-141. 8		
17:30:31						End gyro drift check
17:39:42						Start gyro drift check
18:00:00			51	-141. 7		
18:00:00			61	-141. 8		
18:30:00			51	-141. 6		
18:30:00			61	-141. 6		
19:00:00			51	-141. 6		
19:12:57						End gyro drift check
19:24:15	4					
19:30:00			51	-142. 4		
19:30:00			61	-141. 7		
19:31:42	2	550	51			
19:41:35	5					
20:00:00				-142. 5		

Table 5. 3-1 (continued)

GMT, hr:min:sec	Mode	Bit Rate	DSIF Station	DSIF, AGC-dbm	Telemetry Margin, db	Comments
20:30:00				-142. 9		
21:00:00				-143. 1	+ 0. 6	
21:30:00				-143. 2		
21:35:50	4					
21:38:47	5					
22:00:00				-143. 4		
22:29:00				-143. 6	+ 0. 1	
22:38:03	4					
22:40:15	2					
22:42:50	5					
23:00:00				-144. 3	- 0. 6	
23:24:00						Cmd mod off
23:30:02			51	-144. 3		Xmtr off for transfer to DSS-11
23:30:02			11	-143. 6	+ 0. 1	Xmtr on 23:30:00
23:45:45	4					
23:49:32	2					
23:51:32	1					
23:53:50	5					
23:54:50	None					Gyro speed sig processing on
23:58:03	5					
Day 198						
00:00:00			51	-144. 5		
00:00:58			11			Xpndr pwr off
00:02:31						Xpndr B pwr on
00:04:16			11			DSS-11 two-way
00:21:30			11	-142. 6		) Appear to be
00:21:30			14	-136. 7		) 00:00:00 readings
00:23:59			11	-142. 7		
00:23:59			14	-135. 6		
00:40:50			11	-142. 5		
00:47:00			11	-142. 7		
00:59:30	6					
01:04:51	4					
01:08:00			11	-142. 8		Low pwr
01:09:27				-121. 0		Xmtr B high pwr on; Δ = 21. 8 db
01:09:57		1100		-120. 2		
01:10:38						Summing amps off
01:10:39						Phase sum amp B on
01:11:39	2					
01:13:12	5					
01:17:09	5	1100	11			Xpndr pwr off
01:28:00				-121. 2		After terminal sun and roll
01:36:15				-123. 9		
01:43:42	6					
01:50:00				-123. 8		
01:54:20				-123. 8		
02:02:39						Loss of signal
02:15:00						Loss of data

TABLE 5.3-2. SPACECRAFT CONFIGURATION SHEET

GMT, hr:min:sec	Mission Phase	Transmitter A/B	Power H/L	Omni Antenna A/B	A/D Converter 1/2	Receiver A φL/AFC	Transponder A	Receiver B φL/AFC	Transponder B	Command Decoder A/B	Comments
Day 195											
11:53:29	Launch	B	Low	B	1		Off		On	B	
12:05:57			High								
12:12:24											DSS-72 xmtr on
12:13:53								φL			
12:17:14								NotφL			
12:19:22								φL			Cmd mod on
12:20:50								NotφL			Cmd mod off
12:21:53								φL			
12:26:41										A	Cmd mod on
12:34:15			Low								
13:03:42										B	Cmd mod off for xfer to DSS-51
13:12:44											Cmd mod on DSS-51
16:54:00											Cmd mod off for xfer to DSS-61
17:47:20			High								
18:15:25		B	Low								
18:23:35										A	Cmd mod off for xfer to DSS-51
18:32:20											Cmd mod on DSS-51
20:02:34										B	Indexing from 20:02:34 to
20:03:37										A	20:04:07 due to low signal
20:03:39										B	level into recr A
20:04:07										A	
23:05:00											Cmd mod off for xfer to DSS-11
Day 196											
00:00:00											Start day 196
04:55:20										B	Cmd mod off for xfer to DSS-42
05:04:13								NotφL	On		No overlapping visibility DSS-11/42
05:08:20								φL			DSS-42
14:00:00											Cmd mod off for xfer to DSS-51
14:10:40											Cmd mod on DSS-51
23:29:00										A	Cmd mod off for xfer to DSS-11
Day 197											
00:00:00											Start day 197
01:46:41										B	
02:02:19		B	High								
02:46:03		B	Low								
05:53:30										A	Cmd mod off for xfer to DSS-42
14:53:00											Cmd mod off for xfer to DSS-51
15:11:13											Cmd mod on DSS-51
23:24:00										B	Cmd mod off for xfer to DSS-11
Day 198											
00:00:00											Start day 198
00:00:58								AFC	Off		
02:00:32								NotφL	On		
00:02:47										A	Cmd mod off to reacquire
00:04:16								φL			
00:48:42										B	
01:09:27		B	High								
01:17:09								AFC	Off		
02:02:39											Loss of signal Loss of data

5.3.2 ANOMALY DISCUSSION

This subsection contains a discussion of three mission events that question the RF subsystem performance. It has not been established that two of the three, i.e., 1) simultaneous DSS-51 and DSS-11 loss of lock during station transfer (pass 2), and 2) loss of signal signature during retro burn, were truly spacecraft RF anomalies. However, the spacecraft subsystem has failure modes that could produce the observed signatures. The third topic, degraded receiver B performance, was not considered an operational anomaly since the signal level was within the established tolerance region. However, when considering the mission as a whole, the receiver performance was seen to be biased by approximately -5 db from predicted values.

5.3.2.1 Degraded Receiver B Performance

During Mission D coast periods, deviations from the predicted received signal level curves were noted in both the up and down links. Gyro drift checks performed during these periods account for omnidirectional antenna gain variations that are not taken into consideration when generating predictions. However, deviations in receiver B received signal levels, above those expected due to the gyro drifts, as well as deviations from predictions during maneuvering periods, indicated that an approximate -5 db bias existed in either the performance or calibration of the receiver.

Omnidirectional antenna B up-link gain variations during the transit phase of the mission are illustrated in Figure 5.5-2. This figure shows the earth vector variation superimposed on the omnidirectional antenna B up-link antenna gain contour map. For the most part, the mission was flown with the relative spacecraft/ground station attitude so that the antenna operated in a high-gain region (G $\geq$ -3 db). However, during the Canopus acquisition sequence, the required 360-degree spacecraft roll resulted in gains as low as -18 db. Figure 5.3-6c illustrates measured versus actual gain values for this maneuver and indicates an offset of approximately 5 db between the two sets of data. Figures 5.3-5 and 5.3-7c are similar presentations for the coast phases and midcourse phase, respectively, and indicate the same general bias.

A deviation from the expected performance of receiver B is not unique to Surveyor IV. A -2 db bias was also observed during Mission C (Reference 1). During Mission D, as was the case for Mission C, this degraded behavior could not be considered an anomaly since the combined effect of gyro drift checks and receiver bias caused the signal level to remain at the predicted negative tolerance level which, due to the nature of the negative tolerances on system parameters, is accepted as an expected signal level.

As pointed out in Reference 1, it is unlikely that the bias seen in all the data can be attributed to any uncertainty in the antenna pattern data due to the consistency of the measured data throughout the wide range of sampled antenna gain values.

Two sets of data were available to convert the spacecraft data to engineering units: one taken at the unit level and the other during phase C of the solar thermal vacuum test (References 2 and 3). For the signal level range and temperatures encountered during the mission (approximately 75° F), the two sets of data are within 2 db of each other and the interpretation of mission data using either set yields the same general conclusions. Both sets of calibration data are multivalued for the range of signal levels observed on receiver B for most of the mission. Even though some ambiguity exists as to the determination of absolute signal levels, sufficient evidence is obtained, when considering the mission as a whole, to suspect that the performance or calibration of the receiver was biased.

During the countdown phase of the mission, signal levels at the spacecraft receivers are a function of system test equipment assembly transmitter attenuation and transmission link parameter variations. The concern during this period is not for the absolute signal level readings but that both receivers indicate the same signal power level. Telemetry indicated that this was indeed the case for Surveyor IV, and the receiver bias was not apparent prior to launch. The loss of spacecraft signal at retro burn precluded any lunar calibration attempt which may have provided additional insight into the reason for the above performance deviation.

5.3.2.2 Simultaneous DSS-51 and DSS-11 Loss of Lock During Station Transfer (Pass 2)

During the station transfer from Johannesburg (DSS-51) to Goldstone Pioneer (DSS-11) on GMT day 196, a real-time verbal report from DSS-51 of a loss of receiver lock appeared to be coincident with an observed DSS-11 loss of lock. Transmitter tuning during the time could cause a drop of phase lock in the spacecraft receiver. The spacecraft transmitter would then revert to the narrow-band voltage controlled crystal oscillator and, consequently, a loss of ground receiver lock due to the corresponding spacecraft frequency shift would result. Spacecraft data being processed at the time did not indicate that the tuning rate was too excessive for the spacecraft receiver to track. However, the resolution of the processed data would not allow momentary frequency step functions to be observed. It could not be positively established in real time that the receiver drop locks were simultaneous. The conclusion was that the transmitter tuning at DSS-51 caused the observed glitches.

Subsequent reduction of FR1400 tapes from both DSS-51 and DSS-11 has established that both receivers at both tracking stations lost phase lock simultaneously and that all receivers had identical dynamic phase error glitching signatures leading up to the loss of lock. The glitching observed in the ground station receivers must certainly have been due to the spacecraft transmitted signal. However, since the spacecraft was operating in two-way lock, this signature could have been induced by the ground transmitting station. The spacecraft itself could have been the source of the problem; however, the available data do not indicate any spacecraft disturbance. The ground station was in the process of transmitter tuning at the time, but

no reason for the signature is obvious from their accounts. Neither source can be divorced from the responsibility of causing the situation.

The results of the data investigation do not provide an explanation to the loss of lock at station transfer, but two points in regard to this situation should be made:

1) The event did not reoccur at any other time during the mission.

2) The signature associated with the loss of signal during this event in no way compares to that situation when the signal was lost during retro burn at terminal descent.

Detailed discussions of the investigation associated with this event can be found in Reference 4.

5.3.2.3 Loss of Signal Signature During Retro Burn

Extensive reduction and analysis has been performed on the predetection recordings from both DSS-11 and DSS-14 of the spacecraft RF signal during retro burn, with particular emphasis on signal characteristics at the time the signal was lost.

Figure 5.3.2 in Reference 5 illustrates signature of the behavior of the PCM data, the 7.35-kHz subcarrier, and the carrier at the time of the loss of signal. This information was obtained from the DSS-11 60 ips tape record and processed as follows:

1) The composite signal representing the carrier is 500 kHz IF signal from the receiver operating in the manual gain control mode. This signal was mixed with a 506-kHz signal, subjected to a 1-kHz to 8-kHz bandpass filter, and recorded as illustrated.

2) The 7.35-kHz subcarrier is recorded at the output of the 10-MHz phase detector in the receiver operating in the phase lock mode.

3) The PCM data are the output of the discriminator, having for its input the 7.35-kHz subcarrier derived above.

The reference time code also included on the record is a 1-kHz code, thus representing 1 millisecond per cycle. The loss of PCM data is indicated by the loss of the last bit of word 16 with the loss of both the carrier and subcarrier occurring at the same time — within the resolution of the display (approximately 1/4 millisecond). A similar record from DSS-14 indicates the same signature.

The behavior of the carrier at the loss of signal was investigated by performing a spectral analysis on the 500-kHz IF signal from the open-loop receiver at DSS-11. The 500-kHz signal was divided by 64 by a series of playback record techniques. This was then used as the input to a Rayspan spectrum analyzer. This analyzer consists of 420 filters, each having an

average bandwidth of 32 Hz and a time constant of 12.7 milliseconds. The total bandwidth of the analyzer is 10.5 kHz with a resolution of 60 Hz over the entire band.

The spectrum analyzer was swept every 15 milliseconds of real time, which represents 15/64 millisecond of original data time. The results show the spectrum decaying within two sweeps of the spectrum analyzer, or within less than 1/2 millisecond in original data time. The analyzer time constant is approximately 0.2 millisecond in original data time with this reduction.

The subcarrier is very difficult to see since, with the reduction, it is located approximately 115 Hz from the carrier and therefore approaches the minimum resolution of the analyzer. The amplitude of the carrier was also noted to vary from sweep to sweep. Since the frequency of the carrier was varying due to doppler variations and tape noise, it was assumed that the spectrum was shifting within one of the 420 filters or from one filter to another in the spectrum analyzer. The individual gain characteristics of the filters would influence amplitude variations in the recorded spectrum.

The spectrum investigation was repeated utilizing the same basic data at a frequency reduction of 128. For this case, the subcarrier is not seen at all since it is located 57 Hz from the carrier. The results indicate that the carrier decayed within two sweeps of the spectrum analyzer. This represents less than 1/4 millisecond in original data time, with the corresponding analyzer time constant being approximately 0.1 millisecond.

An extrapolation of the above technique was incorporated to determine if a frequency shift occurred at signal loss. This was done by observing the energy decay in the individual filters of the analyzer rather than the composite output. The input to the analyzer was the 500-kHz IF tape divided by 200. The output of 12 filters covering a bandwidth of 95 Hz (each filter of this analyzer has a bandwidth of 10 Hz) centered about the carrier frequency was examined. This represents a bandwidth of ±9.5 kHz in original data. The carrier and the subcarrier were found to stop at the same time. The decay of energy in the filters was at the rate of the filter time constant. No shift of energy from one filter to another was noted at the loss of signal.

The conclusions reached as a result of this investigation were that, if a frequency shift did occur, it was greater than 10 kHz and occurred in a time corresponding to less than 1/4 of the individual filter time constant. This represents 1/4 millisecond in original data time.

In addition to the above analysis, the signature of the dynamic phase error of receivers at both DSS-11 and DSS-14 prior to and during retro burn were examined from FR1400 recordings. No observable change in the amplitude or characteristic was noted during this period.

Section 4.3 contains further information concerning the failure during retro burn.

5.3.3   SUMMARY AND CONCLUSIONS

Table 5.3-3 contains a summary of the measurable performance parameters compared with applicable requirements and premission predictions. Most subsystem parameters are not directly measurable, and those that are measurable are difficult to summarize due to time variability.

Received signal level, for example, is a function of time and spacecraft attitude. The summary for these parameters reflects wide tolerances, with corresponding wide variations in actual performance in cases when the earth vector was in the omnidirectional antenna null. Performance and predictions outside the null are much more closely bounded. More detailed information is found in the subsections dealing with each mission phase.

The following conclusions can be drawn as a result of the foregoing analysis:

1) RF subsystem performed as expected with the exception of receiver B. In most cases, close to nominal performance was experienced in both the up and down links.

2) Receiver B performance was biased by -5 db from the predicted values. No operational problems resulted since the signal level at no time deviated below the region bounded by the negative tolerances of the predicted values.

3) Mission D again verified the accuracy of the omnidirectional pattern data measured on the JPL range.

4) RF subsystem premission predictions and real-time analysis techniques used during Mission D were relatively accurate.

5) The analysis performed on the predetection recordings from both DSS-11 and DSS-14 of the spacecraft RF signal during retro burn established the following signature:

   a)   The PCM subcarrier (7.35 kHz) had modulation present at the time it went off. Loss of subcarrier occurred during the last bit (parity) of commutator word 16.

   b)   There is no distinguishable time difference between loss of carrier and loss of subcarrier.

   c)   The carrier decayed in less than 1/4 millisecond.

   d)   There is no observable frequency shift at the loss of signal.

   e)   There is no observable change in the amplitude or characteristic of the dynamic phase error prior to and during retro engine burn.

TABLE 5.3-3. RF PERFORMANCE PARAMETER SUMMARY

Parameter	Predicted Value	Requirement	Actual Performance
Transmitter frequency at acquisition	2294.994959 MHz	2295 MHz ± 23 kHz	2294.995899 MHz
Receiver B frequency at acquisition	2113.29328 MHz	2113.31 MHz ± 21 kHz	2113.335744 MHz
Receiver A signal levels during coast phases*	Time variable predictions. Predicts are some nominal value ±10 db.	>-114 dbm**	Level between +8 and -12 db of nominal and ≥-120 dbm
Receiver B signal levels during coast phases*	Time variable predictions. Predicts are some nominal value ±5 db.	>-114 dbm**	Level between -2 and -5 db of nominal and ≥-99.0 dbm
Receiver A signal levels during star maneuver	Time variable predictions. Predicts are some nominal value ±10 db.	>-114 dbm**	Level between +8 and -7 db of expected and ≥-105 dbm
Receiver B signal levels during star maneuver	Time variable predictions. Predicts are some nominal value ±8 db.	>-114 dbm**	Level between 0.0 and -9 db of expected and ≥-104 dbm
Receiver A signal levels during post-midcourse maneuver	Time variable predictions. Predicts are some nominal value ±10 db.	>-114 dbm**	Level between +4 and -9 db of expected and ≥-107.4 dbm
Receiver B signal levels during post-midcourse maneuver	Time variable predictions. Predicts are some nominal value ±3.3 db.	>-114 dbm**	Level between -3 and -7 db of expected and ≥-98.7 dbm
Receiver A signal levels during terminal maneuver	Time variable predictions. Predicts are some nominal value ±10 db.	>-114 dbm**	Level variations of 8 db and >-116.5 dbm (predicted variations of 16 db)

Table 5. 3-3 (continued)

Parameter	Predicted Value	Requirement	Actual Performance
Receiver B signal levels during terminal maneuver	Time variable predictions. Predicts are some nominal value ±6.4 db.	>-114 dbm**	Level variations of 11 db and >-106 dbm (predicted variations of 11 db
DSS signal levels during coast phases*	Time variable predictions. Predicts are some nominal value ±5 db.	>-157.4 dbm (carrier power) (17.2 bps threshold)	Level between +2 and -4 db of nominal and >-145 dbm at 550 bps
DSS signal levels during star maneuver	Time variable predictions. Predicts are some nominal value ±10 db.	None	Level between +5 and -4 db of expected and ≥-147.9 dbm (carrier power at 4400 bps)
DSS signal levels during midcourse maneuver	Time variable predictions. Predicts are some nominal value ±2.8 db.	>-136.0 dbm (carrier power at 4400 bps/ high power	Level between +0 and -2.5 db of expected and >-126.9 dbm
DSS signal levels during terminal maneuver and descent	Time variable predictions. Predicts are some nominal value ±2.8 db.	>-130.4 dbm (carrier power at 1100 bps/ high power	Level between +2.5 and -1 db of expected and >-124.4 dbm (carrier power at >-124.4 bps)
Transmitter A high power output	40.8 dbm $^{+0.3}_{-0.4}$ db	>39.6 dbm	Not available
Transmitter A low power output	20.6 dbm $^{+1.0}_{-1.9}$ db	>19.1 dbm	Not available
Transmitter B high power output	41.1 dbm $^{+0.3}_{-0.0}$ db	>39.6 dbm	Output between 40.9 and 41.4 dbm
Transmitter B low power output	21.1 dbm $^{+0.1}_{-0.8}$ db	>19.1 dbm	Output between 19.6 and 20.4 dbm

Table 5. 3-3 (continued)

Parameter	Predicted Value	Requirement	Actual Performance
Phase jitter 12 Hz bandwidth	<36 degrees	<36 degrees (3 σ)	Not available
Phase jitter 152 Hz bandwidth (thrust phase)	<22 degrees	<22 degrees (3 σ)	<6 degrees during retro engine burn
Command reject rate	<1/2000	≤1/2000 at signal level >-114 dbm	No known rejected commands sent at signal levels greater than -100 dbm
Telemetry bit error rate	<3/1000	≤3/1000 at input SNR ≥ 10 db	Minimum BER = 3 × 10^{-3} at input SNR ≏ 9.2 ± 0.7 db

*Gyro drift checks during coast phases caused antenna gain variations not taken into account in the predicted signal levels.

**Threshold value applies to command threshold and, as such, only requires one of the two receivers to be above -114 dbm at any one time.

5. 3. 4   SUBSYSTEM PERFORMANCE ANALYSIS

5. 3. 4. 1   General Discussion

Before specific phases are discussed, a general treatment of the mission will be undertaken. Information applicable to all mission phases is included in this subsection.

Subsystem Parameters

Most quantitative estimates of performance are based on received signal levels which, in turn, are determined from individual link parameters. Those parameters used in the performance predictions and the subsystem analyses are tabulated in Table 5. 3-4. Equations using these data are derived here; parameters discussed in later portions can be evaluated from these data. Tables 5. 3-4 and 5. 3-5 consist of measured data taken from flight acceptance (FAT), solar thermal vacuum (STV), and command and data handling console (CDC) tests or specification values where measurements were not available.

TABLE 5.3-4. UPLINK PARAMETERS FROM FAT, STV, AND CDC TESTS

Description	Value
Transmitting system (DDS)	
RF power	$70.0 \, ^{+0.5}_{-0.0}$ dbm
Antenna gain	
SAA	20.0 ± 2.0 db
SCM	$51.0 \, (+1.0, \, -0.5)$ db
Circuit loss	
SAA	-0.5 ± 0.0 db
SCM	-0.4 ± 0.1 db
Receiving system (Surveyor IV)	
Circuit loss	
Receiver A	-3.9 ± 0.5 db
Receiver B	-4.5 ± 0.5 db
Up-link carrier tracking loop	
Equivalent noise	
Bandwidth	240 ± 24 Hz
Threshold SNR	12 db
Up-link channel	
Threshold SNR	9 db
System noise	
Temperature	$2700°$ K
Equivalent noise	
Bandwidth (predetection)	13430 Hz
Data/subcarrier modulation index	7.2
Subcarrier/carrier modulation index	1.6 ± 0.16

TABLE 5.3-5. DOWNLINK PARAMETERS FROM FAT, STV, AND CDC TESTS

Description	Value
Transmitting system (SC-4)	
RF power	
Transmitter A (low power)	20.6 (+1.0, -1.9) dbm
Transmitter B (low power)	21.1 (+0.1, -0.8) dbm
Transmitter A (high power)	40.8 (+0.3, -0.4) dbm
Transmitter B (high power)	41.1 (+0.3, -0.0) dbm
Planar array gain	27.0 ± 0.5 db
Circuit loss	
Transmitter A Omnidirectional antenna A	-2.84 (±0.5) db
Transmitter B Omnidirectional antenna A	-3.0 (±0.5) db
Transmitter A Omnidirectional antenna B	-3.4 (±0.5) db
Transmitter B Omnidirectional antenna B	-3.4 (±0.5) db
Planar array	-2.3 (+0.0, -0.22) db
Carrier frequency	2295 MHz
Receiving system (DSS)	
Antenna gain	
SAA (acquisition aid antenna)	21.0 ± 1.0 db
SCM (85-foot antenna)	53.0 (+1.0, -0.5) db

Table 5.3-5 (continued)

Description	Value
Circuit loss	
SAA	-0.5 ± 0.0 db
SCM	-0.18 ± 0.05 db
Effective noise temperature	
Maser	55 ± 10° K
Parametric amplifier (SAA antenna)	
All DSS except Johannesburg	270 ± 50°K
Johannesburg	320 ± 50°K
Lunar temperature	110 ± 25° K
Carrier channel	
Equivalent noise bandwidth for maneuvers (at threshold)	152 Hz
Equivalent noise bandwidth for coast mode (at threshold)	12 Hz
Threshold SNR	
Acquisition	9.0 db
Maneuvers	14.0 ± 1.0 db
Coast mode	11.4 db
Subcarrier oscillator	
Equivalent predetection noise bandwidth, Hz ± 10 percent	
4400 bits/sec	5160
1100 bits/sec	1290
550 bits/sec	685
137.5 bits/sec	169
17.2 bits/sec	26.7
Strain gauge 1	168
Strain gauge 2	169
Strain gauge 3	169
Reject/enable	405
Gyro speed	948

Table 5.3-5 (continued)

Description	Value
Subcarrier oscillator center frequencies, kHz	
4400 bits/sec	33.0
1100 bits/sec	7.35
550 bits/sec	3.90
137.5 bits/sec	0.96
17.2 bits/sec	0.56
Strain gauge 1	0.96
Strain gauge 2	1.30
Strain gauge 3	1.70
Reject/enable	2.3
Gyro speed	5.4
Threshold signal-to-noise ratio for telemetry data, ±1.0 db	
4400 bits/sec	9.0
1100 bits/sec	9.0
550 bits/sec	9.0
137.5 bits/sec	9.0
17.2 bits/sec	9.0
Strain gauge 1	7.0
Strain gauge 2	7.0
Strain gauge 3	7.0
Reject/enable	10.0
Gyro speed	10.0
Subcarrier oscillator modulation indices, ±10 percent	
4400 bits/sec	1.6
1100 bits/sec	0.935
550 bits/sec (acquisition)	0.3
550 bits/sec	1.15
137.5 bits/sec	1.45
17.2 bits/sec	1.45
Strain gauge 1	0.65
Strain gauge 2	0.65
Strain gauge 3	0.65
Reject/enable	0.655
Gyro speed	1.600

Computations Used

In this subsection, reference is made to received signal levels and quantities computed from these levels. The equations used are listed below and will not be derived again:

1) Spacecraft transmitter high power output is

$$P_{xmtr}(dbm) = 10 \log (P_{tm} \times 10^3) + L$$

where

P_{xmtr} = transmitter power (dbm) = P_{high}

P_{tm} = telemetered power output (watts)

L = loss from transmitter to power monitor. (Value for transmitter B/omnidirectional antenna B $\simeq$ as determined from STV calibration data.)

2) Spacecraft transmitter low power output is

$$P_{low} = P_{high} - P_{DSS_H} + P_{DSS_L} \quad (dbm)$$

where

P_{low} = transmitter low power output

P_{high} = telemetered transmitter high power output

P_{DSS_H} = DSS received signal level at high power

P_{DSS_L} = DSS received signal level at low power

3) Spacecraft omnidirectional antenna gain (up-link) is

$$G_R = \frac{P_R}{P_T \, G_T \left(\frac{\lambda}{4\pi R}\right)^2 L}$$

where

G_R = received omnidirectional antenna gain (up-link gain)

P_R = received signal level (determined from spacecraft AGC)

P_T = DSS nominal transmitter power

G_T = DSS nominal antenna gain

λ = wavelength of up-link signal

R = slant range at time of computation

L = nominal spacecraft and DSS losses

(Note: For down-link gain, appropriate down-link parameters are inserted in a similar equation.)

4) Signal-to-noise ratio (SNR) for any subcarrier is

$$SNR = \frac{P_S}{P_N} = \frac{MP_R}{KT_{eff}BW_{sc}}$$

where

P_S = signal power in predetection noise bandwidth

P_N = total noise power in predetection noise bandwidth

M = carrier to subcarrier modulation loss adjustment constant based on subcarrier oscillator modulation index on the carrier

P_R = received carrier power reported by the DSS

K = Boltzmann's constant

T_{eff} = DSS system temperature reported by the DSS

BW_{sc} = subcarrier equivalent predetection noise bandwidth

When using these equations, attention must be given to the desired accuracy of the answer. Since several parameters not measurable in flight, spacecraft telemetry, and DSS station reports are used, computed parameters

have potentially large errors. Their validity is thus weighed against similar test data and/or is judged quite subjectively based on past experience. These equations are not used so much for their numerical results as for the total picture of subsystem performance generated. Any gross subsystem problems or computation errors will tend to be uncovered in this analysis, but subtle errors will not.

Bit Error Rate Calculations

One subsystem parameter of interest is the telemetry bit error rate (BER). This parameter serves as an example of the problems encountered when attempting to evaluate postmission data. BER is required to be less than 3×10^{-3} at input SNR ratios of 9 ± 1 db. BER cannot be measured in flight, but word error rate can. On day 196 at approximately 6 hours GMT, DSS-42 began counting parity errors. Based on the assumption that a bad parity word represented a single bit error, a BER of 3×10^{-3} was observed at a reported -138.5 dbm ground station received carrier power (7 hours 45 minutes).

The SNR at this time of the observed 3×10^{-3} BER was computed as shown below:

DSS AGC/1100 bits/sec = -138.5 dbm

System noise temperature = 53.3° K = 17.3 db
(DSS-42 post-track)

Boltzmann's constant = -198.6 dbm/deg/cps

Bandwidth = 1290 Hz ± 10 percent = 31.1 (+0.41, -0.46) db

Noise power = -150.20 (+0.41, -0.46) dbm

Modulation loss
   Carrier   -2.01 (+0.40, -0.46) db
   Subcarrier -4.56 (+0.62, -0.73) db

Δ modulation loss = -2.55 (+0.22, -0.27) db

Subcarrier power = -141.05 (+0.22, -0.27) dbm

SNR = subcarrier power − noise power = 9.15 ± 0.68 db

The tolerance in this computation is only approximate and is probably greater. Based on the SNR requirement of 9 ± 1.0 db, the measured parameter (BER) meets the specification.

Omnidirectional Antenna Gain Maps

In order to better visualize and interpret the significance of the signal level data, traces of the earth vector on the omnidirectional antenna gain contour maps are presented. Figures 5.3-2 and 5.3-3 show the antenna up and down links. Since signal level variations are, for the most part, the result of increasing range (i.e., more space loss) and changing omnidirectional gain, these plots allow visualization of the expected signal level changes for comparison with plots of up-link and down-link signal levels versus time.

5.3.4.2 Mission Phase One: Prelaunch to Spacecraft Acquisition

During the prelaunch phase, subsystem performance is assessed during the launch pad systems readiness test and prelaunch countdown test. Next to assuring normal system performance prior to launch, the most important subsystem data taken during this phase are transmitter and receiver frequency data. Frequency data are used to predict the frequencies at initial acquisition and are transmitted from the Cape prior to launch. The DSS, in turn, uses these data to tune the DSS receiver for one-way lock and the DSS transmitter for eventual two-way lock.

The measured transmitter and receiver frequency data are tabulated in Table 5.3-6. Compartment temperature during the prelaunch period was increasing, thus causing a transmitter frequency decrease and a receiver frequency increase, as expected. The temperature directly affecting the frequency is not actually measured since the telemetered sensor is in the thermal tray and not at the voltage controlled crystal oscillator. Relative temperature versus frequency information is thus considered to be most reliable. Based on this judgment, the measured frequency data were consistent with previous Surveyor IV test data.

Acquisition frequencies are determined by extrapolating the measured values by essentially predicting the compartment temperature increase due to the high-power operation from just prior to Centaur/Surveyor separation to the time of initial spacecraft acquisition. However, the frequency drift for the scheduled launch azimuth was insignificant since the spacecraft would be in high power for only 5 minutes prior to DSS-72 acquisition. Therefore, the acquisition frequencies used were not biased from the measured values.

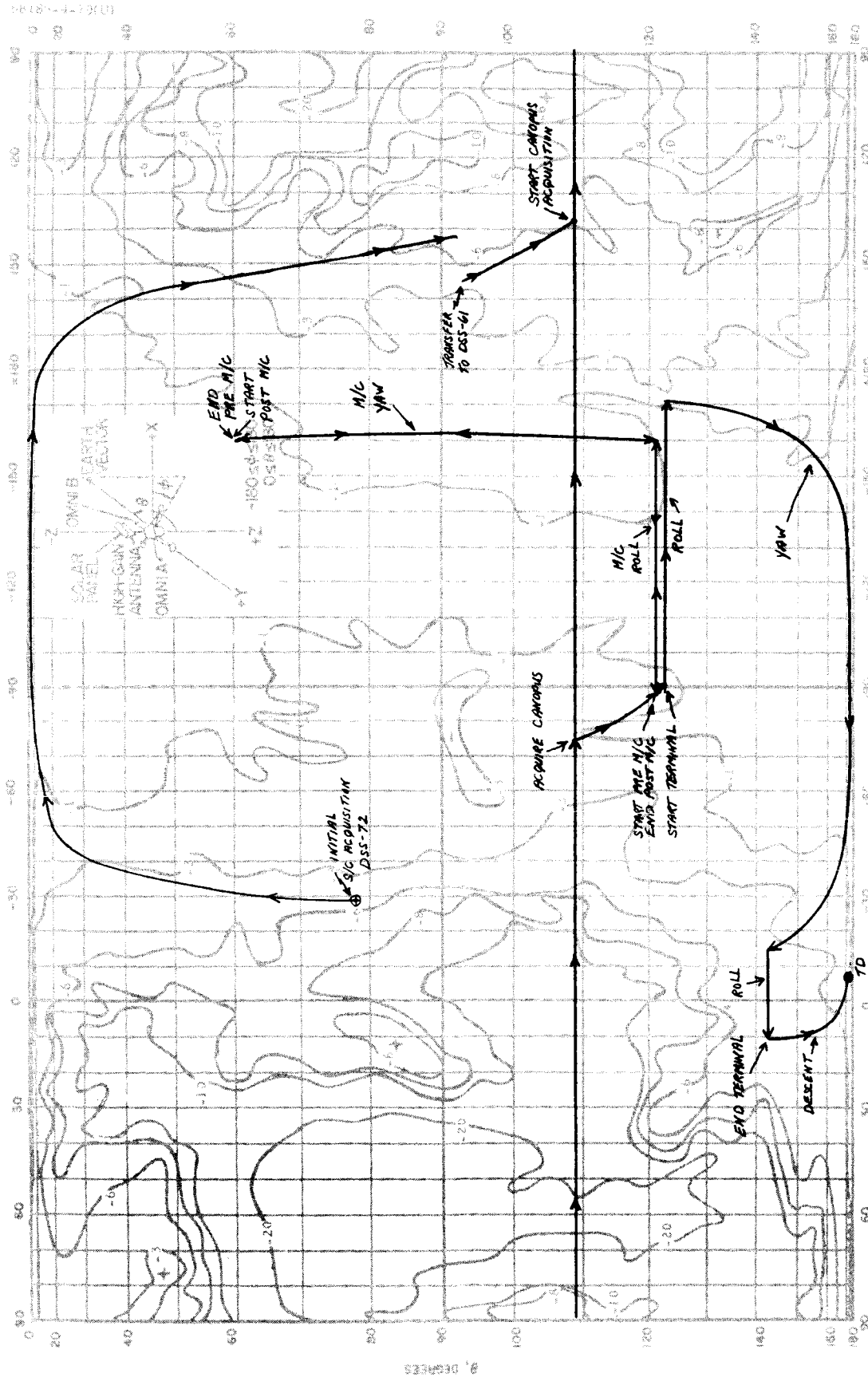The actual frequencies at initial DSS-72 acquisition were as follows:

Transmitter (one-way) = 2294.995899 MHz

Receiver (two-way)   = 2113.335744 MHz

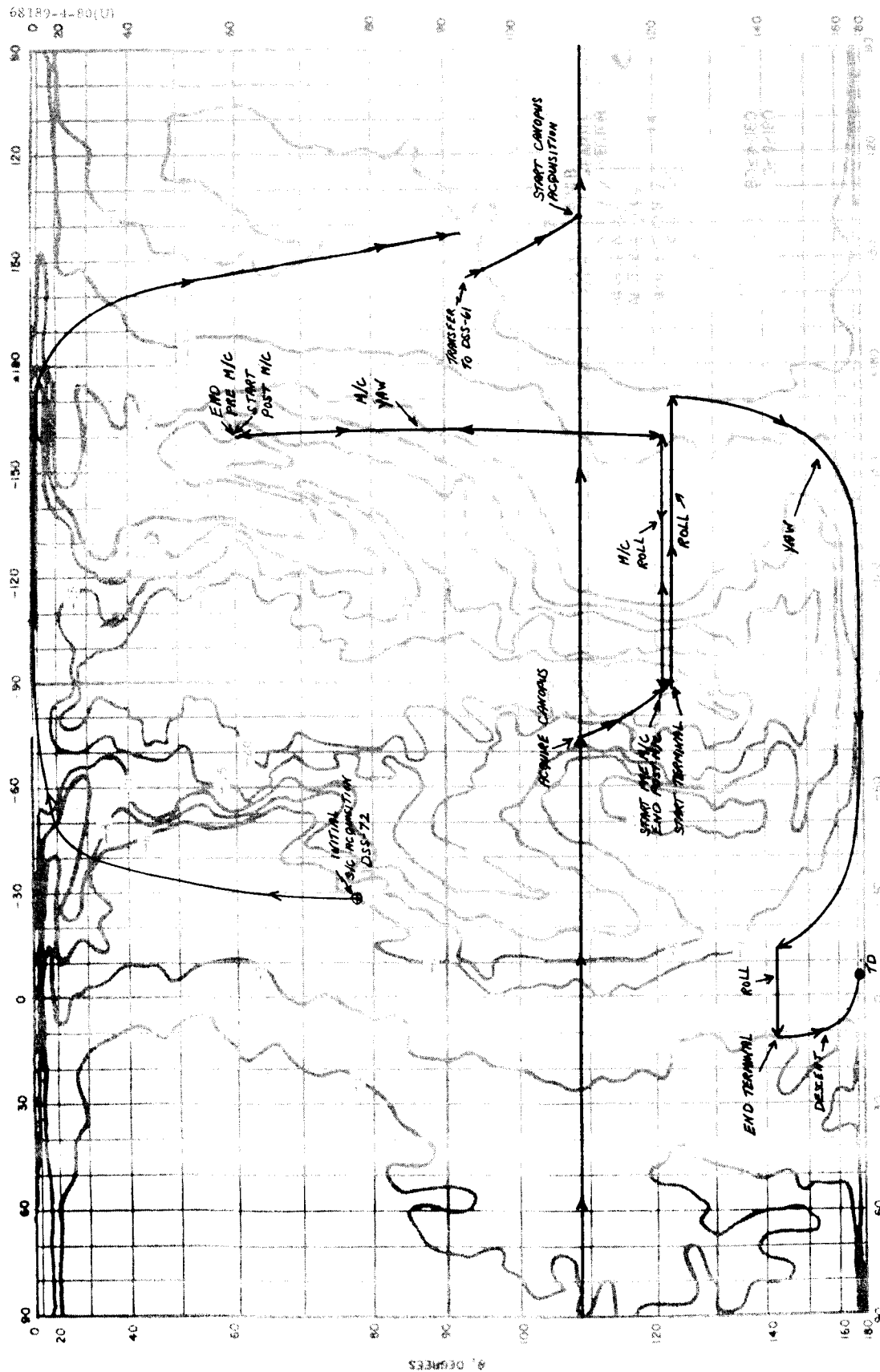The difference between predicted and actual was as follows:

Transmitter = 940 Hz

Receiver   = 6416 Hz

a) Omnidirectional Antenna A

Figure 5.3-2. Up-link (2113 MHz) Omnidirectional Antenna Gain Map

b) Omnidirectional Antenna B (continued). Up-link (2113 MHz) Omnidirectional Antenna Gain Map

Figure 5.3-2 (continued).

a) Omnidirectional Antenna A

Figure 5.3-3. Down-link (2295 MHz) Omnidirectional Antenna Gain Map

5.3-32

b) Omnidirectional Antenna B. Down-link (2295) MHz) Omnidirectional Antenna Gain Map

Figure 5.3-3 (continued).

TABLE 5.3-6. PRELAUNCH FREQUENCY SUMMARY[*]

Frequency Message, time in minutes	Measured Frequencies, mc		Lower Tray Temperature, °F
	One-Way Narrowband Voltage Controlled Crystal Oscillator	Best Lock	
T-555 (transmitter A)	2295.014463	2113.312016	75
T-494 (transmitter B)	2295.000058	2113.328800	77
T-274 (transmitter B)	2295.008145	2113.310808	80
T-83 (transmitter B)	2295.002040	2113.328456	77
T-49 (transmitter B)	2294.997753	2113.329744	78
T-23 (transmitter B)	2294.994959	2113.329328	83

[*]Final frequencies used by Flight Path Analysis and Command for initial DSS-72 acquisition.

Table 5.3-7 is a summary of the significant events during initial RF acquisition at DSS-72 (Ascension Island). One-way acquisition was accomplished 11 seconds later than the predicted first visibility, and good two-way lock was accomplished 16 minutes and 14 seconds later. Telemetry data indicated a signal in the passband of both spacecraft receivers at DSS transmitter turn-on. However, two-way lock was delayed due to a pointing problem associated with the ground station antenna system (Reference 6). The spacecraft received signal levels for both receivers A and B were greater than -80 dbm during the initial acquisition phase.

With the exception of the ground station antenna pointing problem, the initial spacecraft acquisition was nominal. The spacecraft high-power transmitter was turned off 30 minutes and 34 seconds after being commanded to high power by the Centaur. The maximum allowable time to accomplish turnoff is 1 hour.

5.3.4.3 Mission Phase Two: Coast

The coast phases consist of the following:

1) Pre-Canopus acquisition — Period from initial spacecraft acquisition until Canopus acquisition. During this time, the spacecraft attitude is uncertain in roll, and the spacecraft -Z axis is pointed toward the sun.

TABLE 5.3-7. ACQUISITION EVENTS

Event	GMT (Day 195), hr:min:sec	Comments
Transmitter B high power on	12:05:55.18	Spacecraft commanded to high power by Centaur
DSS-72 acquires spacecraft in one-way mode on SAA (acquisition aid antenna)	12:09:56	Accomplished 11 seconds later than predicted first visibility and 16 minutes and 27 seconds after launch
DSS-72 switch from SAA to SCM (30-foot antenna)	12:12:08	
DSS-72 transmitter turn on	12:12:24	
Signal in passband of both spacecraft receivers	12:12:31	(From telemetry) receiver B not phase locked. Receiver A in AFC capture.
Receiver B phase locked	12:13:52	From telemetry
DSS-72 reports two-way	12:14:06	
DSS-72 auto tracking on SCM	12:18:50	
DSS-51 reports one-way lock	12:19:00	
DSS-72 turned on command modulation	12:19:22	DSS-72 could not confirm two-way. Telemetry data indicated receiver B not phase locked at 12:17:24
DSS-72 turned off command modulation	12:20:50	Accomplished to reacquire the spacecraft in two-way

Table 5.3-7 (continued)

Event	GMT (Day 195), hr:min:sec	Comments
DSS-72 reacquired two-way	12:21:46	Telemetry indicates receiver B phase locked at 12:21:43
DSS-72 reported momentary out of locks	12:25:48 12:25:52	
DSS-72 reported good two-way lock	12:26:10	Solid two-way acquisition in 32 minutes and 41 seconds from launch
DSS-72 turned on command modulation	12:26:41	
Spacecraft commanded to 1100 bits/sec data	12:29:58	Necessary for low-power data reception at DSS-72
Transmitter B high power off		Spacecraft was in high power for 30 minutes and 34 seconds for initial acquisition phase (1-hour maximum allowed)

2) Premidcourse — Period from Canopus acquisition until midcourse maneuvers.

3) Postmidcourse — Period from completion of midcourse maneuvers until terminal maneuvers.

Figures 5.3-4 and 5.3-5 are plots of DSS, receiver A, and receiver B signal levels from launch to touchdown. The premission predicted signal level after Canopus acquisition is shown in each figure. Since the spacecraft attitude in roll is uncertain to ±60 degree about an estimated reference point prior to Canopus acquisition, no premission predictions are made for this period.

Referring to Figures 5.3-3 and 5.3-4, which show traces of the earth vector relative to omnidirectional antenna B down link and omnidirectional antennas A and B up-link gain contours, it can be noted that changes in signal levels during the pre-Canopus acquisition phase and right at Canopus acquisition are in complete agreement with the antenna gain contour maps. The approximate antenna gains during the pre-Canopus phase are noted in Table 5.3-8.

5.3-36

TABLE 5.3-8. ANTENNA GAIN VARIATIONS PRE-CANOPUS

	Gain Variations (Coast), db		Pre-Canopus Gain, db		Gain at Canopus, db	
	Predicted	Actual	Predicted	Actual	Predicted	Actual
Omni B down link	0.0 to -6.0	-1.0 to -6.0	-5.5	-5.5	-1.0	-1.0
Omni A up link	+1.0 to -10.0	+1.0 to -12.0	+1.0	-1.5	-7.5	-9.0
Omni B up link*	+1.0 to -3.0	-3.0 to -8.0	+0.2	-3.8	+1.0	-4.0

*Actual gain values are calculated assuming nominal receiver perform-ance. Mission data indicate a -5 db bias in receiver B as discussed in the contents of this report.

Figures 5.3-5 and 5.3-6 indicate that, during the premidcourse and postmidcourse coast periods, received signal levels deviated from the pre-dicted values in both the up and down links. Gyro drift checks performed during these two periods account for earth vector variations not taken into consideration when generating the predictions. As pointed out in Reference 1, these minor look angle variations can cause the observed signal level vari-tions. However, the data indicate that the tolerances on the nominal predicted signal level, which also includes antenna gain variations, found those values seen in the mission data.

5.3.4.4   Mission Phase Three: Canopus Acquisition Maneuver

At approximately L + 6 hours, the star acquisition maneuver was initiated. One roll about the Z-axis was required to make a star map and adequately identify Canopus. An additional 212 degrees of roll were required to finally acquire the star.

Real-time analysis indicated that the roll maneuver would take the earth vector through deep antenna nulls on both the up and down links of omnidirectional antenna A and the down link of antenna B. The maneuver would pass through the low gain region of antenna B, but the deep null region would not be entered. Based on this and the fact that predicted signal level values would not exceed the two-way tracking threshold, two-way trans-ponder B operation was recommended for the Canopus acquisition phase. The analysis also indicated that no significant stars would be in the region where possible data outages would be expected with the spacecraft trans-mitting via omnidirectional antenna B at a data rate of 4400 bits/sec.
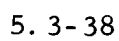
Figure 5.3-4.   DSS-Received Carrier Power (dbm)

5.3-38

Figure 5.3-5. Spacecraft Receiver Signal Level Profile

At 17 hours 46 minutes 35 seconds GMT, transmitter B was commanded to high power with the ground received signal indicating an increase of 21.3 db. Star mapping was initiated at 17 hours 51 minutes 27 seconds GMT from DSS-61 with the spacecraft operating in the transponder B mode and transmitting data at 4400 bits/sec in mode 5. The 360-degree roll produced down-link signal variations of approximately 35 db which agreed with the premaneuver predictions. Minor difficulties were experienced in maintaining decommutator lock; however, no significant data outages occurred. Spacecraft received signal levels during the roll maneuver indicated deviations of approximately 25 db on receive A and 20 db on receiver B. This again agreed with premaneuver predictions. Phase lock on receiver B was maintained throughout the maneuver, and Canopus lock-on was accomplished at 18 hours 10 minutes 22 seconds GMT.

Transmitter B high power was commanded off at 18 hours 14 minutes 49 seconds GMT, which resulted in 28 minutes and 14 seconds of high-power operation for star acquisition. DSS-61 received signal level for low-power operation was -129.8 db, with a resulting +8.8 db nominal telemetry margin for 1100 bits/sec data.

The spacecraft was 212 degrees in a positive roll sense from Canopus prior to the initiation of the Canopus acquisition/verification sequence. With this information and the antenna contour patterns, the variations in antenna gain seen in the data are compared to predicted variations and are illustrated in Figure 5.3-6 which compares omnidirectional antenna B down link, omnidirectional antenna A up link, and omnidirectional antenna B up link, respectively. Both omnidirectional antenna B up and down link signal level variations agree well with antenna gain variations. However, it was during this maneuver that the first evidence of the -5 db bias in receiver B performance was noted.

Relatively good agreement existed between omnidirectional antenna A up-link gain values and the actual signal level variations, except for those values in the region between the -Y axis and the -X axis. A deep null is indicated in mission data which cannot be explained from the analysis of antenna pattern data at points in the vicinity of this region. It has been noted in previous missions that the degree of correlation between antenna pattern data and mission data is not as good on omnidirectional antenna A as on omnidirectional antenna B. However, the presence of an unexplained null of this magnitude would indicate a condition not caused by normal configuration differences which result from assembly tolerances. A similar condition was apparent during this phase of the Surveyor III mission (Reference 1).

5.3.4.5   Mission Phase Four: Midcourse Maneuvers

The L + 39 hours standard roll-yaw was selected from 16 possibilities as the midcourse maneuver. Real-time analysis predicted the following variations in nominal omnidirectional antenna gain during the maneuver:
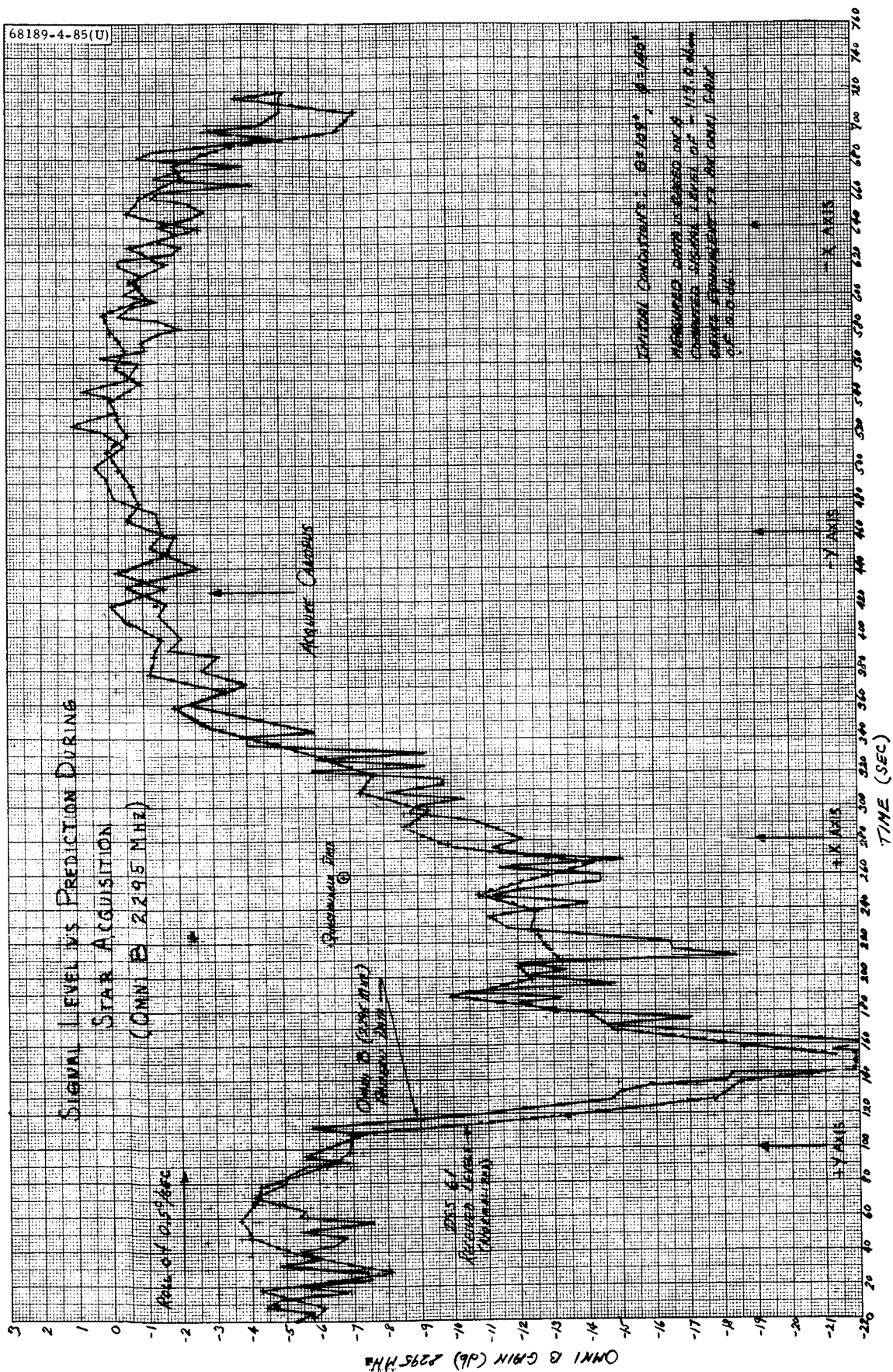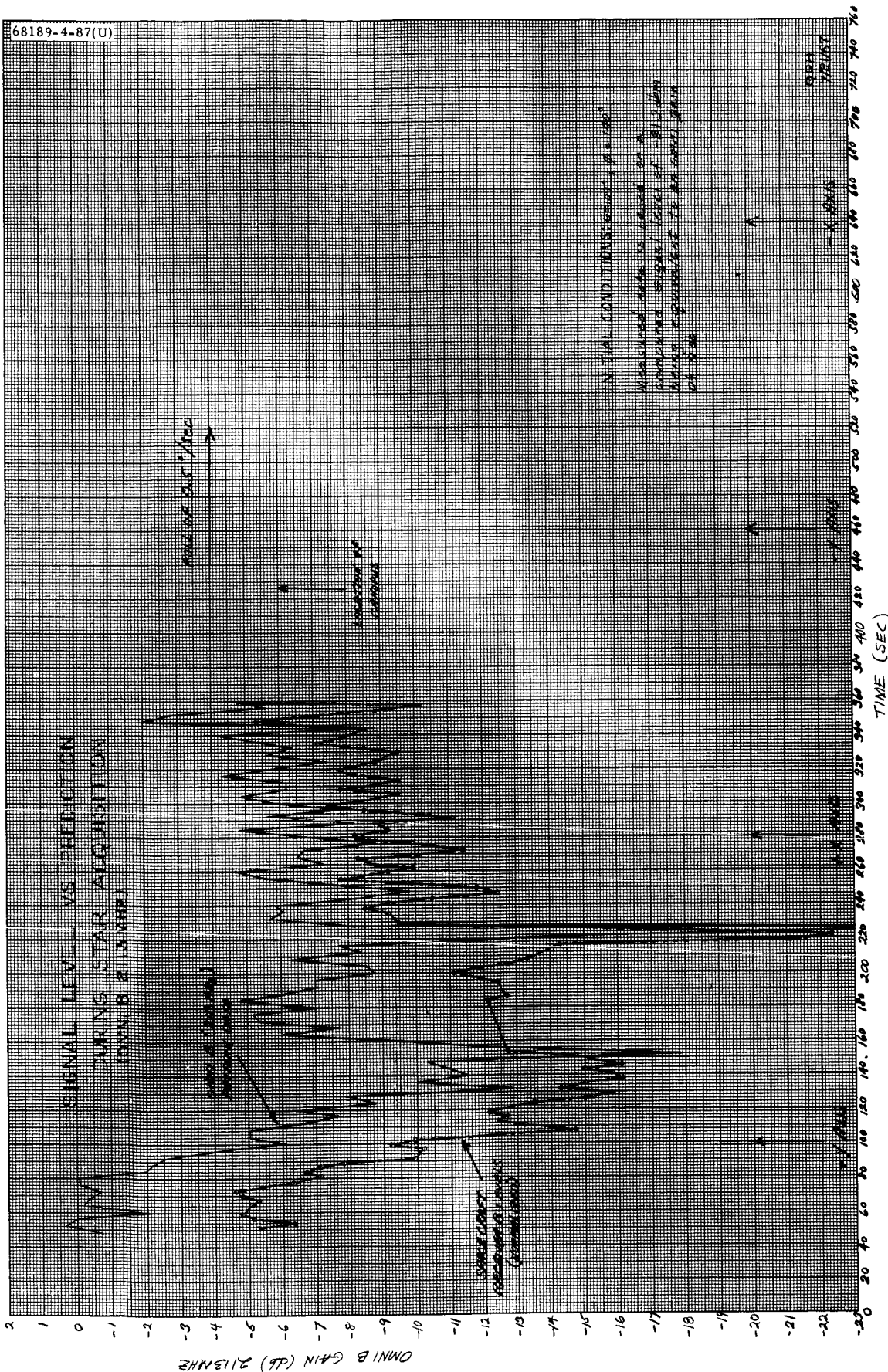
a) Omnidirectional Antenna B Down Link (2295 MHz)

Figure 5.3-6   Signal Level Versus Predictions During Star Acquisition

5.3-41
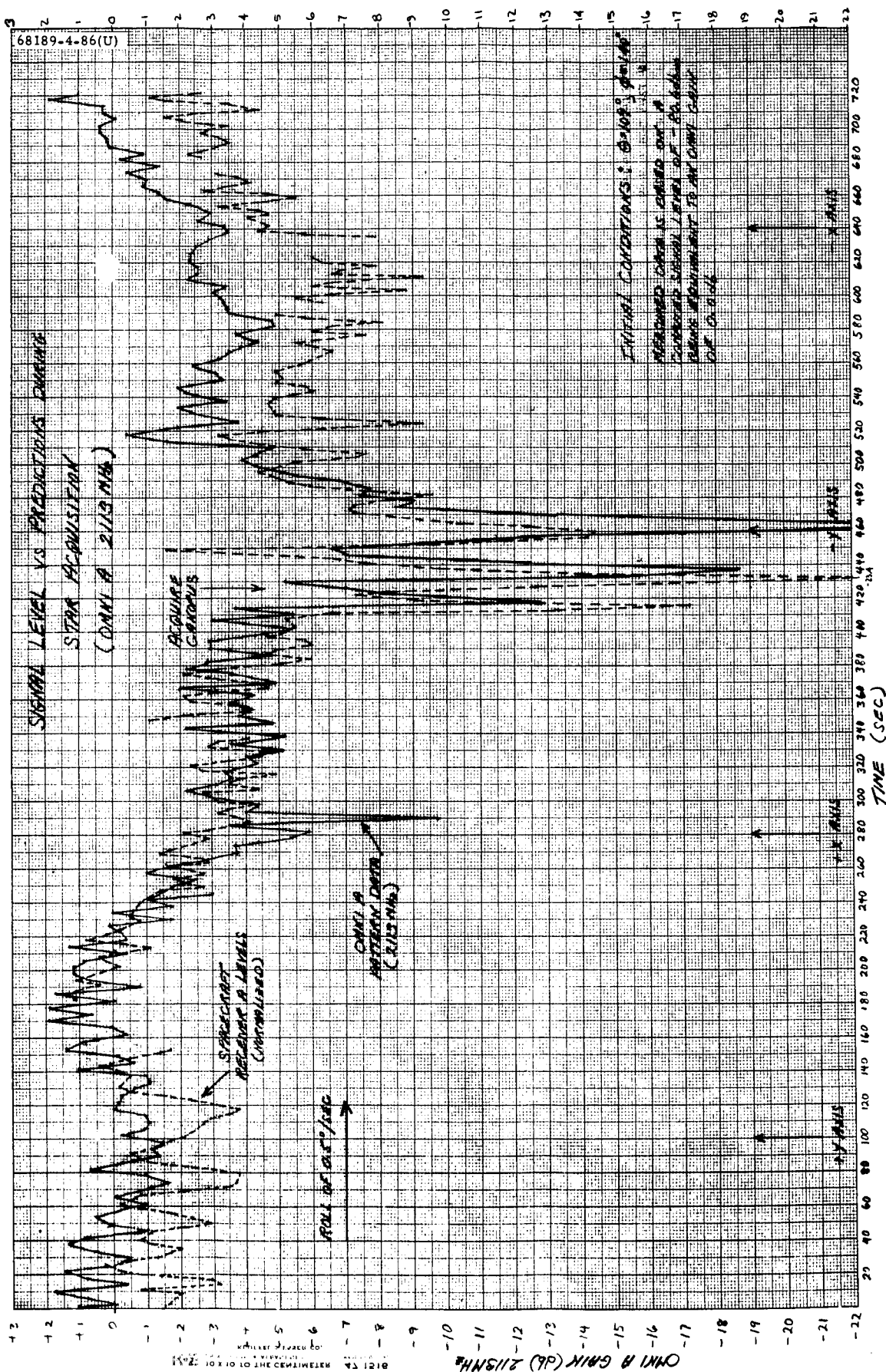
b) Omnidirectional Antenna A Up Link (2113 MHz). Signal Level Versus Predictions During Star Acquisition

Figure 5. 3-6 (continued).

c) Omnidirectional Antenna B UpLink (2113 MHz)

Figure 5.3-6 (continued). Signal Level Versus Predictions During
Star Acquisition

5.3-43
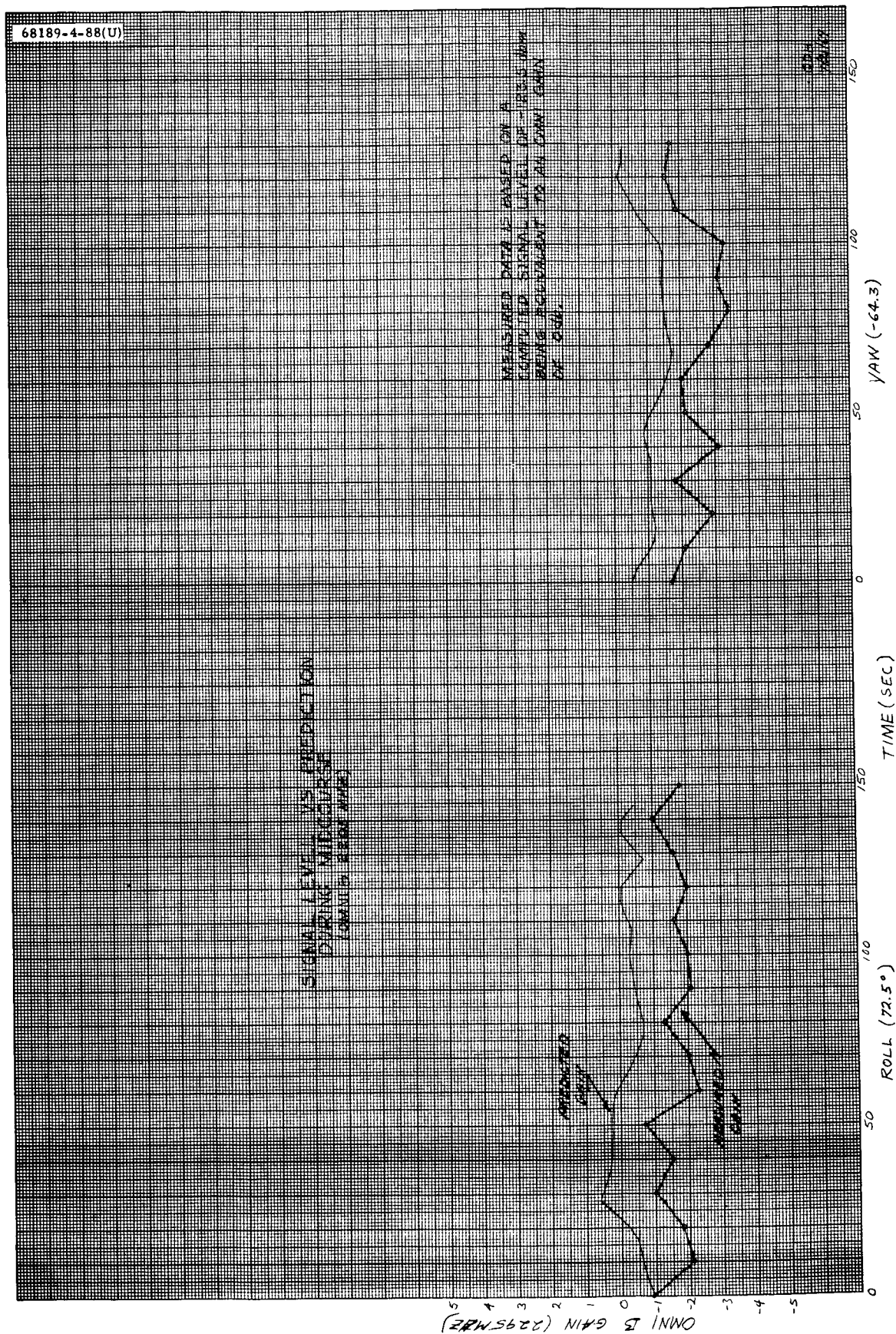
1)   Omnidirectional antenna B down link: -1.7 < G < +0.6 db

2)   Omnidirectional antenna A up link: -19.8 < G < 1.8 db

3)   Omnidirectional antenna B up link: -1.6 < G < +2.3 db

Predicted minimum margins were 12.3 db for 4400 bits/sec telemetry, 1.9 db on receiver A, and 20.1 db on receiver B command links. Two-way (transponder) mode was recommended.

At 2 hours 2 minutes 18 seconds GMT, the spacecraft was commanded to high power, and, at 2 hours 3 minutes 18 seconds GMT, the 4400 bits/sec data rate was selected. The ground received signal increased by 20.7 db when the spacecraft was commanded from low power to high power, with DSS-11 reporting a received carrier power of -124.5 dbm prior to maneuvering. Maneuver initiation times were 2 hours 15 minutes 29 seconds GMT for the roll and 2 hours 21 minutes 10 seconds GMT for the yaw. The premidcourse maneuver ended at 2 hours 23 minutes 20 seconds GMT with the DSS-11 received carrier power reading -125.3 dbm and having indicated approximately a 2.7-db variation during the maneuver, as predicted.

Variations in omnidirectional antenna B down-link antenna gain seen in the data are compared to predicted variations and are illustrated in Figure 5.3-7a. The premidcourse maneuver was executed in mode 1; therefore, no spacecraft receiver signal values were available.

At 2 hours 30 minutes 2 seconds GMT, midcourse thrust was executed. DSS-11 received carrier power was steady with reported 0.1-db variations during the thrusting period.

At 2 hours 31 minutes 24 seconds GMT, mode 5 data were selected in preparation for the postmidcourse maneuver. Maneuver initiation times were 2 hours 32 minutes 53 seconds GMT for the yaw and 2 hours 37 minutes 25 seconds GMT for the roll. The postmidcourse maneuver ended at 2 hours 39 minutes 51 seconds GMT with the DSS-11 received carrier power indications essentially retracing those seen during the premidcourse maneuver. Since the postmidcourse maneuver was executed in data mode 5, spacecraft received signal levels were available.

Variations in omnidirectional antenna A and B up-link antenna gains, as seen in the data, are compared to predicted variations and are illustrated in Figures 5.3-7b and 5.3-7c. The approximate -5 db bias in receiver B is again apparent in Figure 5.3-7c.

Canopus lockon was indicated at 2 hours 40 minutes 18 seconds, and preparations were made to return the spacecraft to its cruise configuration. At the end of the midcourse sequence, the DSS-11 received carrier power (-124.7 dbm) indicated that a nominal 550 bits/sec telemetry margin should exist with the spacecraft in low power. At 2 hours 45 minutes 3 seconds GMT, the 550 bits/sec data rate was selected, and at 2 hours 46 minutes 10 seconds GMT, the spacecraft was returned to low power. The spacecraft

operated in high power for 43 minutes and 52 seconds during the midcourse maneuver sequence. Approximately a 21.1-db decrease from high to low power was noted. The resulting -142.5 dbm received carrier level produced a +1.3 db telemetry margin for 550 bits/sec data.

5.3.4.6   Mission Phase Five: Terminal Maneuver and Descent

The roll-yaw-roll standard maneuver was selected from eight possibilities as the terminal maneuver, and was optimum for the communications link. Real-time analysis predicted the following variations in nominal omnidirectional antenna gains during the maneuver:

1)   Omnidirectional antenna B down link: $-4.5 < G < +1.3$ db

2)   Omnidirectional antenna A up link: $-18.0 < G < -2.0$ db

3)   Omnidirectional antenna B up link: $-12.0 < G < -1.0$ db

Predicted minimum margins were 5.2 db for 1100 bits/sec telemetry, 1.5 db on receiver A, and 7.5 db on receiver B command links. One-way mode was recommended even though adequate margins were available for the transponder operation. This recommendation was made since one-way configuration was desired for the terminal descent sequence and, operationally, it was safer to establish before the terminal maneuver.

The spacecraft was commanded to high power at 1 hour 9 minutes 27 seconds GMT (day 198) and 1100 bits/sec data selected at 1 hour 7 minutes 56 seconds GMT. The resulting -121.0 dbm received signal level indicated an increase of 21.8 db over low-power operation. Transponder B was turned off at 1 hour 17 minutes 9 seconds GMT, establishing the terminal sequence spacecraft configuration. Maneuver initiation times were 1 hour 24 minutes 44 seconds GMT for the first roll, 1 hour 29 minutes 34 seconds GMT for the yaw, and 1 hour 35 minutes 5 seconds GMT for the second roll. The terminal maneuvers ended at approximately 1 hour 35 minutes 57 seconds GMT with the DSS-11 received carrier power reading -123.8 dbm and having indicated approximately a 4.6-db variation during the maneuver, as compared to a predicted variation of 5.8 db.

Up-link signal level variations observed in the telemetry data, as compared to predicted variations, are summarized as follows:

	Gain Variations, db	
	Actual	Predicted
Omnidirectional antenna A	8.0	16.0
Omnidirectional antenna B	11/0	11.0

68189-4-88(U)

a) Omnidirectional Antenna B Down Link

Figure 5.3-7. Omnidirectional Antenna Gains During Midcourse Maneuver
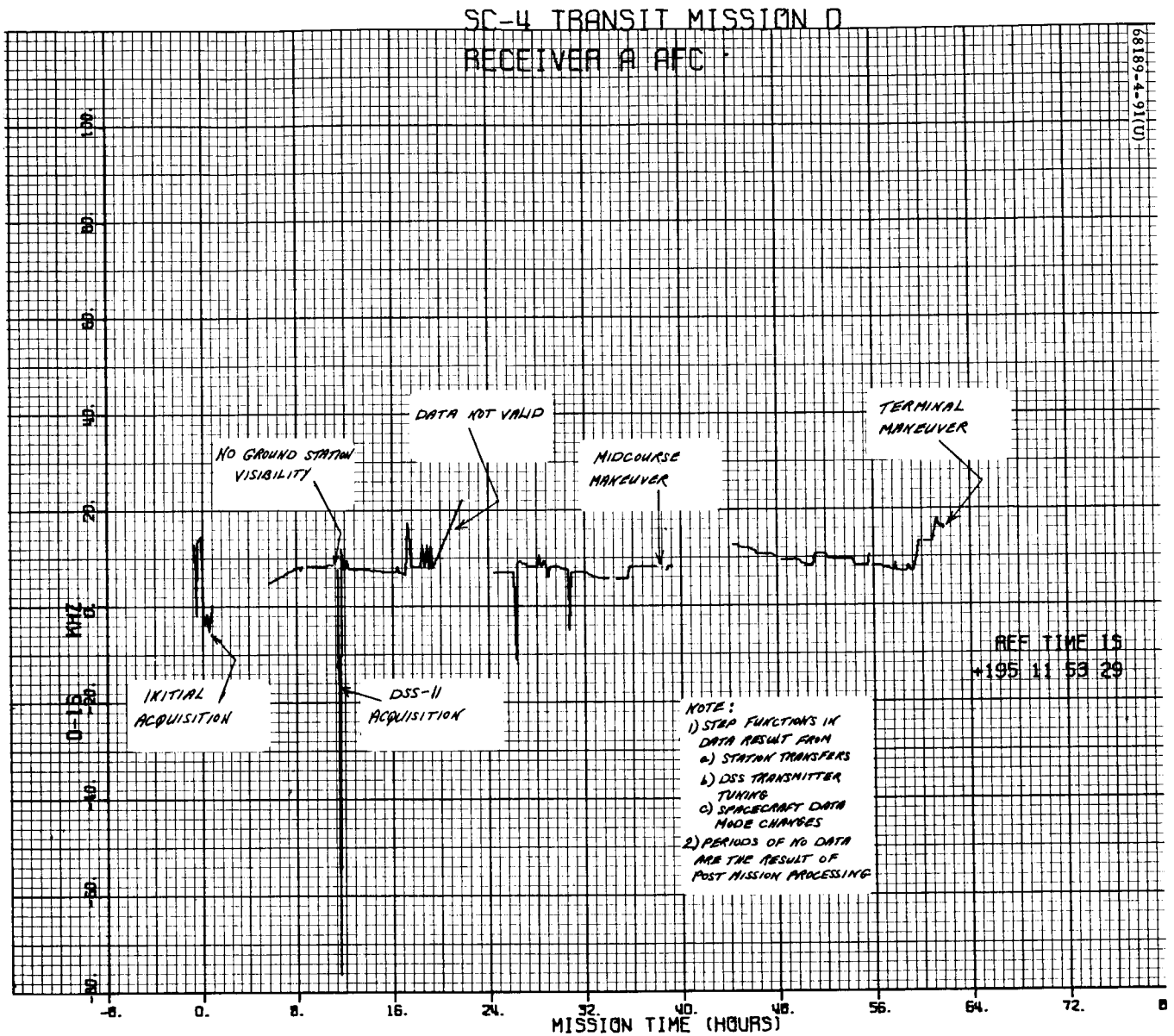
b) Omnidirectional Antenna A Up Link

Figure 5.3-7 (continued). Omnidirectional Antenna Gains During Midcourse Maneuver

5.3-47

Figure 5.3-8.   Received Automatic Frequency Control

NOTE:
1) STEP FUNCTIONS IN
   DATA REPRESENT
   STATION TRANSFERS OR
   TRANSMITTER TUNING
2) PERIODS OF NO DATA
   ARE THE RESULT OF
   POST MISSION PROCESSING

TRANSPONDER B OFF

N3VCXO   TERMINAL
CHECK   MANEUVER

REF TIME IS
+195 11 53 29

NO GROUND STATION
VISIBILITY

INITIAL
ACQUISITION

DSS-11
ACQUISITION

MIDCOURSE
MANEUVER

MH²
O=8

MISSION TIME (HOURS)
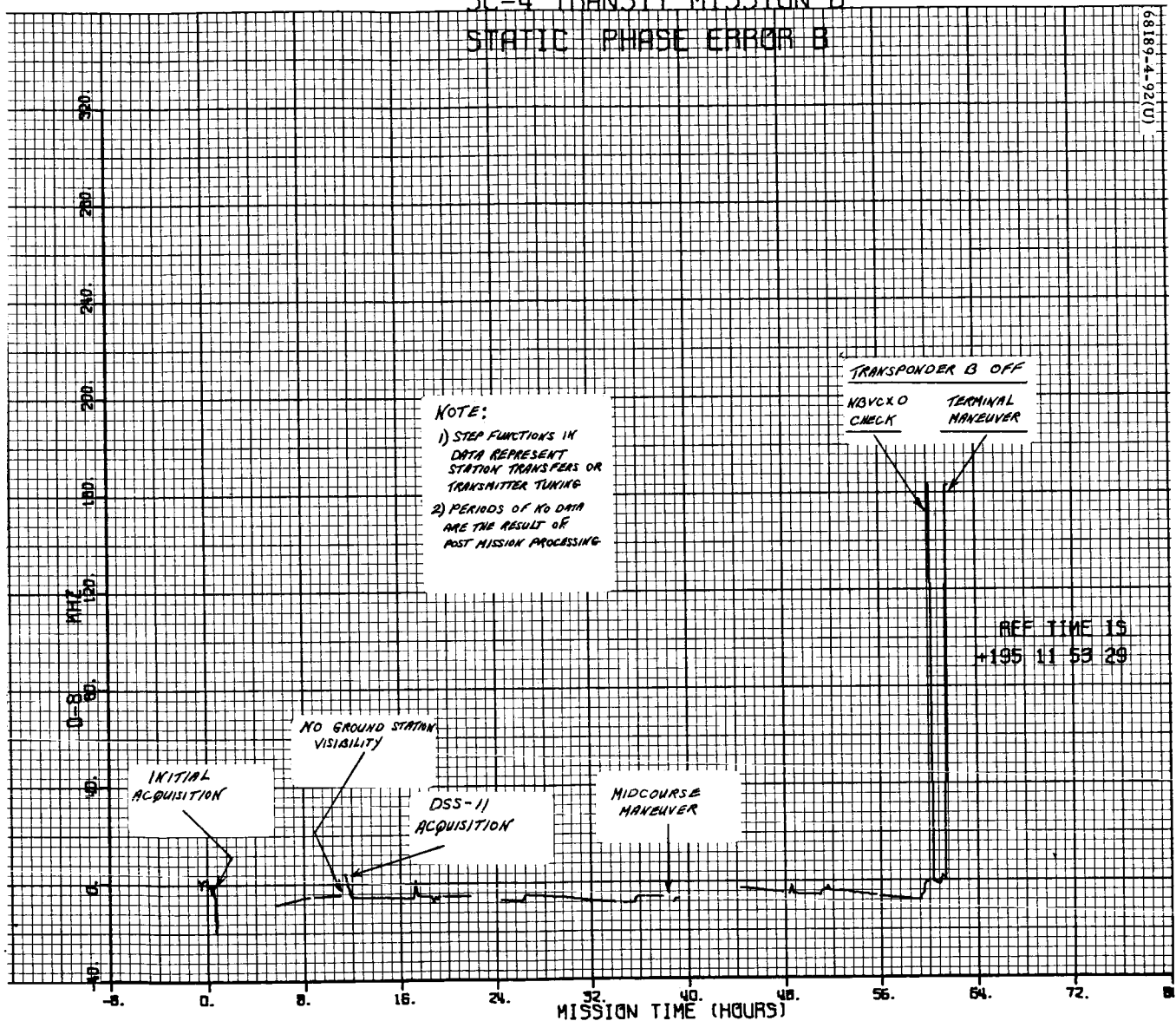
Figure 5.3-9.   Receiver B Static Phase Error

Receiver B Static Phase Error (Figure 5.3-9) — Receiver B was used for transponding through most of the mission. These data thus represent the DSS transmitter frequency offset from the receiver phase lock center frequency. Since these data are analogous to the automatic frequency control data discussed above, the comments apply equally well to these data. It should be noted, however, that this signal is not as sensitive to signal processing effects.

Transmitter B Traveling-Wave Tube Temperature (Figure 5.1-2) — These data represent the temperature of the traveling-wave tube used for high-power transmitter operation during transit.

5.3.5 REFERENCES

1) "Surveyor III Flight Performance Final Report," Hughes Aircraft Company, SSD 68189-3, July 1967.

2) G. A. Tadler, "Telemetry Calibration Data for SC-4," Hughes Aircraft Company, IDC 2294.2/81.

3) J. L. Hoose, "The Effects of Vacuum and Temperature on AGC for SC-4 Receivers," Hughes Aircraft Company, IDC 2294.2/91.

4) J. O. Votaw, "Simultaneous DSS-51 and DSS-11 Loss of Lock at Station Transfer During Pass 2 of Surveyor Mission D," Hughes Aircraft Company, IDC 2292/369.

5) "SC-4 Preliminary Post Flight Data Analysis," Hughes Aircraft Company, 1 August 1967.

6) "Surveyor Mission D Space Flight Operations Report," Hughes Aircraft Company, SSD 74109, August 1967.

5.3.6 ACKNOWLEDGMENTS

1) J. O. Votaw was the coordinator and author of this section.

2) Q. D. Howard and W. Mitchell for their assistance in reducing, formatting, and analyzing much of the data contained in this section.

3) The DSS tracking advisors at JPL for supplying ground station data.

4) The Spacecraft Performance/Analysis/Command Telecommunications Team, consisting of V. S. Amstadter, W. Mitchell, W. G. Moore, and M. R. Weiner, for maintaining accurate mission records and logs.

5) F. K. Rickman who, although not officially a member of the Spacecraft Performance/Analysis/Command Telecommunications Team, significantly contributed to the real-time operational support of the subsystem.

5.4 SIGNAL PROCESSING

5.4.1 INTRODUCTION

The signal processing subsystem is composed of the following units:

1) Engineering signal processor (ESP)

2) Auxiliary engineering signal processor (AESP)

3) Central signal processor (CSP)

4) Signal processing auxiliary (SPA)

5) Low data rate auxiliary (LDRA)

These units contain two electronic commutators with a total of 6 operational modes, 2 analog-to-digital converters that have available 5 digital bit rates, 17 subcarrier oscillators for transmission of pulse coded modulation data and continuous real-time data, 9 summing amplifiers, and signal conditioning subsystem performed normally throughout the mission.

A summary of test and flight values for signal processing telemetry can be found in Table 5.4-1. Values for the Surveyor I, II, and III flights have been included for comparison.

5.4.2 ANOMALIES

There were no anomalies in the signal processing subsystem throughout the flight. The loss of all data during terminal descent was not due to signal processing, and has been discussed in Section 4.3.

5.4.3 SUMMARY

The signal processing subsystem performed properly throughout the flight until loss of data during terminal descent. At this time, all data and communications with the spacecraft were lost.
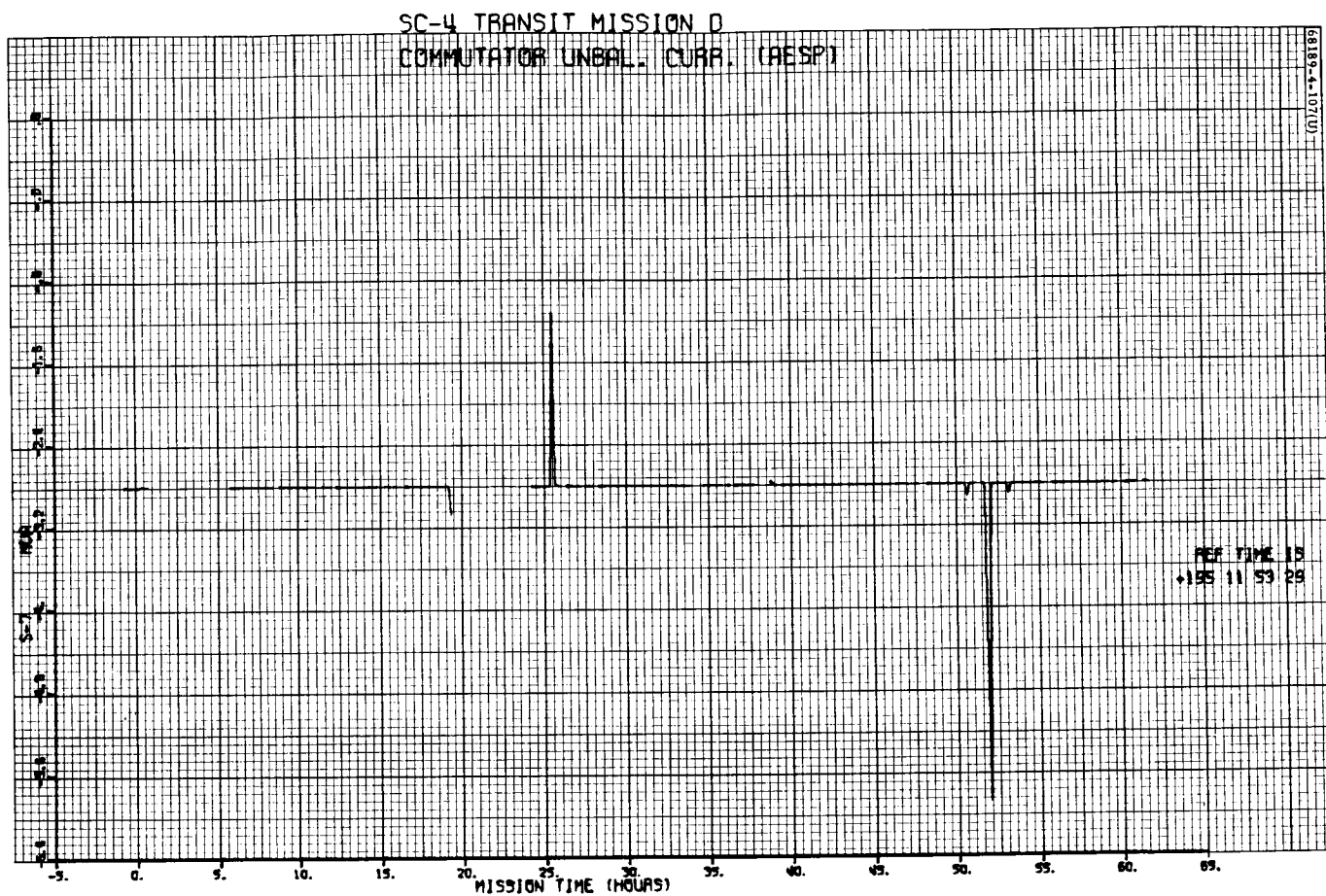
Figure 5.4-1. Commutator Unbalance Current (AESP)

TABLE 5.4-1. COMPARISON OF SIGNAL PROCESSING VALUES
FROM TEST AND FLIGHT

Telemetry Signal	Surveyor IV Retest Values, STV	Surveyor IV Flight Values, Day 197	Surveyor III Retest Values, STV-C4	Surveyor III Flight Values, Day 107	Surveyor II Flight Values	Surveyor I Flight Values
S-1* reference voltage, volts	4.88	4.875	4.86 to -4.9	4.86	4.9	4.88
S-2* reference return, volts	0	0	0	0	0.003	0.0024 to 0.0072
S-5* ESP commutator unbalance current, microamperes	-1.7	-1.714	-2.2 to -2.6	-2.1	-1.4	-3.1
S-7** AESP commutator unbalance current, microamperes	-3.0	-2.813	-1.0 to -1.2	-1.3	-1.7	-2.8

*Mode 4
**Mode 5

5.4.4 SIGNAL PROCESSING ANALYSIS

5.4.4.1 Unbalance Current Corrections

In each telemetry commutator, transistor switches connect each analog output voltage (representing a spacecraft voltage, current, or temperature) with a common commutator line connected to the input of one of two analog-to-digital converters. A bootstrap unloader circuit is connected to this common line to reduce the stray capacitance, equalize the load impedance, and provide bias currents for the commutator and master switches. Since these bias currents are not exactly equal, a difference or unbalance current exists. The telemetry circuit being sampled must supply this current, causing an error in the measured voltage proportional to the output impedance of the circuit.

The unbalance current for a specific telemetry channel in each commutator (S-5 for ESP and S-7 for AESP) is measured in telemetry modes 2, 4, and 5. Figure 5.4-1 shows S-7 up to terminal descent. Although no plot of S-5 has been included, typical values have already been given in Table 5.4-1.

5.4.4.2 Potentiometer Reference Voltage Corrections

The nominally 4.85 reference voltage is supplied by either the ESP or AESP units to the landing gear and solar panel position potentiometers, to the propulsion pressure transducers, and to the secondary sun sensors. This reference voltage, derived from the 29-volt nonessential bus, varies

due to load and input supply voltage changes. The ESP voltage is telemetered in modes 2 and 4, and can be used to correct the affected signals whose calibrations are based on a reference voltage of exactly 4.85 volts. Since the AESP voltage is never telemetered, it must necessarily be obtained through computation.

The mechanism position signals do not normally change in flight after initial deployment since they are mechanically held. Therefore, any apparent difference in a given signal reading from the ESP commutator to the AESP can be due only to a corresponding change in commutator-supplied reference voltage. Based on this assumption, Table 5.4-2 shows the calculation of the AESP reference voltage. At this point in the mission (Launch + 39 hours), the AESP reference voltage was computed to be 1011 BCD (4.938 volts) which is the average of the three sensor calculations in Table 5.4-2.

TABLE 5.4-2. AESP REFERENCE VOLTAGE CALCULATION

GMT, day:hr:min:	Mode	Signal	Telemetry Value, BCD	AESP Reference Voltage Calculation	AESP Reference Voltage
197:02:45	5	M3	628	NA	NA
		M4	374	NA	NA
		M7	504	NA	NA
197:02:43	4	M3	620	$\dfrac{X}{998} = \dfrac{628}{620}$	1010.9
		M4	369	$\dfrac{X}{998} = \dfrac{374}{369}$	1011.6
		M7	498	$\dfrac{X}{998} = \dfrac{504}{498}$	1010.0
		S-1 reference voltage	998		

5.4.4.3 Current Calibration Signals

Current measurements are accomplished by measuring the voltage drop across a low resistance shunt which is in series with the power line being monitored. This measurement is in the range of 0 to 100 millivolts. Since this voltage is not referenced to ground and is not scaled to the 0- to

5-volt telemetry input level range, it is necessary to amplify it with a differential amplifier. The nominal gain of this amplifier is 50, but its actual gain linearity and stability are not specified to a tight tolerance. To determine the current amplifier parameters and thereby increase the accuracy of current measurements, three calibration signals (with 0.2-percent stability) are amplified and telemetered in each commutator. These signals can thus be used by postmission processing for a continual in-flight calibration of the current amplifier.

The majority of the Surveyor IV data was obtained in modes 5 and 6, and therefore only the AESP current calibration signals were investigated. Table 5.4-3 shows that these signals have changed by no more than 0.5 percent since being initially set at the unit flight acceptance test. It is also seen that the gain of the AESP current amplifier was reasonably constant over the mission.

TABLE 5.4-3.   SUMMARY OF CURRENT CALIBRATION
SIGNAL DATA IN AESP

Signal	Function, percent	Flight Data, percent	Remarks
EP-27	90	0.32	Coast phase 1
		0.48	Coast phase 2
EP-28	50	0.1	Coast phase 1
		0.49	Coast phase 2
EP-29	10	0.32	Coast phase 1
		0.48	Coast phase 2

The AESP midscale current calibration sensor, EP-28, is shown in Figure 5.4-2 as a typical representative of the AESP calibration telemetry. It can be seen that the signal value is a function of bit rate. This effect was noted previously as occurring on Surveyors II and III.

5.4.5   ACKNOWLEDGMENTS

This section was coordinated by A. W. Dittmer.
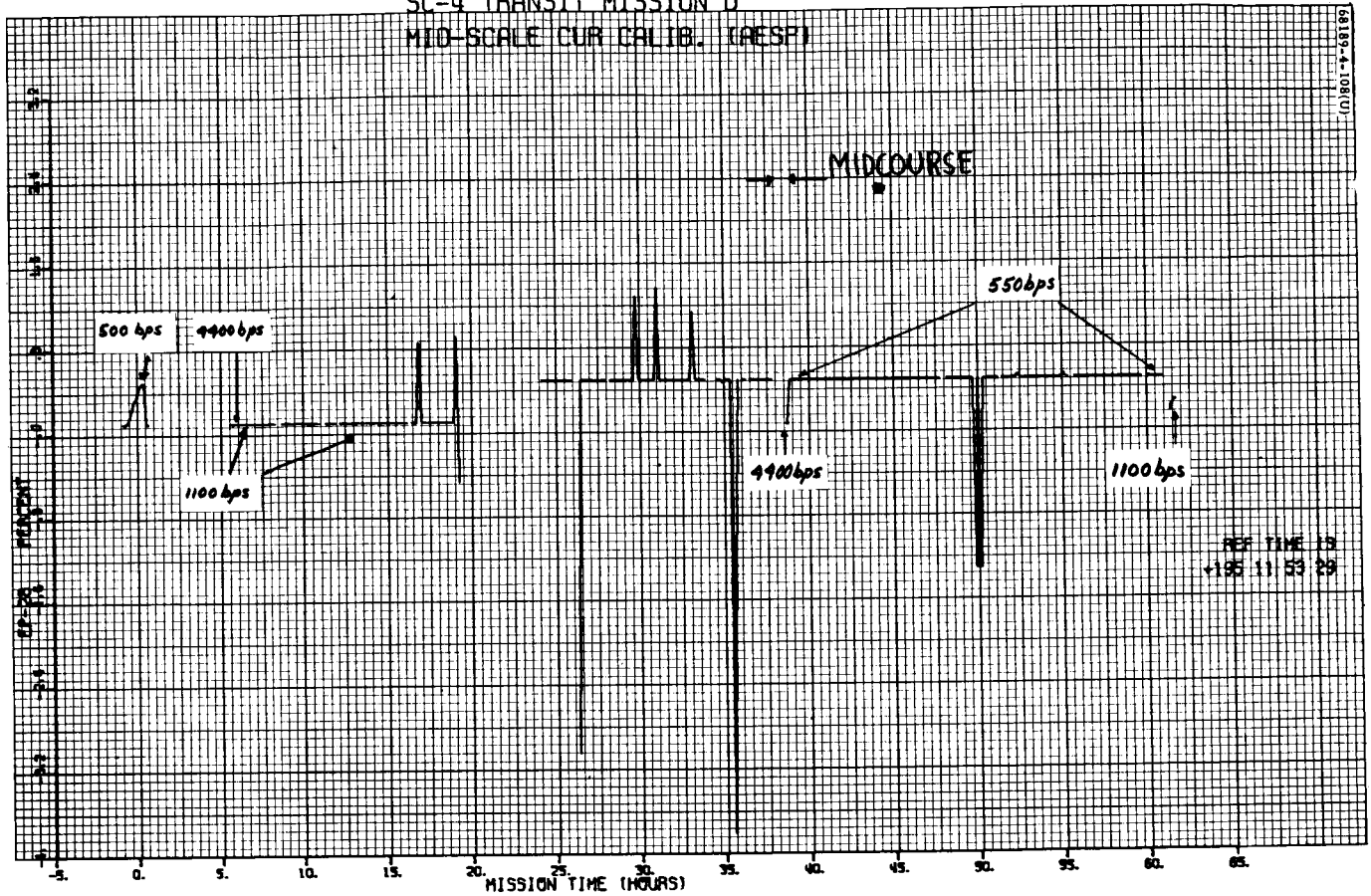
Figure 5.4-2. Midscale Current Calibration (AESP)

5.5   FLIGHT CONTROL

5.5.1   INTRODUCTION

The principal requirements of the Surveyor flight control system are attitude control, accurate angular maneuvers, precision velocity corrections, and a soft lunar landing. In order to accomplish these functions, the control system utilizes such hardware as gyros, gas jets, a solid fuel engine, liquid fuel engines, optical sensors, timing devices, radars, and acceleration sensing mechanisms.

5.5.1.1   Attitude Control

Attitude control is accomplished by two basic types of active control systems. During coast phase, a bang-bang type of attitude gas jet system is employed which utilizes artifical rate feedback for loop stabilization. During periods of potentially large moment disturbances, such as the main retro phase, the throttle-controlled vernier engine system is used. The error signals required for controlling the propulsion systems are derived from optical sensors or rate integrating gyros which are mounted on the spacecraft in such a way as to provide a three-axis control system. During coast phase, when the gas jet system is used, two modes of operation are available. One is the celestial referenced mode using the sun and Canopus, and the second is self-contained inertial referencing (gyros). The first mode is used to establish accurate spatial attitude, and the second mode is generally used when momentary inertial reference is desired; such an instance occurs during an attitude maneuver.

5.5.1.2   Angular Maneuvers

The rate integrating gyros are also used for accurate angular maneuvers, accomplished by precessing the gyros at precise rates for given time intervals and slaving the spacecraft to the gyros through the gas jet system.

5.5.1.3   Velocity Correction

A midcourse velocity correction capability is provided by a system consisting of three vernier engines, a precision timer, and an accurate acceleration sensing device. The difference between the commanded acceleration level and the output from an accelerometer provides the error signal that commands the vernier engines to the required thrust levels. The constant

acceleration and variable time concept used by the Surveyor flight control system provides the flexibility of choosing velocity corrections from 0 to 50 m/sec.

5.5.1.4 Soft Landing

Surveyor's soft landing capability is provided by a sophisticated technique utilizing radars to compute velocities and range. The range information is then used by an on-board computer to provide vertical velocity commands to the vernier engine system according to an approximate, constant acceleration, V^2/R function. The velocity information is used by the vernier engine attitude control loop to produce a near-gravity turn descent by aligning the spacecraft thrust axis to the true velocity vector. The velocity information is also used, along with velocity commands, to generate error signals for the velocity control loop.

To provide the required condition of low velocity for the soft landing phase, a large amount of approach velocity is removed by a solid fuel rocket engine during the initial portion of the terminal descent phase. Spacecraft attitude during this phase is inertially stabilized by the gyro vernier engine control system.

5.5.1.5 Mission Performance

Surveyor IV performance was satisfactory until approximately 2 seconds before burnout of the main retro engine when all data was lost.

5.5.1.6 Analysis

Subsection 5.5.4 contains the analysis effort. The analysis items are categorized under major mission phases for easier identification and performance evaluation. A log of time and events is presented in Table 5.5-1, and a table of results (Table 5.5-2) is given in subsection 5.5.3.

5.5.2 ANOMALY DESCRIPTION

The only flight control anomaly that occurred during the mission is described briefly below.

Vernier Engine Thrust Command Modulation

Following ignition of the vernier engines and main retro engine, the vernier engine thrust commands were modulated at a frequency between 1.5 and 25 cps. The peak-to-peak amplitudes were approximately 7.0 pounds on engines 1 and 2 and 2.0 pounds on engine 3. A detailed discussion of this anomalous behavior is presented in subsection 5.5.4.12.

TABLE 5.5-1. SURVEYOR IV TIME AND EVENTS LOG

Event	Date, GMT	Mission Time	
		GMT, hr:min:sec	From Launch
Launch	14 July 1967	11:53:29	0
Injection		12:05:05	11M36S
Separation			
Electrical		12:06:01	12M32S
Mechanical		12:06:06	12M37S
Automatic sun acquisition			
Start		12:06:54	13M23S
Completed		12:10:24	16M55S
Automatic solar panel			
Deployment completed		12:11:59	18M30S
Canopus verification, started		17:51:28	5H57M59S
Canopus acquisition, completed (Canopus lockon)		18:10:21	6H16M52S
Gyro drift check No. 1			
Start		18:46:01	6H52M32S
Stop		20:54:14	9H0M45S
Gyro drift check No. 2			
Start		20:57:43	9H4M14S
Stop		22:37:24	10H43M55S
Gyro drift check No. 3			
Start	15 July 1967	00:09:25	12H15M56S
Stop		02:09:24	14H15M55S
Gyro drift check No. 4 (roll only)			
Start		02:18:52	14H25M23S
Stop		07:54:56	20H01M27S

Table 5.5-1 (continued)

| Event | Date, GMT | Mission Time | |
		GMT, hr:min:sec	From Launch
Gyro drift check No. 5			
Start		08:00:56	20H07M27S
Stop		09:58:27	22H04M58S
Gyro drift check No. 6			
Start		10:20:12	22H26M43S
Stop		11:47:01	23H53M32S
Gyro dirft check No. 7			
Start		16:08:33	28H15M04S
Stop		17:38:33	29H45M04S
Gyro drift check No. 8			
Start		18:03:17	30H09M48S
Stop		19:42:36	31H49M07S
Gyro drift check No. 9 (roll only). No data			
Start		21:39:49	33H46M20S
Stop		22:27:26	34H33M57S
Premidcourse (+) roll of 72.5 degrees	17 July 1967		
Start		02:15:31	38H22M02S
Stop		02:17:56	38H24M37S
Premidcourse (-) yaw of 64.3 degrees			
Start		02:21:12	38H27M43S
Stop		02:23:20	38H29M51S
Midcourse thrust			
Start		02:30:04.1	38H36M34.9S
Stop		02:30:14.6	38H36M50.4S
Sun reacquired		02:34:40	38H41M11S
Canopus reacquired		02:40:18	38H46M49S

Table 5.5-1 (continued)

Event	Date, GMT	Mission Time GMT, hr:min:sec	Mission Time From Launch
Gyro drift check No. 10			
Start		04:15:58	40H22M29S
Stop		05:50:44	41H57M15S
Gyro drift check No. 11 (roll only)			
Start		08:50:59	44H57M30S
Stop		14:36:18	50H42M49S
Gyro drift check No. 12			
Start		15:40:34	51H47M05S
Stop		17:30:30	53H37M01S
Gyro drift check No. 13			
Start		17:39:40	53H46M11S
Stop	18 July 1967	19:13:00	55H19M31S
Preretro (+) roll, 80.4 degrees			
Start		01:24:47	61H31M18S
Stop		01:27:28	61H33M59S
Preretro (+) yaw, 92.7 degrees			
Start		01:29:37	61H36M08S
Stop		01:32:42	61H39M13S
Preretro (-) roll, 25.3 degrees			
Start		01:35:07	61H41M38S
Stop		01:35:58	61H42M03S
AMR mark		02:01:56.1	62H08M26.9S
Vernier ignition		02:01:58.8	62H08M29.6S
Retro ignition		02:01:59.9	62H08M30.7S
Loss of data		02:02:41	62H09M11.8S

TABLE 5.5-2. FLIGHT CONTROL RESULTS

	Controlling Specification	Specification Value	Results	Comments
Prelaunch				
Proper gyro temperature control			Roll 167. 2°F Pitch 161. 2°F Yaw 161. 5°F	Time was 195:10:38 GMT
Verification of N_2 loading	224832A	4. 6 pounds	4. 56 pounds	(FC-4) = 4568 psi (FC-48) = 75. 8°F
Centaur separation	(3. 5. 2. 1)			
Time required to null rates to less than 0. 1 deg/sec		<0. 1 deg/sec within 50 seconds	<13 seconds	
Magnitude of angular rate at separation		≤3. 0 deg/sec	<0. 2 deg/sec	
Sun acquisition	(7. 3. 3. 3. 4)	Minus roll maneuver until activation of acquisition sun sensor and then a plus yaw maneuver until primary sun sensor illumination		
Proper sun acquisition				
Roll			-59. 4 degrees of roll	
Yaw			42. 1 degrees of yaw	
Total time			203 seconds	
N_2 gas used	Design	0. 054 pound (average)	<0. 1 pound	Tank temperature may not have been at steady state
Star acquisition	(7. 3. 3. 3. 5)	Positive roll maneuver sufficient to produce an adequate star map for Canopus verification. Provide a lockon signal when Canopus appears in the sensor field of view		
Proper acquisition and verification of Canopus			Automatic lockon	
Roll angle from beginning of maneuver to Canopus			210. 5 degrees	
Stars identified			Eta U Majoris, Delta Veldrum, Gamma Casiopeiae, Canopus, earth, and moon	
Mean roll rate during star map phase		0. 5 deg/sec	0. 5003 deg/sec	
Effective gain (relative to nominal Canopus) of Canopus sensor			1. 16 X Canopus	
N_2 gas used	Design	0. 048 pound (average)	0. 03 pound	
Coast mode	(7. 3. 3. 3. 6)	Roll axis shall be held to within 0. 20 degree of sun-spacecraft line, plus a ±0. 30 degree limit cycle		Sun and star error signal noise level were low enough to have no effect on the limit cycle performance
		Same magnitude as above for Canopus-spacecraft line		
Limit cycle (gas jet system)	(7. 3. 3. 3. 3)			
Optical mode/inertial mode	(7. 3. 3. 3. 5)	±0. 30 degree		Values are that of the total deadband. Predicted values were:
Average amplitude – roll			0. 6/0. 48 degree	0. 44/0. 44 degree
Average amplitude – pitch			0. 44/0. 46 degree	0. 44/0. 44 degree
Average amplitude – yaw			0. 41/0. 53 degree	0. 44/0. 44 degree
Average period			64 (optical) and 61 sec/pulse (inertial)	80 (optical) and 117 sec/pulse (inertial)
Average N_2 usage	Design	0. 0012 lb/hr (average)	0. 0012 lb/hr	
Gyro drift	(7. 3. 3. 3. 3C)	<1 deg/hr		
Roll			Roll -0. 5 deg/hr	
Pitch			Pitch -1. 0 deg/hr	
Yaw			Yaw +0. 15 deg/hr	
Gas jet thrust level		>0. 052 pound	0. 072 pound (roll)	Design value is 0. 057 pound
Premidcourse maneuvers				
Maneuver angles	(7. 3. 3. 3. 7)	Rates shall be controlled to be 0.5±0.0011deg/sec		Assuming a precession level of 0. 5000 deg/sec
Roll			+72. 37 degrees	
Yaw			-64. 37 degrees	
Precession command times		0. 2 second plus 0. 02 percent of command interval magnitude		These times were obtained from the gyro error signal response profile
Roll			144. 74 seconds	
Yaw			128. 74 seconds	
Attitude maneuver accuracy (includes drift, initial attitude errors, and limit cycle)			-0. 12 degree (yaw) -0. 15 degree (pitch)	Calculated using actual data of drift, attitude errors, and execution errors
Max. midcourse accel. error	224832A	ΔV error <± 1. 3 ft/sec		
Expected ΔV/tracking ΔV			33. 81 fps 33. 24 fps	
Shutdown impulse	(8. 3. 1. 3. 2. 4. 1)	<5 lb-sec/engine Δ impulse <0. 66 lb/sec		
Engine 1			-0. 18 lb-sec	
Engine 2			+0. 03 lb-sec	
Engine 3			+0. 15 lb-sec	

Table 5.5-2 (continued)

	Controlling Specification	Specification Value	Results	Comments
Preretro maneuvers				
Maneuver angles	(7.3.3.3.7)	Rates shall be controlled to be 0.5 ± 0.0011 deg/sec		Values only include execution error. The desired values were:
Roll			+80.8 degrees	Roll (+) 80.9 degrees
Yaw			+92.7 degrees	Yaw (+) 92.7 degrees
Roll			-25.4 degrees	Roll (-) 25.3 degrees
Precession command times		0.2 second plus 0.02 percent of the command interval magnitude		The command values were:
Roll			161.6 seconds	162 seconds
Yaw			185.34 seconds	185.6 seconds
Roll			50.75 seconds	50.8 seconds
Pointing accuracy (includes drift, initial attitude errors, and limit cycle)		Within ±1 degree	0.14 degree	
Gyro drift compensation values				
Roll			-0.5 deg/hr	
Pitch			-1.0 deg/hr	
Yaw			+0.15 deg/hr	
Terminal descent				
AMR marking altitude	(7.6.1)	Nominal slant range of 60 miles		
Main retro				
Burn time (from ignition to 3.5 g switch)	(7.3.3.3.9)	Approximately 42 seconds	≈42 seconds at time of data loss	
Maximum retro thrust		<10,000 pounds	≈9250 pounds	Computed using retro accelerometer data
Peak attitude transient at vernier ignite — retro ignite	(7.3.3.3.10)			
Roll			-0.47 degree	
Pitch			≈0 degree	
Yaw			-0.39 degree	
Main retro thrust vector to spacecraft center of gravity offset	(8.3.5.3.2.8)	<0.18 inch		Exact values were limited by telemetry accuracy of the parameters
Thrust vector pointing accuracy during retro burn	(8.3.5.3.2.9)	Within ±1 degree	0.17 degree	Based on estimated versus actual lateral velocities
Mean attitude error during burn				
Roll			≈0 degree	
Pitch			≈0 degree	
Yaw			-0.28 degree	
Roll actuator position				
Peak at retro ignition			+0.58 degree	
Mean value during burn			≈0 degree	
Time between major events	(7.3.3.3.9)			
AMR mark and vernier inition		0 to 20 seconds	2.73 seconds	
Vernier and retro ignition		1.1 ± 0.1 seconds	1.115 seconds	
Data loss condition	224832A			
Altitude/slant range			57,000 feet (SR)	
Velocity			V_z = 1100 ft/sec	V_x = -87 ft/sec and V_y = -20 ft/sec
Angle between thrust vector and velocity vector				
Additional information				
Total nitrogen gas used	Design	0.65 ± 0.22 pound	0.64	See coast mode gas consumption
Gyro speeds	235159	Telemetry value ≈ 50 cps for all three gyros		
Roll gyro			Roll = 50 cps (average)	
Pitch gyro			Pitch = 50 cps (average)	
Yaw gyro			Yaw = 50 cps (average)	
Gyro heater duty cycle				
Roll			Roll = 20 percent (on)	
Pitch			Pitch = 35 percent (on)	
Yaw			Yaw = 19 percent (on)	

5.5.3 SUMMARY

A summary of flight control system performance is presented in Table 5.5-2.

Performance was completely normal until shortly after vernier and retro engine ignition when a low level thrust modulation appeared on the vernier engine thrust commands. Subsequent investigation revealed that the most probable cause of the modulation was the excitation of a spacecraft structural mode by the retro, or retro and vernier engine combination, with amplitude sufficient to cause an attitude control system response. The induced loads on the spacecraft at the determined frequency are not of sufficient magnitude to normally cause a structural failure.

5.5.4 SUBSYSTEM PERFORMANCE ANALYSIS

5.5.4.1 Prelaunch

Gyro Temperatures

The gyro temperatures at the turn-on of flight control 29-volt coast phase power and just prior to launch at 10 hours 38 minutes GMT are shown below in Table 5.5-3.

TABLE 5.5-3.   PRELAUNCH GYRO TEMPERATURES (°F)

Gyros	Prelaunch, 10:38 GMT
Roll	167.2
Pitch	161.2
Yaw	161.5

Nitrogen Weight

The estimated on-board nitrogen weight at launch was 4.56 pounds based on a telemetered tank pressure of 4568 psi at a tank temperature of 75.8°F. This agreed closely with the best estimate of 4.6 pounds of nitrogen loaded. All subsequent nitrogen weight estimates were corrected for this 0.04-pound difference.

5.5.4.2 Launch Through Separation From Centaur

After extending its landing legs, Surveyor is separated from the Centaur booster. When the three legs-down signals and the separation signal have been generated, the programmer removes the logic signal which has

been inhibiting operation of the gas jet amplifiers. At this same instant, the magnitude register begins to count down 1024 counts for a 51-second interval; the start of sun acquisition is inhibited for this interval to give the cold gas attitude control system opportunity to rate stabilize the spacecraft. Table 5.5-1 presents these events in time reference.

Rate stabilization is accomplished by using the three-axis attitude control system to torque the spacecraft and drive the caged integrating rate gyros error signals to within the deadband of each gas jet amplifier. Thus, at the end of a nominal rate stabilization maneuver, the spacecraft has achieved a low angular velocity at a random orientation in inertial space. The system response is dependent upon the magnitude and direction of the initial velocity vector and the gas jet thrust levels, and is essentially dead-band in nature.

Flight control system performance just after Centaur separation was evaluated for proper nulling of the separation rates, the time required to null rates to less than 0.1 deg/sec, the total angular excursion, and magnitude of angular rates due to separation. The events observed from launch through separation and sun acquisition are depicted in Figure 5.5-1.

Separation transients based on data received via the Space Flight Operations Facility are plotted in Figure 5.5-2. The roll transient appears normal and indicates that any separation-induced rate was essentially zero. While the pitch and yaw transients also indicate very small separation-induced rates, it appears that an impulse disturbance caused a transient motion away from null about both axes at mechanical separation. In order to better understand the nature of this disturbance, the initial conditions at separation were used as inputs to a three degree-of-freedom analog simulation. The results of the simulation for the case where no external forces are present at mechanical separation is shown in Figure 5.5-3a. The roll transient agrees closely with the Space Flight Operations Facility data, while the pitch and yaw transients do not. A good match for the pitch and yaw transients was obtained by introducing a negative 8.2 ft-lb-sec disturbance about the yaw axis and a 2.5 ft-lb-sec disturbance about the pitch axis at mechanical separation (Figure 5.5-3b). It is assumed that the separation springs apparently were the source of the disturbance even though Centaur data indicated that extension of the three separation springs was essentially simultaneous.

All three body rates were reduced to ≤0.1 deg/sec in less than 13 seconds. The total attitude change of the spacecraft from the time of mechanical separation until each body rate was less than 0.1 deg/sec is simply the time integral of the plots in Figure 5.5-2 over the applicable time range. Graphical integration provided the following results:

Roll: 0 degree

Pitch: +0.35 degree

Yaw: -2.0 degrees

The expected nitrogen usage for rate dissipation is small. A typical rate dissipation transient will require the use of 0.040 pound of nitrogen. Because the measurement uncertainties are large compared to the usage, no quantitative measurement of nitrogen gas consumption during rate dissipation was attempted.

5.5.4.3 Sun Acquisition

Fifty-one seconds after electrical separation, sun acquisition is initiated by a command from the flight control programmer which causes a vehicle roll maneuver of -0.5 deg/sec and continues until the sun comes into the acquisition sun sensor field of view which is aligned approximately to the spacecraft roll-pitch plane. When this occurs, the roll command is removed and a plus yaw maneuver is initiated to point the primary sun sensor line of sight toward the sun. When the sun falls into the primary sun sensor field of view, a lockon signal is generated. This signal switches vehicle attitude control to the primary sun sensor and also serves to indicate (via telemetry) the completion of sun acquisition.

The automatic sun acquisition mode was initiated at 12 hours 6 minutes 54.193 seconds GMT as indicated by setting of the sun mode "on" latch. The estimated magnitude of the roll maneuver based on a constant gyro precession rate of 0.5 deg/sec was 59.4 degrees, while the yaw maneuver was estimated to be 45.6 degrees. The primary sun sensor lockon signal was generated at a primary sun sensor pitch error of approximately -3.0 degrees and a yaw error of -12.6 degrees, which is within the expected lockon field of view range of the sensor. The sun acquisition phase is depicted in Figure 5.5-4.

Nitrogen Utilization

Following sun acquisition, the remaining nitrogen was estimated at 4.45 pounds, indicating that 0.11 pound was consumed during the separation rate dissipation and sun acquisition maneuvers. This is quite close to the expected nominal value of 0.094 pound.

5.5.4.4 Canopus (Star) Acquisition

As defined in Reference 1 (Specification 224510, Revision E) paragraph 3.4.2:

". . . the spacecraft is commanded to roll up to 720 degrees in one continuous roll. During this roll, the unthresholded star intensity signal, as well as the normal thresholded signal, is monitored. From these signals, a star map is made and Canopus identified. The capability for performing at least four of these verifications shall be provided. This verification shall be performed before the normal star acquisition mode is initiated. The star acquisition command starts a vehicle positive roll of 0.5 deg/sec until a star of the correct brightness falls into the sensor field of view. When this occurs, a lockon signal is generated which stops the 0.5 deg/sec roll rate and switches the vehicle roll control to the star sensor error signal. "
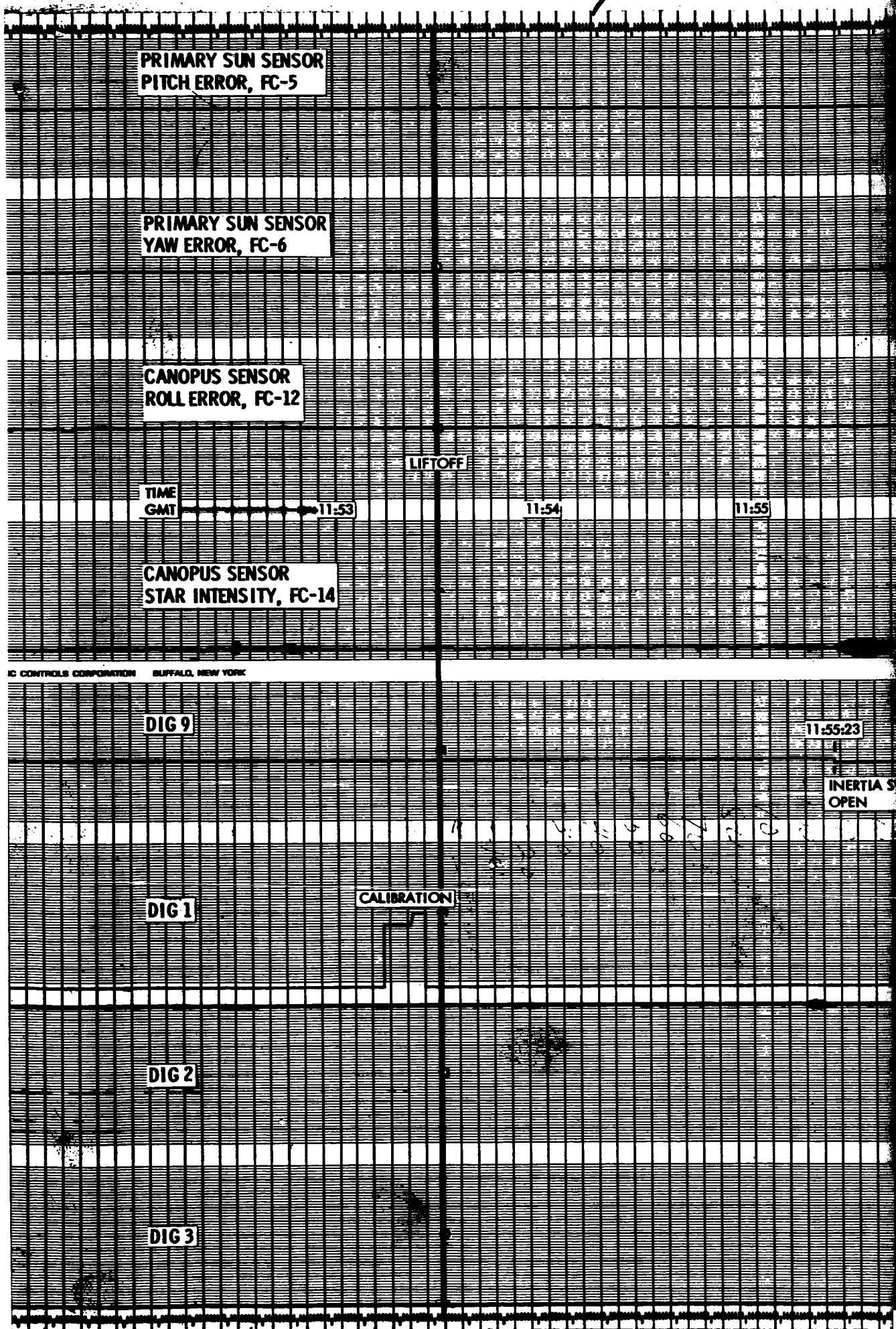
Figure 5.5-1. Launch Through Sun Aquisition

FOLDOUT FRAME 1

11:56:55

MARK 4

11:56   11:57   11:58   11:59   ·12:00

NOSE FAIRING JETTISON
MARK 4

PRINTED IN U.S.A.   RECORDED CHARTS   GRAPHIC CONTROLS CORPORATION   BUFFALO, NEW YORK
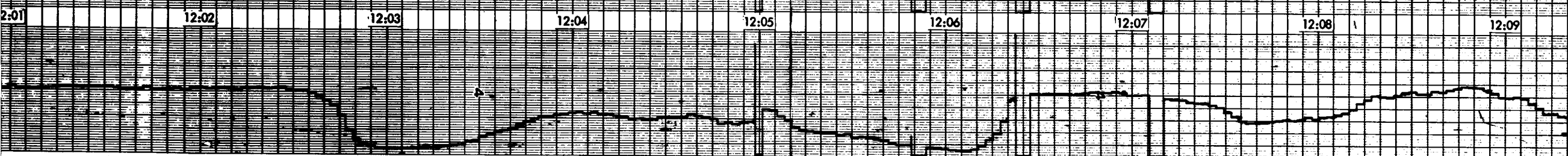
55:52

CAL

12:01   12:02   12:03   12:04   12:05   12:06   12:07   12:08   12:09

PRINTED IN U.S.A.   RECORDING CHARTS GRAPHIC CONTROLS CORPORATION   BUFFALO, NEW YORK   PRINTE

INERTIA
SWITCH

OPEN   CLOSE

RATE MODE RESET
SUN MODE SET

LEGS
EXTENDED

GAS JETS
ENABLED

ELECTRICAL
SEPARATION

ACQUISITION SUN SENSOR
"ON"

CLOCK
COUNTING
DOWN

START OF SUN
ACQUISITION ROLL

END OF CHART

12:10 12:11 12:12

RECORDING CHARTS GRAPHIC CONTROLS CORPORATION BUFFALO, NEW YORK

PRINTED IN U.S.A.

CALIBRATION
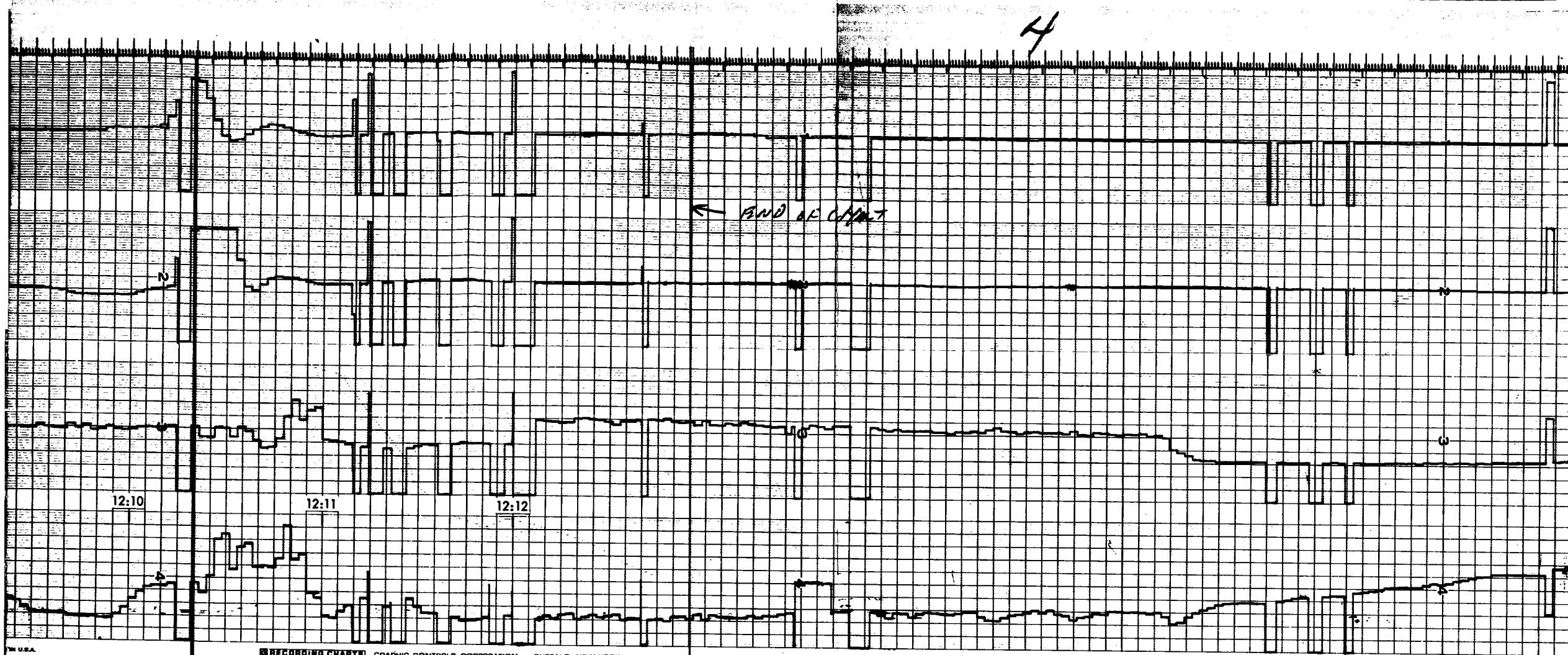
SUN LOCK ON

Figure 5.5-1 (continued). Launch Through Sun Aquisition

FRAME 3

FOLDOUT FRAME 1

DOUT FRAME

N LOCKON)

12:11   12:12   12:13

← END OF CHART

BUFFALO, NEW YORK   PRINTED IN U.S.A   Ⓖ RECORDING CHARTS   GRAPHIC CONTROLS CORPORATION   BUFFALO, NEW YORK
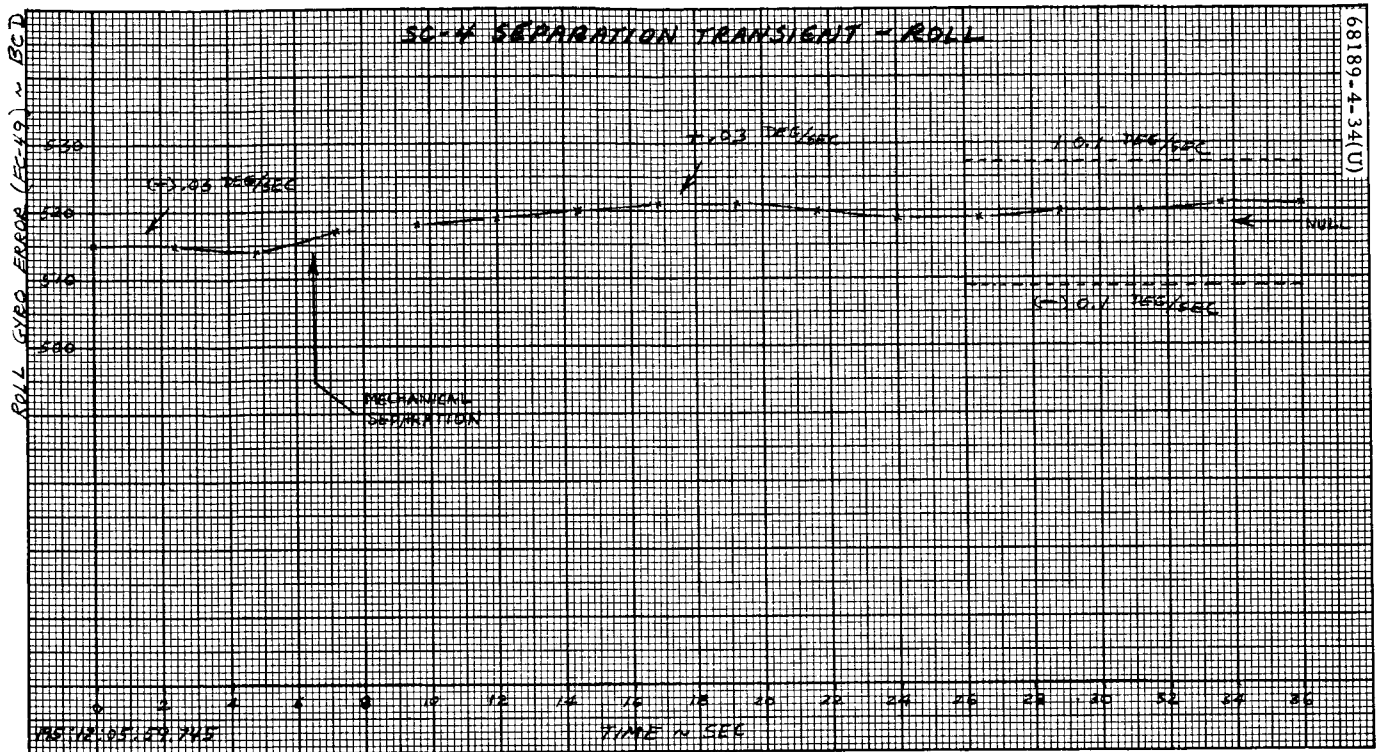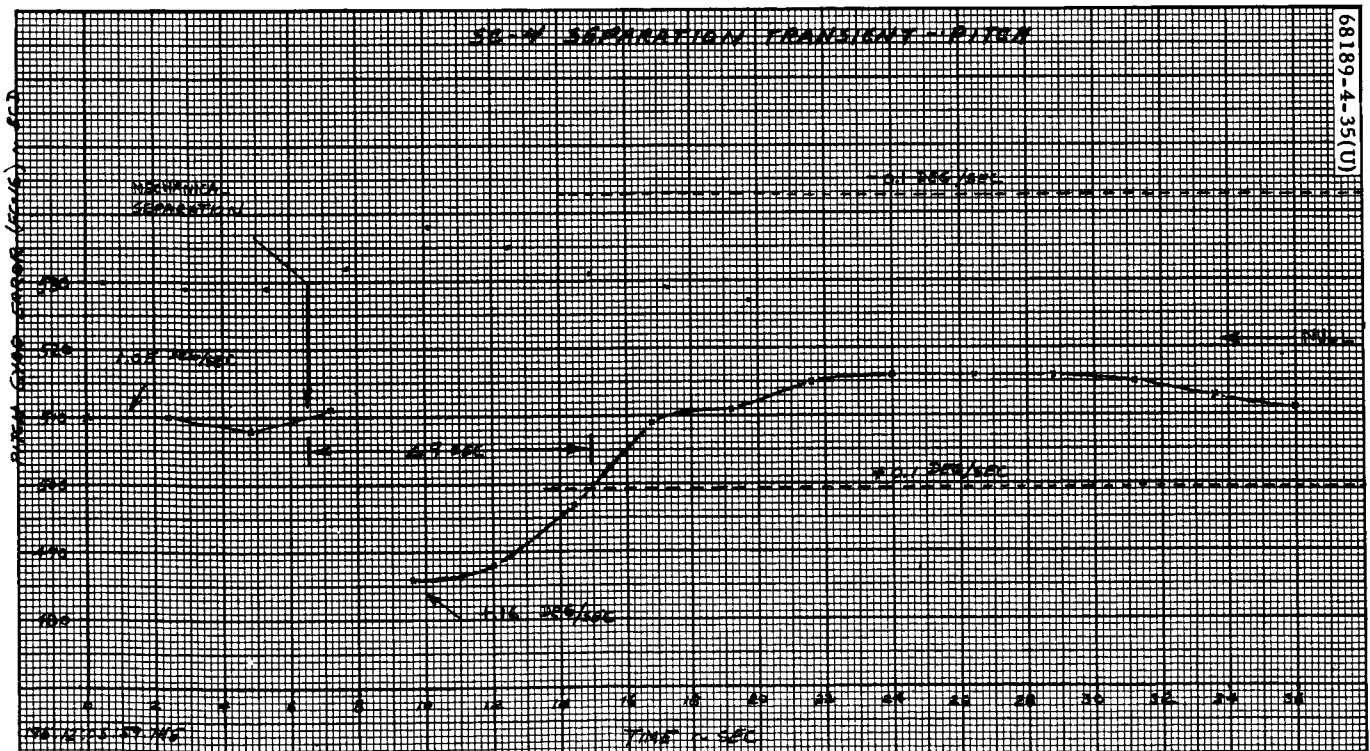
a) Roll

b) Pitch

Figure 5.5-2 (continued). Separation Transient

5.5-15

c) Yaw

Figure 5.5-2 (continued). Separation Transient
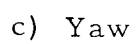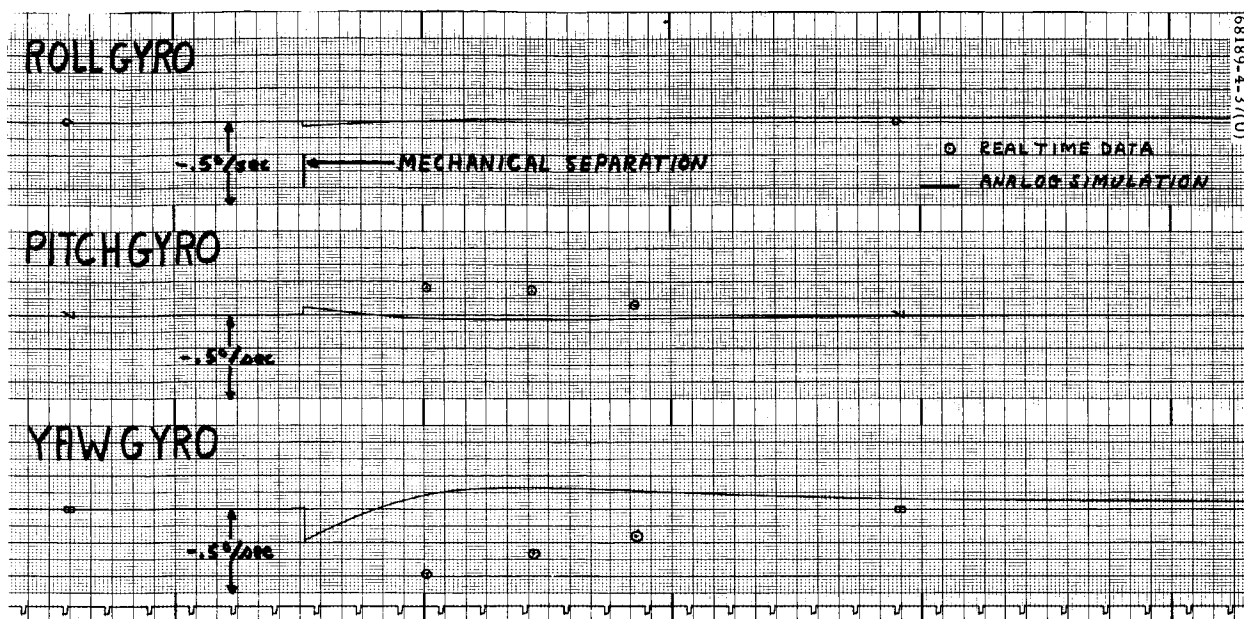
a) Without Induced Disturbance
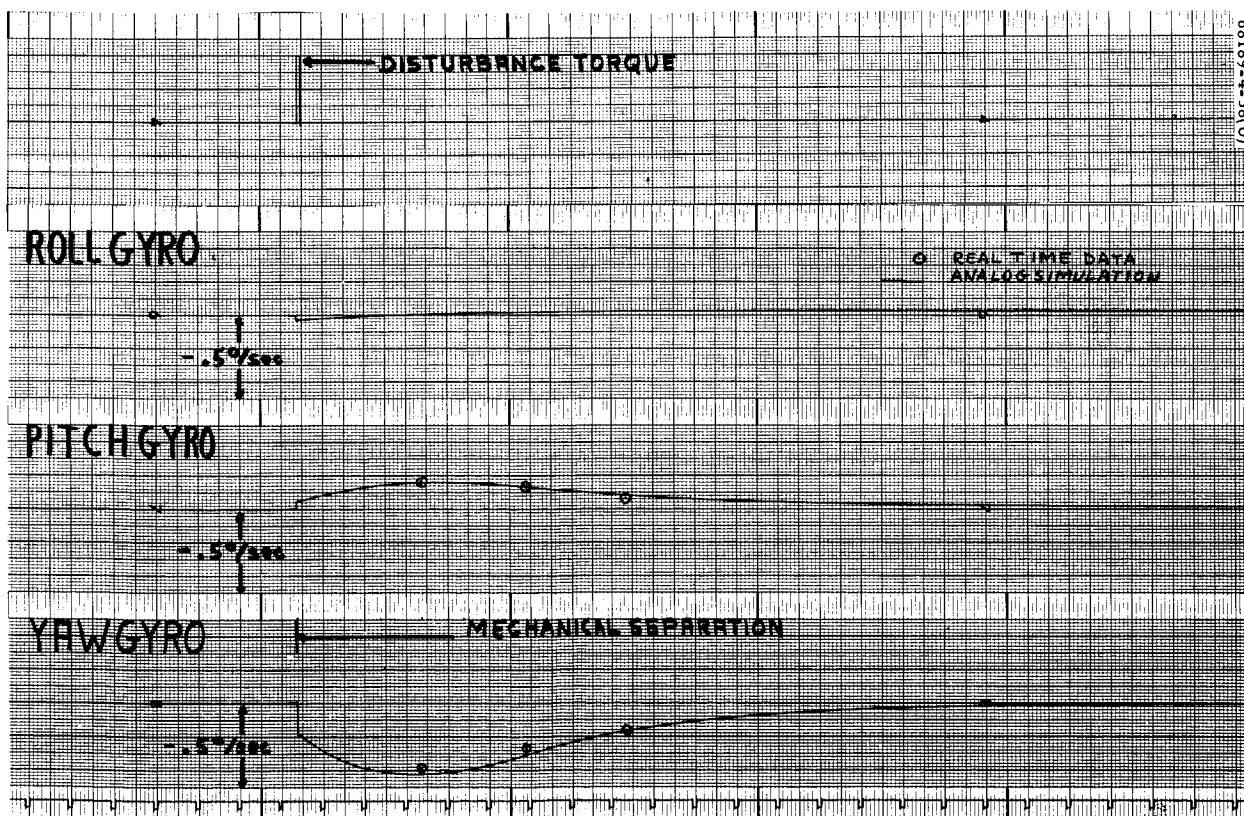
b) With Induced Disturbance

Figure 5. 5-3. Rate Dissipation Transient Simulation
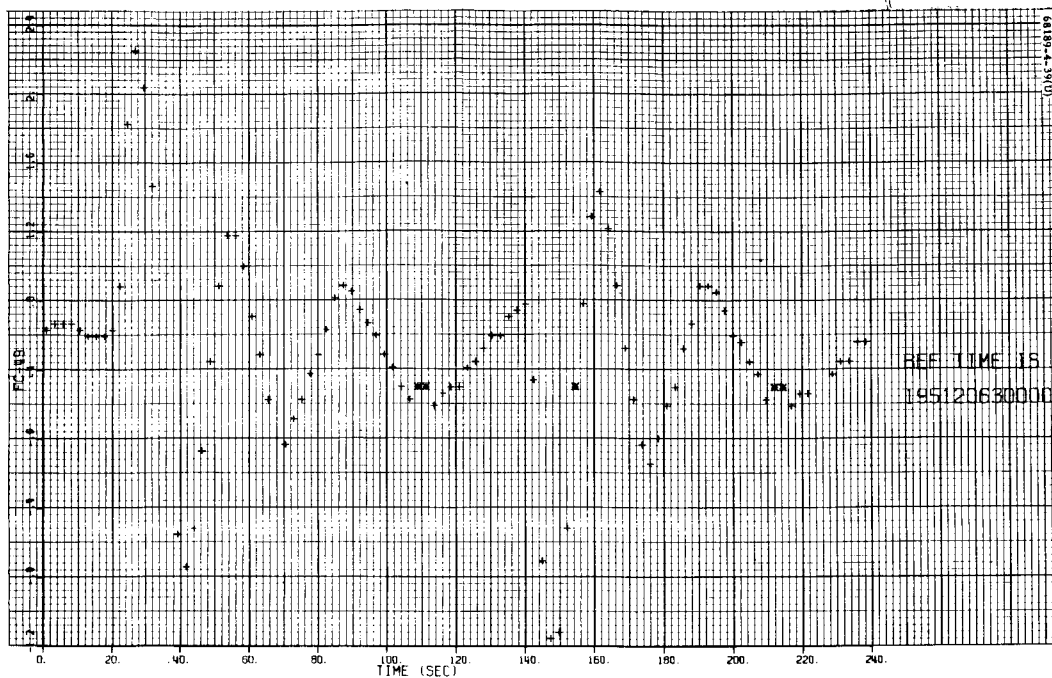
a) Roll Precession Command (FC-49)
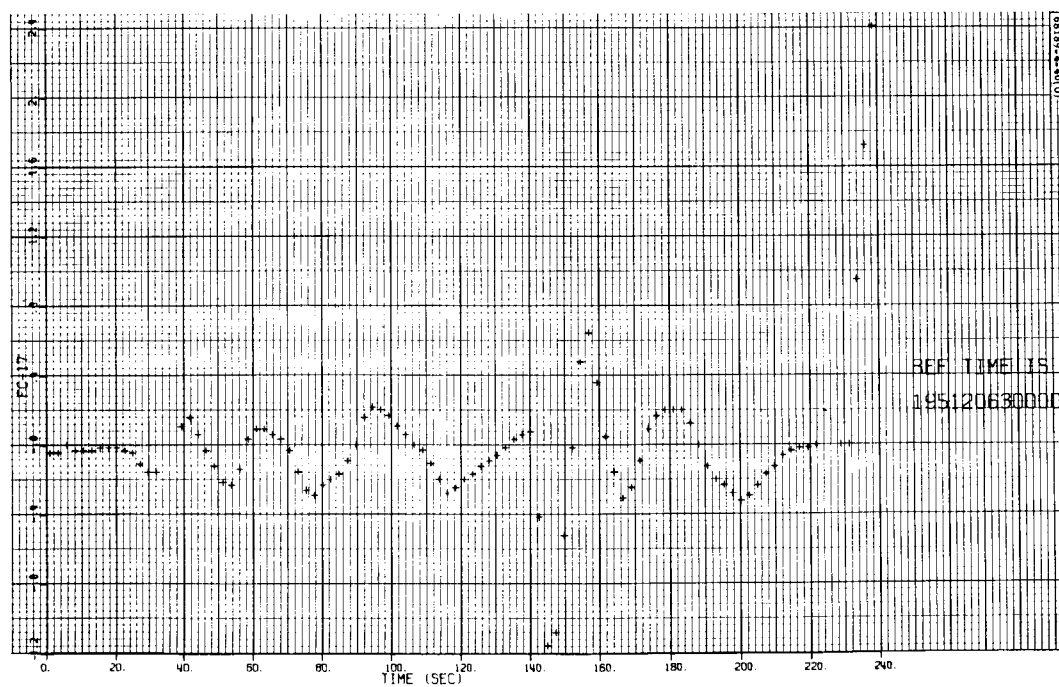
b) Yaw Gyro Error (FC-17)

Figure 5.5-4.   Sun Acquisition Phase

5.5-18
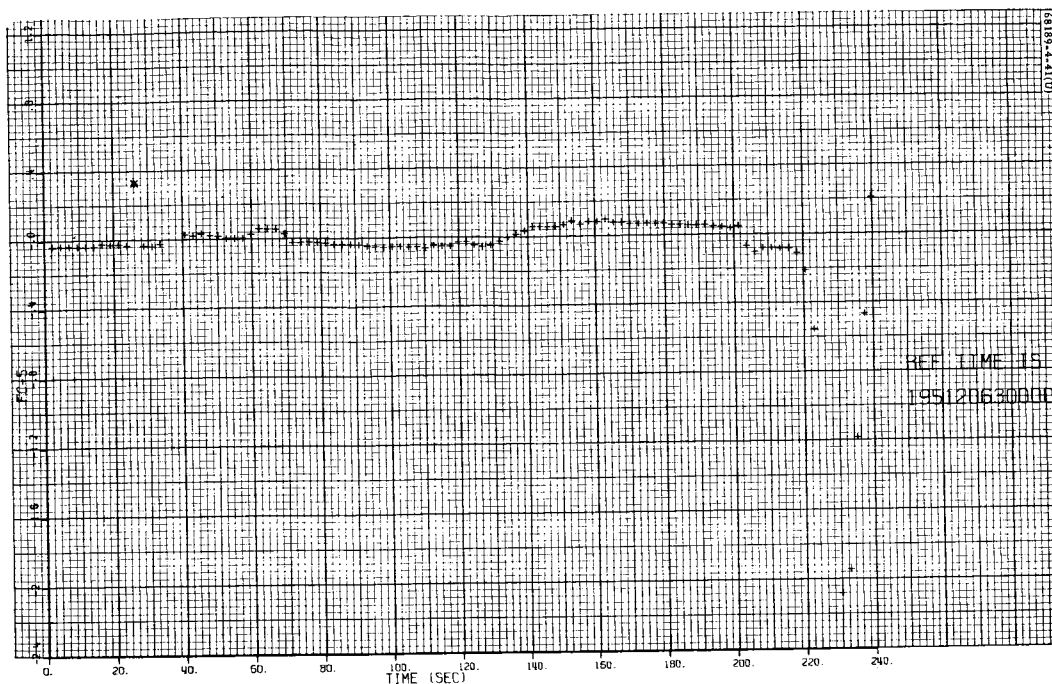
c) Primary Sun Sensor Pitch Error (FC-5)
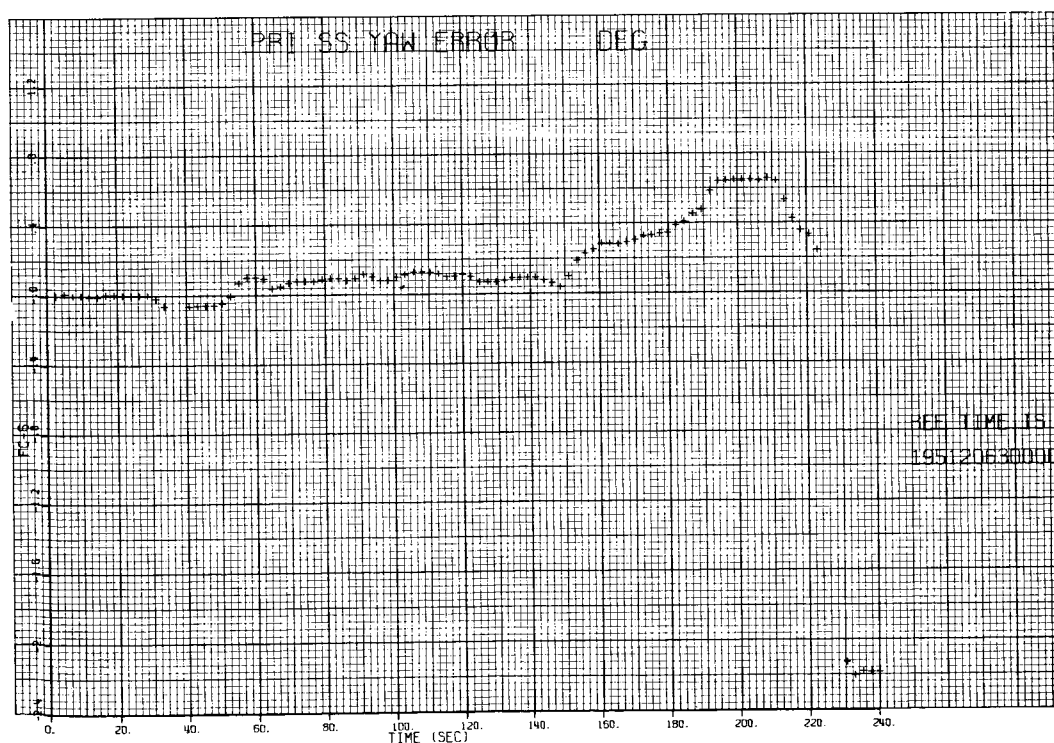
d) Primary Sun Sensor Yaw Error (FC-6)

Figure 5.5.4 (continued). Sun Acquisition Phase
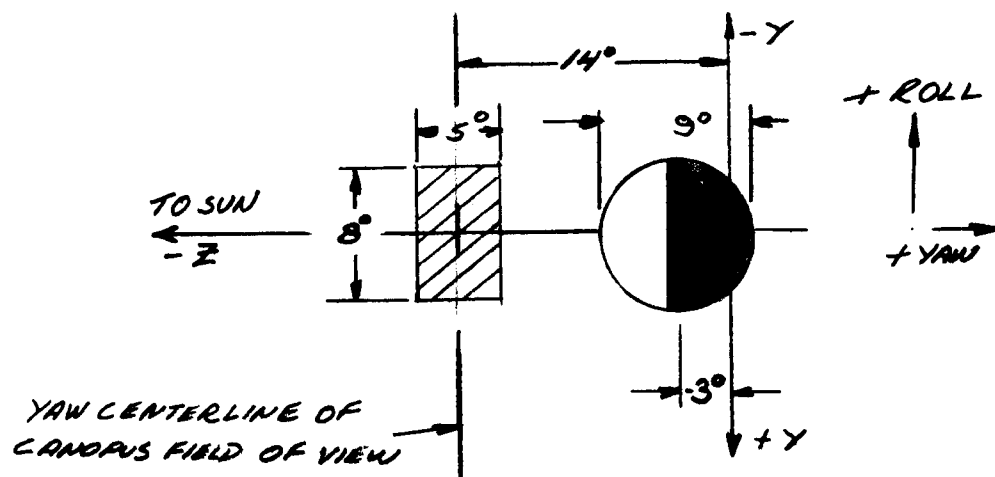
a) Canopus Line-of-Sight Orientation to X-Y Plan
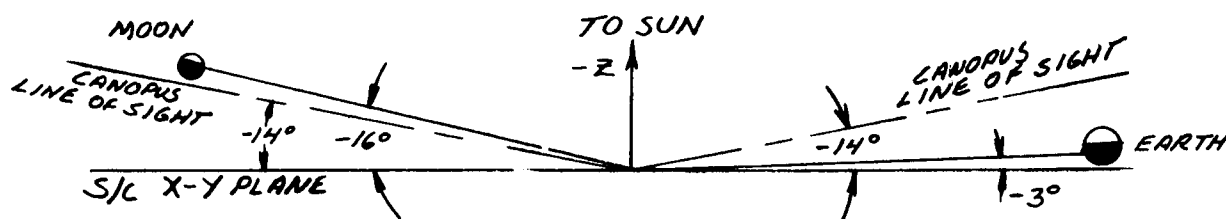
b) Relative Position
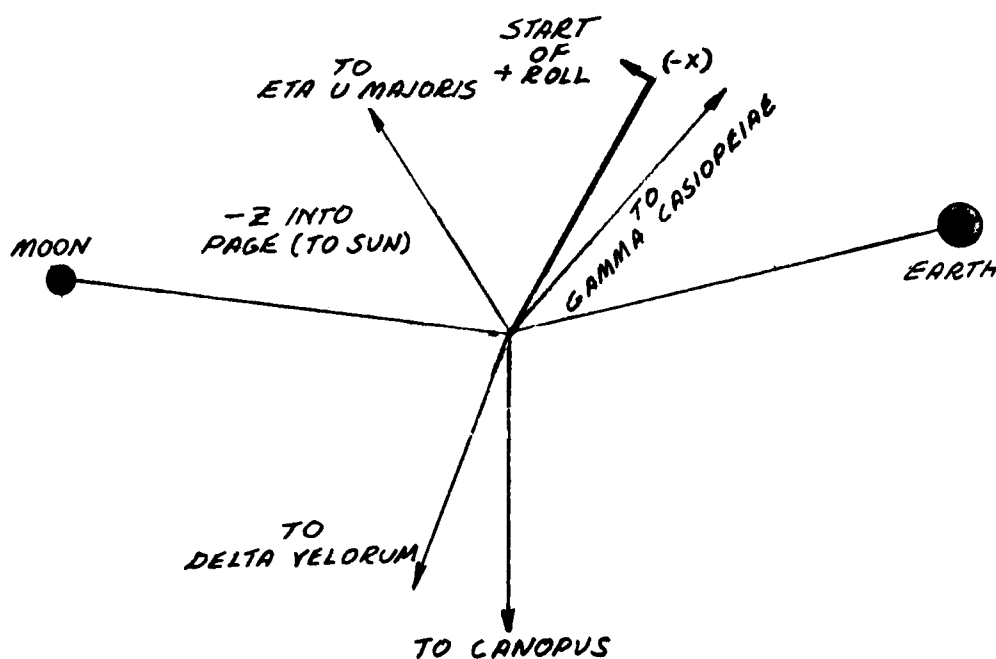
c) Angular Spacing (in Roll) of Observed Objects

Figure 5. 5-5.   Canopus Field of View Versus Earth

During Mission D, the spacecraft was commanded on day 195 to roll at +0.5 deg/sec at 17 hours 51 minutes 26.9 seconds GMT. Telemetered confirmation occurred at the received time of 17 hours 51 minutes 27.5 seconds, corresponding to L + 5 hours 57 minutes 58.3 seconds. During the ensuing roll, a star map was generated by recording the analog signals star intensity (FC-14) (i.e., unthresholded star intensity) and star angle or roll error (FC-12) (i.e., thresholded star intensity) on a strip chart recorder. From this map, Canopus was positively identified (based on identifying the angular spacing of Canopus plus five other objects) during the first 360 degrees of roll. While the spacecraft was still rolling, it was decided to continue the roll and acquire Canopus when the star entered the field of view during the second revolution, i.e., beyond 360 degrees. It had been observed during the first roll revolution that the Canopus lockon signal was present when Canopus was in the field of view. Therefore, it was possible to effect the acquisition of Canopus by employing the single sun and star command. The spacecraft was commanded to the sun and star modes at 18 hours 7 minutes 58.8 seconds, and telemetered confirmation occurred at the received time of 18 hours 7 minutes 59.4 seconds. Canopus lockon (FC-13) telemetry was received at 18 hours 10 minutes 19.4 seconds, after which it required approximately 44 seconds for both the star intensity and roll error signals to stabilize to their deadband limits.

Star Map

At this point in time, the spacecraft, moon, sun, and earth relationships in the ecliptic plane are as shown in Figure 5.5-5a. The center of the moon would pass approximately 0.5 degree inside the field of view in a plus yaw direction, and the center of the earth would pass approximately 8.5 degrees outside the field of view in a plus yaw direction. As shown in Figure 5.5-5a, the spacecraft is behind the moon and earth and would therefore "see" less than a half-moon and a half-earth. Figure 5.5-5b depicts the relationship of the sensor field of view and the earth as the spacecraft's -X axis points toward the earth during spacecraft roll.

Since large area bright objects within approximately 35 degrees of the sensor's line of sight will reflect light into the sensor from baffles in the sensor's light shield, it was expected that some star intensity signal would result when the sensor was rolling past both the moon and the earth. In addition, 21 stars, with intensities greater than 0.37×10^{-14} w/cm^2, come within the Canopus sensor's field of view during a complete roll revolution. However, based on laboratory measurements of star intensity signals versus star intensity on this particular sensor (S/N 4), it was predicted that only four stars would be observed.

Figure 5.5-5c depicts the calculated angular (roll angle) spacing of the moon, earth, Canopus, and the other three stars actually observed when looking towards the sun.

FC-12, FC-13, and FC-14 signals were sampled by telemetry once every 0.3 second, equivalent to +0.15 degree of roll at the mapping roll rate of +0.5 deg/sec.

Figure 5.5-6 depicts analog traces of primary sun sensor pitch angular error (FC-5), primary sun sensor yaw angular error (FC-6), roll precession command (i.e., roll gyro error (FC-49)), star angle, star intensity, digital word 1, digital word 2, and digital word 3 from the start of roll through Canopus acquisition. The traces of star angle and star intensity which comprise what is referred to as the "star map" indicate five clearly distinguishable star-type objects, plus an 18-degree-wide, low-intensity signal and a 45-degree-wide, high-intensity signal. The angular spacing of these signals was compared with the previously calculated object angles as shown in Figure 5.5-5c, thus permitting positive identification of Canopus, Eta U Majoris, Gamma Casiopeiae, and Delta Velorum, plus the moon and earth.

Table 5.5-4 indicates the responses received versus predicted responses. Roll angle is measured to the nearest 0.15 degree based on peak star intensity amplitudes as digitally recorded at the Madrid (DSS-61) site.

One object appeared in the field of view during the first roll (at 145 degrees), and two objects appeared during the second roll (at 50 and 137 degrees). Figure 5.5-7 shows for comparison purposes the star angle and star intensity telemetry signals (FC-16) for Eta U Majoris and the first object during the first roll. Figure 5.5-8 shows the telemetry signals for the third object (the second object appearing in the second roll). Both of these objects have telemetry signatures shaped like celestial body responses, but they remain in the sensor field of view for a shorter time than do the stars observed. Therefore, it is concluded that these objects were particles moving in space with a roll velocity component somewhat faster than the spacecraft roll rate of 0.5 deg/sec. The small perturbation in the third object's telemetry signals (see Figure 5.5-8) is ascribed to the possibility that the particle itself is rotating and presents a brighter reflection at that time. As noted in Figure 5.5-6, the star angle telemetry signal for the second object exhibits only half the normal star signature of a sawtooth. Such a signal would result if the object were moving diagonally across the left half of the field of view. Therefore, it is concluded that all three objects were particles and are labeled as first, second, and third particle even though it is possible that the first and third particle are one and the same.

As noted in Table 5.5-4, the correlation between post- and preflight calculated angles from Canopus of Eta U Majoris, Delta Velorum, and Gamma Casiopeiae ranges from +0.1 to -0.3 degree, which is considered well within the capabilities of the analyst to determine the exact center of the weaker star's signals coupled with the basic sampled data resolution of 0.15 degree. The correlation on moon and earth angles ranges from +0.5 to +1.5 degrees, which is considered well within the capabilities of the analyst to determine the exact center of broad varying signals.

The mean roll rate, as determined from the incremental times Eta U Majoris and Delta Velorum are at the center of the field of view, is 720/((18:05:30.9 - 17:53:31.4) + (18:09:45.9 - 17:57:46.2)) = 720/(11:59.5 + 11:59.7) = 720/1439.2 = 0.5003 deg/sec. This rate is 0.06 percent faster than 0.5 deg/sec. The error due to sampling time is 0.3 sec/720 sec = 0.004 percent.

Figure 5.5-6. Surveyor IV Star Map
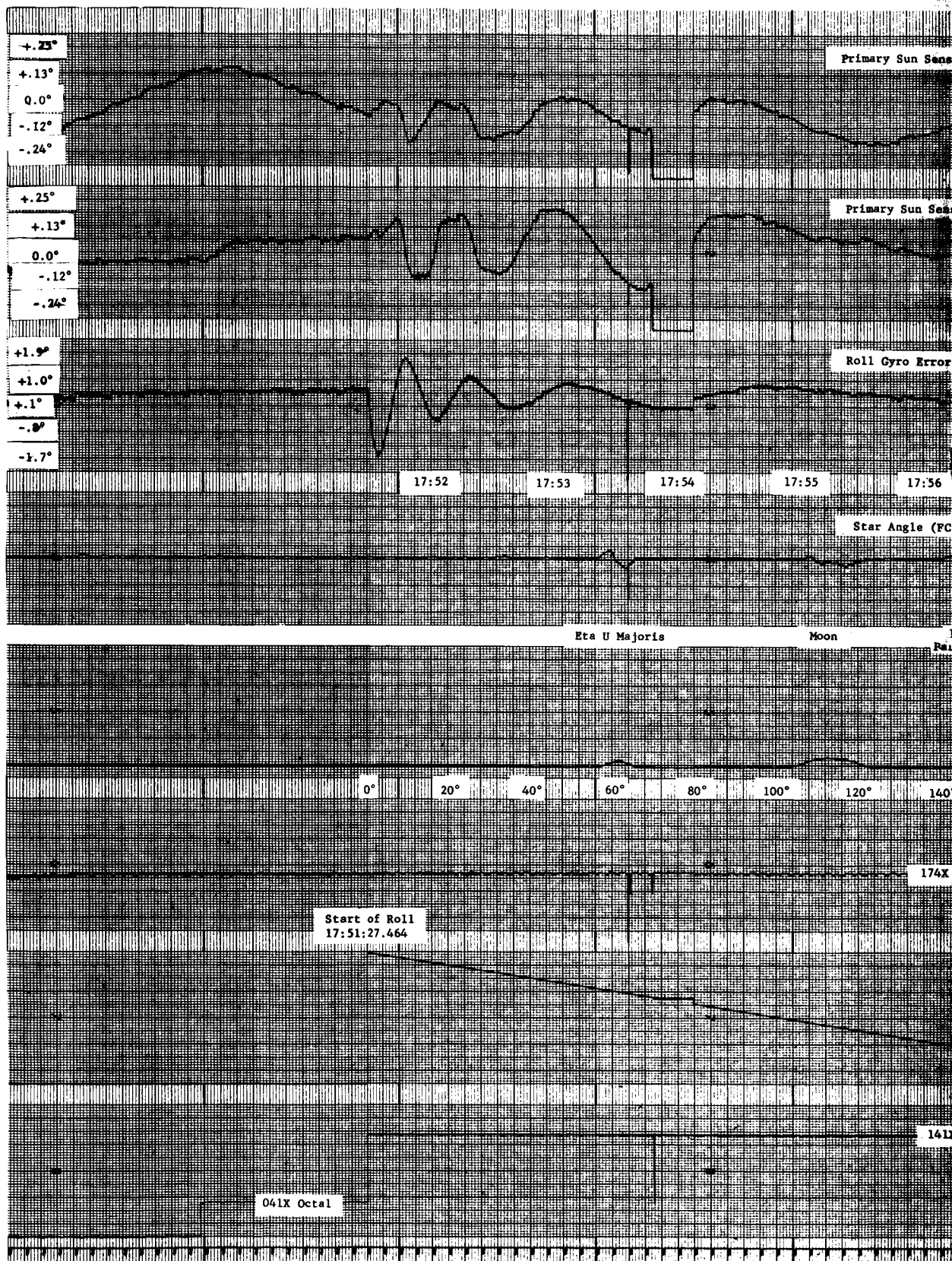
FOLDOUT FRAME 1

r Pitch Error (FC-5)

r Yaw Error (FC-6)

(FC-49)

| 17:57 | 17:58 | 17:59 | 18:00 | 18:01 | 18:02 | 18:03 | 18:04 | 18:0 |

12)

BRUSH INST Delta Velorum Canopus LEVITE CORPORATION   CLEVELAND, OHIO   PRINTED IN U.S.A.   Earth   Gamma Casiopeiae   Partic

cle

Star Intensity (FC-14)

| 160° | 180° | 200° | 220° | 240° | 260° | 280° | 300° | 320° | 340° | 360° | 380° | 400° |

Digital Word 1

Lock-On   Lock-On Lock-On Lock-On

Octal

1023 BCD   Digital Word 2

0 BCD

Digital Word 3

Octal

FOLDOUT FRAME 2

5 | 18:06 | 18:07 | 18:08 | 18:09 | 18:10 | 18:11 | 18:12

Eta U
Majoris   Moon   3rd Particle   Delta Velorum   Canopus   **BRUSH INST**

420°   440°   460°   480°   500°   520°   540°   560°

Lock-On

176X Octal

Sun & Star Mode
18:07:59.378

000X Octal
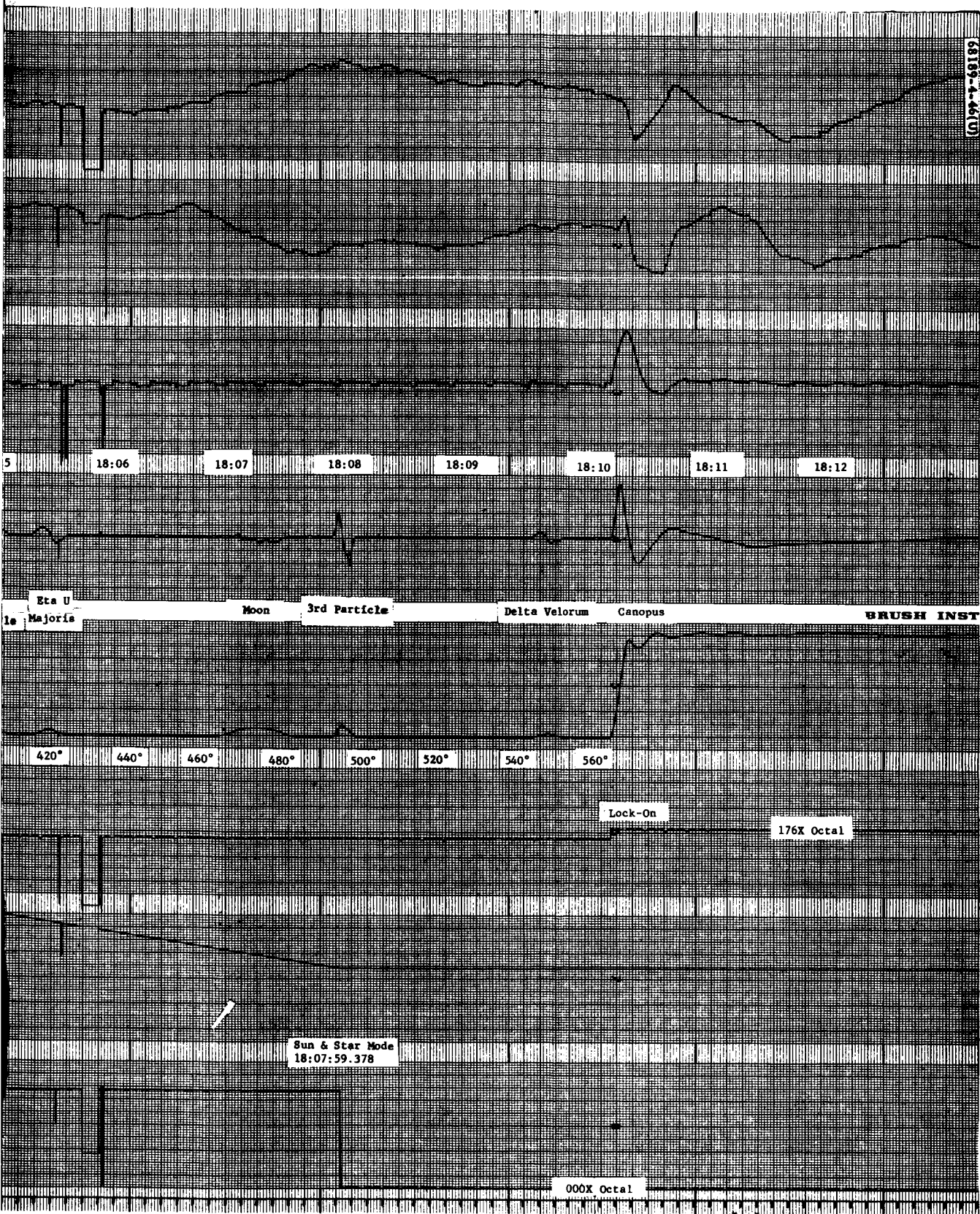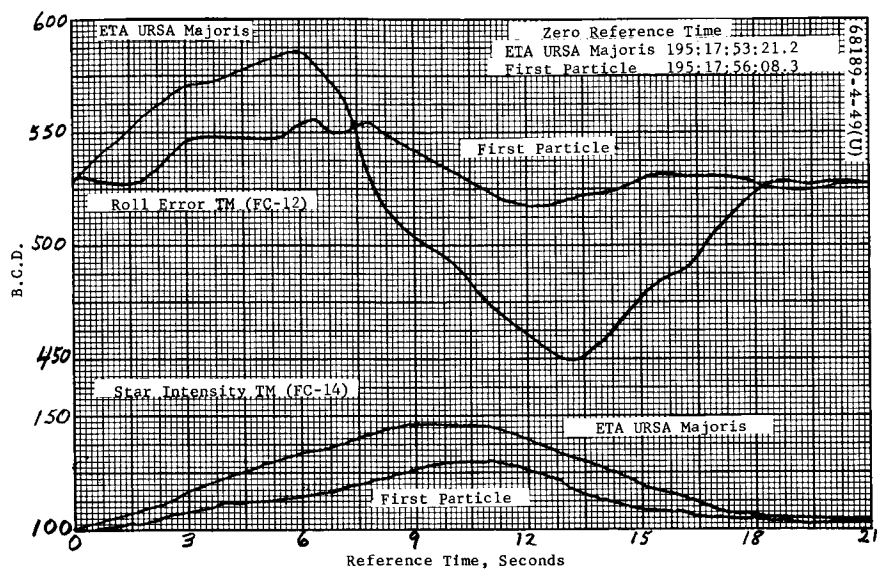
Figure 5.5.-7. Comparison of Eta Ursa Majoris
and First Particle Responses
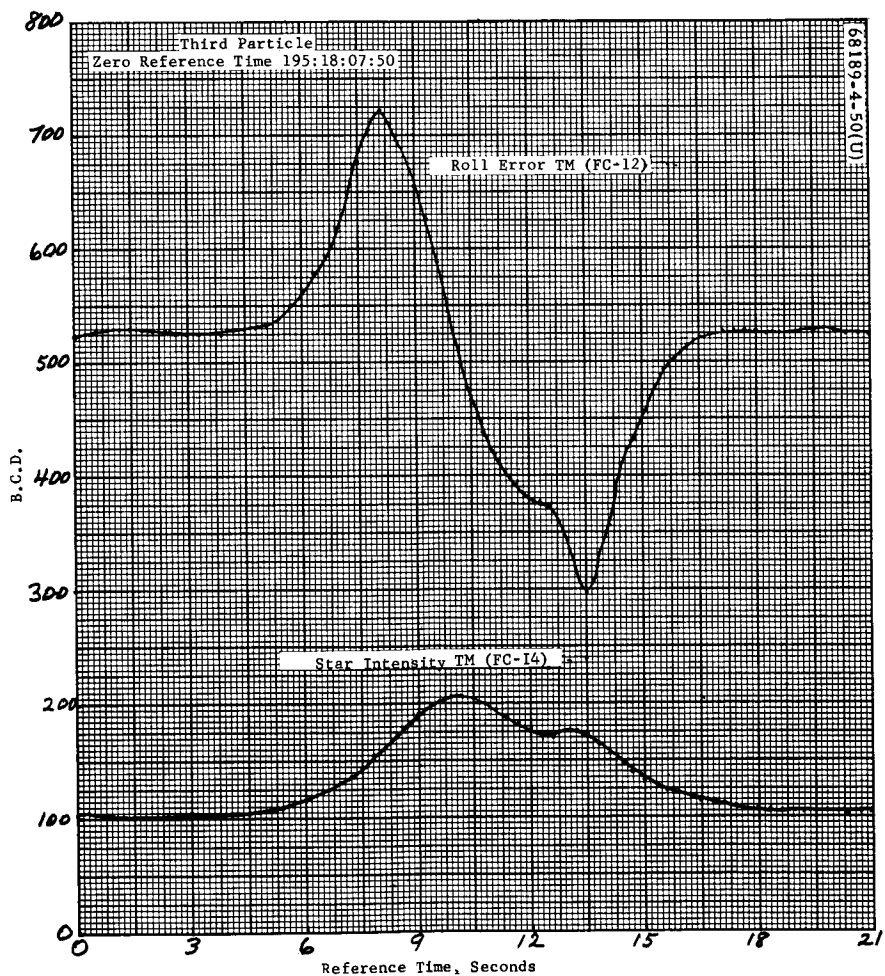
Figure 5.5-8. Third Particle Responses

TABLE 5.5-4.   STAR MAP — RECEIVED VERSUS PREDICTED RESPONSE

GMT, hr:min:sec	Postflight Calculated Roll Angle, degrees = Δ time × 0.5 deg/sec	Object	Postflight Calculated Angle From Canopus, degrees	Preflight Calculated Angle From Canopus, degrees	Measured Peak Intensity During Roll, telemetry volts	Predicted Peak Intensity During Roll, telemetry volts	Measured Peak Intensity at 0 Roll Rate, telemetry volts	Predicted Peak Intensity at 0 Roll Rate, telemetry volts	Occurrence of Canopus Lockon, digital word 1
17:51:27.5	0	(Start of roll)	-210.6						
17:53:31.4	62.0	Eta U Majoris	-148.6	-148.7	0.71	0.57			No
17:55:15.6	114.1	Moon	-96.5	-97.0	0.88				No
17:56:18.5	145.5	First particle	-65.1		0.63				No
17:57:46.2	189.4	Delta Velorum	-21.3	-21.1	0.65	0.49			No
17:58:28.7	210.6	Canopus			4.32	4.11			Yes
18:01:57.6	315.1	Earth	104.5	103.0	4.42				Yes
18:03:06.8	349.7	Gamma Casiopeiae	139.0	139.2	0.64	0.47			No
18:05:08.5	410.5	Second particle	199.9		0.60				No
18:05:30.9	421.7	Eta U Majoris	211.1	211.3	0.75	0.57			No
18:07:15.8	474.2	Moon	263.5	263	0.86				No
18:07:61.5	497.0	Third particle	286.4		1.22				No
18:09:45.9	549.2	Delta Velorum	338.6	338.9	0.69	0.49			No
		Canopus					4.68	4.42	Yes
		No star					0.51	0.37	No

Star Sensor Performance

The star sensor provides three outputs: star angle or roll error, Canopus lockon, and star intensity. A comparison of inflight and preflight measurements is used to determine how well the sensor performed in flight.

The star angle signal is designed to increase from a quiescent level, close to 512 BCD when no star is in the field of view, to a maximum, close to 1023 BCD, when Canopus is approximately +2 degrees from the X-Z plane. It returns to its quiescent level when Canopus is in the X-Z plane, then to a minimum, close to 0 BCD when Canopus is approximately -2 degrees from the X-Z plane, and finally increases to its quiescent level as Canopus leaves the field of view.

The star intensity signal is designed to increase from a quiescent level when no star is in the field of view to a maximum when Canopus is in the X-Z plane. It then decreases to its quiescent level as Canopus leaves the field of view. No star and maximum intensity values are listed in Table 5.5-4.

Figure 5.5-6 depicts the star angle and star intensity signals for all stars observed during the star map. Figure 5.5-9 depicts an enlarged view of these signals during the time Canopus was in the field of view in the first revolution. From these figures, it can be seen that the star angle and star intensity signals perform as designed.

Since the star intensity signal is a measure of the effective gain of the star sensor, the measurements, as recorded in Table 5.5-4, are analyzed to determine effective gain. Star sensor gain is a function of the photomultiplier tube scale factor which is controlled by the intensity of the sunlight actually reaching the tube through a sun filter in the sun channel optics. All preflight star sensor measurements are made with a unit sun intensity illuminating the sun channel. For flight, a flight filter is installed with a transmission factor that will admit more, equal, or less than a unit sun into the sensor. Mission A was flown with a sun filter calculated to increase the sensor gain so that Canopus would respond as 1.5 X Canopus. Analysis of inflight measurements indicated the effective gain was even greater than 1.5 X Canopus. Mission B was flown with a 1.17 X Canopus sun filter, and analysis of inflight measurements indicated the effective gain was still greater than 1.5 X Canopus, or 28 percent larger than expected. Mission C was flown with a 0.80 X Canopus sun filter, and analysis of in-flight measurements indicated the effective gain was in the vicinity of 1.17 X Canopus versus a prediction of 1.02 X Canopus.

Based on Missions A, B, and C, it was decided to install a 0.8 X Canopus sun filter for Mission D which should result in an effective gain close to the 1.17 X Canopus determined in Mission C. The actual observed peak intensity of Canopus, in a low roll rate condition after acquisition, is 4.678 volts compared to the Mission C value of 4.111 volts and the average preflight 1.0 X Canopus measurement of 3.77 volts. The 3.77-volt value is the weighted mean of 27 intensity measurements using four different star simulators, ranging from 3.10 to 4.20 volts. Using these values, the effective gain of the sensor has a range of 1.51 to 1.11, with a weighted mean of 1.24 X Canopus versus the 1.17 X Canopus value determined in Mission C. The difference of 0.07 X Canopus is attributed primarily to the inaccuracies inherent in preflight intensity measurements.

The third sensor output, Canopus lockon, is shown in Figure 5.5-6. as part of digital word 1 and is listed in Table 5.5-4. Since the earth's intensity signal is between the lockon triggering levels, the lockon signal is present for an extended period. Based on these observations, it can be seen that the Canopus lockon signal performed as desired.

Canopus Acquisition Sequence

Since Canopus was identified during the first revolution and Canopus lockon was present when Canopus was in the field of view, it was decided to send the sun and star command after the earth had sufficiently cleared the field of view. The automatic acquisition sequence could then occur.
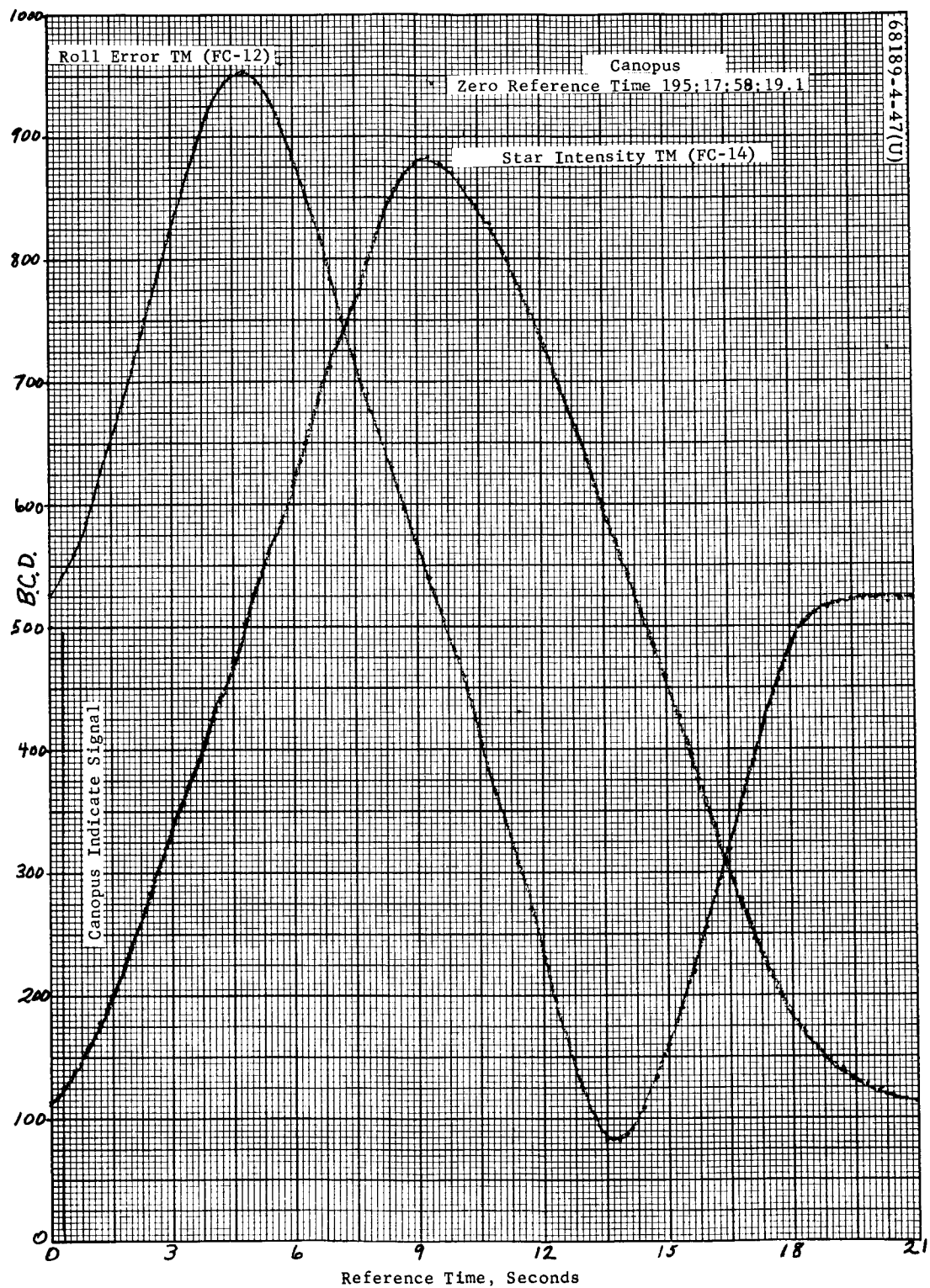
Figure 5.5-9. Canopus Responses
First revolution

Figure 5.5-10 depicts the response of the star intensity, star angle, and roll error, signals after Canopus lockon has put the spacecraft in a closed-loop roll error controlled mode. When lockon occurs, the spacecraft is rolling at +0.5 deg/sec, and the roll error signal is increasing to a maximum, which commands the spacecraft to roll positive to obtain a nulled roll error signal. Thus, the positive command causes the plus roll rate to increase until the roll error signal crosses its null position into the lower area, at which time it commands the spacecraft to roll negative. This negative roll command slows the roll rate to zero and reverses the roll direction such that the roll error again crosses its null position into the upper area, which commands the spacecraft to roll positive. After several such cycles, the spacecraft settles down to a slow roll oscillation which causes the roll error signal to oscillate above and below its null position. This oscillation is bounded, and the bounds are referred to as the roll optical limit cycle.

As noted in Figure 5.5-10, the star intensity peak value increases as the roll rate decreases. This is the normal response of a signal having a time constant in the vicinity of 1 second.

Conclusions

The Canopus sensor performed as designed without malfunction. The star intensity signal, with Canopus in the field of view, was higher than the nominal predicted, but within the accuracy of the preflight measurements. The automatic star acquisition capability was successfully utilized.

5.5.4.5 Coast Phase

Gas Jet Thrust Level

Reference 2 developed the following expression for the gas jet thrust level, T:

$$T = \frac{I_z \dot{\varphi}_c}{R t_p}$$

where

I_z = roll inertia = 224 slug-ft^2

$\dot{\varphi}_c$ = commanded precession rate = 0.5 deg/sec

R = gas jet moment arm = 6.47 feet

t_p = thrusting time of the gas jet from initiation of precession command to point at which $\varphi_{gyro} = 0$

Using the premidcourse roll maneuver data (Figure 5.5-11), the time from command initiation until $\dot{\varphi}_{gyro} = 0$ was 5.5 seconds. Since the No. 1 gas jet amplifier is off 1.3 seconds of this time (Reference 3), $t_p = 5.5$ seconds - 1.3 seconds = 4.2 seconds.
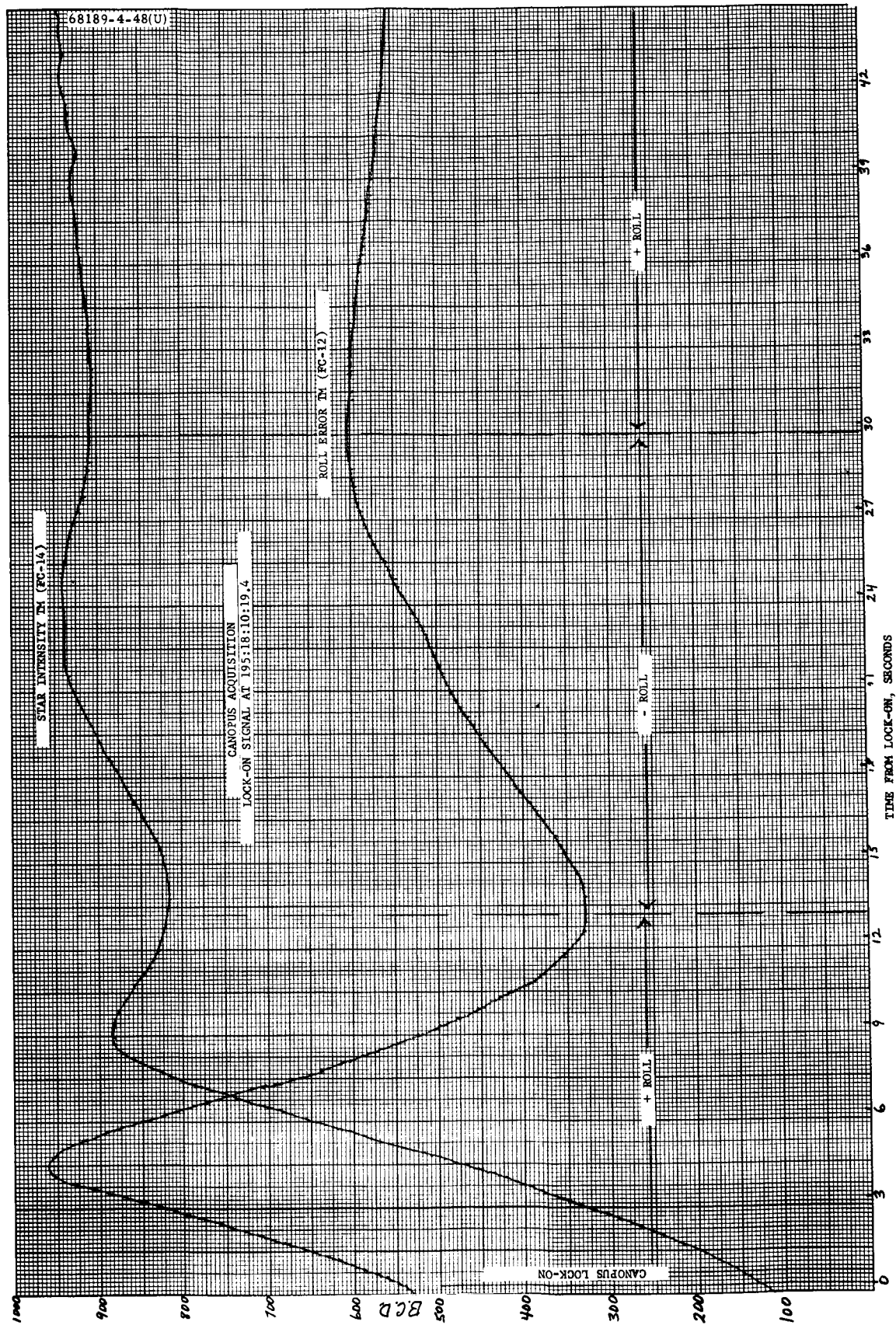
Figure 5.5-10. Canopus Response
Acquisition phase

Figure 5.5-11. Gas Jet Thrust Level
Determination of firing

$$T = \frac{(224 \text{ slug-ft}^2)(0.5 \text{ deg/sec})}{(6.47 \text{ feet})(4.2 \text{ seconds})} = 0.072 \text{ pound}$$

Section 13 of Reference 4 shows that the thrust levels for all six jets during test were within 2.0 percent of each other. On this basis, it can be assumed that the nominal thrust level for the six gas jets was 0.066 pound.

Nitrogen Consumption

Nitrogen consumption for the period from launch to preretro maneuvers was 0.64 pound. This number compares favorably with predicted usage when measurement uncertainties and postgyro drift lockon transients are taken into account. Mission nitrogen usage was obtained from pressure and temperature information telemetered on flight control signals FC-4 and FC-48.

The predicted nitrogen usage for each maneuver was determined from the simulation defined in Reference 5; a detailed breakdown of the predicted impulse and weight expenditures is documented in Reference 6.

For the number and sequence of Mission C maneuvers, Attachment 1 of Reference 6 yields the following nominal impulse consumption budget:

	lb-sec
Leakage	3.40
Vernier phase of midcourse maneuver	2.00
Limit cycle operation	4.50
Sun acquisition	3.25
Inertial roll maneuvers (3)	4.50
Star verification	1.50
Star acquisition	1.40
Inertial yaw maneuvers (2)	2.50
Rate dissipation	2.75
Postmidcourse rate dissipation	1.00
Total	26.80

Assuming an average I_{sp} of 60 seconds yields a nominal nitrogen usage prior to the preretro maneuvers of approximately 0.45 pound. Reference 6 also predicts a 3σ usage uncertainty of 0.22 pound for this particular mission profile.

The fuel consumption due to the post-gyro drift check lockon transients was determined by using the final angular attitude positions of each drift check as initial conditions to the simulation documented in Reference 7 yield the following:

1) The average impulse expenditure for a post-three-axis drift transient was 0.90 lb-sec.

2) The average impulse expenditure for a post-roll-axis-only drift transient was 0.55 lb-sec.

So there is an increase in the nitrogen consumption prediction of

$$\frac{3 \ (0.55) \ \text{lb-sec} + 10 \ (0.90) \ \text{lb-sec}}{60 \ \text{seconds}} = 0.178 \ \text{pound}$$

The net prediction would be

$$(0.45 + 0.18) \pm 0.22 = 0.63 \ \text{pound} \pm 0.22 \ \text{pound}$$

5.5.4.6 Premidcourse Attitude Maneuvers

In order to orient the spacecraft thrust axis properly prior to vernier engine ignition, a positive roll maneuver of 72.6 degrees and a negative yaw maneuver of 64.4 degrees were commanded. Although these were the values entered into the magnitude register, the desired maneuvers per the midcourse and terminal guidance system calculations were 72.4518 degree of roll and 64.3196 degree of pitch.

Several variables affect the accuracy of an angular maneuver: precession rate accuracy, precession command time, gyro drift, and initial attitude errors due to biases and limit cycle. When several maneuvers are performed with large time intervals between them, attitude errors due to gyro drift must be included. A list of all parameters affecting the midcourse attitude maneuver accuracy is presented in Table 5.5-5 along with their allowable 3σ values and actual performance values wherever possible.

Determination of Precession Times

The register was loaded with 363 bits for roll and 322 bits for yaw. For a clock rate of 2.5 cps, the respective times are 145.2 and 128.8 seconds with a maximum error of 0.20 second ± 0.02 percent. An attempt was made to reduce the optical mode limit cycle contribution to the pointing error by initiating the attitude maneuvers at the limit cycle null point. The following table indicates the optical errors that existed at the start of each maneuver.

TABLE 5.5-5.   PREMIDCOURSE ATTITUDE ERROR SUMMARY

Parameter	3σ Requirement	Reference Number	Measured Value	Comments
Primary sun sensor null with respect to FCSG roll axis	0.2 degree	1 (paragraph 4.3.1.1)	Pitch = +0.009 degree Yaw = +0.08 degree	
Canopus sensor null with respect to FCSG roll/pitch plane	0.2 degree	1 (paragraph 4.3.1.2)	+0.104 degree	
Pitch/yaw limit cycle	0.3 degree	1 (paragraph 4.3.1.1)	-0.06/-0.1 degree	Based on sun sensor error signals at start of yaw
Roll limit cycle	0.3 degree	1 (paragraph 4.3.1.2)	+0.05 degree	Based on Canopus error signal at start of roll
Gyro torquer scale factor	0.15 percent	11 (paragraph 3.2.5.1.3)	} 0.2 percent	
Precession current source accuracy	0.13 percent			
Precession current source drift	0.1 percent			
Timing source accuracy	0.2 second ±0.02 percent		Roll = -0.15 degree Yaw = +0.08 degree	Based on timing errors determined in subsection 5.5.4.6
Gyro alignment to FCSG roll axis	0.14 degree	11 (paragraph 3.2.5.1.4)	Pitch = +0.042 degree Yaw = +0.119 degree	
FCSG/spacecraft roll axis alignment	0.1 degree	1 (paragraph) 4.1.3.7.1)		
Gyro non-g sensitive drift	1.0 deg/hr	1 (paragraph 4.3.1.5	Roll = -0.12 degree Yaw = +0.02 degree Pitch = -0.15 degree	Based on measured -0.5 deg/hr in roll for 14 minutes and 33 seconds, +0.15 deg/hr in yaw, and -1.0 deg/hr in pitch for 8 minutes and 52 seconds
Total attitude error prior to ignition			0.19 degree with 0.15-degree uncertainty	

5.5-34

Maneuver	Error, degree	Limit Cycle Peak, degree
Roll	+0.06	±0.3
Yaw	-0.06 pitch	±0.23
	-0.10 yaw	±0.27

As can be seen, the roll and pitch optical errors were close to the null point, while the yaw optical error was approximately halfway between its limit cycle peak and its null (Figure 5.5-12).

The telemetered gyro error signal data were used in determining the actual precession time. The sampling rate during the maneuvers was 20 times/sec, giving a resolution of 0.05 second. The results are as follows (Figure 5.5-13):

144.74 seconds, or 72.37 degrees of roll

128.74 seconds, or 64.37 degrees of yaw

Precession Rates. The accuracy of the precession rates imposed by the "Surveyor Spacecraft Model A-21 Equipment Specification" is 0.5000 ±0.0011 deg/sec. The roll precession rate obtained during the star mapping phase indicated that the positive precession rate was 0.5011 deg/sec.

Attitude Maneuver Error

Reference 8 develops two orthogonal equations that specify the spacecraft thrust axis pointing error during midcourse thrusting. The equations were derived for the roll-yaw rotation sequence which applies here.

Neglecting error sources that are present only after engine ignition:

$$\text{Error about yaw axis} = -\psi_{R_E} + -\psi_{A_E} \cos \varphi - \theta_{A_E} \sin \varphi$$

$$\text{Error about pitch axis} = \left(\varphi_{A_E} + \varphi_{R_E} \right) \sin \varphi + \theta_{A_E} \cos \psi \cos \varphi$$

$$- \psi_{A_E} \sin \varphi \cos \psi$$

where

$$(\varphi, \ \theta, \ \psi)_{A_E} = \text{spacecraft inertial reference alignment errors}$$

$$(\psi, \ \varphi)_{R_E} = \text{rotation errors}$$

Use of $\varphi = 72.6$ degrees, $\psi = -64.4$ degrees, and the errors listed in the summary chart results in an 0.12-degree attitude error about the negative yaw axis and an 0.15-degree error about the negative pitch axis. The resultant pointing error has a 99-percent circular probable uncertainty of 0.15 degree.

5.5.4.7 Postmidcourse Attitude Maneuvers

The postmidcourse attitude maneuvers are used to realign the space-craft to the celestial reference after performing a midcourse velocity correction. To accomplish this, two reacquisition schemes are available. One method is to perform the premidcourse attitude maneuvers in reverse, and the other is to perform another automatic sun acquisition sequence. The first method is more desirable since real-time monitoring of optical sensor signals provides a good indication of premidcourse maneuver accuracy and attitude control during the thrust period. If reacquisition of the sun and Canopus is not achieved to within a fair degree of accuracy, one or more of the following conditions must have existed:

1) Nonsymmetrical precession commands

2) Spacecraft attitude change occurred between maneuver periods

3) Premidcourse maneuvers were not accurate

4) Postmidcourse maneuvers were not accurate

5) Vernier engine shutoff transients excessive

The first method was chosen for the Surveyor IV mission, and the celestial reference was successfully reacquired.

Determination of Precession Times

For the postmidcourse attitude maneuvers, the magnitude register was loaded with 322 bits for yaw and 363 bits for roll. This corresponds to 128.8 and 145.2 seconds, respectively.

The precession times, using gyro error signal data, were found to be as follows:
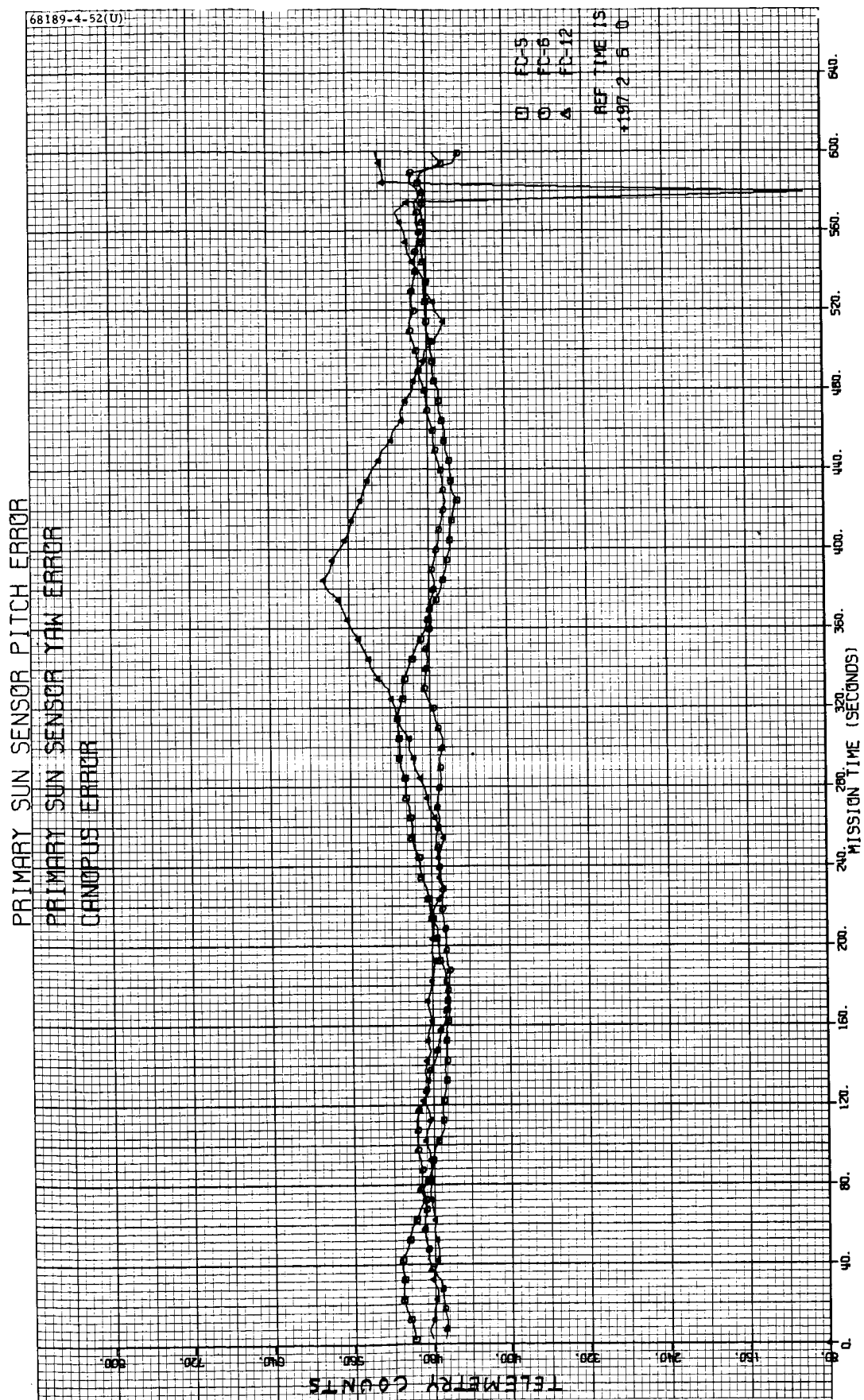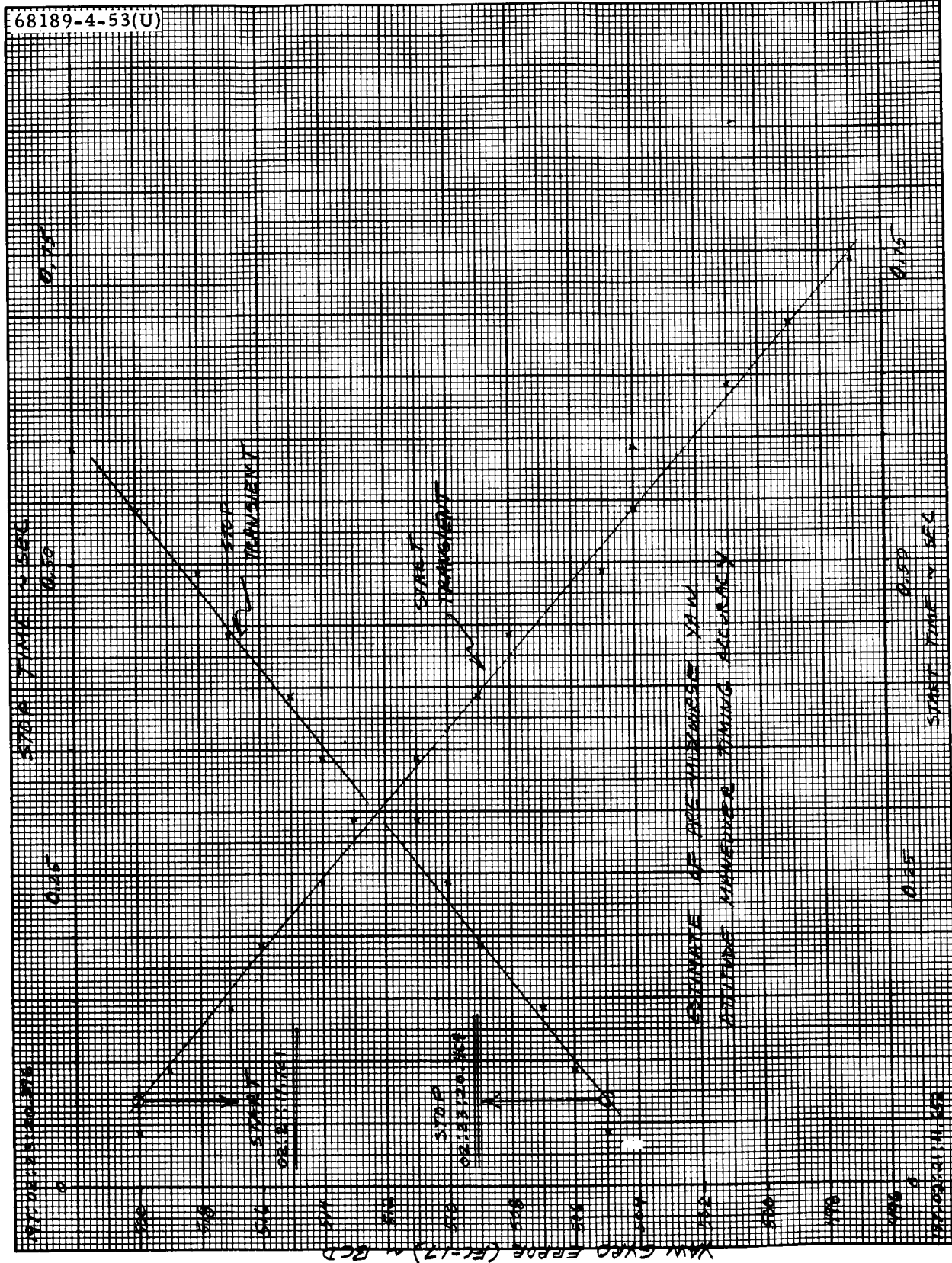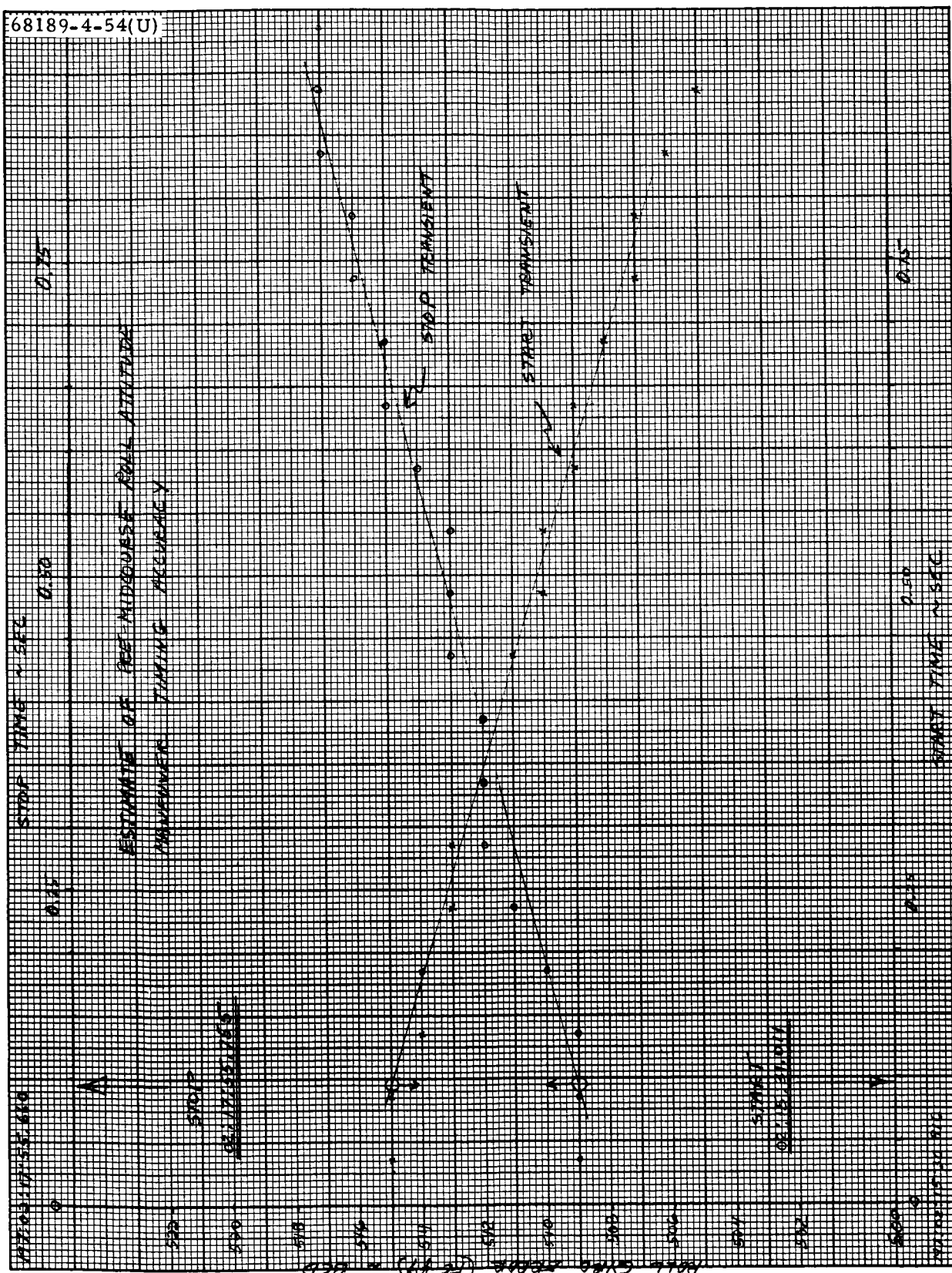
127.6 seconds (yaw)

144.0 seconds (roll)

Figure 5.5-12. Premidcourse Maneuver Errors — FC-5, -6, and -12

a) Roll

Figure 5.5-13. Gyro Error

b) Pitch

Figure 5.5-13 (continued). Gyro Error

The postmidcourse maneuvers were performed using the coast mode commutator at 4400 bits/sec, thereby increasing the data granularity to 0.3 second from the 0.05 second obtained for the premidcourse attitude maneuvers which were performed using the mode 1 commutator at 4400 bits/sec.

5.5.4.8 Midcourse Velocity Correction

The midcourse velocity correction was successfully executed starting at 2 hours 30 minutes 4.140 seconds GMT on 17 July. From orbit determination, the actual magnitude of the velocity change was estimated to be 10.1316 m/sec compared to the commanded value of 10.305 m/sec. This constitutes a ΔV execution error of -0.17 m/sec. Also from orbit determination, the midcourse thrust vector pointing error was within the accuracy of two-way doppler tracking system and estimated to be <0.2 degree. Using prelaunch alignment information and inflight data, the preignition pointing error was calculated to be 0.19 degree in subsection 5.5.4.6.

Midcourse Engine Ignition Characteristics

Vernier ignition was smooth; it was followed by a nominal, uneventful thrusting phase (Figure 5.5-14). Peak pitch and yaw gyro errors during thrusting were -0.174 degree during the ignition transient and less than +0.188 degree, respectively, thereafter until engine cutoff. A summary of the midcourse pitch and yaw gyro errors is given in Table 5.5-6.

TABLE 5.5-6. MIDCOURSE IGNITION TRANSIENT
CONTROL SUMMARY

Gyro error telemetry resolution = 0.016 degree

Initial (preignition) gyro errors, degrees:
Pitch = -0.04
Yaw = -0.22
Maximum change in attitude, degrees:
Pitch = -0.17
Yaw = +0.19
Peak angular rates, deg/sec:
Pitch = -0.50
Yaw = +0.34
Vernier engine startup time = <0.15 second

HELIUM
PRESSURE

VERNIER PRESSURIZATION
GMT 02:27:35

ACCELERATION
ERROR FC-15

THRUST COMMAND
ENGINE NO. 1
FC-25

THRUST COMMAND
ENGINE NO. 2
FC-26

ONTROLS CORPORATION   BUFFALO, NEW YORK

THRUST COMMAND
ENGINE NO. 3
FC-27

VERNIER ENGINE NO. 1
STRAIN GAUGE

VERNIER ENGINE NO. 2
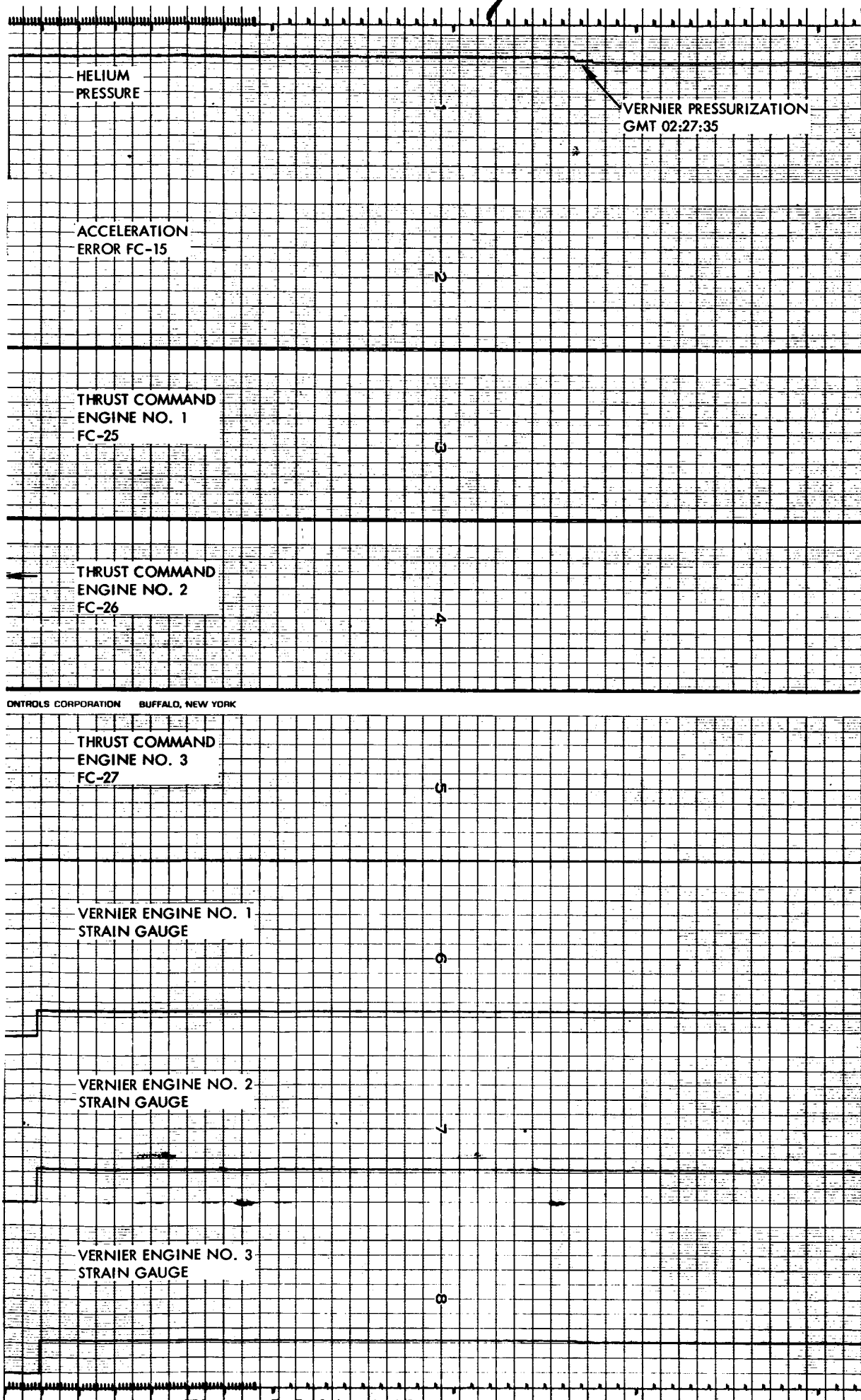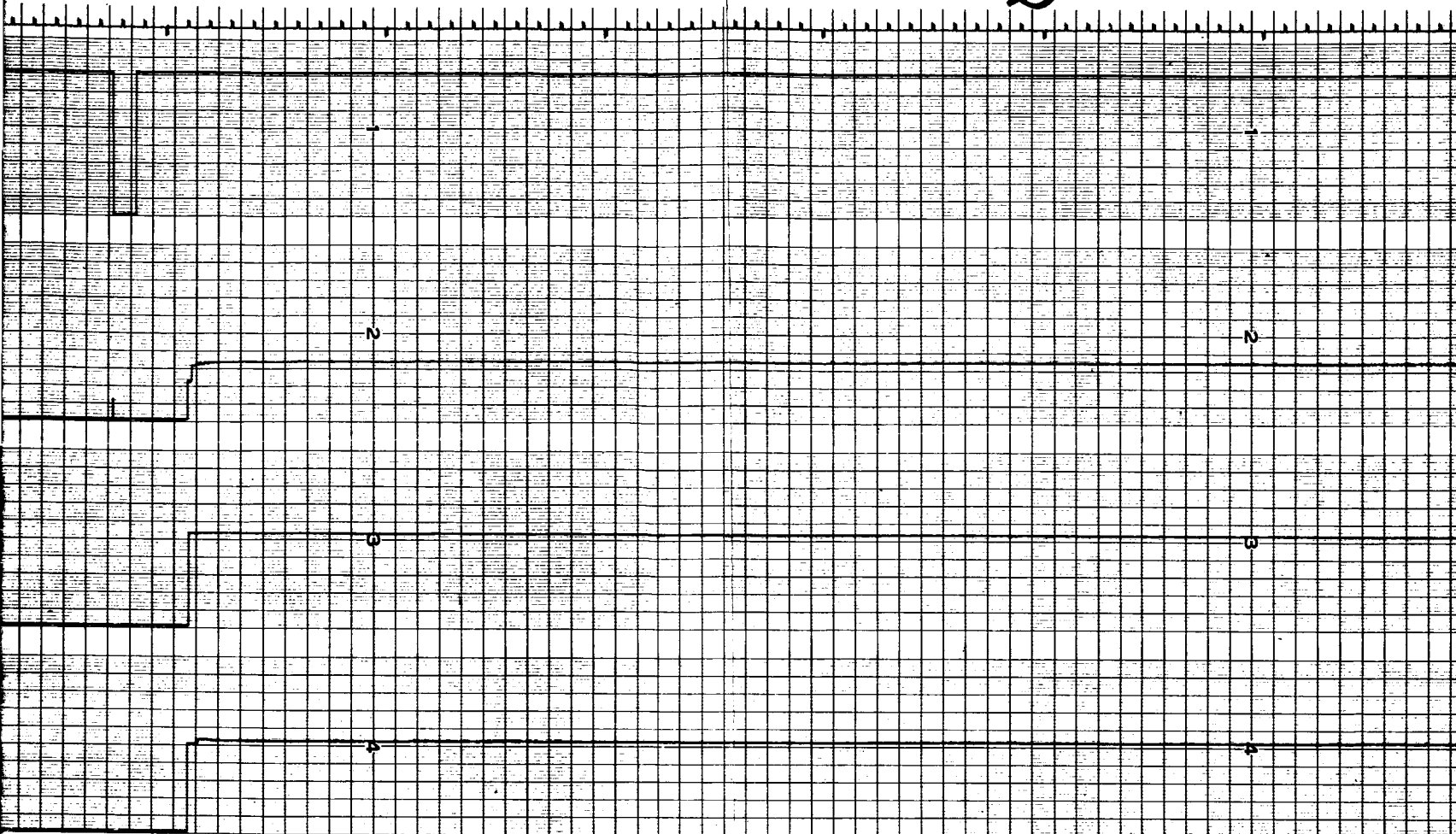STRAIN GAUGE

VERNIER ENGINE NO. 3
STRAIN GAUGE

Figure 5.5-14. Midcourse Velocity Correction

PRINTED IN U.S.A.   ⑤RECORDING CHARTS GRAPHIC CONTROLS CORPORATION   BUFFALO, NEW YORK

THRUST PHASE
POWER "ON"
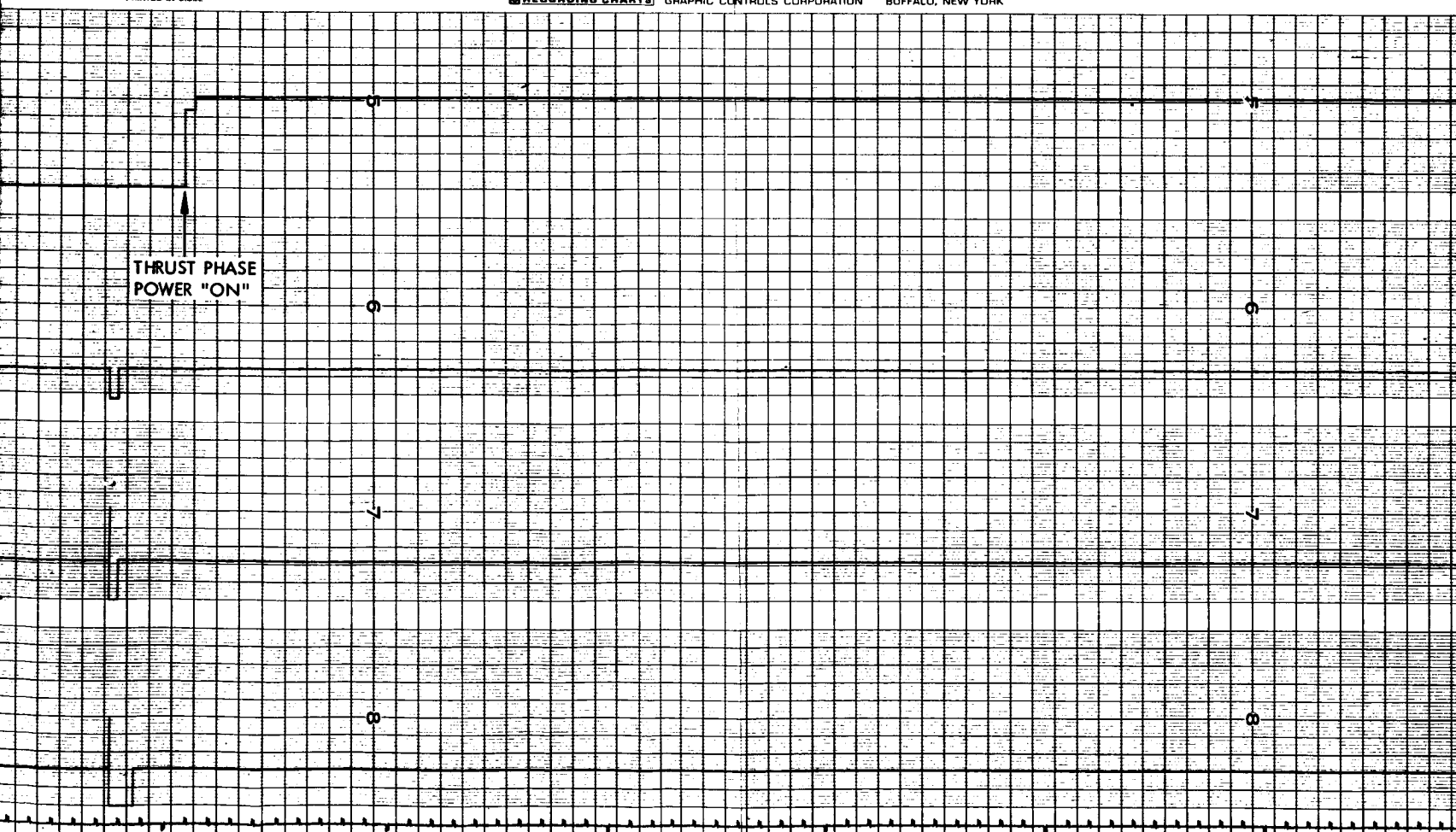
FOLDOUT FRAME 3

02:30:08.629

348
155
0.0993 g's
531
662
77.5 LBS
531
659
77.7 LBS

PRINTED IN U.S.A.   RECORDING CHARTS GRAPHIC CONTROLS CORPORATION   BUFFALO, NEW YORK

520
655
78.25 LBS

10.3

242
450
66 LBS

225
580
81 LBS

72 LBS

PRIMARY SUN SENSOR
PITCH ERROR, FC-5

PRIMARY SUN SENSOR
YAW ERROR, FC-6

CANOPUS SENSOR
ROLL ERROR, FC-12

CANOPUS SENSOR
STAR INTENSITY, FC-14

MODE 5 →

SUN
SHUTTER
OPEN

530

533

523

PRINTED IN U.S.A.   ⊗RECORDING CHARTS GRAPHIC CONTROLS CORPORATION   BUFFALO, NEW YORK

DIG 9

DIG 1

SUN
LOCK-ON

START OF
(+) YAW

END
YAW

DIG 2

MAGNITUDE REGISTER
LOADED

DIG 3

(+) ANGLE

-5   -10 -15 -20 -25 -30 -35 -40 -45 -50 -55 -60 63.7

PARTICLES
OR
REFLECTIONS

RECORDING CHARTS   GRAPHIC CONTROLS CORPORATION   BUFFALO, NEW YORK

PRINTED IN U.S.A.

PRINTED IN U.S.A.

MODE 2

SUN MODE
"ON"

CRUISE MODE "ON"

RESCALE
5MM

CAN. L.O.

CANOPUS
LOCK-ON

OF

START OF
(-) ROLL

END OF
ROLL

-5
-10
-15
-20
-25
-30
-35
-40
-45
-50
-55
-60
-65
-70
73

(+) ANGLE
RESET

FC-16 PITCH GYRO ERROR

FC-17 YAW GYRO ERROR

FC-49 ROLL PRECESSION COMMAND

GMT 02:15:30:884

START
+ YAW

PRE-MIDCOURSE ROLL

-10 -20 -30 -40 -50

FC-43 ROLL ACTUATOR POSITION

PRINTED IN U.S.A.

SECONDARY SUN SENSOR

FC-7 CELL A

PRE-MIDCOURSE
(MODE 1 4400 B

FC-8 CELL B

FC-9 CELL C

FC-10 CELL D

Figure 5.5-14 (continued). Midcourse Velocity Cor

GMT 02:21:11.87

START OF (-) YAW

PRE-MIDCOURSE YAW

-10 -20 -30

GMT 02:17:55.878

END -70.5 ROLL -70

-60

10 SEC
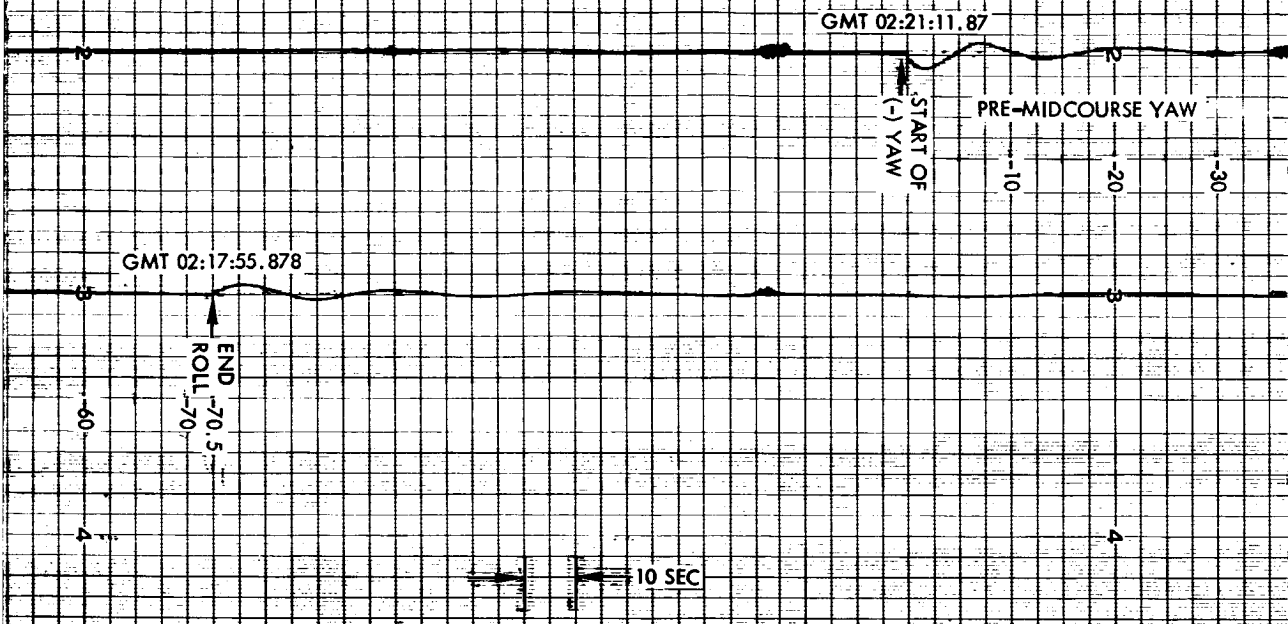
RECORDING CHARTS GRAPHIC CONTROLS CORPORATION   BUFFALO, NEW YORK

ATTITUDE MANEUVERS

ection
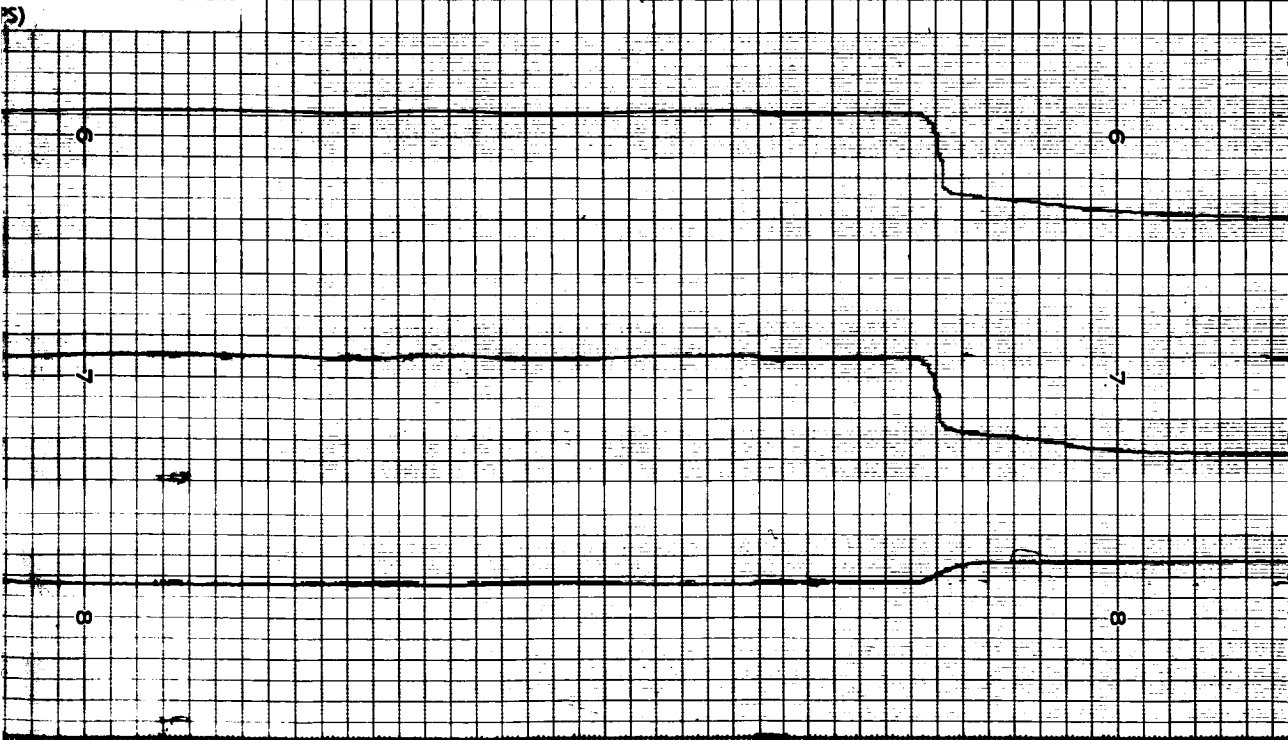
02:23:20.565

END OF YAW

-64

-50

-60

-40

PRINTED IN U.S.A. [RECORDING CHARTS] GRAPHIC CONTROLS CORPORATION   BUFFALO, NEW YORK

GMT 02:27:58

THRUST PHASE POWER ON

UNREGULATED
OUTPUT CURRENT
EP-4
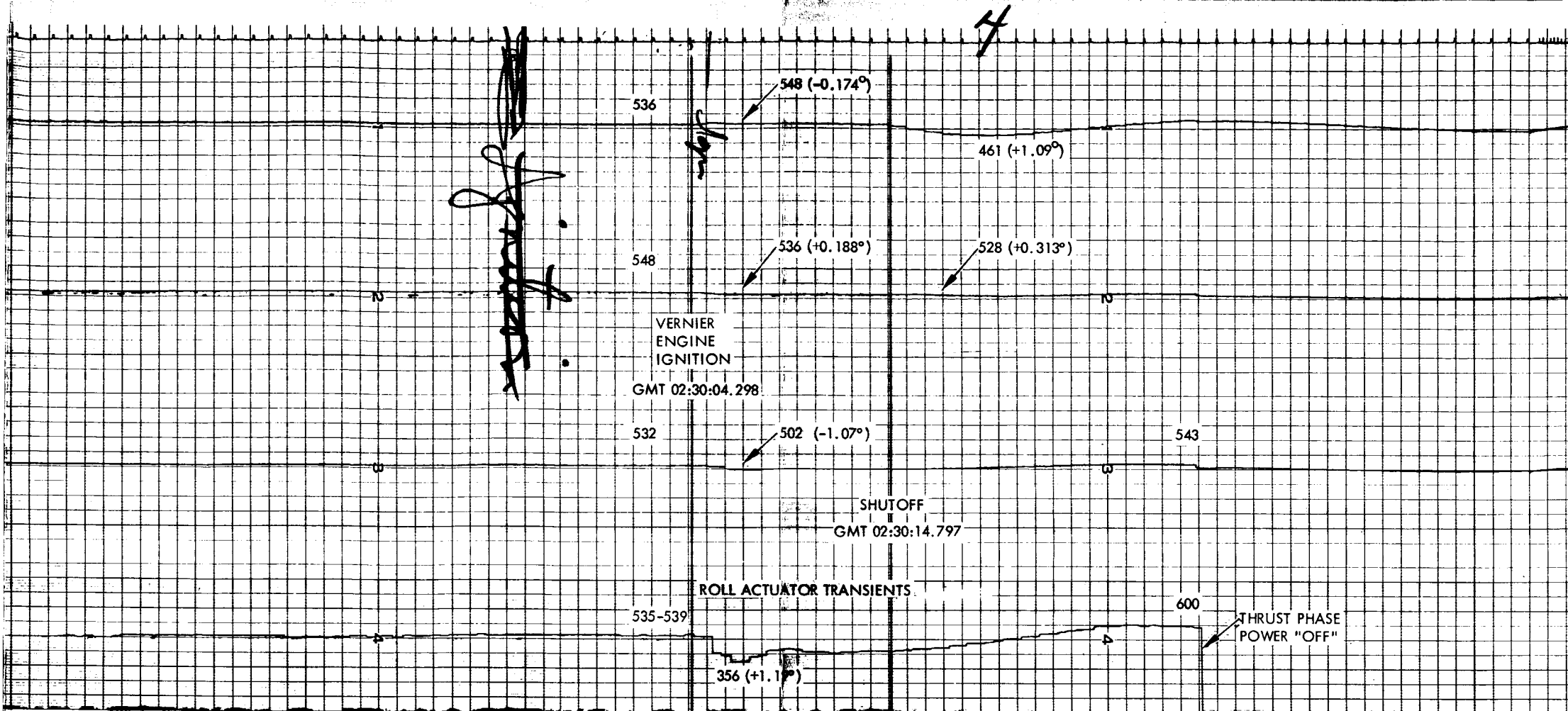
536

548 (−0.174°)

461 (+1.09°)

548

536 (+0.188°)

528 (+0.313°)

VERNIER
ENGINE
IGNITION
GMT 02:30:04.298

532

502 (−1.07°)

543

SHUTOFF
GMT 02:30:14.797

ROLL ACTUATOR TRANSIENTS

535-539

600

THRUST PHASE
POWER "OFF"

356 (+1.1°)

EP4 UNREGULATED
OUTPUT CURRENT

≈1.7 AMPS
MIDCOURSE THRUST
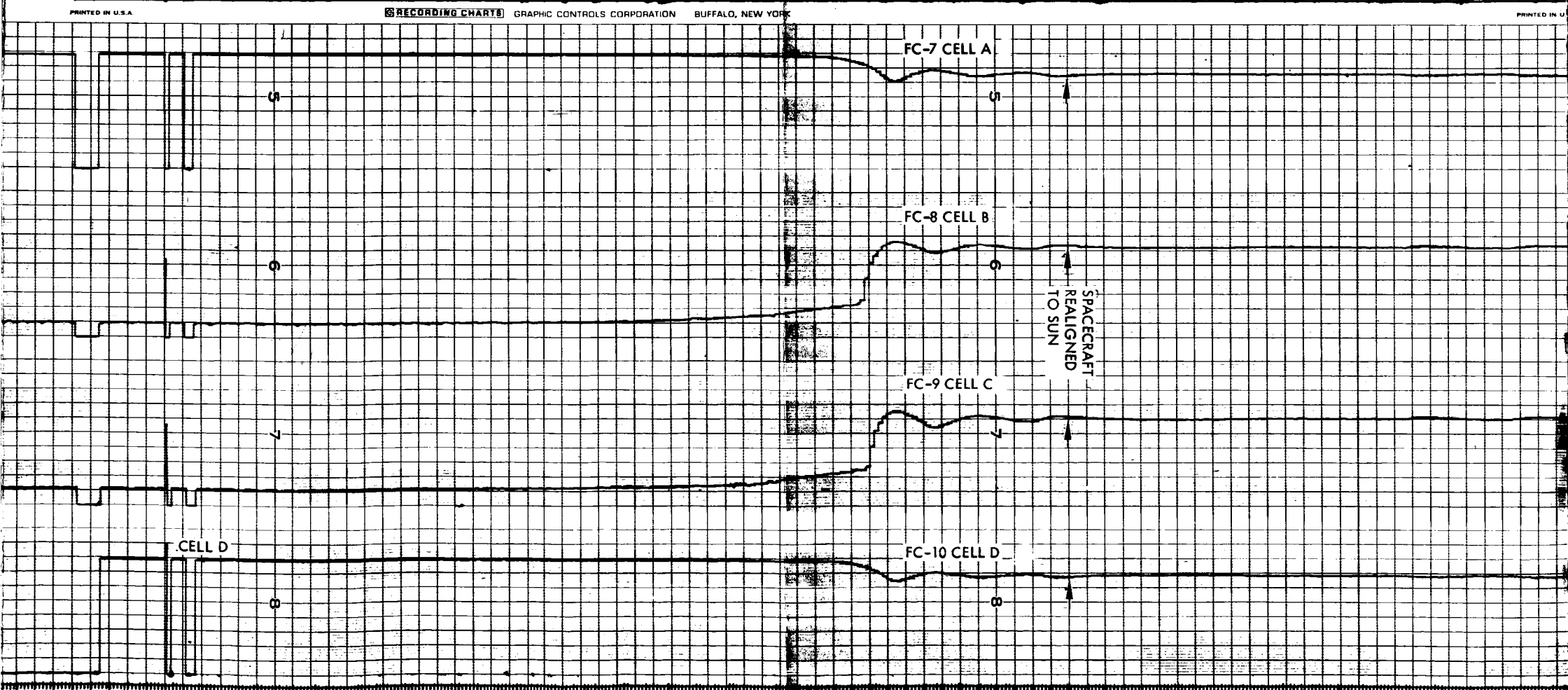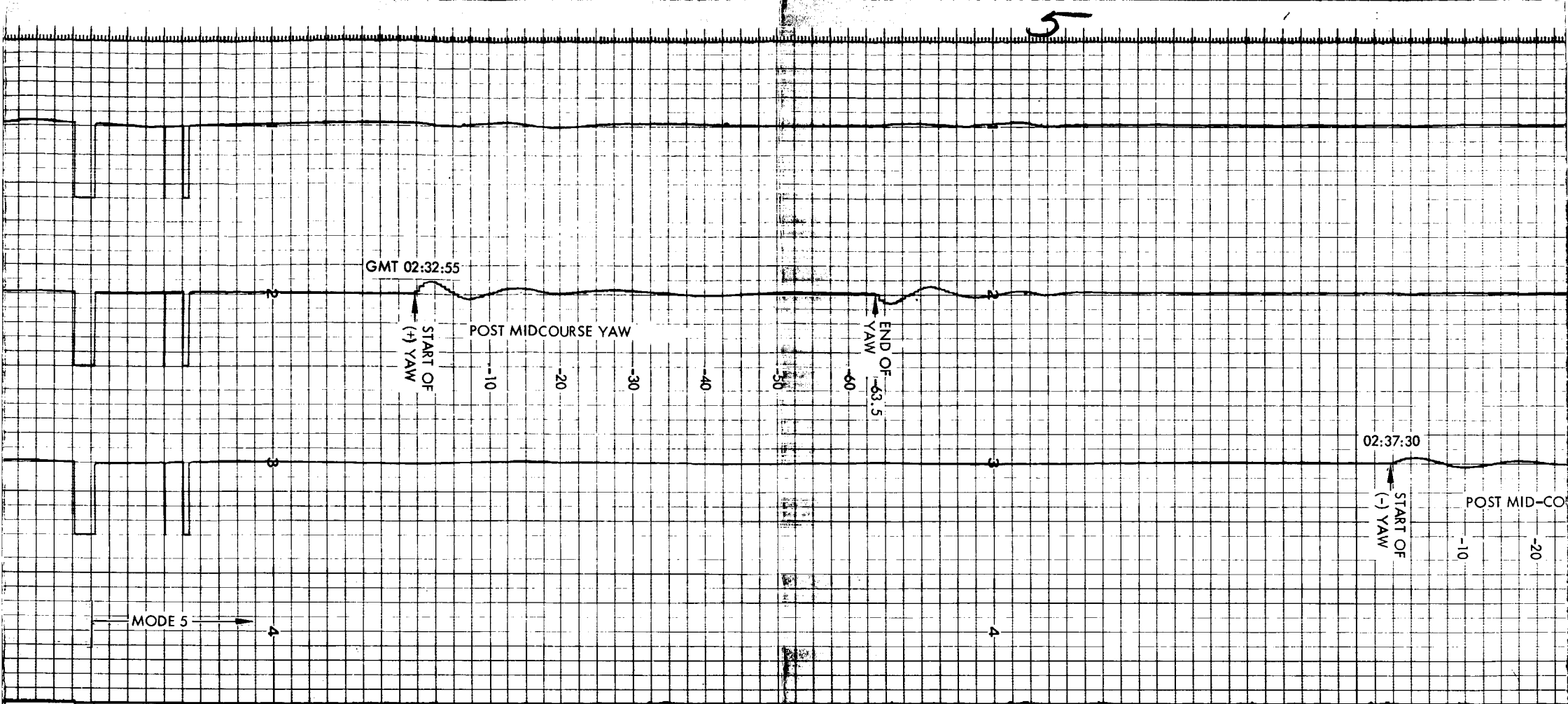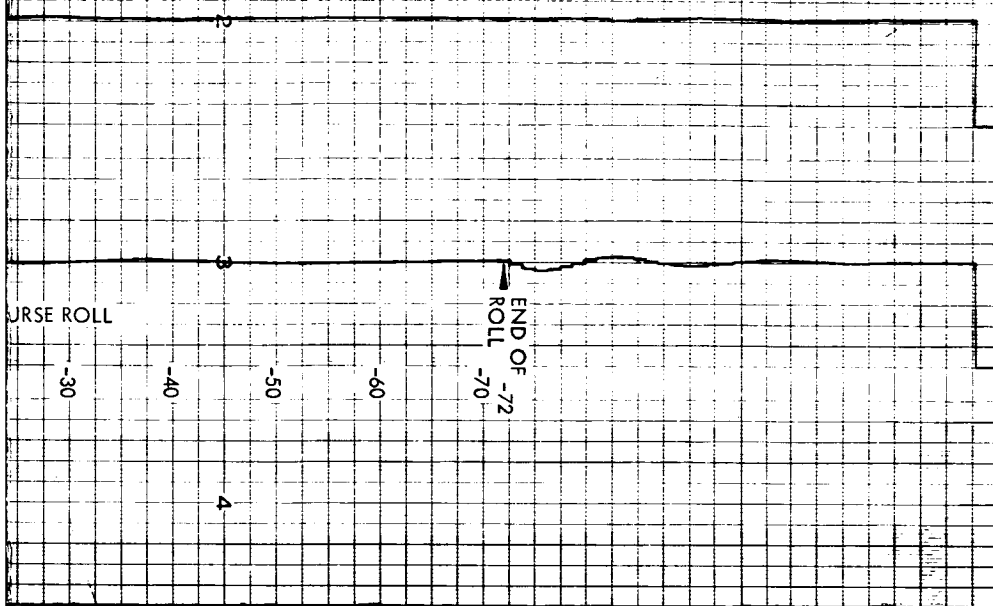
GMT 02:32:55

POST MIDCOURSE YAW

START OF (+) YAW

END OF YAW 63.5

02:37:30

START OF (-) YAW

POST MID-CO

-10 -20 -30 -40 -50 -60

-10 -20

MODE 5

PRINTED IN U.S.A.

RECORDING CHARTS GRAPHIC CONTROLS CORPORATION BUFFALO, NEW YORK

PRINTED IN U

FC-7 CELL A

FC-8 CELL B

SPACECRAFT REALIGNED TO SUN

FC-9 CELL C

CELL D

FC-10 CELL D

URSE ROLL

-30 -40 -50 -60 -70 -72

END OF ROLL

RECORDING CHARTS GRAPHIC CONTROLS CORPORATION   BUFFALO, NEW YORK
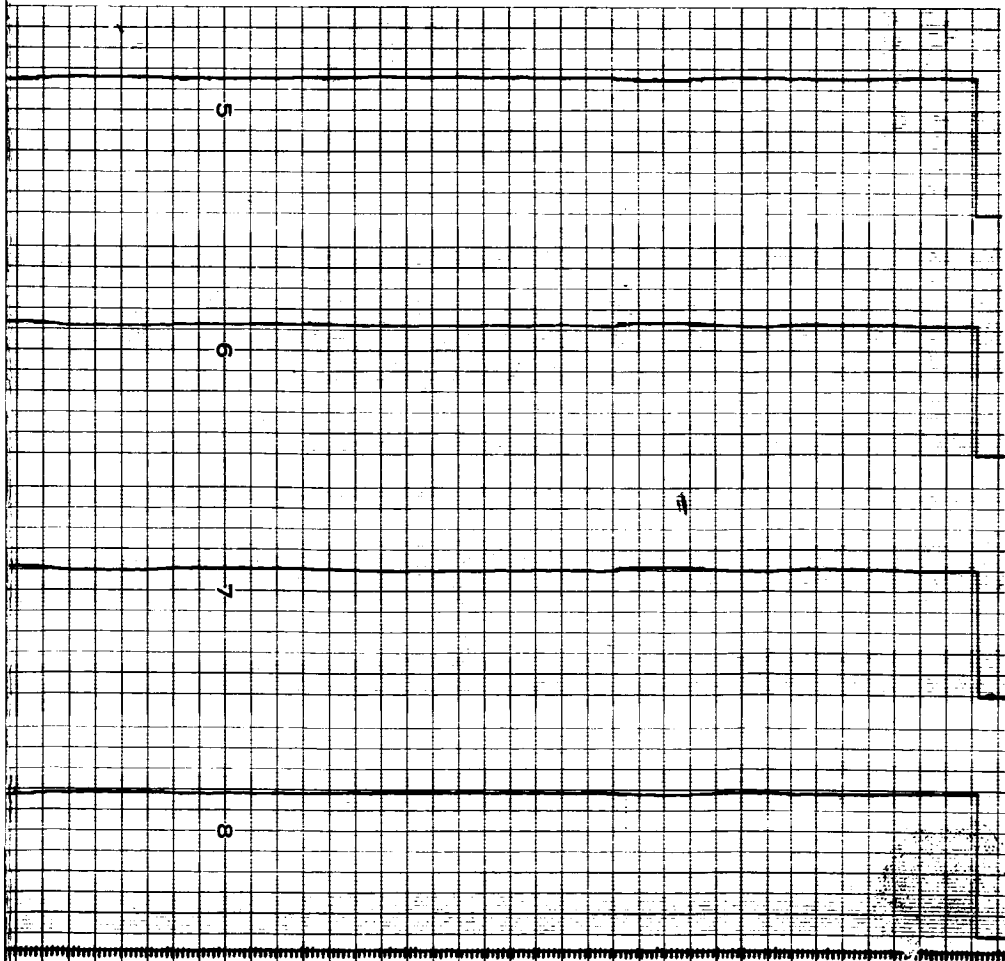
Prior to vernier ignition, pitch and yaw gyro errors were maintained within the inertial deadband of ±0.22 degree by the gas jet system. At the instant of ignition, these errors were -0.04 and -0.22 degree for pitch and yaw, respectively. The subsequent transient at ignition was reduced to zero in approximately 2 seconds. The change in yaw attitude was +0.19 degree, while the pitch attitude change was -0.17 degree. The transient behavior of both responses was dominated by the 1.0-second time constant of the attitude control loops.

Peak angular rates of (approximately) -0.5 deg/sec in pitch and +0.34 deg/sec in yaw occurred at vernier ignition. The startup impulse dispersions (deviations from average startup impulse) of the three engines were calculated by the procedure outlined in Reference 9 to be approximately as follows:

Leg 1: +0.267 lb-sec

Leg 2: +0.188 lb-sec

Leg 3: -0.455 lb-sec

These figures imply a maximum startup impulse variation (between legs 2 and 3) of 0.72 lb-sec. However, at engine ignition, the control system null reference changes from that which existed for the gas jet attitude control system to that which exists for the vernier engine attitude control system. This change in reference produces a significant portion of the gyro motion at ignition and tends to mask any effects due to uneven engine startup.

Based on the acceleration error telemetry signal (FC-15) (Figure 5.5-15), it was concluded that all three engines were producing controlled thrust within about 0.150 second of the ignition command signal. Therefore, acceleration signal amplifier saturation, which requires a startup delay of 0.26 second, did not occur, and no ΔV error information was lost.

Midcourse Engine Shutdown Dispersions

A summary of the peak spacecraft angles and angular rates and computed vernier engine shutdown impulse dispersions are given in Table 5.5-7.

It should be noted that peak gyro angles were less than 2 degrees and well within the required travel range of ±10 degrees. Inertial reference was therefore retained, and reacquisition of the sun and Canopus was accomplished via the reverse maneuver sequence.

Vernier engine shutdown impulse dispersions (relative to mean impulse of the three engines), calculated from pitch and yaw angular rate data as per the procedure outlined in the "Midcourse Engine Startup Characteristics," were well within the specification limit of ±0.63 lb-sec (Reference 10).
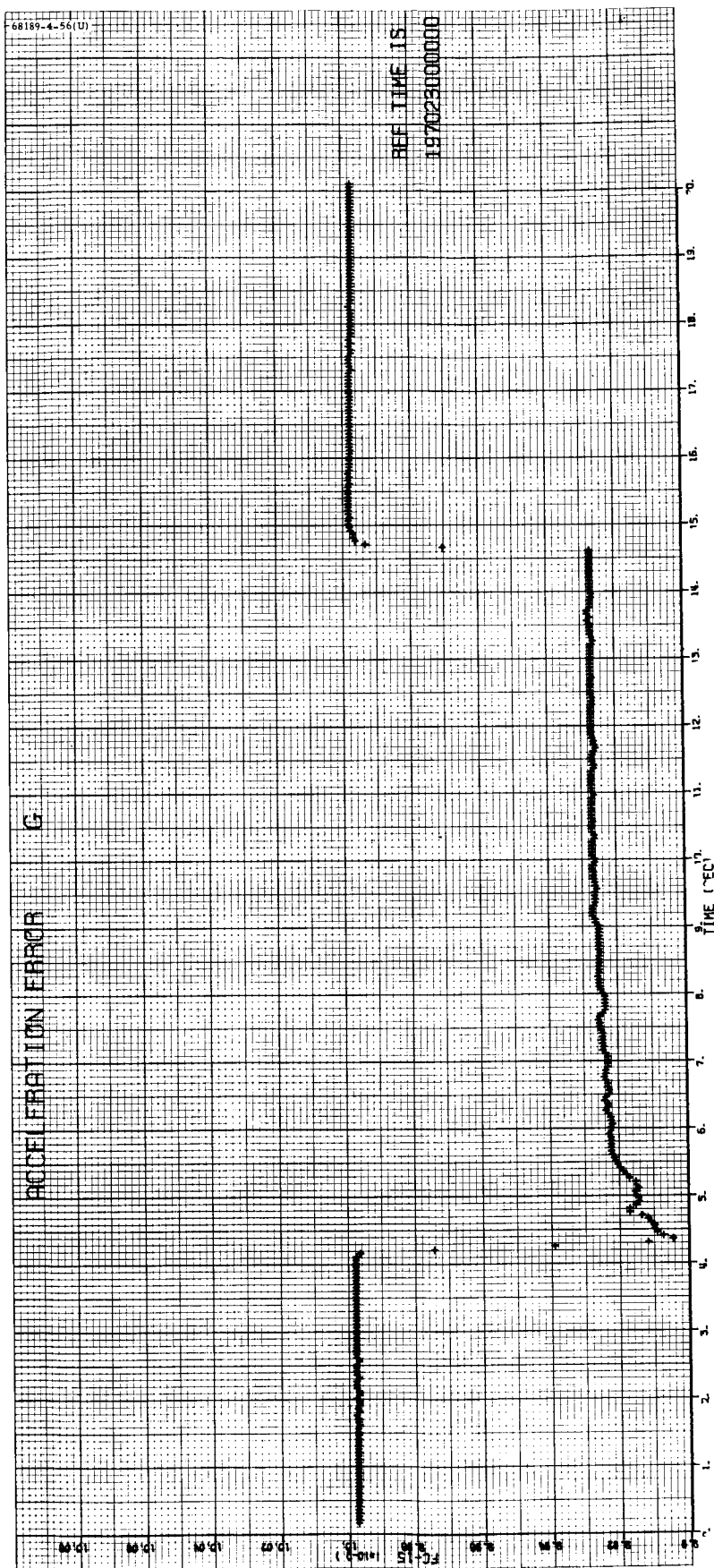
Figure 5.5-15. Acceleration Error

TABLE 5.5-7. MIDCOURSE SHUTDOWN SUMMARY

Maximum change in attitude, degrees:

Pitch   = +1.09

Yaw   = +0.10

Roll   = +1.18

Roll
actuator   = -1.22

Peak angular rates, deg/sec:

Pitch   = +0.24

Yaw   = -0.01

Vernier shutdown impulse dispersions, lb-sec:

Leg

1   = -0.18

2   = +0.03

3   = +0.15

Midcourse Velocity Determination

The general concept of midcourse correction capability employed by Surveyor is to apply a constant acceleration for a finite period of time. Thus, in theory, once the magnitude of the velocity correction is known, the exact duration of the constant acceleration phase can be determined. In practice, this approach is slightly altered to account for such error sources as engine ignition transients, shutdown impulse, and hysteresis. Thus, the actual command time ΔT is slightly higher.

The desired values during flight were as follows:

1) Desired ΔV = 10.272 m/sec (33.69 fps)

2) Desired ΔT = 10.4628 seconds

Duration of Burn Time. The acceleration error signal data were used in an attempt to determine the actual burn time. The results (Figure 5.5-16) indicated that the burn time was 10.479 seconds for a timing error of 0.02 second. (The magnitude register was loaded with 210 counts or ΔT = 10.5 seconds.)
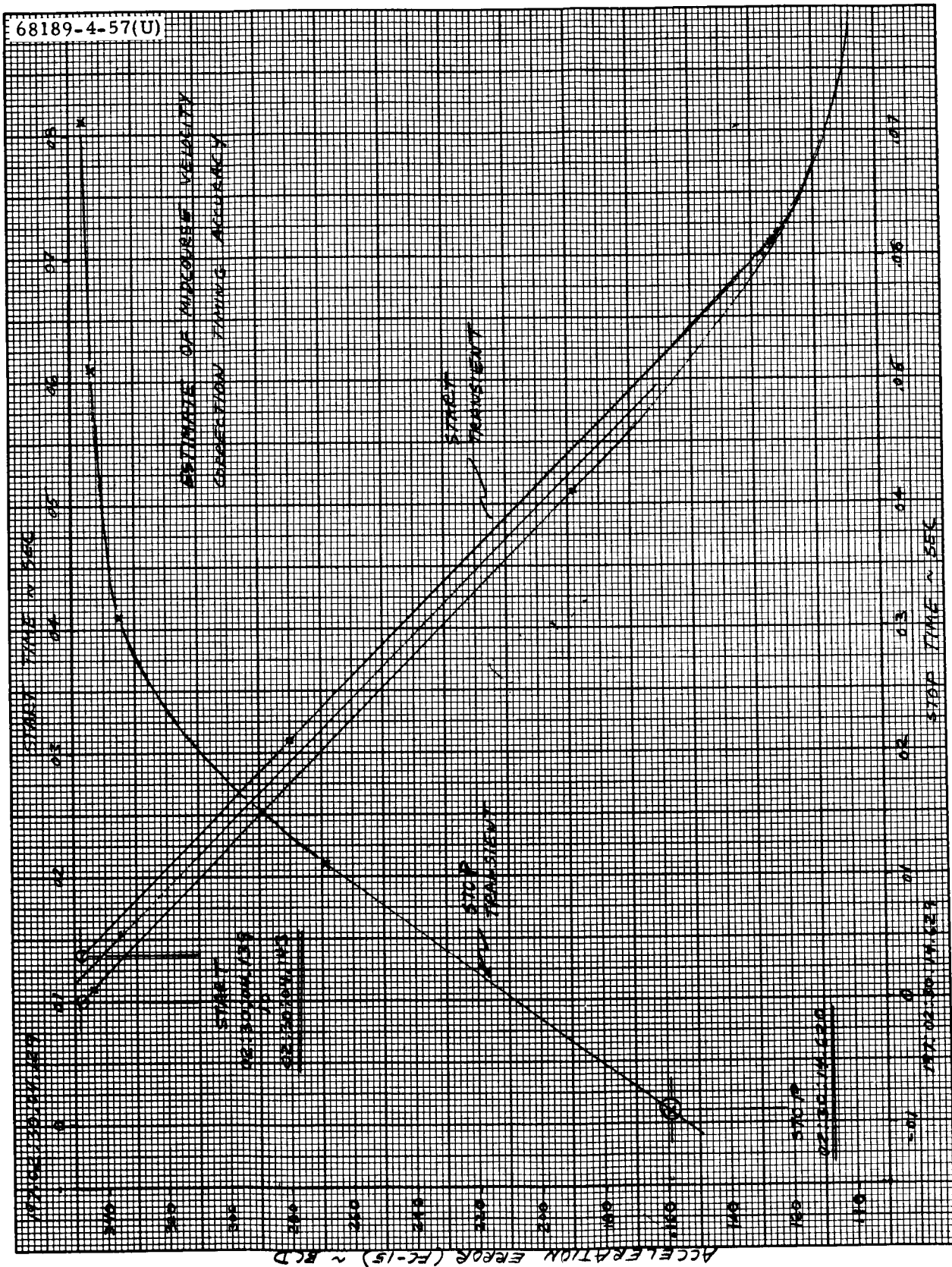
Figure 5.5-16. Midcourse Velocity Correction
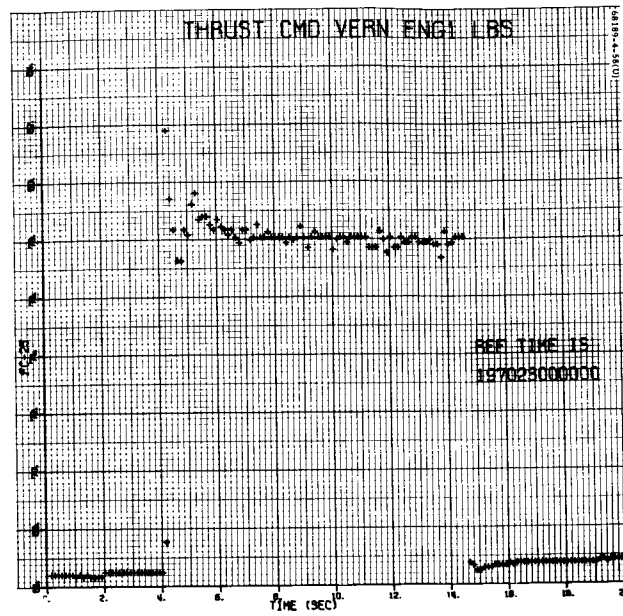Timing accuracy using acceleration error (FC-15)

Estimate of ΔV

The output of the acceleration amplifier (FC-15) remained essentially constant during the burn period at a value equivalent to 3.19 ft/sec^2. Therefore, the midcourse ΔV was 3.19 X 10.479 = 33.46 fps. From orbit determination, it was concluded that the actual midcourse ΔV was 10.1316 m/sec (33.24 fps). The ΔV value obtained from the telemetered acceleration amplifier output data is within 1.0 percent of the value obtained by means of orbit determination techniques.
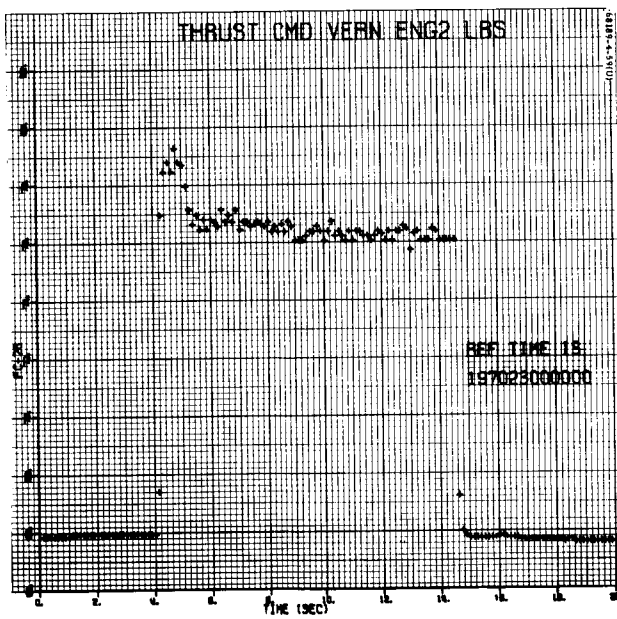
A list of parameters affecting the accuracy of the velocity correction is presented in Table 5.5-8 along with the values of maximum allowable errors. Actual performance values were used wherever possible.

### TABLE 5.5-8. SURVEYOR IV MIDCOURSE VELOCITY CORRECTION ACCURACY

Item	Parameter	Requirement 3σ or Limit	Equivalent Error, fps	Requirement Specification	Performance Value, ft/sec	Comments
1	Errors proportional to maneuver magnitudes					Much of the error was anticipated and was included in the calculation of the desired burn time
	Accelerometer accuracy	1.1 percent	0.15	234632C		
	Reference signal	0.5 percent	0.068	234600E		
	Flight control electronics null	0.15 percent	0.02	234600E		The difference between the actual value of ΔV from orbit determination and the commanded value was -0.57 fps
	Thrust bias variation	0.09 percent	0.01	287105		
	Control channel gain variation	0.07 percent	0.009	234600E	0.17	
	Accelerometer misalignment	0.06 percent	0.008	234600E		This value is more meaningful than the 0.18 fps given as performance value
	Total proportional errors (RSS)	1.22 percent	0.17			
2	Errors independent of maneuver magnitude					
	Shutdown impulse dispersion	±0.63 lb-sec	±0.016	287015	-0.004	$\Delta V = \dfrac{\Delta I}{M}$
	Hysteresis limit cycle	3 milliamperes	0.035	287105	0	
	Ignition transient	—	0.47	—	0	
	Timing granularity	0.05 second	0.16	224832A 7.2.1.9	-0.06	
	Total independent errors		0.497		-0.064	
3	Total magnitude errors (RSS)		0.525		0.18	

a) Engine 1

b) Engine 2
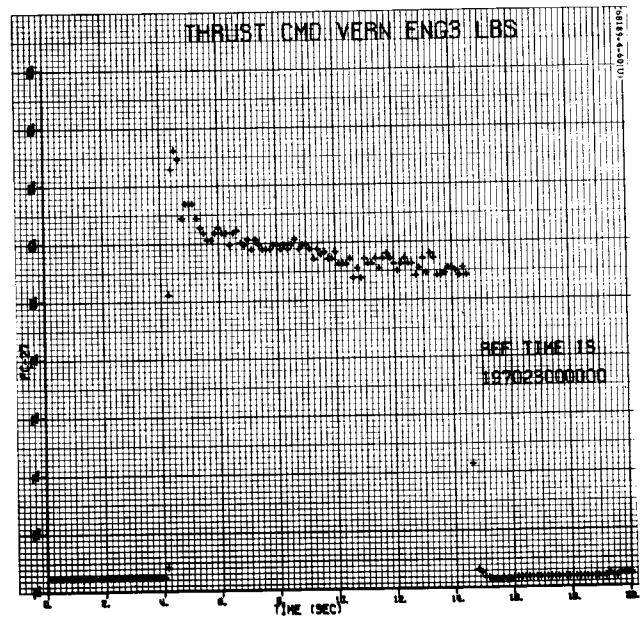
c) Engine 3

Figure 5.5-17. Vernier Engine Thrust Commands

Telemetered Thrust Levels

The vernier engine thrust levels were determined from vernier engine thrust command calibration data which were obtained using the improved calibration techniques (Figures 5.5-17 and 5.5-18).

The approximate steady-state vernier engine thrust levels were as follows:

Engine		Pounds
(FC-25)	=	77.5
(FC-26)	=	77.7
(FC-27)	=	78.25

Based on a spacecraft weight at injection of 2295 pounds and an estimated constant acceleration of 0.09917 g, the expected total thrust is 227.6, which compares favorably with the total thrust of 233.4 pounds obtained from the telemetered vernier engine thrust commands.
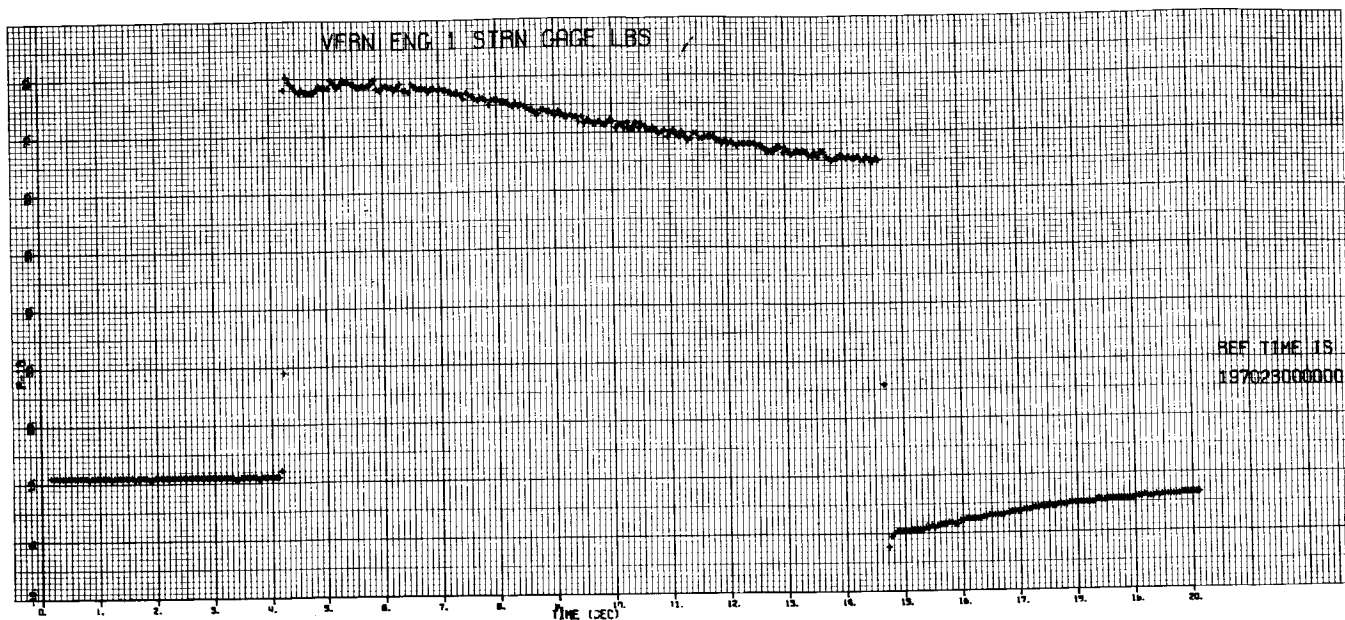
5.5.4.9 Preretro Maneuvers

Before retro ignition, it is required that the spacecraft thrust axis (roll axis) be aligned to the translational velocity vector of the spacecraft as part of the gravity turn terminal descent phase guidance. The alignment is performed by means of two sequential rotations about the spacecraft body (gyro) axes. A third roll rotation may be required to align the high-gain planar array with the spacecraft-earth line to secure a favorable omnidirectional antenna pattern or to satisfy a RADVS sidelobe constraint (Reference 12).

These maneuvers are accomplished by using the cold gas attitude control system, with the body-fixed integrating rate gyros as inertial references. To accomplish a rotation, the appropriate gyro torquer winding is driven by a constant current source for a precise length of time; the spacecraft is slaved to this changing reference at a constant rate of 0.5 deg/sec.

The major events and times associated with the preretro maneuvers are given in Table 5.5-9.

The preretro maneuvers were analyzed in terms of the following:

1) The gyro precession times were determined from gyro error signals and precession logic signals and compared to commanded times.

2) Using these attitude errors and the initial sun and Canopus error signals, the terminal pointing accuracy was determined.
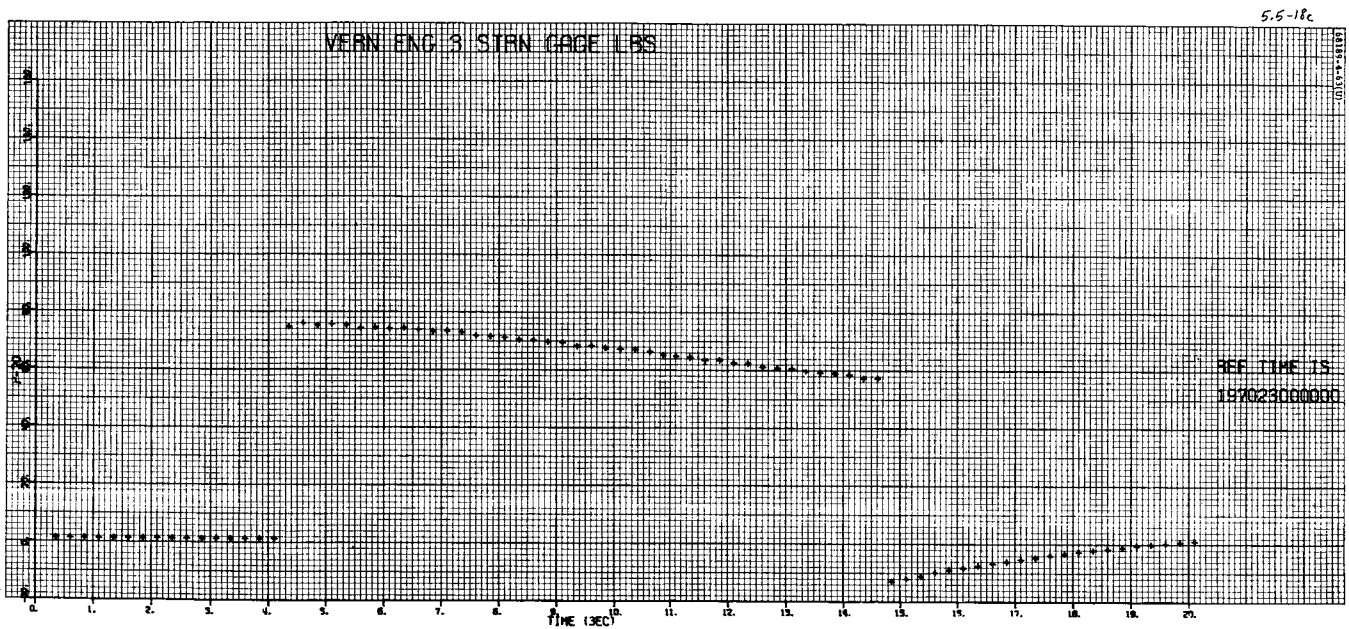
a) Engine 1
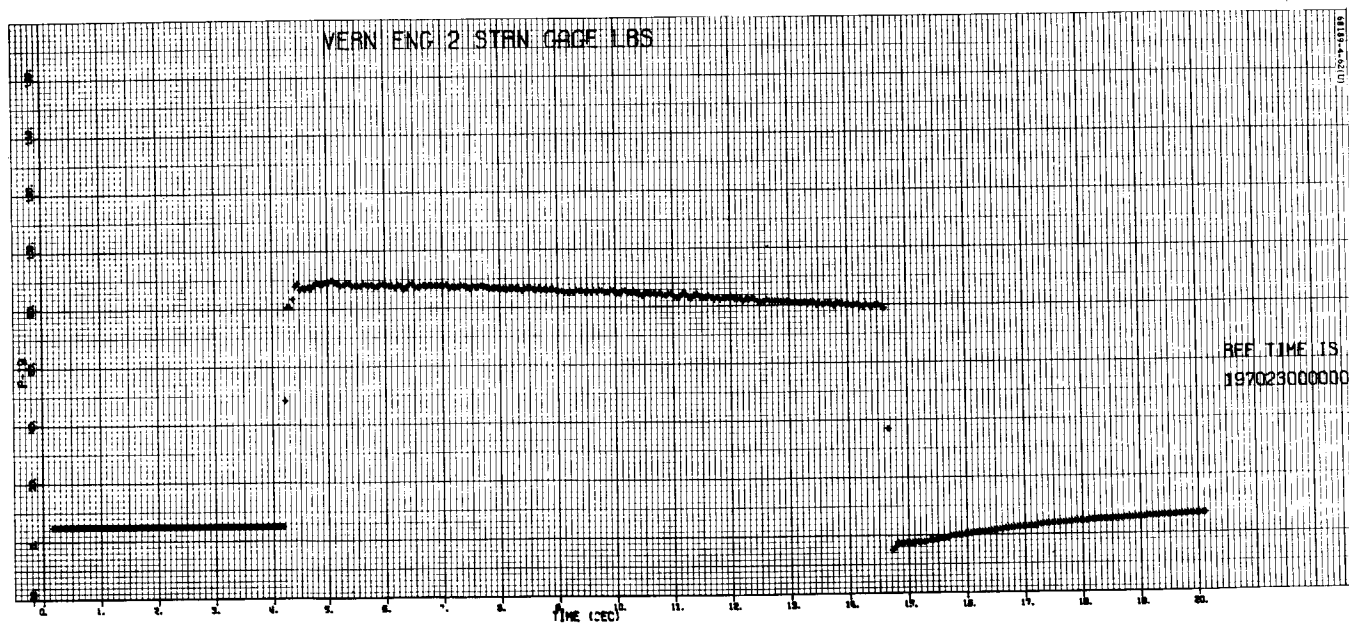
b) Engine 2

Figure 5.5-18. Vernier Engine Strain Gauges

c) Engine 3

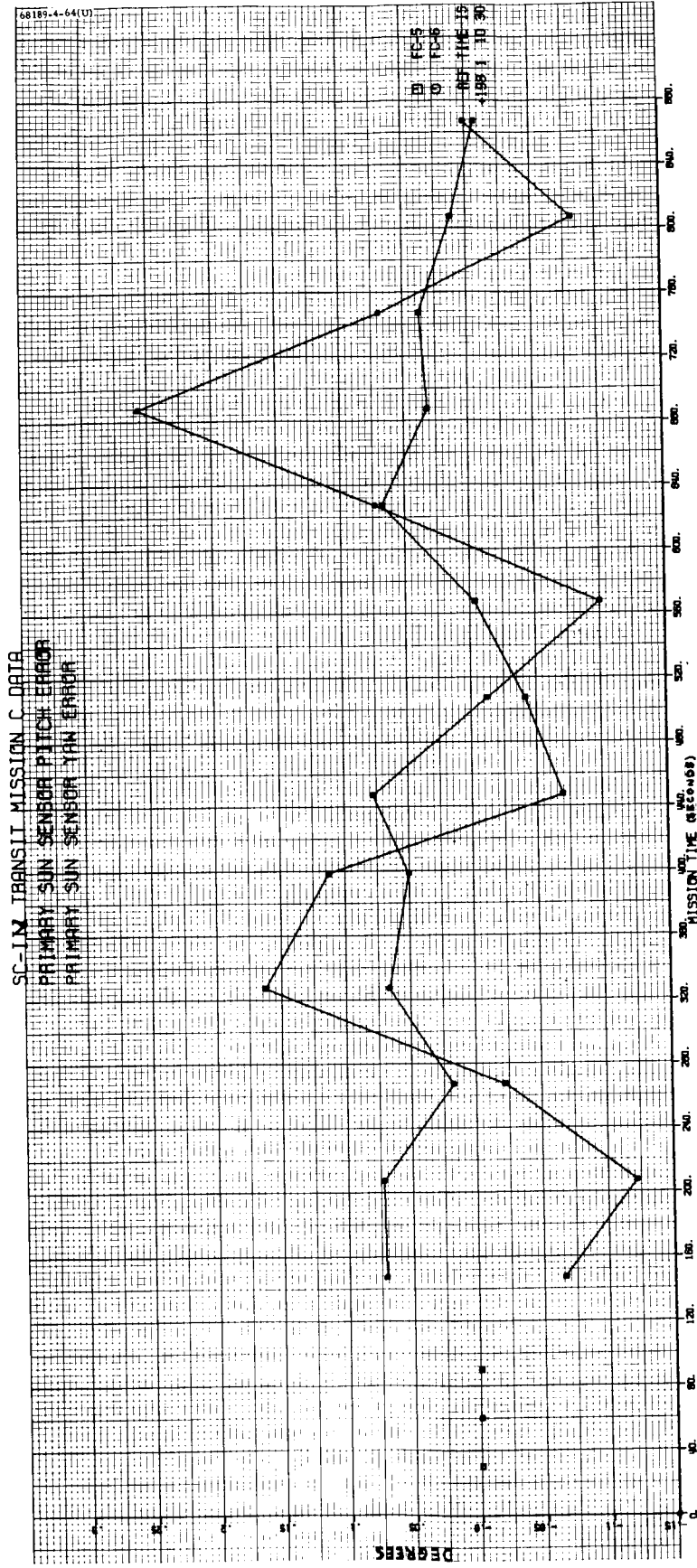Figure 5.5-18 (continued). Vernier Engine Strain Gauges

Figure 5.5-19. Primary Sun Sensor Error Signals

TABLE 5.5-9.   MAJOR EVENTS AND TIMES (DAY 198)
FOR PRERETRO MANEUVERS

Event	Command	GMT, hr:min:sec
Begin roll	0714	01:24:46.812
End roll		01:27:28.415
Begin yaw	0713	01:29:36.660
End yaw		01:32:42.002
Begin roll	0711	01:35:07.045
End roll		01:35:57.793
Retro ignition		02:01:59.915

The first attitude maneuver (roll) was initiated 37 minutes and 13 seconds before retro ignition. Normally, the time constraint on break of optical lock is 33 minutes based on an allowable 1 deg/hr gyro drift contribution to the pointing error (Reference 1). Since the attitude maneuver magnitudes were compensated for in flight measurements of gyro drift, the earlier maneuver time was acceptable.

As in the case of the premidcourse attitude maneuvers, an attempt was made to initiate the maneuvers at the limit cycle null points. The roll maneuver was initiated within approximately -0.05 degree of null while the pitch and yaw optical errors at the start of yaw were -0.07 and -0.14 degree, respectively (Figure 5.5-19).

Gyro Precession Times

The attitude maneuvers entered into the flight control programmer magnitude register were as follows:

Maneuvers	Degrees	Bits
+Roll	80.9	405
+Yaw	92.7	464
-Roll	25.3	127

Table 5.5-10 presents the estimated gyro precession times.

Figure 5.5-20. Gyro Error Signals

TABLE 5.5-10.   ESTIMATED GYRO PRECESSION TIMES

Attitude Maneuver	Commanded Time, seconds	Observed Time, seconds	ΔT, seconds	Rotation Error, degrees
Roll	162.0	161.60	-0.4	$\Delta\varphi$ = -0.20
Yaw	185.6	185.34	-0.26	$\Delta\psi$ = -0.13
Roll	50.8	50.75	-0.05	$\Delta\varphi$ = -0.02

Since the gyro error signals are only sampled once every 1.2 seconds (coast mode at 1100 bits/sec) during the preretro maneuvers, it was assumed that the shapes of roll and yaw gyro transients were the same as those observed during the premidcourse attitude maneuvers when the gyro error signals were sampled once every 0.05 second. The precession times were then estimated graphically based upon the intersection points of the start and stop transients with the steady-state gyro error values (Figure 5.5-20).

Gyro Drift Measurements

Ten three-axis gyro drift checks were made during the mission, eight of them prior to the midcourse velocity correction. Two roll-axis-only drift checks were also made. A summary of gyro drift measurement is presented in Table 5.5-11. Two techniques were used to measure the drift rates. The first was based on average slopes of the optical error signals obtained from analog Brush recorder and Milgo plots. In the second technique, iterated calculations were made as described in Reference 13.

The preterminal attitude maneuvers were compensated for by the following gyro drift rates:

Roll = -0.5 deg/hr

Pitch = -1.0 deg/hr

Yaw = +0.15 deg/hr

The gyro drift values selected for preterminal maneuver compensation were based essentially upon an average of all measurements made during the mission. The gyro drift measurements are depicted versus mission time in Figure 5.5-21. The fixed drift history of each gyro is shown in Figure 5.5-22. Although all three gyros indicate a tendency to drift in a negative direction, no predictable trend is apparent.
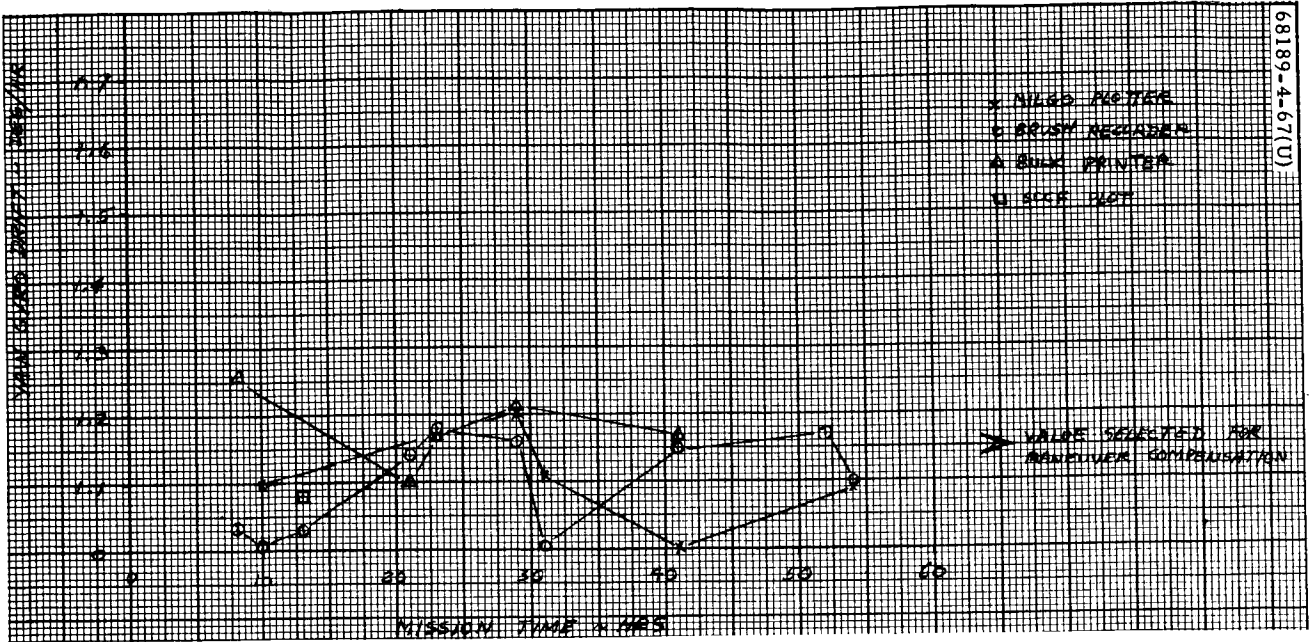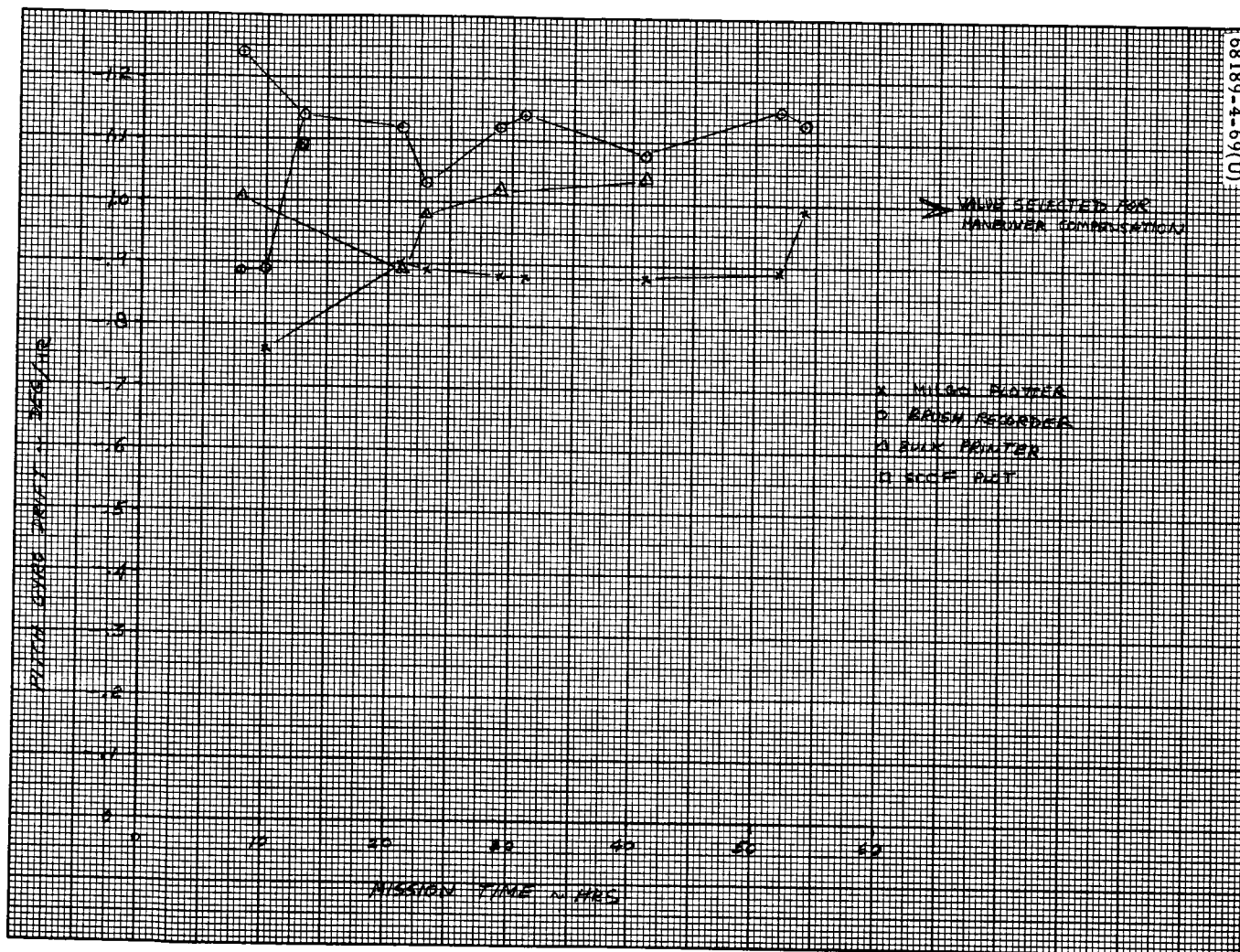
a) Yaw
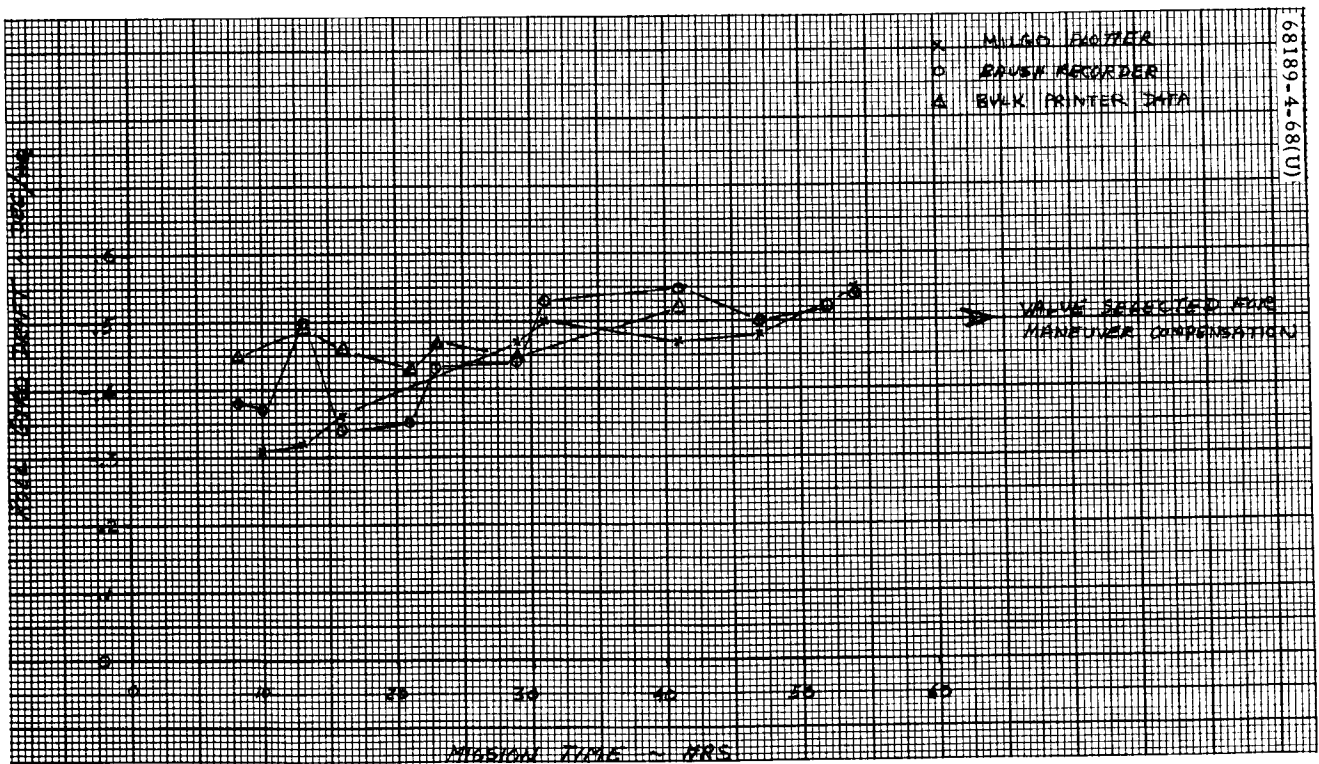
b) Roll

Figure 5.5-21. Gyro Drift Measurements Versus Mission Time

c) Pitch

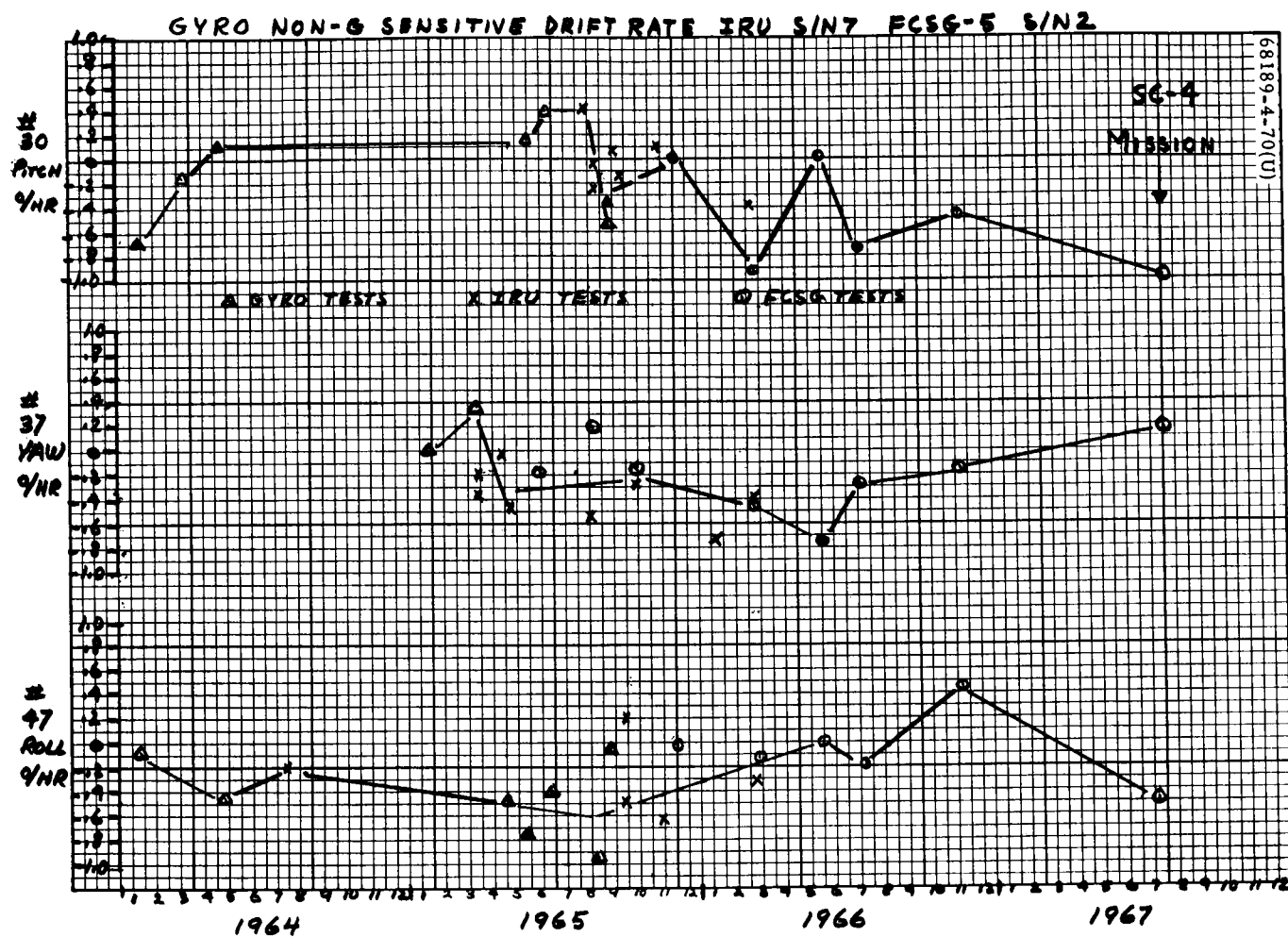Figure 5.5-21 (continued). Gyro Drift Measurements Versus Mission Time

Figure 5.5-22. History of Gyro Fixed Drift

TABLE 5.5-11. GYRO DRIFT SUMMARY

Number	Day	Time	Type	Roll			Pitch			Yaw		
				Milgo	Analog	Bulk	Milgo	Analog	Bulk	Milgo	Analog	Bulk
1	195	18:46 to 20:54	3 axis	No data	-0.384	-0.445	No data	-1.24 0.885	-1.04	No data	+0.032	+0.26
2		20:58 to 22:37	3 axis	-0.31	-0.372		-0.76	-0.89		+0.10	0	
3	196	00:09 to 02:09	3 axis	-0.32	-0.50	-0.49		-1.14	-1.09		+0.03	+0.08
4		02:19 to 07:55	Roll	-0.36	-0.34	-0.46						
5		08:00 to 09:58	3 axis		-0.35	-0.43	-0.90	-1.12	-0.88		+0.14	+0.10
6		10:20 to 11:47	3 axis		-0.43	-0.467	-0.89	-1.03	0.975		+0.18	+0.172
7		16:08 to 17:39	3 axis	-0.47	-0.438	-0.45	-0.88	-1.12	-1.02	+0.20	+0.16	+0.209
8		18:03 to 19:43	3 axis	-0.50	-0.53		-0.88	-1.14		+0.11	≈0	
9				Data Not Available								
10	197	04:15:56 to 05:50:43	3 axis	-0.47	-0.55	-0.52 (-0.26)	-0.875	-1.08	-1.04	0	+0.13	+0.17
11		08:50:57 to 14:36:19	Roll	-0.48	-0.50							
12		15:40:30 to 17:30:30	3 axis	NA, wrong format	-0.52		-0.89	-1.15			+0.17	
13		17:39:40 to 19:12:08	3 axis	-0.55	-0.54		-1.09	-1.13		+0.09	+0.1	

5.5.4.10   Main Retro Phase

Main retro phase began at day 198, 2 hours 1 minute 56.080 ± 0.03 second GMT with the indication of altitude marking radar mark and ended at 2 hours 2 minutes 41.018 seconds.

During this phase, the function of the flight control system is to maintain the attitude of the spacecraft inertially fixed and to provide and execute a fixed sequence of commands to establish the necessary initial conditions for the vernier descent phase. The following analysis reveals that these functions were performed satisfactorily up to the time data were lost.

The range and longitudinal velocity telemetry signals remained saturated at the time of data loss, which was consistent with predicted values of $R = 57,000$ feet and $V_z = 1100$ fps at this time.

A list of retro phase events and their corresponding time of occurrence is given in Table 5.5-12 along with expected time intervals. These results confirm the performance of the magnitude register and programmer.

Observation of telemetry signal FC-64 confirmed that the altitude marking radar mark occurred prior to emergency altitude marking radar since FC-64 can only be set high by the true mark signal.

Ignition of the vernier engines during the main retro phase was executed smoothly, with impulse dispersions between engines well within the specification values. As discussed previously, the change in gyro angles due to a shift in reference null at engine ignition limits the accuracy of the startup impulse dispersion calculations.

Retro Phase Attitude Control

During the main retro phase, from vernier ignition until the loss of data, spacecraft attitude motion was small in all three axes (Figure 5.5-23). Peak pitch and yaw inertial attitude motion, as read directly from gyro error telemetry data (FC-16 and FC-17), occurred at vernier ignition and amounted to -0.35 degree in yaw and -0.09 degree in pitch. Following ignition, static attitude error was virtually zero about the pitch axis and approximately -0.24 degree about the yaw axis. Roll inertial attitude error was less than 0.05 degree throughout the main retro phase (less than 1.0 degree is required).

Since all gyro error signals were maintained to within ±1.0 degree (during retro burn), each gyro was exercised less than 10 percent of the available travel range of more than ±10 degrees. A summary of pitch and yaw inertial attitude angles produced at various points in the retro phase is given in Table 5.5-13.

RETRO ACCELEROMETER
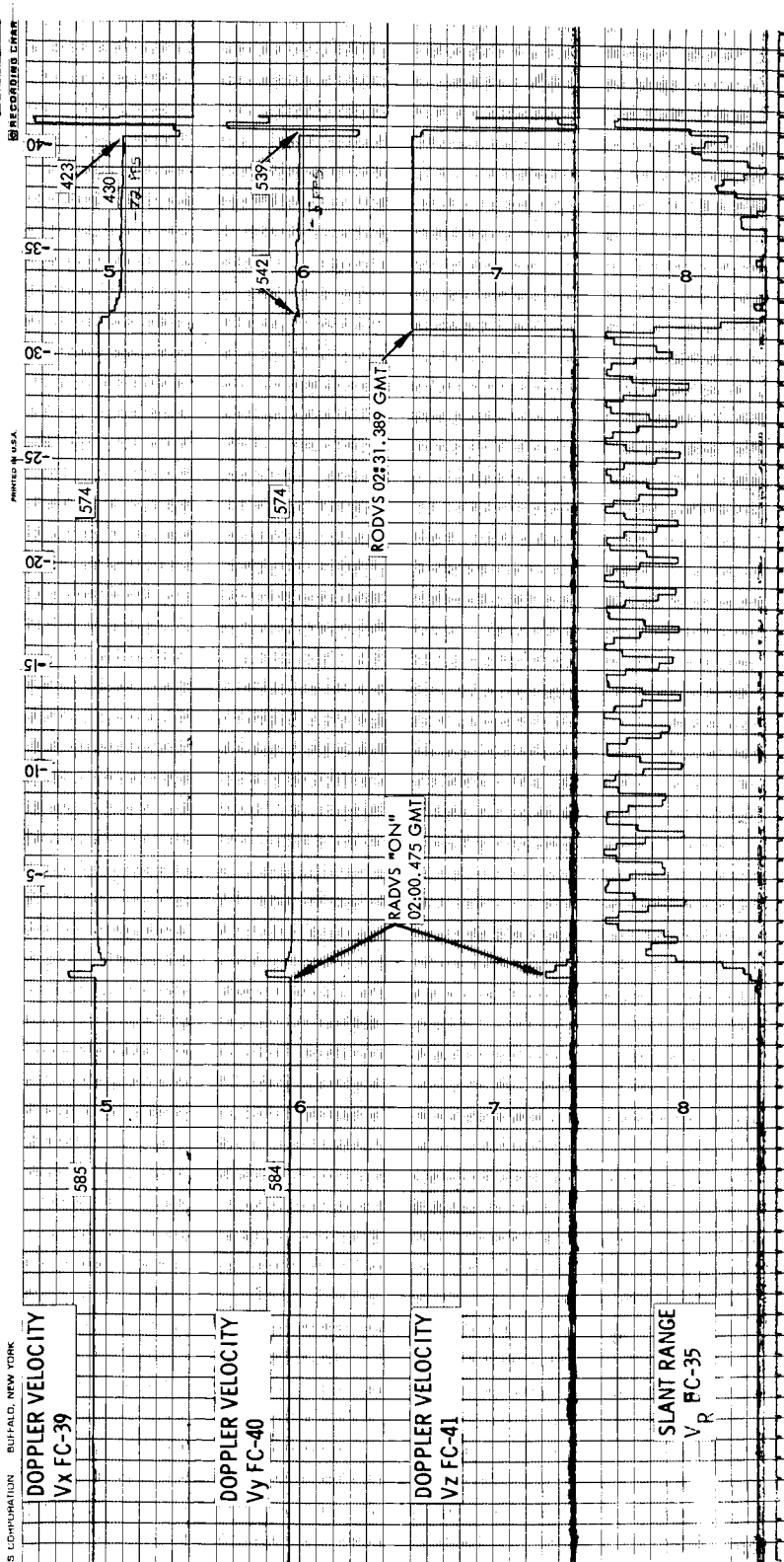FC-32

8.5g
580
251 (365 gs)
22

ACCELERATION ERROR
FC-15

THRUST COMMAND
VERN. ENG. NO. 1
FC-25

(67 lbs)
536
≈ 7.0 lbs
583 (70.9 lbs)
616 (73.8 lbs)
511
(64.7 lbs)
538-40 (67 lbs)

THRUST COMMAND
VERN. ENG. NO. 2
FC-26

(70 lbs)
571
≈ 7.0 lbs
587 (71.4 lbs)
499 (64 lbs)
534 67 lbs

THRUST COMMAND
VERN. ENG. NO. 3
FC-27

(64 lbs)
491
≈ 3.0 lbs
536 (67.8 lbs)
499 (65 lbs)
526-8

ENG. NO. 1
STRAIN GAUGE
P-18

VERNIER IGNITION
01:58.815 GMT
RETRO IGNITION
01:58.915
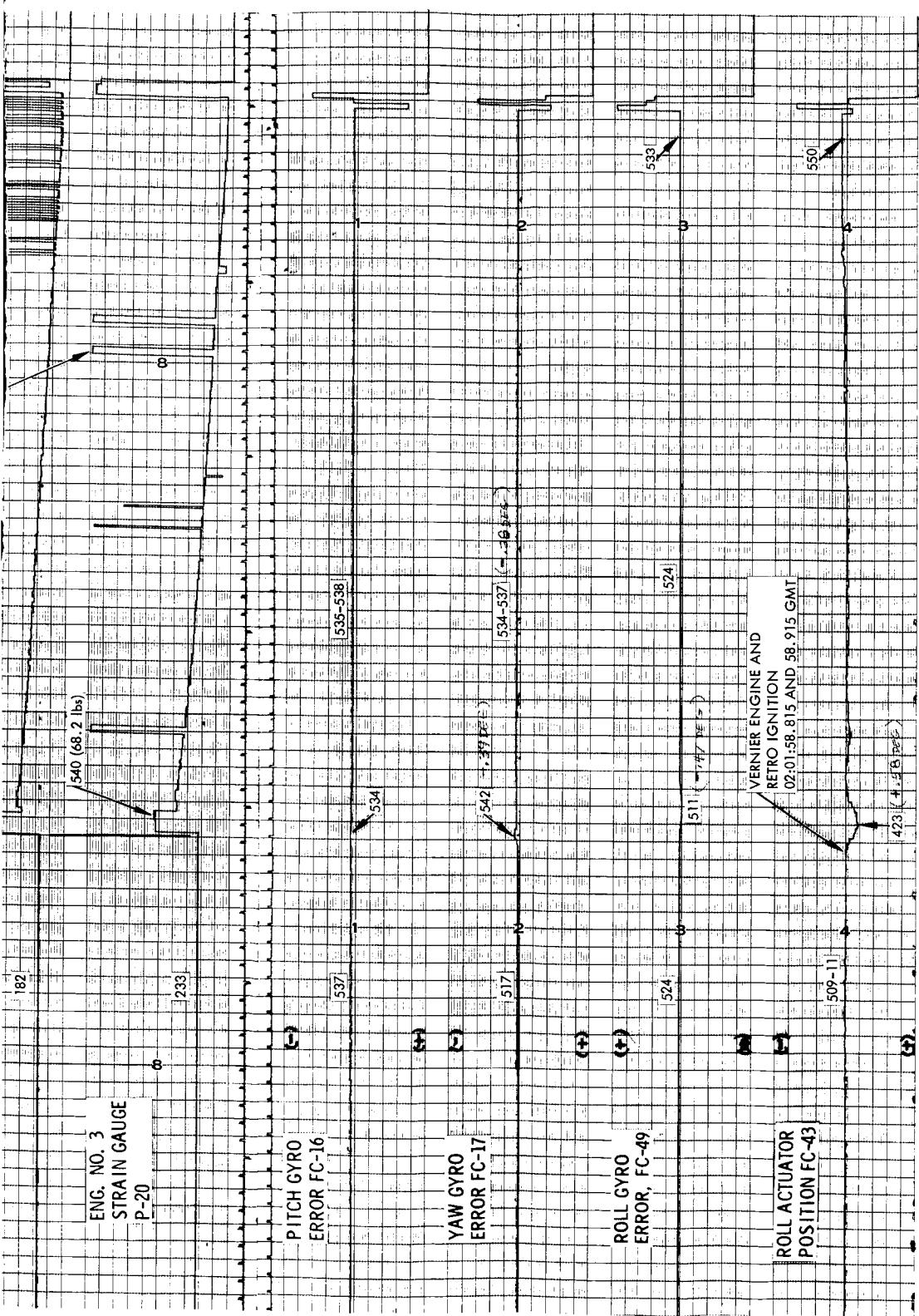442 (71)
253

ENG. NO. 2
STRAIN GAUGE
P-19

502 (69.2)

BAD DATA

1 2 3 4 5 6 7

Figure 5.5-23. Surveyor IV Terminal Descent

TABLE 5.5-12.   TIME AND EVENTS LOG, RETRO PHASE

Main Retro Phase Event	Time of Occurrence, Day 198, GMT, hr:min:sec	Time Between Events, seconds	Expected Time Intervals, seconds
Altitude marking radar signal (FC-64)	02:01:56.080 ± 0.005		
Vernier ignition (FC-28)	02:01:58.810 ± 0.025	2.735 ± 0.055	2.725
Retro ignition (FC-29)	02:01:59.925 ± 0.025	1.115	1.1 ± 1
RADVS on	02:02:00.475 ± 0.025	0.55	0.55
Inertia switch "opened"	02:02:02.685 ± 0.6	2.210	
RODVS	02:02:31.484	28.799	
Last bit of data	02:02:41.018	9.534	

TABLE 5.5-13.   RETRO PHASE ATTITUDE CONTROL SUMMARY

Event	Pitch	Yaw
Vernier ignition	-0.09	-0.35
Retro ignition	+0.08	-0.17

Pitch and yaw control moments generated by the vernier engines were estimated by means of the following equations:

$$L_x = -2.969\ T_1 + 0.5723\ T_2 + 2.397\ T_3$$

$$L_y = -1.053\ T_1 + 3.098\ T_2 - 2.045\ T_3$$

where L_x and L_y are pitch and yaw control torques (ft-lb), respectively, and T_1, T_2, and T_3 are thrusts (pounds) generated by engines 1, 2, and 3,

respectively. Values for the average value of T_1 = 65.8 pounds, T_2 = 62.7 pounds, and T_3 = 67.9 pounds were estimated from the thrust command telemetry signals (FC-25, FC-26, and FC-27). Shortly after retro ignition, differential throttling equivalent to approximately 14.0 ft-lb of control torque were produced.

The maximum thrust vector to center of gravity offset can be estimated using this maximum control torque magnitude of 14 ft-lb. Assuming a 9150-pound retro thrust, the offset was estimated as

$$\text{Maximum center of gravity offset} = \frac{14.0 \text{ ft-lb}}{9150 \text{ pounds}} \times \frac{12 \text{ inch}}{\text{feet}}$$

$$= 0.016 \text{ inch}$$

This compares to the required value of 0.18 inch (Reference 1).

The maximum attitude error produced by the retro disturbance torques was also determined from the maximum torque magnitude of 14 ft-lb. Since the nominal static gain (stiffness) of the pitch and yaw attitude control loops is

$$\text{static gain} = 1200 \text{ ft-lb/deg}$$

the maximum static attitude error is estimated to be

$$\text{maximum static error} = \frac{14}{1200} = 0.012 \text{ degree}$$

which is less than the allowable value of 0.12 degree.

Vernier Engine Thrust Command Modulation

During the retro phase, vernier engines 1 and 2 thrust commands (Figure 5.5-23) were modulated at an indicated 7.0 pounds peak-to-peak amplitude and a frequency of at least 1.5 Hz. The peak-to-peak amplitude of vernier engine 3 (Figure 5.5-23) thrust command was between 2 and 3 pounds peak-to-peak. The thrust command telemetry signals, FC-25 and FC-26, indicated that the commands to engines 1 and 2 were in phase because of signal processing effects. The in-phase condition is not possible because of the attitude control system mixing network which is designed to provide a constant total thrust. In-phase thrust commands imply a varying total thrust. An intensive investigation was undertaken to determine the actual frequency and amplitude of the modulation which is masked by the telemetry signal processing techniques. The results of this investigation are presented in Reference 14. Since there were no abnormal disturbances noted during the midcourse velocity correction (when the attitude control system configuration is identical to that which exists during the retro phase except that the accelerometer is not in the loop), it was considered

possible that either the retro engine or retro/vernier engine combination excited a spacecraft structural mode with amplitudes sufficient to cause a response by the attitude control system or a structural failure occurred to produce the effects observed.

Investigation revealed that the most probable frequency of oscillation was 18.33 cps, with the indicated peak-to-peak thrust command levels of 7 pounds being representative of the actual levels. Since the flight control sensor group and retro engine structural resonance range includes this frequency, it is suspected that either or both structural modes were excited during the retro phase to produce the thrust command modulation. At this frequency, however, the induced loads on the spacecraft are not of sufficient magnitude to normally cause a failure of any structural elements. Additional structural vibration tests are planned on the S-9 test vehicle to provide more information on attitude control system response to structural resonances.

Radar Performance

Operation of the radar system was completely normal up until the time data were lost, as described in Reference 15. Both the range (FC-35) and vertical velocity (FC-41) telemetry signals were saturated at this time, as expected, since the predicted range and velocity were 57,000 feet and 1100 fps, respectively.

All three doppler velocity system beams acquired lunar signals, and RODVS occurred within less than 1 second of the predicted time. The lateral velocities at data loss were approximately V_x (FC-39) = -87 fps and V_y (FC-40) = -20 fps compared to predicted velocities of -109 and -26 fps, respectively. The differences between the predicted and actual lateral velocities imply an average pointing error during retro burn of

$$\text{pointing error} = \frac{\sqrt{\Delta V_x^2 + \Delta V_y^2}}{\Delta V_z} \times 57.3$$

$$\text{pointing error} = \frac{23}{7705} \times 57.3 = 0.17 \text{ degree}$$

where

$\Delta V_x, \Delta V_y$ = difference between actual and predicted, fps

ΔV_z = vertical velocity removed by retro, fps

5.5.5 REFERENCES

1. "Functional Requirements," Hughes Specification 224510, Revision E.

2. K. Kobayashi, "A Method for Determining Gas Jet Thrust Level —
    Post Mission Analysis," Hughes Aircraft Company IDC 2253.4/25,
    1 March 1966.

3. "Surveyor III Flight Performance Final Report," Hughes Aircraft Company,
    SSD 68189-3, July 1967.

4. G. L. Puckett, "SC-4 Flight Control Data Package," Volume II,
    15 July 1967.

5. R. H. Bernard, "Restoration and Updating of Surveyor Coast Phase
    Analog Computer Mechanization," Hughes Aircraft Company
    IDC 2223/77, 29 July 1964.

6. R. H. Bernard, "Revised Gas Jet Fuel Consumption for 66-hour
    Mission," Hughes Aircraft Company IDC 2223/843, 19 February 1965.

7. R. H. Bernard, "Surveyor Sun Acquisition With the Sun Sensor Oriented to
    Include the Roll and Pitch Uses," Hughes Aircraft Company
    IDC 2223/540, 14 December 1964.

8. E. I. Axelband, "Analysis of Inertial Pointing Accuracy of Surveyor
    Midcourse Thrust Vector," Hughes Aircraft Company IDC 2242/2706,
    17 June 1963.

9. H. D. Marbach, "Angular Rates at Midcourse Shutdown," Hughes
    Aircraft Company IDC 2223/731, 3 February 1963.

10. "Interface Document, Surveyor Vernier Propulsion Thrust Chamber
    Assembly," Hughes Specification 287015.

11. "Spacecraft Flight Control Subsystem," Revision E, Hughes
    Specification 234600.

12. "Standard Transit Sequence of Spacecraft Operations," Hughes
    Specification 224550.

13. "Flight Control SPAC Handbook," Hughes Aircraft Company.

14. O. N. Hertzmann, "SC-4 Thrust Command Modulation Study,"
    Hughes Aircraft Company IDC 2223/3055, 25 August 1967.

15. "SC-4 Preliminary Post Flight Data Analyses Report," Hughes
    Aircraft Company, 1 August 1967.

5.5.6 ACKNOWLEDGMENTS

5.6 VERNIER PROPULSION

5.6.1 INTRODUCTION

5.6.1.1 System Description

The Surveyor vernier propulsion system (VPS) (Figure 5.6-1) is a bipropellant, variable thrust, liquid rocket system utilizing an oxidizer composed of 90 percent nitrogen tetroxide and 10 percent nitric oxide (Mon 10) and a fuel composed of 72 percent monomethyl hydrazine and 28 percent water. The VPS consists of three regeneratively-cooled thrust chamber assemblies (TCAs) with radiation-cooled expansion cones. Each TCA has a variable thrust range of from 30 to 104 pounds vacuum thrust.

Propellant is supplied to the TCAs from six tanks employing positive expulsion bladders. One fuel tank and one oxidizer tank supply each TCA and are located adjacent to the TCA near each of the three spacecraft landing legs.

Propellant expulsion is accomplished by pressurizing the propellant tanks on the gas side of the bladders with helium gas. The helium is stored under high pressure in a spherical pressure vessel. The helium tank, together with the pressure regulator, dual check and relief valves, and servicing connections, is mounted outboard of the spaceframe between landing legs 2 and 3.

Thermal control of the VPS is both active and passive. Electric heaters are installed on two oxidizer tanks, one fuel tank, and all propellant feedlines to the TCAs. Passive thermal control consists of the application of black and white paint and vapor-deposited aluminum to selected portions of the VPS, together with super insulation applied to the propellant tanks. The feedlines are wrapped with aluminum foil to deter heat loss.

5.6.1.2 System Purpose

The VPS has three main functions during the mission:

1) Midcourse velocity correction and attitude control

2) Attitude control during retro phase

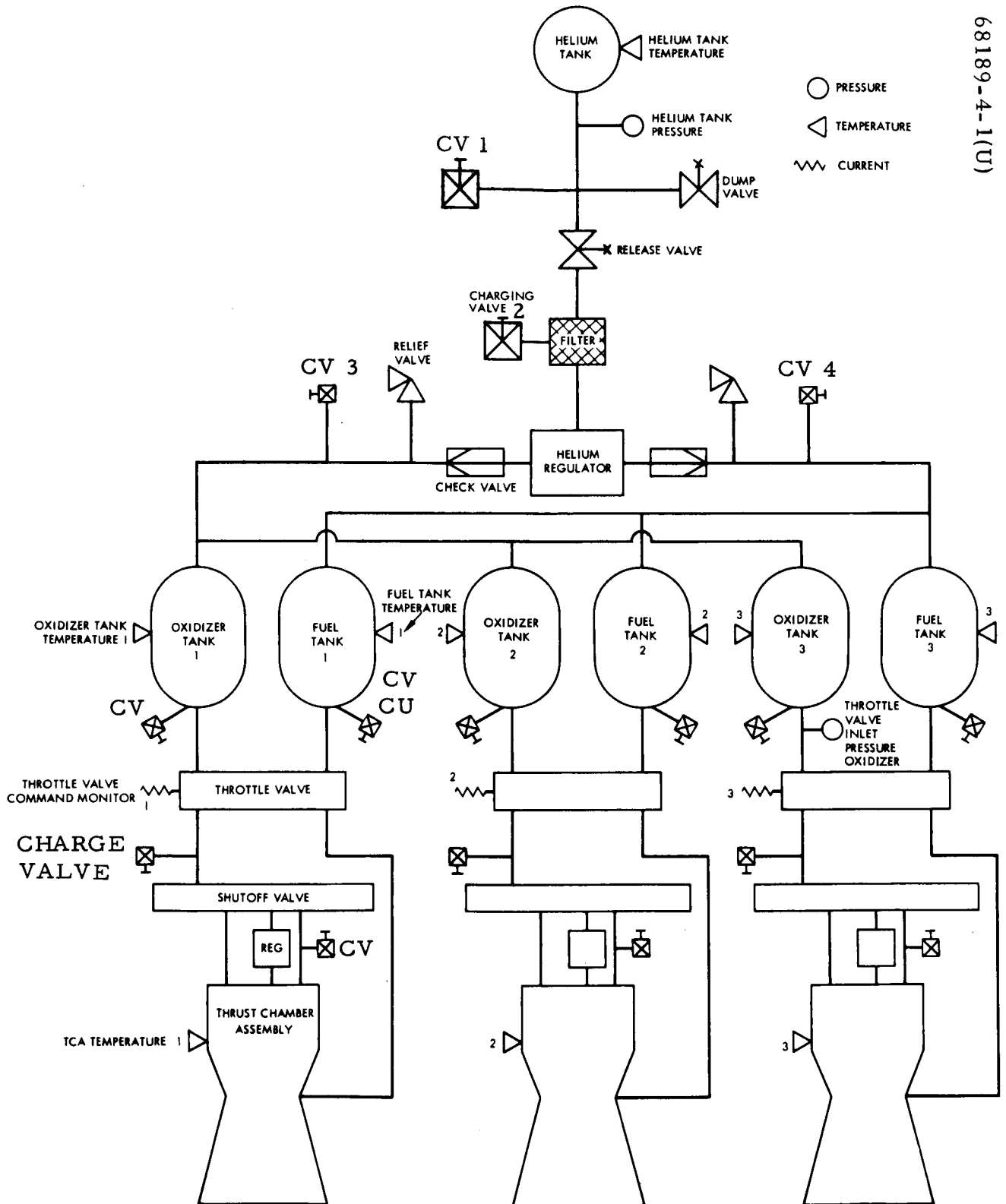3) Attitude control and velocity correction during the final descent maneuver

Figure 5.6-1. Vernier Propulsion System Schematic

The midcourse velocity correction may be required to correct initial launching and injection errors. The VPS provides velocity corrections up to 50 m/sec with sufficient propellant remaining to successfully land the spacecraft on the moon. The required correction is transmitted to the spacecraft in the form of a desired burn time at a constant acceleration of 0.1 g, which results in a thrust level of approximately 75 pounds for each TCA. In addition to providing the required velocity change, the VPS also provides spacecraft attitude control during the maneuver.

Attitude control during firing of the spacecraft retro motor is provided by the VPS. The VPS is ignited approximately 1.1 seconds prior to retro ignition. Attitude control by the VPS is biased around a total vernier thrust level of either 150 or 200 pounds, depending on predictions of spacecraft attitude and velocity at retro burnout. The desired vernier thrust level is transmitted to the spacecraft several minutes prior to initiation of the retro maneuver sequence. Following retro burnout, the vernier thrust level is increased to 280 pounds total thrust to further slow the spacecraft to allow the ejected retro motor case to fall clear.

Following retro motor ejection, the VPS is throttled to approximately 110 pounds total thrust under radar control. When the spacecraft intersects the first descent segment, the VPS, operating in the closed-loop mode with the radar system, acquires the predetermined altitude-velocity profile and keeps the spacecraft on the profile. Each succeeding segment of the profile is acquired in a similar manner. At an altitude of 14 feet, the VPS is shut down, and the spacecraft free falls to the lunar surface.

5.6.2 ANOMALIES

Two anomalies were observed during the earth/lunar transit:

1) A 5-degree temperature rise was indicated by the leg 1 oxidizer temperature sensor during the first coast mode period (see subsection 5.1.2)

2) During the retro burn sequence of terminal descent, a ±3-pound thrust oscillation was observed on vernier engines 1 and 2 thrust commands and strain gauges (see subsections 5.5.2 and 4.3).

All data were lost abruptly at GMT 02:02:41 (retro ignition plus 41 seconds) and not regained. A detailed discussion of this loss of data is presented in Section 4. With the exceptions noted above, all vernier propulsion signals were normal.

5.6.3 SUMMARY AND RECOMMENDATIONS

At the time of data loss, the vernier propulsion system was performing in an essentially nominal manner and could have brought the spacecraft

to a successful lunar landing; consequently, no modifications to system design, instrumentation, or procedures are recommended.

Table 5. 6-1 lists the time of occurrence of the major events concerning or influencing the vernier engine system. A summary of the vernier engine system performance parameters, as determined from postflight analysis, is given in Table 5. 6-2, along with the predicted values.

TABLE 5. 6-1. SURVEYOR IV PROPULSION EVENTS

Event	GMT, day:hr:min:sec	Mission Time, hr:min:sec	Command
Pressurize propellant tanks	197:02:27:25	38:27:39	0605
Engine ignition — midcourse	197:02:30:01	38:37:01	0721
Engine shutdown — midcourse	197:02:30:12	38:37:12	—
Engine ignition — terminal descent	198:02:01:59	62:08:59	—
Data loss	198:02:02:41	62:09:41	—

5. 6. 4   SUBSYSTEM PERFORMANCE ANALYSIS

5. 6. 4. 1   Prelaunch

Final propulsion preparations for the Surveyor IV launch were begun on 22 June when propellant loading of the vernier system was initiated. The desired and actual loadings are given in Table 5. 6-3 and show that the spacecraft was loaded within the specified tolerance in Reference 1.

The helium tank was charged on 5 July to a pressure of 5200 psig at 72°F. Prelaunch telemetry readings of the tank temperature and pressure were taken over a 6-day period. These data indicate a helium leakage rate of 76. 6 std cc/hour, well within the limit of 237 std/cc hour called out in Reference 2.

TABLE 5.6-2. MISSION PARAMETERS — PREDICTED AND ACTUAL

Parameters	Predicted	Actual
VPS midcourse thrust, pounds	229.4***	229.1***
Midcourse shutdown impulse dispersion, lb-sec		
Leg 1	-0.28*	-0.18**
Leg 2	+0.20*	+0.03**
Leg 3	-0.09*	+0.15**
VPS retro phase thrust, pounds	200	198

*From TCA flight acceptance test
**See Section 5.5
***Reference 3

TABLE 5.6-3. ACTUAL VERSUS PREDICTED SURVEYOR IV
PROPELLANT LOADING (POUNDS)

	Predicted at 105°F		Predicted at 70°F		Actual at 70°F	
	Oxidizer	Fuel	Oxidizer	Fuel	Oxidizer	Fuel
Total loaded gross	109.99	75.35	113.59	76.84	115.55	76.73
3 σ loading tolerance	0.75	0.75	0.75	0.75	0.75	0.75
Offload	0	0	3.60	1.49	5.42	1.20
Total loaded net	109.24	74.60	109.24	74.60	109.38	74.78
Unusable at 0°F	1.29	0.86	1.29	0.86	1.29	0.86
Total usable	107.95	73.74	107.95	73.74	108.09	73.92

The spacecraft was initially thermally conditioned to 75°F. Two hours prior to launch, the shroud temperature was increased to 85°F. Table 5.6-4 compares the predicted propulsion temperatures with the actual stabilized

values at launch. Temperature differences are due to thermal gradients within the shroud. All temperatures were within tolerances, and all propulsion parameters appeared normal at launch.

TABLE 5.6-4.   ACTUAL VERSUS PREDICTED TEMPERATURES (°F)

Temperature Sensor	Launch		Midcourse		Terminal Descent	
	Actual	Predicted	Actual	Predicted	Actual	Predicted
P4, leg 2 line	84	85	20	18 - 26	20	18 - 26
P5, leg 2 fuel tank	76	78	38	42	33	35
P6, leg 3 oxygen tank	76	77	45	46	42	40
P7, leg 1 TCA	85	85	50	57	53	57
P8, leg 1 line	84	84	39	31	39	30
P9, leg 3 line	84	85	19	18 - 26	20	18 - 26
P10, leg 2 TCA	85	85	80	76	82	76
P11, leg 3 TCA	85	85	66	60	68	60
P13, leg 1 fuel tank	76	76	57	55	56	53
P14, leg 3 fuel tank	76	76	51	56	51	53
P15, leg 1 oxygen tank	75	75	48	47	42	42
P16, leg 2 oxygen tank	75	75	27	32	19	22.5
P17, helium tank	84	84	76	68	78.5	68

5.6.4.2   Coast Phase I (L + 30 Minutes to L + 37 Hours)

Following launch, an assessment of the propulsion functions was made and all conditions were normal. All temperatures decreased approximately as predicted. The leg 2 line temperature decreased to 19.4°F at L + 1 hour, 50 minutes and the heater started cycling between that temperature and 24.7°F at that time. The initial heater duty cycle was approximately 22 percent, based on thermal data. Another duty cycle calculation was made at L + 7 hours with a resulting duty cycle of 36 percent.

Helium pressure increased from 5170 psia at 71.1°F at L - 1 hour, 40 minutes to 5181 psia at 75.5°F at L + 13 hours. Leakage calculations over this period are not meaningful since the helium is not in thermal equilibrium with the tankage; however, the data indicate no significant leakage. Stabilized

TCA temperatures during coast phase 1 were: leg 1 — 51°F, leg 2 — 84°F, and leg 3 — 65°F. Gyro drift checks conducted during this period caused insignificant TCA temperature changes as compared to the Surveyor I and III flights.

At L + 31 hours, the leg 1 oxidizer tank temperature increased 5 degrees from 49° to 54°F. The sensor is located at the base of the propellant tank and indicates the temperature of the coldest strata of oxidizer rather than the average tank bulk temperature. The cause of the temperature increase is not definitely known, but it is thought that bladder movement associated with relaxation of propellant surface tension forces caused propellant movement. This movement changed the local liquid temperature as seen by the temperature sensor. Subsequent to the temperature rise, the temperature decayed to the previously defined temperature-time profile and followed it until midcourse. The line 3 heater started cycling at L + 32 hours.

5.6.4.3 Midcourse Operations (L + 38 Hours to L + 40 Hours)

Propulsion system status just prior to the midcourse correction was nominal. All temperatures were within the predictability range of the thermal analysis (Table 5.6-4).

The helium release squib was actuated at L + 38 hours, 27 minutes, and the propellant tank pressure increased from 178 to 772 psia (corrected for mode) within 2.5 seconds (Figure 5.6-2). It remained at this pressure until engine ignition at midcourse. The observed helium tank pressure drop was 217 psi (Figure 5.6-3).

Ignition of all three engines was smooth and well controlled. The average corrected commanded thrust levels for TCAs 1, 2, and 3, determined from telemetry, were: 75.3, 73.8, and 80.0 pounds, respectively. These values agree with the predicted levels for each TCA within 3 pounds and within 0.3 pound for the thrust total (Table 5.6-5). The shutdown impulse dispersions are shown in Table 5.6-2.

Helium pressure at vernier ignition was 5175 psia (Figure 5.6-3); following the midcourse maneuver of 10.5 seconds, the helium pressure dropped to 4750 psia and then stabilized at 4826 psia 7 hours after midcourse.

Propellant and helium usage are summarized in Table 5.6-6.

5.6.4.4 Coast Phase II (L + 40 Hours to L + 61 Hours)

Subsequent to post-midcourse stabilization, the helium tank pressure and temperature remained at a constant 4826 psia and 79°F, respectively. Regulator lockup pressure during this period remained constant at 772 psia. All propulsion temperatures remained within specified limits throughout the entire coast phase.
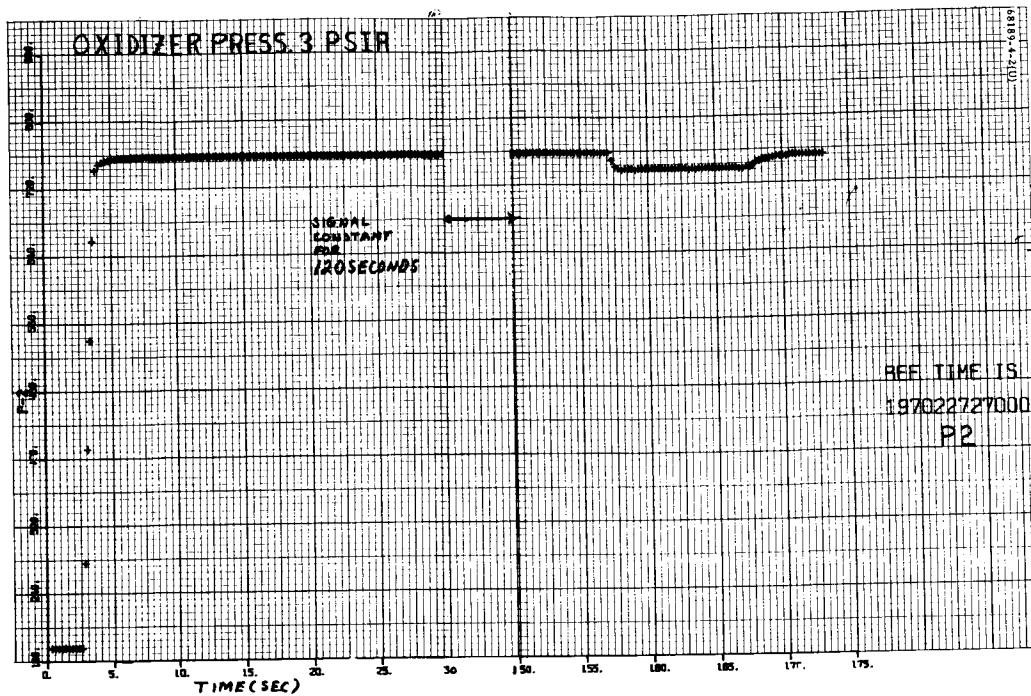
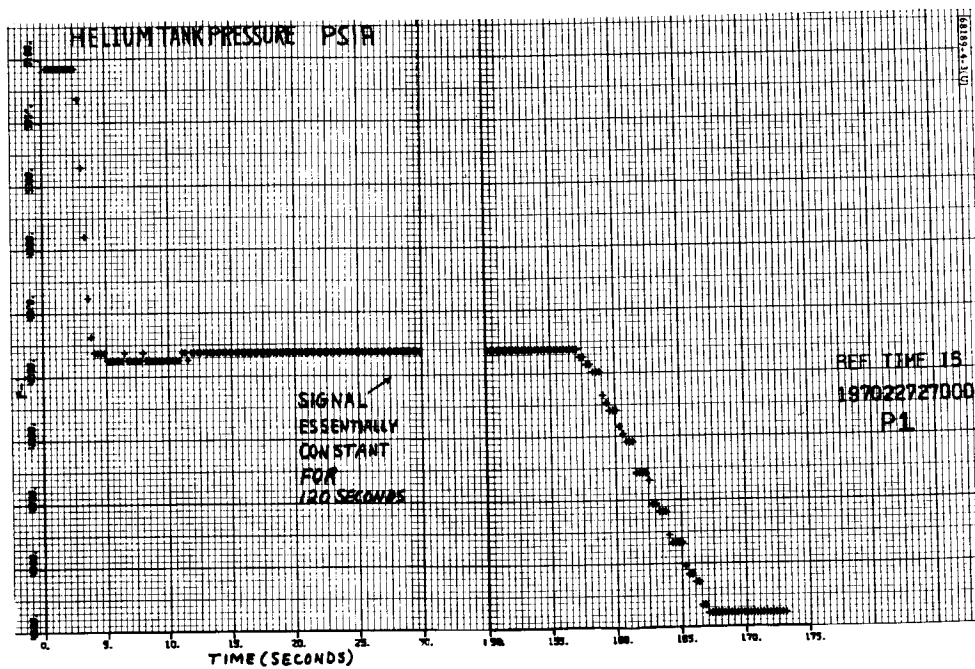Figure 5. 6-2   Oxidizer Pressure During Midcourse

Figure 5. 6-3   Helium Tank Pressure During Midcourse

TABLE 5. 6-5. MIDCOURSE THRUST LEVELS (POUNDS)

Engine Number	Average Thrust Command Last 5 Seconds of Midcourse	Thrust Command Off-Set Before Midcourse	Corrected Average Thrust	Predicted Thrust for Midcourse	Error
1	78. 0	2. 7	75. 3	75. 3	0
2	76. 3	2. 5	73. 8	76. 9	-3. 1
3	81. 6	1. 6	80. 0	77. 2	2. 8
			Total 229. 1	Total 229. 4	Total -0. 3

TABLE 5. 6-6. PROPELLANT AND HELIUM USAGE

Event	Helium, psi		Propellant, pounds		
				Actual	
	Predicted	Actual	Predicted	From Helium Usage	From Thrust Command
Squib release	206	217	0	0	0
Midcourse	215	208	8. 5	8. 2	8. 7
Terminal descent to data loss	711	711	29. 6	29. 6	30. 2

5. 6. 4. 5   Terminal Descent (L + 61 Hours to L + 62 Hours)

Terminal operations were initiated at GMT 198:01:07 (L + 61 hours, 14 minutes) when transmitter filaments were turned on.

The pre-ignition maneuvers were uneventful. Vernier ignition occurred at GMT 198:02:01:59 and retro ignition at GMT 198:02:02:00, as programmed. Helium tank pressure at vernier ignition was 4728 psia. A preterminal descent VPS data summary is shown in Table 5. 6-7. All signals appeared normal during retro burn, with the exception of the leg 1 and leg 2 thrust command, which indicated a ±3 pound oscillation. This modulation was also noted on the corresponding strain gauge signals. Corrected thrust

TABLE 5.6-7. PRETERMINAL DESCENT PROPULSION DATA

Launch +	59H58M	60H28M	61H10M	61H18M
GMT	23H52M	00H22M	01H03M	01H11M
Mode	1	5	6	2
Bit Rate	550	550	550	1100
Parameter				
P_1 helium, psia	4740	4826	4826	4722
P_2 oxidizer, psia	758	772	772	755
P_3 upper retro, °F				65.8
P_4 leg 2 line, °F	19.4	19.4		
P_5 fuel tank 2, °F				32.6
P_6 oxidizer tank 3, °F		42.4		41.5
P_7 TCA 1, °F		52.5	51.6	
P_8 leg 1 line, °F	38.4	38.4		
P_9 leg 3 line, °F	20.8	19.9		
P_{10} TCA 2, °F		82.2	82.2	
P_{11} TCA 3, °F		67.8	67.0	
P_{12} lower retro, °F		44.7		43.8
P_{13} fuel tank 1, °F		56.1		
P_{14} fuel tank 3, °F		51.1		
P_{15} oxidizer tank 1, °F		42.3		
P_{16} oxidizer tank 2, °F		19.3		18.4
P_{17} helium tank, °F		78.2	Mode 4 78.2	
P_{18} strain gage 1, pounds	-62.7		-63.1	
P_{19} strain gage 2, pounds	-43.6		-43.8	
P_{20} strain gage 3, pounds	-39.9		-40.1	

levels are shown in Table 5.6-8. The computed total thrust of 197.7 pounds agrees well with the 200-pound thrust desired.

TABLE 5.6-8. TERMINAL THRUST LEVELS

Engine Number	Average Thrust Command, pounds	Thrust Command Off-set Before Terminal, pounds	Corrected Average Thrust, pounds
1	67.5	+1.8	65.7
2	66.8	+1.3	65.5
3	67.1	+0.6	66.5
			Total 197.7

Helium and oxidizer pressure histories up to the time of data loss are shown in Figures 5.6-4 and 5.6-5.

All data were lost abruptly at GMT 02:02:41 (retro ignition plus 41 seconds), and not regained. With the exception noted above, all propulsion signals appeared normal and offered no insight into the cause of data loss.

5.6.5 REFERENCES

1. R. Laird to Distribution, "A21 and A21A/114 Vernier Propulsion Systems Propellant Inventory," Hughes Aircraft Company, IDC 2227.1/1110, 29 September 1966.

2. G. F. Pasley to Distribution, "Revised Helium Leakage Rates for the Surveyor Vernier System," Hughes Aircraft Company, IDC 2227.1/1331, 31 March 1966.

3. T. B. Shoebotham to L. Gee, "Transmittal of Propulsion SPAC Mission D Report," Hughes Aircraft Company, IDC 2227.1/2108, 27 July 1967.

5.6.6 ACKNOWLEDGMENTS

The following people aided in the preparation of this report:

G. F. Pasley, Coordinator

T. B. Shoebotham
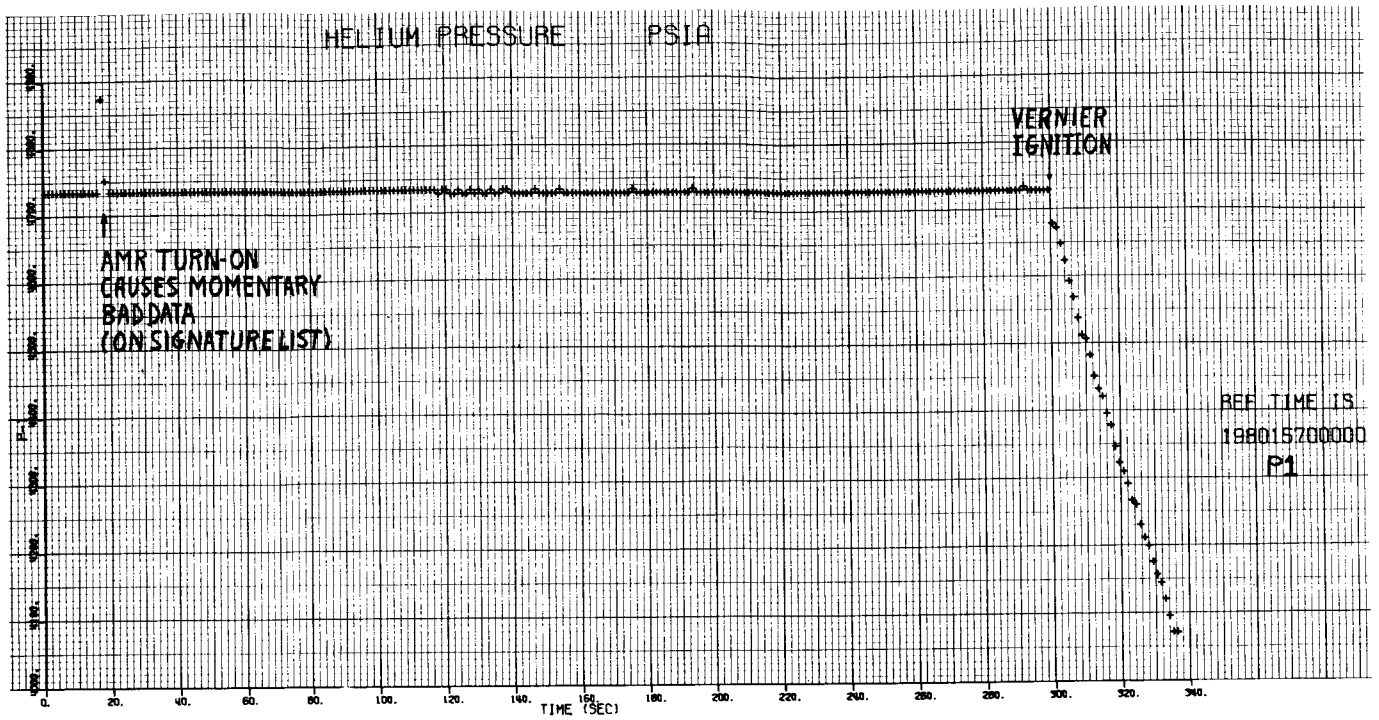
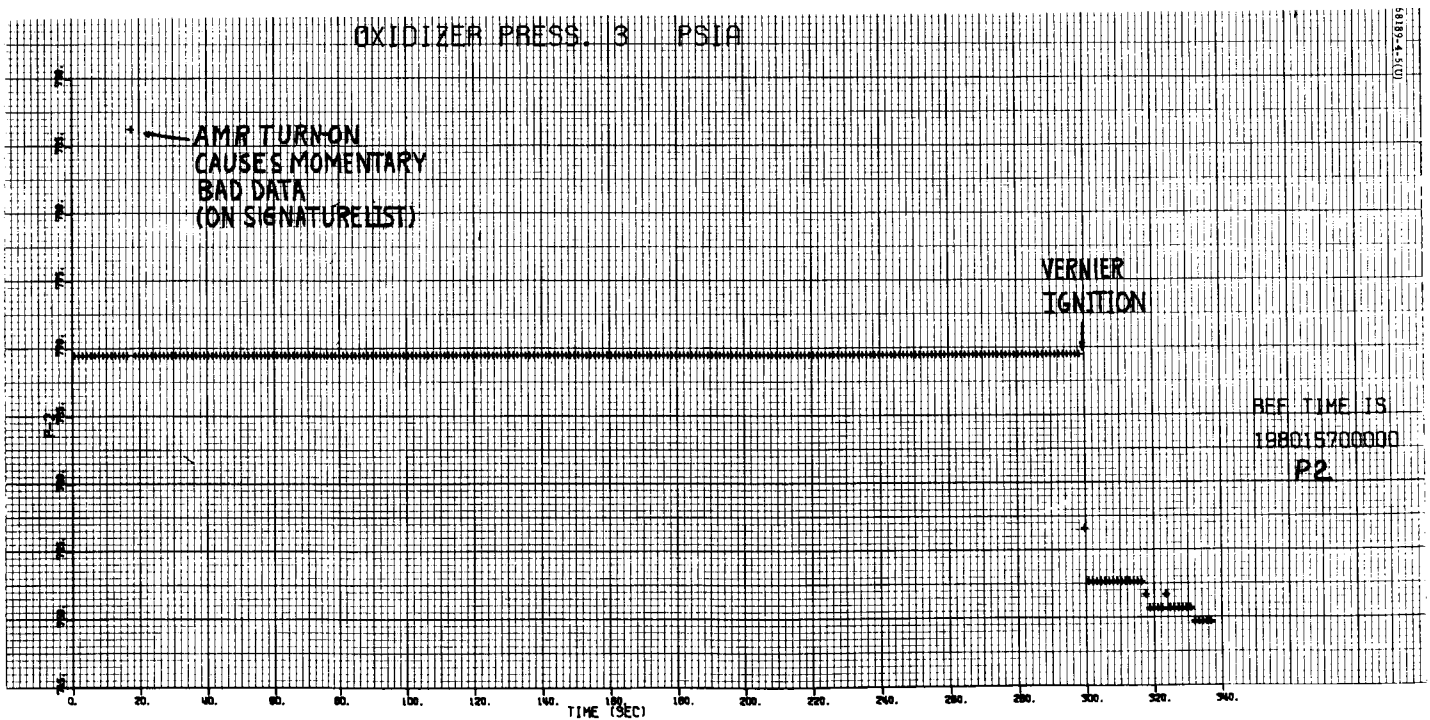Figure 5. 6-4   Helium Tank Pressure During Terminal Descent

Figure 5. 6-5   Oxidizer Pressure During Terminal Descent

5.7 PROPULSION — MAIN RETRO

5.7.1 INTRODUCTION

The main retro-rocket, which performs the major portion of space-craft deceleration during terminal descent, is a spherical solid propellant unit with a partially submerged nozzle.

The unit is attached at three points to the spacecraft near the landing leg hinges, with explosive nut disconnects for postfiring ejection. Friction clips around the main retro-rocket engine nozzle flange provide attachment points for the altitude marking radar. The igniter gas pressure ejects the altitude marking radar when the retro firing sequence is initiated. The main retro-rocket engine ignition squibs and retro release explosive nuts operate from a pulsed, 19-ampere, constant-current source. Commands are initiated by the flight control system.

The nozzle is partially submerged to minimize overall length. It has a graphite throat insert backed up by laminates of carbon cloth phenolic with a fiberglass exit cone lined with bulk carbon phenolic. The case is of high strength steel and is insulated with asbestos and inorganic fiber filled buna-N rubber to maintain the case at a low temperature level during burning.

The main retro-rocket engine with propellant weighs approximately 1445 pounds. The engine utilizes an aluminum, ammonium perchlorate, polyhydrocarbon, case-bonded, composite-type propellant, and conventional grain geometry. The engine thrust may vary between 8000 to 10,000 pounds over a temperature range of 50° to $70^\circ F$.

Two thermal sensors are installed on the main retro-rocket engine case for telemetering engine temperature during transit. One thermal sensor is installed for monitoring the nozzle temperature during transit.

The main retro-rocket engine employs a safe and arm device that has dual firing and single bridgewire squibs for the engine igniter. In addition, provisions for local and remote safe and actuation and remote indication of inadvertent firing of the squibs are included. Both mechanical and electrical isolation exists between squib initiator and pyrogen igniter in the safe condition.
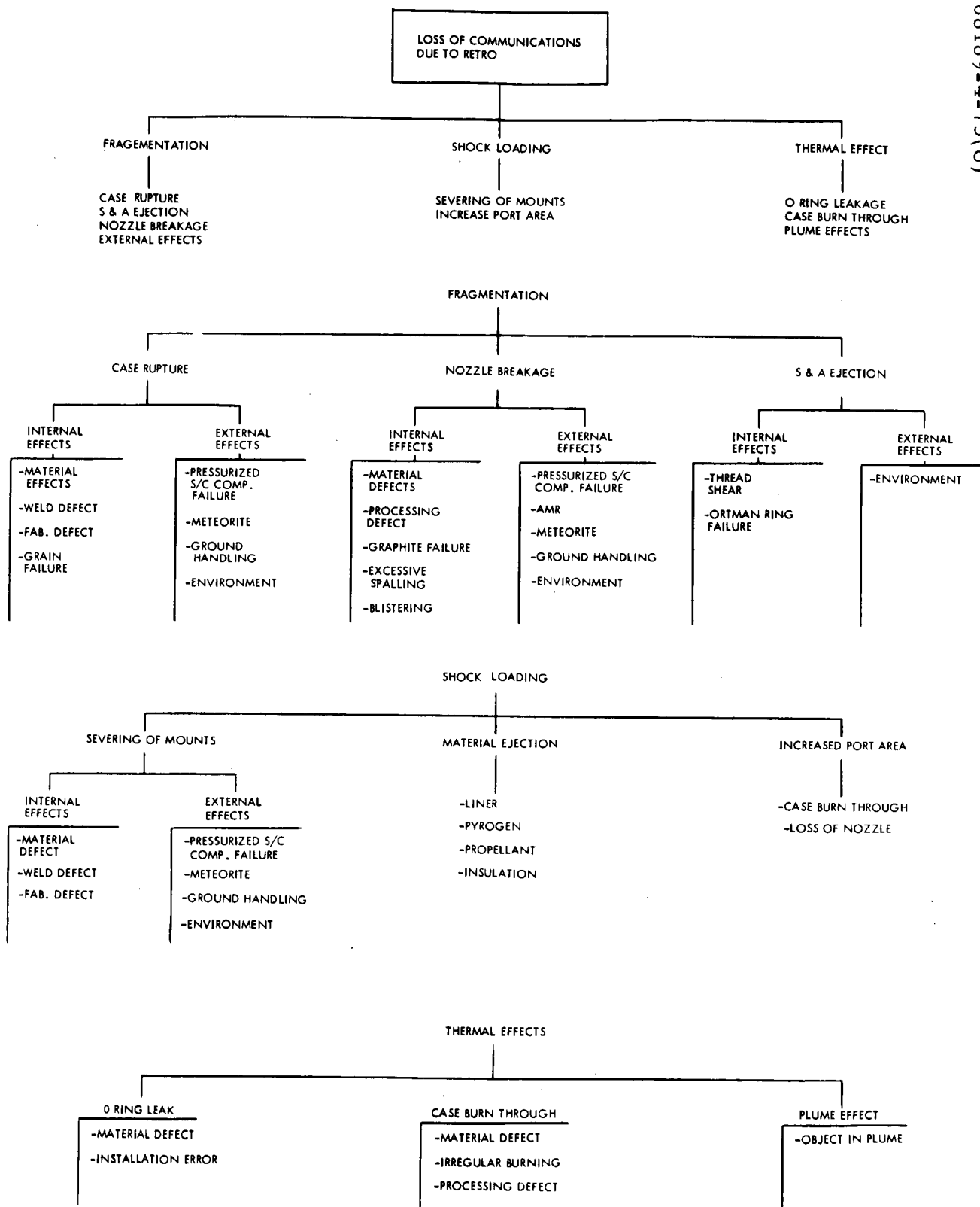
LOSS OF COMMUNICATIONS
DUE TO RETRO

FRAGEMENTATION

CASE RUPTURE
S & A EJECTION
NOZZLE BREAKAGE
EXTERNAL EFFECTS

SHOCK LOADING

SEVERING OF MOUNTS
INCREASE PORT AREA

THERMAL EFFECT

O RING LEAKAGE
CASE BURN THROUGH
PLUME EFFECTS

FRAGMENTATION

CASE RUPTURE

INTERNAL EFFECTS

-MATERIAL EFFECTS

-WELD DEFECT

-FAB. DEFECT

-GRAIN FAILURE

EXTERNAL EFFECTS

-PRESSURIZED S/C COMP. FAILURE

-METEORITE

-GROUND HANDLING

-ENVIRONMENT

NOZZLE BREAKAGE

INTERNAL EFFECTS

-MATERIAL DEFECTS

-PROCESSING DEFECT

-GRAPHITE FAILURE

-EXCESSIVE SPALLING

-BLISTERING

EXTERNAL EFFECTS

-PRESSURIZED S/C COMP. FAILURE

-AMR

-METEORITE

-GROUND HANDLING

-ENVIRONMENT

S & A EJECTION

INTERNAL EFFECTS

-THREAD SHEAR

-ORTMAN RING FAILURE

EXTERNAL EFFECTS

-ENVIRONMENT

SHOCK LOADING

SEVERING OF MOUNTS

INTERNAL EFFECTS

-MATERIAL DEFECT

-WELD DEFECT

-FAB. DEFECT

EXTERNAL EFFECTS

-PRESSURIZED S/C COMP. FAILURE

-METEORITE

-GROUND HANDLING

-ENVIRONMENT

MATERIAL EJECTION

-LINER

-PYROGEN

-PROPELLANT

-INSULATION

INCREASED PORT AREA

-CASE BURN THROUGH

-LOSS OF NOZZLE

THERMAL EFFECTS

O RING LEAK

-MATERIAL DEFECT

-INSTALLATION ERROR

CASE BURN THROUGH

-MATERIAL DEFECT

-IRREGULAR BURNING

-PROCESSING DEFECT

PLUME EFFECT

-OBJECT IN PLUME

Figure 5.7-1. Retro Failure Tree

5.7.2 ANOMALIES

No anomalies were noted in the main retro subsystem up to the time of data loss.

5.7.3 SUMMARY AND RECOMMENDATIONS

Immediately upon the failure of Surveyor IV a Propulsion Analysis Group was formed and a detailed investigation was launched in the retro engine area. All flight data were carefully screened, and the history of the retro engine was reviewed. Table 5.7-1 presents a summary of the pertinent main retro performance parameters. The history included the development, qualification, and flight program. The records associated with the Surveyor IV retro engine, A22-9, and engines A22-8 (Surveyor III retro) and A22-10 (lot acceptance test) were all reviewed since they were processed during the same period of time. All Material Review Board reports, trouble and failure reports, quality assurance records, and X-rays (see Table 5.7-2) were re-examined. It should be noted that the X-ray technique located separations prior to fabrication of A22-9 (Surveyor IV retro) and that the retros made in the same period of time, A22-8 (Surveyor III retro) and A22-10 (static test), performed satisfactorily after passing the X-ray examination. A detailed failure analysis tree was generated for all possible retro engine failure modes (Figure 5.7-1). This investigation concluded that a very low probability existed that the retro engine failed.

The Propulsion Analysis Group recommended the following action be taken to give greater confidence for future successful flights:

1) Conduct a test program to confirm the adequacy of current techniques for reading X-rays of the retro engine. (This effort has been conducted.)

2) Investigate alternate techniques for determining if the propellant/liner/insulation/case bond is satisfactory. (This effort has been conducted.)

3) Increase in-flight instrumentation

a) Add more thermocouples on retro engine with readout during engine firing (under investigation).

b) Investigate use of subcarrier oscillator to give continuous reading of spacecraft acceleration (under investigation).

c) Add a strain gauge to the retro engine case to measure chamber pressure (under investigation).

TABLE 5.7-2.   SUMMARY OF A-22 RETRO X-RAY RESULTS USING
IMPROVED TECHNIQUES

Retro Designation	X-ray and Firing Results
A22-5	Rejected because X-ray at AFETR showed a headend separation between insulation and case.
A22-6	Passed Thiokol X-ray and static fired successfully.
A22-7	Rejected because visual examination at Thiokol indicated poor bond between liner and insulation. Mechanical inspection showed that poor bonding existed throughout the motor.
A22-8	Passed X-ray at AFETR and fired successfully on Surveyor III.
A22-9	Passed X-ray at AFETR and fired on Surveyor IV.
A22-10	Passed X-ray at Allegheny Ballistics Laboratory (same as AFETR equipment) and successfully static fired at Thiokol.
A22-11	Questionable (ABL) X-ray at 20°F.
A22-12	Questionable shadow at ambient temperature in one view of AFETR X-ray.

5.7.4.1   Thrust Versus Time

The technique used in the reconstruction of the thrust versus time trace from both accelerometer and doppler data is discussed in subsection 5.15.6.2 of Reference 1.   This reconstructed trace varies from the predicted trace, as shown in Figure 5.7-2.   The maximum difference is 4 percent, and it occurs 6 seconds after ignition.   This agreement is very comparable to Surveyors I and III.

5.7.4.2   Specific Impulse

The main retro-rocket engine specific impulse was obtained by correcting the predicted nominal specific impulse used in the preflight descent trajectory computer program by the change in velocity measured during retro burning on Surveyor IV up to the time of data loss.   The difference between the actual and predicted change in velocities, 7705 and 7746, respectively, amounts to 0.53 percent low versus the 1 percent

TABLE 5.7-3. MAJOR EVENT TIMES FOR
RETRO OPERATION, DAY 198

Event	GMT, hr:min:sec	Maximum Error, second
Vernier ignition	01:58.810	±0.025
Retro ignition	01:59.925	±0.05
Time of data loss	02:41.018	+0.05, -0.06
Predicted 3500-pound thrust level	02:42.689	—

allowed. This approach is conservative from the retro-rocket engine point of view since the velocity difference is actually due to a number of sources in addition to the main retro-rocket engine. Some of these other sources are as follows:

1) Uncertainty in vernier engine specific impulse

2) Uncertainty in vernier engine thrust level

3) Uncertainty in vernier engine weight versus time

4) Uncertainty in retro-rocket engine specific impulse versus time

5) Uncertainty in retro-rocket engine weight versus time

6) Uncertainty in doppler data

The average value of retro specific impulse obtained by this method was 288.0 seconds, which compares within the allowable tolerance with the predicted value of 289.5 seconds.

5.7.5 REFERENCES

1. "Surveyor I Flight Performance Final Report," Volume III, Hughes Aircraft Company, SSD 68189R, October 1966.

Other

"Surveyor Spacecraft A21 Model Description," Hughes Aircraft Company, Document No. 224847B, 1 March 1965.

"Surveyor Main Retro Engine A22-8 Support Documentation," Thiokol Chemical Corporation.

"Surveyor III Flight Performance Report (Preliminary)," Hughes Aircraft Company, SSD 78079, May 1967.

"Surveyor IV Propulsion Analysis Group Report," Hughes Aircraft Company, SSD 78132R-1, August 4, 1967.

5.7.6 ACKNOWLEDGMENTS

5.8 ALTITUDE MARKING RADAR

5.8.1 INTRODUCTION

The Surveyor altitude marking radar (AMR) is a small, conventional, pulsed, X-band, fixed dual-range gate, marking radar designed and supplied by Hughes Division 27. The purpose of the AMR is to provide, with high accuracy and reliability, a positive indication that slant range from the Surveyor spacecraft to the lunar surface has decreased through a preset value, nominally 60 statute miles for the A-21 series of engineering models. This signal starts an on-board timer, whose run-out time is set by ground command earlier in flight to initiate vernier and main retro engine ignition. Since the AMR is installed in the exhaust cone of the main retro engine and has served its purpose in providing ignition timing, it is forcibly jettisoned from the spacecraft when that engine is ignited.

The AMR is a conventional noncoherent radar, employing a pulsed magnetron, single antenna, duplexed mixer, crystal-controlled, solid-state local oscillator, wideband IF amplifier, noncoherent detector, and video processing circuitry. Dynamic range is extended by automatic gain control (AGC) of the IF amplifier; AGC voltage is telemetered and provides an indication of received signal power. The video circuitry is of special design to mark at a preset range with high accuracy and reliability. Two fixed, adjacent range gates continuously examine the video signal. Their outputs are continuously summed and differenced. When the sum exceeds a fixed threshold and the difference simultaneously crosses zero with positive slope, the mark signal is generated. Sum threshold is set for an extremely low probability of marking on noise (false mark) throughout the operating time, while video integration plus a very substantial radar gain margin ensure a high probability of marking successfully.

Two separate ground commands, whose timing is controlled, are required to fully activate the AMR. The first signal, called simply AMR on, commands on the primary power to the AMR, which includes all internal power except high voltage to the transmitter. The video signal is inhibited from reaching the marking circuits until the second command, thus eliminating any residual probability of false marking on noise during this warmup interval. The second signal, called AMR enable, commands on the transmitter high voltage and also removes the video inhibit. This enabling function is timed not only for favorable thermal conditions at the expected marking time but also to preclude premature marking on second-round echoes at

much longer ranges. In a lunar mission, FPAC supplies a marking time prediction based upon trajectory data. The prescribed times for SPAC transmission of these two commands are "on" at 280 ± 10 seconds, and "enable" at 100 ± 10 seconds before predicted marks.

For proper analysis, complete trajectory information is required. While either known or assumed for preflight predictions, it must be known or derived for postflight evaluation. Spacecraft attitude and velocity data are supplied by FPAC from tracking and trajectory computations. Residual range uncertainty, however, exceeds that of the AMR itself, which is assumed to have marked with mean value and dispersion predicted by radar analysis prior to each mission. In conjunction with approach velocity and attitude conditions from FPAC, the trajectory can then be extrapolated backward with high accuracy by a special two-body program. This program derives all the significant AMR parameters throughout the nominally 100-second interval from enable to mark, and calculates correction factors to be applied to observed telemetry data before comparison with predicted received signal power.

AMR telemetry includes three digital and three analog signals, plus analog temperature data. The digital signals confirm on-board discrete events: prime power application (R-1, AMR on), high voltage and video enabling (R-11, AMR enable), and slant range trigger (FC-64, AMR mark). It should be noted that FC-64 is telemetered only when the on-board mark is generated, and not in response to the backup command from earth. The three analog signals (besides temperature) are magnetron current (R-12), AGC voltage level (R-14), and late gate detected video voltage level (R-29). The AGC not only confirms receiver response to RF return, but is also useful in evaluating terrain reflectivity. The magnetron current confirms pulsing of the magnetron after enable, and is useful primarily as a transmitter failure mode indication. The late gate signal, primarily a receiver failure mode indication, normally confirms presence of gated video signal rising quickly to a peak at the time of mark and decaying quickly thereafter. All but a few of its values are normally at the quiescent noise level, and in no way constitute repeated events.

5.8.2 ANOMALIES

The only instance of unanticipated AMR behavior concerned the AMR AGC quiescent level (before enable) which was somewhat higher than in preflight testing. There was, however, no apparent correlation with events and no apparent effect on the mission. It rose from the quiescent level before the mark, and appeared about normal at mark (refer to TFR 29462).

5.8.3 SUMMARY AND RECOMMENDATIONS

The Surveyor IV AMR functioned normally. The AMR magnetron current was properly off until enable, then jumped properly to on, but at a slightly lower than test level. The true altitude mark was generated at the

expected time and initiated the automatic terminal descent sequence as planned. Routine emergency mark backup command transmission was received after the on-board mark had been generated. AGC indicated signal strength within 2 to 3 db of predicted value throughout the operating time (Figure 5.8-1); while a little weaker than expected, these values are within normal tolerances and may actually indicate weaker than nominal terrain. The late gate signal was normal, confirming the presence of RF return signal and detected video within the gate at the proper time relative to the mark.

As described below, significant pulse-stretching of the return signal occurs; it also varies widely during the AGC observation interval. Calibration has shown the AGC to be only roughly proportional to pulse energy. While wholly satisfactory for functional operation, the nonlinearity involved requires separate treatment of peak power and of stretched pulse length for proper AGC interpretation. For this reason, additional preflight calibration at longer pulse lengths, predicted for Surveyor IV, has been recommended for all remaining missions.

Continued use of the AMR on future spacecraft is required for reliable terminal descent initiation. The backup command may be retained for residual reliability as long as its timing continues to be tightly controlled.

5.8.4   AMR SUBSYSTEM PERFORMANCE ANALYSIS

5.8.4.1   Event Timing

From Table 5.9-1, Surveyor IV radar event times, the following can be determined: The warmup time (on to enable) was 180.0 ± 1.2 seconds, well within the nominal 180 ± 10 seconds. The enabled time was 99.1 ± 0.60 seconds, also within the nominal 100 ± 10 seconds.

The AMR mark was received on day 198 at 2 hours 1 minute 56.080 ± 0.005 seconds. The mark was determined from telemetry and magnitude register extrapolation. Table 5.8-1 demonstrates that the backup command arrived after the AMR mark had been produced, although it was uncomfortably close (0.27-second difference). The time from FC-64 to FC-28 (vernier ignition) was the commanded and stored 2.7 seconds, also indicating that the onboard clock (magnitude register) was started by the true mark, not by the backup command.

5.8.4.2   Late Gate Signal

Concerning the trajectory reconstruction for AGC evaluation, the total stretched pulse length as received was about 20.8 microseconds and the effective closing rate was 8597 fps, both at the time of mark. The corresponding video pulse closing rate was therefore about 17.5 microseconds per second. The nominal video late gate is 20 microseconds (20 ± 1, required). It should therefore have produced output within 3 db of peak for (20.8 + 20.0)/17.5 = 2.33 seconds, ensuring that one of the samples at 1.2-second (mode 6)
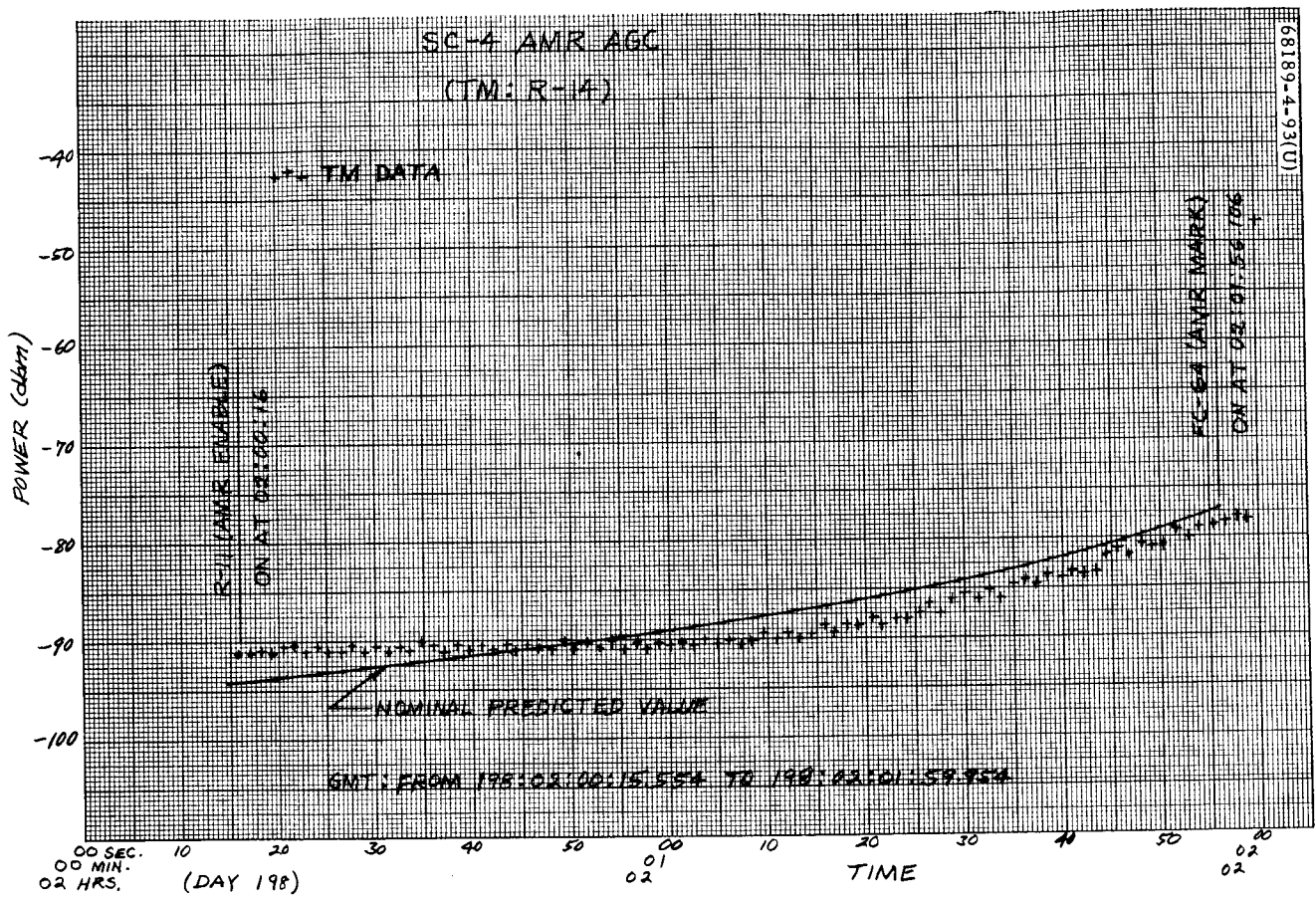
Figure 5.8-1.   Surveyor IV AMR AGC

TABLE 5.8-1.   VERIFICATION OF AMR MARK, DELAY, AND
VERNIER IGNITION FROM TELEMETRY

All times given are in seconds after 198:02:01

AMR Mark

Mark time (from DSIF-14 telemetry)	56.075 to 56.175
Magnitude register = 37	56.985
Extrapolate register back to initial setting (55)	56.035 to 56.085
Most probable AMR mark time (intersection of above events)	56.080 ± 0.005

AMR Backup Command

Command sent, DSIF-14	53.91
Command at spacecraft	55.13
Effect of command received by DSIF-14 (comparable with above mark time)	56.35
Message enable from command (telemetry)	56.59 ± 0.60
Margin, time from actual mark to command	0.27 ± 0.02
Predicted mark time at DSIF-14	55.21
Margin if prediction was correct	1.14

Vernier Ignition

FC-28 (from DSIF-14 telemetry)	58.775 to 58.875
Magnitude register = 13	58.185
Extrapolate to 0	58.785 to 58.835
Most probable vernier ignition time	58.810 ± 0.025

Ignition Delay

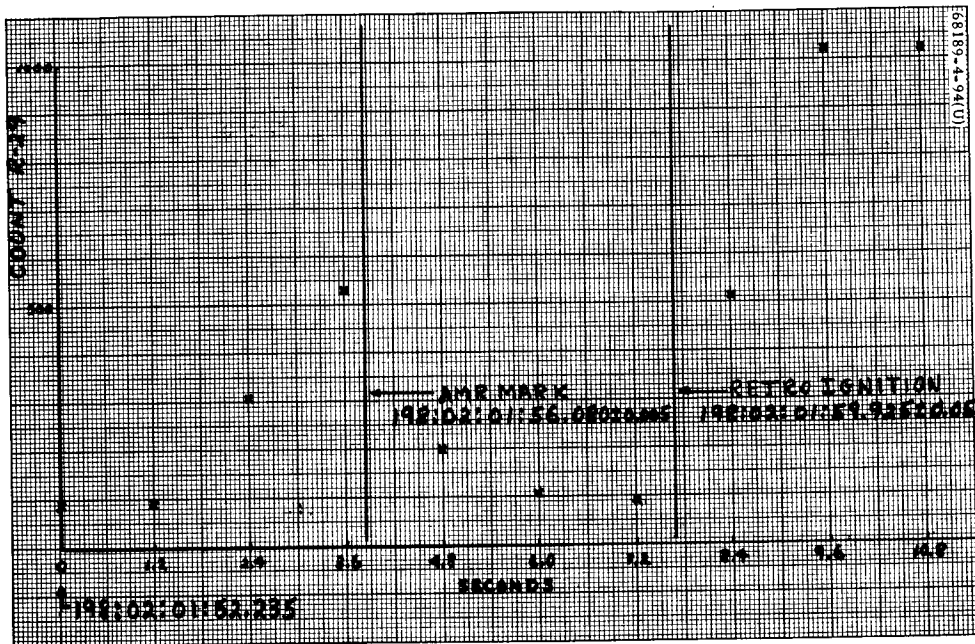|	
Actual delay	2.73 ± 0.03
Intended delay	2.725 ± 0.025

Figure 5.8-2. Surveyor III AMR Late Gate R-29

intervals of telemetry channel R-29 should be close to peak amplitude. In Surveyor IV, this sample occurred on day 198 at 2 hours 1 minute 55.835 seconds or within 0.25 second of the mark, with one partial amplitude sample on each side, as is proper. This confirms presence of proper radar return at the mark. Figure 5.8-2 shows this channel for Surveyor IV. (All AMR channels go full scale at engine ignition.)

5.8.4.3 AMR AGC Evaluation

Because of the significant distance traveled during the nominal 100 seconds from enable to mark, the AMR slant range (Figure 5.8-3), the pulse length of the received signal (Figure 5.8-4), and the calibration for pulse length (Figure 5.8-5) all vary significantly. The received pulse stretching effect varies as a function of slant range. The incidence angle is remarkably constant. References 1 and 2 outline techniques used to evaluate accurately the parameters presented in Figures 5.8-3 and 5.8-4.

5.8.4.4 Evidence Showing Failure Was Not Due to Lunar Impact

1) Orbit Determination

Predicted AMR mark time agreed with actual AMR mark time within 0.87 second. Uncertainty in OD timing is 0.8 second (1 σ). OD timing would have had to be 6.6 seconds (8 σ) off to result in premature impact at the time of the data loss.

2) AMR Performance

AMR late gate confirmed presence of the signal at the time of the mark and appeared normal in its behavior. AMR mark did occur, as confirmed by telemetry signal FC-64, which is generated only by the true mark (not by the backup). The mark was caused by a signal in the gate. The AMR is a fixed gate system. The delay from the main bang to the gate would have had to shift over 100 microseconds to cause the mark to be generated late.

3) RADVS Received Signal Strength

Received signal strength in all three beams that locked was within 3 to 4 db of the expected strength for the nominal altitude (and was weaker than nominal, not stronger). Had the altitude been lower, such that impact occurred at the time of data loss, the signal strengths on the beams should have been 60 db higher than indicated.

4) Altimeter Lockon

The altimeter beam did not lock on, and it should not have locked on as the return frequency was still too high. Had the altitude been lower, the altimeter beam would have acquired.
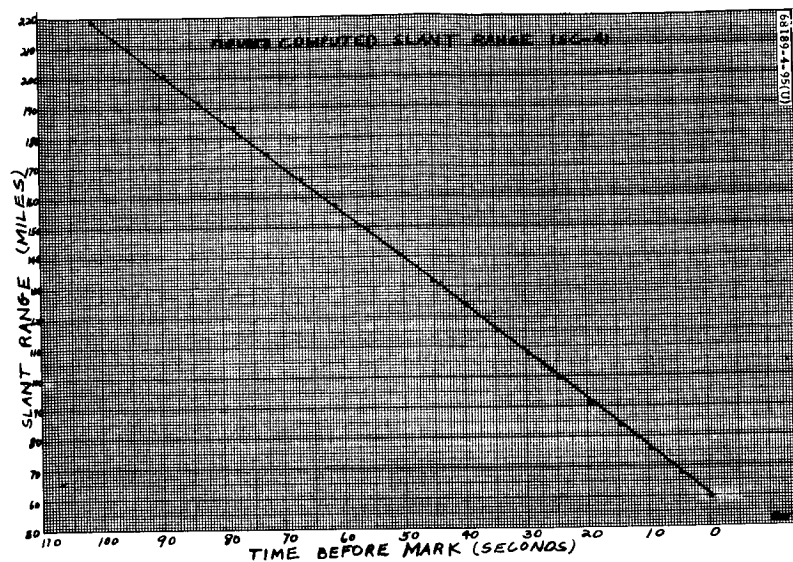
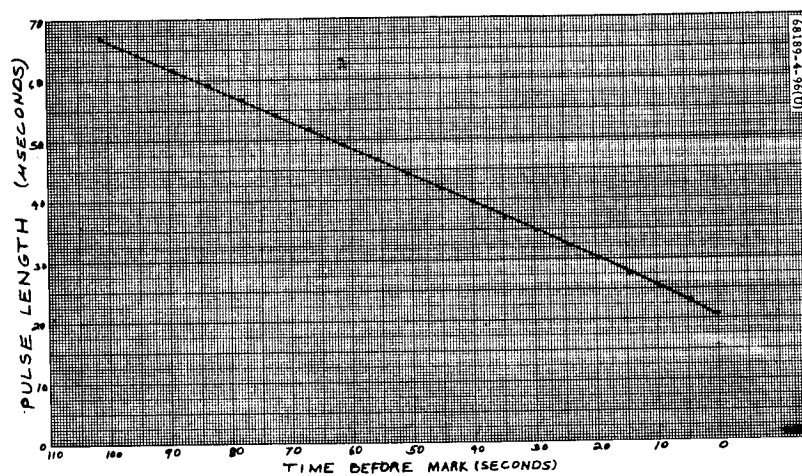Figure 5.8-3.   Surveyor IV Computed Slant Range

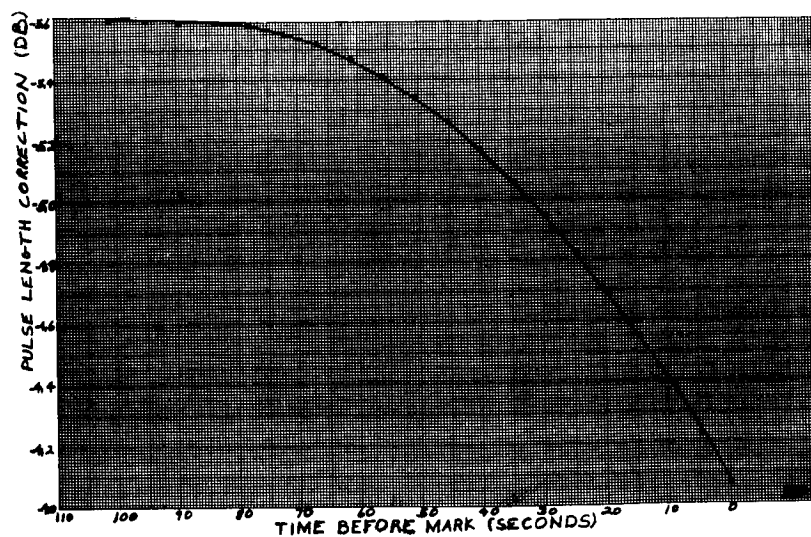Figure 5.8-4.   Surveyor Pulse Length of Received Signal

Figure 5.8-5.   Calibration Correction for Pulse Length

5) Conclusion

Lunar impact was not the cause of spacecraft signal loss. Independent items that would have had to be simultaneously wrong in order for premature impact to have occurred are as follows:

a) OD timing 6.6 seconds off (over 8 σ error).

b) AMR failed to mark at proper range ($< 10^{-4}$ probability).

c) AMR incorrect mark at a time correlated with the incorrect OD time ($< 10^{-6}$ probability).

d) Failure of altimeter beam to acquire (despite its normal sweep pattern and operable receiver).

e) Lunar reflectivity weaker than expected by a varying amount increasing up to 60 db at time of impact and varying in a very special way so as to match the predicted slope (amplitude versus time).

5.8.4.5 <u>DB Budget</u>

Recalling that the peak instantaneous received power is (Reference 2):

$$Pr\,(max) = \frac{P_t \lambda^2 G^2 L_F}{(4\pi)^3 R^4}\,\sigma(\theta)\,A_P$$

But

$$A_P = (\beta_1 R)\left(\frac{c\,\tau}{2}\cot\theta\right)$$

and

$$P_t = \frac{P_{AV}}{\tau f_r}$$

so that

$$Pr\,(max) = \left(\frac{1}{2}\right)\left(\frac{c}{4\pi}\right)^3 \left(\frac{P_{AV}G^2 L_F}{f^2 f_r R^3}\right)(\beta_1 \cot\theta)\,\sigma(\theta) \qquad (1)$$

where

$$c = f\lambda$$

$$P_t = \text{transmitted power peak}$$

$$P_{AV} = \text{average transmitted power}$$

$$\lambda = \text{wavelength}$$

$$f = \text{frequency}$$

$$G = \text{peak gain (one-way)}$$

$$R = \text{slant range along beam axis}$$

$$L_F = \text{loss factor (drifts)}$$

$$\theta = \text{incidence angle}$$

$$\sigma(\theta) = \text{effective radar cross section per unit projected area}$$

$$f_r = \text{repetition rate}$$

$$\beta_1 = \text{equivalent beamwidth}$$

The Surveyor IV AMR db budget at a slant range of 59.96 miles and an incidence angle of 31.8 degrees is given in Table 5.8-2.

5.8.5 REFERENCES

1) "Surveyor III Flight Performance Final Report," Hughes Aircraft Company, SSD 68189-3, July 1967.

2) R. A. Dibos, "AMR AGC Post-Mission Evaluation," Hughes IDC 2253.4/88, 27 June 1967.

5.8.6 ACKNOWLEDGMENTS

This section was compiled by W. McIntyre and R. H. Leuschner primarily from material generated by R. A. Dibos and M. R. Weiner.

TABLE 5.8-2. DB BUDGET AT 59.96 MILES

P_t (average)	+ 33.42 dbm
G^2	+ 69.0 db
β_1	- 13.57 db
nK_1	- 1.17 db
R^{-3}	- 53.33 db
f^{-2}	-199.37 db
f_r^{-1}	- 25.52 db
$1/2 \left(\dfrac{c}{4\pi}\right)^3$	+122.12 db
cotan (31.8 degrees)	2.08 db
F (31.8 degrees)	- 10.92 db
	+226.62
	-303.88
P_r dbm	- 77.26 dbm
P_{min} (10 microseconds)	- 97.2 dbm (worst case)
P_{min} (10 microseconds)	-103.7 dbm (measured)
P_{min} (30 microseconds)	-101.5 dbm (worst case)
P_{min} (30 microseconds)	-105.7 dbm (measured)
P_{min} (20.8 microseconds)	-100.6 dbm (worst case)
P_{min} (20.8 microseconds)	-104.8 dbm (predicted)
DB margin	+ 27.5 db

5.9 RADVS PERFORMANCE

5.9.1 INTRODUCTION

The radar altimeter and doppler velocity sensor (RADVS) is a coherent CW microwave radar designed and supplied by Ryan Electronics, San Diego. Its primary function is to measure velocity and slant range relative to the lunar surface during the terminal descent of the Surveyor spacecraft. These quantities are measured directly in spacecraft coordinates, allowing direct utilization by the spacecraft flight control system for both attitude steering and deceleration thrust control.

The doppler velocity sensor (DVS) portion of the system is essentially a three-beam coherent CW autodyne doppler radar. A single klystron (two-cavity type) provides undeviated output at a nominal frequency of 13,300 MHz. Its output is divided equally among the transmitting horns for beams 1, 2, and 3. Each beam has a separate receiving horn, with adequate RF isolation against direct leakage, and a separate and independent receiver utilizing a small sample of the transmitted signal as a local oscillator (bias). Associated with each receiver is a separate and independent frequency tracker capable of acquiring and tracking the doppler signal corresponding to that component of velocity associated with the spacecraft orientation of that particular beam. The spacecraft beam orientations are such that the nominal velocity components V_i (i = 1, 2, 3) along the axes of these three beams are determined by the spacecraft coordinate components of velocity according to the matrix multiplication:

$$\begin{pmatrix} V_1 \\ V_2 \\ V_3 \end{pmatrix} = \begin{pmatrix} +A & +A & +B \\ -A & +A & +B \\ -A & -A & +B \end{pmatrix} \begin{pmatrix} V_x \\ V_y \\ V_z \end{pmatrix}$$

where

$A = \sin 45 \text{ degrees} \sin 25 \text{ degrees} = 0.29884$

$B = \cos 25 \text{ degrees} \qquad\qquad = 0.90631$

and the spacecraft coordinates are a Cartesian right-handed triad with +z along the roll axis in the normally descending direction.

The frequency outputs of these three frequency trackers are properly scaled and summed in three converters whose outputs are analog voltages representing the spacecraft velocity components:

$$V_x = \frac{V_1 - V_2}{2A} \; ; \quad V_y = \frac{V_2 - V_3}{2A} \; ; \quad V_z = \frac{V_1 + V_3}{2B}$$

The radar altimeter (RA) portion of the system is basically a single-beam coherent FM-CW microwave radar altimeter. Beam 4, fixed along the spacecraft +Z axis, also contains separate transmit and receive horns, a fourth receiver, and a fourth frequency tracker. The same kind of transmitter-derived local oscillator (bias) signal configuration is used, but the RA uses a reflex klystron whose frequency is sawtooth deviated in standard FM-altimeter fashion. The operating portion of the sawtooth has negative slope (with time) to avoid any range-velocity ambiguities. The beam 4 receiver and frequency tracker therefore operate at a frequency which is the sum of scaled slant range and scaled doppler velocity inevitably appearing along that beam. The RA converter corrects the frequency output of the beam 4 tracker by a properly scaled term (V_z compensation), obtained from the DVS V_z converter, to provide an analog output voltage proportional to R_z, the slant range along the spacecraft +Z axis. (The nominal RA operating frequency is 12,900 MHz. Deviation is nominally 40 MHz at 800 MHz/sec below 1000 feet, and 4 MHz at 800 MHz/sec above 1000 feet.)

Each receiver is actually two parallel receiving channels, each with separate microwave mixers and audio preamplifiers. Microwave mixer signal and bias inputs are phased so that the parallel audio channels are essentially in phase quadrature, and with equal amplitudes, for all normal doppler signals. Each frequency tracker uses these quadrature audio signals to single-sideband modulate an internal reference signal held at 600 kHz, thus reproducing doppler frequencies unambiguously. In Surveyor, this serves primarily to reject negative velocity at tracker IF, thereby preserving the sense of the velocities. (In a more general application, this would permit measuring negative and positive beam velocities including the unwanted radar return from the main retro engine after separation from the spacecraft.) Each frequency tracking loop is closed by a voltage controlled oscillator whose frequency is controlled by a discriminator-integrator combination, whose output is a direct measure of the frequency being tracked.

To preserve the high degree of both amplitude and phase balance between the parallel quadrature channels of each receiver over the full dynamic range of signals and over the region of operating temperatures, the preamplifier gains are switched in discrete steps by wideband (at audio) gain-switching threshold circuits. Automatic gain control is not used. A set of discrete outputs is provided and telemetered to indicate the gain state of each receiver, as follows:

	Gain Switch 1	Gain Switch 2
High gain (DVS, 90 db; RA, 80 db)	Off	Off
Mid gain (DVS, 65 db; RA, 60 db)	Off	On
Low gain (DVS and RA, 40 db)	On	On

Other discrete outputs are also provided and telemetered. One is a confirmation of application of prime power. This initiates a warmup interval ended by an internal timer which applies high voltage to both klystrons. A set of tracker-lock signals indicates the search or track status of each of the four frequency trackers. A reliable operate doppler velocity sensor (RODVS) discrete indicates, both prior to 3.5 g + 3.7 seconds and subsequent to the 1000-foot mark, that all three DVS beams are locked; between these two times (in Surveyor IV and subsequent spacecraft), it indicates that any one or more of the DVS beams is locked. RODVS causes the flight control to switch attitude steering inputs from gyros to lateral velocities. A RORA (reliable operate radar altimeter) discrete is on when and only when beams 1, 3, and 4 are locked, thus providing reliable V_z and R_z for the flight control acceleration control loop. From the analog range output, the RADVS itself derives and supplies two discrete range mark signals, one at 1000 feet (used to change flight control loop parameters), and the other at 12 feet (used to cut off vernier engines).

The latter is termed the 14-foot mark for RADVS purposes, since it is measured from the RADVS antenna boresight reference, which is 24 inches above the legs-extended position of the landing pads on the spacecraft structure (whose position at vernier engine cut off, in turn, has been used in landing stability analyses).

The RADVS hardware is packaged in five units, each of which is a control item in Hughes Spacecraft Configuration Control. Since temperature is measured separately for most of these units, their basic composition is indicated below:

A/VS antenna	— beams 1 and 4 antenna, mixer, and preamplifier components
DVS antenna	— beams 2 and 3 antenna, mixer, and preamplifier components
Klystron power supply modulator (KPSM)	— includes all components for both DVS and RA
Signal data converter	— all frequency trackers and data converters
Waveguide assembly	

5.9.2 ANOMALIES

During the Surveyor IV mission, all radar events occurred essentially at their predicted times up to loss of data. All analog channels were close to nominal up to loss of data with two exceptions as follows:

1) RADVS reflectivity signals, while DVS beams were reported locked, followed their predicted relative values and time dependencies, but were 3 to 4 db lower than nominal. This is attributed to terrain reflectivity uncertainty and possibly to minor calibration errors.

2) RADVS lateral velocities were well within accuracy and noise requirements, but suggest a possible spacecraft attitude oscillation up to perhaps ±0.1 degree, which was not noted in lateral velocities in previous missions.

5.9.3 SUMMARY AND CONCLUSIONS

The most notable conclusion is that the data indicate, in several independent ways, that the Surveyor IV terminal descent trajectory was close to nominal up to loss of data. All these indications would have to be simultaneously in exorbitant error, far outside design capabilities in fact, to satisfy a hypothesis that lunar impact occurred at loss of data. The probability of this hypothesis being valid is therefore immeasurably small.

The only other significant conclusion from radar data is possible confirmation of a small attitude oscillation of the spacecraft in the few seconds after the RODVS signal.

The following summarizes the most important items of RADVS performance which could be determined from the data up to the time of signal loss:

1) All digital events occurred at times which were normal up to data loss.

2) RADVS power on and high-voltage time-in occurred at times which are normal relative to ignition.

3) RA sweep was normal during KPSM time-in, depressed sharply as is normal with lockup to large V_z, and began rising again as is also normal with continuously decreasing true V_z.

4) All three DVS beams acquired lunar signals within less than 1 second of their predicted times. These were based upon the six degree-of-freedom predicted trajectory and RADVS values. This confirms the retro velocity decrement to that point in time, since tracker acquisition was constrained by the upper sweep limit in frequency, related to velocity, not by signal strength. RODVS appeared properly.

5)   DVS beam signal strengths between RODVS and loss of data were actually 3 to 4 db below predicted nominal. (Acquisition margins were still close to 30 db.) If Surveyor IV had impacted the moon at the time of data loss, all three DVS signal strengths should have been about 60 db above their indicated levels.

6)   RA acquisition did not occur and RORA did not appear up to loss of data; both were normal. Predicted RA acquisition was not until separation, 14 seconds after data loss, when RA frequency should have decreased to its upper sweep limit of about 90 kHz. RA frequency predicted at time of data loss was over 121 kHz, well above that. RORA requires lock of beams 1, 3, and 4, and beam 4 (RA) did not have a chance to lock before data loss.

7)   Predicted slant range of 57,000 feet at time of data loss corresponds to 6.64 seconds of flight time at 8600 fps prior to ignition. This would have been over 8σ of O.D. error, or 116 μs of AMR gate setting error (measured to 0.1 μs accuracy (preflight) to have caused lunar impact at data loss). RADVS data confirms that these exorbitant errors did not exist.

8)   While range cannot be accurately assessed without altimeter readings, all radar data indicate a normal descent trajectory up to loss of data. Predicted conditions at that time were $V_Z = 1000$ fps and $R_Z = 57,000$ feet.

9)   Telemetry V_Z saturated at RODVS and remained saturated at data loss. This was normal for predicted conditions. Doppler frequencies within the velocity converters are correct for all values tracked. True V_Z decreased as indicated by the rising RA sweep pattern. The predicted 1100 fps at time of data loss was still above the 800 fps (minus FC-77) telemetry saturation level.

10) Telemetry V_X and V_y indicated about the right spacecraft orientation, with perhaps 0.2-degree pointing error, well within tolerances. Relative strengths of the DVS beams confirmed a correct spacecraft geometry (to the degree their accuracy permits).

11) Telemetry V_X suggests a small yaw oscillation after RODVS, and did not develop quite the expected time slope.

12) Telemetry V_y appears erratic after RODVS, a situation not seen in Surveyors I or III. This suggests unusual pitch motion. Amplitude is about ±5 fps; at 3000 fps, this would be equivalent to about ±0.1 degree. While well within RADVS accuracy and noise requirements, hence inconclusive, this does suggest unusual lateral motion.
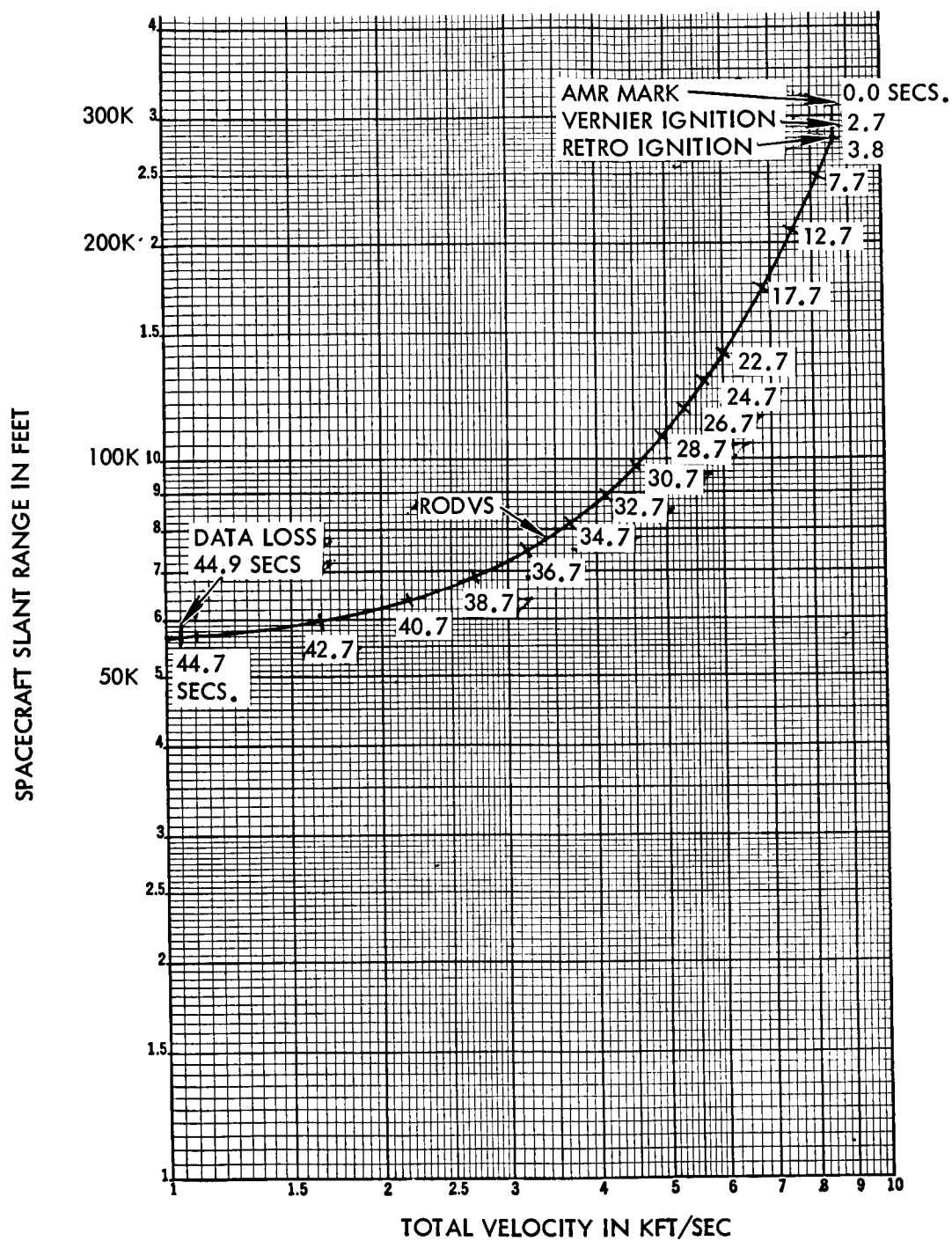
Figure 5.9-1. Six Degree-of-Freedom Program Predicted Trajectory

13) Fluctuation in DVS signal strengths was perfectly normal, and is related only to terrain variation, not to any lateral rates that may have existed. (Even at maximum steering rate, beam rotation contributes only infinitesimally to normal Rayleigh scintillation.)

There are no radar recommendations related to the Surveyor IV loss of data.

5.9.4 RADVS PERFORMANCE ANALYSIS

5.9.4.1 RADVS Turnon

RADVS turnon occurred properly at retro ignition as indicated by altimeter search sweep on the range signal telemetry output. Subsequent time-in of the high voltage occurred approximately 19 seconds after turnon, as indicated by the change in current on the radar squib current telemetry channel, EP-17.

5.9.4.2 Telemetered Event Times

Table 5.9-1 shows discrete events associated with Surveyor IV radar operation. Times are derived from postmission processing of DSIF-14 magnetic tapes, accounting for individual word and bit locations within the commutation frame. In certain cases, it has been possible to refine these times beyond the telemetry values by considering independent sources of timing information (magnitude register counting).

### 5.9.4.3 Predicted Trajectory and Geometry

One of the large scale Surveyor simulation programs is a six degree-of-freedom terminal descent flight program. It includes all significant propulsion, vehicle, flight control, and radar parameters. It is used both for postmission reconstruction by iteration against all pertinent telemetry data, and for preflight prediction of nominal performance.

Such a prediction was performed before the Surveyor IV terminal descent. It produced a complete printout at 1-second (maximum) intervals and a complete set of plots of pertinent information.

Table 5.9-2 is a summary of such predictions for Surveyor IV. Figure 5.9-1 is an artificial-scale representation of the R_z, V_z trajectory in time. Figure 5.9-2 represents the RADVS beam geometry of Surveyor IV as predicted at the time of data loss.

5.9.4.4 RADVS Beam Frequencies

Figure 5.9-3 shows the predicted values versus time (in the region of interest) of the signal frequencies on all four RADVS beams.
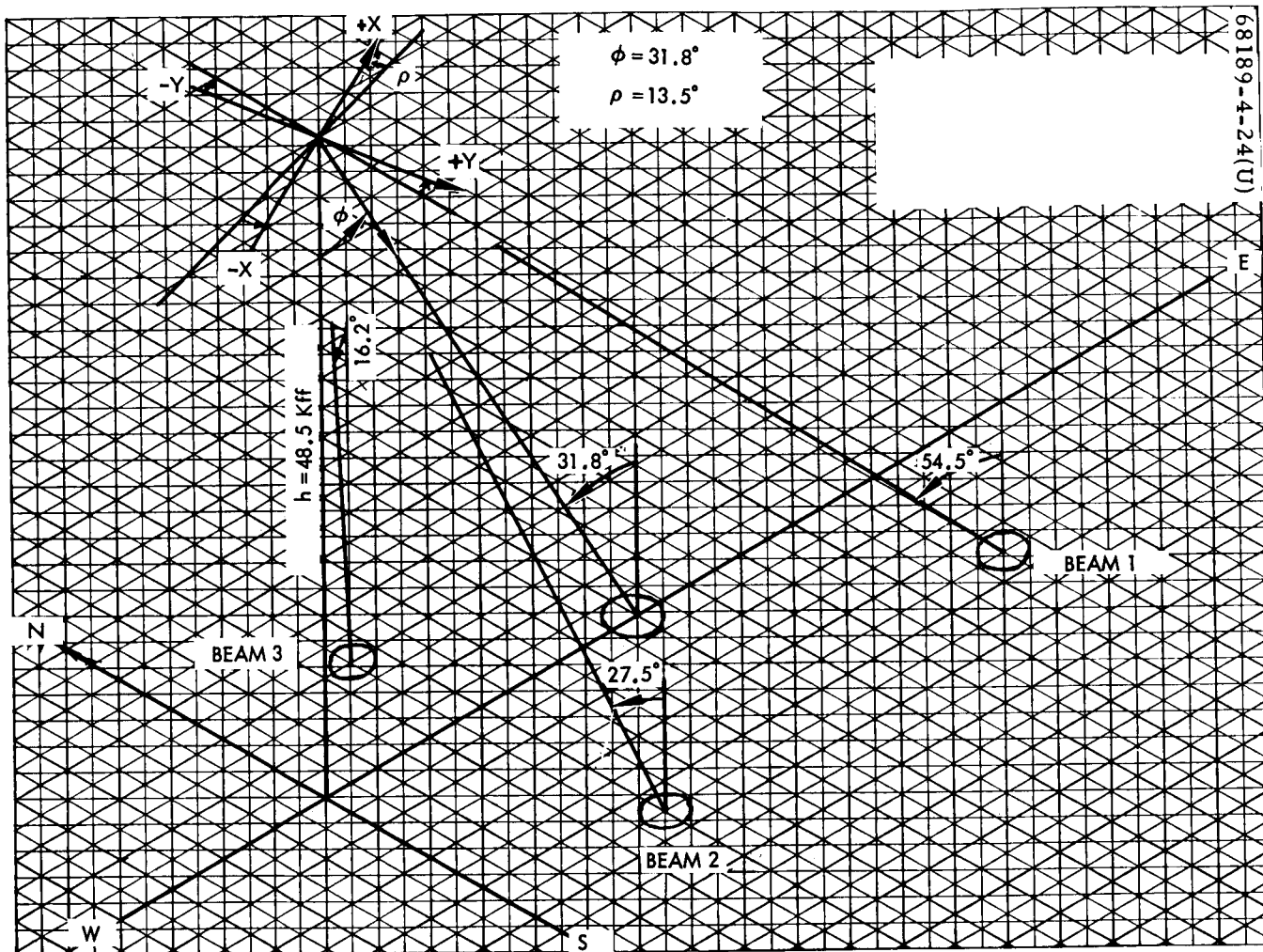
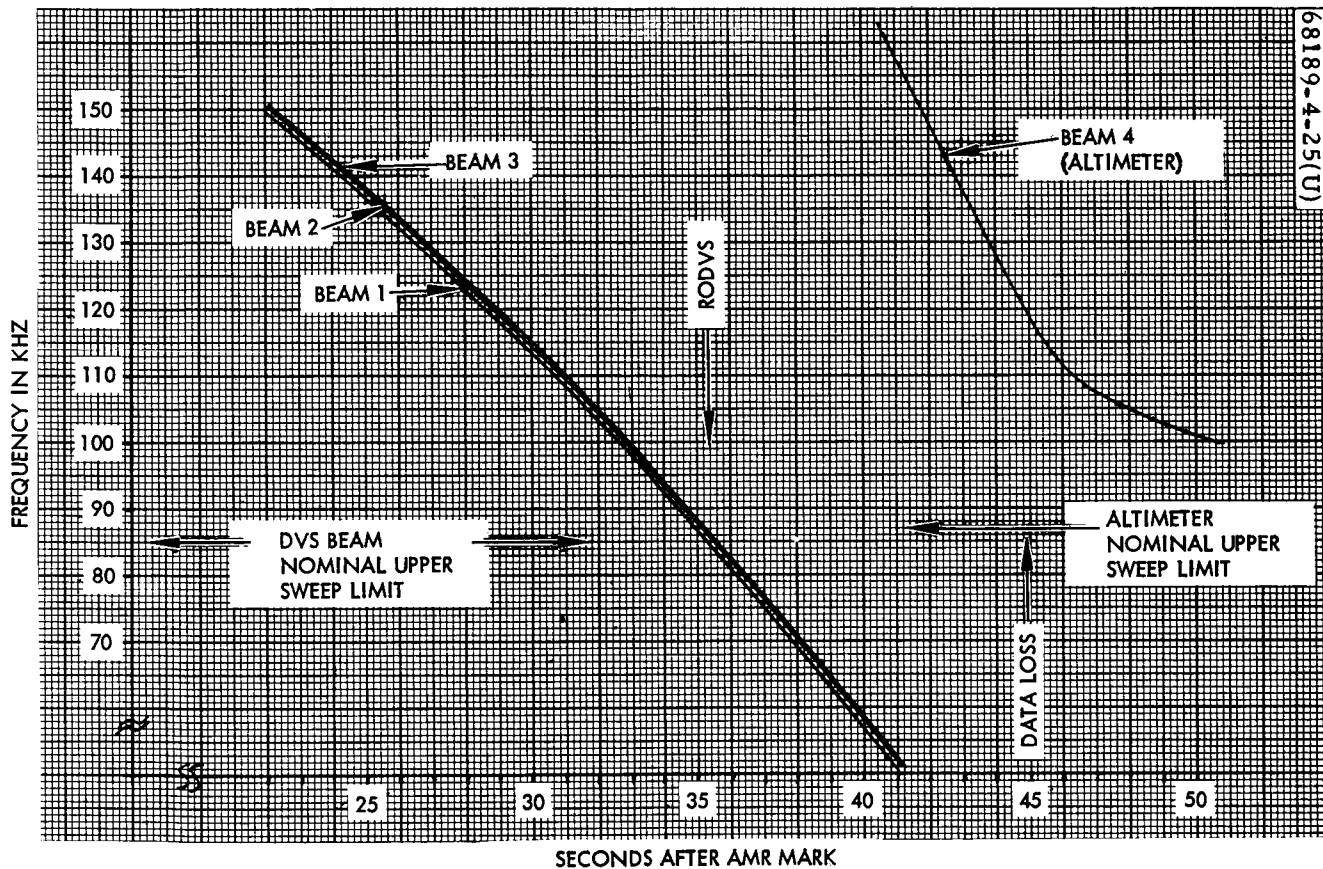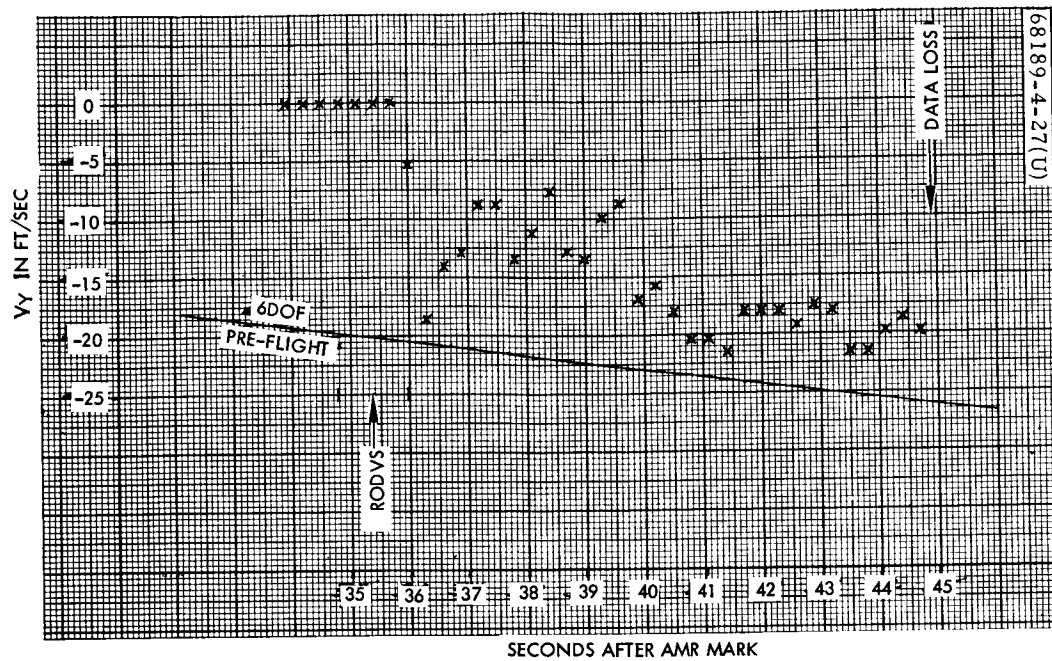Figure 5.9-2. Surveyor IV Beam Geometry of Data Loss

Figure 5.9-3. Preflight RADVS Predictions (Six Degree-of-Freedom Program)
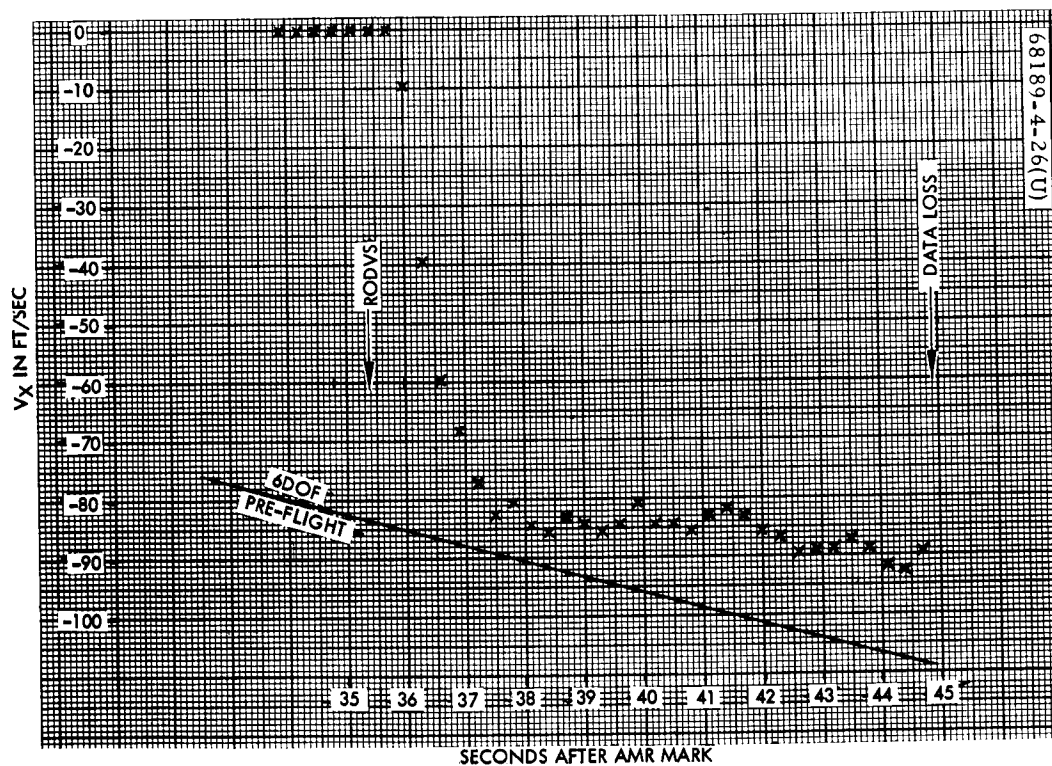
TABLE 5.9-1.   RADAR EVENT TIMES

Signal	Nomenclature	GMT, hr:min:sec
R-1	AMR on	01:57:16.996 ± 0.6
R-11	AMR enable	02:00:16.992 ± 0.6
FC-64	AMR mark	01:56.080 ± 0.005
FC-28	Vernier ignition	01:58.810 ± 0.025
FC-29	Retro ignition (also FC-64 off)	01:59.925 ± 0.05
EP-33	RADVS pyro on	02:00.585 ± 0.6
R-28	RADVS on	02:00.785 ± 0.6
FC-63	Inertia switch off	02:02.685 ± 0.6
R-17	D3 lock	02:31.384 ± 0.6
FC-34	RODVS	02:31.484 ± 0.6
FC-36	10 fps off	02:31.524 ± 0.05
R-15	D1 lock	02:31.684 ± 0.6
R-24	D3 gain state 2	02:31.684 ± 0.6
R-16	D2 lock	02:31.684 ± 0.6
Data loss		02:41.018
V-4	Retro not ejected remained on	
R-18	R lock remained off	
	No other gain state changes occurred	
	Momentary RADVS locks and analog glitches are normal at power on.	

TABLE 5.9-2. SURVEYOR IV SIX DEGREE-OF-FREEDOM PROGRAM PREFLIGHT PREDICTIONS

Time, seconds	Total Velocity, fps	Altitude, feet	Slant Range, feet	Angle from Z-Axis to Vertical, degrees	Comments
0.0	8606	248.5K	288.7K		Vernier ignition
1.0				30.64	Retro ignition
33.0	3414	66.4K	78.0K	31.65	DVS:82.6 - 84.37 kHz predicted lock
56.0	514	40.5K	47.6K	31.78	RA:90.36 kHz predicted lock
57.9	503	39.5K	46.5K	31.79	Start RADVS-controlled descent: V_x = -151.4 fps V_y = -36.3 fps V_z = +478.2 fps
65.0	503	36.0K	37.0K	12.83	V_x = -3.37 fps V_y = -0.70 fps V_z = +503 fps
89.0	510	24.1K	24.5K	9.83	Segment acquisition
114.0	392.8	13,015	13,122	7.33	First segment corner
141.0	203.1	5,016	5,031	4.49	
168.24	104.8	998	998	1.54	1000-foot mark
176.0	61.6	355	355	0.52	
186.24	8.54	44.9	44.9	0.03	10-fps mark
192.09	5.18	13.4	13.4	0.03	14-foot mark
193.57	12.62	0	0		Touchdown

a) V_x

b) V_y

Figure 5.9-4. RADVS Lateral Velocity

Every DVS beam acquired its lunar signal, and RODVS appeared within a second of the predicted time. Since signal power margin was confirmed as close to the nearly 30-db acquisition margin, the acquisition constraint is the upper sweep limit of each frequency tracker. This has consistently been true of every beam in each mission to date. This not only confirms proper DVS operation, but also indicates strongly an essentially nominal velocity decrement during retro engine burning to that point in time. The RA sweep pattern also confirms a continually decreasing velocity thereafter to loss of data, as described in the conclusions, subsection 5.9.3.

Altimeter lockup did not occur because its frequency was still too high (see subsection 5.9.3). RA acquisition has been predicted to occur some 14 seconds after time of data loss, essentially at separation.

5.9.4.5 RADVS Lateral Velocities

Figure 5.9-4 shows both predicted and telemetered values of V_x and V_y, respectively, from RODVS to loss of data.

Spacecraft orientation and velocity vector magnitude and direction were essentially confirmed to within perhaps 0.2 degree pointing error after the roll-yaw-roll preretro maneuvers.

Surveyor IV lateral velocities were not quite typical, however, compared with Surveyor I and III data. Noted elsewhere herein are the possible oscillation of V_x and the unusual variation of V_y. While well within radar accuracy and noise requirements, they suggest a possible spacecraft attitude variation of up to about ±0.1 degree.

5.9.4.6 RADVS Reflectivity Signals

Table 5.9-3 shows hand-calculated individual db budgets for each of the four RADVS beams prior to the computer predictions. The angles in this table were earlier predictions refined in the computer simulation. RADVS test values were common to both.

Figures 5.9-5a, b, and c apply to DVS beams 1, 2, and 3, respectively. Each shows both computer predicted and Surveyor IV telemetry values, bias-corrected and hand-converted to dbm, for the signal strength indication of each velocity tracker. Each is also associated with pertinent event times. It is noted that relative amplitudes of the three beams and the time variation of each were essentially as predicted. Absolute levels were 3 to 4 db lower than nominal in all cases, however. This is attributable to uncertainties in lunar reflectivity and perhaps to minor calibration errors. Such variation is still well within design performance margin requirements. Beam 4 reflectivity data are meaningless because its tracker had not yet acquired its lunar signal.
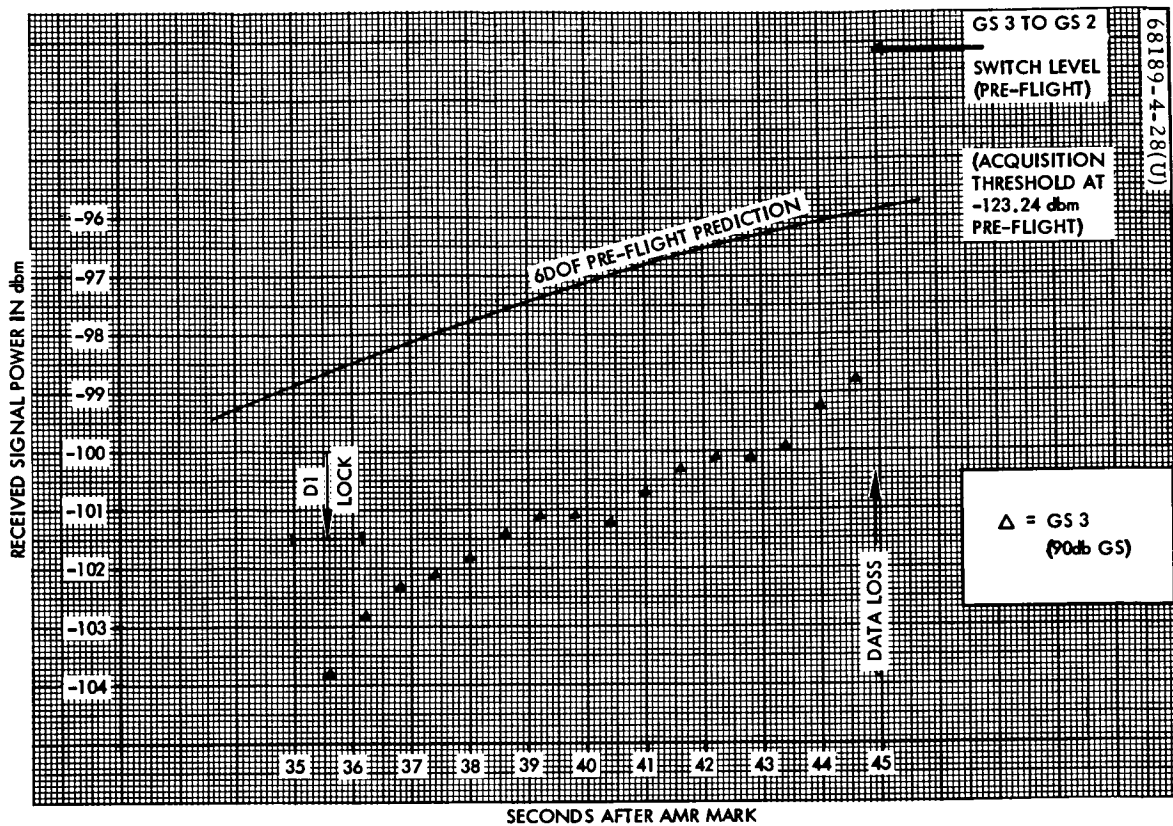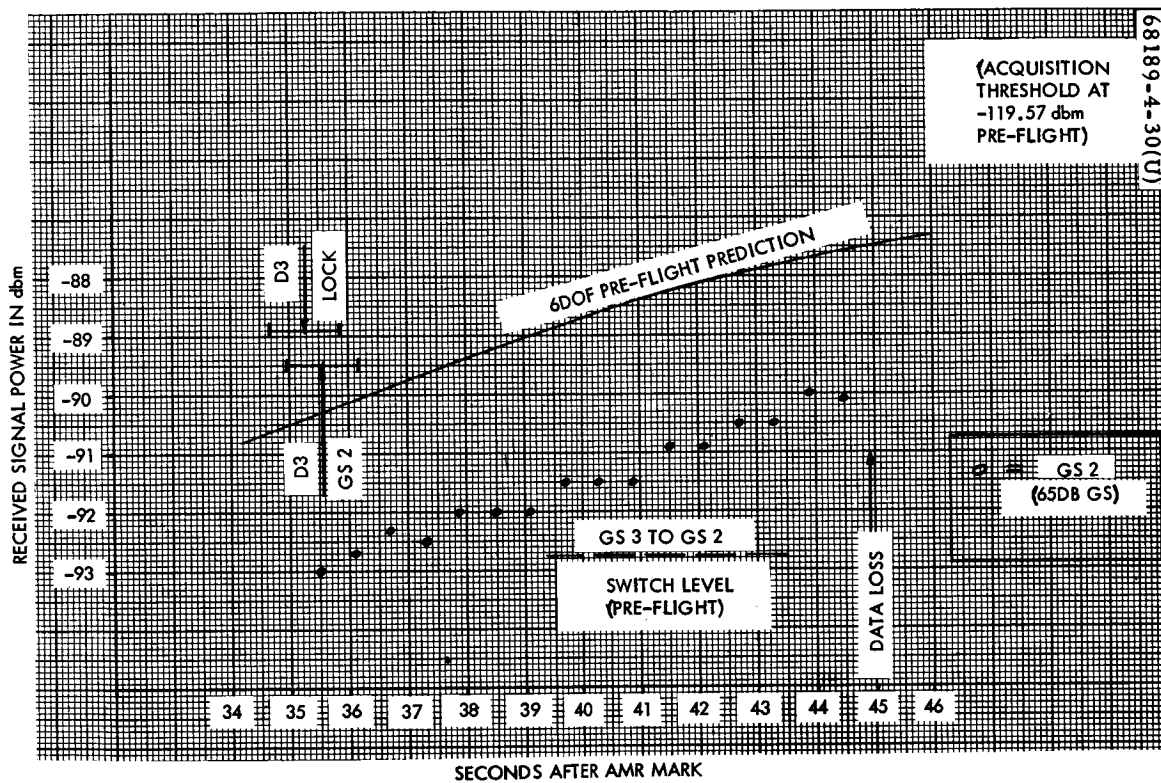
a) Beam 1
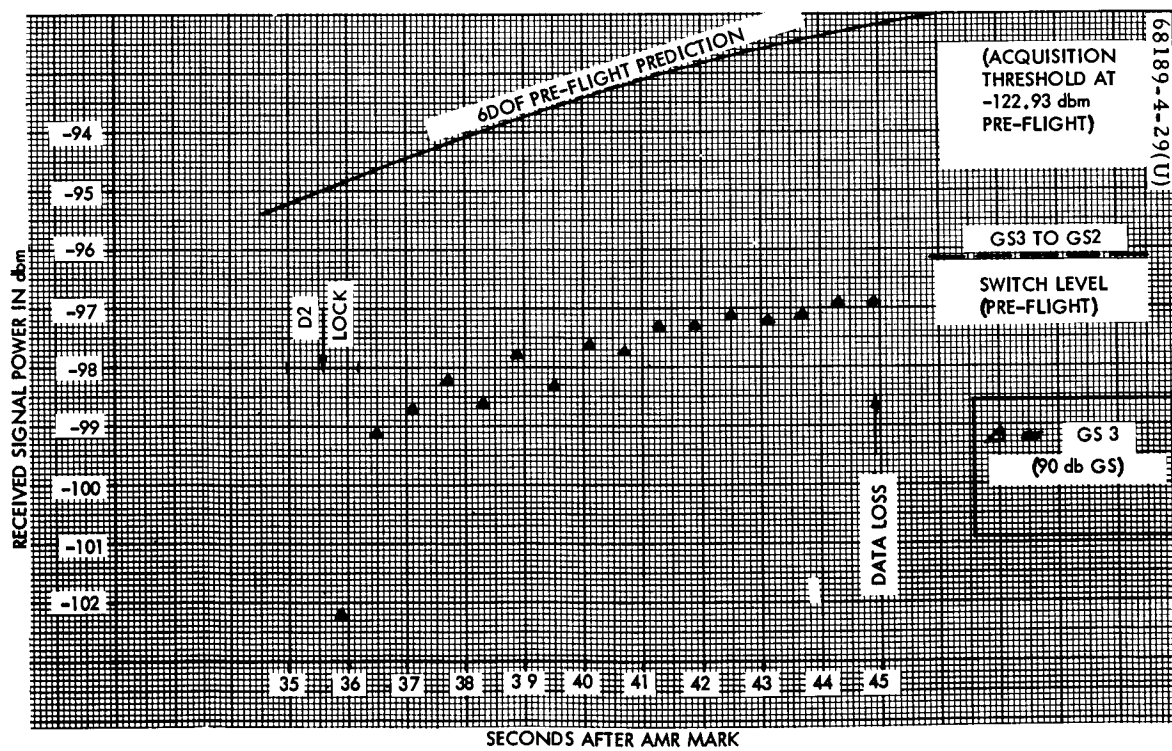
b) Beam 2

Figure 5.9-5. RADVS Reflectivity

c) Beam 3

Figure 5.9-5 (continued). RADVS Reflectivity

TABLE 5.9-3. RADVS INDIVIDUAL BEAM DB BUDGETS BEFORE STEERING

Using measured Pt and G values and nominal reflectivity model

For $\varphi = 31.2$ degrees, $\dot{p} = +346$; $R_z = 30$ kilofeet

Values	Beam 1	Beam 2	Beam 3	Beam 4
Pt, dbm	+ 34.65	+ 32.93	+ 34.43	+ 25.38
G, db	+ 30.0	+ 28.45	+ 28.2	+ 30.1
(1/2), db	- 3.01	- 3.01	- 3.01	- 3.01
λ^2, db	- 22.64	- 22.64	- 22.64	- 22.36
$(4\pi)^{-2}$, db	- 21.98	- 21.98	- 21.98	- 21.98
$(25.6 \text{ kilofeet})^{-2}$, db	- 88.18	- 88.18	- 88.18	- 88.18
$\cos^2 \theta i$, db	- 4.60	- 1.04	- 0.32	- 1.36
$F(\theta i)$, db	- 12.74	- 9.46	- 7.13	- 10.17
$\eta(K/\alpha^3)$, db	- 1.72	- 1.72	- 1.72	- 1.72
Sum of + values	+ 64.65	+ 61.38	+ 62.63	+ 55.48
Sum of - values	-154.87	-147.03	-144.98	-148.78
P_r, dbm	- 90.22	- 85.65	- 82.35	- 93.30
θi, degrees	54.0	27.4	15.7	31.2
$\sigma(\theta)$, db	- 14.46	- 11.18	- 8.85	- 11.89
R, kilofeet	43.6	28.9	26.6	30.0

5.9.5 ACKNOWLEDGMENTS

This section has been principally compiled from the RADVS portion of the "SC-4 Preliminary Post Flight Data Analysis" report written by R. A. Dibos.

APPENDIX A
TO SECTION 5.9

SURVEYOR III BEAM 4 STUDY

As reported after the Surveyor III mission and as duscussed in the final postmission report (Reference A-1), there were two dropouts of the radar altimeter (beam 4) in the region of retro separation. Each was occasioned by a gain switch (GS) from GS 3 (80-db gain state) to GS 2 (60-db gain state). The lunar signal was above threshold in GS 3, but was below threshold in GS 2, so that dropout was normal given the gain switch. The second occurrence was just after retro separation, and is attributed to the retro case itself as a radar target. The first occurrence, about 6 seconds after 3.5 g, exhibited similar radar characteristics. It was desirable that the parameters necessary to this behavior be examined. (It is emphasized that no false lock occurred.)

The events of present interest and the GMT (minutes and seconds only) of their receipt at DSIF-11 were as follows:

	Min:sec
FC-63 inertia switch	02:00.183 ± 0.6
FC-30 retro burnout	00.523 ± 0.05
Beam 4 GS 3	05.782
R-18 beam 4 unlock	06.083 ± 0.6
Beam 4 GS 2	06.982
Beam 4 GS 3	08.182
R-18 beam 4 lock	08.483 ± 0.6
FC-31 retro eject	12.523 ± 0.05
Beam 4 GS 3	12.982
V-4 retro ejected	13.282 ± 0.6
R-18 beam 4 unlock	13.283 ± 0.6
Beam 4 GS 2	14.182
FC-42 start RADVS descent	14.624 ± 0.05

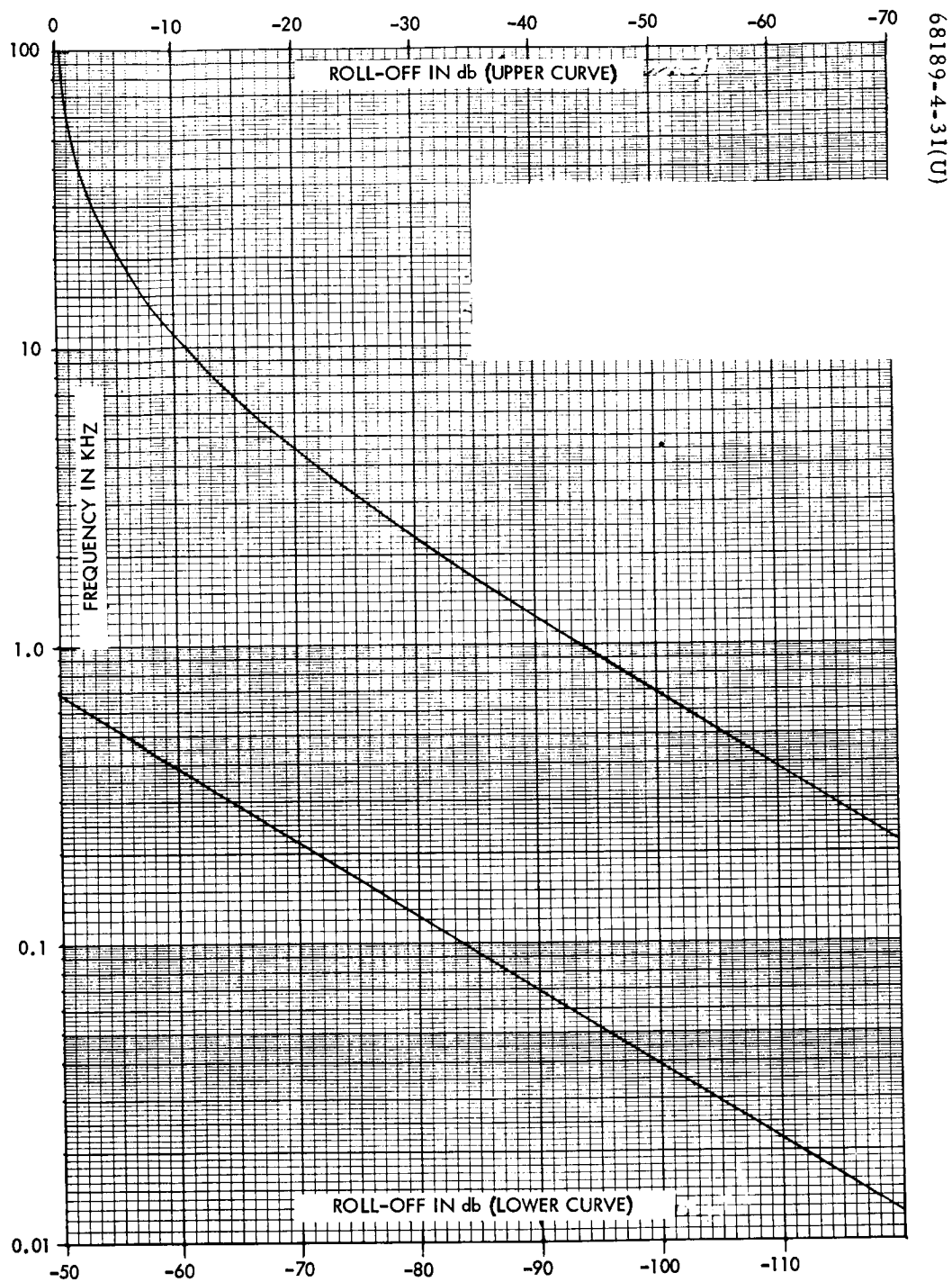Figure A-1. A-21 RADVS Radar Altimeter (Beam 4) Nominal Roll-Off

A-2

Beam 4 GS 3   02:15. 382

R-18 beam 4 lock   15. 683 ± 0. 6

(Note: GS are shown at times of sampling. Events are interpolated between on-off or off-on samples.)

   Lock and GS digital signals are sampled once per frame in telemetry mode 6, or at 1. 2-second intervals at 1100 bits/sec. It is noted that exactly one GS 2 sample was associated with each dropout. Each GS 2 interval was therefore of indeterminate length less than 2. 4 seconds and greater than zero (gain-switching can occur in less than 0. 1 second). Each dropout was marked by two successive off samples; since the sampling interval is less than the RA tracker sweep and relock time of about 1. 75 seconds, either one or two off samples could occur during one sweep; it is also possible, but less likely, that two sweeps may have occurred (2 X 1. 65 + 0. 1 = 3. 4 is less than 3 X 1. 2 = 3. 6).

   Considerable care was taken in the material prepared for the final postmission report to point out the analog reflectivity signal voltages are not always capable of proper dbm interpretation, particularly near gain-switching. This is also decidedly the case during intervals of tracker underlock, especially in wideband mode (above 1000 feet for beam 4). For this reason, dbm values have been omitted where the sweeping tracker saw only noise.

   Several aspects of RADVS design are significant to the observed data. First, gain-switching is done in the preamplifiers; these are essentially flat to 100 kHz but have pronounced roll-off added for mixer noise and retro case suppression. This roll-off is graphed in Figure A-1; it always includes both a 30-kHz corner and a 5-kHz corner as seen by the gain-switching circuits; there is no band-limiting as such. Second, the two quadrature preamplifier channels have similar main signal paths to a high order of gain and phase balance, but each responds equally well to either positive or negative "doppler" frequencies; single sideband discrimination does not occur until these signals are combined in the tracker. Third, negative doppler frequencies can cause gain-switching without actually being acquired by the single sideband tracker. Whether the nominal 25-db unwanted sideband suppression was indeed adequate in these cases cannot be positively determined because of uncertainty about the actual peak amplitude of extraneous signal, its frequency, and its duration relative to the sweep cycle. (By Ryan design, retro case acquisition is precluded for a relative acceleration of 1 fps^2.) Fourth, the range and velocity scale factors for beam 4 frequency are such as to ensure a negative doppler frequency for any high-speed particles in the retro plume, according to the equation:

$$F_R \text{ (kHz)} = 0.001626 \text{ R (feet)} - 0.0262 \text{ V (fps)}$$

given that V is an opening rate and that the RA is in wideband (as it is until the 1000-foot mark). It is seen that F_R is negative for all:

$$R \text{ (feet)} < 16.1 \text{ V (fps)}$$

and the F_R equation above, with its assumptions, has been used throughout in the following analysis.

The major approximation used is an abrupt transition from far-field asymptotic signal power equations to near-field asymptotes based upon an assumed cylindrical region of uniform power density. The results are equivalent to uniform power density in any plane normal to the beam axis, bounded by and vanishing outside a region formed by a combined cylindrical near-field and conical far-field.

The two-way gain of Surveyor III's beam 4 was +59.25 db in flight acceptance test. The equivalent one-way gain of +29.12 db corresponds with an effective aperture of 0.378 ft^2 at 12.9 GHz, or at 60 percent aperture efficiency (typical) to a physical aperture of 0.63 ft^2. If this were perfectly circular, the diameter would be 0.896 foot. Projecting this outward along the beam axis, at 8.5 feet it intersects a cone of 6.09 degrees total angle, the one-way far-field equivalent to the flight acceptance test two-way total beam-width at -3 db of 4.30 degrees. This cone has a cross section of 1 square foot 10.6 feet from the aperture, and 10 square feet at 33.6 feet from the aperture.

The beamwidth-limited range equation consistently used with RADVS has been well documented as

$$Pr = \frac{Pt(G/2) \lambda^2}{(4\pi R)^2} \text{ (Refl)}$$

where (Refl) is a lunar surface cross section model relative to a lossless isotropic surface. For an effective radar cross section large enough to fill the far-field beamwidth, this factor goes to unity.

For an effective radar cross section σ not large enough to fill the far-field beamwidth, the classical radar equation is

$$Pr = \frac{Pt \ G^2 \ \lambda^2 \ \sigma}{(4\pi)^3 \ R^4}$$

Equating the results for the case where σ just fills the far-field beamwidth produces

$$\sigma = \frac{2\pi R^2}{G}$$

For $\sigma = 10$ ft^2, R = 36.0 feet (versus 33.6 feet in the geometric model); for $\sigma = 1$ ft^2, R = 11.4 feet (versus 10.6 feet in the geometric model). The correlation is rather good, and the models were not refined further, considering the approximations used and the wide ranges of variables considered. The db budget for Surveyor III beam 4 using the R-4 equation is

$$
\begin{array}{ll}
P_t & +24.90 \text{ dbm} \\
G^2 & +58.25 \text{ db} \\
\lambda^2 & -22.36 \text{ db} \\
(4\pi)^{-3} & -32.97 \text{ db} \\
\hline
& +27.82 \text{ dbm}
\end{array}
$$

which is 109.7 db above the measured GS 3/2 switch level of -81.9 dbm. Therefore

$$
\frac{\sigma}{R^4} + \text{roll-off} = -109.7 \text{ db}
$$

relates σ, R, and V in the far-field when not beamwidth limited. Figure A-2 shows solutions in this region for five values of σ in decade intervals from 10^{+1} to 10^{-3} ft^2.

It is emphasized that σ is an effective radar cross section, lossless and isotropic. A thin splinter of still burning solid fuel could conceivably have an effective area much larger than that of the splinter itself. Along the beamwidth limited boundary, the sharpness of the model used says that a still larger σ would return no more power. This is not as gross as it may appear, since the geometric envelope model has been matched to the R^{-2} equation, which is valid for the entire lunar surface. For the R < 8.5 feet, return power is assumed constant in the cylindrical near-field model, which is asymptotically correct within 3 db as the isotropic σ approaches the aperture.

The true return power variation is a smoother curve to the right of the sharp corners shown at 8.5 feet, fairing into both asymptotes. Precise evaluation in the transition region involves complicated integrals at each distance, and was not deemed worth the effort.

The above db budget represents just enough signal to gain-switch, whereas it cannot be determined how much more may have existed. The contours therefore represent maximum ranges and minimum velocities for which the indicated σ is just enough to have gain-switched beam 4 of Surveyor III.

REFERENCE

A-1.   "Surveyor III Flight Performance Final Report," Section 5.9.3,
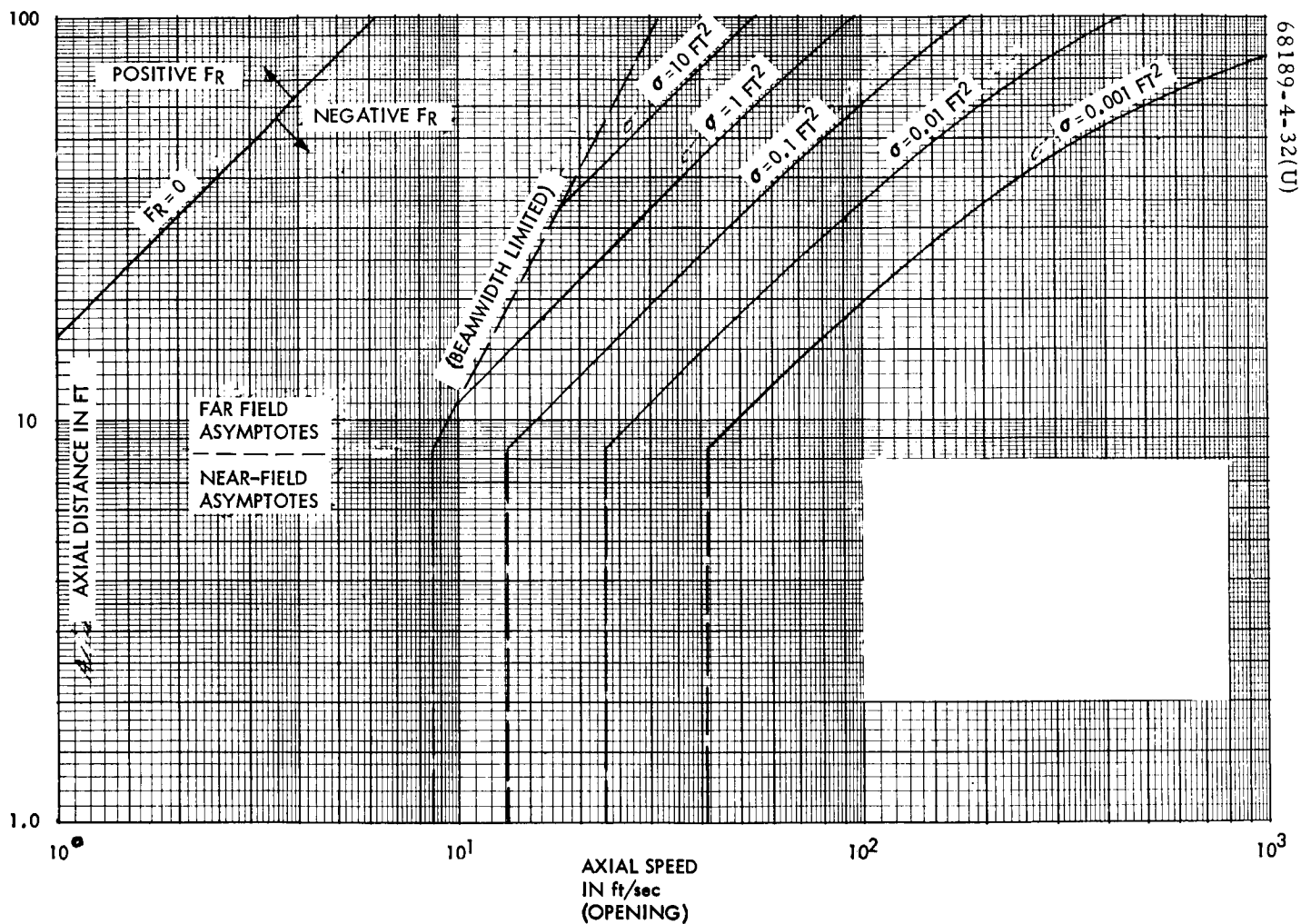   Hughes Aircraft Company, SSD 68189-3, July 1967.

Figure A-2.   Surveyor III RADVS Radar Altimeter (Beam 4) Asymptotic
Contours of Range and Velocity

5.10 MECHANISMS SUBSYSTEM

5.10.1 INTRODUCTION

This section deals with the mechanical performance of the spacecraft landing legs, omnidirectional antennas, and antenna/solar panel positioner (A/SPP). For purposes of this report, these mechanisms are collectively defined as the mechanisms subsystem.

1) **Landing gear deployment** — When each landing gear is fully deployed, it opens an electrical switch on the telescoping strut. The actuation of these switches indicates that the landing gear is deployed, and is required for initiation of automatic sun acquisition at separation from Centaur. The telemetry designations for these functions are V-1, V-2, and V-3 for each landing leg, respectively.

2) **Omnidirectional antenna deployment** — When each omnidirectional antenna is fully deployed, it opens an electrical switch to produce a change of state for telemetry purposes only. The telemetry designation for omnidirectional antenna A is M-1, for omnidirectional antenna B, M-2.

3) **A/SPP automatic solar panel deployment** — The A/SPP function after separation is to deploy the solar panel surface perpendicular to the roll axis to achieve maximum receipt of solar energy during transit.

The A/SPP has four rotation axes which are moved in steps upon command from earth. The axes are polar, solar, elevation, and roll. The polar axis rotates 1/16 degree per command; the other axes rotate 1/8 degree per command. Figure 5.10-1 illustrates the A/SPP with the polarity of rotation for each axis. The telemetry designation for the A/SPP axis positions are as follows:

Solar panel	M-3
Polar axis	M-4
Elevation axis	M-6
Roll Axis	M-7

SOLAR
PANEL
AXIS

MINUS

PLUS

PLANAR ARRAY/SOLAR
PANEL ANGLE 90° TO 355°

SOLAR PANEL

PLANAR ARRAY
ANTENNA

ZERO

90°

90°

PLUS

PLUS

ELEVATION
AXIS

96°

POLAR
AXIS

MINUS

MINUS

ZERO

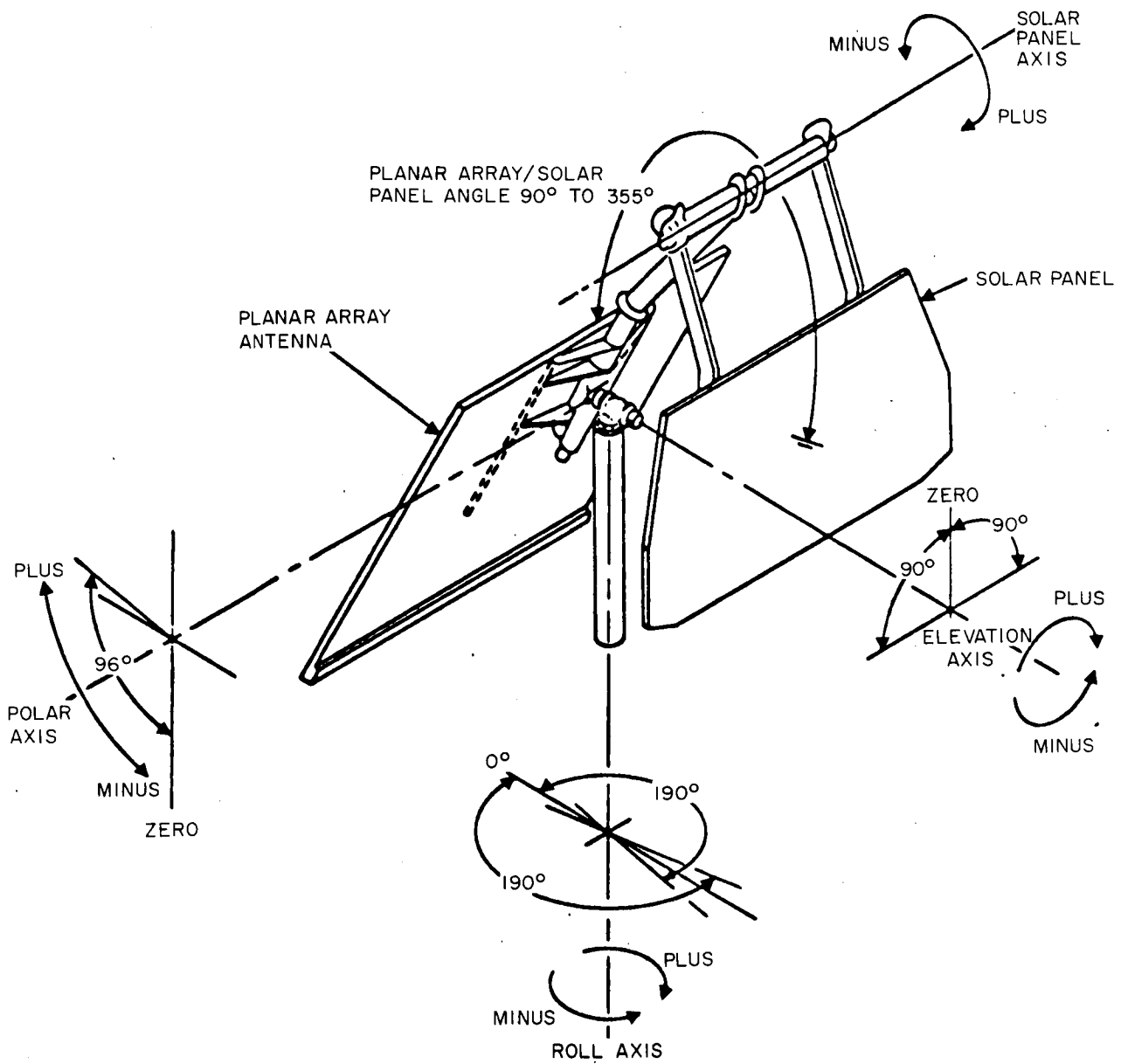0°

190°

190°

PLUS

MINUS

ROLL AXIS

Figure 5.10-1.   Antenna and Solar Panel Positioner

5.10.2 ANOMALY DESCRIPTION

No anomalies were detected in the mechanisms subsections during separation. Telemetry data during transit indicated no anomalous conditions.

5.10.3 SUMMARY AND RECOMMENDATIONS

All mechanism functions performed properly and at the correct times.

5.10.4 SUBSYSTEM PERFORMANCE ANALYSIS

Table 5.10-1 shows the occurrence of major events for the mechanisms subsystem. Table 5.10-2 presents a summary of the subsystem parameters reduced from telemetry data. The expected values were obtained from flight acceptance, type approval, and solar thermal vacuum testing, and from specified design performance values.

5.10.4.1 Landing Gear Deployment

Table 5.10-2 shows the nominal expected deployment time for the landing gear to be about 2.3 seconds. Flight data show the deployment time to be 0.4 ±1.2 second, which is slightly below the expected value. The leg deflection signals (V5-7) also indicated normal and complete extension of the landing gear. Total variation in these signals after deployment was less than 0.2 degree (7 BCD).

5.10.4.2 Omnidirectional Antenna Deployment

The nominal expected omnidirectional antenna deployment time is 2.4 seconds. The mission deployment time was 2.3 ±1.2 seconds, which indicates nominal deployment performance. Data show that both omnidirectional antennas were deployed at the same time.

5.10.4.3 A/SPP Performance

Automatic Solar Panel Deployment

Automatic solar panel deployment begins upon closure of the 22-volt switch in the separation sensing and arming device at vehicle separation. The solar panel launch lock is unlocked and the solar panel is stepped from 355 to 270 degrees where it is relocked. At this point, the roll axis is stepped from -60 to 0 degrees and relocked. Both positions are locked until after touchdown.

TABLE 5.10-1. MECHANICAL EVENTS AT SEPARATION

Event	Mission Time, GMT, Day 195, hr:min:sec
Launch	11:53:29.215
Extend landing gear (Centaur command)	12:05:25*
Landing gears extended (V-1, V-2, V-3 on)	12:05:25.422 ±1.2
Extend omnidirectional antennas (Centaur command)	12:05:34.5*
Omnidirectional antennas extended (M-1, M-2 on)	12:05:36.821 ±1.2
Spacecraft electrical separation (Centaur command)	12:06:00.5*
Spacecraft electrical separation (M-9 on)	12:06:01.419 ±1.2
Spacecraft mechanical separation	12:06:06.1*
A/SPP solar panel unlocked (M-14 on)	12:06:05.619 ±1.2
A/SPP solar panel locked in transit position (M-11 on)	12:11:53.622 ±1.2
A/SPP roll axis locked in transit position (M-13 on)	12:16:05.6 ±1.2

*Reported times from Centaur data (see "SC-4 Flight Path Analysis and Command Operation Report," Hughes Aircraft Company, SSD 74108, 10 August 1967.

TABLE 5.10-2. PERFORMANCE PARAMETERS SUMMARY

Parameter	Expected Value, Nominal	Measured Value
Time from Centaur extend landing gear command to legs extended indications (V-1, V-2, and V-3 on)	< 2.3 seconds	0.4 ±1.2
Time from Centaur extend omni-directional antenna command to omnidirectional antennas extended (M-1 and M-2 on)	< 2.4 seconds	2.3 ±1.2
Solar axis deployment time (A/SPP solar panel autodeployment)	340 seconds*	348 seconds
Roll axis deployment time (A/SPP solar panel autodeployment)	248 seconds*	252 seconds
Total A/SPP solar panel auto-deployment time	588 seconds*	600 seconds
Solar axis launch position (355 degrees)	356.8 degrees*	357.0 degrees
Polar axis launch position (0 degree)	0.99 degree*	1.07 degrees
Elevation axis launch position (0 degree)	1.3 degrees*	-0.11 degree
Roll axis launch position (-60 degrees)	-60.23 degrees*	-58.5 degrees
Solar axis transit position	270 degrees	270.5 degrees
Roll axis transit position	0 degree	0.1 degree
Leg deflection signals, prelaunch:		
Leg 1		24.6 degrees 1 BCD
Leg 2	24 degrees 0 BCD	23.1 degrees 2 BCD
Leg 3		23.9 degrees 3 BCD
Leg deflection signals, postlaunch:		
Leg 1	0 degree 952 BCD	-0.21 degree 960 BCD
Leg 2	0 degree 947 BCD	0.15 degree 942 BCD
Leg 3	0 degree 942 BCD	-0.27 degree 953 BCD

*Solar thermal vacuum test phase B.

The Surveyor IV mission solar panel deployment time was 600 seconds. Comparing this mission deployment time to that in solar thermal vacuum phase B (588 seconds), the agreement is better than 98 percent.

Table 5. 10-3 shows the positions of the A/SPP axis before and after the automatic solar panel deployment. These all fall within the required limits when corrections are applied to the telemetry data.

5.10.5 ACKNOWLEDGMENTS

W. McIntyre, Technical Coordinator.

TABLE 5.10-3. A/SPP AXIS POSITIONS FOR PRELAUNCH
AND POST-AUTODEPLOYMENT CONDITIONS

| | | Post-autodeployment* | | | | Prelaunch** | | | |
| | | Telemetry | | Corrected Data | | Telemetry | | Corrected Data | |
		Counts	Indicated Angle, degrees	Counts	Angle, degrees	Counts	Indicated Angle, degrees	Counts	Angle, degrees
Solar axis	M-3	620	269.8	616.9	270.5	864	357.5	859.7	357
Polar axis	M-4	369	-0.53	367.2	-0.35	373	0.89	371.1	1.07
Elevation axis	M-6	526	-0.53	523.4	-0.11	526	-0.53	523.4	-0.11
Roll axis	M-7	498	-0.46	495.5	-0.10	337	-58.27	335.3	-58.46
Reference voltage	S-1	998	—	—	—	998	—	—	—

Nominal reference voltage, BCD: 993.

*Post-autodeployment data time: 197:02:43:20.

**Prelaunch data time: 195:10:05:09.

5.11   TERMINAL DESCENT TRAJECTORY PERFORMANCE

5.11.1   INTRODUCTION

The terminal descent and landing phase begins with the transition from coast mode II to the terminal descent phase. Terminal descent itself starts with the preretro attitude maneuvers. These maneuvers reposition the attitude of the spacecraft from the sun-star reference so that the expected direction of the retro thrust vector will be aligned with respect to the velocity vector. This alignment achieves the desired retro burnout conditions. Following completion of the attitude maneuvers, the altitude marking radar (AMR) is activated. The AMR is preset to generate a mark signal when the range to the lunar surface is 60 miles. A backup mark signal, delayed a short interval after the time the AMR mark should occur, is transmitted to the spacecraft to initiate the automatic sequence in the event the AMR mark is not generated. The desired delay between the altitude mark and retro ignition is stored in the flight control programmer by ground command. Vernier engine ignition is automatically initiated 1.1 seconds prior to retro ignition.

During the retro phase, spacecraft attitude is maintained in the inertial direction established at the end of the preretro maneuvers by the vernier attitude control system, and the total vernier thrust is maintained at midthrust. As the mass of the vehicle decreases due to expenditure of retro and vernier propellant, the spacecraft thrust to mass ratio (T/M) increases from approximately 4 g_e (g_e = 32.2 ft/sec^2) at ignition to 10 g preceding burnout. Prior to burnout, the inhibit is removed from the acceleration switch output, and the doppler radar and altimeter (RADVS) is activated.

As the thrust decays during retro burnout, the acceleration switch signals when the T/M level has dropped to 3.5 g_e. At this time, the vernier engine thrust command is automatically changed to high thrust, and a counter in the flight control programmer is initiated. After 12.0 seconds following receipt of the burnout signal, the explosive bolts attaching the retro to the spacecraft are activated, allowing the retro case to separate from the spacecraft. Following a programmed delay of 2.15 seconds after separation begins, the vernier thrust command is changed from the open-loop mode to a closed-loop acceleration control mode. Nominal acceleration commanded at this point is 4.82 ft/sec^2.

When reliable radar operation occurs, attitude control of the vehicle is switched from inertial to radar control, and the spacecraft maneuvers to align the vernier thrust axis to the velocity vector. When the combined range and velocity, as measured by the radar, indicates that the spacecraft has descended to the programmed range/velocity descent profile, the total vernier engine thrust is controlled to achieve a trajectory along this profile. When a velocity of 10 fps is reached, attitude control of the spacecraft is switched to inertial reference, and thrust control is servoed to maintain descent velocity at 5 fps. At 14 feet above the surface, the radar generates a signal commanding vernier engine cutoff, and the vehicle free falls to the lunar surface. The touchdown impact is absorbed by the spacecraft landing system, completing the terminal descent phase.

The Surveyor IV performance was near perfect from launch to the main retro phase; however, just prior to retro burnout, the spacecraft's signal was lost. Attempts to re-establish contact with the spacecraft were unsuccessful. During the terminal phase of the mission in which the spacecraft's return signals were available, the performance was close to nominal with no anomalies or problems indicated other than a larger than expected modulation in the vernier engine thrust commands.

The preretro maneuvers properly oriented the spacecraft for the start of the retro phase sequence. The AMR mark occurred and the vernier engines ignited at the desired time delay of 2.7 seconds from the AMR mark, indicating that the start of the terminal descent was generated by the true mark and not the backup command. The main retro engine ignited at the 1.1-second programmed delay after vernier ignition. The vernier engines maintained inertial attitude during the retro phase and, as the end of the expected retro burning phase was approaching, the loss of signal occurred. During the main retro burning phase the reliable operate doppler velocity sensor (RODVS) signal was generated, indicating acquisition by all three velocity radar beams. The predicted retro burn time was 42.53 seconds; the loss of signal occurred 1.43 seconds prior to the predicted burnout time.

As a result of the loss of data, the postflight analysis in this section will be presented only up to the loss of signal.

5. 11. 2   ANOMALY DESCRIPTION

An anomaly during the terminal descent phase is defined as any deviation from the expected mission or system performance. The major anomaly during this phase was the loss of signal prior to retro burnout. Detailed review and analysis of preflight and postflight data have not yet revealed the cause or reason for this event. The only other anomalous behavior was the vernier engine thrust command modulation of all three engines during the retro burn phase. This anomaly is discussed in detail in subsection 5.5.4.10.

5.11.3 SUMMARY

Table 5.11-1 lists the significant terminal descent events up until the loss of signal and the most accurate determination of each event's time of occurrence. The time, as determined from SFOF tape 2087, is either plus or minus the one-way transit time delay (approximately 1.222 seconds), depending on whether the event is a command or a telemetered spacecraft action.

The significant terminal descent parameters are summarized in Table 5.11-2. The actual or best estimates of the Surveyor IV performance values are listed to loss of signal; the predicted values include significant parameters to touchdown. The table shows that performance during available signal return was nearly as predicted.

TABLE 5.11-1. BEST ESTIMATE TIMES FOR SURVEYOR IV TERMINAL DESCENT

Event	At SFOF (DSS-14)	At Spacecraft
Initiation of roll maneuver	01:24:44	01:24:45.2
Initiation of yaw maneuver	01:29:34	01:29:35.2
Initiation of roll maneuver	01:35:05	01:35:06.2
AMR power on	01:57:16	01:57:17.2
AMR mark	02:01:56.080 ± 0.005	02:01:54.858 ± 0.005
Vernier engine ignition	02:01:58.815 ± 0.025	02:01:57.593 ± 0.025
Retro engine ignition	02:01:59.924 ± 0.05	02:01:58.702 ± 0.05
RODVS on	02:02:31.484 ± 0.6	02:02:30.262 ± 0.6
Signal loss	02:02:41.018	02:02:40.796

5.11.4 PERFORMANCE ANALYSIS

5.11.4.1 Introduction

The Surveyor IV terminal phase performance has been investigated and analyzed from the telemetry and spacecraft transmitter one-way doppler data available up to loss of signal (42.2 seconds after vernier ignition). The performance reconstruction during this phase, as determined from postflight data, is compared with predicted preflight data reconstruction. This reconstruction is accomplished with the aid of digital computer programs and simulations as described in subsection 5.11.4.2.

TABLE 5.11-2. SUMMARY OF TERMINAL DESCENT PERFORMANCE PARAMETERS

Parameter	Nominal Value	Best Estimate Value
Retro phase initial condition		
Time, hr:min:sec	02:01:56.723	02:01:57.593
Altitude, feet	250,907.5	250,907.5
Velocity, fps	8,605.9	8,605.9
Attitude, degrees	30.38	30.38
Signal loss		
Altitude, feet	49,830	49,420
Velocity, fps	1,049	1,092
Attitude, degrees	31.54	31.54
Flight path angle, degrees	25.5	26.8
Vernier propellant consumed, pounds	38.79	38.69
Thrust-induced velocity change, fps	7,747	7,705
Retro burnout conditions		
Altitude, feet	40,896	—
Velocity, fps	503.8	—
Attitude, degrees	31.57	—
Flight path angle, degrees	13.68	—
Misalignment angle during retro		
In-plane, degrees	0	0.03
Out of plane, degrees	0	0.136
1000-foot mark conditions		
Slant range, feet	1,000	—
Velocity, fps	105	—
Attitude, degrees	1.5	—
10-fps mark conditions		
Slant range, feet	44	—
Velocity, fps	8.6	—
Attitude, degrees	0.12	—
Vernier engine cutoff conditions		
Slant range, feet	13	—
Velocity, fps	5	—
Attitude, degrees	0.02	—

Reconstruction of the terminal descent phase is primarily dependent on telemetered spacecraft velocities V_x, V_y, and V_z, slant range, and discrete time events. However, due to the loss of signal, much of these data were not available. Even though all three velocity radar beams acquired lock (RODVS), the spacecraft Z-axis velocity component was above the 800 fps telemetry saturation level at the time of signal loss. Radar altimeter acquisition did not occur, and reliable operate radar altimeter was not generated up to loss of signal. Only the lateral component of spacecraft velocity was available for terminal phase reconstruction. Most of the reconstruction presented here was determined from preflight data and spacecraft transmitter one-way doppler data.

The one-way doppler data, as received from the spacecraft by the tracking station, is utilized to determine the retro thrust-time curve, the total ΔV during the retro phase (up to data loss), and the spacecraft total velocity at the time of signal loss. The retro thrust-time curve is also reconstructed from retro accelerometer telemetry data.

The total vernier propellant consumption is determined by utilization of the vernier engine flight acceptance data of specific impulse and mixture ratio as a function of engine thrust for the midcourse and retro phases.

Included in this section is the expected soft landing location based on best estimate orbit determination data.

5.11.4.2 Digital Computer Programs Utilized

PREPRO

PREPRO is a preprocessing program utilized to reduce the telemetry data from raw BCD counts into appropriate engineering units. The Surveyor IV preflight calibration coefficients are utilized for the conversion of the telemetry signals, except for the SR, V_x, V_y, and V_z coefficients which are determined from postmission RADVS and telemetry channel assessment. Prior to conversion to engineering units, the FC-77 correction is made to the appropriate signals. The engineering data, significant to terminal descent reconstruction, are then interpolated into preselected equal time interval steps. PREPRO then outputs two tapes: tape No. 1 of the interpolated engineering data, and tape No. 2 of the signals in proper engineering units as telemetered.

POSTPR

POSTPR provides machine plots (CALCOMP) of input data tapes. The program has been modified to accept both PREPRO tape No. 1 and 6DOF data tape. This provides the capability of superimposing 6DOF and PREPRO parameters on the same plot.

6DOF

6DOF is a precision six degree-of-freedom digital program that simulates RADVS and flight control system and rigid body dynamics, including weight and moment of inertia changes. Preflight assessments of Surveyor IV parameters are inputs into the program.

TD1

TD1 is a two-dimensional, three degree-of-freedom digital computer program. It can be utilized to a limited extent for terminal descent trajectory reconstruction. The main utilization of TD1 is to determine the vernier propellant consumption. The program models the spacecraft to the extent necessary for accurate propellant consumption determination. Both mixture ratio and specific impulse, as a function of thrust, are included for each Surveyor IV engine from engine flight acceptance test data.

TTC

TTC reconstructs the retro thrust-time curve from raw accelerometer telemetry data. Corrections are made to the telemetry data by removing bias, scale factor, and hysteresis errors.

DOPP

DOPP reconstructs the main retro thrust-time curve from the spacecraft transmitter's one-way doppler data. This reconstruction technique is especially accurate since the frequency of the transmitter is very stable. Various error sources can exist in the doppler data, such as temperature sensitivity drift; however, they have been accounted for in the final reconstruction.

5.11.4.3 Velocity Change Due to Thrusting During Retro Phase

Determination of Ignition Conditions

Ignition velocity V_O, flight path angle γ, and roll angle φ serve as initialization parameters and are determined from tracking data. The 3σ uncertainty in free flight velocities is < 0.5 fps. Since ignition altitude has a calculated 3σ inaccuracy of 2240 feet due to marking range errors (with a $V = 8600$ fps and an incidence angle with respect to local vertical of 31 degrees), the equivalent ignition velocity uncertainty due to this error source is

$$\Delta V = gt = 5 \times \frac{2240}{8600} = 1.3 \text{ fps}$$

Hence, the total uncertainty in ignition velocity is 1.4 fps when these two independent error sources are combined. The direction of V_O at ignition has an uncertainty of < 0.07 degree. Therefore, the best estimate ignition conditions are

$$V_O = 8605.9 \pm 1.4 \text{ fps}$$

$$\gamma_O = -59.62 \pm 0.07 \text{ degree}$$

Gravity-Induced Component of Velocity

During the retro phase (from vernier ignition to signal loss), gravity contributes to the spacecraft velocity by an amount $\int g\ dt$. Lunar gravity varies in magnitude from 4.9 ft/sec² (at vernier ignition) to 5.23 ft/sec² (at signal loss). In addition, g varies in direction since the spacecraft has horizontal motion. The change in direction of g over the retro phase (to signal loss) is about

$$\int_0^t \sin^{-1}\left[\frac{V\ \sin\ \psi\ dt}{R_\ell}\right] = 1.16 \text{ degrees}$$

where

t = retro time

ψ = velocity vector incident angle

V = spacecraft velocity

R_ℓ = moon centered radial distance

Since the vehicle spends more time at lower altitudes than at higher ones, the average value of g for the retro phase will be closer to 5.23 ft/sec². The average value of g over the retro phase was 5.10 ft/sec². The time duration of the retro phase is 42.2 seconds (see Table 5.11-1). Actual numerical integration of $\int g\ dt$ gives gt = 215.7 ± 1 fps.

Thrust-Induced Velocity Change

The thrust-induced velocity change of the spacecraft is determined from the spacecraft one-way doppler data by the DOPP program. These data are input into DOPP and are corrected for the transmitter's temperature-dependent frequency drift within the program. This correction is determined by comparing postflight doppler data prior to vernier ignition with a simulated determination of the expected doppler shift, since at this period in the flight the actual doppler shift is well defined.

Figure 5.11-1 shows a comparison of actual and predicted Surveyor IV ΔV (retro plus verniers) versus time from vernier engine ignition to the time of signal loss. The ΔV during this phase is found by dividing the sum of the radial velocity change as determined from the doppler data and the gravity-induced velocity component in the same radial direction by the cosine of the angle between the tracking station-spacecraft line and the spacecraft thrust axis. A correction is made to the doppler data to account for the radial velocity change, ΔV_{ROT}, due to the earth's rotation. The thrust-induced velocity change, ΔV, can therefore be determined as follows:
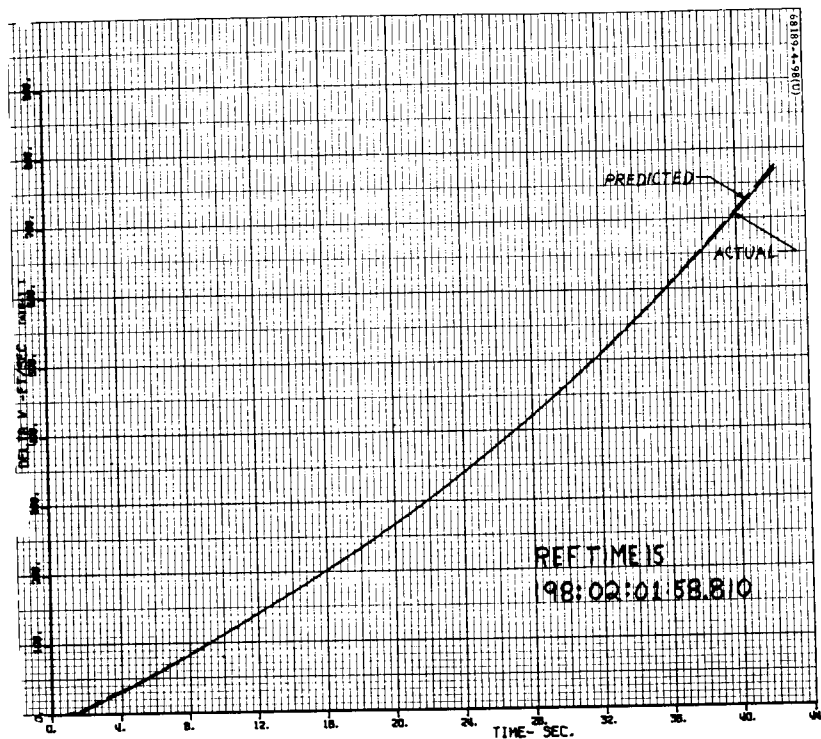
Figure 5.11-1. Surveyor IV ΔV of Retro Plus Vernier Engines From Vernier Ignition to Loss of Signal

$$\Delta V = \frac{\Delta V_{DOPP} + g\, t \cos \varphi + \Delta V_{ROT}}{\cos \xi}$$

where

ΔV_{DOPP} = velocity change seen by tracking station

$g\, t$ = gravity-induced velocity change

φ = angle between tracking station-spacecraft line and lunar gravity direction

ξ = angle between tracking station-spacecraft line and thrust direction

Therefore

$$\Delta V = \frac{5990 + 215.7 + 3.3}{\cos 36.3 \text{ degrees}} = 7705 \text{ fps}$$

There exists an uncertainty in the angle ξ of ±0.12 degree due to lateral translation of the spacecraft during the descent. There also exists an uncertainty in the temperature dependent doppler frequency drift of ±5 fps. The above uncertainties result in an uncertainty of ±12 fps in ΔV.

The nominal predicted ΔV of 7747 fps was computed by two methods for comparison purposes. Both methods assume the preflight vernier engine thrust level of 196.7 pounds total. One method consisted of numerically integrating the spacecraft acceleration by the 6DOF computer simulation in which predicted retro thrust versus time curve was an input. The other method consisted of converting simulated doppler data generated by the DOPP program using a predicted thrust versus time curve to spacecraft ΔV in the same manner as the flight data conversion was made. Since 7747 fps was obtained by both methods, added confidence can be given to the doppler ΔV conversion method.

The 42 fps difference between predicted and actual ΔV is comparable to Surveyor I and III results. Actual ΔV was 33 fps less than predicted for Surveyor I and 16 fps less than predicted for Surveyor III. Table 5.11-3 shows actual and predicted ΔV's for all three spacecraft. The ΔV's for Surveyors I and III are from vernier engine ignition to the beginning of RADVS-controlled descent, while the ΔV for Surveyor IV is from vernier engine ignition to the time corresponding to the loss of telemetry.

Assuming a nominally performing main retro and vernier system resulting in the total ΔV of 7747 fps, the vernier system would have contributed a ΔV of 171 fps. The average value of the modulated telemetry signal of the vernier engine thrust commands indicates the engines to be thrusting at their expected levels; therefore, by assuming nominally
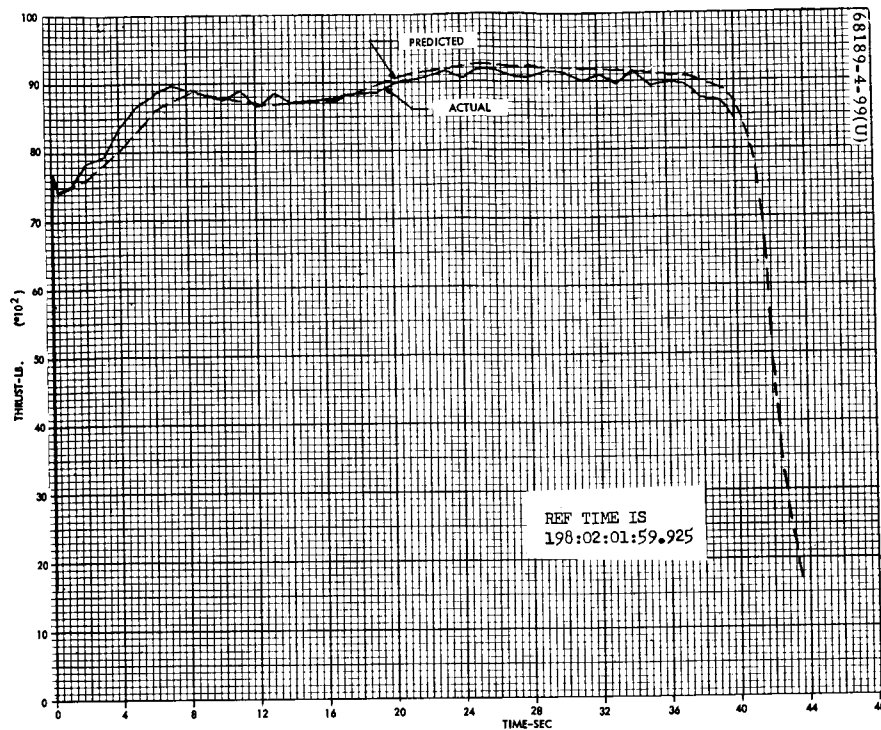
Figure 5.11-2. Surveyor IV Retro Thrust Versus Time as Reconstructed
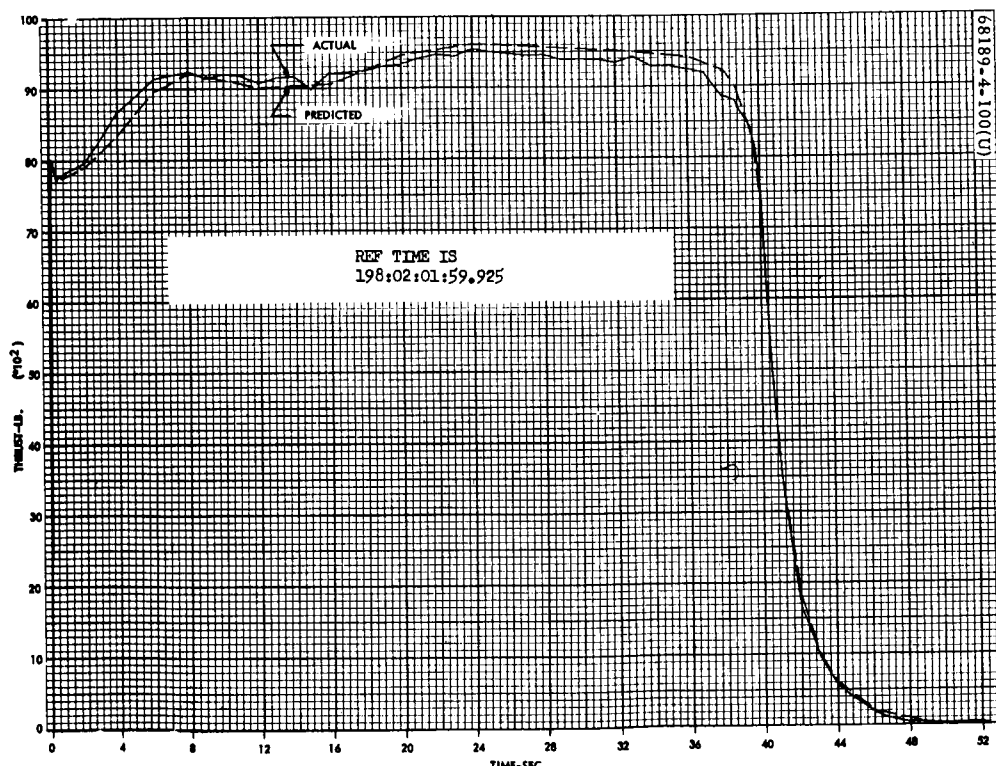From Tracking Station Doppler Data

Figure 5.11-3. Surveyor III Retro Thrust Versus Time as Reconstructed
From Tracking Station Doppler Data

TABLE 5.11-3. COMPARISON OF ACTUAL TO PREDICTED ΔV REMOVED BY RETRO PLUS VERNIERS (FPS)

	Surveyor I	Surveyor III	Surveyor IV
Predicted	8453	8438	7747
Actual	8420	8422	7705

performing vernier engines, the percentage loss in retro performance up to the time of signal loss can be determined as follows:

$$\frac{\delta V}{\Delta V} \times 100 \text{ percent} = \frac{7705 - 7747}{7747 - 171} \times 100 = 0.55 \text{ percent loss}$$

It cannot be determined if this indicates a 0.55-percent loss in retro specific impulse since data were not available throughout the entire retro burn. If the data had been available, it might have shown that the Surveyor IV retro operated at a lower than predicted thrust for a longer than predicted burn time, thereby making up the ΔV lost up to the time of telemetry loss.

5.11.4.4   Main Retro Thrust Versus Time Curve

Two methods used to calculate the retro's thrust versus time curve were as follows:

1)   Thrust/time from doppler data

The Surveyor IV retro thrust versus time reconstruction from one-way tracking station doppler data indicates a nearly normal performing retro up to the time when data were lost. This reconstruction (Figure 5.11-2) was made by the DOPP computer simulation which perturbed the Surveyor IV nominal thrust time curve by an iterative procedure until doppler data simulated by this program agreed with the actual spacecraft transmitter frequency doppler shift measured by the tracking station. For comparison purposes, the Surveyor III doppler thrust versus time reconstruction along with the predicted Surveyor III curve is shown in Figure 5.11-3.

The unevenness in the Surveyor IV reconstruction is apparently caused by noise in the doppler data. Figure 5.11-4 shows a comparison of doppler noise levels for Surveyors III and IV for a 10-second period prior to retro ignition. The data shown here are available every second and are doppler count data which represent twice the frequency shift measured by the tracking station. These data prior to ignition represent the spacecraft velocity change caused by lunar gravity and would appear as smooth straight lines if no noise existed. It can be seen that the Surveyor IV data are noisier than the Surveyor III data.
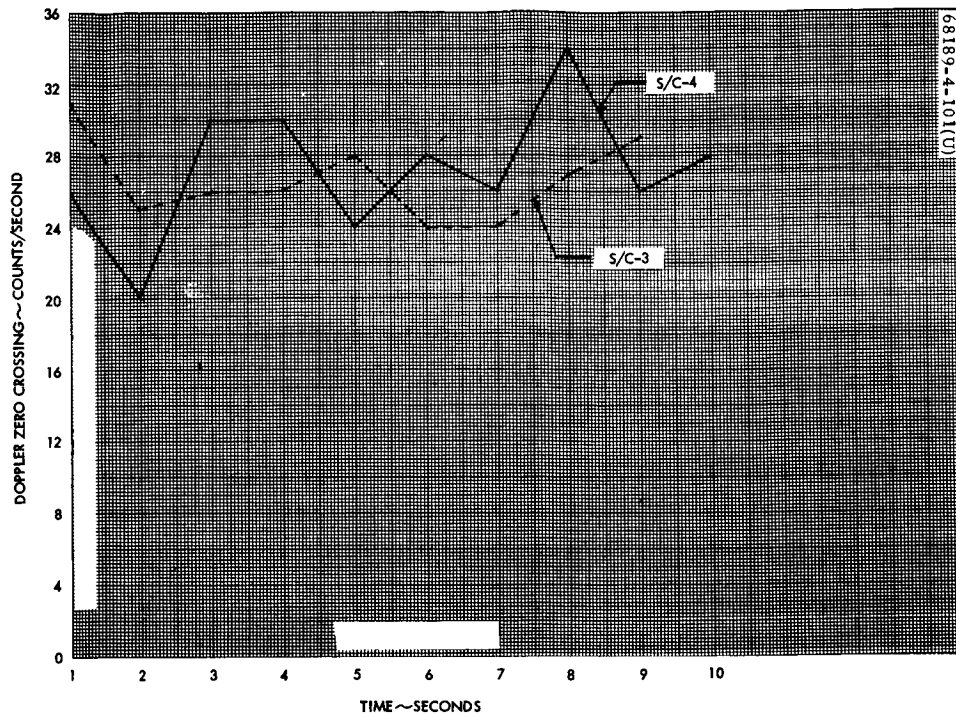
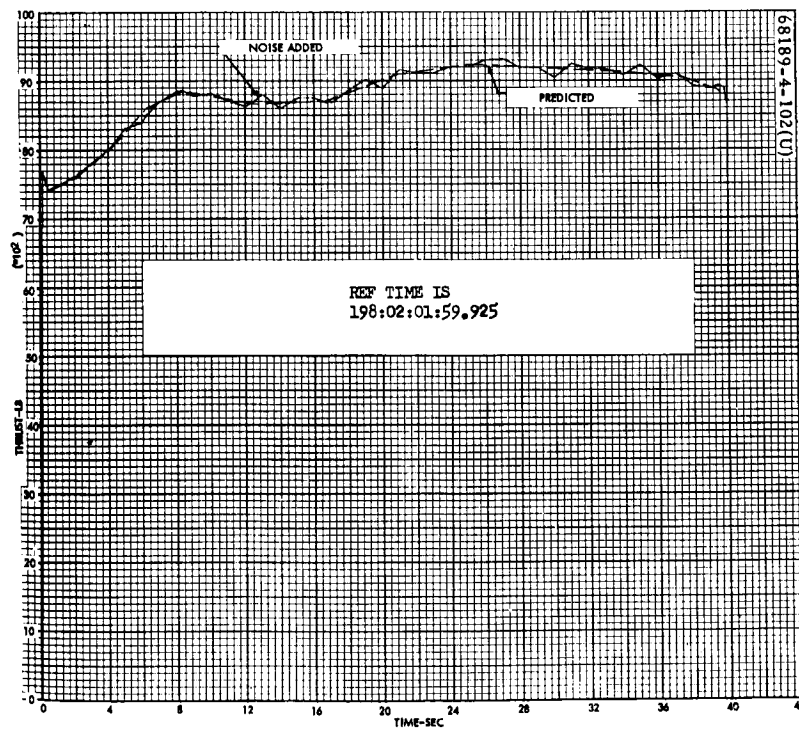Figure 5.11-4. Doppler Count Data 10 Seconds Prior to Retro Ignition

Figure 5.11-5. Surveyor IV Thrust Versus Time History — Predicted and With Preretro Doppler Noise Added

To determine the effect of Surveyor IV doppler noise, a thrust versus time curve was reconstructed from doppler data simulated by a predicted Surveyor IV thrust versus time curve from pre-ignition Surveyor IV doppler noise superimposed on the data. This reconstruction (Figure 5.11-5) shows that the unevenness caused by doppler noise superimposed on the predicted curve is the same as the unevenness in the actual Surveyor IV doppler reconstruction (Figure 5.11-2), indicating that the variations in the Surveyor IV reconstruction are due to doppler noise.

2) Thrust/time from retro accelerometer data

Before being used to calculate a thrust curve, the raw accelerometer data were given the following two corrections:

a) A bias, as determined from preretro ignition telemetry data, was removed.

b) A scale factor error was removed. This was done by integrating the unbiased accelerometer data over time and comparing the resulting integral with the ΔV computed from doppler data.

The corrected acceleration, a(t), was then used in the equation

$$T(t) = \frac{a(t)}{go} \left[W_o - \int_o^t \frac{T(t)}{I_{sp}} dt \right]$$

which is integrated numerically to obtain total thrust (W_o is weight at retro ignition). Vernier engine thrust is then subtracted out to obtain the retro thrust.

Figure 5.11-6 shows the Surveyor IV retro thrust versus time curve as reconstructed by the TTC program with the retro accelerometer telemetry data as input. The oscillations in this reconstruction are caused by accelerometer stiction and were seen in thrust-time reconstructions of Surveyors I and III. Figure 5.11-7 shows the Surveyor IV accelerometer telemetry data (FC-32) plotted versus time, while the Surveyor III accelerometer telemetry data (FC-32) are shown in Figure 5.11-8 for comparison purposes.

Comparison of Two Methods for Retro Thrust/Time Curve

Both reconstructions show the same general shape with the curve beginning slightly higher than predicted and ending slightly lower than predicted. A similar trend was seen in the Surveyor I and III reconstructions.

The two methods of reconstruction are not completely independent since the accelerometer data were scaled to give the same ΔV as the doppler
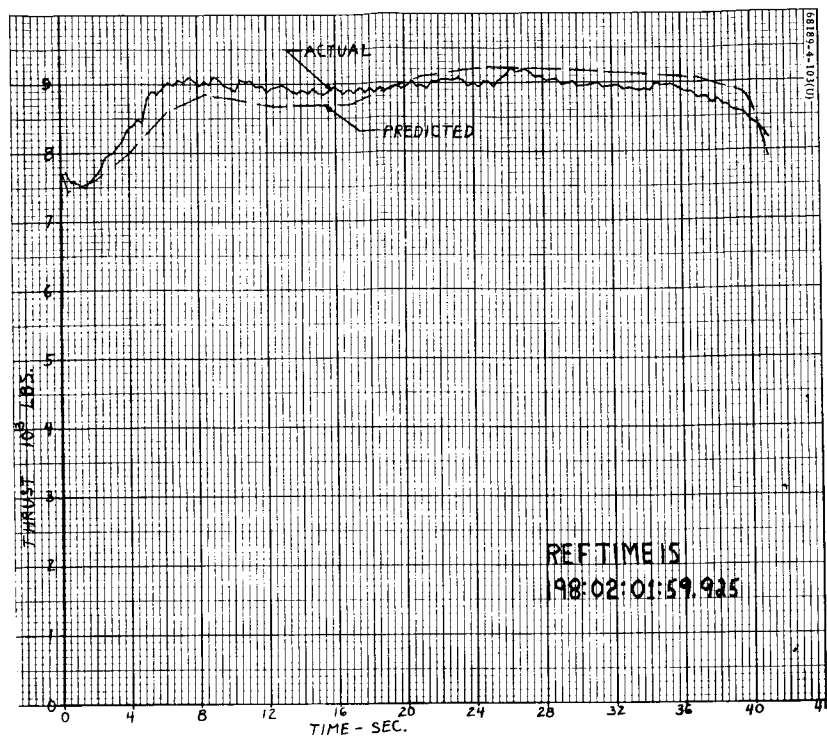
Figure 5.11-6. Surveyor IV Retro Thrust Versus Time Reconstructed From Retro Accelerometer Data
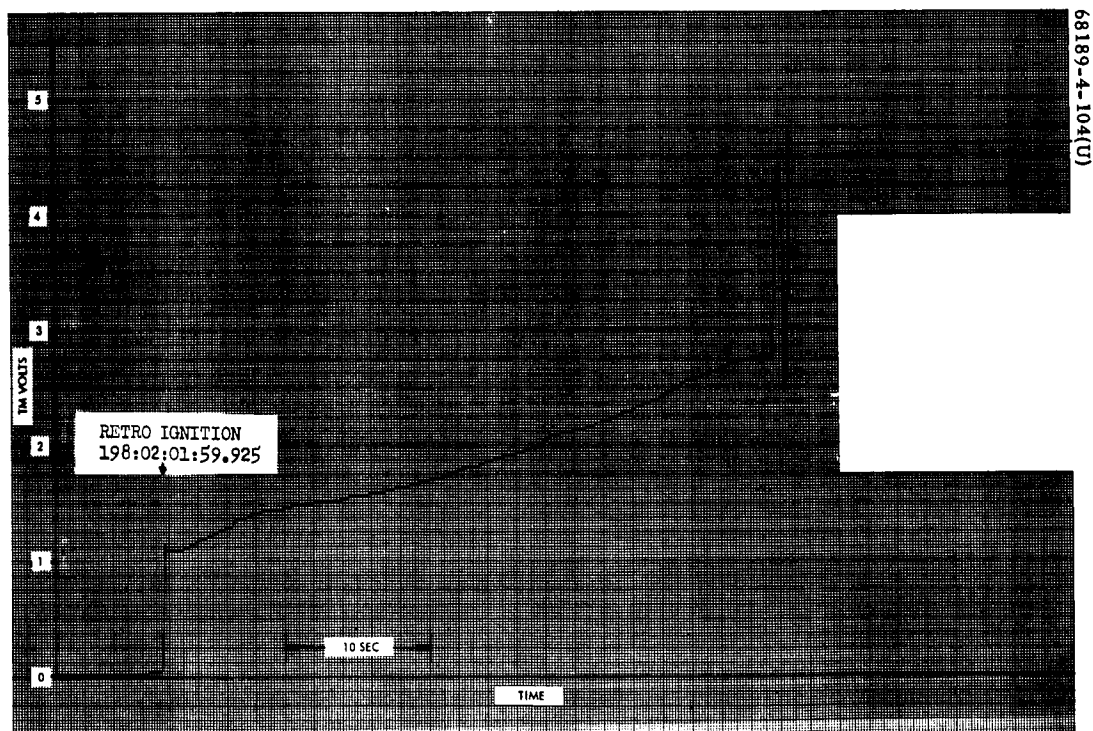

Figure 5.11-7. Surveyor IV Terminal Phase — Retro Accelerometer FC-32

data. The nominal predicted retro specific impulse was used in both recon-
structions, since the ΔV difference of 42 fps up to the time of data loss could
not be attributed directly to a loss in retro specific impulse.

5.11.4.5 Altitude and Velocity at Time of Signal Loss

Spacecraft altitude and total velocity could not be determined from
telemetry data since RORA had not appeared before the time of signal loss
and the spacecraft's Z-axis velocity was telemetry saturated. However, the
total velocity at loss of signal can be obtained by vectorially adding ignition
velocity V_O, thrust-induced ΔV, and lunar gravity-induced velocity component
gt.
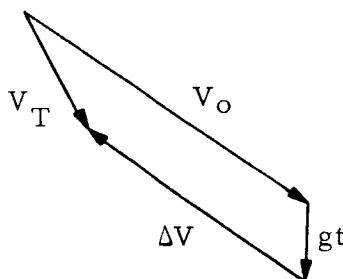
Since the thrust misalignment was primarily in the trajectory plane
(see Figure 5.11-9), the four vectors in the above illustration can be assumed
coplanar, and the total spacecraft velocity, V_T, at signal loss is computed to
be 1092 fps.

At the time of signal loss, the telemetered values of spacecraft
lateral velocity components were

$$V_x = -20 \text{ fps}$$

$$V_y = -91 \text{ fps}$$

Therefore

$$V_z^2 = V_T^2 - V_x^2 - V_y^2$$

or

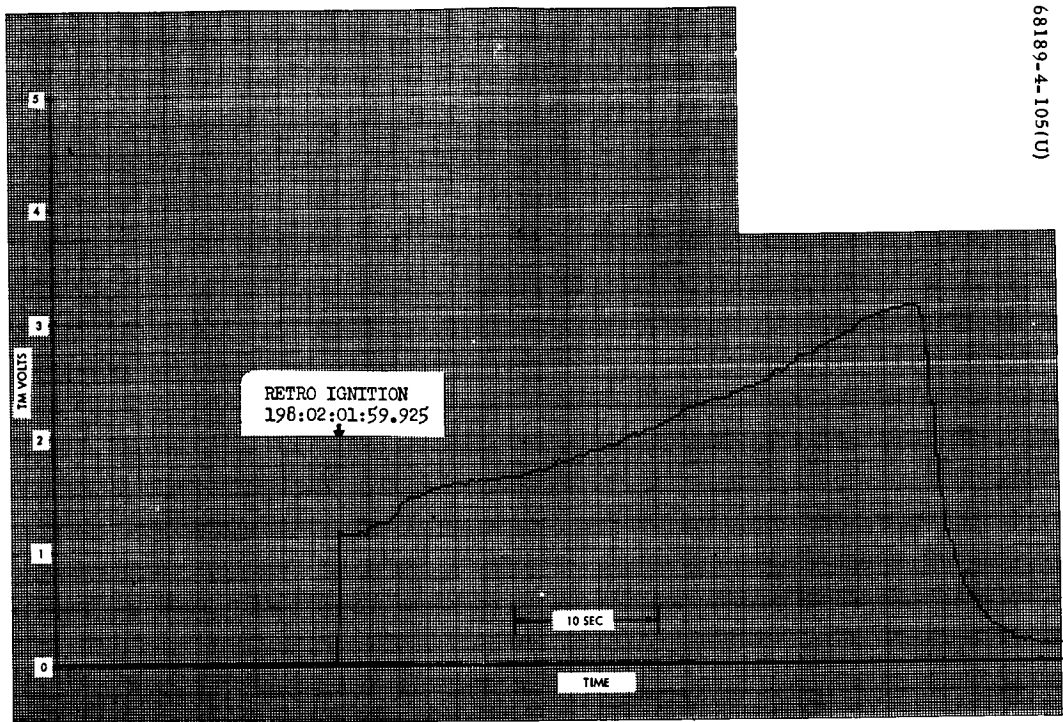$$V_z = 1088 \text{ fps at time of signal loss}$$

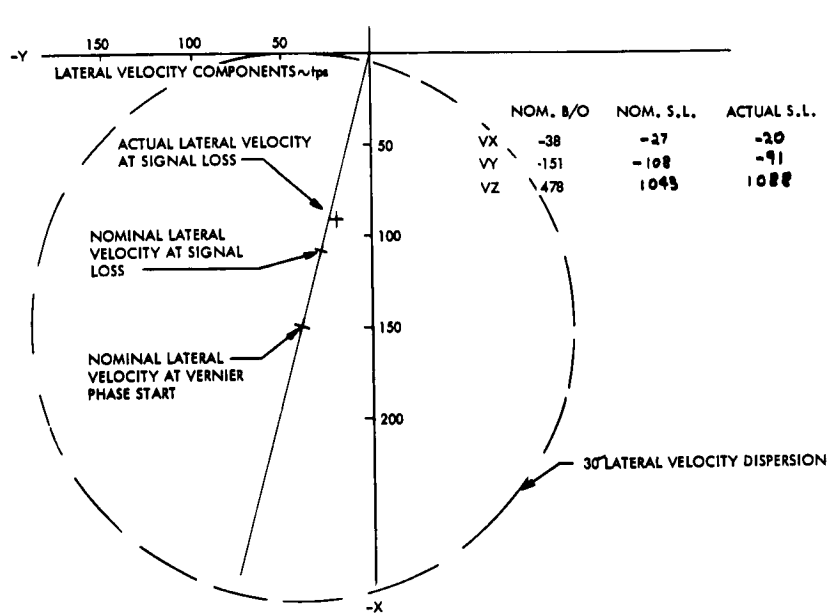Figure 5.11-8. Surveyor III Terminal Phase — Retro Accelerometer FC-32

Figure 5.11-9. Lateral Velocity

The total velocity of 1092 was also obtained from the TD1 computer program using the doppler reconstructed thrust versus time curve and a retro thrust vector pointing error of 0.14 degree as determined in subsection 5.11.4.6. The spacecraft altitude, as determined by TD1, was 49,420 feet at time of signal loss. Predicted altitude at this time using this program with the predicted retro thrust-time curve as an input was 49,830 feet.

5.11.4.6 Thrust Vector Pointing Accuracy

Figure 5.11-9 presents data used to compute the average error in spacecraft thrusting direction during the Surveyor IV retro phase. The 6DOF computer program was used to predict the expected spacecraft lateral velocity at retro burnout. In Figure 5.11-9, this value is plotted and listed in the accompanying table. Also shown is the expected 3σ lateral velocity dispersions caused by 1-degree attitude uncertainty.

From the same computer program, the expected lateral velocity at signal loss was also plotted. Comparing the nominal velocity conditions with actual obtained from telemetry indicates an error of 19 fps. The average attitude error (μ) in degrees required to generate a 19-fps lateral velocity error (EV_L) is

$$\mu \cong \frac{EV_L}{\Delta V} \times 57.3 \text{ deg/rad}$$

where ΔV is the integral of the thrust acceleration at the time of signal loss. Therefore

$$\mu = \frac{19 \text{ fps}}{7705 \text{ fps}} \times 57.3$$

$$\mu = 0.14 \text{ degree}$$

The above average attitude error is less than the equivalent values computed for Surveyors I and III and is considerably better than the 3σ maximum.

5.11.4.7 Vernier Propellant Consumption

The total vernier propellant consumption during the midcourse and terminal phase portion to loss of signal is based on vernier engine acceptance test performance data of both specific impulse and mixture ratio as a function of engine thrust.

Based on post-touchdown orbit determination data, the desired midcourse maneuver of 10.27 m/sec is apparently accurate for propellant computational purposes. Based on this ΔV correction, the total vernier propellant consumed was calculated to be 8.83 pounds.

The main retro phase propellant consumption computations are inherently the most inaccurate because of the open-loop nature of the thrust commands. While at midcourse, the change in spacecraft velocity is a very accurate measure of engine impulse; during the retro phase, the main retro engine overshadows any expected variation in vernier performance.

From vernier ignition to loss of signal (42.2 seconds duration), the propellant consumption, based on premission computations of the expected vernier thrust level of 196.7 pounds, is 29.96 pounds. However, by averaging the modulation of the telemetered vernier engine thrust commands and integrating these values over time results in a total propellant consumption of 29.86 pounds. This discrepancy between premission expectation of vernier engine thrust levels and telemetered thrust commands also existed in Surveyors I and III. The explanation for this discrepancy has not yet been determined.

5.11.4.8 Predicted Spacecraft Touchdown Location

The original targeted landing site for Surveyor IV was 0.58°N latitude and 0.83°W longitude. The computed midcourse correction of 10.27 m/sec would enable the spacecraft to soft land at 0.417°N latitude and 1.333°W longitude. Had Surveyor IV successfully soft landed, the current best estimate of the landing location as determined from postretro phase orbit determination data would have been 0.43°N latitude and 1.61°W longitude with a 3σ dispersion ellipse of 6.0-km semimajor axis and 4.5-km semiminor axis. This results in an 8.6-km miss between the final best estimate of the soft landing location and the premidcourse estimate. This final point is almost at the 3σ limits of the premidcourse aim point. However, based on Lunar Orbiter photos of the Surveyor I amd III landing locations, there was a consistent 3-km difference in an almost easterly direction between the orbit determination data and the Lunar Orbiter photos. Therefore, an apparent bias seems to exist in the orbit determination program. An investigation is under way to determine a probable bias in the orbit determination program. If a 3-km bias is assumed, the final landing location would only be 5.6 km off, which is well within the 3σ limits of the premidcourse prediction.

If it is assumed that Surveyor IV proceeded along a ballistic path after loss of signal, the impact point based on orbit determination data would have been 0.452°N latitude and 1.39°W longitude with a 3σ uncertainty of 3 km.

5.11.5 ACKNOWLEDGMENTS

Victor Marelia, Coordinator

Eddy White, retro thrust-time curve reconstruction; ΔV determination

Leonard Davids, thrust vector pointing accuracy